Postglacial relative sea-level changes and the deglaciation of northwest Iceland

BRADER, MARTIN,DAVID

Martin David Brader

Postglacial relative sea-level changes and the deglaciation of northwest Iceland

Abstract

Iceland provides an important opportunity to investigate relative sea-level (RSL) changes and Last Glacial Maximum (LGM) glaciation in a sensitive area of the North Atlantic. This project employs new and existing RSL data, coupled with glacio-isostatic adjustment (GIA) modelling, to resolve the current debates surrounding the extent of the LGM Icelandic ice sheet (IIS). Robust understanding of the LGM IIS is important, because there are two markedly different maximum and minimum ice loading scenarios, with very different implications for global thermohaline circulation. Previous studies of glacial geomorphology and sedimentology have failed to differentiate between these scenarios. Reconstructing RSL changes in northwest Iceland can address this issue because the two LGM glaciation scenarios yield significantly contrasting RSL histories. Northwest Iceland is also an important location in which to determine Earth models for Iceland. In this study, a series of new sea-level index points (SLIPs) have been generated for northwest Iceland from isolation basin and coastal lowland sediment samples along two perpendicular transects. Diatom, tephrochronological and radiocarbon analyses have allowed the generation of new RSL curves for the region, showing higher marine limit elevations close to loading centres and differing influences of Younger Dryas ice re-advance. Mapping of the marine limit has shown differences in the pattern of deglaciation due to fjord width and morphology. The contrasting LGM glaciation scenarios have been tested using the GIA modelling, with the new and existing RSL dataset as a constraint. Both field data and GIA model outputs support the maximum glaciation hypothesis.

Postglacial relative sea-level changes and the deglaciation of northwest Iceland

Martin David Brader

Thesis submitted for the degree of Doctor of Philosophy

Department of Geography

Durham University

2015

Contents

List of Tables

List of Illustrations

Copyright Declaration

Acknowledgements

I would like to thank my supervisory team, Dr Jerry Lloyd, Prof. Mike Bentley, Dr Anthony Newton and Dr Natasha Barlow, for their support and guidance throughout this research project. They have been a constant source of encouragement and advice over the course of the PhD and I am very grateful for all that they have done to support me. I have been very fortunate to work with them.

I would also like to acknowledge the assistance of my excellent field assistants – Sam Gunter, Harry Inman, Christopher Darvill and Matthew Edwards – who provided valuable help in the collection of the field samples, as well as sharing some spectacular field cuisine and Icelandic confectionary, which of course was marked competitively!

I would also like to thank Dr Hreggviður Norðdahl (University of Iceland) who advised on and assisted in the collection of samples from Breiðavik, Látrar. The valuable advice provided by Prof. Giorgio Spada and Dr Daniele Melini on SELEN is also greatly appreciated. I would also like to acknowledge the provision of the three Icelandic Ice Sheet models employed within this research by Dr Henry Patton and Prof. Alun Hubbard and the assistance of Dr Pippa Whitehouse with gfortran queries.

A number of people have offered additional support as part of this PhD research. I would like to thank Prof. Andrew Dugmore, the University of Edinburgh and the North Atlantic Biocultural Organisation (NABO) for the use of a Land Rover for fieldwork in Iceland. Dr Chris Hayward (University of Edinburgh) provided valuable discussions on tephra analysis. In addition, I would like to thank Dr Karen Milek and the participants of the Forneifastöfnun Íslands (FSI) Field School at Vatnsfjörður, for their welcome whilst undertaking fieldwork in the area, as well as providing an insight into the human use of some of the field locations.

The welcome and generosity of Birna Mjöll Átladóttir and the staff at Breiðavik was much appreciated during both field seasons – thank you for the fantastic Icelandic lamb and for the Vitamin C when I was unwell! I would also like to thank the many Icelandic landowners with whom we had contact, for the permission granted to access their respective properties, the much-welcome coffee on wet Icelandic field days and their interest in my research.

The support of several funding bodies is also gratefully acknowledged – the Quaternary Research Association Dudley Stamp Memorial Award, British Society for Geomorphology Postgraduate Award, Royal Geographical Society (with IBG) Postgraduate Research Award, Van Mildert College Postgraduate Award, Durham University Faculty of Social Sciences PhD Projects and Initiatives Scheme, Van Mildert College Principal's Award, NERC Radiocarbon Allocations (Alloc. No. 1689.0313 and 1748.1013) and NERC TAU Support (NERC TAU78/1012). I would also like to thank RANNÍS (The Icelandic Centre for Research) and Umhverfisstofnun Íslands (The Environment Agency of Iceland) for permission to undertake the research in Iceland.

I have been fortunate to have a fantastic time in Durham both in the Department and my College. Thank you to everyone for making the experience so enjoyable.

I would also like to thank my examiners, Professor Roland Gehrels and Dr Mark Tamisiea, for reviewing this research and generating insightful discussions within the viva. Both examiners provided constructive comments on the original manuscript which have improved this thesis.

Finally, I would like to acknowledge the support and encouragement from my family, without which this research would not have been possible.

CHAPTER 1

Introduction

1.1 Introduction

Undertaking RSL study in Iceland provides an opportunity to investigate RSL changes in a sensitive area of the North Atlantic, where the input of freshwater during deglaciation could have had important consequences for global thermohaline circulation and climate (e.g. Hubbard *et al*., 2006). Despite this, limited research has been undertaken to determine accurate reconstructions of postglacial relative sea-level (RSL) change and the deglacial history of northwest (NW) Iceland (e.g. Rundgren *et al.*, 1997; Gehrels *et al.*, 2006; Lloyd *et al.*, 2009). As a result, NW Iceland continues to pose questions when conducting geophysical and ice sheet modelling of the former Icelandic Ice Sheet (IIS) (e.g. Hubbard *et al.*, 2006), particularly as several of the existing RSL records suffer from a lack of dateable material, weak assumptions surrounding feature formation and limited sea-level index point (SLIP) datasets. Where research has been undertaken, there has been a focus on geomorphological mapping of the local marine limit and raised shorelines (e.g. Einarsson, 1968; Hjort *et al.*, 1985; Hansom and Briggs, 1991; Ingólfsson, 1991; Ingólfsson and Norðdahl, 2001; Norðdahl and Pétursson, 2005; Principato, 2008), which are often limited by poor spatial coverage (Lloyd *et al.*, 2009). More recently, a small number of isolation basin and saltmarsh studies have been completed in northern and western Iceland, providing more comprehensive records of environmental and RSL changes for particular regions (e.g. Rundgren *et al.*, 1997; Gehrels *et al.*, 2006; Lloyd *et al.*, 2009; Brader, 2012; Saher *et al.*, 2015).

This thesis will provide a series of accurate RSL reconstructions for NW Iceland, with the principal aim of resolving the ice loading histories and crustal structure of the region. The principal drivers for RSL change on a local and regional scale will be investigated, with implications for global reconstructions of postglacial RSL changes. The current debates surrounding the extent and scale of the Last Glacial Maximum (LGM) IIS will be resolved, through the employment of a comprehensive high spatial density RSL dataset to establish accurate patterns of glacio-isostatic adjustment (GIA) in the region. The response of the Icelandic lithosphere to ice loading and removal will be explored, with implications for studies in similar plate boundary locations elsewhere. At present, there are two contrasting hypotheses of the LGM glaciation of Iceland, with differences in ice volume and distribution (e.g. Hansom and Briggs, 1991; Hubbard *et al.*, 2006). The RSL data presented will therefore also allow the testing of the two glaciation

scenarios, including the proposed secondary ice loading centre in NW Iceland (e.g. Hansom and Briggs, 1991).

Understanding the glacial history of Iceland is of particular importance due to its position close to a sensitive area of deepwater formation in the north Atlantic; meltwater from the LGM IIS has the potential to affect global thermohaline circulation and therefore global climate (Hubbard *et al.*, 2006). As a result, determining the patterns of deglaciation and scale of the LGM IIS would allow more accurate predictions of meltwater volume and the potential effects on global thermohaline circulation.

In this study, sedimentological, geomorphological and microfossil analyses will provide sufficient high quality data to produce RSL curves for four areas of NW Iceland, highlighting variations in the RSL histories both across and away from hypothesised ice loading centres at the LGM. Although mapping of the marine limit has been undertaken (e.g. Norðdahl and Pétursson, 2005), few sites are accurately dated and so the implications for deglacial history are difficult to interpret. Isolation basin studies are also relatively scarce (Rundgren *et al.*, 1997; Lloyd *et al.*, 2009; Brader, 2012), which could provide more complete records of postglacial RSL. Therefore, there are currently relatively few reliable reconstructions of ice loading history, with several modelling studies reliant on limited data and assuming synchroneity between features without robust chronological constraints (e.g. Le Breton *et al.*, 2010). Furthermore, there is relatively little published mapping of the former ice limits in Iceland, much of which may lie offshore, such as the Breiðarfjörður moraine (e.g. Ólafsdóttir, 1975; Syvitski *et al.*, 1999). A recent mapping study has identified a series of potential ice streams and moraine features within major Icelandic fjord systems (Spagnolo and Clark, 2009). However, many of the conclusions drawn in previous modelling studies rely on the mapping of undated marine limit elevations. This thesis will therefore provide the first critical test of the maximum and minimum glaciation hypotheses through the construction and testing of GIA models for the region. In doing so, the ice loading history and crustal structure of NW Iceland will be investigated, with important consequences for future study.

1.2 Aims and Objectives

This research aims to resolve the current debates surrounding the Last Glacial Maximum (LGM) ice loading histories and crustal characteristics of northwest Iceland, using a suite of new and existing relative sea-level (RSL) data.

In order to meet this research aim, a series of objectives will be realised:

1. Collection of field data (isolation basin sediments and marine limit elevations)
2. Palaeoenvironmental reconstruction (sediment and microfossil analyses, radiocarbon dating and tephrochronology) to provide RSL records
3. Assessment of the spatial patterns of relative sea-level (RSL) changes in northwest Iceland
4. Modelling of glacio-isostatic adjustment (GIA) to test regional ice models and rheological characteristics

The principal research question explored within this thesis is:

Did Iceland experience a maximum or minimum glaciation at the Last Glacial Maximum?

1.3 Thesis outline

Following the Introduction, this thesis is divided into a further eight chapters. Chapter 2 provides an overview of the present published research on the glacial, deglacial and RSL histories of Iceland since the LGM. The chapter includes an overview of the hypotheses of the LGM glaciation of Iceland, stages of deglaciation and RSL history, alongside the evidence for a RSL lowstand in the early Holocene. The application of tephrochronology in environmental reconstruction is explored, alongside the current modelling of the LGM IIS and rheological profile in Iceland. It is concluded that there are limitations to the existing RSL dataset, with northwest Iceland having the potential to differentiate between ice loading scenarios due to the contrasting implications for the RSL changes experienced in the region.

Chapter 3 provides an overview of the research design and location of the field and GIA modelling locations. The justification of site selection is outlined, alongside the implications for the testing of the contrasting glaciation hypotheses. Site descriptions are provided by field research area, comprising an overview of the geographical location, site elevation and morphology.

Following this outline, Chapter 4 summarises the methodology employed to address the research objectives. The chapter is divided into three distinct sections: field methods, laboratory methods and GIA modelling. The chapter provides an overview of the chosen techniques, alongside their principal limitations, justifying the approaches adopted. The methods outlined relate to the results presented in Chapters 5, 6 and 7.

Chapter 5 summarises the results of geochemical analyses on tephra samples from a number of sediment cores extracted from sites in NW Iceland as part of this research. Correlations with previous study and known tephra horizons, or isochrones, are presented in order to assist in the interpretation of the environmental data presented in the next chapter. The tephrochronological

results allow the construction of an overview figure of the tephra analyses completed in isolation basin and coastal lowland sites in NW Iceland.

The results of sediment and diatom analyses are outlined in Chapter 6, which includes a summary of the site stratigraphy, core sediment log, diatom assemblage and environmental interpretation. Results are outlined for each site by field research area and integrated with tephra results from Chapter 5. At the end of the chapter, a table of sea-level index points (SLIPs) for NW Iceland is presented, providing an overview of the data employed in the testing of GIA models outlined in Chapter 7. The SLIPs are also presented in graphical format for each field area to provide a visualisation of the key trends within the dataset.

Chapter 7 contains the results of GIA modelling in Iceland, using a suite of ice and Earth models. Model outputs from ICE5G (VM2) (Peltier, 2004) and Icelandic ice models (Patton, unpub.; e.g. Hubbard *et al*., 2006) and viscosity profiles are presented. Initial results on an Iceland-wide scale are presented for each model, followed by outputs for the NW. For each model, chi^2 testing provides a measure of fit between the field-based RSL reconstructions and modelled RSL predictions for each research area, allowing the determination of likely ice loading, lithospheric thickness and mantle viscosity scenarios.

Chapter 8 discusses the implications of the results outlined in Chapters 5, 6 and 7 both in a global and regional context during the LGM deglaciation. Potential factors affecting the disintegration of the LGM IIS are outlined, alongside the consequences for the deglaciation of the ice sheet and associated patterns of RSL change. In addition, the preferred GIA model characteristics are explored, including the preferred lithospheric thickness, mantle viscosity profile and ice loading scenario.

Chapter 9 summarises the principal conclusions of the thesis. In addition, limitations of the present research are outlined, alongside areas for future research and development.

CHAPTER 2

Background and Rationale

2.1 Introduction

This chapter provides a rationale for the current study through the exploration of existing research and literature into the glacial, deglacial and RSL histories of Iceland. The chapter will provide an overview of the Last Glacial Maximum (LGM) Icelandic Ice sheet (IIS) and the stages of deglaciation identified in Iceland. In turn, the consequences of deglaciation on RSL change in Iceland will be explored, alongside the evidence for a RSL lowstand during the mid-Holocene. The use of tephrochronology will also be explored, both in terms of delimitation of the LGM IIS and the production of RSL records. Finally, glacio-isostatic adjustment modelling in Iceland will be evaluated to determine the key areas for future research.

2.2 The Last Glacial Maximum Icelandic Ice Sheet

2.2.1 Last Glacial Maximum (LGM) ice extent

Previous investigation of the LGM Icelandic Ice Sheet (IIS) has been undertaken using a range of methods, including geomorphological mapping (e.g. Ólafsdóttir, 1975; Egloff and Johnson, 1979; Norðdahl and Pétursson, 2005), glacial striation identification (e.g. Thorodssen, 1905-1906; Keith and Jones, 1935; Einarsson, 1967; Hoppe, 1968; 1982), sedimentological analyses (e.g. Syvitski *et al.,* 1999; Andrews *et al.*, 2000) and ice sheet modelling (e.g. Bingham *et al.*, 2003; Hubbard *et al.*, 2006). Despite this body of evidence, there remains uncertainty surrounding the vertical and lateral extent of the LGM IIS, with estimations varying between studies (e.g. Rundgren and Ingólfsson, 1999; Hubbard *et al.*, 2006). It is however clear that Iceland was covered by a considerable ice mass at the LGM (Ingólfsson *et al.*, 2010).

Initial research into the extent of the LGM IIS concentrated on glacial striations in Eyjafjörður, where striae running parallel to the fjord led to the proposition of a single ice mass hypothesis (Thorodssen, 1905-1906; Fig. 2.1). Later research identified glacial striations (Einarsson, 1967) and smoothed bedrock (Keith and Jones, 1935) on Grímsey, north Iceland providing evidence for glaciation 40 km from the present coastline. Additional research into sedimentology and seismic profiling has provided additional evidence to support this assertion in North Iceland (e.g. Andrews *et al.*, 2000). Andrews *et al.* (2000) analysed a number of sediment cores from north of Vestfirðir,

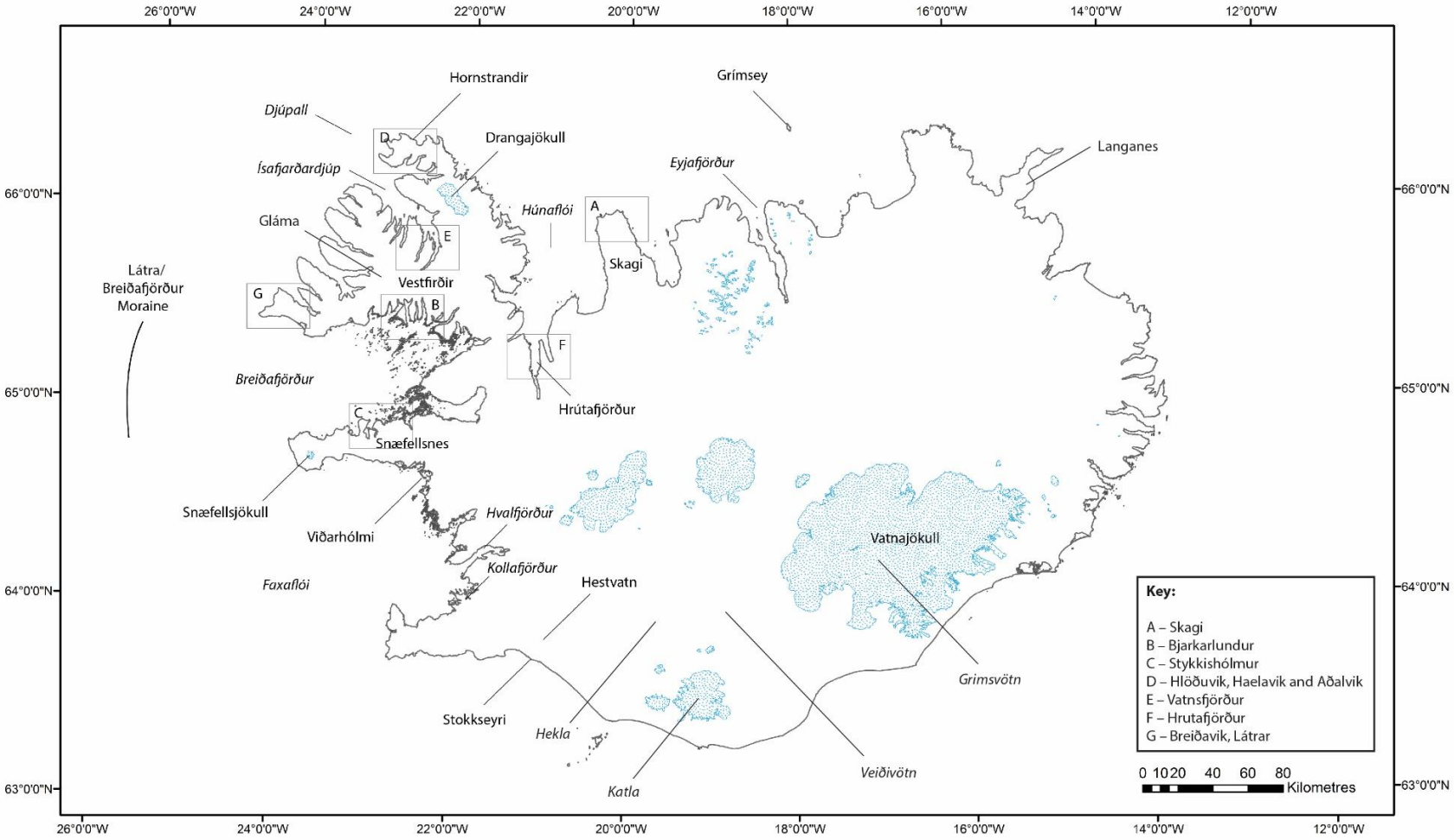

Figure 2.1 – Locations mentioned in the text, with the exception of volcanic systems (see Fig. 2.14) and tide gauge locations (see Fig. 4.3A).

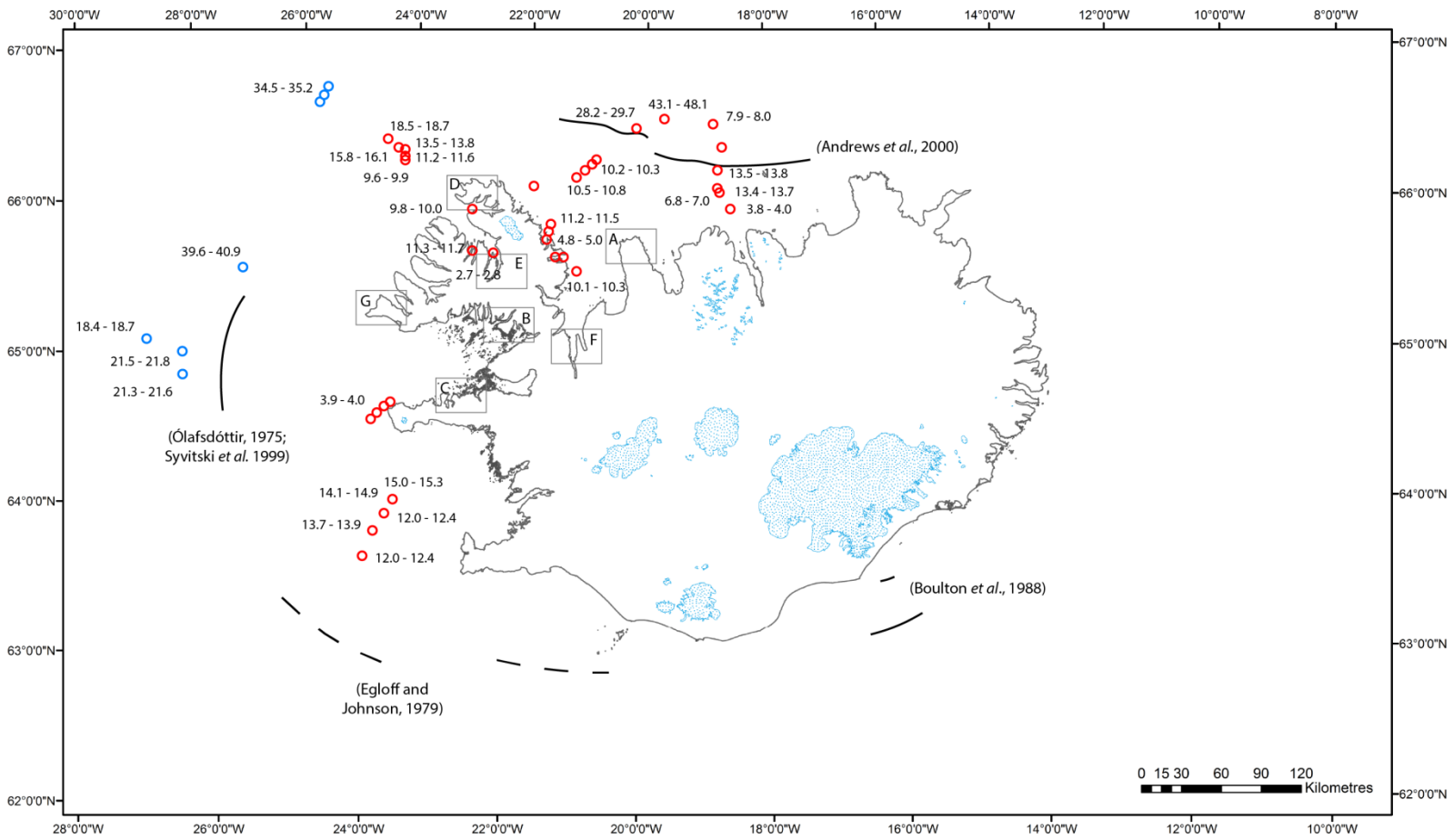

Figure 2.2 – Previous sedimentological studies in Iceland, alongside the proposed ice sheet limits. Boxes A-G represent research areas explored within this thesis in northwest Iceland. Blue and red circles represent coring locations of two cruises outlined in Andrews et al. (2000).

generating 32 AMS radiocarbon ages from basal peat deposits ranging from 10 cal. ka BP to 16 cal. ka BP (Fig. 2.2). Within this thesis, all published radiocarbon dates have been calibrated using CALIB7.1 (Stuiver *et al.*, 2014) and the IntCal13 and Marine13 datasets (Reimer *et al.*, 2013). These basal dates provide a useful constraint on the extent of glaciation of the Iceland shelf, highlighting that glacial sedimentation occurred on the Inner and Mid-Shelf during the Bølling-Allerød (Andrews *et al.*, 2000). In addition, Helgadóttir and Thors (1998) identified a series of undated, submerged end moraines north of Vestfirðir, providing a maximum extent for the LGM IIS (Fig. 2.2).

In western Iceland, various techniques have been employed to delimit the LGM IIS, with the mapping of submerged features (e.g. Ólafsdóttir, 1975) and sedimentological analyses (e.g. Syvitski *et al.*, 1999) proving particularly beneficial. Breiðafjörður, a major fjord separating Vestfirðir and Snæfellsnes, has been an important site for such investigations due to its potential as a route for a former ice stream (Hubbard *et al.*, 2006). An extensive end moraine was identified within Breiðafjörður (Ólafsdóttir, 1975; Ingólfsson, 1991; Sykitski *et al.*, 1999) which has been dated to between 18.8 and 23.5 cal. ka BP (Andrews *et al.*, 2000) with a maximum age of 41.2 cal. ka BP (Norðdahl and Pétursson, 2005). The position of the Breiðafjörður or Látra Moraine is taken as a limit of the LGM glaciation in western Iceland, suggesting that ice terminated ~150 km from the present coastline (Fig. 2.2).

Seismic profiling has also assisted in the delimitation of the LGM IIS in southwest Iceland (e.g. Egloff and Johnson, 1979; Syvitski *et al.*, 1999). Egloff and Johnson (1979) conducted analyses at the shelf edge and a series of intermediate locations towards the present coastline, providing evidence for ice extending tens of kilometres beyond the present coastline. A series of moraine ridges were identified during the analyses (Fig. 2.2; Egloff and Johnson, 1979). It should be noted here that some seismic profiling studies are limited due to a lack of chronological control and therefore the age assigned to particular features relies on stratigraphic correlations with samples analysed elsewhere. Thus, the features should be considered as evidence of glacial action rather than the extent of the ice sheet at a particular time.

Despite evidence in western and northern Iceland suggesting an LGM ice sheet extending beyond the present coastline, a number of studies have highlighted the possibility of ice free regions or nunataks (e.g. Steindórsson, 1962; 1963; Hjort *et al.*, 1985; Buckland and Dugmore, 1991; Andrews *et al.*, 2000; Ægisdóttir and Þórhallsdóttir, 2005). Trimlines on nunataks have long been thought to represent the maximum elevation reached by an ice sheet and therefore to provide a measure of former ice thickness (e.g. Wright, 1927; Farrington, 1947; Warren, 1979; Rae *et al.*, 2004). However, more recent studies in Scotland and Ireland have highlighted the potential for trimlines to represent an englacial thermal transition from warm-based erosive ice at low

elevations to cold-based passive ice at higher elevations and summits (Ballantyne *et* al., 2006, 2007, 2008; Fabel *et al*., 2012; Ballantyne and Stone, 2015). It is possible therefore that the proposed nunataks in Iceland were in fact ice covered at the LGM, which could have significant consequences for the proposed extent of the LGM IIS.

In addition to nunataks, ice free areas have been posited both in the mid and outer shelf of Djúpall by 15 cal. ka BP (Andrews *et al.*, 2000), with ice free coastal areas also being hypothesised by biologists (Steindórsson, 1962; 1963). Hence, these areas may have been situated outside of the LGM ice limit. However, there is only limited geological evidence to support these claims at the LGM (Ingólfsson, 2009). Hjort *et al.* (1985) do provide some geomorphological evidence for ice free areas in northwest Iceland, however it is accepted that these areas were likely rare, with an ice sheet likely covering the majority of present day Iceland (Norðdahl and Pétursson, 2005). Several studies have highlighted the potential for ice free areas at the LGM, such as Langanes (Buckland and Dugmore, 1991), which could have important implications for the configuration and extent of the LGM IIS. However, evidence for such ice-free locations remains elusive.

2.2.2 Hypotheses of the LGM glaciation of Iceland

Previous research into the LGM glaciation of Iceland has led to the proposition of two contrasting glaciation hypotheses: maximum (extensive; e.g. Buckland and Dugmore, 1991; Hubbard *et al.*, 2006) and minimum (restricted; e.g. Hjort *et al.*, 1985) as outlined in Fig. 2.3. The two hypotheses are associated with very different lateral and vertical ice extents, ice volumes, styles of glaciation and patterns of deglaciation. Under the maximum hypothesis, Iceland was covered by a single mono-domed ice sheet (Hubbard *et al.*, 2006), which extended between 50 and 120 km from the present coastline (Andrews *et al.*, 2000; Norðdahl and Pétursson, 2005; Hubbard *et al.*, 2006). By contrast, the minimum glaciation hypothesis suggests multiple ice loading centres, with ice terminating within 15 km of the present coastline (Hjort *et al.*, 1985). In particular, this hypothesis supports a separate ice loading centre in Vestfirðir, which is supported by limited geomorphology-based RSL reconstructions that suggest a different pattern of RSL change compared to the rest of Iceland (e.g. Hansom and Briggs, 1991).

Figure 2.3 – The contrasting maximum (blue) and minimum (red) glaciation hypotheses in Iceland, demonstrating the differences in ice sheet configuration and extent under each scenario.

In recent decades, the maximum glaciation hypothesis has gained increasing support from studies of submerged (e.g. Ólafsdóttir, 1975) and raised marine features (e.g. Einarsson and Albertsson, 1988), sediment analyses (e.g. Andrews *et al.*, 2000), seismic profiling (e.g. Egloff and Johnson, 1979) and ice sheet modelling (e.g. Hubbard *et al.*, 2006). Despite this, contradictory evidence in northwest Iceland remains unexplained (e.g. Hjort *et al.*, 1985) thus continuing limited support for the minimum hypothesis (Fig. 2.3).

2.2.3 The deglaciation of Iceland

Ice sheet modelling suggests that the deglaciation of Iceland was relatively rapid (Hubbard *et al.*, 2006), due to destabilisation of the large marine based component of the ice sheet by rising eustatic sea level leading to extensive calving (Hubbard, 2006). Subglacial heating of the ice sheet from volcanic activity also helped drive rapid collapse (Hubbard, 2006), with several studies having examined the links between deglaciation and increased volcanism (e.g. Jakobsson *et al.*, 1978; MacLennan *et al.*, 2002). Links between increased eruption rates, meltwater production and glacial unloading have been suggested (e.g. Gudmundsson, 1986; Jull and McKenzie, 1996), with the order of particular drivers for ice sheet collapse being debated. At present, modelling and sedimentological studies favour the maximum glaciation hypothesis, as follows:

During deglaciation, two stadials and two interstadials have been identified (Einarsson, 1973; 1979), with limited evidence for a third stadial event. At the LGM, a recent ice sheet model (Hubbard *et al.*, 2006) suggests that 81% of the IIS base was situated below sea level (Hubbard, 2006). Initial deglaciation occurred rapidly during the Bølling Interstadial (13-12 cal. ka BP) (Ingólfsson and Norðdahl, 2001), when rising eustatic sea level (Fairbanks, 1989) likely led to rapid ice sheet collapse (Ingólfsson and Norðdahl, 2001).

A brief Older Dryas stadial then led to glacial advance (Einarsson and Albertsson, 1988; Ingólfsson, 1985; 1987; 1988; Ingólfsson *et al.,* 1997; Le Breton *et al.*, 2010; Fig. 2. 4). Evidence of the Older Dryas is limited in Iceland (Principato, 2008), although some evidence has been gathered in Borgarfjörður, western Iceland (Ingólfsson, 1987; 1988). Following this glacial advance, a second retreat phase occurred during the Allerød (11.8 – 11 cal. ka BP) leading to ice free coastal areas (Ingólfsson, 1991). During the Allerød, environmental conditions improved, with increases in grass and shrubland pollen being identified within sediment records (e.g. Rundgren, 1995; 1999). There is also evidence for a marine transgression during this period in western Iceland (Ásbjörnsdóttir and Norðdahl, 1995) as a result of eustatic sea-level rise and crustal subsidence due to expansion of the inland IIS (Norðdahl and Pétursson, 2005).

The Younger Dryas stadial led to an extensive glacial readvance in Iceland (Norðdahl and Hjort, 1987; Hjartarson, 1991; Ingólfsson, 1991; Ingólfsson *et al.*, 2010; Fig. 2.4). This readvance was rapid in its onset (Hjartarson, 1991), extending beyond the present coastline in several locations (Ingólfsson, 1987; Ingólfsson and Norðdahl, 2001). In western Iceland, evidence suggests that glaciers terminated onshore or close to the present coastline (Vikingsson, 1978; Eiríksson *et al.*, 1997; Geirsdóttir *et al.*, 1997; Norðdahl and Pétursson, 2005). The extent of the Younger Dryas has been delimited through mapping raised marine features (e.g. Norðdahl and Pétursson, 2005) and tephra deposits, such as the Skógar-Vedde ash (Grönvold *et al.*, 1995; Fig. 2.4), although precise dating of a number of features is currently limited.

A final relatively short-lived readvance has been identified in the Preboreal (11500 – 10100 cal a BP; see Fig. 2.4; Ingólfsson *et al.*, 2010). The extent of the Preboreal IIS is relatively poorly constrained except in southwest Iceland (Hjartarson and Ingólfsson, 1988; Ingólfsson *et al.*, 1995). Following this final readvance, the IIS disintegrated rapidly, retreating to the present ice caps such as Drangajökull in NW Iceland and Vatnajökull in SW Iceland (Ingólfsson *et al.*, 2010). The deglacial history of Iceland is a key area for future research, both in terms of the style and pattern of deglaciation and the associated meltwater volume generated. The deglacial history of Iceland is relatively poorly constrained at present, partly due to the limited data available to test current models of the IIS.

In contrast, the minimum glaciation hypothesis sees a secondary ice loading centre at the LGM situated in northwest Iceland, centred over the Vestfirðir peninsula (Hansom and Briggs, 1991). It is proposed that this ice centre was either independent (Sigurvinsson, 1983) or coalesced with the main ice sheet (e.g. Norðdahl and Pétursson, 2005). Deglaciation would likely have still been rapid under minimum glaciation, although the pattern of freshwater input to the north Atlantic may have been very different due to the ice loading configuration.

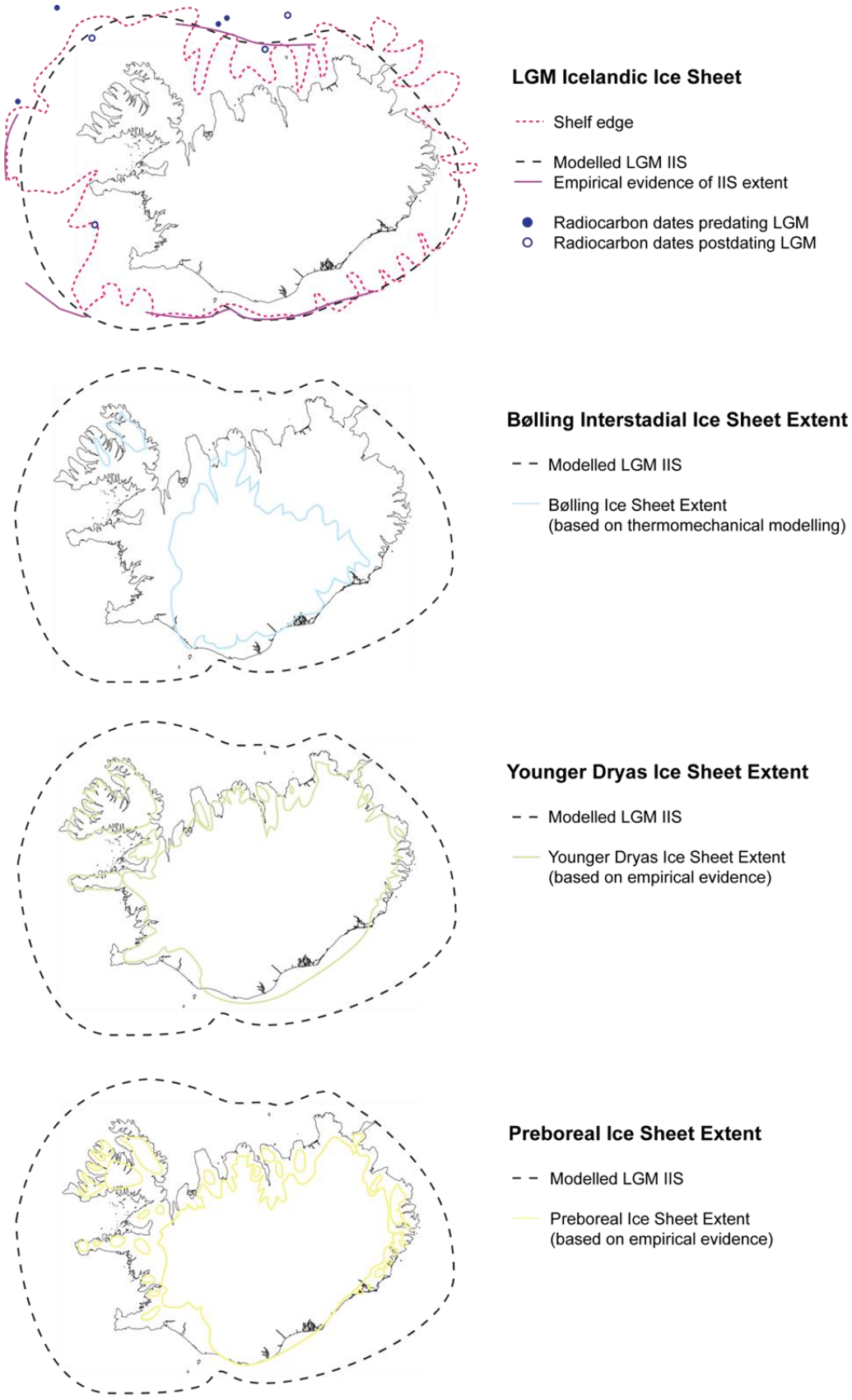

Figure 2.4 – Ice sheet extent at the Last Glacial Maximum (LGM), Bølling Period, Younger Dryas and Preboreal Readvance in Iceland under the maximum glaciation scenario, demonstrating changes in ice sheet extent over time (adapted from Ingólfsson et al., 2010).

2.3 Relative sea level change in Iceland

Relative sea level (RSL) change is the result of eustatic processes, via changes in the global ocean volume following deglaciation (Fleming *et al.*, 1998), and isostatic processes, resulting from regional scale changes in ice mass balance (Mitrovica *et al.*, 2001) and water (un)loading (hydro-isostacy). The patterns of RSL change in a particular location can therefore be very different from the global eustatic value (Tamisiea and Mitrovica, 2011). It is usual practice for RSL to be defined as relative to present (BP, 1950) (Shennan, 2015). RSL change can therefore be represented as:

$$RSL\ (Ø, t_{past}) = SL\ (Ø, t_{past}) - SL\ (Ø, t_{present}) \qquad \text{Shennan (2015)}$$

$$Ø = \text{location} \qquad t = \text{time}$$

The combination of eustatic and isostatic processes results in RSL being situated higher than present in Iceland immediately following deglaciation and into the early Holocene (e.g. Rundgren *et al.*, 1997; Lloyd *et al.*, 2009). RSL can also be affected by movement of mantle material following the deglaciation of proximal ice sheets, such as Laurentia, Greenland and Fennoscandia (Fjeldskaar, 1994), deformation of the ocean geoid (Farrell and Clark, 1976) and local tectonic effects (Shennan *et al.*, 2012). The influence of these factors will differ spatially and temporally, leading to a complex pattern of RSL changes. This section outlines the geomorphological and biostratigraphical evidence for RSL change in Iceland, which record the effects of these processes.

2.3.1 Marine Limit in Iceland

The marine limit, defined as the highest elevation reached by postglacial RSL at a particular location (Andrews, 1970), has been frequently employed to reconstruct deglacial and RSL histories (e.g. Evans, 1990). The marine limit has been extensively mapped in Iceland (e.g. John, 1975; Hjort *et al.*, 1985; Ingólfsson, 1991; Hansom and Briggs, 1991; Norðdahl and Pétursson, 2005; Principato, 2008). The marine limit in Iceland varies both in age and elevation (Hjartarson and Ingólfsson, 1988)because of differences in ice thickness and deglacial processes, style and age (Ingólfsson, 1991; Jennings *et al.*, 2000; Fig. 2.5). Mapping of geomorphological evidence has identified the highest marine limits in southern and western Iceland, occurring at 110 m asl (Ingólfsson, 1991; Ingólfsson *et al.*, 1995) and 120-135 m asl respectively (Principato and Geirsdóttir, 2002). Several studies have hypothesised a similar age for marine limit formation at c. 10000 yr BP (e.g. Ingólfsson, 1988; Le Breton *et al.*, 2010). This contrasts with other studies which suggest that RSL was highest during the Bølling Interstadial (15400 – 13900 cal. a BP; e.g. Einarsson, 1968; Rundgren *et al.*, 1997; Ingólfsson and Norðdahl, 2001; Norðdahl and Pétursson, 2005). Subsequent glacio-isostatic adjustment (GIA) modelling studies have therefore assumed synchroneity between these features, masking regional differences (Le Breton *et al.*, 2010).

However, there is clear evidence to contradict this approach, through dated terrace sequences (e.g. Ingólfsson and Norðdahl, 2001).

Alongside this reported variability in marine limit elevation and age, it is important to recognise the limitations of marine limit investigation. The marine limit is frequently difficult to constrain, with Andrews (1970) stating that unequivocal evidence is only provided through the presence of marine shells within deltaic sediments. However, previous sedimentological and geomorphological research has highlighted the use of non-deltaic coastal geomorphological evidence and deposits for determining the elevation of the marine limit and subsequent lower raised shorelines (e.g. Sandgren *et al.,* 1999; Principato, 2008).

Attaining an accurate date from marine limit deposits can often be challenging however, due to a lack of dateable material (Fleming and Lambeck, 2004; Lloyd *et al.*, 2009). In Iceland, several studies have reported a lack of suitable dateable material in order to constrain the age of shoreline formation (e.g. Principato, 2008). Previous research in the Arctic and North America has demonstrated the potential for detailed chronologies where dateable material is available, typically from the radiocarbon dating of driftwood, whalebone or marine shells (e.g. Bell, 1996; Dyke *et al.*, 1996; Zeeberg *et al.*, 2001; Long *et al.*, 2012). Such studies have highlighted the requirement for accurate age and elevation data for marine limit deposits in order to provide the most robust and reliable RSL reconstructions (Evans, 1990). There are also frequent difficulties in the identification of the marine limit surface elevation and reference to the tidal frame (Andrews, 1970). Accordingly, marine limit elevations often suffer from large elevation errors, which limit the data employability.

Despite these limitations, the elevation and age of the marine limit in Iceland has been used to denote regional patterns of ice loading and deglaciation (e.g. Norðdahl and Pétursson, 2005). Studies in northwestern Iceland have highlighted the potential for a secondary ice loading centre in Vestfirðir, based on the recorded elevation of the marine limit (Hansom and Briggs, 1991). Furthermore, the collation of marine limit data in particular regions can begin to denote differences in glacial unloading over short distances, such as in Hornstrandir (Fig. 2.6). However, due to the lack of dateable material, the correlation of sediment sequences has been employed in Iceland in order to assess the patterns of ice loading. Thus, sediment sequences have been determined as diachronous in several locations, despite the lack of direct evidence for timing of formation. It is therefore essential that the marine limit evidence in Iceland is treated with some caution, due to the lack of accurate chronological control on several features.

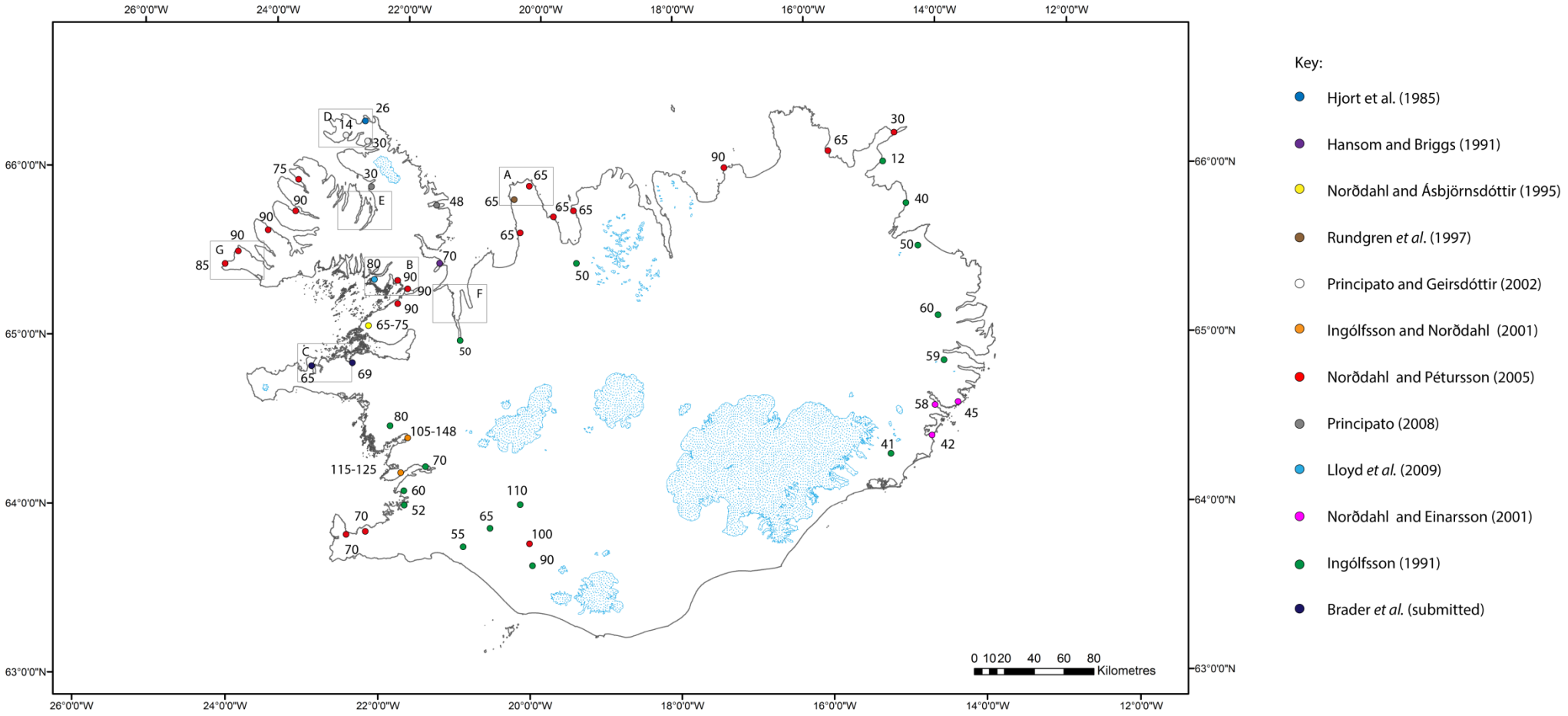

Fig. 2.5 – Marine Limit in Iceland (m asl) highlighting the key trends within the current dataset (adapted from Brader, 2012). Boxes A-G represent the research locations associated with this theses in NW Iceland, including previous research (A: Rundgren et al., 1997; B: Lloyd et al., 2009; C: Brader, 2012) and new research locations (D, E, F and G).

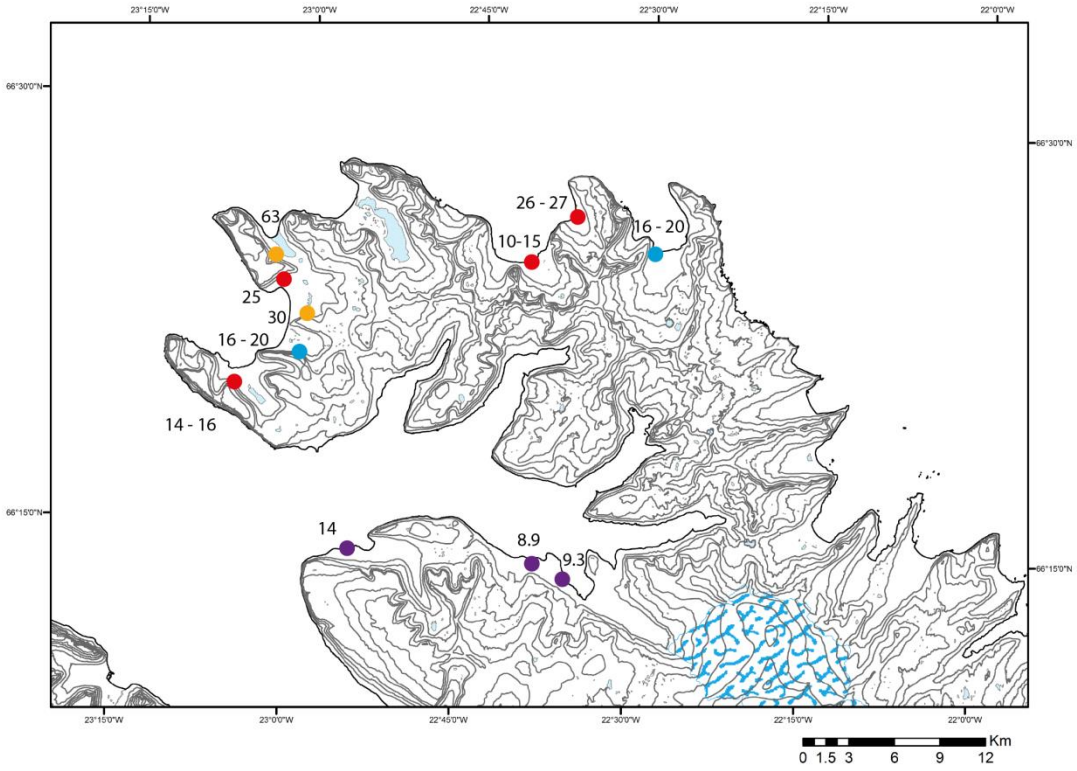

Figure 2.6 – Marine Limit in Hornstrandir (m asl) highlighting differences in the measured elevation (m), including Thoroddsen (1892; orange), Simonarson (1979; blue), Hjort et al. (1985; red) and Principato (2008; purple). The present ice cap at Drangajökull is outlined by the blue hatched area in the bottom left of the image. Base Map: National Land Survey of Iceland (Landmælingar Íslands).

In addition to the mapping of the marine limit, previous research has focussed on lower elevation raised marine terraces, which have provided important information on the patterns and style of deglaciation and postglacial RSL (e.g. Hansom and Briggs, 1991; Principato, 2008). In Vestfirðir, Hansom and Briggs (1991) identified several raised shorelines on the coast of Hunáflói, providing a constraint on postglacial RSL changes following marine limit formation at 70 m asl. Similarly, sixteen raised terrace deposits were identified in eastern Vestfirðir by Principato (2008).

Unfortunately, the available dateable material limited the scope of the two research projects, but the recorded elevations provide a useful insight into the differences in raised terrace formation within northwest Iceland. In addition, several studies have identified *Nucella* beach deposits in Iceland, first identified by Bárðarson (1910), which ranges from c. 4 m asl in Hrútafjörður (John, 1975; Hansom and Briggs, 1991; Eiríksson *et al.*, 1998) to c. 5 m asl in eastern Vestfirðir (Principato, 2008) and c. 6 m asl in Stokkseyri, southern Iceland (Símonarson and Leifsdóttir, 2002). *Nucella* is a marine gastropod mollusc and the eponymous beaches contain a distinct layer of the species, which is taken to represent former RSL. Unlike other raised shorelines in Iceland, the *Nucella* beach has been widely dated to c. 3000 cal. a BP (Símonarson and Leifsdóttir, 2002; Principato, 2008). As a result, the *Nucella* beach acts as an important deposit for the comparison

of environmental and RSL changes throughout western Iceland. Previous studies have also highlighted the importance of raised terrace deposits when employed alongside other datasets, with the combination of isolation basin and raised shoreline data being particularly effective in the determination of patterns of deglaciation in Iceland (e.g. Rundgren *et al.*, 1997; Lloyd *et al.*, 2009).

2.3.2 Isolation Basin Studies

Until recently, geomorphological mapping was the principal method employed in the investigation of RSL change in Iceland (e.g. Hansom and Briggs, 1991; Ásbjörnsdóttir and Norðdahl, 1995; Ingólfsson and Norðdahl, 2001; Norðdahl and Pétursson, 2005; Principato, 2008). Although less common, isolation basin studies have subsequently been employed in northwest and southwest Iceland, providing comprehensive records of postglacial RSL and environmental changes (e.g. Rundgren *et al.*, 1997; Hardardóttir *et al.*, 2001; Lloyd *et al.*, 2009).

Isolation basins are defined as basins which have been isolated from marine conditions and have subsequently accumulated freshwater sediments, which can undergo re-inundation, changing from freshwater to marine conditions (Kjemperud, 1986; Svendsen and Mangerud, 1987; Shennan *et al.*, 1994; Lowe and Walker, 1997; Long *et al.*, 2011). The preservation of an accurate record of environmental change is dependent on the presence of an impervious rock sill (Lloyd and Evans, 2002; Long *et al.*, 2011), which prevents seepage into the basin once RSL has fallen below the sill elevation. The elevation of former RSL depends on this sill elevation and accurate determination of this feature is therefore essential. A series of stages have been identified in the basin isolation process, which are summarised in Fig. 2.7. It is important to note that following a decrease in marine influence, the salinity of an isolation basin can vary during the brackish phase, rather than following a simple linear decrease to freshwater dominance. The isolation basin can also experience several re-inundation and isolation events depending on the speed and direction of vertical land motion and sea-level changes.

The sediment and microfossils preserved within the isolation basin can provide a comprehensive record of environmental change at a particular site. Analysis of these data can lead to the identification of three isolation contacts (Kjemperud, 1986):

a) Diatomological isolation contact - the point at which freshwater diatom flora dominate the basin assemblage;
b) Sedimentological isolation contact - the point at which sediment changes from allochthonous clastic to autochthonous organic sediments, suggesting a shift from marine to freshwater influences and;
c) Hydrological isolation contact - the point at which the water column becomes entirely freshwater.

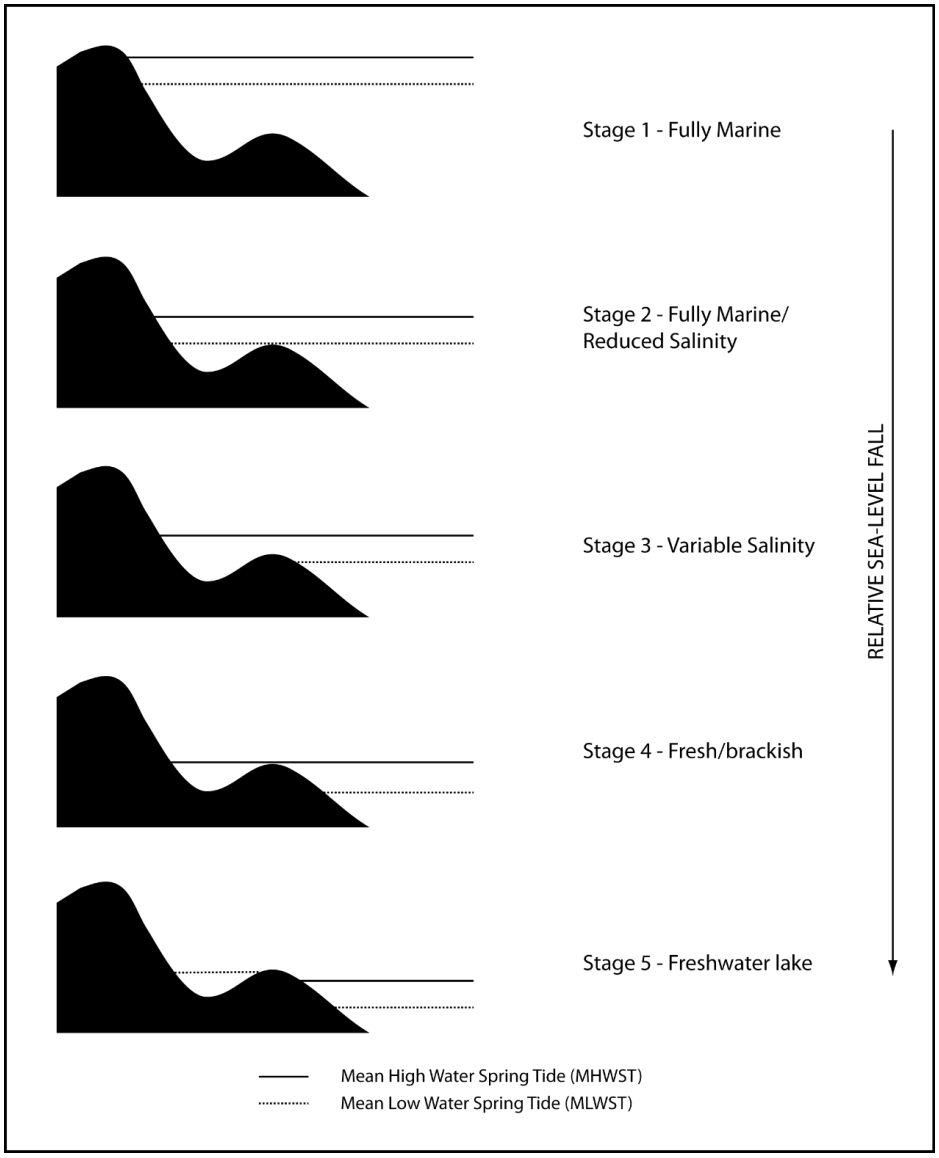

Figure 2.7 – Stages of basin isolation demonstrating the transition from fully marine (Stage 1) to brackish (Stages 2-4) and subsequent freshwater dominance (Stage 5). Adapted from: Lloyd and Evans (2002).

Isolation basins therefore have the potential to provide useful data regarding environmental and RSL changes and thus offers an opportunity to determine differences in the rate of isostatic rebound and subsidence in particular regions (Rundgren *et al.*, 1997). They have been widely used in formerly glaciated landscapes where numerous natural basins are preserved, for example Greenland (Long *et al.*, 1999; Long *et al.*, 2011), Norway (Corner *et al.*, 2001; Balascio *et al.*, 2011; Romundset *et al.*, 2014), Sweden (Hedenström and Risberg, 1999), Scotland (Shennan *et al.*, 1994; Shennan *et al.*, 1995; Lloyd and Evans, 2002) and Antarctica (Bentley *et al.*, 2005; Verleyen *et al.*, 2005).

The first isolation basin based RSL reconstruction in Iceland was completed by Rundgren *et al.* (1997) in northernmost Skagi (Figure 2.1). Rundgren *et al.* (1997) identified three raised shorelines and sampled seven isolation basins in order to develop a RSL curve for the region, highlighting a rapid RSL fall following deglaciation (Fig. 2.8). RSL fell 45 m between 13 cal ka BP

and 10.2 cal. ka BP, during which two transgressions also occurred both of 5 m amplitude (Rundgren *et al.*, 1997). The most rapid period of RSL fall occurred between the two marine transgressions (11.4 cal ka BP – 11.25 cal. ka BP) with a fall of c. 20 m. The rates of RSL fall generated for the region provide an insight into the rates of crustal rebound following the removal of glacial load, being calculated at 27.5 mm cal. yr^{-1} between 13 and 10.2 cal. ka BP, rising to 150 mm cal. yr^{-1} between the two marine transgressions.

In addition, the RSL record from the region provides an insight into the positions of ice sheet margins and associated crustal loading, with the two transgressions being assigned to ice sheet readvance during the Younger Dryas and Preboreal (Rundgren *et al.*, 1997). The RSL record from Skagi correlates well with other studies, which have highlighted similar ice readvances at the Younger Dryas and Preboreal (e.g. Ingólfsson and Norðdahl, 1994; Norðdahl and Ásbjörnsdóttir, 1994; Norðdahl and Pétursson, 2005). It is however worth noting here that the timing of the second transgression should be treated with caution, due to a hiatus present in the sedimentary record (Rundgren *et al.*, 1997). The RSL record from Skagi also provides information regarding a mid-Holocene RSL lowpoint in northern Iceland, with RSL falling below present at c. 10 cal. ka BP (Rundgren *et al.*, 1997).

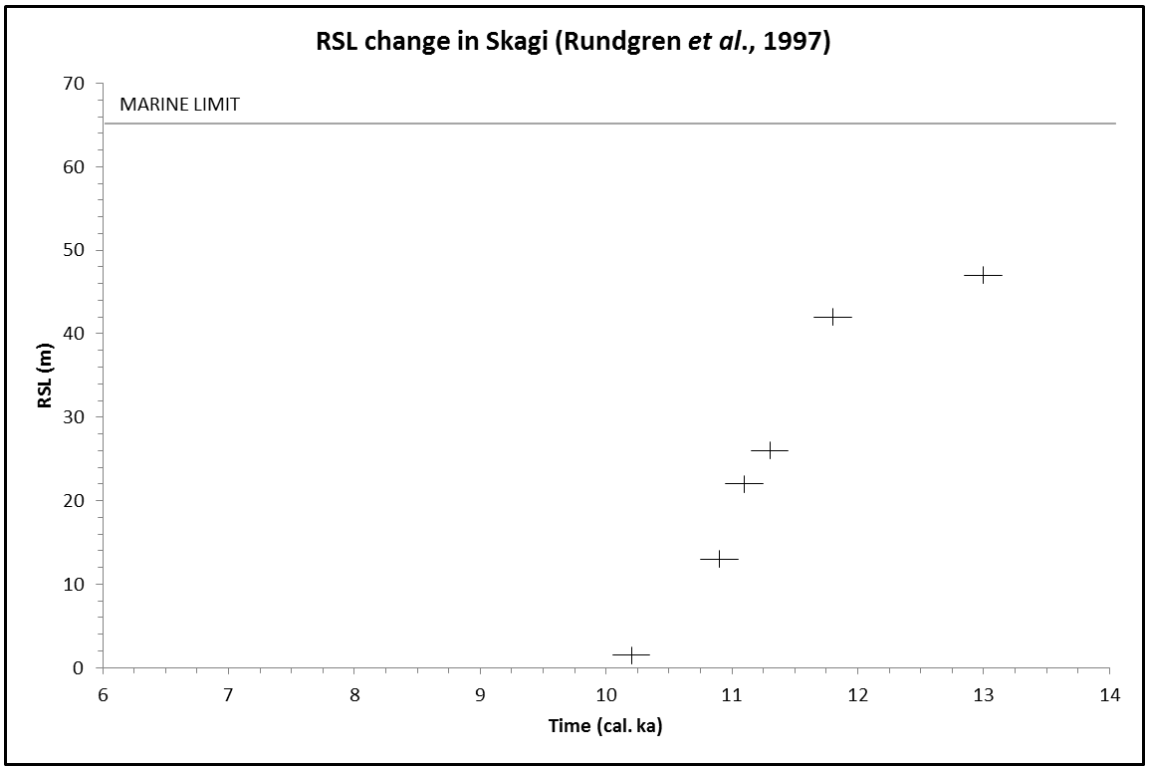

Figure 2.8 – RSL change in northernmost Skagi (1σ error), northern Iceland (Rundgren et al., 1997).

More recently, isolation basins and raised shorelines have been employed to determine postglacial RSL changes in southern Vestfirðir (Lloyd *et al.*, 2009; Fig. 2.9). A limiting elevation for postglacial RSL was determined at c. 94 m asl, with an entirely freshwater sequence recorded at the highest basin examined (Lloyd *et al.*, 2009). Lloyd *et al.* (2009) demonstrate a continuous RSL

fall from 14 cal. ka BP to the early Holocene. In Bølling-Allerød times, RSL fell at a rate of c. 38 mm cal. yr^{-1} (Lloyd *et al.,* 2009). During the Younger Dryas, the rate of RSL fall declined to c. 4 mm cal. yr^{-1}, increasing to c. 16 mm cal. yr^{-1} in the early Holocene (Lloyd *et al.*, 2009). Lloyd *et al.* (2009) note the potential for a RSL rise during the Younger Dryas, but insufficient data is available to unequivocally delimit this RSL change. It was however possible to constrain the Younger Dryas fluctuation to 10 m (Lloyd *et al.*, 2009). This constraint provides an insight into the extent of the Younger Dryas readvance in Vestfirðir, which could have important implications on RSL change in the region. It is unlikely that the sea-level index points (SLIPs) generated at 25 m asl, c. 13.7 cal. ka BP are correct, with the site likely suffering from poor chronological control (Lloyd *et al*., 2009).

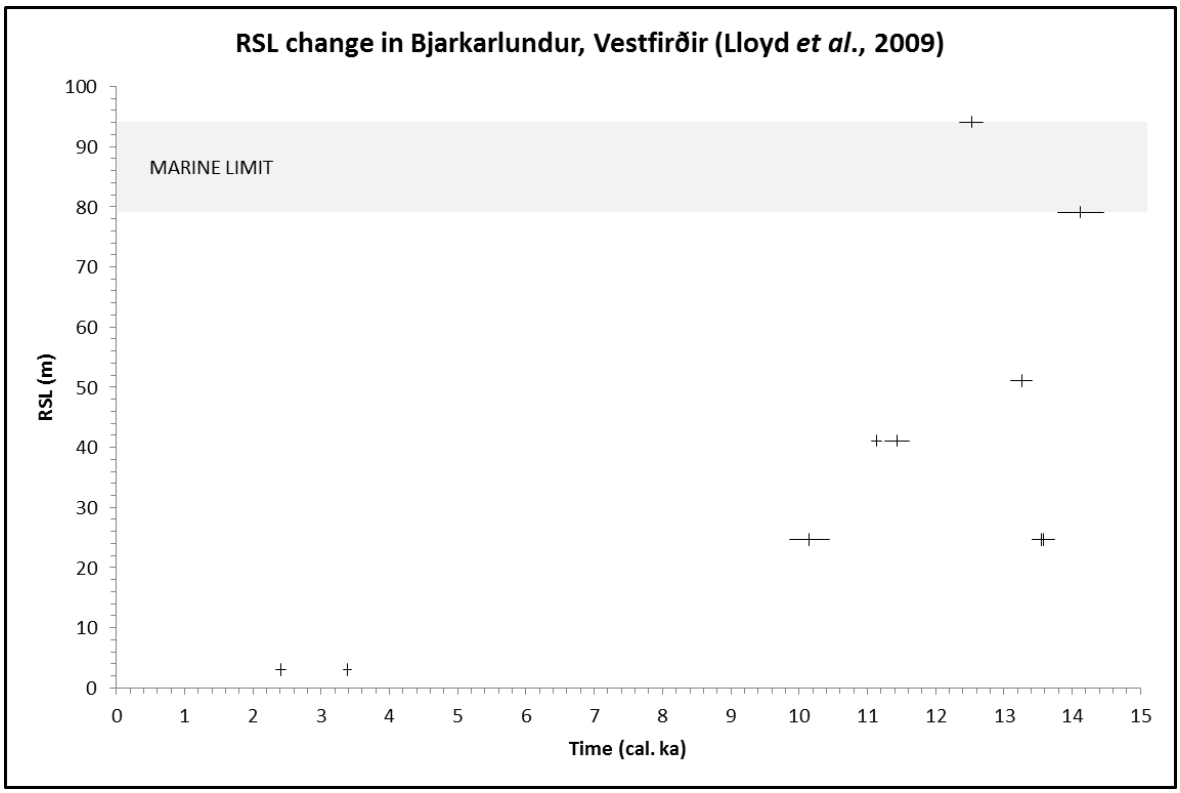

Figure 2.9 - RSL change at Bjarkarlundur (1σ error), southern Vestfirðir (Lloyd et al., 2009).

In addition, isolation basin study has been undertaken to determine the RSL changes in northern Snæfellsnes, west Iceland (Brader, 2012; Fig. 2.10). Six isolation basin and two coastal lowland sediment cores were analysed, with the marine limit being identified at 65-69 m asl (Brader, 2012). The study demonstrated a rapid RSL fall of 30 mm cal. yr^{-1} between 14 cal. ka BP and 12.6 cal. ka BP. After 12.6 cal. ka BP, the rate of RSL fall reduced, falling below present by c. 7ka cal. BP (Brader, 2012). The investigation highlighted a limited influence of Younger Dryas ice advance at the site, providing a contrasting RSL record to that demonstrated by Lloyd *et al.* (2009) on the northern coast of Breiðafjörður.

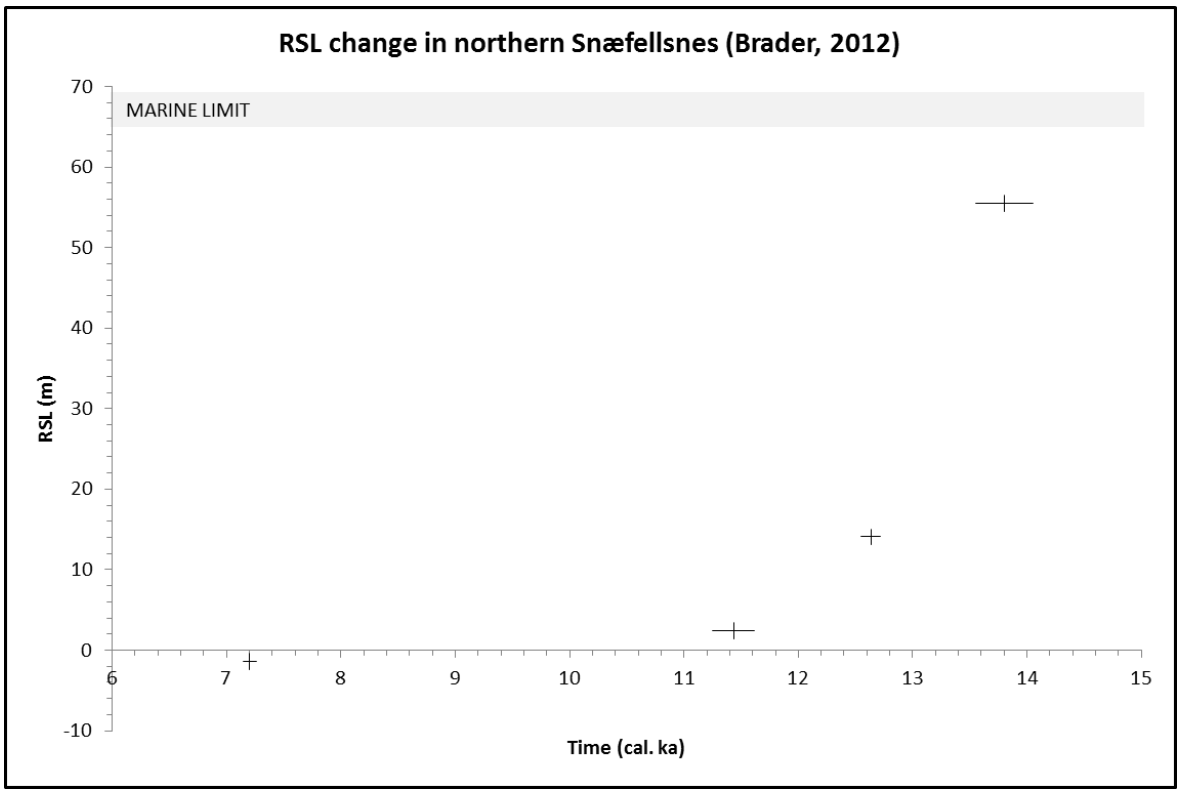

Figure 2.10 – Initial RSL curve (1σ error) from Stykkishólmur, northern Snæfellsnes (Brader, 2012).

Furthermore, studies in individual basins have provided additional constraints on postglacial RSL changes in Iceland (e.g. Hardardóttir *et al.*, 2001). Lake Hestvatn (49.5 m asl) in southern Iceland demonstrates a transition from marine to freshwater sediment deposition following seismic surveys, sediment and microfossil analyses (Hardardóttir *et al.*, 2001). Diatom and foraminiferal assemblages demonstrate a transition from marine to freshwater dominance, with basin isolation being dated to 9 ^{14}C ka BP (Hardardóttir *et al.*, 2001).

In the majority of cases, the principal benefit of isolation basin studies is the provision of complete RSL curves for particular locations (e.g. Rundgren *et al.*, 1997; Lloyd *et al.*, 2009; Brader, 2012) rather than individual point measurements provided by alternative techniques, such as marine limit studies (e.g. Ingólfsson, 1988). Where individual basin sequences are investigated, the results generated are still beneficial, as they provide a higher precision sea-level index point than marine limit data. There are however limitations to the technique which should be considered when interpreting isolation basin data, such as hiatuses within sedimentary sequences, a lack of lake basins at particular elevations and in certain locations, as well as the lack of preservation of microfossil evidence.

2.3.3 Saltmarsh Studies

Two saltmarsh deposits from Viðarhólmi, southern Snæfellsnes, have provided important evidence for late Holocene RSL changes in western Iceland (e.g. Gehrels *et al.*, 2006). Gehrels *et al.* (2006) generated a rate of RSL rise of 0.65 m ka^{-1} over the past 2 ka. The study produced four basal sea-level index points (SLIPs) for the late Holocene, providing an elevation for MSL with limited influence from sediment compaction. The RSL record from Viðarhólmi highlighted a c. 1.3 m rise in RSL since AD 100, with a 0.4 m increase over the past 150 – 200 years based on foraminiferal datasets (Gehrels *et al.*, 2006). This recent rise in RSL is reported as a consequence of isostatic subsidence and eustatic sea-level rise (Gehrels *et al.*, 2006).

In addition to the foraminiferal analyses conducted at Viðarhólmi, southern Snæfellsnes, Saher *et al.* (2015) conducted subsequent diatom analyses at the site, providing an additional reconstruction of RSL change over the past 500 years. Diatom analyses highlighted a c. 0.6 m RSL rise since AD 1570, with three periods of particularly rapid RSL rise (Saher *et al.*, 2015). Saher *et al.* (2015) outline how the increased rate of RSL rise noted by Gehrels *et al.* (2006) over the past 150 – 200 years is not replicated by the new age-depth model. The diatom record from Viðarhólmi demonstrates greater variability in the sea-level record, possibly as a consequence of changes in wind patterns from the North Atlantic Oscillation (NAO) (Saher *et al.*, 2015). Such saltmarsh studies, whilst uncommon in Iceland, provide useful constraints on late Holocene RSL changes, alongside the potential drivers for such changes on a local and regional basis (Saher *et al.*, 2015). In particular, saltmarsh and coastal lowland sediment studies could be of great benefit in areas with limited numbers of isolation basins at lower elevations.

2.3.4 Low postglacial RSL in Iceland

It has been long proposed that RSL fell below present in north and western Iceland during the mid-Holocene (e.g. Bárðarson, 1923; Thórarinsson, 1956). Various methods have been employed to investigate this RSL lowstand, including seismic profiling (e.g. Thors and Boulton, 1991) and submerged peat analyses (e.g. Meyer and Venzke, 1987; Moriwaki, 1990; Thors and Helgadóttir, 1991; Ingólfsson *et al.*, 1995). Despite this, there remains uncertainty about the scale and feasibility of such a lowstand, due to limited spatial coverage, conflicts with alternative evidence sources and methodological issues.

The most extensive study of low postglacial RSL was undertaken in western Iceland, where Thors and Helgadóttir (1991) reported a RSL fall to a lowstand of -30 m around 9.9 cal. ka BP using submerged peat evidence from Faxaflói, Hvalfjörður and Kollafjörður. However, the results of radiocarbon analyses on the dredged peat samples may not be truly correct, providing a sensible age but likely being affected by post-depositional reworking (Thors and Helgadóttir, 1991). In addition, the results generated in western Iceland (e.g. Thors and Helgadóttir, 1991; Ingólfsson *et*

al., 1995) contrast with nearby isolation basin studies, with Hardardóttir *et al.* (2001) demonstrating that the Southern Lowlands were likely submerged until 9.9 cal. ka BP. Similar low RSL values were generated in northern Iceland, with a recorded low point of -20 m (Thors and Boulton, 1991) and -30 m (Meyer and Venzke, 1987; Moriwaki, 1990). Hence, there is a body of evidence in support of low postglacial RSL in Iceland. Additional constraints on this lowstand are required in order to determine the likelihood of such an event. However, these data, alongside other RSL studies, may prove beneficial in the testing of GIA models in Iceland.

2.4 Glacio-isostatic adjustment modelling in Iceland

Glacio-isostatic adjustment (GIA) models have been used on a range of spatial and temporal scales to explore both rheological characteristics and patterns of horizontal and vertical deformation following the addition or removal of load (e.g. Tushingham and Peltier, 1991; Lambeck and Purcell, 2001; Peltier, 2004; Le Breton *et al.*, 2010; Bradley *et al.*, 2011; Shennan *et al.*, 2012; Whitehouse *et al.*, 2012; Argus *et al.*, 2014; Peltier *et al.*, 2014). Several studies have demonstrated the effectiveness of GIA modelling in determining estimations for lithospheric thickness and mantle viscosity values in Iceland (e.g. Fleming *et al.*, 2007) and elsewhere (e.g. Argus *et al.*, 2014). GIA models are comprised of three key elements: the glaciation history, upper mantle viscosity and lithospheric thickness (Argus *et al.*, 2014). These model components are inherently linked and so the uncertainty or error associated with a particular element of the GIA model can lead to misrepresentation of ice sheet or rheological characteristics (see Argus *et al.*, 2014). In order to test models of GIA, RSL databases are frequently employed, often based on dated raised shoreline deposits or isolation basin data (e.g. Peltier, 1998). The following sections summarise the existing published ice sheet models and proposed rheological characteristics for Iceland, which influence the approach adopted by this research.

2.4.1 Models of the Last Glacial Maximum (LGM) Icelandic Ice Sheet (IIS)

At present, only two Iceland-specific ice sheet models have been produced with suitable climate and precipitation forcing mechanisms (Bingham *et al.*, 2003; Hubbard *et al.*, 2006), although the global model ICE5G also contains data for Iceland (Peltier, 2004).

ICE5G provides a global model of GIA, containing ice loads for each of the principal ice sheets at the LGM, including an ice load in Iceland (Peltier, 2004). The Icelandic ice load within the global model is taken from previous modelling experiments, ICE2 and ICE3G, with a maximum ice thickness of 1900 m (Tushingham and Peltier, 1991). The ice load is constrained by geomorphological data, principally end moraine locations (e.g. Einarsson, 1973) and three RSL curves (Tushingham and Peltier, 1991). Whilst the ice load provides improved outputs to the ICE2 model, the limited number of data points used to constrain the ice load means that there is potential for some uncertainty in the configuration of the LGM IIS. The ICE5G model therefore

provides an initial, relatively coarse resolution (one degree), depiction of the LGM IIS, with a maximum extent at 21000 ^{14}C a BP (c. 25000 cal. a BP) (Peltier, 2004).

In contrast, Bingham *et al.* (2003) developed a three-dimensional numerical ice-sheet model of the southern extent of the IIS since the LGM, which was set at 20 ^{14}C ka BP (c. 24000 cal. a BP) (Mineter and Hulton, 2001; Bingham *et al.*, 2003). Through an ELA lowering of 500 m, consistent with a c. 5°C lowering of temperature or 15 m a^{-1} increase in precipitation at the LGM, glacier ice covered the entirety of the modelled area (Bingham *et al.*, 2003). This modelled ice coverage suggests that ice calved directly into the sea and that there were no ice free areas during the LGM in southern Iceland (Bingham *et al.*, 2003). As a result, the alpine landforms found in the area (e.g. Sigbjarnarson, 1983) were likely generated by less effective ice sheet erosion, rather than the presence of glacial refugia (Bingham *et al.*, 2003).

Bingham *et al.* (2003) also explored the extent of the YD readvance in southern Iceland, with model outputs agreeing with geomorphological data from the region (e.g. Jóhannesson, 1985). Whilst the modelling study highlights the possibility of an ice free zone between the present coastline and the YD Ice Sheet, the region would have likely been submerged due to the higher RSL during the period (Bingham *et al.*, 2003). The ice sheet models produced by Bingham *et al.* (2003) provide useful information about the possible configuration of the LGM and YD IIS in southern Iceland.

More recently, Hubbard *et al.* (2006) produced a suite of LGM IIS models using different temperature and precipitation forcing scenarios. The ice sheet model was developed to determine the glacial susceptibility of Iceland and the extent of the LGM IIS (Hubbard *et al.*, 2006). Hubbard *et al.* (2006) highlight the complexity of modelling the LGM IIS due to the large number of potential internal and external variables with limited empirical field constraints for testing. There is therefore potential for various scenarios that are compatible with the existing field evidence (Hubbard *et al.*, 2006). The climatologically-driven ice sheet models therefore employ the available evidence to produce a sensible suite of scenarios (Fig. 2.11) for additional testing with later chronological constraints, such as tephra distributions or cosmogenic isotope analyses (Hubbard *et al.*, 2006).

Hubbard *et al.* (2006) present an optimum model for the LGM IIS, with an east-west ice divide, leading to half of the ice mass draining to the north and half to the south. The Hubbard *et al.* (2006) ice sheet model is dynamic, with several accumulation centres and nunataks present in upland areas, particularly in the south and south east of the ice sheet (Hubbard *et al.*, 2006; Hubbard, 2006; Fig. 2.11). The ice sheet model has a substantial marine component, with ice extending beyond the present coastline in the north, west and south (Hubbard *et al.*, 2006; Hubbard, 2006).

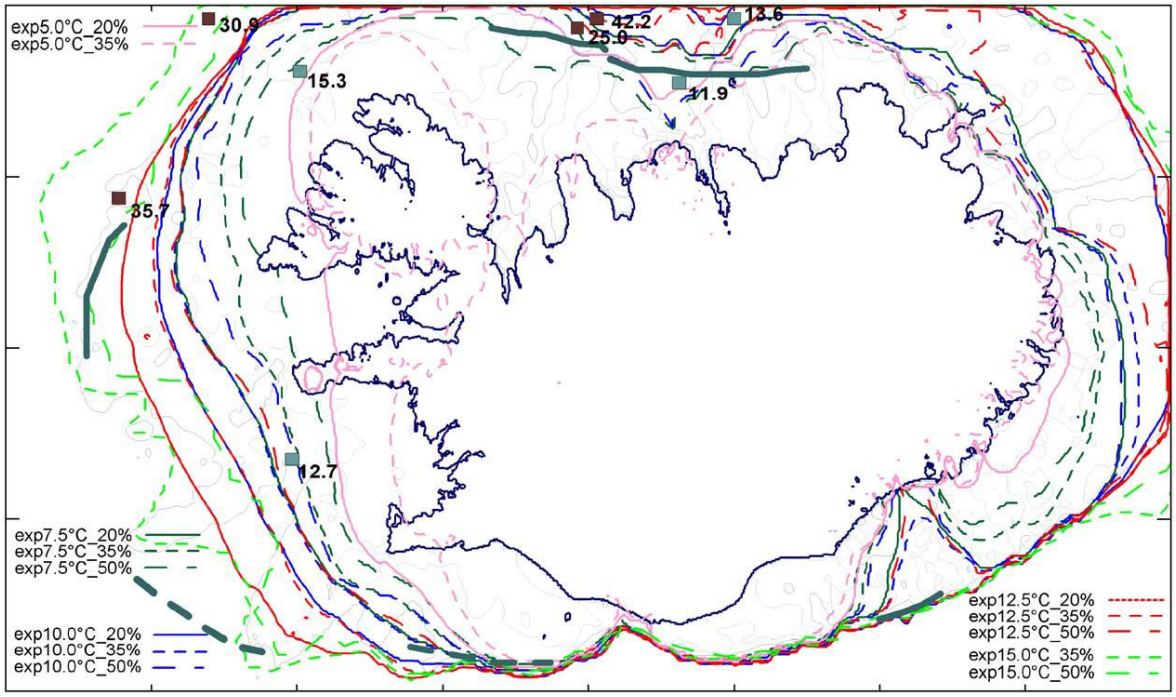

Figure 2.11 – Suite of ice sheet models showing maximum ice extent at 21000 cal ka BP developed by Hubbard et al. (2006). Each model corresponds to individual forcing experiments: temperature decrease (°C) and precipitation suppression (%). Individual model outputs demonstrate the potential for ice free areas (northeast Iceland) under more extreme forcing scenarios.

However, the Langanes peninsula in northeast Iceland remains ice-free, with ice terminating close to the present coastline in eastern Iceland (Hubbard *et al.*, 2006). The optimum model corresponds well with the majority of field evidence available in Iceland, particularly with ice contact and directional features (Hubbard *et al.*, 2006). Hubbard *et al.* (2006) provide support for the maximum glaciation hypothesis, with the minimum glaciation being untenable even under minimal climatic forcing at the LGM.

2.4.2 Icelandic rheological structure

In order to effectively model solid Earth response to changes in ice load following deglaciation, it is essential to employ a glacio-isostatic adjustment (GIA) model which includes informed estimates of the Earth's rheology and structure. Numerous studies have been undertaken to investigate crustal structure in various regions of Iceland (e.g. Du and Foulger, 1999; 2001; Darbyshire *et al.*, 2000; Du *et al.*, 2002; Foulger, 2006; Kumar *et al.* 2007; Barnhoorn *et al.*, 2011), Two models of the Icelandic crust have been posited: thin and hot crust (e.g. Pálmason, 1971; Flóvenz, 1992) and thick crust (e.g. Bjarnason *et al.*, 1993; Darbyshire *et al.*, 1998; Weir *et al.*, 2001), which have consequences for crustal structure and uplift rates.

Mantle viscosity studies have concentrated on Vatnajökull, close to the proposed mantle plume, meaning viscosity values generated are particularly low (~10^{16} - 10^{18} Pa s) (e.g. Sigmundsson, 2006; Fleming *et al.*, 2007; Barnhoorn *et al.*, 2011; Schmidt *et al.*, 2012). Only a limited number of

studies have been undertaken elsewhere in Iceland (e.g. Sigmundsson, 1991; Pollitz and Sacks, 1996). The establishment of the lithospheric thickness and mantle viscosity characteristics of Iceland is important, as the relatively low mantle viscosity and thin crust presented in previous studies would result in rapid uplift responses to the removal of glacial load (Barnhoorn *et al.*, 2011). Similar response is seen in other plate margin locations with low viscosity, such as Alaska (Motyka, 2003; Larsen *et al.*, 2005), Patagonia (Ivins and James, 2004) and Cascadia (Clague and James, 2002). Previous studies have generated significantly different estimations of the Icelandic lithospheric thickness (10-100 km) and mantle viscosity (10^{16}- x 10^{20} Pa s; Table 2.1). When compared to mid-continental locations employed in global GIA models, such as Fennoscandia and Laurentia under VM2 (Peltier, 2004) or VM5a (Peltier *et al.*, 2015), it is clear that the Icelandic rheology has low values for both the lithospheric thickness and upper mantle viscosity (Table 2.1).

Location	**Time Period**	**Lithospheric thickness (km)**	**Upper mantle viscosity (Pa s)**	**Source**
Iceland	LGM	10-20	1 x 10^{19}	Sigmundsson (1991)
Vatnajökull	Historical	5-25	1 x 10^{18}-5 x 10^{19}	Sigmundsson and Einarsson (1992)
NE Iceland	Present	N/A	3 x 10^{18}	Pollitz and Sachs (1996)
Vatnajökull	Present	10-20	7 x 10^{16}-3 x 10^{18}	Thoma *et al.* (2002)
Vatnajökull	Present	10-20	5 x 10^{17}	Sjöberg *et al.* (2004)
Vatnajökull	Present	20-30	1-2 x 10^{18}	Fleming *et al.* (2007)
Vatnajökull	Present	10-20	4-10 x 10^{18}	Pagli *et al.* (2007)
Iceland	N/A	N/A	5 x 10^{19}-2 x 10^{20}	Biessy *et al.* (2008)
Iceland	Present	40	6 x 10^{18}-2 x 10^{19}	Árnadóttir *et al.* (2009)
Iceland	Holocene	N/A	2.1-3.2 x 10^{19}	Le Breton *et al.* (2010)
Iceland	Present	27-40	2 x 10^{18}-10^{19}	Barnhoorn *et al.* (2011)
Iceland (200km from ridge axis)	Present	100km	N/A	Barnhoorn *et al.* (2011)
Iceland	LGM (10 cal. ka BP)	100	1 x 10^{19}	Barnhoorn *et al.* (2011)
Iceland	1890-2004	N/A	8 x 10^{18}	Schmidt *et al.* (2011)

Table 2.1 – Lithospheric thicknesses and upper mantle viscosities in Iceland.

The lithospheric thickness and mantle viscosity in Iceland has large lateral variability because of Iceland's location on a ridge axis (Barnhoorn *et al.*, 2011). It is therefore important to consider

the implications of lithospheric thicknesses and mantle viscosities employed in GIA studies, as the uplift rates produced will likely under- or over-represent rebound in particular locations. Argus *et al*. (2014) has highlighted the potential for additional model uncertainty due to lateral homogeneity of viscosity characteristics. Previous research has highlighted the impact of lateral variability of viscosity, particularly in Antarctica (e.g. A *et al*., 2013, van der Wal *et al*., 2015).

Several studies have focussed on the presence of a hotspot or mantle plume beneath Iceland (e.g. Schilling, 1973; Tryggvason *et al.*, 1983; Vogt, 1983; Wolfe *et al.*, 1997; Shen *et al.*, 2002; Foulger and Anderson, 2005). There remains debate on the extent of the influence of this feature, with research highlighting differing effects on the lower mantle. The inclusion or exclusion of the proposed mantle plume has varied between studies, often relating to whether the modelling is conducted in two or three dimensions.

2.4.3 Modelling glacio-isostatic adjustment (GIA)

Models of ice sheet and earth structure developed in previous studies have been employed to determine the effects of the addition or removal of glacial load in Iceland over different periods (e.g. Sigmundsson, 1991; Ingólfsson *et al.*, 1995; Le Breton *et al.*, 2010; Schmidt *et al.*, 2012; Auriac *et al.*, 2013). A number of studies have centred on the Vatnajökull ice cap over recent decades to determine rates of residual rebound (e.g. Sigmundsson and Einarsson, 1992) although a limited number of studies have focussed on postglacial rebound over the Lateglacial to Holocene (Le Breton *et al.*, 2010). The majority of studies have assumed a two dimensional model of postglacial rebound, but recent studies have begun to develop three dimensional representations of the Icelandic mantle and residual rebound (e.g. Schmidt *et al.*, 2012).

The majority of rheological studies in Iceland are focussed on recent changes in rates of uplift surrounding Vatnajökull, central Iceland (e.g. Compton *et al.*, 2015). Such studies have demonstrated a significant upward velocity (30 mm a^{-1}) because of recent glacial melt using Global Positioning System (GPS) datasets (Compton *et al.*, 2015). Compton *et al.* (2015) demonstrate a relationship between mass balance and uplift at Vatnajökull, with the commencement of upward velocity correlating with the onset of ice mass balance loss. Although research into recent uplift provide a useful insight into the rheological response to the removel of loading, investigations of Icelandic rheology over the postglacial will be of greatest importance to this research and will therefore be the focus of this discussion.

Le Breton *et al.* (2010) compiled a range of data of vertical motions in Iceland over the course of the Holocene. Through analysis of a digital elevation model (DEM), Le Breton *et al.* (2010) determined uplift of 40-170 m between 10 ka BP and 8150 BP equating to a rate of 21-92 mm a^{-1}. This rapid rate of uplift is taken to represent the response of the Icelandic lithosphere and mantle to the removal of glacial load after the LGM (Le Breton *et al.*, 2010). Spatial variability in the rate

of uplift is noted and ascribed to differences in glacial load and patterns of deglaciation, rather than differences in geodynamics (Le Breton *et al.*, 2010). It was noted that the relaxation time varied considerably around Iceland, with uplift data suggesting a period of 4167 a in western Iceland and 2000 in southwest Iceland (Le Breton *et al.*, 2010). This variability is thought to result from differences in lithospheric thickness away from the rifting centre and therefore Le Breton *et al.* (2010) suggest a uniform mantle viscosity.

Whilst these estimations of uplift provide useful insights into the potential differences in patterns of deglaciation, there are some limitations to the approach adopted. A number of the marine limit features employed to develop the model are without chronological control and are assigned a similar timing of formation based on their elevation (Le Breton *et al.*, 2010). In order for marine limit data to be employed effectively, accurate chronological control is required (Andrews, 1970). In turn, the assumption of synchronous formation by Le Breton *et al.* (2010) may mask patterns in marine limit formation which could have important implications for uplift rate calculation and determination of the influences of mantle viscosity and lithospheric thickness. The incorporation of additional data sources, such as tephra distributions, may assist in the determination of likely patterns of deglaciation.

2.5 Tephrochronology in Iceland

Tephrochronology involves the identification and correlation of pyroclastic deposits produced by volcanic eruptions or tephra (Thórarinsson, 1944; 1981). Tephrochronology is reliant on three key principles: a) sedimentological sequences occurring in one location can be correlated to similar sequences elsewhere (superposition), b) tephra deposits can be characterised through field or laboratory analyses, and c) if a deposit can be accurately dated, the age can be applied to identical deposits in other locations (Lowe, 2011). These principles are a consequence of the rapid and widespread nature of tephra deposition, particularly in terrestrial, marine and lacustrine settings (Lowe, 2011). Hence, tephrochronology has the potential to identify a series of deposits based on physical or geochemical characteristics with chronological resolution as high as annual, which can be applied in multiple locations, known as isochrones (Lowe, 2011).

In Iceland, tephrochronology has been employed to constrain environmental and RSL changes (e.g. Dugmore *et al.*, 2009; Lloyd *et al.*, 2009; Dugmore and Newton, 2012), reconstruct eruption histories (e.g. Larsen and Eiriksson, 2008), investigate influences on human activity and populations (e.g. Streeter *et al.*, 2012), test ice sheet models (e.g. Hubbard *et al.*, 2006) and correlate sediment sequences and samples through the establishment of individual marker horizons (e.g. Þórarinsson, 1954, 1956, 1958, 1967, 1975; Westgate and Gorton, 1981; Hafliðason *et al.*, 2000). The length of available chronology is dependent on sediment type, with the shortest

chronology in terrestrial soils (e.g. Larsen and Eiríksson, 2008) and longer records in marine deposits (e.g. Eiríksson *et al.*, 2000).

With an increase in environmental research, the numbers of tephra horizons being discovered and dated has increased, with distinct marker horizons being identified throughout the Lateglacial and Holocene in marine, lacustrine and terrestrial deposits (e.g. Björck *et al*, 2002; Table 2.2). Over the past 1100 year period, ~ 200 tephra layers have been identified in Iceland (Thórdarson and Larsen, 2007). Extensive, well-preserved basaltic deposits make up the majority of tephra layers in Iceland, although they are less numerous elsewhere during the Late Quaternary (Mangerud *et al.*, 1984; Davies *et al.*, 2001).

Tephra deposit	Source	Age (1 σ)	Reference
Landnám	Veiðivötn	871±2 AD	Sigurgeirsson *et al.* (2013)
Hekla 3	Hekla	2958 - 3061 cal. a BP	Dugmore *et al*. (1995b)
Hekla 4	Hekla	4177 - 4231 cal. a BP	Dugmore *et al.* (1995b)
Snæfellsjökull	Snæfellsjökull	Est. 7000 - 9000 ^{14}C a BP	Hafliðason *et al.* (2000)
Saksunarvatn	Grímsvötn	10175 - 10245 cal. a BP	Lohne *et al*. (2014)
Vedde Ash	Katla	12016 - 12112 cal. a BP	Lohne *et al*. (2014)

Table 2.2 – Key Lateglacial to Holocene tephra deposits found in NW Iceland for use in this study, calibrated using CALIB7.0 from the original source where possible.

Tephra deposits can have a distinct geochemical signature, in many cases allowing the determination of both source area and the individual eruption event. In total, c. 30 volcanic systems have been identified in Iceland (Gudmundsson, 2000; Larsen and Eiríksson, 2008; Figure 2.12). Whilst the majority of systems can be differentiated, several studies have highlighted problems with the identification of individual eruption events from the same or geochemically-similar systems (Larsen *et al.*, 1999; Larsen and Eiríksson, 2008). A number of tephra geochemical signatures have been collated in *Tephrabase* (Newton, 1996; Newton *et al.*, 2007), which provides geochemical results from electron microprobe analyses (EPMA).

Whilst tephrochronology offers many advantages, such as chronological control when the accuracy of ^{14}C dating is insufficient (Lowe, 2011), there are some limitations and key assumptions of the technique which must be considered. Post-depositional chemical alteration of the deposit can be problematic (e.g. Pollard *et al.*, 2003; Swindles *et al.*, 2010), with surrounding sediment (Hodder *et al.*, 1991) and bacteria (Thorseth *et al.*, 1995) affecting sample geochemistry. In addition, deposition is not uniform throughout the fallout region (Dugmore *et al.*, 1996; Swindles *et al.*, 2010), meaning that key horizons may not always be present where expected. Furthermore, issues of tephra reworking must be considered, particularly in peat deposits (Payne and Gehrels, 2010; Swindles *et al.*, 2010).

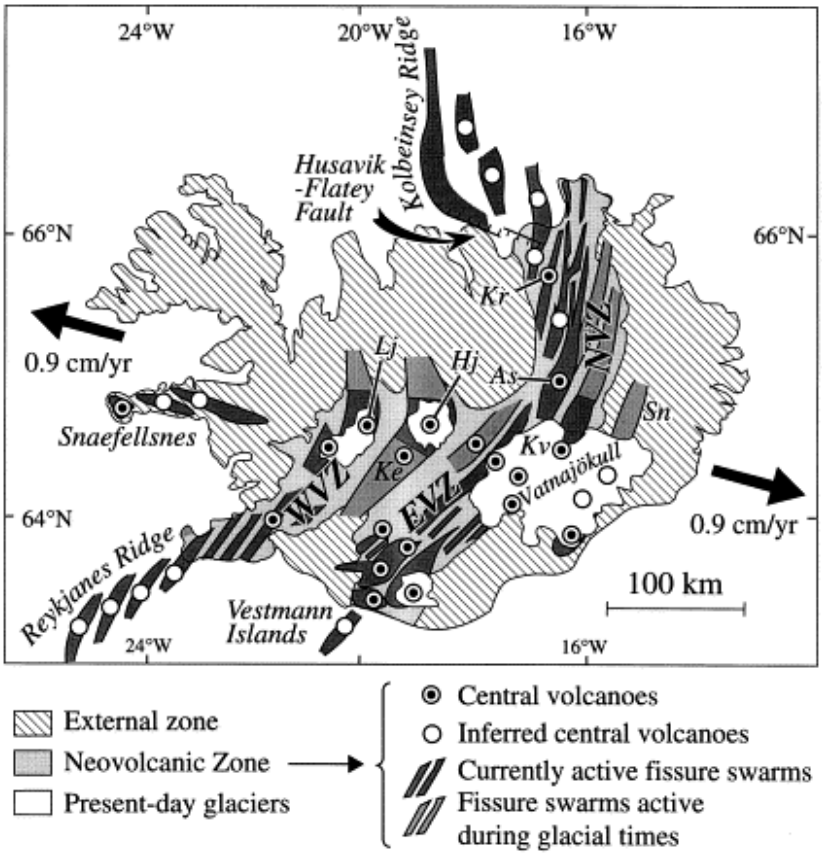

Figure 2.12 – Volcanic systems of Iceland, highlighting the principal volcanic zones, alongside major tephra production centres. As: Askja; Hj: Hofsjökull; Ke: Kerlingarfjöll; Lj: Langjökull; Sn: Snaefell (different to Snaefellsjökull); Kr: Krafla; Gr: Grimsvotn; Ve: Veiðivotn; SVB: Snæfellsnes Volcanic Belt (including Ljósfjöll Volcanic System); NVZ: Northern Volcanic Zone; WVZ: Western Volcanic Zone; EVZ: Eastern Volcanic Zone. Adapted from Bourgeois et al. (1998).

2.6 Summary

This chapter has provided an overview of the glacial, deglacial and RSL histories of Iceland, demonstrating key patterns within the existing dataset. In doing so, limitations to previous studies have been highlighted, alongside key areas for future research. Conflicting data and evidence have been identified and analysed to determine drivers for divergence in reconstructions from particular techniques. An overview of the principal methods in the determination of patterns of glacial rebound and chronological control has also been provided. In the next chapter, the site locations are outlined, justifying the approach adopted in the development of a series of new RSL curves for northwest Iceland.

CHAPTER 3

Site Locations

3.1 Introduction

This chapter introduces the field areas investigated and is divided into five sections: Iceland and the North Atlantic, Northwest Iceland, Site Selection, Previous Research Locations and New Research Locations. The chapter aims to provide location information and to justify the research design and individual site selection.

3.2 Iceland and the North Atlantic

Iceland is situated in the mid North Atlantic between 63°23'N to 66°32' N and 13°30'W to 24°32'W (Einarsson, 1984), covering an area of 103100 km^2. The country can be sub-divided into eight regions, with this study located within Vesturland (Western Region), Vestfirðir (Westfjords) and Norðurland vestra (Northwestern Region) (Fig. 3.1).

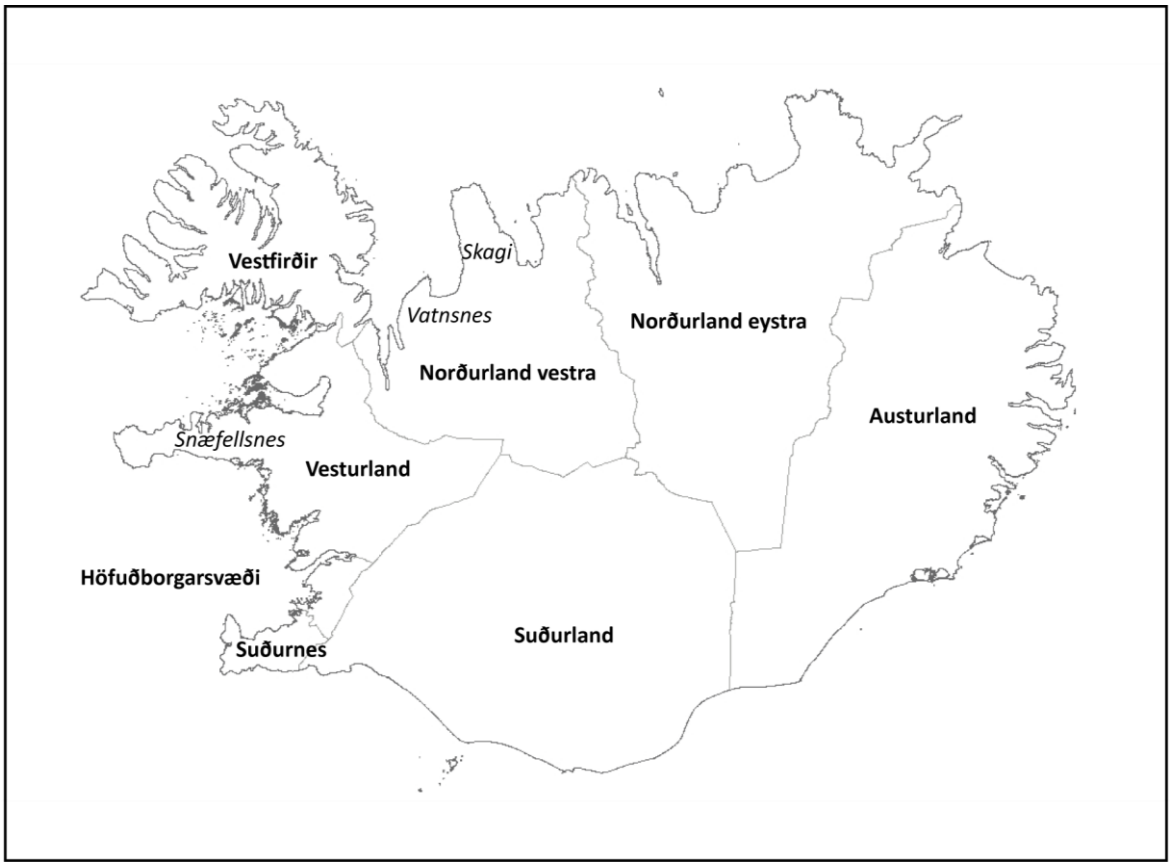

Figure 3.1 – The regions of Iceland (bold) and the principal peninsulas being investigated as part of this study

As a result of Iceland's location in the mid North Atlantic, the climate is dominated by the interaction between relatively warm and cold oceanic currents (Fig 3.2) and Arctic and sub-tropical air masses (Einarsson, 1984). The interface between cooler and warmer water has led to the establishment of temperature fronts close to Iceland and large temperature and pressure gradients around the country. The climate is classified as cold oceanic (Cfc) climate but because of the temperature fronts, it is particularly sensitive to oceanographic and atmospheric change (Ingólfsson *et al.,* 1997; Eiríksson *et al.*, 2000; Norðdahl and Pétursson, 2005). The sensitivity of Iceland to such changes means that the response of ice masses would be relatively rapid and therefore records of ice sheet extent should provide a robust constraint on the response to climatic and oceanographic change.

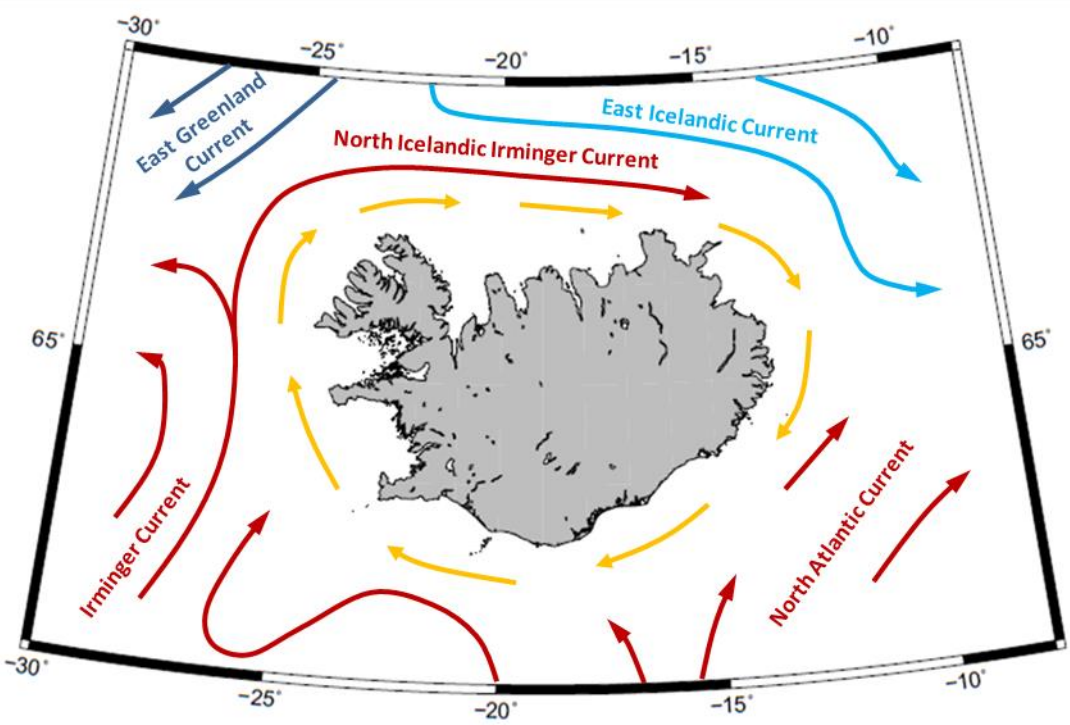

Figure 3.2 – Oceanic circulation in the North Atlantic, showing present circulatory patterns. Orange arrows represent coastal waters, which have varying influences on local salinity throughout the year.

Iceland is also situated close to an area of deepwater formation in the North Altantic that is sensitive to change (Dickson *et al.*, 2002). Therefore the deglaciation of the LGM IIS had the potential to affect global thermohaline circulation through the input of large quantities of freshwater into the region (Hubbard *et al.*, 2006). Iceland is situated in a critical and sensitive area of the North Atlantic for oceanographic and climatic change, with terrestrial records having the potential to record the response of the Icelandic climate to such adjustments.

3.3 Northwest Iceland

Northwest Iceland is here defined as comprising the Snæfellsnes, Vestfirðir, Vatnsnes and Skagi peninsulas (Fig. 3.1, 3.3). In order to determine the patterns of former ice loading, investigation of isolation basin and raised terrace deposits was undertaken in seven areas within northwest Iceland along two perpendicular transects of research (Fig. 3.3).

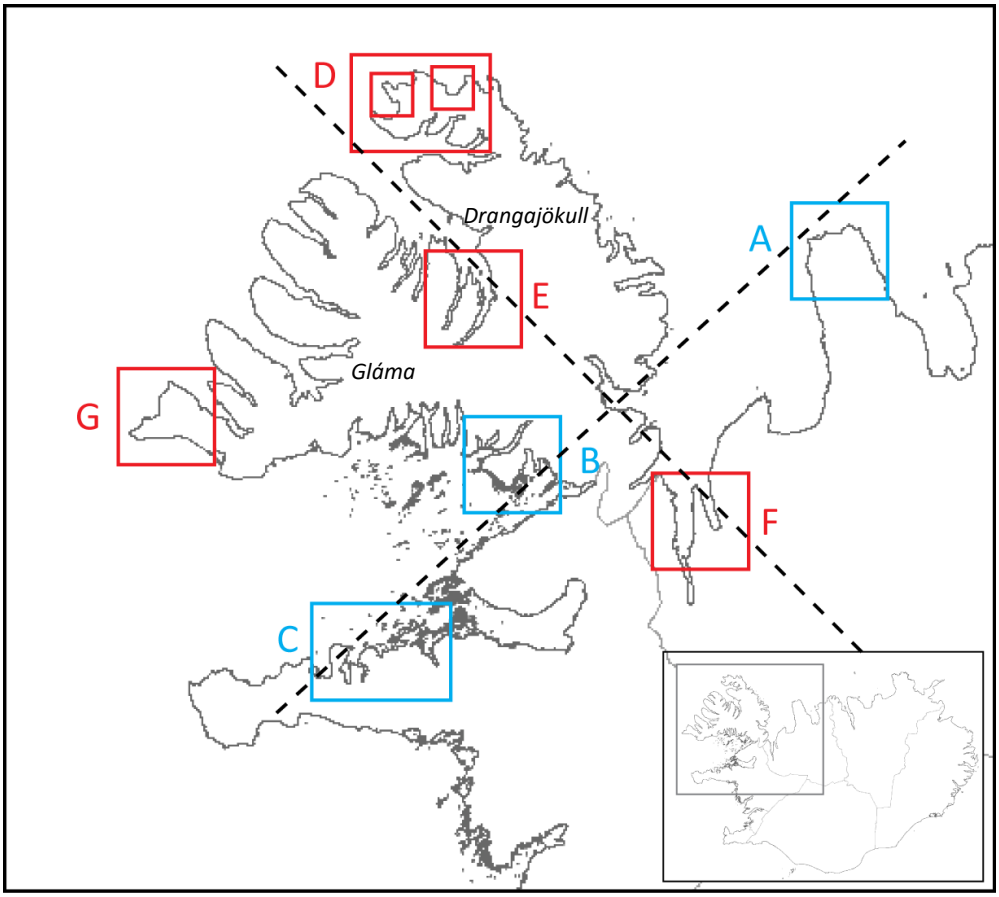

Figure 3.3 – Distribution of RSL study sites in NW Iceland, highlighting previous (blue) and new (red) research locations alongside the two principal transects of research. The research locations are: A – Skagi (Rundgren et al., 1997); B – Bjarkarlundur, Vestfirðir (Lloyd et al., 2009); C – Snæfellsnes (Brader, 2012; Brader et al., 2015; this thesis); D – Aðalvik and Hornstrandir; E – Vatnsfjörður, F – Hvammstangi, Vatnsnes; G – Breiðavik, Vestfirðir.

The two transects are made up of a series of sites, with Transect 1 comprising Areas A (Skagi), B (Bjarkarlundur), and C (Snæfellsnes) and Transect 2 being made up of Areas D (Hornstrandir), E (Vatnsfjörður) and F (Hvammstangi), as outlined in Fig. 3.4A. Area G (Breiðavik) was investigated due to the marine limit elevations reported in the area (Norðdahl and Pétursson, 2005), which are high (85 - 90 m asl) in comparison to other distal locations from the proposed former ice loading centres (Fig 3.4A). In addition, Area G may assist in the assessment of the proposed ice stream within Breiðafjörður (Bourgeois *et al*., 2000; Hubbard *et al*., 2006). The two transects were designed to determine RSL changes across and away from hypothesised ice loading centres in Gláma/Drangajökull and Vatnajökull (Fig. 3.4A). Under the two LGM glaciation hypotheses, the

resultant pattern of RSL changes along each transect would contrast, providing an opportunity to differentiate between the potential ice loading scenarios (Fig. 3.4B). Under the maximum glaciation scenario, it is anticipated that marine limit elevations will increase with proximity to the principal ice loading centre (Fig. 3.4B). In contrast, the highest marine limits in northwest Iceland would be found in Area E under the minimum scenario, which is closest to the proposed secondary ice loading centre (Fig. 3.4B).

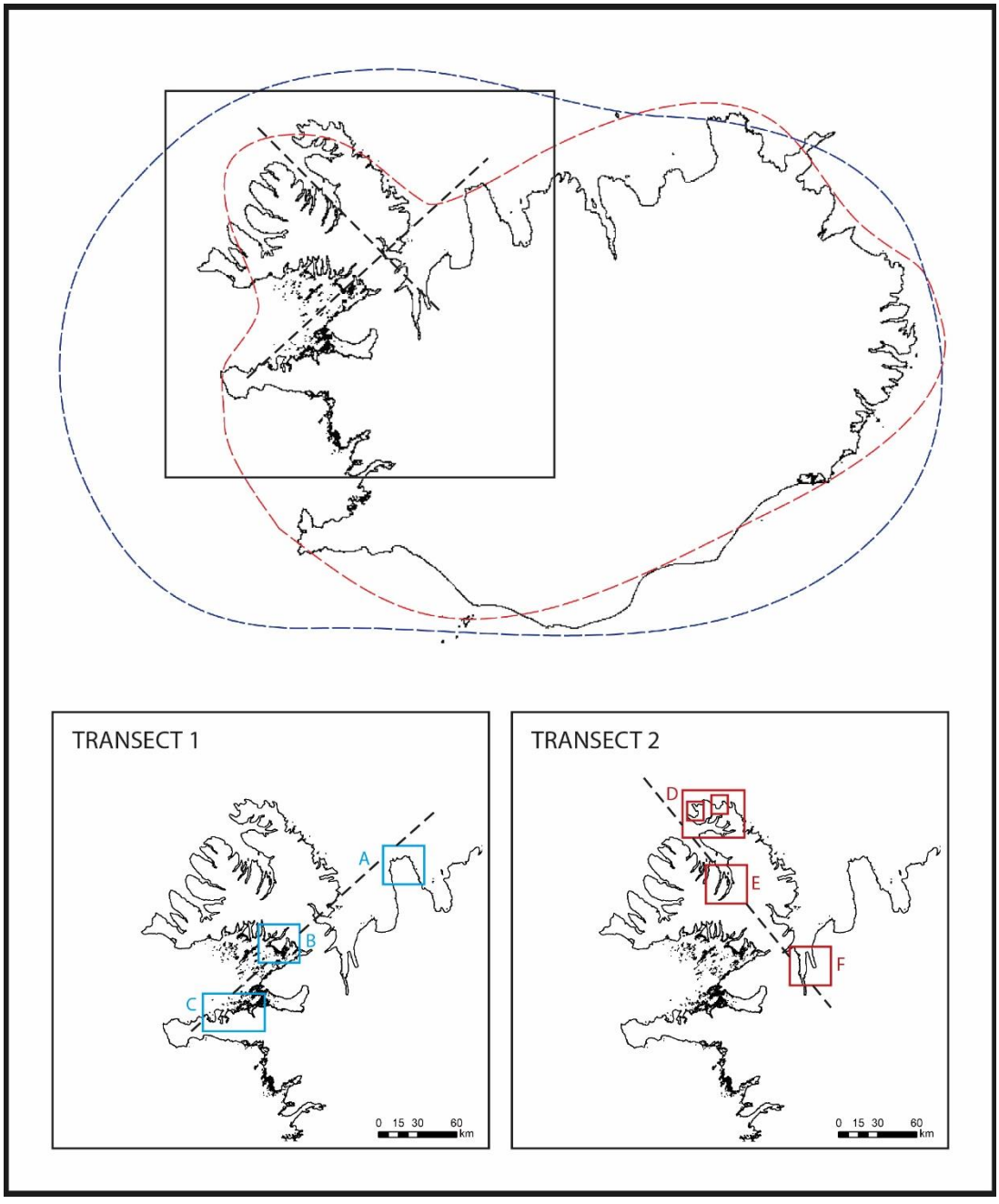

Figure 3.4A - Contextual information for Fig. 3.4B including the proposed glaciation scenarios (maximum - blue dashed line - and minimum - red dashed line) and transects of research in northwest Iceland. Transect 1 (light blue boxes) comprises Locations A (Skagi; Rundgren et al., 1997), B (Bjarkarlundur; Lloyd et al., 2009) and C (Snaefellsnes; Brader, 2012). Transect 2 (dark red boxes) includes Locations D (Aðalvik and Hornstrandir), E (Vatnsfjörður) and F (Hvammstangi, Vatnsnes). The proposed patterns of RSL change for each locations are outlined in Fig. 3.4B.

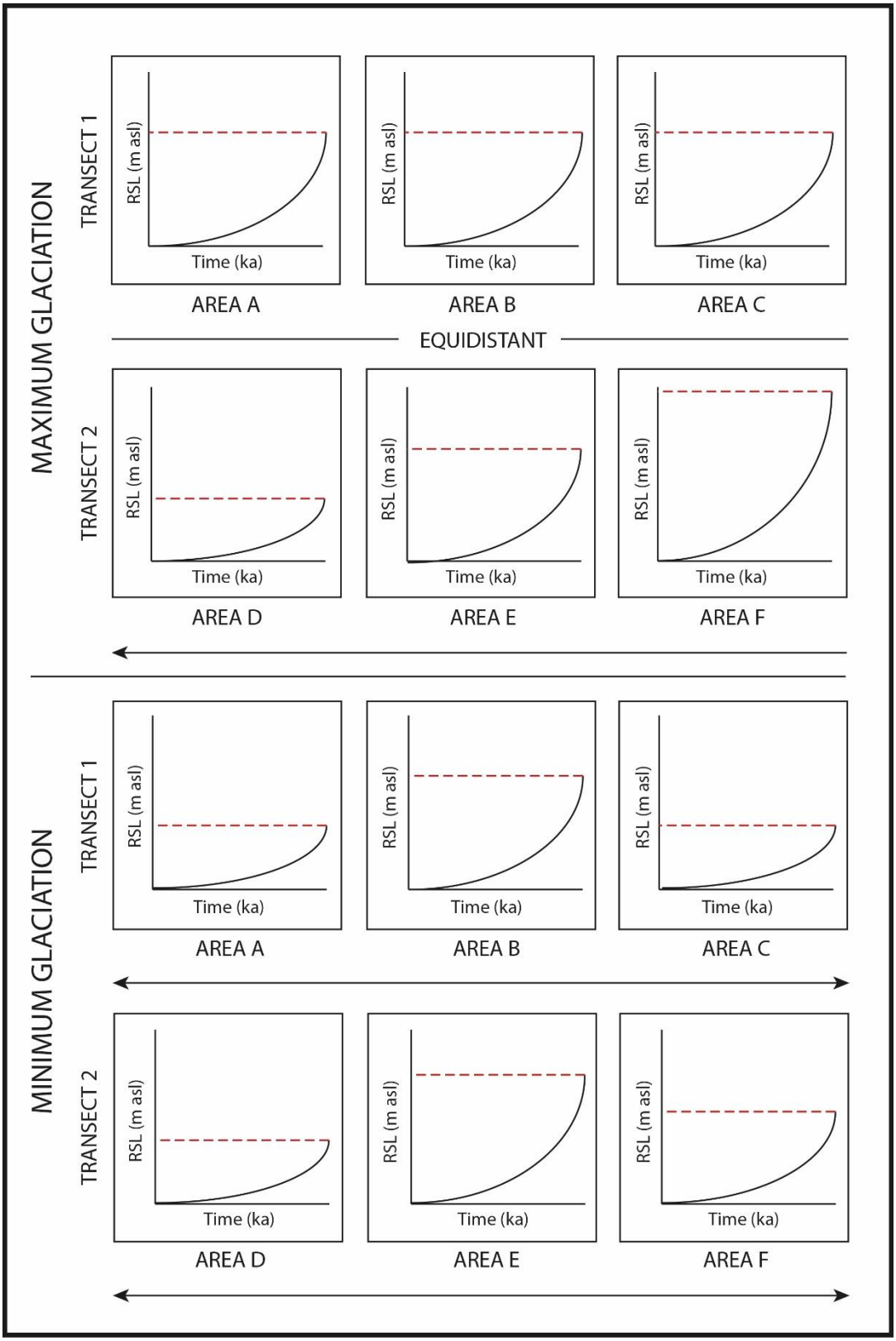

Figure 3.4B - Proposed patterns of RSL change for the two LGM glaciation scenarios in NW Iceland. Arrows denote distance from the loading centre and red dashed lines show the marine limit (relative elevations). Under the maximum scenario, Transect 1 experiences similar patterns of RSL change due to equidistance from the proposed loading centre. Transect 2 sees a decrease in the marine limit elevation with distance away from the loading centre. Under the minimum scenario, highest marine limit elevations will be recorded at the centre points of both research transects due to the secondary loading centre in Vestfirðir. See Fig. 3.4A for contextual information regarding the transect locations and glaciation scenarios.

3.4 Site Selection

3.4.1 Isolation Basins and Coastal Lowlands

Prior to the commencement of fieldwork, potential isolation basin and coastal lowland sites were identified from aerial imagery. These sites were then visited in the field and a series of criteria were employed to assess their suitability for inclusion within the study (c.f. Long *et al.*, 2011):

1. *Site elevation:* it is necessary to sample sites ranging in altitude from the marine limit to present in order to provide a comprehensive record of postglacial RSL change. Sites were therefore selected at a range of elevations to avoid duplication and allow the potential for RSL records from deglaciation to present. The number of isolation basins sought in a particular location was dependent on the elevation of the local marine limit and lower raised shorelines. Sites were chosen to provide possible sea-level index points at a range of elevations, with regular elevation intervals used where possible.
2. *Site location:* the nature of the Icelandic crust means that differential isostatic rebound is an important issue in reconstructing former environmental change. In order to minimise the effects, individual study areas were kept as small as possible (~ 5 km^2).
3. *Basin depth:* shallow basins suffer from poor sediment preservation (Smith *et al.*, 2005), particularly in sub-polar climates, where lake ice can disturb underlying sediments. Sediment records from deep basins can also be problematic, as sediments are easily reworked by currents (Smith *et al.*, 2005). When used for RSL study, isolation basins tend to have water depths <10 m (Long *et al*., 2011). Basins with <2 m water depth are best avoided, as they can suffer from ice freezing to the lake bed and subsequent disturbance to underlying sediments (Long *et al*., 2011).
4. *Post-isolation alteration:* basins with obvious signs of alteration were avoided.
5. *Sill identification:* the ability to identify an impervious, ideally bedrock, sill was an important factor in determining basin suitability. Sites with gravel or sand barriers were avoided, as they permit the ingression of marine water even following RSL fall below the elevation of the barrier. Therefore these systems give the potential for an inaccurate representation of environmental change over time.
6. *Practicality of sampling:* individual sites with poor access or too large to sample safely from the inflatable boat were avoided.

Coastal lowland sites were selected primarily based on their elevation, accessibility and location. Such sites were particularly useful when isolation basins did not occur close to present sea level. Isolation basin or coastal lowland samples were extracted from Areas A, C, D, E, F and G as part of this research project (Fig 3.3), which are described in Sections 3.5 and 3.6.

3.4.2 Raised shorelines

Raised shoreline sites were selected to complement the isolation basin and coastal lowland sites from the majority of the project's research areas (Fig 3.3). Sites were selected based on terrace preservation or a lack of evidence for post-depositional alteration, the availability of isolation basins in the study area and the availability of material for analysis. The majority of new raised beaches were identified within Areas D, E, F (Fig. 3.3). Raised shorelines frequently provided the elevation of highest postglacial RSL at each field site through the identification of the marine limit. Information regarding the surveying of these features is presented in Section 4.2.2.

3.5 Previous research locations

3.5.1 Area A – Skagi

Skagi is situated in northern Iceland (Fig. 3.3) and is characterised by the many lakes found at its northernmost point. Rundgren *et al.* (1997) investigated five isolation basins and one open section in northern Skagi (Fig. 3.5; Table 3.1) and identified three distinctive raised beach terraces in the region. In order to further develop the RSL curve for the region, an isolation basin close to the marine limit was investigated in this study at Tjörn (TJ1). Tjörn (71.25 m asl) is situated higher than any of the sites investigated by Rundgren *et al.* (1997) and is intended to provide a limiting date for deglaciation (Fig. 3.5, 3.6 and Table 3.2).

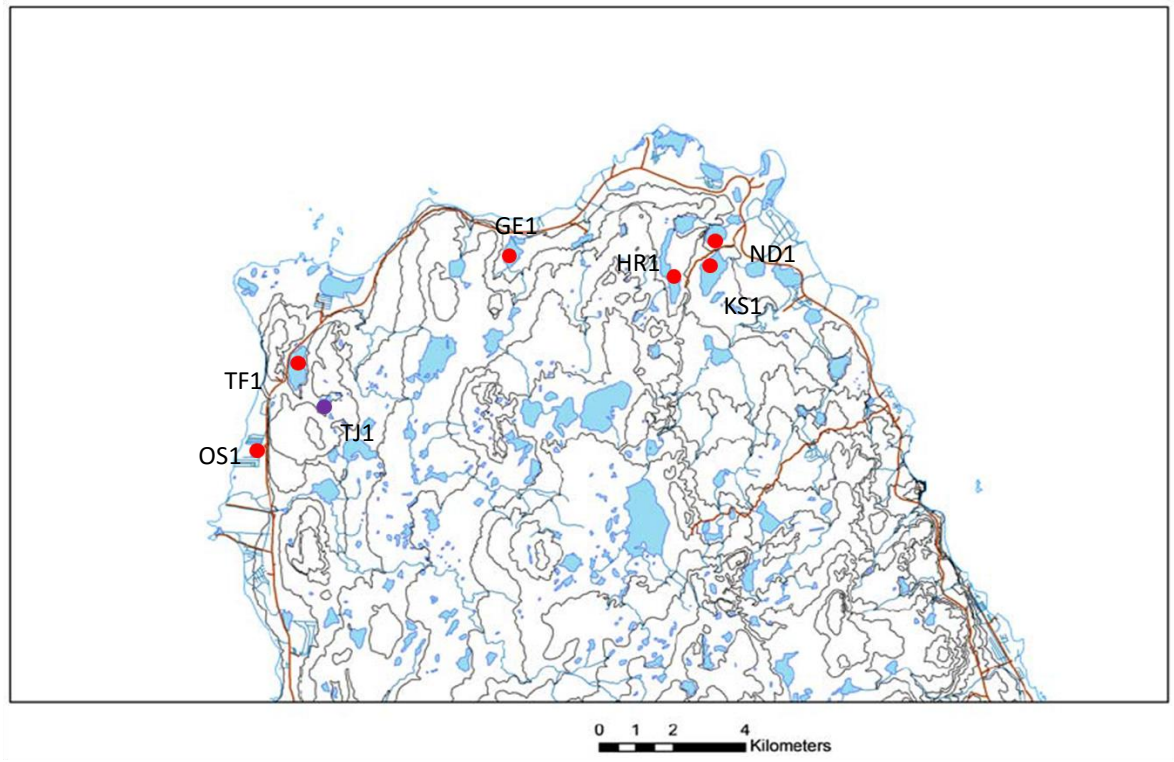

Figure 3.5 – Site locations in northernmost Skagi including previous research (red; Rundgren et al., 1997) and current research sites (purple). Contour interval: 20 m.

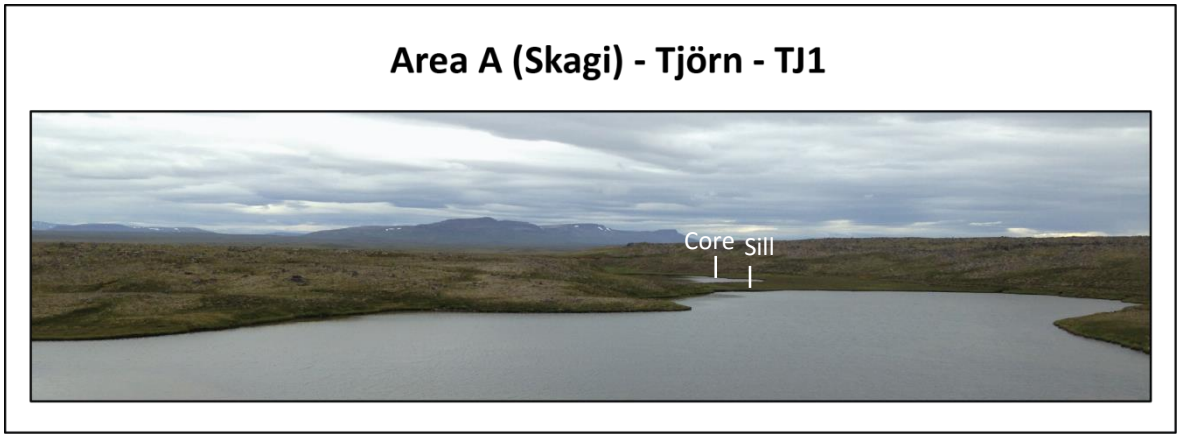

Figure 3.6 – Site location at Tjörn, showing the position of the sampled basin above the larger lake at Tjörn.

Site Name	Site Code	Grid Reference		Sill or Section Elev. (m asl)	
Open Section	OS1	66°02'N	20°25'W	1.5	Rundgren *et al.* (1997)
Neðstavatn	ND1	66°06'N	20°08'W	13	
Kollusátursvatn	KS1	66°05'N	20°08'W	22	
Geitakarlsvötn	GE1	66°05'N	20°16'W	26	
Hraunsvatn	HR1	66°05'N	20°10'W	42	
Torfadalsvatn	TF1	66°04'N	20°23'W	47	
Tjörn	**TJ1**	**66°03.050'N**	**20°22.072'W**	**71.25**	

Table 3.1 – Location and elevation information for previous research sites (Rundgren et al., 1997) and the new site, Tjörn, marked in bold.

3.5.2 Area B – Bjarkarlundur, Vestfirðir

Previous research in Area B (Fig. 3.3) has highlighted a number of isolation basins and raised terraces, which can be exploited to investigate RSL changes over the Lateglacial and Holocene (Lloyd *et al.*, 2009). These basins are summarised in Table 3.2 and range in elevation from the marine limit to present sea level. In addition, these sites will form part of a sea-level database for Iceland, which can be used to test glacio-isostatic adjustment (GIA) models of the region. No additional isolation basin, coastal lowland or raised terrace sites were sampled in Area B as part of this research.

Site Name	Grid Reference		Sill or Core Elev. (m asl)	
Skerðingsstaðir	65°27.240'N	22°16.780'W	3.00	Lloyd *et al.* (2009)
Mávavatn	65°26.612'N	22°13.478'W	3.00	
Hafrafellsvatn	65°30.301'N	22°02.786'W	24.7	

Hríshólsvatn	65°31.827'N	22°04.624'W	41.1	
Berufjarðarvatn	65°33.064'N	22°06.329'W	51.1	
Hríshóll 1	65°32.373'N	22°05.516'W	79.1	
Hríshóll 2	65°32.561'N	22°05.073'W	94.1	

Table 3.2 - Location and elevation information for existing sites in Bjarkarlundur, Vestfirðir (Lloyd et al., 2009).

3.5.3 Area C – Stykkishólmur, Snæfellsnes

The Snæfellsnes peninsula is situated in western Iceland (Fig. 3.3) and is dominated by the Snæfellsjökull volcanic system at its westernmost point, part of which remains glaciated. In addition to the principal peninsula, two smaller peninsulas encroach into Breiðafjörður: Setberg (Barar) and Thorsnes (Fig. 3.7). The Snæfellsnes Volcanic Belt (SVB) gives the region a distinct landscape, with extensive lava fields near Stykkishólmur (Fig. 3.7).

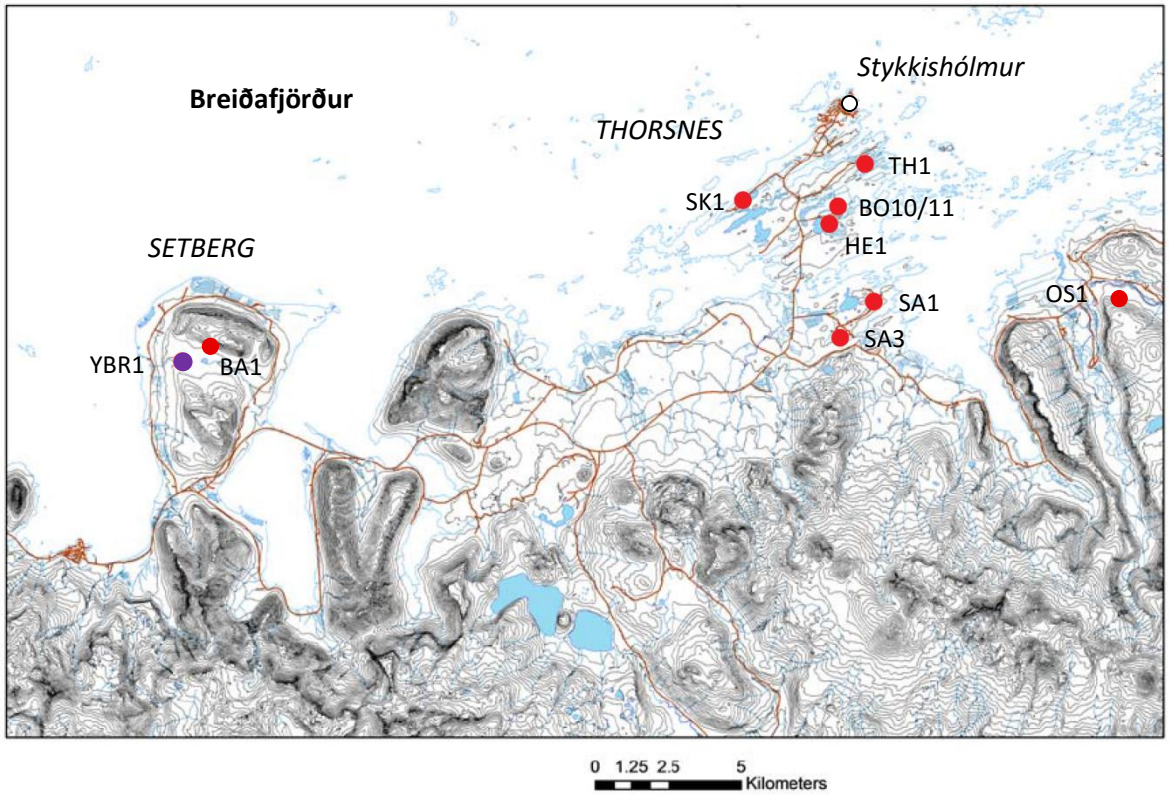

Figure 3.7 – Site locations in northern Snæfellsnes, including previous research (red; Brader, 2012) and current research (purple). Contour interval: 20 m.

Brader (2012) investigated seven isolation basin and coastal lowland sites on the Thorsnes peninsula, alongside mapping the marine limit in Barar (BA1) and Ós (OS1). The sites are summarised in Fig. 3.7 and Table 3.3.

Site Name	Site Code	Grid Reference		Elevation (m asl)	
Borgarland 10	BO10	65°2.680'N	22°43.592'W	1.74 ± 0.30	Brader (2012)
Borgarland 11	BO11	65°2.667'N	22°43.670'W	3.08 ± 0.30	
Skjaldarvatn	SK1	65°2.845'N	22°47.189'W	4.57 ± 0.30	
Þingvallavatn	TH1	65°3.555'N	22°42.719'W	5.34 ± 0.30	
Saurar 1	SA1	65°1.076'N	22°41.785'W	8.97 ± 0.30	
Helgafellsvatn	HE1	65°2.314'N	22°44.387'W	12.77 ± 0.30	
Saurar 3	SA3	65°0.313'N	22°43.103'W	16.20 ± 0.30	
Barar	BA1	64°59.337'N	23°11.651'W	68.87 ± 2.00	
Ós	OS1	65°0.103'N	22°33.264'W	62.84 ± 2.00	
Ytra Baravatn	**YBR1**	**64°59.056'N**	**23°11.579'W**	**57.60 ± 0.30**	

Table 3.3 – Location and elevation information for existing (Brader, 2012) and new research locations (bold) in Snæfellsnes.

One new site, Ytra Baravatn (YBR1) was sampled as part of this project in order to provide a timing for marine limit formation in northern Snæfellsnes (Fig. 3.8 and Table 3.3). The site is situated close to the local marine limit in the Barar region (Fig. 3.7; 3.8).

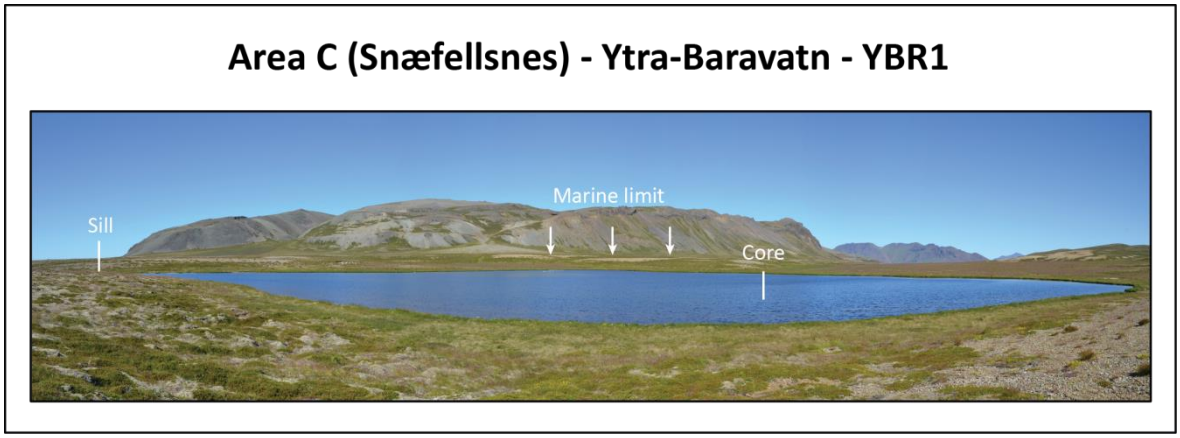

Figure 3.8 – Ytra-Baravatn showing the locations of the basin sill and analysed core sample. The marine limit recorded at Barar is seen behind the lake in the image.

3.6 New research locations

3.6.1 Area D – Hornstrandir and Aðalvik

Within northernmost Vestfirðir, two research locations were chosen: Hornstrandir and Aðalvik (Fig. 3.3). Isolation basins and raised terraces were investigated in both areas, with samples collected from six sites in Hornstrandir and one site in Aðalvik. The locations of these are summarised in Fig. 3.9 and 3.12 and Tables 3.4 and 3.5. Hornstrandir and Aðalvik were selected in order to provide information on RSL change at the most distal locations from the principal former

ice loading centre at Vatnajökull (Fig. 2.2). In addition, both Hornstrandir and Aðalvik provide an opportunity to determine patterns of RSL change close to the potential secondary loading centre within northwest Iceland (Fig. 2.2).

In Hornstrandir, Hlöðuvik and Hælavik are characterised by expansive valleys surrounded by steep hillslopes, corries and extensive geomorphological eivdence of glaciation (Hjort *et al.*, 1985). Numerous small basins can be found in the valley floor, particularly towards the mouth of both valleys (Fig. 3.9). Although this is the case, relatively few basins were suitable for RSL research due to thin, clastic-rich sediment profiles within the basins.

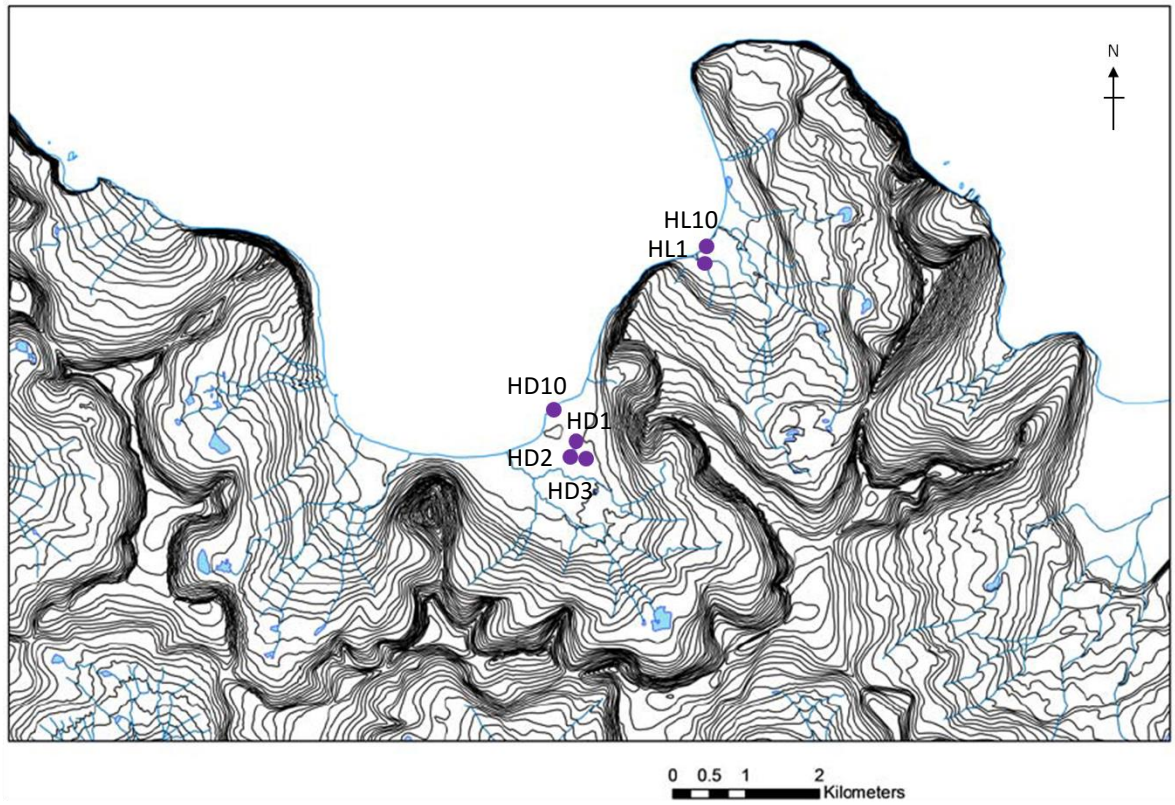

Figure 3.9 – Site locations within Hlöðuvik (HD) and Hælavik (HL), Hornstrandir. Contour interval: 20 m.

Site Name	Site Code	Grid Reference		Elevation (m asl)
Hlöðuvik 3	HD3	66°24.965'N	22°38.857'W	18.01 ± 0.30
Hlöðuvik 1	HD1	66°25.156'N	22°38.846'W	18.13 ± 0.30
Hlöðuvik 2	HD2	66°25.142'N	22°38.776'W	18.71 ± 0.30
Hælavik 1	HL1	66°26.379'N	22°36.686'W	30.58 ± 0.30
Hlöðuvik Terrace	HD10	66°25.354'N	22°38.857'W	7.48 ± 1.00
Hælavik Terrace	HL10	66°26.460'N	22°36.792'W	12.61 ± 1.00

Table 3.4 – Location and elevation information for new sites in Hornstrandir (Hlöðuvik and Hælavik).

In addition to the lake basins, extensive raised terraces are evident in both valleys and were sampled as part of this research (Fig. 3.10 and 3.11). In particular, the sequence at Hlöðuvik was both long and easily accessible, offering an opportunity to collect several samples of tephra and silt (Fig. 3.10). Both of these terrace sequences are found at the mouth of the valley, with no evidence for additional raised marine features at higher elevations.

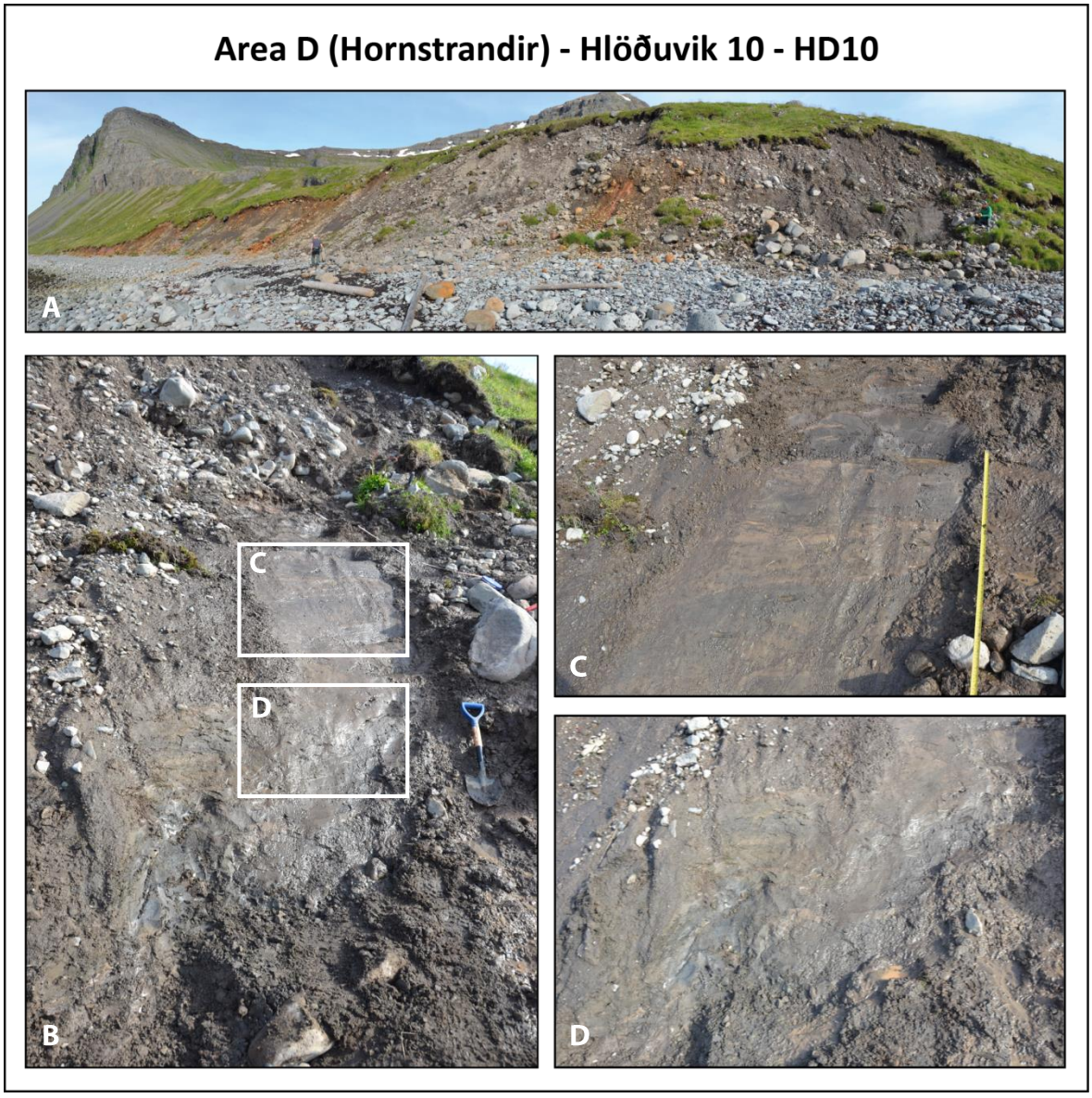

Figure 3.10 – Hlöðuvik 10 showing the extent of the raised terrace deposits (A), cleaned exposed section (B) and layered silt and proposed tephra deposits (C and D) found at the location. The location of the site within Hornstrandir can be seen in Fig.3.9.

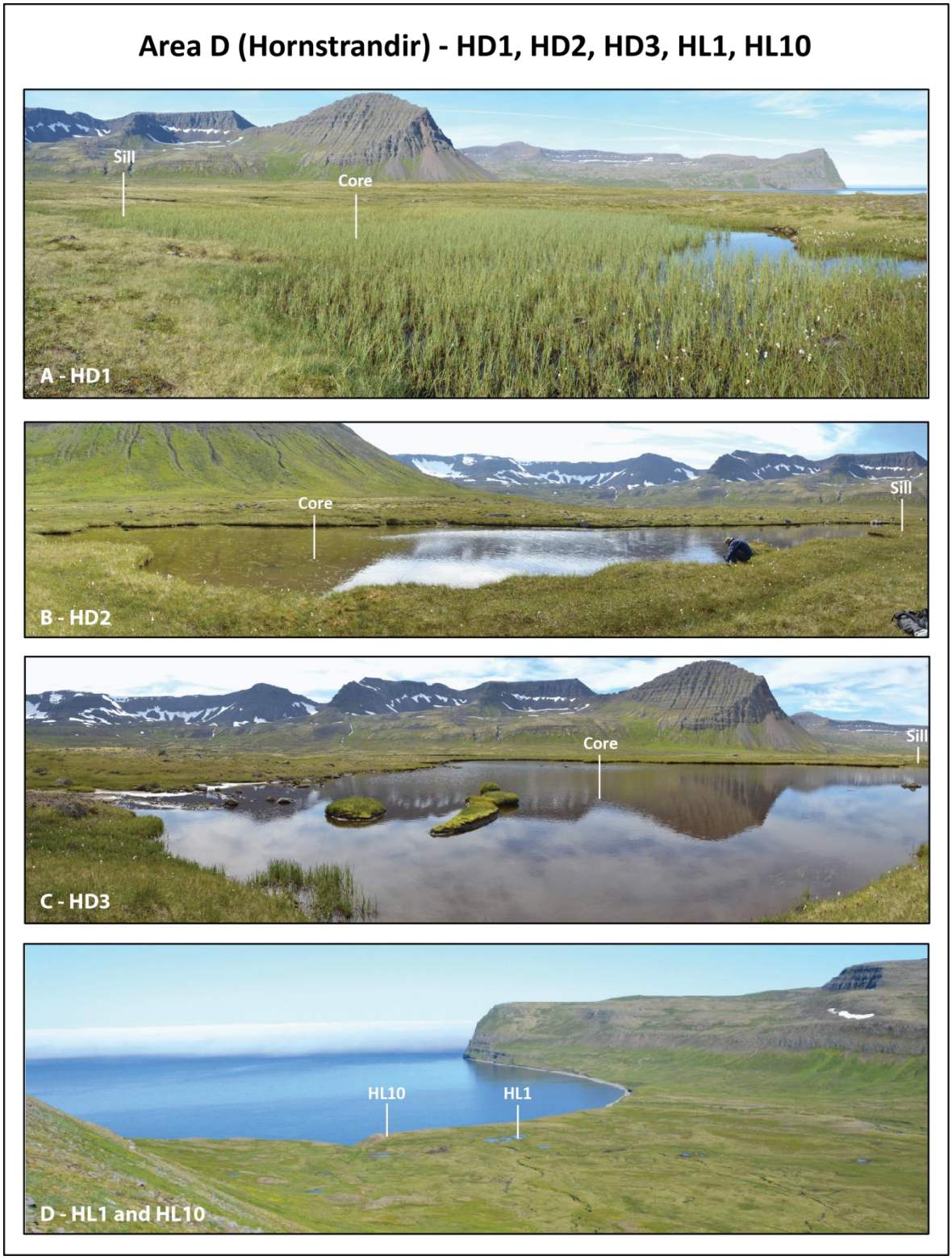

Figure 3.11 – Site locations in Hlöðuvik (A, B, C) and Hælavik (D), highlighting the location of core samples and sills for basins in Hlöðuvik.

Aðalvik is situated at the northwesternmost point of Iceland and is characterised by numerous fjord valleys and extensive dune systems. Lake basins were sampled in a number of locations, with Rekavik being the only site to yield suitable sediments for RSL research (Fig. 3.12, 3.13 and Table 3.5).

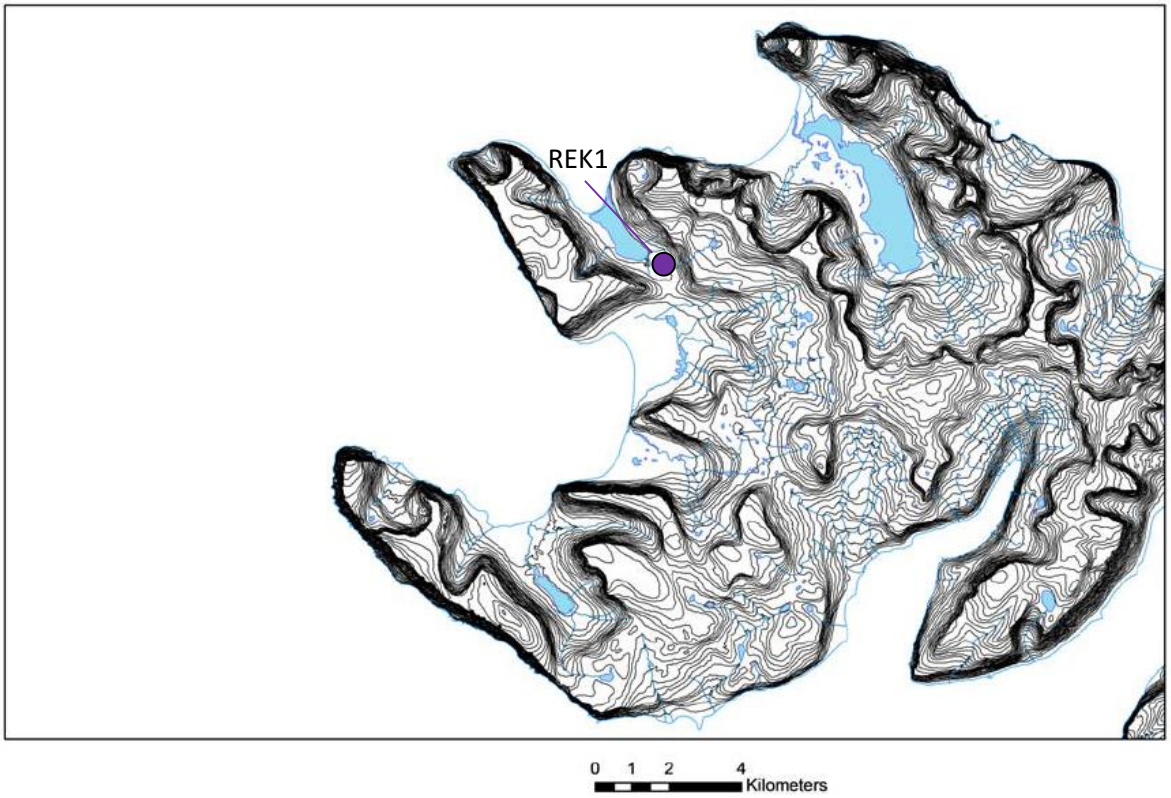

Figure 3.12 – Site location of the new site in Aðalvik, northwest Iceland. Contour interval: 20 m.

Site Name	Site Code	Grid Reference		Elevation (m asl)
Rekavik	REK1	66°24.500'N	23°0.441'W	18.63 ± 0.30

Table 3.5 – Location and elevation information for the new site in Aðalvik, Iceland.

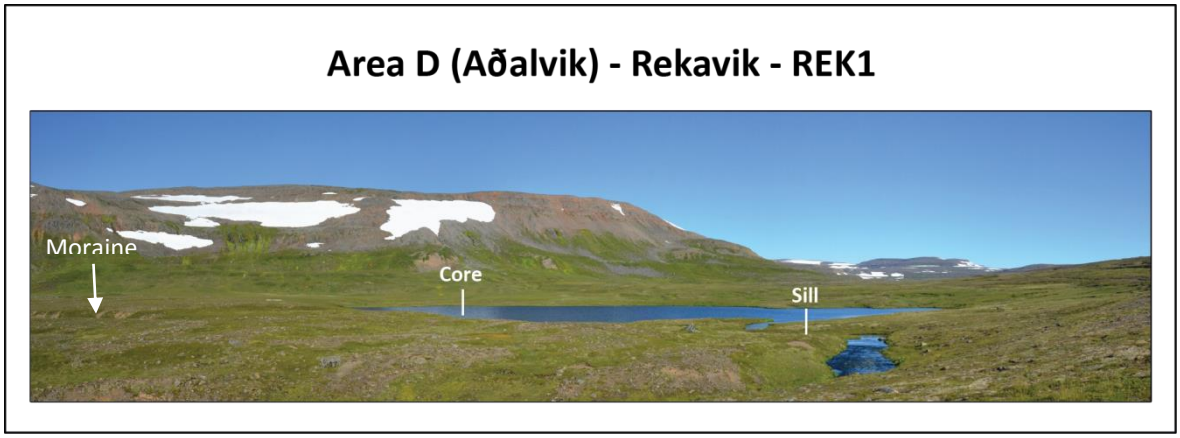

Figure 3.13 – Rekavik 1, showing the location of the sampled core and isolation basin sill. The washed moraine close to the site can be seen to the left of the image.

3.6.2 Area E – Vatnsfjörður, Vestfirðir

Vatnsfjörður is an important Viking settlement site located in central Vestfirðir (Fig. 3.3) and is characterised by a number of small lake basins at low elevation. Area E was chosen to provide an area of investigation close to Drangajökull and Gláma (Fig 3.3). In total, 11 isolation basin, one raised marsh and one raised terrace site were investigated (Figs. 3.14, 3.15, 3.16, 3.17; Table 3.6).

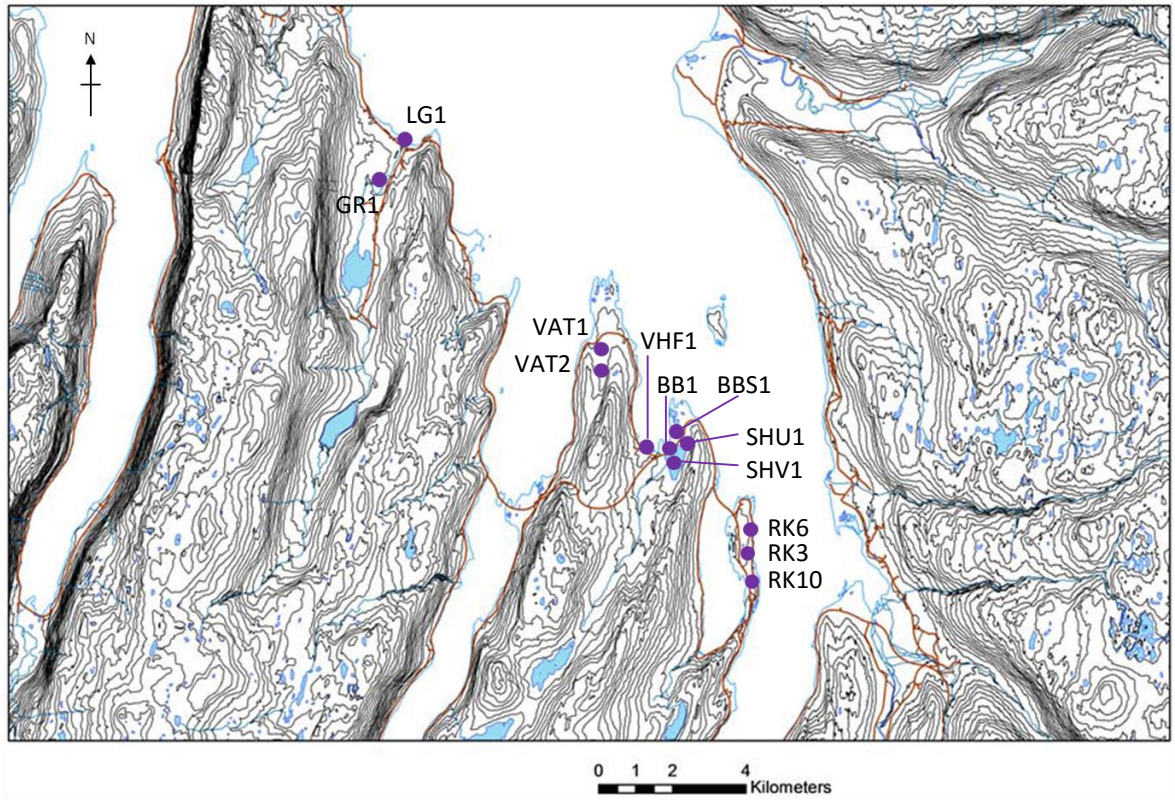

Figure 3.14 – Location of sites within the Vatnsfjörður region of Vestfirðir, northwest Iceland. Contour: 20 m.

Site Name	Site Code	Grid Reference		Elevation (m asl)
Bolsvik Bay	BB1	65°56.392'N	22°29.029'W	-0.50 ± 0.25
Sveinhusvatn	SHV1	65°56.210'N	22°28.193'W	1.24 ± 0.30
Bolsvik Bay Staircase	BBS1	65°56.448'N	22°28.767'W	1.55 ± 0.30
Reykjanes 6	RK6	65°55.193'N	22°25.588'W	2.30 ± 0.30
Sveinhusvatn Upper	SHU1	65°56.571'N	22°27.907'W	3.38 ± 0.30
Vatnsfjörður Home Field	VHF1	65°56.324'N	22°30.000'W	4.50 ± 0.30
Reykjanes 3	RK3	65°54.171'N	22°25.069'W	6.19 ± 0.30
Reykjanes 10	RK10	65°54.321'N	22°25.184'W	16.49 ± 0.30
Vatnsfjarðarnes 1	VAT1	65°57.823'N	22°31.174'W	22.22 ± 0.30
Vatnsfjarðarnes 2	VAT2	65°57.553'N	22°30.956'W	28.52 ± 0.30
Grimhólsvatn	GR1	66°0.053'N	22°39.353'W	29.59 ± 0.30
Laugardalur Terrace	LG1	66°0.600'N	22°38.322'W	18.54 ± 1.00

Table 3.6 – Location and elevation information for new sites in Vatnsfjörður, Vestfirðir, Iceland.

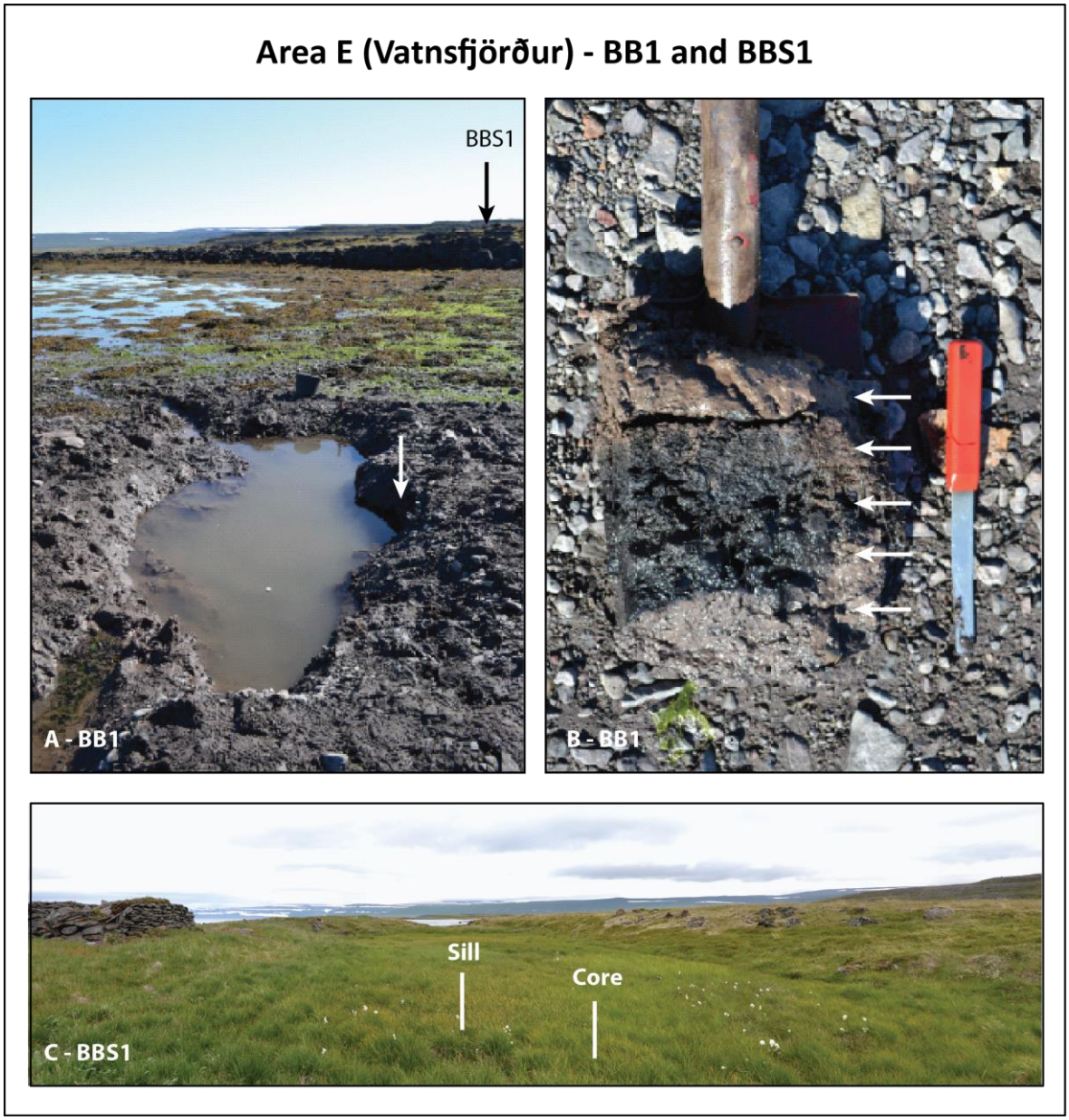

Figure 3.15 – Lower elevation sites in Vatnsfjörður, including Bolsvik Bay (A and B) and Bolsvik Bay Staircase (C). 'A' shows a pit dug on the beach at Bolsvik Bay. The sample for analysis at the site was taken at the edge of this pit, as marked by the white arrow in 'A'. Samples were taken at regular intervals through the sediment sequence presented in 'B' (red arrows). Bolsvik Bay Staircase is a small basin located above Bolsvik Bay (BB1), on the higher ground seen in 'A' (marked as BBS1).

A number of the lower elevation sites are situated close to the historic farm at Vatnsfjörður, several of which were likely exploited by early settlers in Iceland (Fig. 3.15). These sites ranged from coastal archaeological excavation sites to small lake basins. Sites which had been intentionally altered by human action were avoided, to avoid misrepresentation of environmental change within the resulting records.

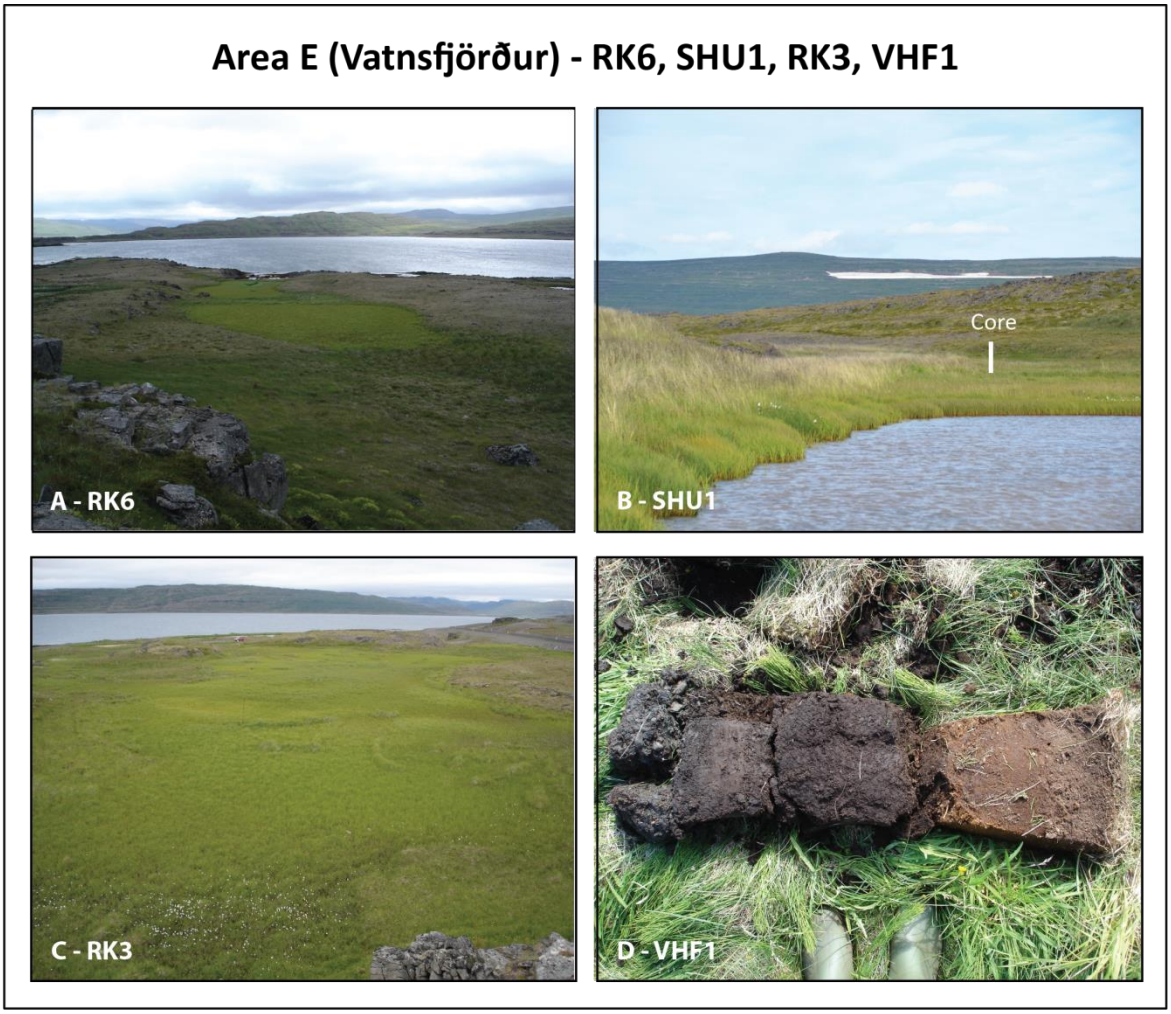

Figure 3.16 – Reykjanes 6 (A), Sveinhusvatn Upper (B), Reykjanes 3 (C) and Vatnsfjörður Home Field (D), showing the sill location and core sample locations at each site.

A number of isolation basin sites were also sampled at higher elevations close to or above the extensive raised terrace deposits found in Laugardalur and Vatnsfjarðarnes (Fig. 3.17). The highest basin at is located at Grimhólsvatn (Fig 3.17C) with sufficient sediment being extracted to allow subsequent laboratory analysis to take place.

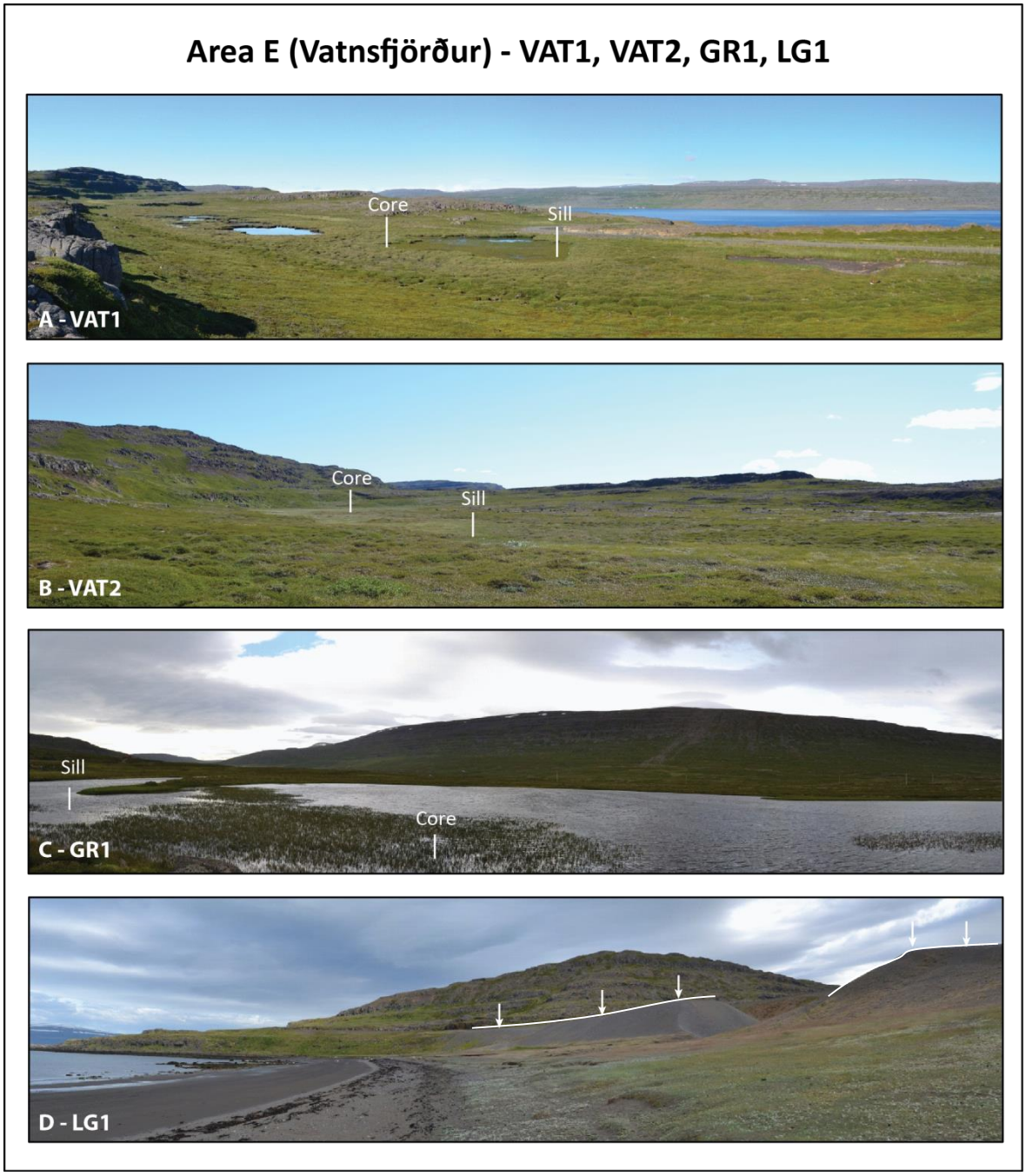

Figure 3.17 - Higher elevation sites within the Vatnsfjörður region, including Vatnsfjarðanes 1 (A), Vatnsfjarðanes 2 (B), Grimhólsvatn (C) and the marine limit at Laugardalur (D), showing the site morphology, sample and sill locations (where appropriate).

3.6.3 Area F – Hvammstangi, Vatnsnes

In total, ten isolation basins and one raised terrace site were investigated in Area F (Figures 3.3, 3.18, 3.19, 3.20 and Table 3.7). Area F was chosen to form part of both perpendicular transects of research, acting as a crossover point. The area is characterised by upland environments, with few basins evident at lower elevations. Indeed, it was not possible to collect a complete sample from between 6.5 and 46 m a.s.l., leading to a gap within the dataset from this region. In addition, the *Nucella* beach in western Hrútafjörður will be useful for inclusion within the RSL reconstruction.

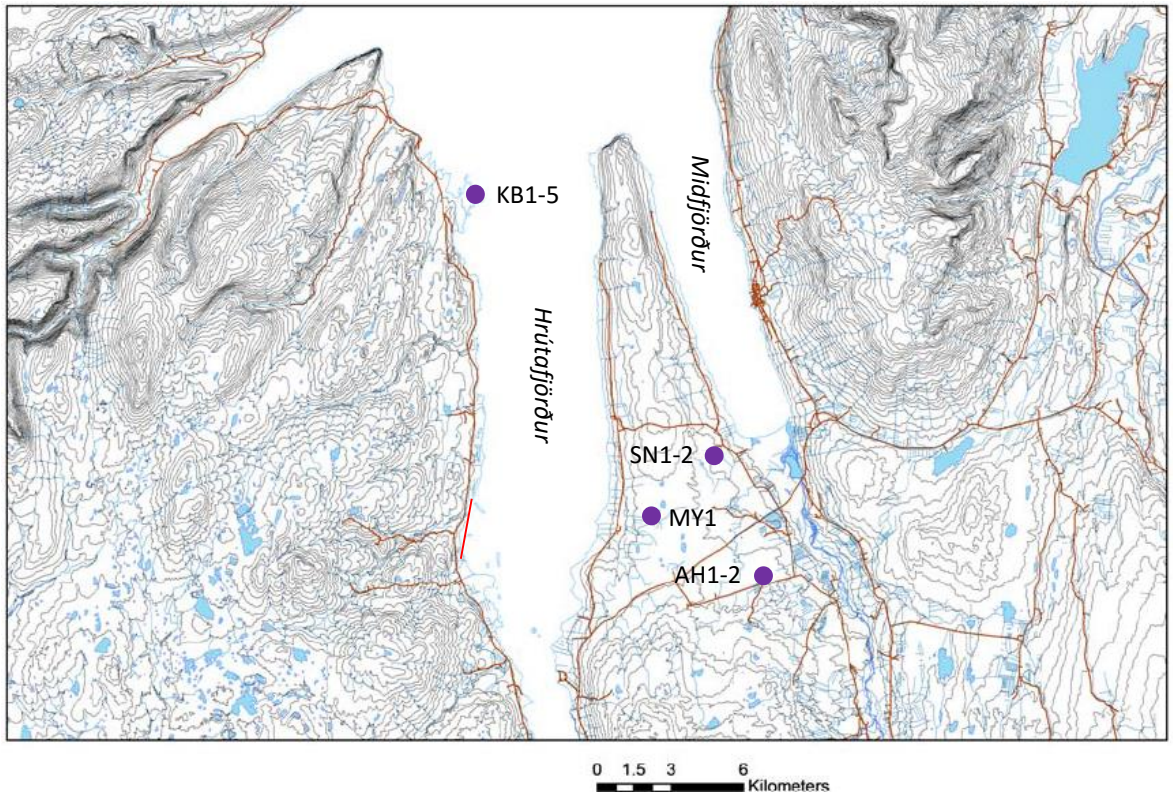

Figure 3.18 – Location of new sites near Hvammstangi, Vatnsnes and southeastern Vestfirðir (purple) and the Nucella beach (red).

Site Name	Site Code	Grid Reference		Elevation (m asl)
Kolbeinsánes 2	KB2	65°25.978'N	21°11.793'W	1.09 ± 0.30
Kolbeinsánes 3	KB3	65°25.945'N	21°11.970'W	1.57 ± 0.30
Kolbeinsánes 4	KB4	65°25.906'N	21°11.992'W	2.24 ± 0.30
Kolbeinsánes 1	KB5	65°25.984'N	21°11.756'W	3.45 ± 0.30
Kolbeinsánes 5	KB1	65°25.813'N	21°13.011'W	6.49 ± 0.30
Sandar 2	SN2	65°20.026'N	20°59.230'W	46.51 ± 0.30
Sandar 1	SN1	65°20.249'N	20°59.381'W	51.02 ± 0.30
Myrar	MY1	65°18.253'N	21°02.401'W	57.90 ± 0.30
Arnhóll 2	AH2	65°17.601'N	20°55.978'W	68.22 ± 0.30
Arnhóll 1	AH1	65°17.657'N	20°55.821'W	70.62 ± 0.30

Table 3.7 – Location and elevation information for new sites within the Hvammstangi region, Vatnsnes.

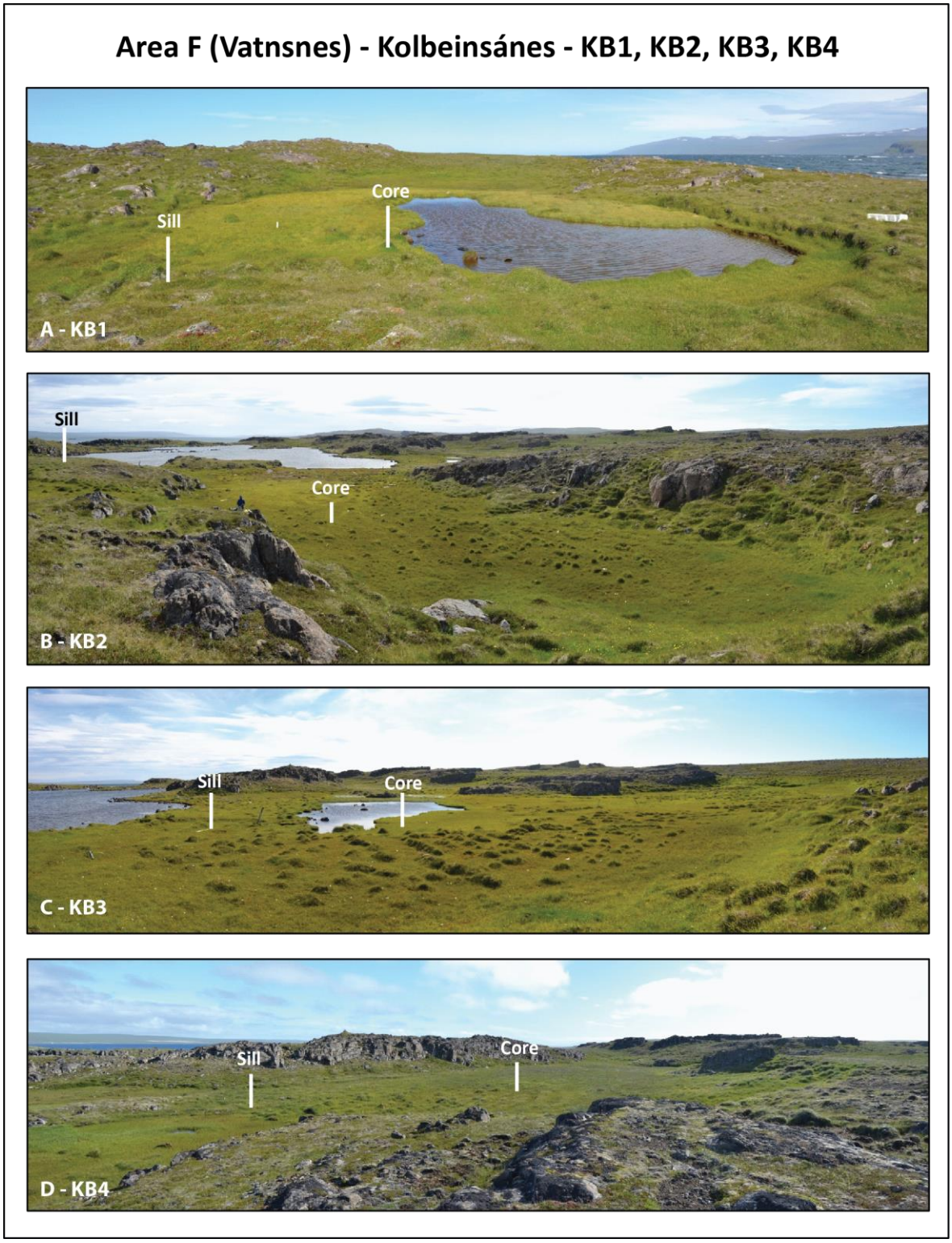

Figure 3.19– Lower elevation sites within Vatnsnes, including Kolbeinsánes 1 (A), Kolbeinsánes 2 (B), Kolbeinsánes 3 (C), Kolbeinsánes 4 (D), showing site morphology, sample and sill locations.

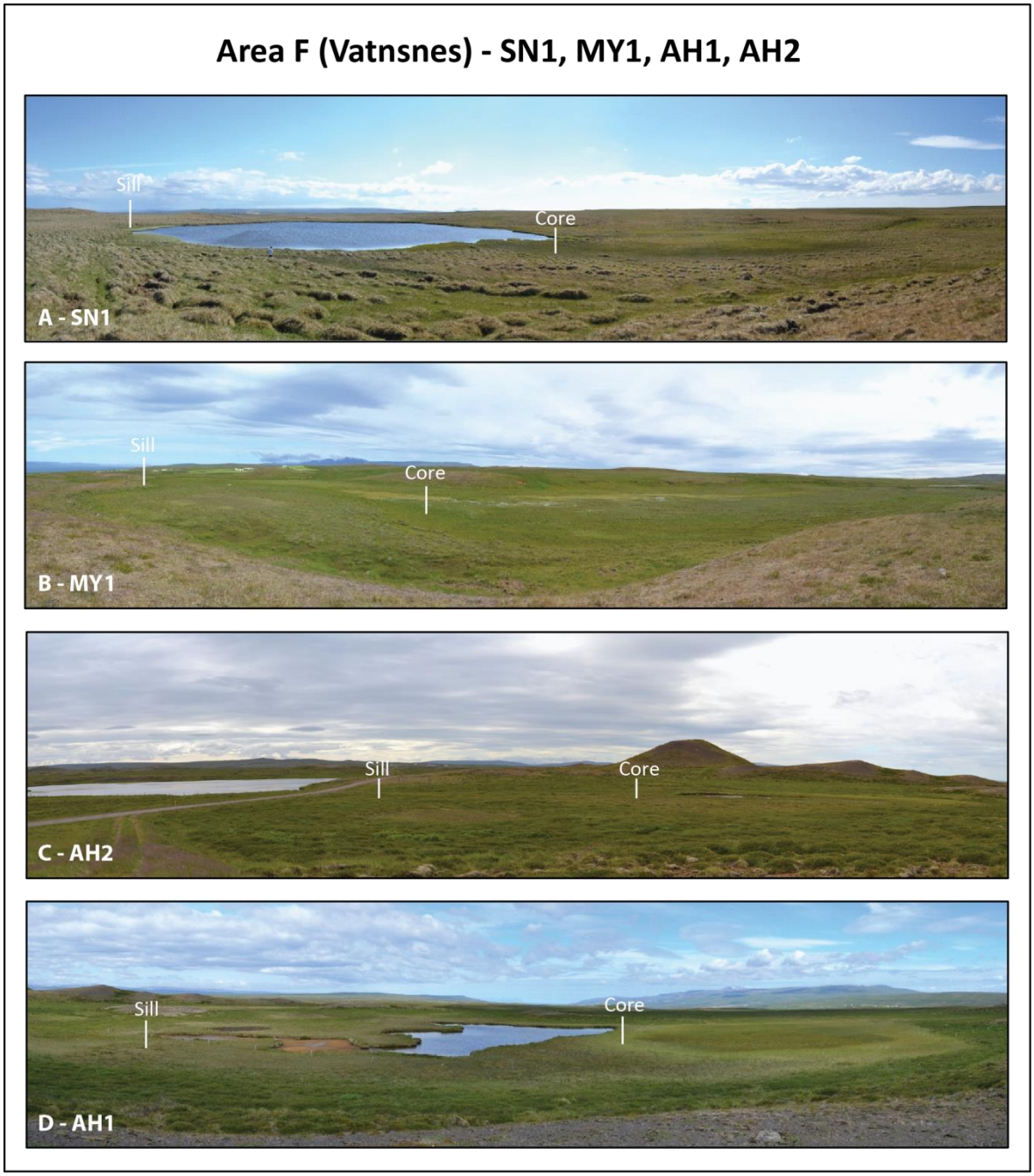

Figure 3.20 – Higher elevation sites in Area F, including Sandar 1 (A), Myrar 1 (B), Arnhóll 2 (C) and Arnhóll 1 (D), showing the position of the sill and core sample at each location.

3.6.4 Area G – Breiðavik, Vestfirðir

In Breiðavik (Fig. 3.3), a total of ten isolation basins were sampled ranging from the marine limit to present sea level (Fig. 3.21, 3.22, 3.23 and Table 3.8). Several other sites were investigated in the region, but were dominated by extensive sand deposits, making sampling challenging. The marine limit is well defined on the western coast of the peninsula and lies between 85 m and 90 m a.s.l. The highest sites sampled in the region were taken from HV1-4, where a series of small basins were found below the marine limit. HV2 failed to produce a suitable sediment record due to the rocky nature of the site. Low and mid-elevation sites were less easily identified in the area.

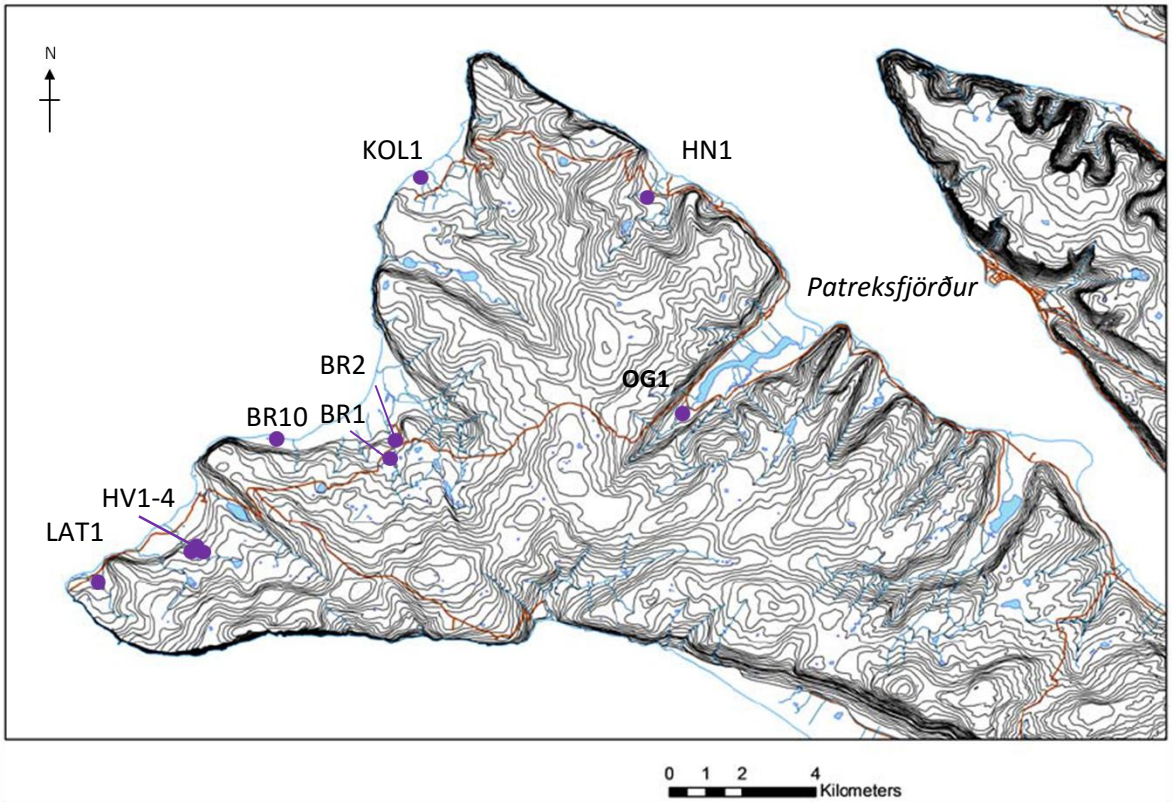

Figure 3.21 – Location of new sites in Area G.

Site Name	Site Code	Grid Reference		Elevation (m asl)
Örlygshöfn	OG1	65°33.533'N	24°10.584'W	4.06 ± 0.30
Kollsvik	KOL1	65°36.597'N	24°21.049'W	4.11 ± 0.30
Breiðavik 10	BR10	65°32.631'N	24°25.081'W	4.42 ± 0.30
Haenuvik	HN1	65°36.515'N	24°12.807'W	25.75 ± 0.30
Látrabjarg 1	LAT1	65°30.180'N	24°30.452'W	38.70 ± 0.30
Breiðavik 2	BR2	65°32.483'N	24°02.480'W	49.96 ± 0.350
Hvallátur 4	HV4	65°30.530'N	24°27.464'W	65.45 ± 0.30
Hvallátur 3	HV3	65°30.543'N	24°27.305'W	68.70 ± 0.30
Breiðavik 1	BR1	65°32.263'N	24°21.720'W	74.70 ± 0.30
Hvallátur 1	HV1	65°30.517'N	24°27.835'W	77.73 ± 0.30

Table 3.8 – Location and elevation information for sites in the Breiðavik region (Area G).

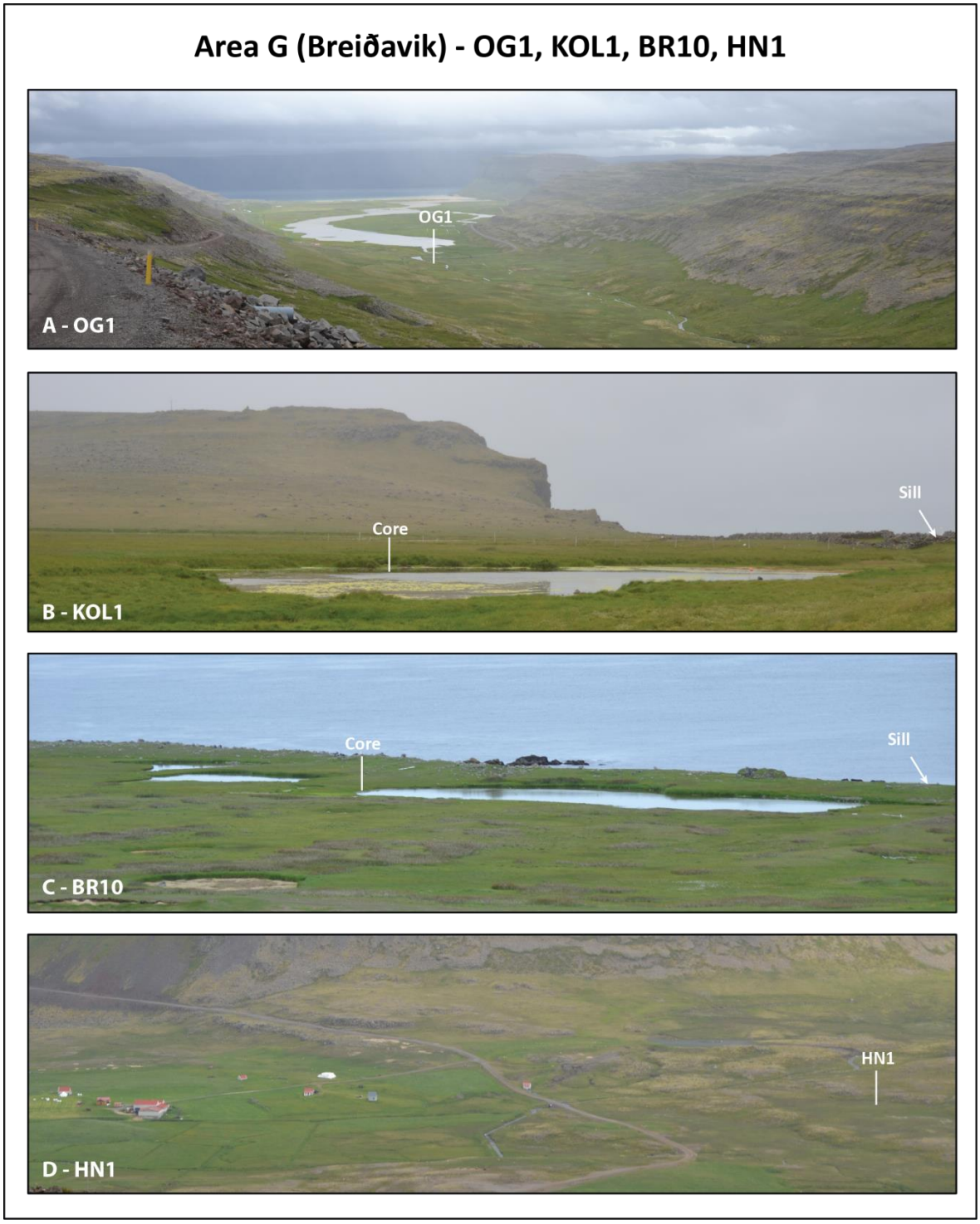

Figure 3.22 – Lower elevation sites at Breiðavik, including Örlygshöfn (A), Kollsvik (B), Breiðavik 10 (C) and Haenuvik 1 (D), showing the location of the sill and/or extracted core sample where appropriate.

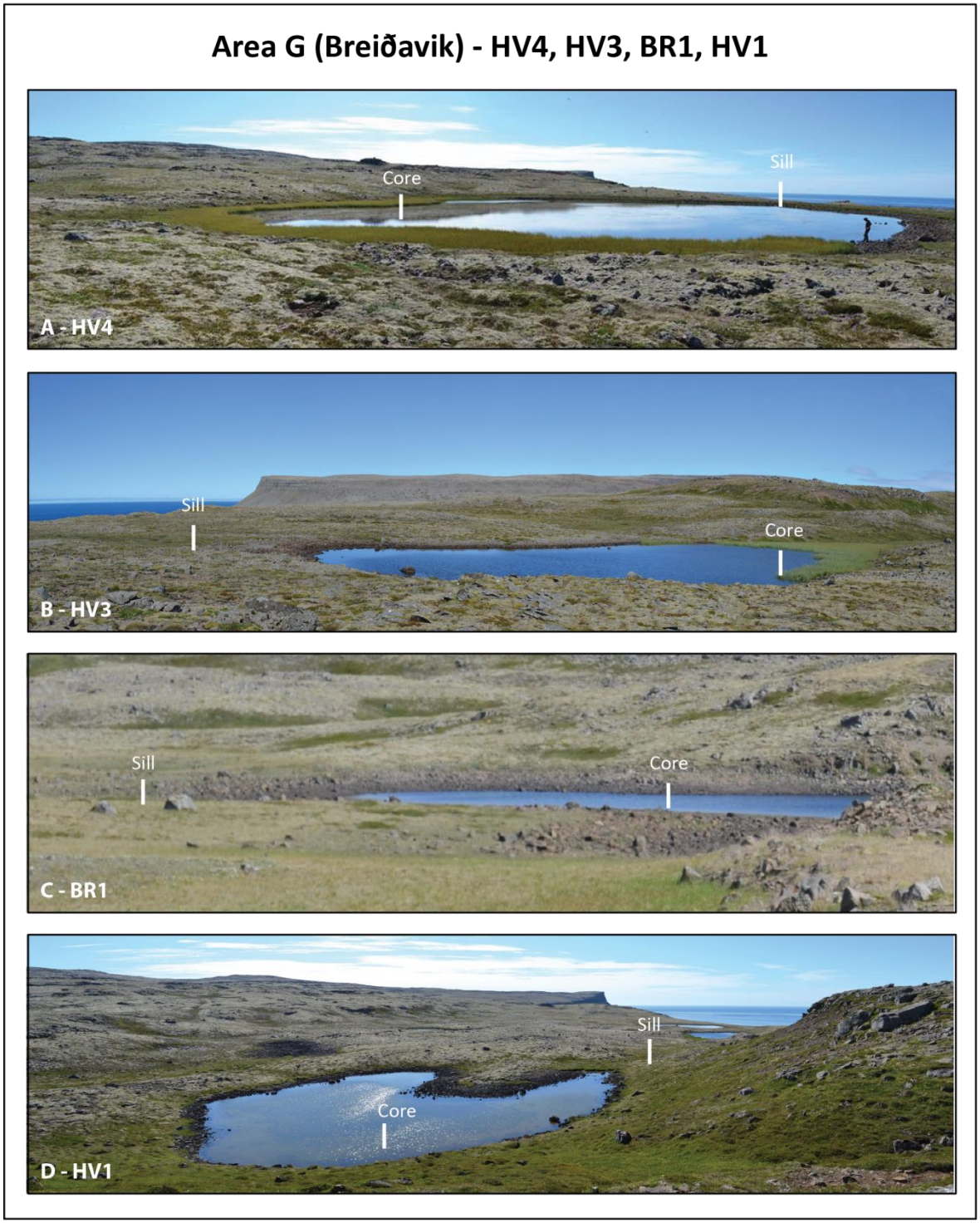

Figure 3.23 – Higher elevation sites in Area G, including Hvallátur 4 (A), Hvallátur 3 (B), Breiðavik 1 (C) and Hvallátur 1 (D), showing the sill and core locations.

3.7 Summary

The research was conducted along two perpendicular transects in northwest Iceland, which were designed to exploit the possibly contrasting RSL changes under the two LGM glaciation scenarios in Iceland. In total, there are seven research areas, with three locations having been the subject of previous study (Transect 1 - Area A – Rundgren *et al*., 1997), Area B – Lloyd *et al*., 2009) and Area C – Brader (2012)). New isolation basins were sought in Areas D, E, F (Transect 2) and G, covering elevations from the marine limit to present sea level. In addition, sites close to the local marine limit were identified in Areas A and C in order to produce a limiting age for deglaciation in these two locations. Raised shoreline deposits have also been located in Area D and E. The next chapter outlines the methods used to extract and analyse samples to produce the RSL dataset, alongside chronological and GIA modelling techniques.

CHAPTER 4

Methods

4.1 Introduction

This chapter outlines the techniques used to address the research objectives and project aims. The chapter is divided into three sections: field methods, laboratory methods, and GIA modelling. Each section aims to provide an overview of the key techniques and associated errors and to justify the choice of approach.

4.2 Field Methods

Fieldwork was conducted over two month-long field seasons, which took place between 21st June – 23rd July 2012 (Field Season 1) and 15th July – 15th August 2013 (Field Season 2). Over the course of the two field seasons, samples were collected from each of the field areas (Fig. 3.3), either to provide RSL histories for new locations or to add new data to existing records. The sites investigated can be divided into three types: isolation basins, coastal lowlands and raised terraces. Within the field, a suite of key methods were employed in order to collect samples and determine the elevation of particular features.

4.2.1 Isolation basins and coastal lowlands

4.2.1.1 Stratigraphic survey and core collection

After establishing site suitability using the criteria outlined in Section 3.4, it was necessary to determine the underlying stratigraphy for each isolation basin or coastal lowland site, as the representativeness of the final sample could then be established with certainty. Site stratigraphy was determined through the coring of a series of transects using a gouge corer, where possible. This allowed the detailed basin geometry to be assessed and selection of the most appropriate spot for coring the basin. When this was not possible, a sample was retrieved from the centre of the basin. The centre of an isolation basin is likely to be the deepest point and thus is likely to preserve the longest, undisturbed record of environmental change. All sediment cores were described in the field using the Tröels-Smith (1955) classification scheme.

Where possible, the site stratigraphy was determined from infilled sections of the basin in order to minimise the difficulties associated with retrieving samples from a boat. When the boat was employed, the oars of the boat were inserted into the basin sediments to keep the boat steady and as such allow the successful extraction of the sample. Examples of the approach can be

found with the site descriptions for each field location, where the location of each core is clearly marked.

After establishing the underlying stratigraphy of each site, representative samples were retrieved using a Russian Corer (Jowsey, 1966). Samples were retrieved from two parallel cores with a five centimetre overlap between samples. This approach overcomes the problems with corer design where the bottom of the corer does not collect material and thus ensures that a complete record is extracted (Fig. 4.1). Each section retrieved was then photographed, packed in plastic tubing and wrapped in airtight film in order to ensure sample preservation. Following the extraction of each core, the elevation of the sample was measured relative to Mean High Water Spring Tide (MHWST) using an Electronic Distance Meter (EDM). MHWST was taken as the highest wet seaweed line where available. Where this was not evident, timed still water measurements were taken and then adjusted to MHWST through consultation with tide predictions (Admiralty Tide Tables, 2006) for the individual field areas.

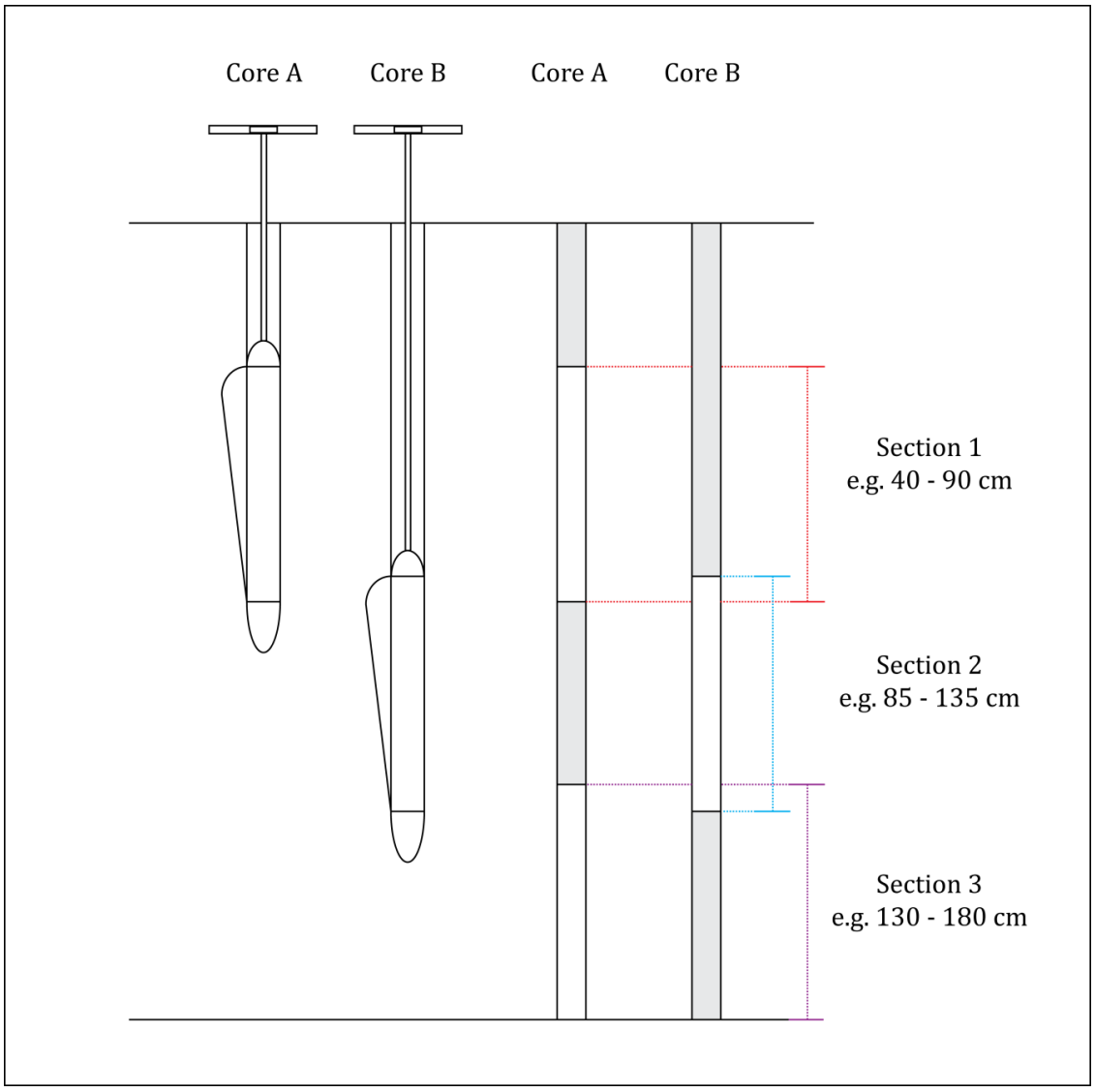

Figure 4.1 – Russian coring technique demonstrating the overlap between core samples (white shading) to ensure a complete sedimentary record is extracted.

4.2.1.2 Sill determination

For isolation basin sites, it is important to accurately determine the elevation of the sill. Initially, potential sill locations were identified through an examination of basin morphology, with the sill being easily identified at the majority of locations. Where multiple potential sill locations existed, detailed surveying of each location was undertaken. The sill of an isolation basin can either be identified as exposed bedrock or by coring through overlying sediments. Where the sill was constrained by exposed bedrock, a grid of points were surveyed using an EDM allowing the determination of the lowest ingression point into the basin identified by the transects. If the sill was covered by sediments, a grid of cores was cored in order to establish the exact location of the sill (Fig. 4.2). The depth reached by each core was recorded, providing an insight into basin morphology, with the lowest high point being identified as the sill (i.e. the sill is a saddle). This approach is only valid if the ground surface is assumed to be level. The elevation of candidate sill locations - those with similar depths - was measured with the EDM. This was undertaken to ensure that the lowest high point was selected, reducing uncertainty over possible undulation of the ground surface. It is essential to ensure that sufficient cores are taken when determining the sill location in order to fully survey the underlying bedrock and avoid misinterpretation of underlying boulders or gravel. The number of points surveyed is dependent on the morphology of the basin. Sill elevations were referenced to Mean High Water Spring Tide (MHWST) or Highest Astronomical Tide (HAT) using the procedure outlined in Section 4.2.1.3.

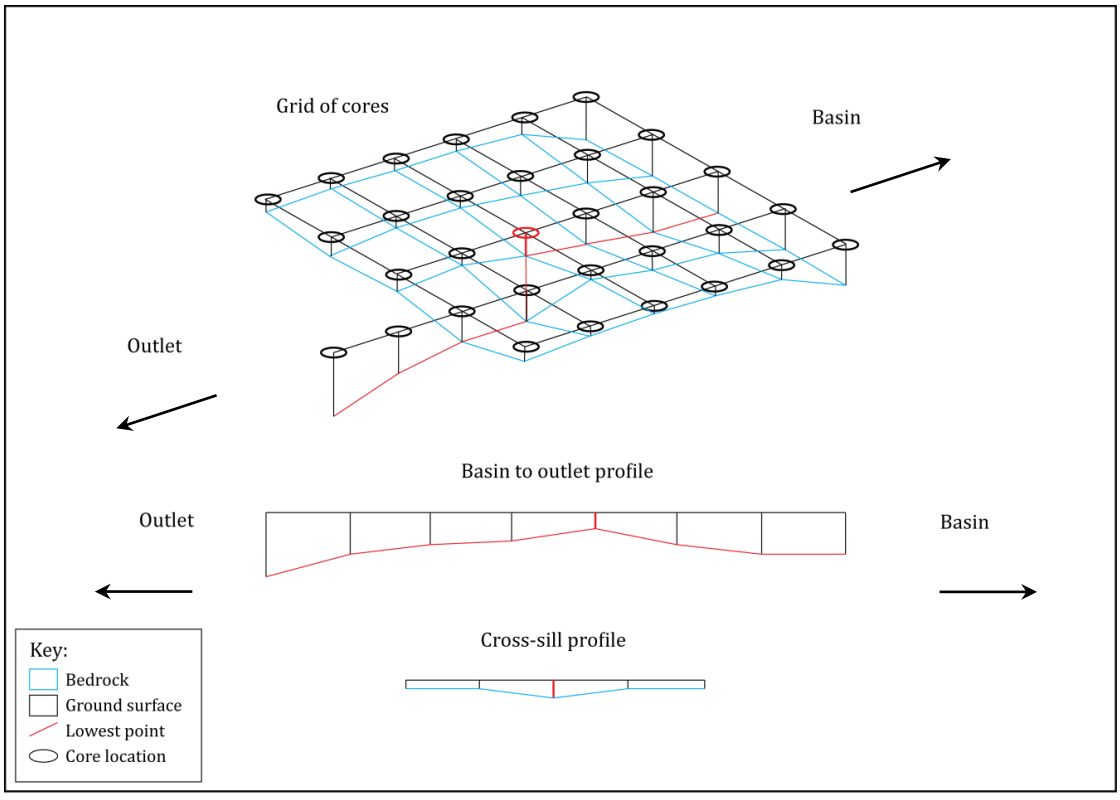

Figure 4.2 – Sill determination technique showing the grid of cores and identification of the lowest high point through the analysis of profile data. Adapted from Brader (2012).

4.2.1.3 Elevation Correction

Following the determination of the elevation of features relative to MHWST, a correction to give an elevation relative to mean sea level (m asl) is required. In order to achieve this correction, tide tables (Admiralty Tide Tables, 2006) were used from the nearest tide station (Table 4.1; Fig. 4.3A). Interpolation was avoided due to the low number of tide gauges in the region and similarity between tidal ranges from sites within the same fjord system (see Location D and E in Table 4.1). The elevation of MSL was calculated through the determination of the mid-point between MHWST and MLWST for each field area (Table 4.1), forming part of the calculation in Fig. 4.3B.

Record	Area	MHWST (m CD)	MHWNT (m CD)	MLWNT (m CD)	MLWST (m CD)
Reykjavik	-	4.0	3.0	1.3	0.2
Skagaströnd	A	1.5	1.1	0.4	0.1
Stykkishólmur	C	4.4	3.3	1.5	0.3
Bolungarvik	D	2.2	1.6	0.7	0.1
Álftafjörður	E	2.2	1.6	0.7	0.1
Hvammstangi	F	1.5	1.1	0.4	0.1
Vatneyri	G	3.2	2.3	1.0	0.2

Table 4.1 – Tidal information used in the elevation correction relative to chart datum (m CD). MHWS – Mean High Water Spring; MHWN – Mean High Water Neap; MLWN – Mean Low Water Neap; MLWS – Mean Low Water Spring. Source: United Kingdom Hydrographic Office/Admiralty Tide Tables (2006).

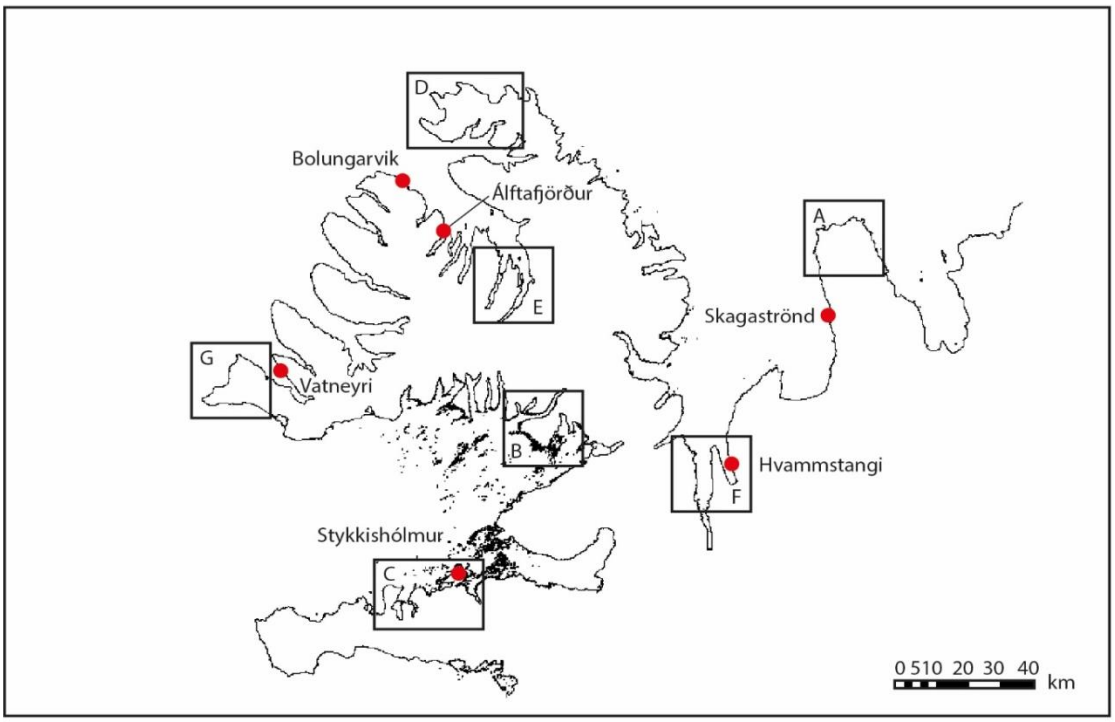

Figure 4.3A - Location of tide gauge stations (red spots) used to correct elevations of individual sites within this study (black boxes).

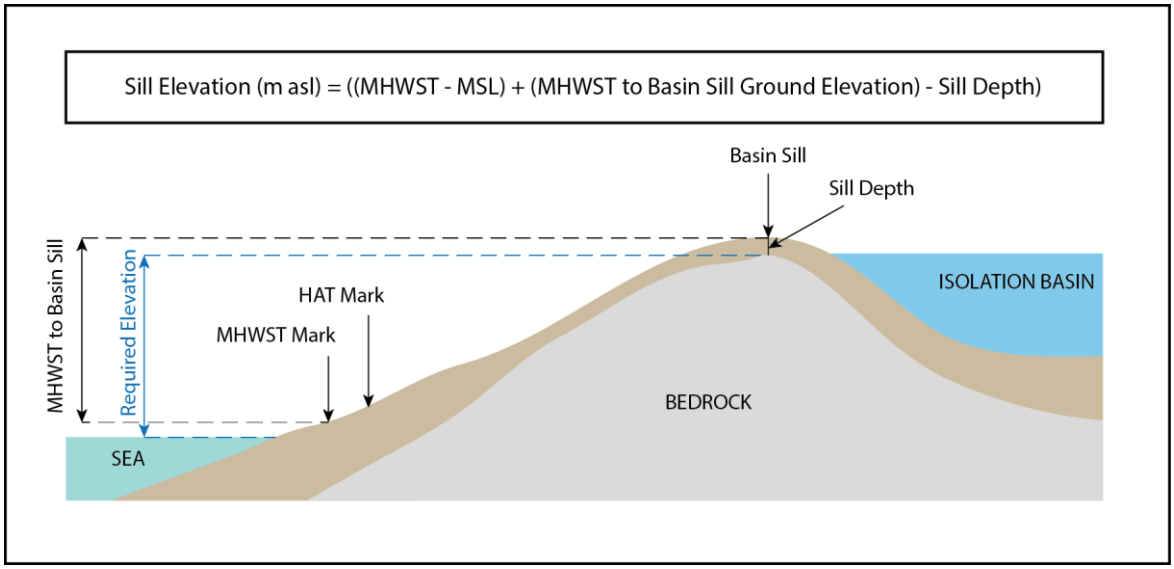

Figure 4.3B – Schematic outlining the process associated with sill elevation calculation, which comprises information from tide gauge data (MHWST-MSL), ground surveying (MHWST to Basin Sill Ground Elevation) and sill depth determination (Fig. 4.2). The elevation of the MHWST and HAT mark are also recorded for information during the surveying process.

In order to calculate the elevation of the isolation basin sill relative to present sea level (m asl), it is necessary to know:

a) The elevation difference (m) between MHWST and MSL (calculated from tide gauge data at the nearest station; Fig. 4.3A);
b) The elevation difference (m) between MHWST and the ground surface at the isolation basin sill (black dashed lines on Fig. 4.3B); and
c) The sediment depth (m) at the basin sill.

Using these pieces of information, the difference in elevation between the basin sill and present sea level (MSL) can be calculated using the formula outlined on Fig. 4.3B. Using these elevation data, a sea-level index point (SLIP) can be generated when biostratigraphic evidence is available and an appropriate indicative meaning is used. The values for these indicative meaning corrections for individual SLIPs are taken from the tidal data at the closest tide gauge station (Table 4.1) and based on the diatom assemblage composition (see Section 4.3.1). All reported elevations within this thesis are relative to MSL.

It is also necessary to assess the elevation uncertainty associated with individual sill elevations. Sill elevation uncertainty stems from a number of factors, including survey error (± 0.10 m), sill identification error (± 0.05 m), uncertainty surrounding the elevation of MHWST (± 0.15 m) and correction to the closest tide gauge. Given the close proximity of a tide gauge to the individual research sites and the similarity in tidal range between locations within the same fjord system, the latter correction is deemed minimal.

4.2.2 Raised shorelines

Raised shorelines were identified on the basis of three characteristics:

a) Evidence of rounded and imbricated clasts;
b) Similar slope angles to the present beach profile; and
c) Topographical steps which occur in parallel to the present coastline.

Raised shoreline deposits were measured using an EDM, following a similar methodology to that outlined in Section 4.2.1.2. Cross sections of raised shorelines were surveyed in the field, with multiple transects undertaken in each location. Survey points were taken at MHWST and HAT, as well as at individual breaks in slope (SB, Fig. 4.4). Where overlying sediments were present, such as glacial till, the highest point was taken at the break between marine and glacial sedimentation (e.g. SB5; Fig. 4.4). Where the beach material extended to the upper ground surface, a number of survey points were taken to identify the elevation of this upper platform (SB7-SB9; Fig. 4.4).

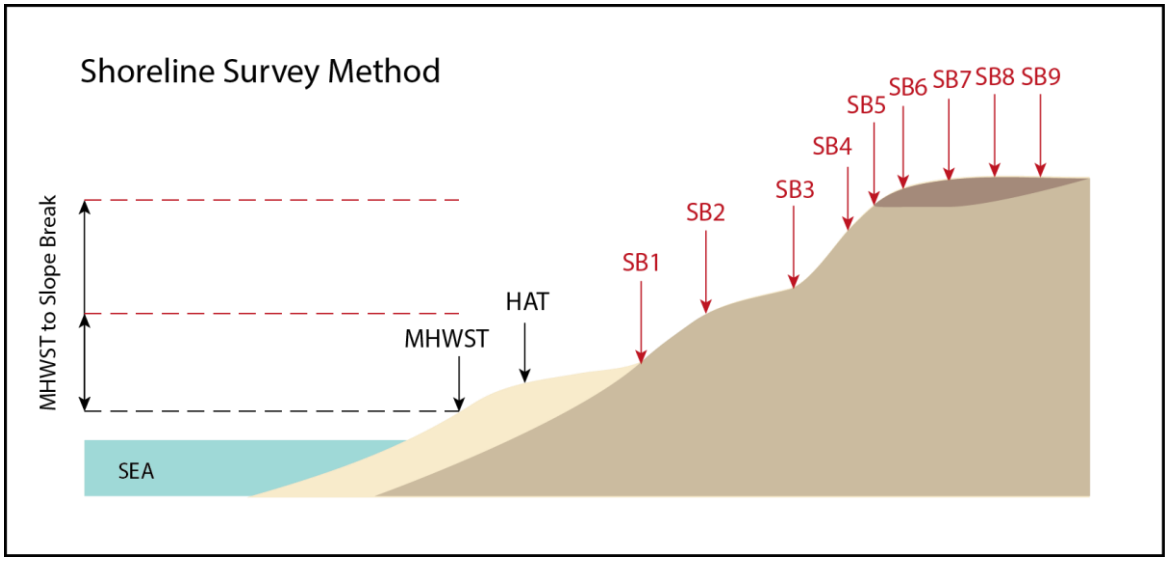

Figure 4.4 – Schematic outlining the method used to determine the elevation of raised shorelines as part of this study. Survey points were taken at the MHWST mark, HAT mark (black arrows) and at subsequent breaks in slope (red arrows), allowing the generation of a cross section for the site. Beach sediments are represented by yellow (present beach) and mid-brown (former beach). Overlying sediments are shown in dark brown.

Raised shoreline elevation measurements were then related to MSL using the tide table from the nearest tide station, as previously outlined for the sill height calculation. Previous study has highlighted the difficulties in relating these features to a known position within the tidal frame (Lloyd *et al*., 2009). However, beach ridges tend to form at or above the highest tide (between MHWST and HAT) or during storm events. Here, the modern beach was employed as an analogue for former conditions where possible.

If the beach is to be used as a sea level limiting point, correction based on the indicative meaning would be required. Studies of raised shoreline deposits tend to provide a single elevation for these features (e.g. Norðdahl and Pétursson, 2005), sometimes presenting large vertical uncertainties. Uncertainty associated with the interpretation of raised shoreline features has been built into the overall elevation uncertainties reported in this thesis.

Where appropriate and permissible, sediment samples were retrieved from raised shorelines, with samples of c. 5 cm^3 being extracted to allow for subsequent diatom and tephra analyses. Sampling occurred throughout the profile at regular intervals and close to changes in sediment composition, as later outlined.

4.3 Laboratory Methods

4.3.1 Diatom Analysis

Previous studies in a number of locations in Iceland have highlighted the effectiveness of microfossil analyses in determining palaeo-sea-level change (e.g. Rundgren *et al.*, 1997; Lloyd *et al.*, 2009). In particular, diatoms provide important information regarding basin salinity, due to their strong depositional patterns (Freund *et al.*, 2004), rapid responses to changes in environmental conditions (Stoermer and Smol, 2001) and the strong influence of salinity on diatom ecology (Guillard and Kilham, 1977). Records of basin salinity can then be used to investigate RSL change through the relation of changes in diatom assemblage to marine inundation or isolation (Kjemperud, 1986) across the elevation of the impervious basin sill.

In order to prepare samples for analysis, the standard techniques outlined by Palmer and Abbott (1986) and Battarbee (1986) were adopted. Samples were taken initially at 8 cm intervals, with subsequent sub-sampling to a maximum resolution of 2 cm in this study. In order to ensure a valid sample for analysis, a minimum of 250 diatoms were counted for each sample. Where a particular species dominated an assemblage (>50%), the count number was increased to 500 diatoms to ensure that the sample was representative. Diatoms were counted systematically using traverses across the slide, ensuring that only valves with greater than 50% preservation were counted. In addition, traverses across the centre and edges of the slide were undertaken to minimise bias in the distribution of diatom species following heating during the slide preparation process.

Classification of diatom taxonomy used Lefébure (1947), Smith (1950), Brun (1965) Foged (1974; 1976; 1977) and Hartley *et al.* (1996), alongside online resources such as *Algaebase* (Guiry and Guiry, 2013). Following the analysis of individual diatom samples, assemblage diagrams were drawn for each site using the software program C2 (Juggins, 2005). Changes in diatom

assemblage identify changes in environmental conditions related to RSL. This analysis allows the identification of critical points within each record for subsequent chronological control.

The diatomological isolation contact results from freshwater within the basin photic zone, denoted by the occurrence of freshwater diatom taxa within the basin assemblage (Lloyd *et* al., 2009). This contact is identified as predominantly freshwater conditions with a minor brackish element (Shennan *et* al., 1994), comprising up to ca. 10 % of the assemblage at this point (e.g. Lloyd *et al*., 2009). Mean High Water Spring Tide (MHWST) is often used to represent the diatomological isolation contact (e.g. Shennan *et al*., 1994; Lloyd *et al*., 2009; Long *et al*., 2011). In turn, the hydrological isolation contact demonstrates the point at which the full water column becomes freshwater – when marine influence has terminated – and is represented by Highest Astronomical Tide (HAT; e.g. Shennan *et al*., 1994). These identification markers are used to position the diatom assemblage within the tidal frame.

4.3.2 Chronology

4.3.2.1 Tephra Analysis

Tephrochronology has been effectively employed in a number of locations to provide a timing for environmental and palaeo-sea-level changes (Lowe, 2011). Several previous studies have applied the technique in Iceland to establish a chronological framework (e.g. Rundgren *et al.*, 1997; Lloyd *et al.*, 2009). Furthermore, the development of the technique has led to the establishment of a series of isochrones throughout the country, which is possible due to the rapid and widespread nature of tephra deposition. This has allowed the comparison of environmental records between core samples from different locations and thus the development of environmental histories for Iceland as a whole (e.g. Ingólfsson and Norðdahl, 1994). The geochemical composition of the glass fraction represents that of the magma produced during an eruption (Barker, 1983) and therefore allows the correlation of a sample with a particular source or eruptive event to the same tephra layer in other locations (Westgate and Gorton, 1981).

Tephrochronology is reliant upon two key assumptions: (1) that the deposition of the tephra layer was instantaneous and (2) that the tephra samples have distinct geochemical compositions, thus generating specific geochemical signals (Hunt and Hill, 1993). The principal limitation of tephrochronology is the geochemical similarity of eruptions from the same volcanic system, which can lead to difficulties when attempting to identify specific eruptive events (Larsen *et al.*, 1999). In addition, the preserved tephra deposits within individual sediment cores may not provide reliable chronological control for the section of interest – the isolation contact - determined by diatom analysis.

Tephra analyses were undertaken in two sets (Set 1: NERC TAU78/1012, Set 2: Van Mildert College Postgraduate Award) following each field season. Electron probe microanalysis (EMPA) was used to determine the geochemical composition of the samples, which benefits from high spatial resolution, precision and accuracy (Hayward, 2012). The samples were analysed for ten key elements and their oxides: Sodium (Na), Magnesium (Mg), Aluminium (Al), Potassium (K), Calcium (Ca), Silicon (Si), Iron (Fe), Phosphorous (P), Titanium (Ti) and Manganese (Mn).

In order to provide a suitable sample for EPMA, the tephra samples were subjected to an acid digestion, similar to that outlined in Persson (1971). The acid digestion is essential for organic rich samples, aiding analysis without affecting tephra geochemistry (Dugmore *et al.*, 1992). Silt-rich samples were sieved between 125 µm and 63 µm sieves, providing tephra grains of a suitable size for EPMA whilst minimising silt particles (e.g. Larsen *et al.*, 1999). Following this initial preparation, the tephra samples were mounted on resin onto slides, ground and polished, using the techniques outlined by Dugmore *et al.* (1995a) and subsequently carbon coated.

The samples were analysed using the five Wavelength Dispersive Spectrometers on a Cameca SX100 electron probe microanalyser (University of Edinburgh) using a voltage of 15 kV and a beam current of 2nA (Si, Al, Fe, Mg, Ca, Na, K) and 80 nA (Ti, Mn, P) and a beam width of approximately 8 µm. The Cameca SX100 allows both manual and automatic analyses and thus samples both rich and poor in crystallites to be analysed alongside unaltered samples. For this research, the BCR2G standard was employed to check the stability of the instrument, due to the basaltic nature of the samples. A minimum of 15 analyses were conducted per sample in order to ensure a valid result, with the combination of automatic and manual analyses allowing a representative sample. At the end of each set of analyses, the BCR2G standard was reanalysed to ensure the measurements were within the acceptance tolerance.

The geochemical composition of each sample was compared to existing Icelandic records using resources such as *Tephrabase* (www.tephrabase.org; Newton, 1996; Newton *et al.*, 2007). A range of additional sources were consulted for specific regions, such as Steinþorsson (1967) in Snæfellsnes (Area A, Fig 3.3). Where it was not possible to match the tephra analysed to a known layer, the sample was radiocarbon dated, providing an age estimation for the eruption.

4.3.2.2 Radiocarbon Analysis

Radiocarbon dating was applied at a number of sites to provide either a timing for basin isolation/inundation or tephra deposition. In total, 34 bulk organic radiocarbon samples were analysed at the NERC Radiocarbon Facility in two sets of analyses (Set 1: 22 samples (Allocation 1689.0313), Set 2; 11 samples (Allocation 1748.1013)) and BETA Analytic (1 sample). The point at which the radiocarbon sample was extracted was informed by the diatom assemblage from each

individual site, providing an opportunity to develop a series of sea-level index points for NW Iceland.

Radiocarbon analyses are affected by the ^{14}C offset or reservoir effect (Stuiver and Braziunas, 1993; Ascough *et al.*, 2011). As a result, some retrieved ages are not truly representative of the age of a particular sediment sample. The offset arises from the differences in residence times between marine and freshwater environments and thus a correction for freshwater or marine reservoir effects must occasionally be employed (Ascough *et al.*, 2011; Section 4.3.2). Within this study, a limited number of samples are affected by reservoir correction, as the need to apply this adjustment has been limited through the dating of the upper contact (freshwater).

4.3.2.3 Radiocarbon Correction and Calibration

Each radiocarbon dated sample has undergone calibration to years before present (where present is AD 1950) using CALIB 7.0 (Stuiver *et al.*, 2014). The IntCal13 dataset was used for terrestrial freshwater samples and MARINE13 for marine samples (Reimer *et al.*, 2013), unless otherwise stated. Marine reservoir corrections were applied where appropriate, using the standard value within MARINE13 (Reimer *et al.*, 2013). Ages for individual sea-level index points are therefore presented as radiocarbon (^{14}C ka) and calibrated ages (ka BP), with the zero point for calibrated ages being defined as 1950 (Stuiver and Polach, 1977).

4.4 Glacial Isostatic Adjustment Modelling

4.4.1 SELEN

SELEN is a freely available Fortran 90 software package designed to solve the sea-level equation (Farrell and Clark, 1976) and investigate associated geophysical processes (Spada and Stocchi, 2007) available from http://www.fis.uniurb.it/spada/SELEN_minipage.html. SELEN has been used in a number of locations to provide an insight into Holocene RSL changes (e.g. Antonioli *et al.*, 2009), crustal deformation and uplift (e.g. Spada *et al.*, 2012) and recent RSL changes at tide gauges (e.g. Stocchi and Spada, 2009). In order to solve the sea-level equation, SELEN assumes a radially stratified and incompressible Earth, with mantle layers having a linear viscoelastic rheology (Spada and Stocchi, 2007). In addition, the ocean function is assumed to remain constant, with no changes in the shape of coastlines during RSL changes (Spada and Stocchi, 2007). It should also be noted that the effects of rotation on RSL change are not included within the model (Spada and Stocchi, 2007). In addition to new codes, SELEN employs routines and code from some additional sources, including the pixelisation code of Tegmark (1996) and the program TABOO (Spada, 2003; Spada *et al.*, 2004), to determine particular elements of the model.

In order to optimise computing capability and output quality, it is necessary to determine the most effective combination of spherical harmonics and Tegmark resolution to address the

problem investigated. Within this research, combinations of spherical harmonics and Tegmark resolutions were tested using the window function, in order to establish the quality of prediction. A viable combination requires the number of Tegmark pixels to exceed the minimum required to generate an optimal quadrature on the globe (Spada and Stocchi, 2007).

Tegmark (1996) outlines this requirement as:

$$N_p = 40RES(RES - 1) + 12 \qquad N_p^{min} = \frac{l_{max}^2}{3}$$

N_p – number of Tegmark pixels

RES – resolution of Tegmark pixels

N_p^{min} – minimum number of Tegmark pixels

lmax – harmonic degree

Figure 4.5 – Tegmark pixelisation of the Earth at Tegmark resolution '44', providing 75692 pixels. The Earth is separated into wet (blue) and dry (green) pixels within SELEN.

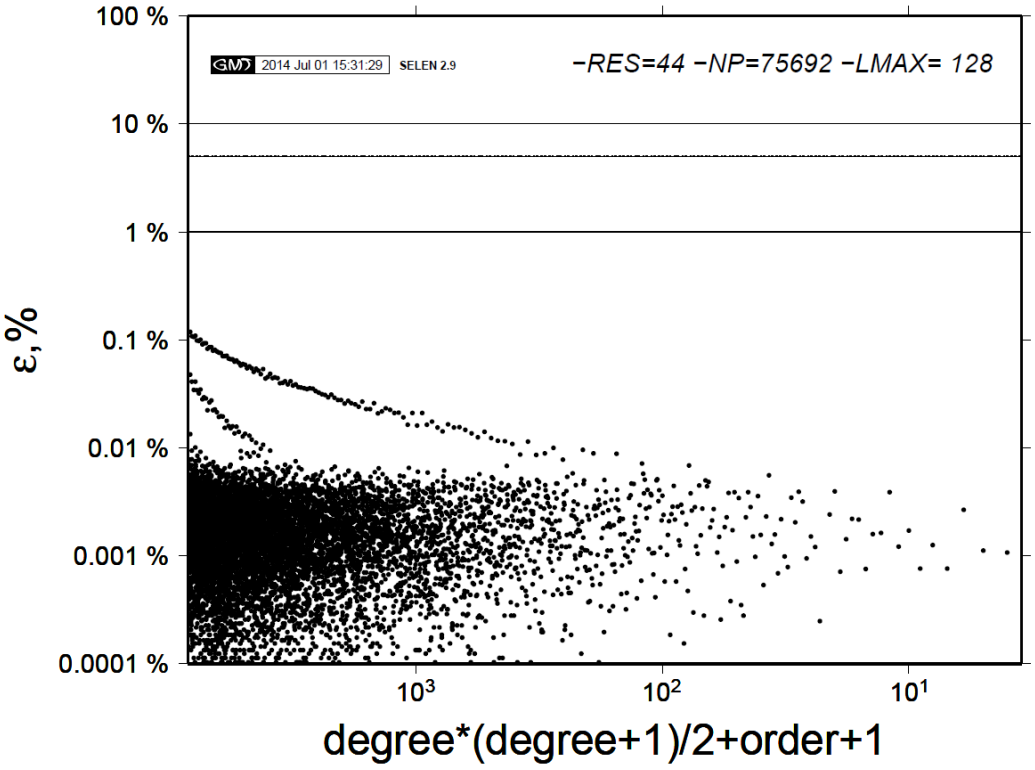

Figure 4.6 – Windows function of an example GIA model run, showing the error of the projection (Ɛ) by degree and order of the spherical harmonics projection. Error increases with the number of harmonic degrees (right to left).

As an example, within this research, the harmonic degree was initially set at 128. With *lmax* = 128, the minimum number of Tegmark pixels is 5461. *RES* was however set at 44, providing an N_p of 75692 (Fig. 4.5), far exceeding the minimum requirement yet still providing good results in the window function outputs (Fig. 4.6). The windows function assesses the error of individual pixelisations and was therefore completed for a range of lmax/Tegmark combinations.

A suite of possible harmonic degree and Tegmark resolution combinations were investigated, with the aim of determining the most effective combination of variables. For a given GIA model, the harmonic degree and Tegmark resolution selected would need to be amended depending on the model disc size at the latitude explored. A number of lmax/Tegmark combinations may provide similar RSL outputs for a given model disc size, but testing is required in order to ensure that the most computationally efficient model can be identified. Suites of lmax/Tegmark resolution combinations were therefore tested, initially for a 1° disc size ice model and subsequently for 0.5° and 0.25° disc size ice models. When the model outputs reached convergence, the least computationally demanding combination was then employed for the investigation of ice loading and subsequent RSL changes for the ice and Earth characteristics specified.

As with any GIA model, SELEN requires an Earth model (the variation of lithospheric thickness and mantle viscosity with depth) and an ice loading model (a record of ice extent and thickness through time). The SELEN model allows the inclusion of pre-defined and user-defined ice and

Earth models, as outlined in Sections 4.4.2 and 4.4.3. An example input file can be found in Appendix A1.

RSL projections for the modelling locations (Fig. 4.7) were generated using a nested approach. Ice loading and viscosity characteristics were adjusted separately for a) Iceland and b) worldwide excluding Iceland ice loading. Accordingly, ice loading and viscosity characteristics were varied for Iceland and integrated with the global ICE5G (excluding Iceland) VM2 outputs. Therefore, the RSL projections for each site are a result of projections from Iceland (ice loading and viscosity) and global models (ICE5G excluding Iceland with VM2) are the pre-defined locations. This approach allows investigation of the impacts of adjustment to Icelandic characteristics within the broader global signal. The ice models and Earth models used in this study are outlined in Sections 4.4.2 and 4.4.3. Thereafter, the GIA modelling strategy is outlined in Section 4.4.4, which details the stages of model interrogation.

4.4.2 Ice Models

Four principal ice models were employed in the investigation of ice loading at the LGM in Iceland: a global ice model: ICE5G (Peltier, 2004); and three regional Iceland models: HP_MAX, HP_MIN and HP_OPT (Patton, unpub.). The four models provide data on ice thickness and extent at different resolutions for individual ice loading scenarios (Table 4.2). Initial modelling was undertaken using ICE5G, as included in SELEN, with subsequent analyses employing the higher-resolution user-defined models (HP_MAX, HP_MIN, HP_OPT) for the Icelandic component of ice loading. ICE5G was retained throughout as the ice loading model for locations outside Iceland. The glaciological background to the four models is outlined within Chapter 2. In order to discriminate between models, a data-model comparison was undertaken between RSL records and model output. Initial modelling explored the RSL changes at four locations around Iceland to determine the effects of changes in ice loading throughout the country, with subsequent modelling focussing on higher spatial resolution outputs from northwest Iceland (Fig. 4.7).

Model	Source	Scenario	Resolution	Equivalent Sea Level (m)
ICE5G	Peltier (2004)	-	1 deg.	0.4
H130c	Patton (unpub.)	Optimum	2km^2	0.75
H128	Patton (unpub.)	Maximum	2km^2	1.0
H153	Patton (unpub.)	Minimum	2km^2	0.67

Table 4.2 – Characteristics of the original ice models used in the investigation of LGM ice loading in Iceland. H130c, H128 and H153 were re-sampled at different resolutions as part of this study.

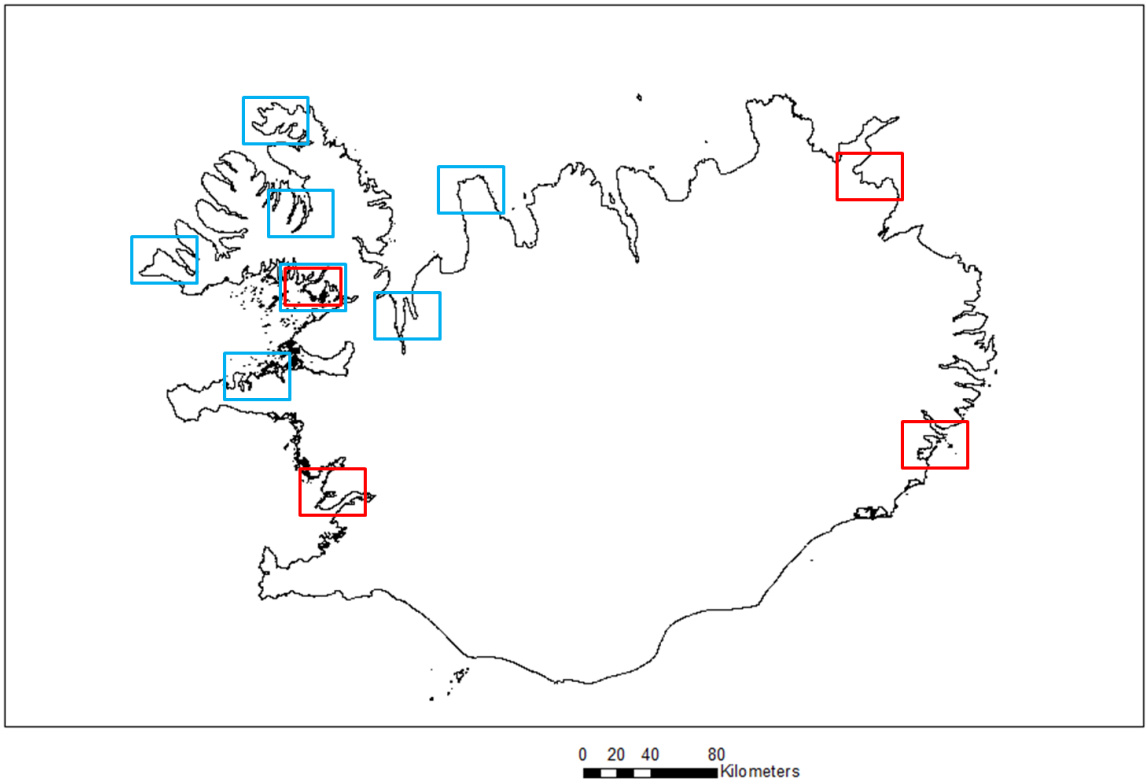

Figure 4.7 – The location of the sites employed for modelling the RSL changes associated with the various ice loading scenarios. Red boxes highlight the initial modelling sites, with blue boxes highlighting the higher-resolution northwestern sites. The initial modelling sites are – Bjarkarlundur (NW) 65.5°N 22.1°W, Stóri-Sandhóll (SW) 64.3°N 21.5°W, Vopnafjörður (NE) 65.6°N 14.5°W and Berufjörður (SE) 64.6°N 14.5°W.

In order to integrate the Hubbard/Patton (HP_MAX, HP_MIN, HP_OPT) models into SELEN, it was necessary to reproject the ice thickness values from Gall's stereographic to WGS 1984 in ArcGIS. This process re-projects the data from metres North and West to degrees longitude and latitude, allowing integration into SELEN as a series of new xyz data files of longitude, latitude and ice thickness (following the format of the alpsc.dat-type file in SELEN; Spada and Stocchi, 2009). Following this data manipulation, the HP_MAX, HP_MIN and HP_OPT models were re-sampled using Generic Mapping Tools (GMT; Wessell and Smith, 1991): this was done at three resolutions (0.25°, 0.5° and 1.0°) and thus provided three ice models for each original HP ice model.

This process used the script bm.gmt (Spada, pers. comm. a) which uses the blockmean tool within GMT to produce a series of block-averaged ice thickness files for individual timeslices at a given resolution – in this case, 0.25°, 0.5° and 1.0°. Within the resulting ice thickness files, the number of data lines denotes the number of data grid squares with an ice thickness of > 0 m within individual models of the IIS. This figure was updated in a number of the SELEN files, as several scripts require this information to run successfully.

In order to produce the ice models, the ice thickness grid data was converted to a series of discs through the build.f90 script (Spada, pers. comm. a) which both creates discs from rectangles and

calculates equivalent sea level (ESL) within the two model types – grid and discs. Build.f90 produces a single ice thickness file for each ice model, using the individual time-slices produced using bm.gmt. The conversion from rectangles to discs follows the formula:

$$\propto^{\circ} = \frac{180^{\circ}}{\pi}\arccos\left[1 - \left(\frac{\Delta^{\circ}}{180^{\circ}}\right) \cdot \sin\left(\frac{\pi(90^{\circ}-\varphi^{\circ})}{180^{\circ}}\right) \cdot \sin\left(\frac{\pi\Delta^{\circ}}{360^{\circ}}\right)\right] \qquad \text{(Spada, pers. comm. b)}$$

$$\Delta = \text{angular width of grid square} \quad \varphi = \text{latitude of disc centre}$$

$$\propto^{\circ} = \text{half amplitude of the disc}$$

The equation for conversion of rectangles to discs is derived from the need to conserve the mass of the original model, wherein load is based on rectangles, and the new model, based on discs. As a result, the area and thickness of the rectangle must equal the area and thickness of the disc (Spada, pers comm. b). Using the conversion equation, α may differ for latitude, but will not change as a function of longitude for a given Δ (Spada, pers comm b). Disc coverage will not therefore necessarily be uniform across the study area, leading to gaps and overlaps between discs. However, the effect of the lithosphere will smooth the short wavelength effects of this phenomenon (Spada, per comm. b).

In order to ensure a true representation of the ice loading within the original HP models, it is essential that the ESL is identical in the grid and disc versions of the ice model, or alternatively that the total ice volume is not affected by resolution or by conversion to discs. Prior to the integration of the resampled HP models into SELEN, the ESL values generated by build.f90 for the disc and grid ice models were compared to ensure that the two values were equal.

Within this thesis, ESL is defined using the following equation, as used in SELEN:

$$ESL_{(t)} = \left(\frac{\rho_i}{\rho_w}\right)\left(\frac{Vi_{(t)} - Vi_{(tp)}}{A_o}\right) \qquad \text{(Spada } \textit{et al.}\text{, 2012)}$$

$$t = \text{time} \quad \rho_i = \text{density of ice} \quad \rho_w = \text{density of water} \quad Vi = \text{ice volume}$$

$$p = \text{present day} \quad A_o = \text{area of the ocean surface}$$

Following confirmation of matching ESLs, a series of ice models were produced to test the LGM glaciation scenarios – HP_MAX, HP_MIN and HP_OPT – at different resolutions. The extent and volumes of ice over time for each model are explored within Chapter 7.

4.4.3 Earth Models

A suite of crustal characteristics were explored in Iceland to test the contrasting hypotheses of the LGM glaciation. Research into the geology of Iceland has demonstrated a complex pattern of mantle viscosities and lithospheric thicknesses for the region (e.g. Sigmundsson, 1991, Pollitz and Sacks, 1996; Foulger *et al.*, 2003; Foulger, 2006). This study used a viscosity profile similar in composition to an average VM2 rheology (Peltier, 2004), with a lithosphere, upper and lower mantle (Fig. 4.8). In Iceland, values for lithospheric thickness and upper mantle viscosity values were varied, but the viscosity of the lower mantle was kept constant at 2.7 x 10^{21} Pa s after VM2 (Peltier, 2004). Testing of adjustment of the lower mantle viscosity value demonstrated no effect on the resulting RSL outputs. For each model run, RSL predictions from Icelandic ice loading and Easrth structure were combined with outputs from the global ICE5G (VM2) model, from which ice loading in Iceland was excluded.

In order to determine the most likely Earth model for Iceland, the consequence of varying lithospheric thickness and mantle viscosity on RSL at particular sites was explored, whilst initially keeping the ice loading constant using ICE5G (Peltier, 2004). Subsequent testing was also undertaken using the HP_MAX, HP_MIN and HP_OPT models outlined in Section 4.4.2. SELEN allows the integration of Earth characteristics through the editing of *vsc.dat* (Spada and Stocchi, 2007). Rather than exploring each of the Earth characteristics outlined in Table 2.1 (Chapter 2), a selection was made covering the range of values published for Iceland, examples of which can be found in Table 4.3.

LITHOSPHERIC THICKNESS	20 - 100 km	Range of Icelandic lithospheric thicknesses
UPPER MANTLE VISCOSITY	1 x 10^{18} - 5 x 10^{20} Pa s	Range of Icelandic upper mantle viscosities
LOWER MANTLE VISCOSITY	2.7 x 10^{21} Pa s viscosity	ICE5G (Peltier, 2004) lower mantle

Figure 4.8 – Rheological profiles explored during GIA modelling in Iceland.

Lithospheric Thickness (km)	Upper Mantle Viscosity (Pa s)	Location	Source
10	1×10^{19}	Iceland	Sigmundsson (1991)
10 - 20	$4 – 10 \times 10^{18}$	Vatnajökull	Pagli *et al.* (2007)
40	$5 \times 10^{18} – 1 \times 10^{19}$	Iceland	Árnadóttir *et al.* (2009)
41	$2.1 – 3.2 \times 10^{19}$	Iceland	Le Breton *et al.* (2010)
27 - 40	2×10^{18}	Iceland	Barnhoorn *et al.* (2011)
100	2×10^{18}	Iceland (LGM)	Barnhoorn *et al.* (2011)

Table 4.3 – Published Earth characteristics in Iceland, illustrating the differences in proposed viscosity and lithospheric thickness.

Using this limited selection, a range of viscosity profiles were explored within the GIA model runs (Fig. 4.8). The lithospheric thickness was adjusted in 10 km steps from 20 km to 100 km and the upper mantle viscosity was increased in regular steps through the range outlined in Fig. 4.8. A suite of Earth model characteristics were therefore applied with each ice model to further test the contrasting hypotheses of the LGM glaciation of Iceland. The specific Earth models employed for individual ice models can be found in Table 4.4.

It should be considered that, at present - and in common with most GIA models - SELEN is not able to deal with 3-D Earth structure and so a clear limitation of the approach is that all Earth models are spherically symmetric whereas in fact lateral variations are likely (e.g. Sigmundsson, 1991). The implications of this factor are discussed further in Chapter 8.

Ice Model	Lithospheric Thickness (km)	Upper mantle viscosity (Pa s)
ICE5G	**90**	**4×10^{20}**
ICE5G (ICELAND)	20, 30, 40, 50, 60, 70, 80, **90**, 100	1×10^{18}, 5×10^{18}, 1×10^{19}, 5×10^{19}, 1×10^{20}, **4×10^{20}**
ICE5G 150% (ICELAND)	**90**	**4×10^{20}**
HP_MAX	**20, 30, 40, 50, 60, 70, 80, 90, 100**	**1×10^{18}, 5×10^{18}, 1×10^{19}, 5×10^{19}, 1×10^{20}**
HP_OPT	**20, 30, 40, 50, 60, 70, 80, 90, 100**	**1×10^{18}, 5×10^{18}, 1×10^{19}, 5×10^{19}, 1×10^{20}**
HP_MIN	**20, 30, 40, 50, 60, 70, 80, 90, 100**	**1×10^{18}, 5×10^{18}, 1×10^{19}, 5×10^{19}, 1×10^{20}**

Table 4.4 – Lithospheric thickness and upper mantle viscosity values employed in the GIA modelling as part of this thesis research. These values were used in the construction of the residual outputs and chi^2 plots (bold) within Chapter 7.

4.4.4 RSL database

In order to test the differing ice loading hypotheses, a database of sea-level index points is required for comparison with modelled outputs of RSL change at particular locations. SELEN contains a global dataset in *sealevel.dat*, which is taken from Tushingham and Peltier (1993). For the purposes of this study, an Icelandic dataset (*icelandsealevel.dat)* was constructed following exploration of RSL literature for Iceland (e.g. Rundgren *et al.*, 1997; Norðdahl and Pétursson, 2005; Lloyd *et al.*, 2009).

In addition to published sea-level index points, the new sea-level index points and limiting ages generated as part of this research were also included within the database, which comprises 28 index points in total. An abridged version of icelandsealevel.dat can be found in Chapter 6 (Table 6.28). This database allows the comparison of field records and modelled RSL outputs and in turn the testing of the contrasting glaciation hypotheses. Initial testing of the GIA model outputs was completed with the complete Iceland sealevel.dat dataset. Subsequently, the database was divided into discrete segments to test outputs from individual regions (see Fig. 3.1). The northwest section of the database was therefore employed to test the majority of model outputs, comprising the *Vesturland*, *Vestfirðir* and *Norðurland vestra* sections (Fig. 3.3), reducing computational time for each model run.

4.4.5 GIA Modelling Strategy

Testing of individual GIA model inputs (ice loading and Earth models) was undertaken through a series of GIA model runs, which kept one variable constant whilst varying the other component i.e. employing different ice models and a fixed rheological profile and vice versa. Following the completion of a GIA model run, the results of the model were compared to field evidence. If there was disagreement between the two datasets, adjustments were made firstly to the ice loading model (e.g. increasing ice thickness uniformly). If the subsequent GIA model run did not lead to an improvement of the fit between datasets, the Earth characteristics were subsequently modified. Additional combinations of ice loading and Earth characteristics were also explored using the adapted versions of the original ice model and Earth structure.

If the poor fit between the model results and field-based RSL reconstruction could not be reconciled, the GIA model was rejected. Once a GIA model, or one of its components (ice model or Earth model), had been rejected, a new process began using alternative ice models and viscosity profiles. If a GIA model produced results with a reasonable fit to the field data, it would be accepted. This was determined through chi^2 or residual testing. Chi2 testing was used for GIA models where variation of the lithospheric thickness and upper mantle viscosity occurred. Where only one Earth model was investigated i.e. the lithospheric thickness or upper mantle viscosity

value was not amended, residuals were explored due to the inability to interpolate a surface plot for these models (see Table 4.4).

The specific procedure adopted within this thesis is summarised in five stages in Fig. 4.9. Initial GIA modelling used ICE5G (VM2) to produce RSL predictions for Iceland (Stage A; Fig. 4.9). Following these tests, the ice thickness for the Icelandic component of ICE5G was increased by 50% and run with VM2. This was then assimilated with the results from a run of ICE5G with Iceland removed with VM2 to produce a revised RSL prediction (Stage B; Fig. 4.9). After, the Iceland component of ICE5G was run with Icelandic viscosity and lithospheric characteristics only, which was then combined with ICE5G (excluding Iceland) with VM2 (Stage C; Fig. 4.9). Subsequently, the Patton (HP_MAX, HP_MIN and HP_OPT) ice models were run with VM2 in Iceland (Stage D; Fig. 4.9). These results were then integrated with the ICE5G (excluding Iceland) VM2 outputs to produce revised RSL predictions. Finally, the Patton models were run with Icelandic lithospheric and viscosity values and combined with the ICE5G (excluding Iceland) VM2 dataset. Thus, a suite of GIA models were tested and produced RSL predictions for Iceland. This systematic approach allowed the examination of a suite of possible scenarios. The results of these model runs are outlined by stage in Chapter 7, providing an overview of the different outputs generated.

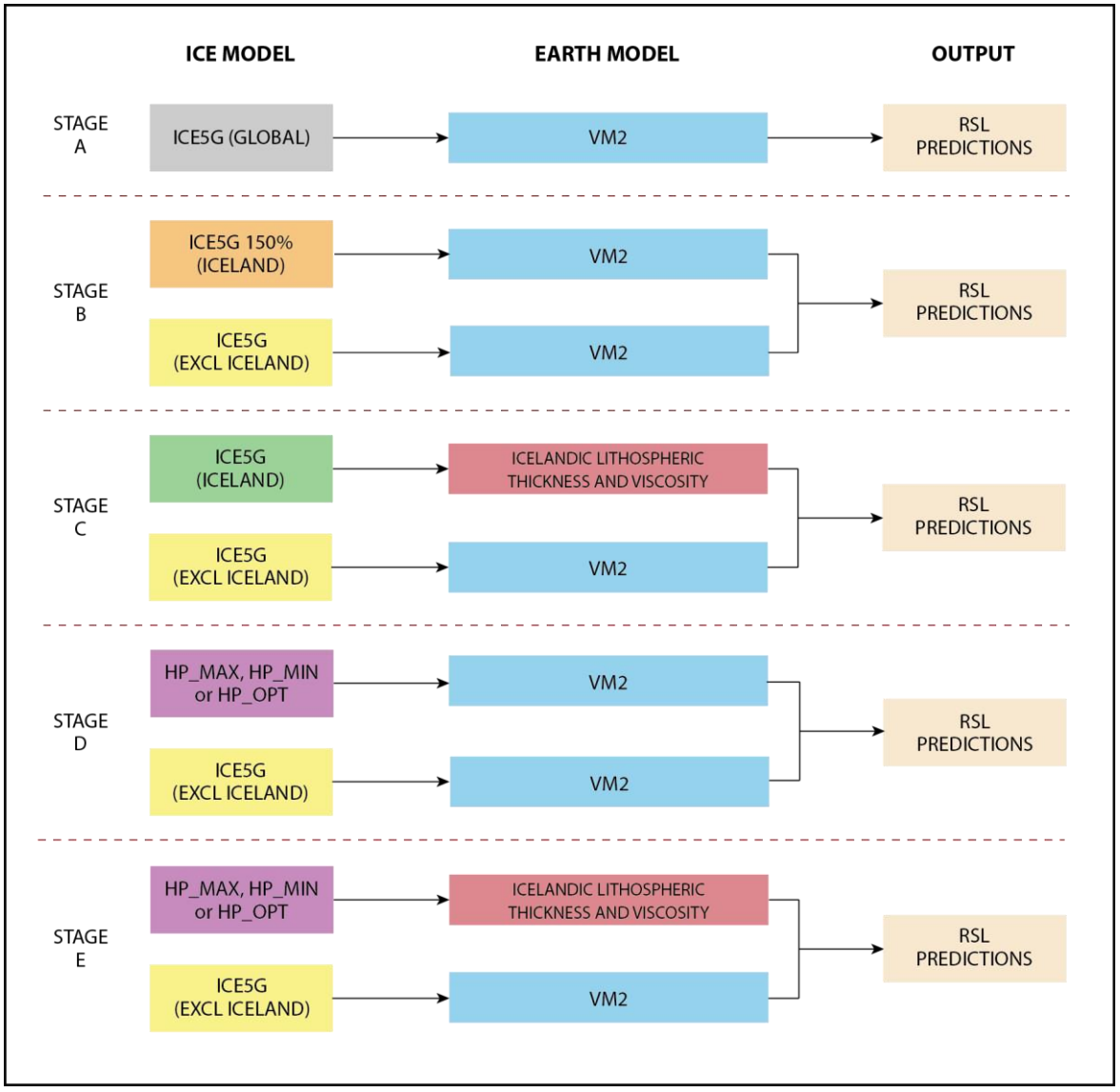

Figure 4.9 – Stages of GIA Modelling undertaken in this thesis – Stage A: ICE5G (Global; grey) with VM2 (blue); Stage B: ICE5G (Iceland at 150%; orange) and ICE5G (excl. Iceland; yellow) with VM2; Stage C: ICE5G (Iceland; green) with Icelandic viscosity (red) and ICE5G (excl. Iceland) with VM2; Stage D: Patton Ice Models (purple) with VM2 and ICE5G (excl. Iceland) with VM2; Stage E: Patton Ice Models with Icelandic viscosity and ICE5G (excl. Iceland) with VM2.

4.5 Summary

The research has adopted three principal methodological types: field methods, laboratory methods and GIA modelling. Within the field, stratigraphic surveys were completed using a gouge corer for each site in order to identify suitable samples for subsequent laboratory analysis. In turn, sediment samples were retrieved from lake basins using a Russian corer. The sill of a lake basin was determined using a grid of cores, which were surveyed using an EDM. This elevation was related to MSL using tide tables from the nearest available station, the elevation change from MHWST and the ground surface at the sill location and the depth of overlying sediment. In turn, this was converted to a SLIP following establishment of the indicative meaning presented in diatom analyses. Each sediment sample underwent diatom analysis to identify principal changes

in environmental conditions at each site, with chronology provided by radiocarbon and tephrochronological analysis. Following generation of individual SLIPs, these data can be used to test GIA model outputs. GIA modelling employed SELEN, an open access computer program, to produce RSL predictions for sites around Iceland. Four ice models – ICE5G, HP_MAX, HP_MIN and HP_OPT – were investigated, alongside a suite of viscosity and lithospheric thickness values. The GIA modelling used a nested approach, with model runs for Iceland combined with global models, which excluded the Icelandic component. The GIA modelling strategy involved five stages in total. Chapters 5, 6 and 7 outline the data generated using these methods.

CHAPTER 5

Tephra Results

5.1 Introduction

Within this chapter, the results of geochemical analyses of tephra deposits are presented. Geochemical results of tephra analyses are presented prior to diatom datasets, as the tephras identified will act as chronological markers in subsequent discussions of environmental changes at individual sites. Samples were taken from tephra layers found in sediment cores from the majority of research locations, with the aim of generating a series of isochrones in NW Iceland. The results of electron microprobe (EPMA) analyses are presented by research area (Fig. 3.3) followed by an analysis of regional patterns of tephra deposition. Each sample is coded to represent the site location and sample depth (e.g. Tjörn at 184 cm - TJ1-184). The tephra results are particularly valuable when adopted as a secondary chronological framework for sites with poor radiocarbon-based chronological control.

Where possible, tephra samples have been correlated with known tephra geochemical signatures using *Tephrabase* (www.tephrabase.org; Newton, 1996; Newton *et al.*, 2007) or suitable previous studies for individual volcanic systems. This association allows the construction of isochrones within and between research areas, allowing the correlation of environmental changes noted within the isolation basin records. These data have been presented prior to the diatom analyses as they form part of the chronological framework for the RSL histories produced.

5.2 Geochemical Results

5.2.1 Area A – Skagi

Two tephra deposits were analysed from Tjörn (TJ1) at 184 cm (TJ1-184) and 187 cm (TJ1-187; Fig. 5.1). Both tephra deposits had similar visual characteristics in the field, being dark grey and having a sharp lower boundary. Both TJ1-184 and TJ1-187 underwent geochemical analysis and demonstrate a distinct geochemical signature, which is consistent with the Vedde Ash (Fig. 5.1).

The identification of the Vedde Ash is important, as it is a key marker horizon for the region, allowing comparison with environmental records from previously published sites in Area A (Rundgren *et al.*, 1997) and more widely in Europe. The Vedde Ash has been widely dated to 12.1 cal. ka BP (Rasmussen *et al*., 2006; Lane *et al.,* 2012).

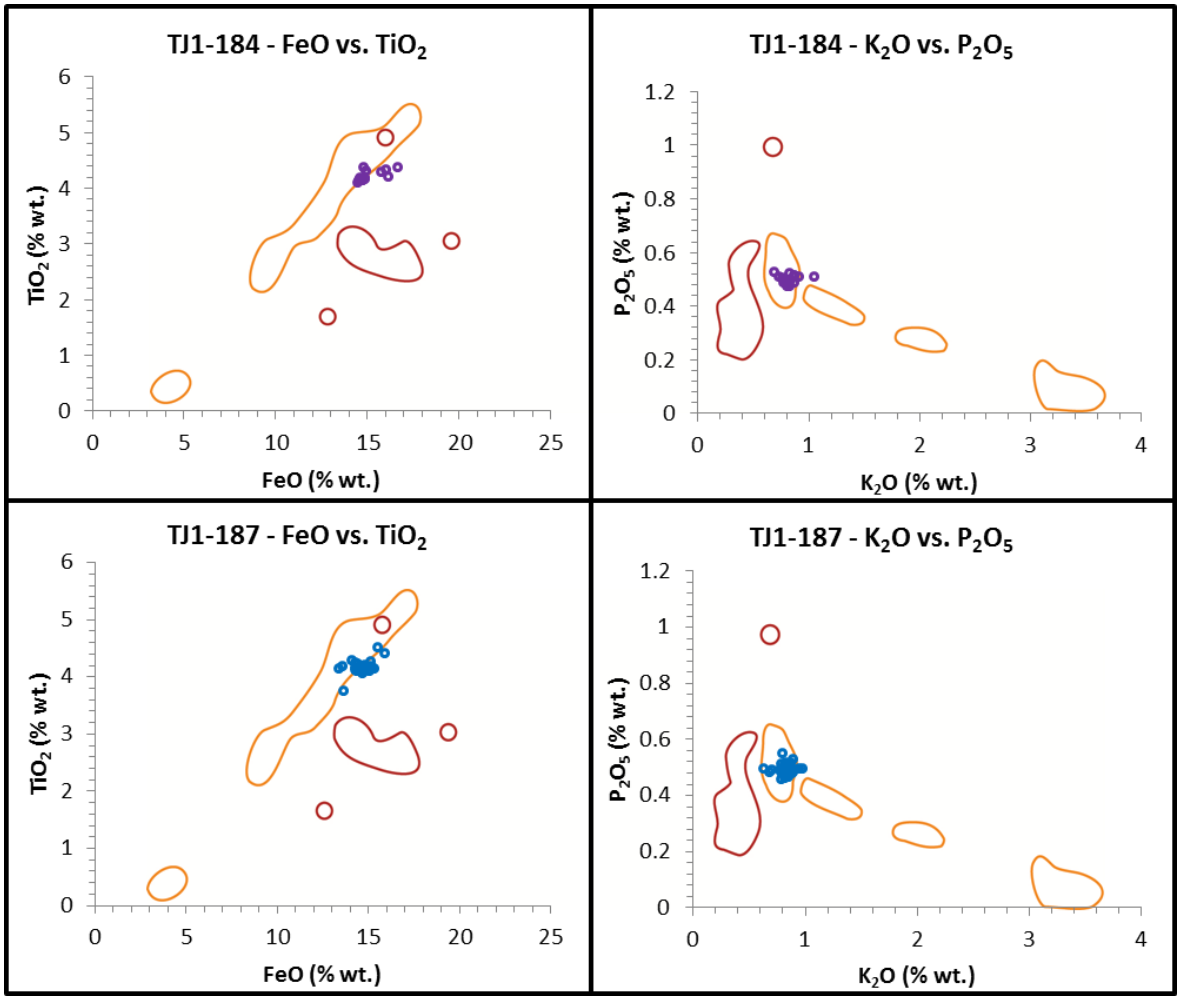

Figure 5.1 – Tephra results from TJ1-184 (purple circle) and TJ1-187 (blue circle) showing the correspondence with the Vedde ash (orange; Lane et al, 2012) and mismatch to Saksunarvatn (red; Tephrabase, www.tephrabase.org).

5.2.2 Area C – Stykkishólmur, Snæfellsnes

Two tephra deposits from the Ytra Baravatn (YBR1) sediment core were analysed (YBR1-210 and YBR1-352; Fig. 5.2). The upper sample, YBR1-210, has a mixed geochemical signature, suggesting the inwashing of tephra deposits from the surrounding landscape (Fig. 5.2). The lower tephra, YBR1-352, has a more distinct cluster, which matches with the Saksunarvatn profile presented in *Tephrabase* (Fig. 5.2).

The Saksunarvatn tephra has been accurately dated to 10210 ± 35 cal. a BP (Lohne *et al.*, 2014) and is found throughout northwest Iceland (e.g. Lloyd *et al.*, 2009). The identification of the Saksunarvatn tephra in Ytra-Baravatn acts as a useful limiting date for the site and will contribute to the development of a chronological framework for this site.

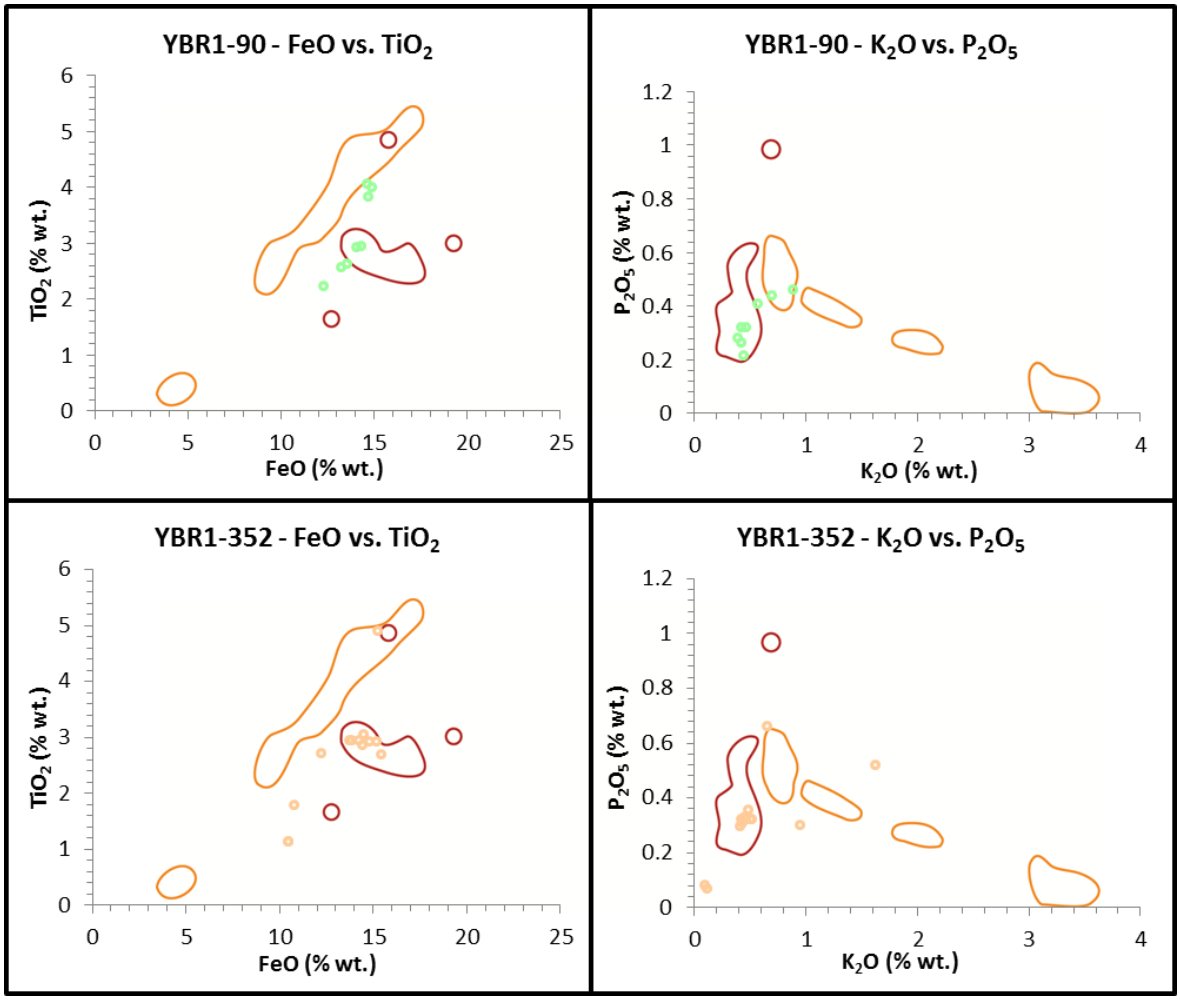

Figure 5.2 – Tephra results from YBR1-210 (light green circles) and YBR1-352 (peach circles). Both datasets are plotted against the Vedde ash (orange; Lane et al, 2012) and the Saksunarvatn tephra (red; Tephrabase, www.tephrabase.org) for reference, demonstrating a clear correlation with YBR1-352.

5.2.3 Area D – Hornstrandir and Aðalvik

A number of tephra samples were analysed from Area D (Fig. 5.3). Unfortunately, samples extracted at Hlöðuvik Terrace (HD10) provided insufficient successful tephra analyses to produce a reliable geochemical signature for each proposed horizon. The results are not therefore presented in full here.

Samples from isolation basins in Hlöðuvik (HD3-134) and Aðalvik (REK-160) provided sufficient tephra grains for analysis, producing geochemical compositions which correlate to the Saksunarvatn tephra (Fig. 5.3). The Saksunarvatn tephra was also identified within deposits from the Hælavik Terrace (HL1; Fig. 5.3). The identification of the Saksunarvatn tephra within Hornstrandir and Aðalvik therefore provides a useful isochrone, as well as an insight into ice position in the early Holocene in Hornstrandir.

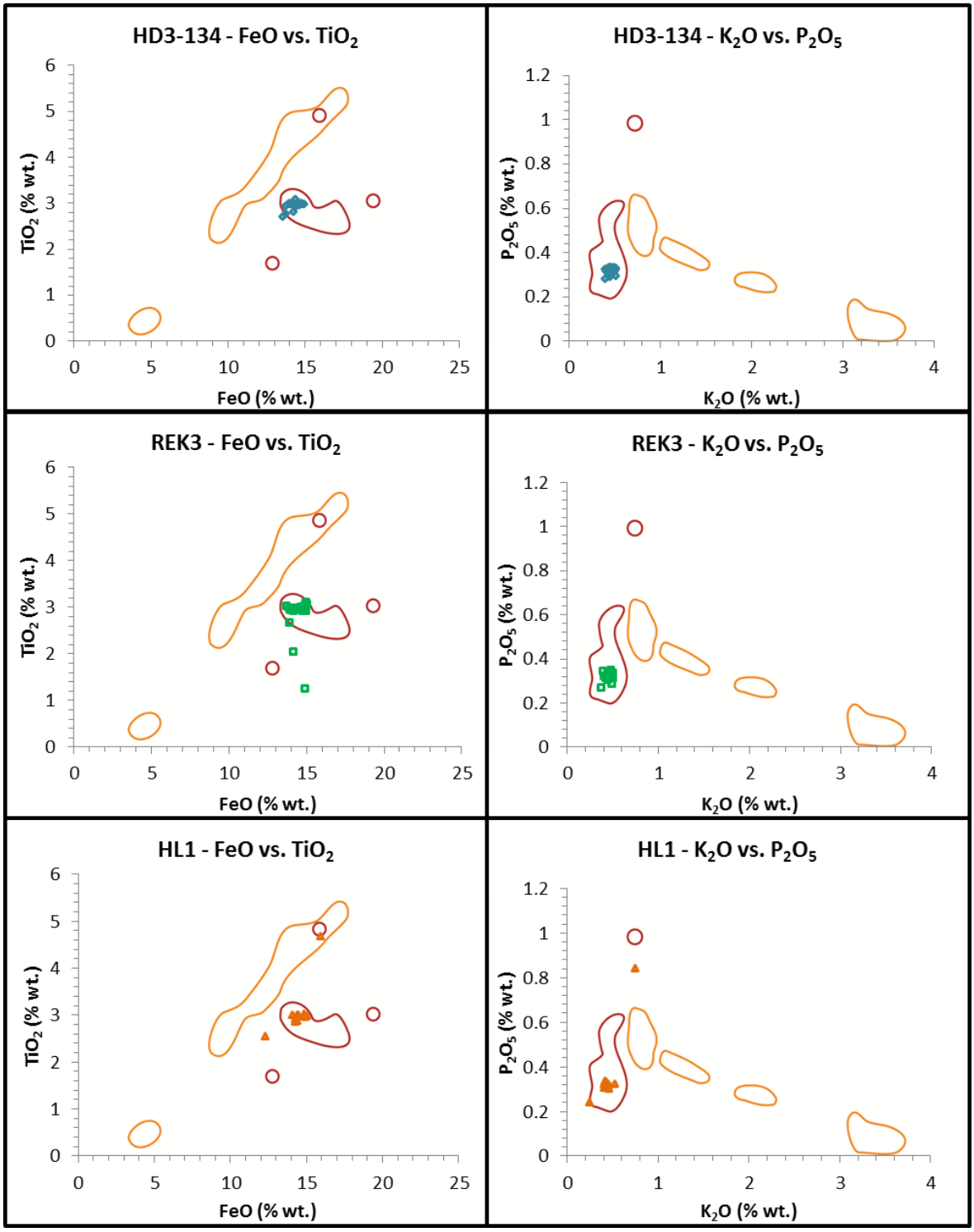

Figure 5.3 – Tephra results from HD3-134 (blue squares), REK3-160 (green squares) and HL1 (orange triangles). All datasets are plotted against the Vedde ash (orange; Lane et al, 2012) and the Saksunarvatn tephra (red crosses; Tephrabase, www.tephrabase.org) demonstrating a clear correlation with the Area D deposits.

5.2.4 Area E – Vatnsfjörður, Vestfirðir

Three tephra deposits were identified at two isolation basin sites in Area E – Reykjanes 10 (RK10) and Vatnsfjarðarnes 1 (VAT1). A total of three tephra deposits were analysed for their geochemical composition, with the RK10-131, RK10-255 and VAT1-163 all correlating with the Saksunarvatn tephra (Fig. 5.4).

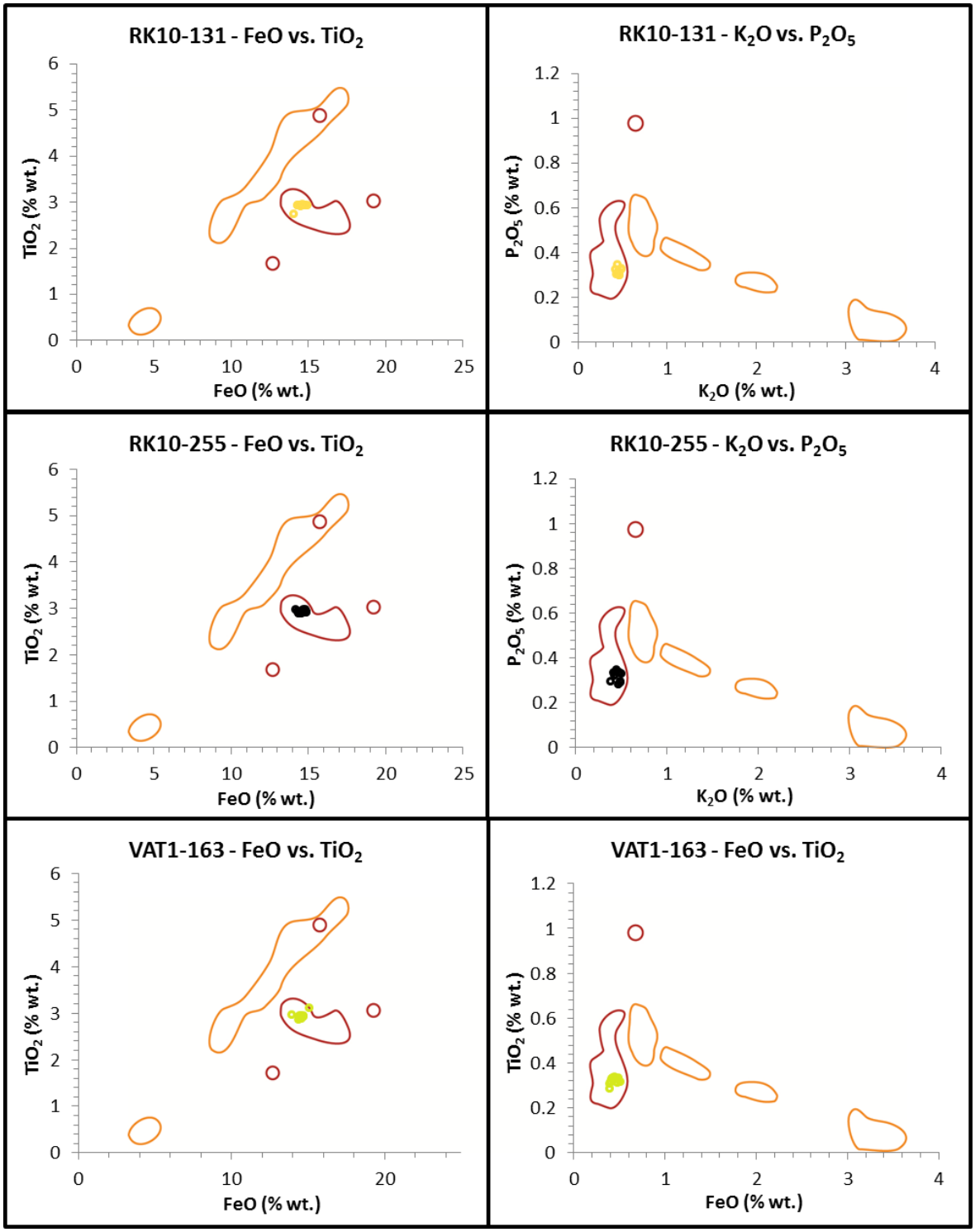

Figure 5.4 – Tephra results from RK10-131 (yellow diamonds), RK10-255 (black circles) and VAT1-163 (green squares) in Area E. All datasets are plotted against the Vedde ash (orange; Lane et al, 2012) and the Saksunarvatn tephra (red crosses; Tephrabase, www.tephrabase.org) for comparison.

At Reykjanes 10 (RK10), the lower tephra deposit is taken to represent the Saksunarvatn tephra. The upper tephra deposit, RK10-131, likely represents the inwashing of material from the local landscape rather than a separate depositional event.

5.2.5 Area F – Hvammstangi, Vatnsnes

Five tephra samples were analysed from Area F (Fig. 5.5 and 5.6). The samples were all collected from high elevation isolation basins, including Sandar 1 (SN1-578), Sandar 2 (SN2-509), Myrar (MY1-594), Arnhóll 2 (AH2-594) and Arnhóll 1 (AH1-612). Each of the analysed tephra deposits correlates with the Saksunarvatn tephra (Figs. 5.5 and 5.6). The tephra layers in this region therefore allow the comparison of RSL changes between sites of similar elevation, as well as between research areas. In addition, the Saksunarvatn tephra helps identify a limiting date for local marine limit formation in the region, due to its presence in the highest site investigated in this study.

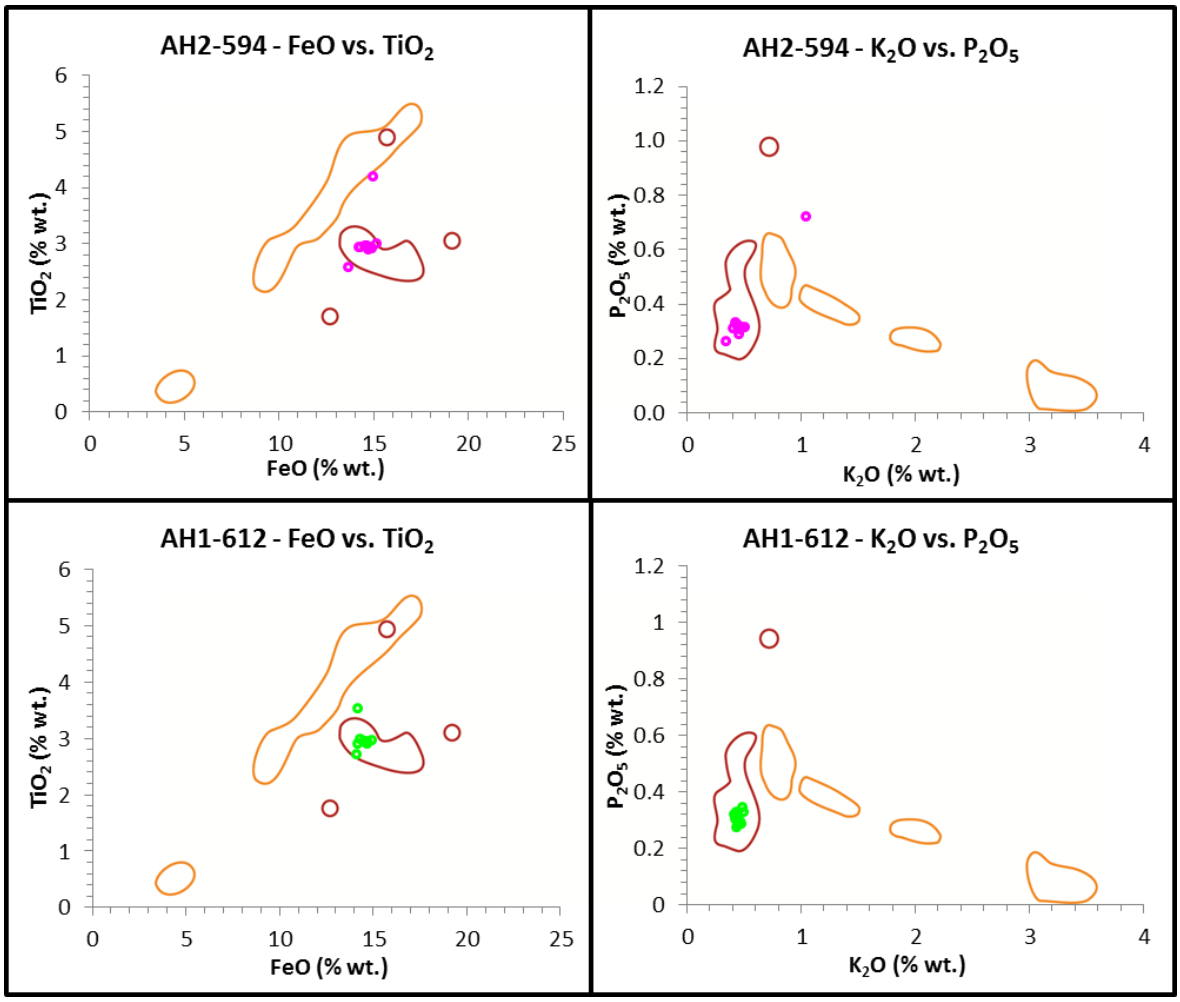

Figure 5.5 – Tephra results from AH2-594 (pink circles) and AH1-612 (green triangles) in Area F. All datasets are plotted against the Vedde ash (orange; Lane et al, 2012) and the Saksunarvatn tephra (red crosses; Tephrabase, www.tephrabase.org) for comparison and correlation.

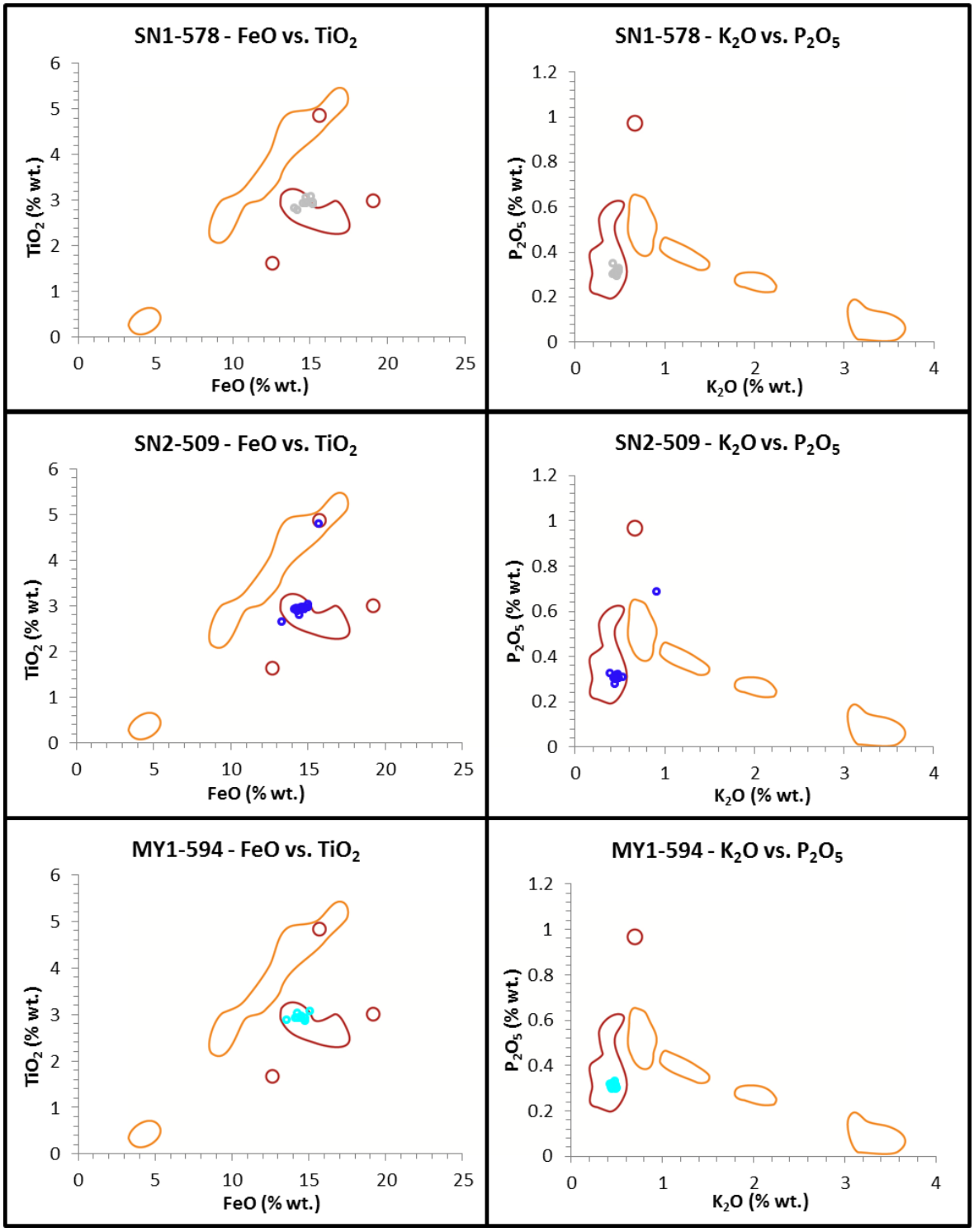

Figure 5.6 – Tephra results from SN1-578 (grey circles), SN2-509 (blue triangles) and MY1-594 (light blue circles) in Area E. All datasets are plotted against the Vedde ash (orange; Lane et al, 2012) and the Saksunarvatn tephra (red crosses; Tephrabase, www.tephrabase.org) for comparison and correlation.

5.3 Tephra Deposits in NW Iceland

The majority of research areas have provided tephra samples which can be correlated with radiocarbon dated tephra layers through *Tephrabase* (www.tephrabase.org; Newton, 1996; Newton *et al.*, 2007). In turn, the tephra samples analysed in this study can be employed to determine ages for environmental change at individual sites, as well as allowing comparison between research areas. In addition to the analyses undertaken as part of this study, previous research has highlighted further tephra deposits in some of the principal research areas (Fig. 3.3; e.g. Rundgren *et al.*, 1997 (Area A); Lloyd *et al.*, 2009 (Area B); Brader, 2012 (Area C)). Interestingly, there is a lack of tephra deposits in Area G, the westernmost research area associated with this study. The distribution of the principal tephra deposits in the field research locations is outlined in Figure 5.7, which highlights the importance of the identification of the Saksunarvatn tephra for correlation of environmental changes between field research locations.

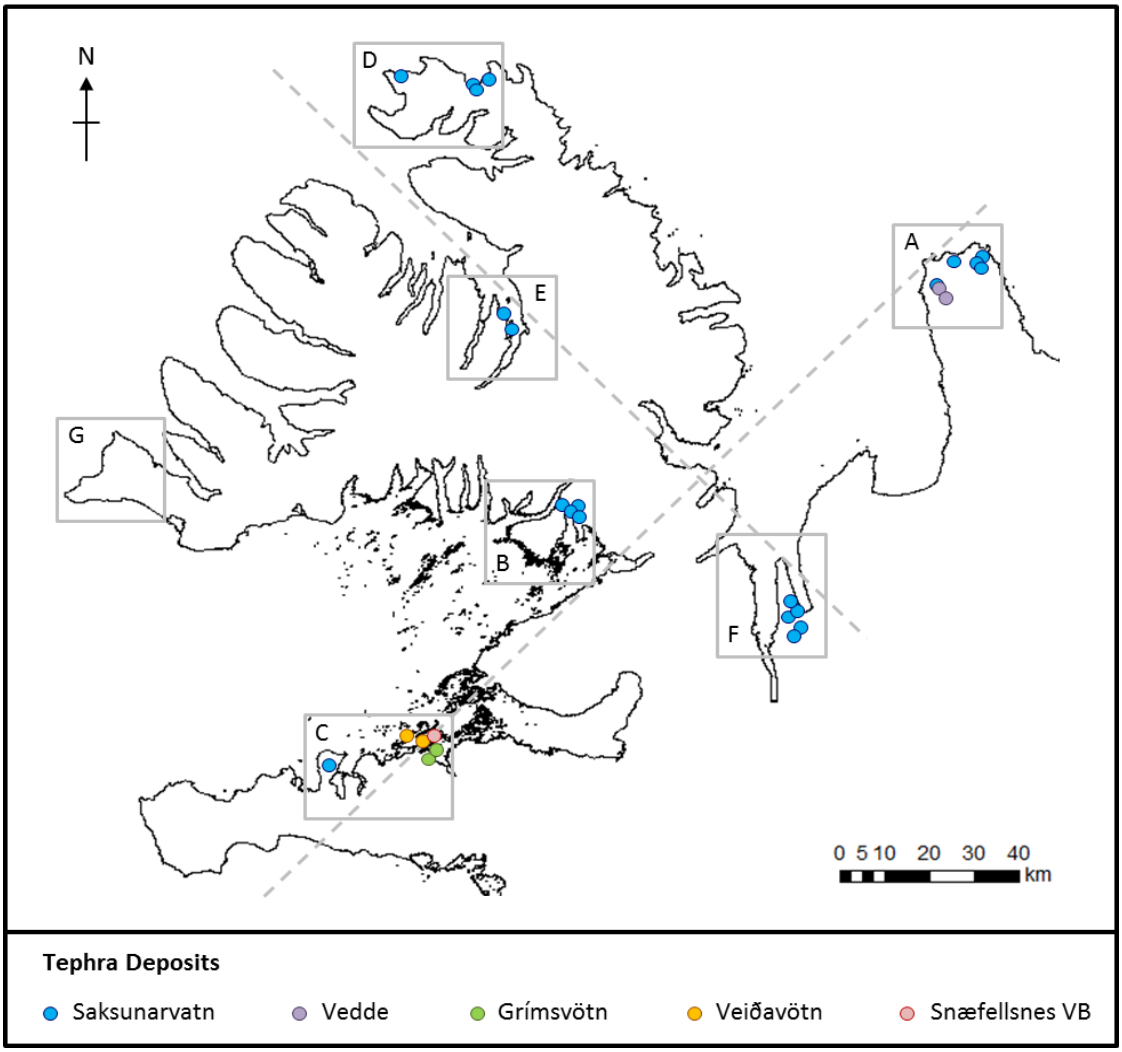

Figure 5.7 – Distribution of tephra layers identified in the seven research locations, highlighting the key deposits. Sources: Area A – Rundgren et al. (1997) and present study, Area B – Lloyd et al. (2009); Area C – Brader (2012) and present study, Area D - G – present study.

5.4 Summary

Tephra samples have been analysed from Areas A, C, D, E and F. Comparison to previously published data has allowed the identification of the Vedde ash in Area A, which will act as a useful chronological marker in the region. The Saksunarvatn tephra is evident in each of the remaining research locations, being widely distributed in northwest Iceland. Geochemical analysis has therefore contributed to the construction of a chronological framework for the research area, which will provide a timing for environmental changes at individual sites and broader regional comparisons. Chapter 6 outlines the environmental data from isolation basin and coastal lowland sediment samples, allowing the development of a series of new SLIPs for northwest Iceland.

CHAPTER 6

RSL changes in NW Iceland

6.1 Introduction

This chapter provides an overview of the environmental changes recorded at each field site investigated as part of this research and are presented from lowest to highest elevation by field area (see Fig. 3.3). Each isolation basin and coastal lowland record will be divided into three sections: site stratigraphy, diatom assemblage and environmental summary. Alongside discussions of stratigraphy and diatom assemblage, chronological analyses on individual core samples will be outlined. At the end of this chapter, the sea-level index points generated as part of this research are presented. The results provided within this chapter will allow the testing of the individual LGM glaciation scenarios, through the subsequent GIA modelling results presented in Chapter 7.

6.2 Key to Figures presented in the Chapter

For the litho- and biostratigraphic figures presented within this chapter, the sedimentological symbols outlined in Fig. 6.1 have been employed.

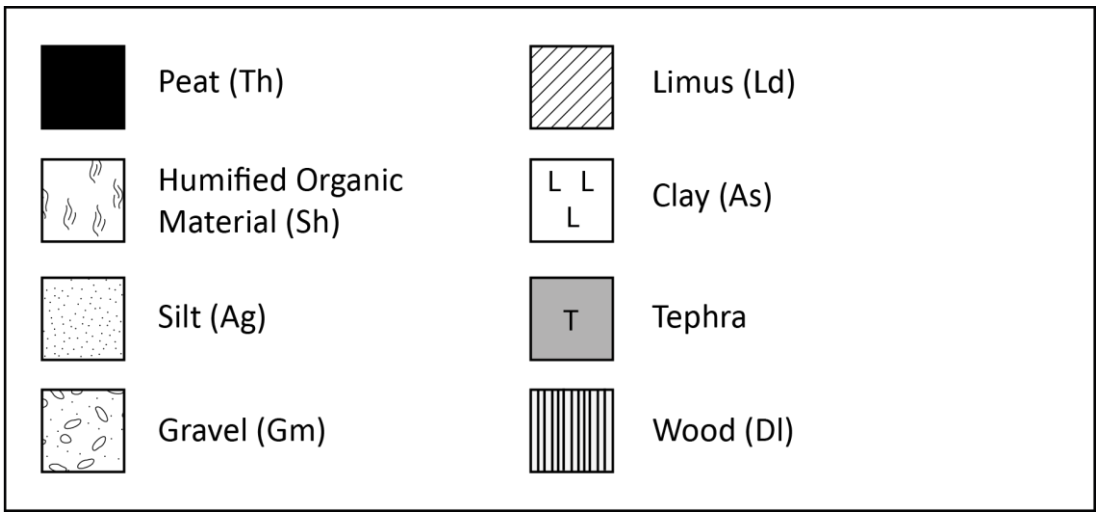

Figure 6.1 – Key to sediment symbols used within the figures presented in Chapter 6.

In addition, diatom figures have been colour coded to represent specific halobian classifications (Hemphill-Haley, 1993; Section 4.3.1): red - salt intolerant (halophobous), orange - freshwater (oligohalobous indifferent), yellow - salt tolerant (halophilous), green - brackish (mesohalobous) and blue - marine (polyhalobous).

6.3 Area A – Skagi

Initial research in Area A was undertaken by Rundgren *et al.* (1997) who investigated five isolation basins and one open section. In addition, three raised shorelines were identified in the region (Rundgren *et al.*, 1997). However, there is uncertainty regarding the timing of marine limit formation, with the published age produced via extrapolation from lower elevation isolation basin records (Rundgren *et al.*, 1997). One isolation basin close to the proposed marine limit was investigated in this study to produce limiting age for marine limit formation.

6.3.1 Tjörn (TJ1)

Sill elevation: 71.25 ± 0.30 m asl Site location: 66°03.050'N 20°22.072'W

Tjörn is situated above the proposed marine limit in Skagi (c. 65 m asl; Rundgren *et al.*, 1997). The location and characteristics of the site are outlined in Section 3.5.1. The sill was calculated based on a grid of cores at the lowest topographical location at the basin edge (S3, Fig. 6.2).

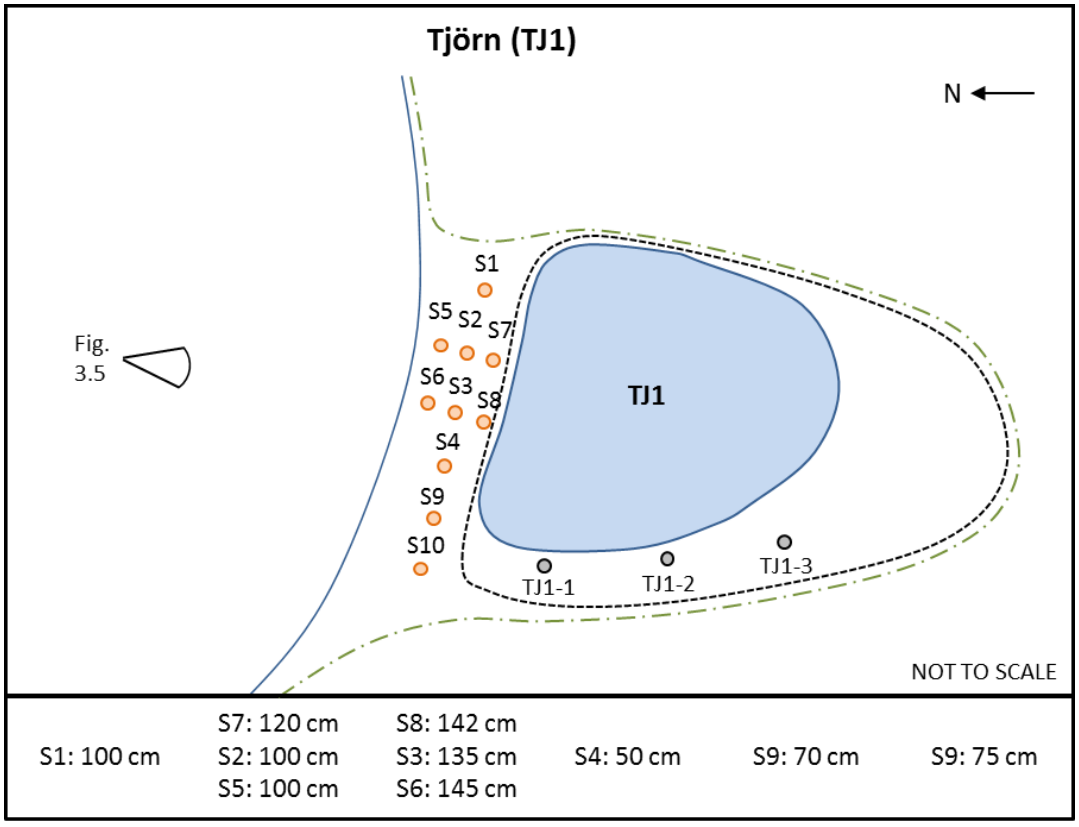

Figure 6.2 – Sill identification at TJ1 (S3) showing the present lake (blue), infilled section (black dashed line), higher surrounding topography (green dashed line), sill cores (orange dots) and sample cores (black dots), alongside the recorded depth for sill cores to underlying bedrock.

6.3.1.1 Site Stratigraphy

In order to establish the stratigraphy of Tjörn (TJ1), a series of cores was extracted from the infilled section of the basin, alongside the present lake, using a gouge corer. The site

demonstrated a consistent overall stratigraphic profile, with some variability in the number of tephra layers recorded at the base of individual core samples. The site stratigraphy has been summarised in Fig. 6.3. A core for diatom analysis was extracted at point TJ1-3 using a Russian Corer. The TJ1-3 sediment core was extracted from the centre point of the transect, which likely represents the deepest point of the basin. It is anticipated that this sediment core provides the most complete record of environmental change at the site and contains two tephra layers at its base. The stratigraphic profile of TJ1-3 is highlighted in Fig. 6.3, with the associated sediment descriptions and Tröels-Smith classifications being presented in Table 6.1.

6.3.1.2 Diatom Assemblage

In total, six diatom samples were analysed from TJ1-3. All of the samples were dominated by freshwater diatom species, such as *Fragilaria construens*, *Fragilaria pinnata* and *Synedra tenera* (Fig. 6.4). Within each of the diatom samples, salt intolerant species were also present, with *Tabellaria fenestrata* being abundant throughout the site assemblage. No brackish or marine species were found at the site and the composition of the diatom assemblage remains roughly constant throughout.

6.3.1.3 Environmental Summary

As demonstrated in Fig. 6.4, the diatom assemblage suggests that the site has not been inundated by the sea, which is consistent with its position close to the highest raised shoreline noted by Rundgren *et al.* (1997). The diatom record supports the interpretation of this feature as the local marine limit and a date at the base of the sediment sample would therefore provide a limiting age on marine limit formation. One bulk radiocarbon sample was taken from the base of the sediment core at 226 cm and produced an age of 6180 ± 37 ^{14}C a BP (6955 - 7174 cal. a BP). This sample appears to suffer from contamination by younger carbon and is contradicted by the geochemical analyses outlined in Chapter 5, as the Vedde Ash (12.1 cal. a BP; Lane *et al.*, 2012) is found within the sediment core at 184 cm and 187 cm (Fig 5.1 and 6.3).

In the absence of any other reliable chronological information, the age of the Vedde Ash is employed as a minimum age for marine limit formation in the region. Using this age, it is possible to estimate a timing of deglaciation, if sedimentation is assumed to be constant throughout the sediment core. This is unlikely to be the case, but difficulties with alternative methods (radiocarbon) mean that this date is the best estimate available for the site. Marine limit formation and therefore deglaciation is estimated at c. 14500 cal. a BP from the sample at Tjörn. Age uncertainty is calculated as a sum of the uncertainty of the Vedde ash age (12121 ± 114 cal. a BP; Rasmussen *et al*., 2006) and a chosen value per centimetre of extrapolation (this study: 1 a cm^{-1}). As a result, the basal age at TJ1 (225 cm) is 14558 ± 152 cal. a BP.

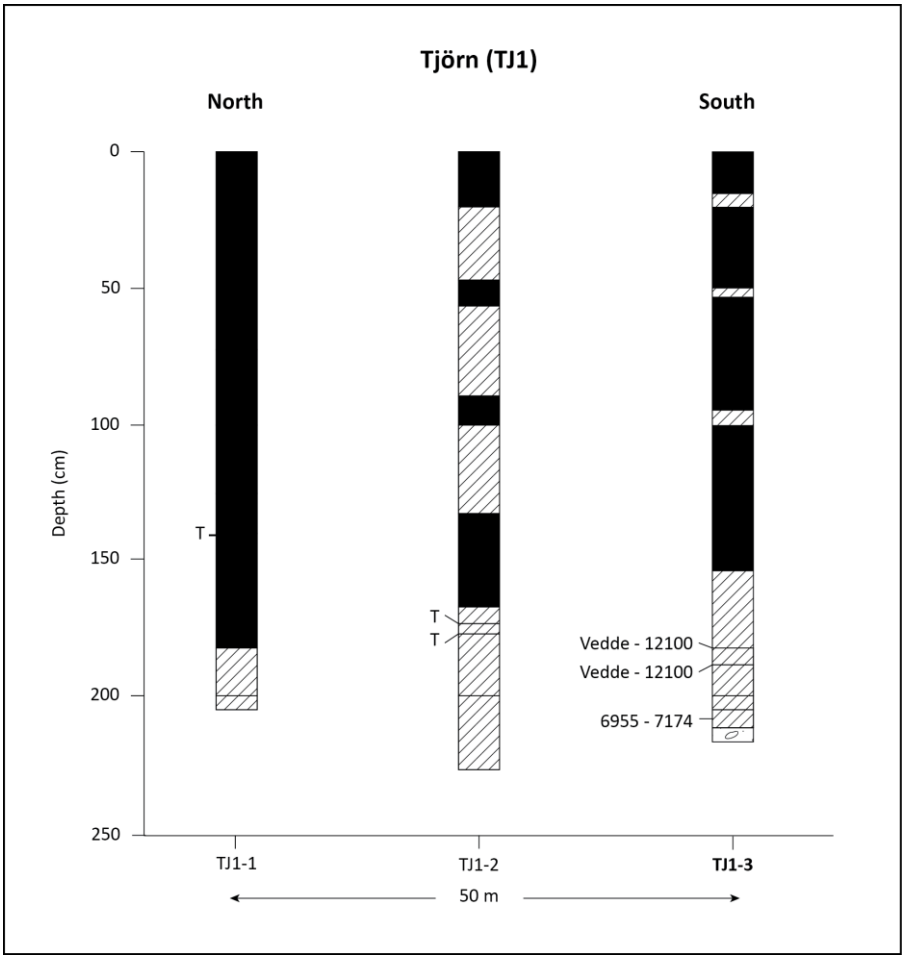

Figure 6.3 – Site stratigraphy at Tjörn (TJ1) showing the dominance of organic sediments at the site. The key to the sediments present can be found in Section 6.2. Ages reported are calibrated ages before present.

Upper Boundary (cm)	Lower Boundary (cm)	Sediment Description	Tröels-Smith Classification
0	15	Sphagnum peat	Tb4
15	19	Beige-brown marl/limus	Lc2 Ld2
19	52	Sphagnum peat	Tb4
52	54	Olive green limus with organic material	Ld3 Sh1
54	89	Sphagnum peat	Tb4
89	100	Beige-brown marl/limus	Lc2 Ld2
100	131	Sphagnum peat with organic material	Tb3 Sh1
131	153	Sphagnum peat	Tb4
153	161	Sphagnum peat with organic material	Tb3 Sh1
161	184	Beige-brown marl/limus	Lc2 Ld2
184	186	Dark grey fine tephra	Ag4
186	187	Beige-brown marl with some tephra	Lc3 Ag1
187	188	Dark grey fine tephra	Ag4
188	200	Beige-brown marl/limus	Lc2 Ld2
200	207	Olive green limus	Ld4
207	226	Beige/olive green limus with marl	Ld2 Lc2
226		Gravel	Gmin4

Table 6.1 – Sediment description and Tröels-Smith classification of the TJ1-3 sediment core sample.

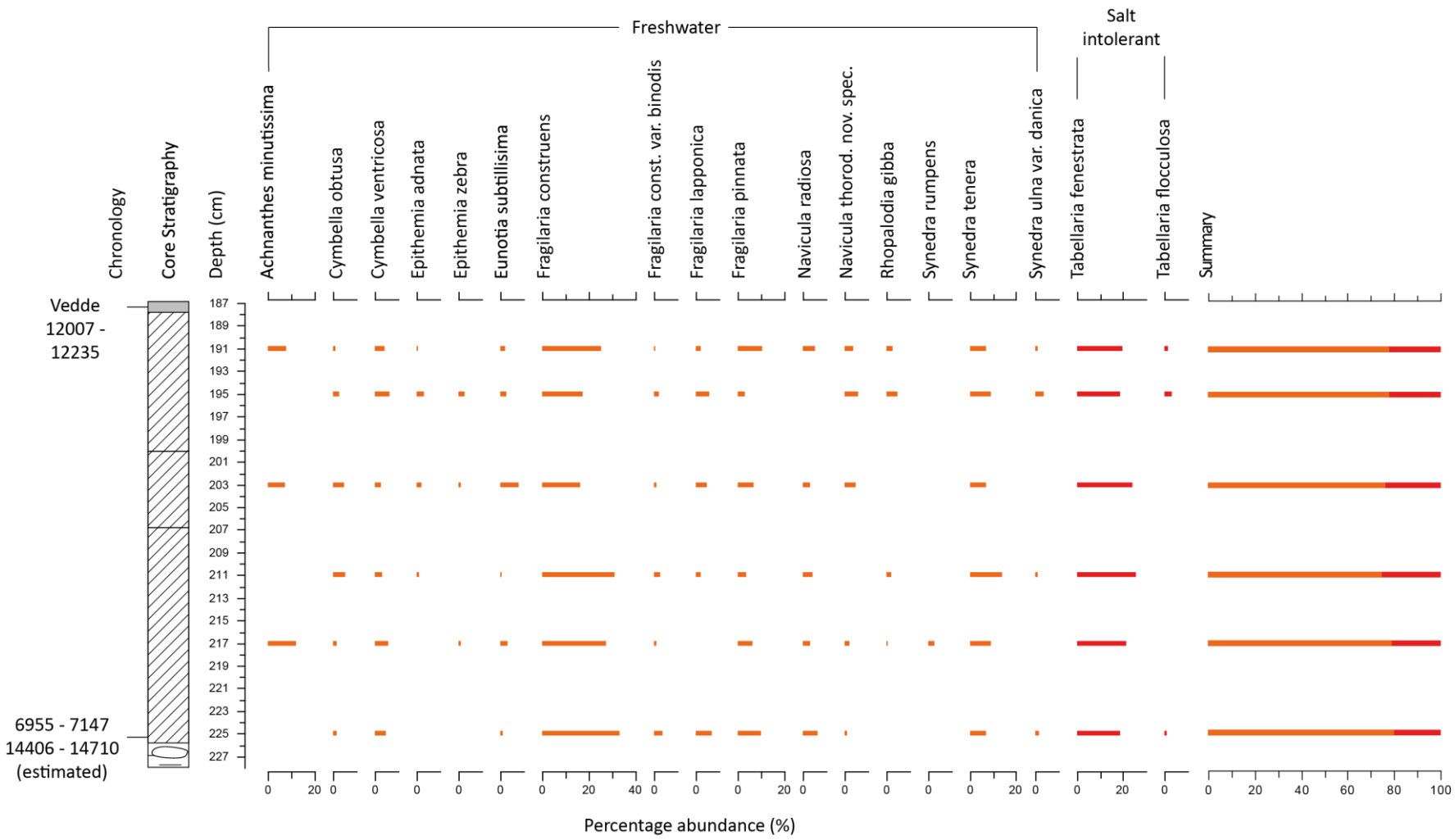

Figure 6.4 – Diatom assemblage at TJ1-3 (>3% of the total diatom count) showing the dominance of freshwater taxa at the site. The key to symbols used can be found in Section 6.2.

6.4 Area C – Snæfellsnes

In Snæfellsnes, six isolation basin and two coastal lowland sites have previously been investigated by Brader (2012). However, the timing of deglaciation and marine limit formation was not established for the region (Brader, 2012). As a result, one isolation basin site was analysed as part of this research, situated close to the proposed marine limit (Brader *et al.*, submitted).

6.4.1 Ytra-Baravatn (YBR1)

Sill elevation: 57.60 ± 0.30 m asl Site location: 64°59.056'N 23°11.579'W

The sill at YBR 1 was identified within the channel exiting west of the present lake basin. The base of the channel was not covered in overlying sediments and as such the sill was determined through surveying the channel with an EDM (S3, Fig. 6.5). Information regarding the morphology of the site can be found in Section 3.5.3.

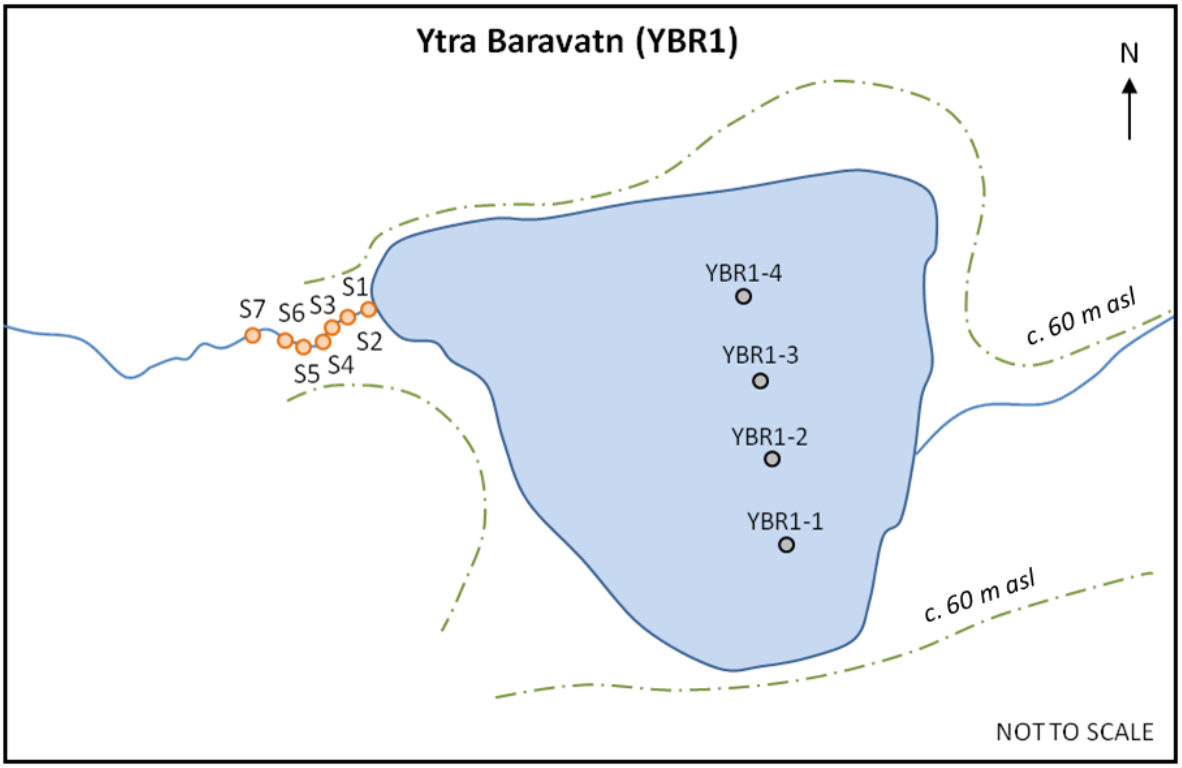

Figure 6.5 – Sill identification at YBR1, showing the location of individual sill measurements (orange dots), sample cores (black dots), present lake (blue) and higher surrounding topography (green dashed line)

6.4.1.1 Site Stratigraphy

Site stratigraphy at Ytra Baravatn (YBR1) was established through the coring of a transect of cores across the present-day lake. No expansive infilled sections are evident within the basin and as such, sediment coring was carried out using the boat. YRB1 shows a generally consistent

stratigraphic profile, with organic-rich limus layers overlying clay rich silts (Fig. 6.6). A sample for analysis was extracted from point YBR1-2, as it provided the longest sediment sequence.

YBR1-2 is comprised of a basal blue-grey clay with silt, overlain by olive green limus. Within the overlying limus deposits, a series of tephra layers were identified at 90 cm, 210 cm and 352 cm. The stratigraphy of the core is summarised in Table 6.2.

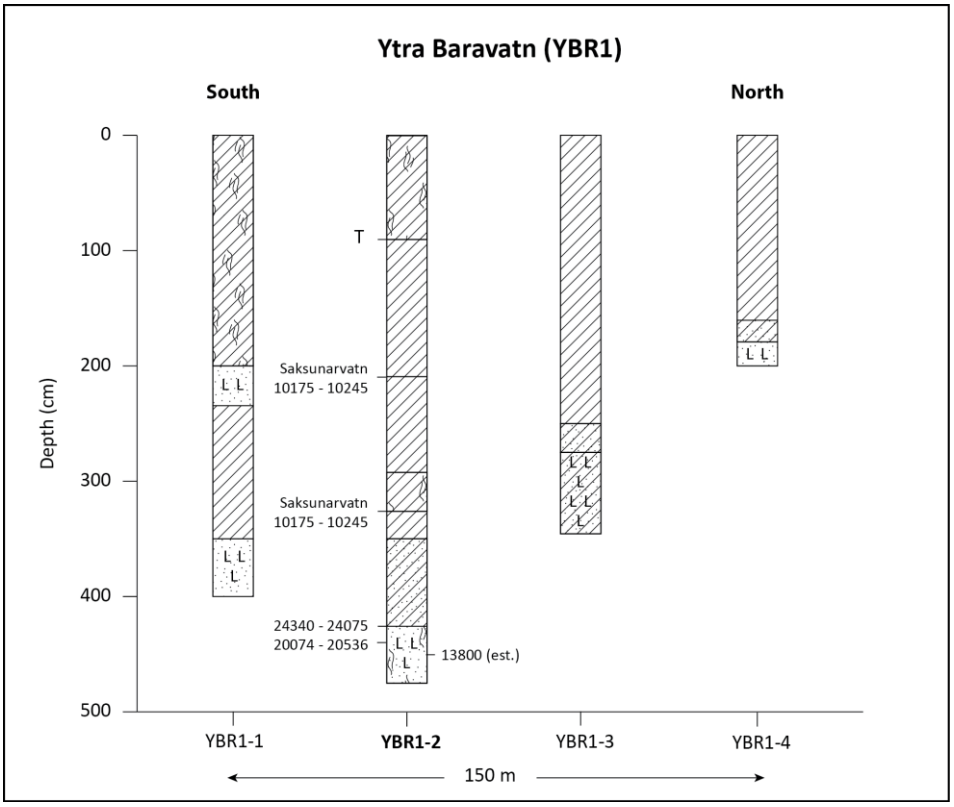

Figure 6.6 – Site stratigraphy at Ytra-Baravatn (YBR1), the highest site in Snæfellsnes. For the key to sediments see Section 6.2. Ages reported are calibrated years before present (cal. a BP).

Upper Boundary (cm)	Lower Boundary (cm)	Sediment Description	Tröels-Smith Classification
0	90	Olive green limus and organic material	Ld3 Sh1
90	91	Light grey fine tephra	Ag4
91	210	Olive green limus	Ld4
210	211	Dark grey fine tephra	Ag4
211	295	Olive green limus	Ld4
295	329	Light brown organic rich limus	Ld3 Sh1
329	352	Olive green limus	Ld4
352	355	Dark grey tephra	Ag4
355	440	Olive green limus with trace of silt	Ld3 Ag1
440	480	Blue grey clay with silt and some organic material	As2 Ag1 Sh1

Table 6.2 - Sediment description and Tröels-Smith (1955) classification of the YBR1-2 sediment core sample.

6.4.1.2 Diatom Assemblage

Twelve diatom samples were analysed through the YBR1-2 core, with ten samples providing sufficient diatoms for a reliable reconstruction. Samples were extracted from the 430-480 cm section of the sediment core in order to establish the diatomological isolation contact (Fig. 6.7). At the base of the YBR1 core sample, brackish and salt tolerant species dominate the assemblage, with *Diatoma tenue var. elongatum* making up a large proportion of the lowermost sample composition (Zone 1, Fig. 6.7). Above this layer dominated by brackish-salt tolerant diatoms, levels of freshwater taxa increase within the diatom assemblage. Increases in *Epithemia zebra*, *Fragilaria construens* and *Synedra sp.* signal a decrease in brackish influence at the site in Zone 2 (Fig. 6.7). There is a minor increase in brackish taxa towards the top of Zone 2, which may result from the proximity of the site to MSL or storm activity. At the top of the analysed section of the sediment core, the diatom assemblage is dominated by freshwater diatom species (Zone 3; Fig. 6.7). The diatomological isolation contact is recorded at 468 cm.

6.4.1.3 Environmental Summary

The diatom assemblage at YBR1-2 demonstrates a decrease in marine-brackish influence through the sediment section, leading to a dominance of freshwater diatom taxa within the uppermost sediment samples analysed. The lowermost diatom samples suggest that the site was located close to MSL and was likely occasionally inundated by marine water, as demonstrated by the limited levels of marine diatoms recorded within the diatom assemblage. The diatom assemblage at YBR1 demonstrates a RSL fall at this site, with the percentage of freshwater diatoms within the record increasing with a lowering of RSL.

Two radiocarbon samples were taken from the site in order to establish the timing of basin isolation at the lowermost point of organic sedimentation. An initial bulk sediment sample at 448 cm produced an age of 16871 ± 76 ^{14}C a BP (20074 - 20536 cal. a BP). A second bulk sample at 440 cm returned an age of 20140 ± 60 ^{14}C a BP (24340 - 24075 cal. a BP; Brader *et al.*, submitted), suggesting a problem with contamination at the site. The ages generated at YBR1 are significantly older than any terrestrial deglacial radiocarbon age previously generated in western Iceland (e.g. Lloyd *et al.*, 2009). The tephra layer at 352 cm has been identified as Saksunarvatn based on the geochemical composition (Fig. 5.2) and so the timing of isolation is taken as 13574 ± 151 cal. a BP at 468 cm (Brader *et al.*, submitted). This timing of isolation is based on the assumption that the sedimentation rate at the site remained constant throughout the core sample, with age uncertainty determined using the method outlined in Section 6.3.1.3. The extrapolated age of basin isolation appears reasonable, when compared to sites close to the marine limit in previously published RSL records (e.g. Rundgren *et al.*, 1997; Brader *et al.*, submitted). RSL studies from

northwest Iceland suggest a deglacial age of c. 14000 cal. a BP (e.g. Rundgren *et al.*, 1997; Lloyd *et al.*, 2009). The preferred age for basin isolation at YBR1 is therefore 13574 ± 151 cal. a BP.

As noted in Section 6.3.1.3, there are likely issues of contamination at the site leading to the anomalous radiocarbon ages. This may be a consequence of the limited vegetation in the surrounding landscape during deglaciation, which would have allowed sediment transport into the basin. This is consistent with the interpretation of the surrounding landscape, which suggests that YBR1 was the highest basin to be inundated by marine water. The site is located close to the marine limit and the timing of isolation at the site can therefore be used as a minimum date for marine limit formation in Area C. It is likely that the marine limit in Snæfellsnes formed ~ 13600 ± 150 cal. a BP.

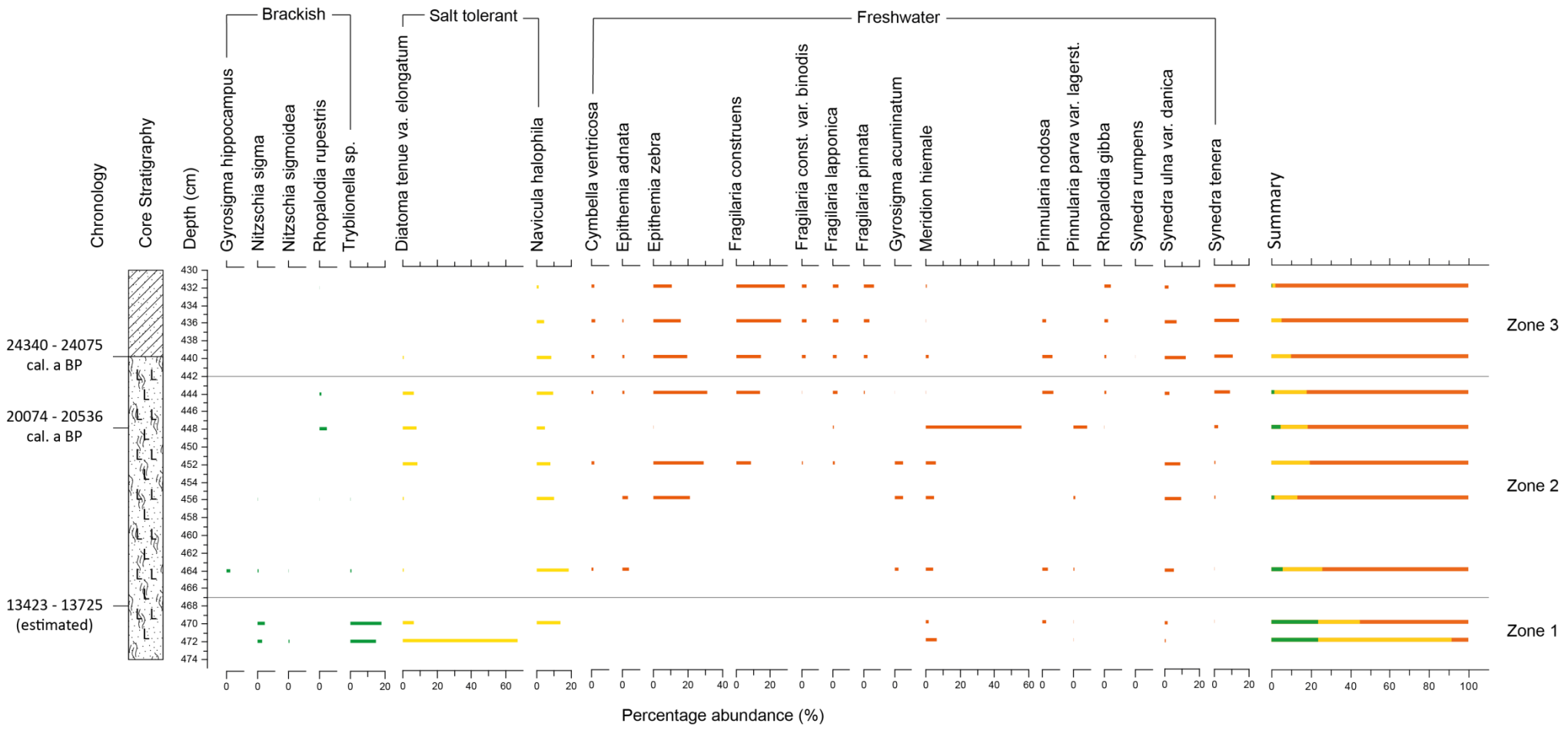

Figure 6.7 – Diatom assemblage from YBR1-2 (>3% of the total diatom count) showing the transition from brackish to freshwater dominance within the core sample. The key to the sediment symbols and colour classifications can be found in Section 6.2.

6.5 Area D – Hornstandir (Hlöðuvik and Hælavik) and Aðalvik

Three isolation basin and two raised terrace sites were investigated in Area D, which has not previously been the subject of RSL study. Hjort *et al.* (1985) identified a marine limit in Hlöðuvik and Hælavik, but were unable to determine an age of formation in either location. In Aðalvik, a range of marine limit elevations have been proposed, which are occasionally contradictory (see Fig. 2.5). Isolation basin study has not previously been conducted in Aðalvik. Thus, isolation basins were sought in both locations in order to investigate the timing of deglaciation and patterns of postglacial RSL change.

6.5.1 Hlöðuvik 3 (HD3)

Sill elevation: 18.01 ± 0.30 m asl Site location: 66°24.965'N 22°38.857'W

HD3 is the lowest isolation basin cored in Hornstrandir but situated furthest from the present day coastline. The sill elevation was based on a grid of cores to the northwest of the lake basin (Fig. 6.8), with the lowest high point taken to represent the sill (see S4, Fig. 4.2). An overview of the site topography and location can be found in Section 3.6.1 and Fig. 3.11.

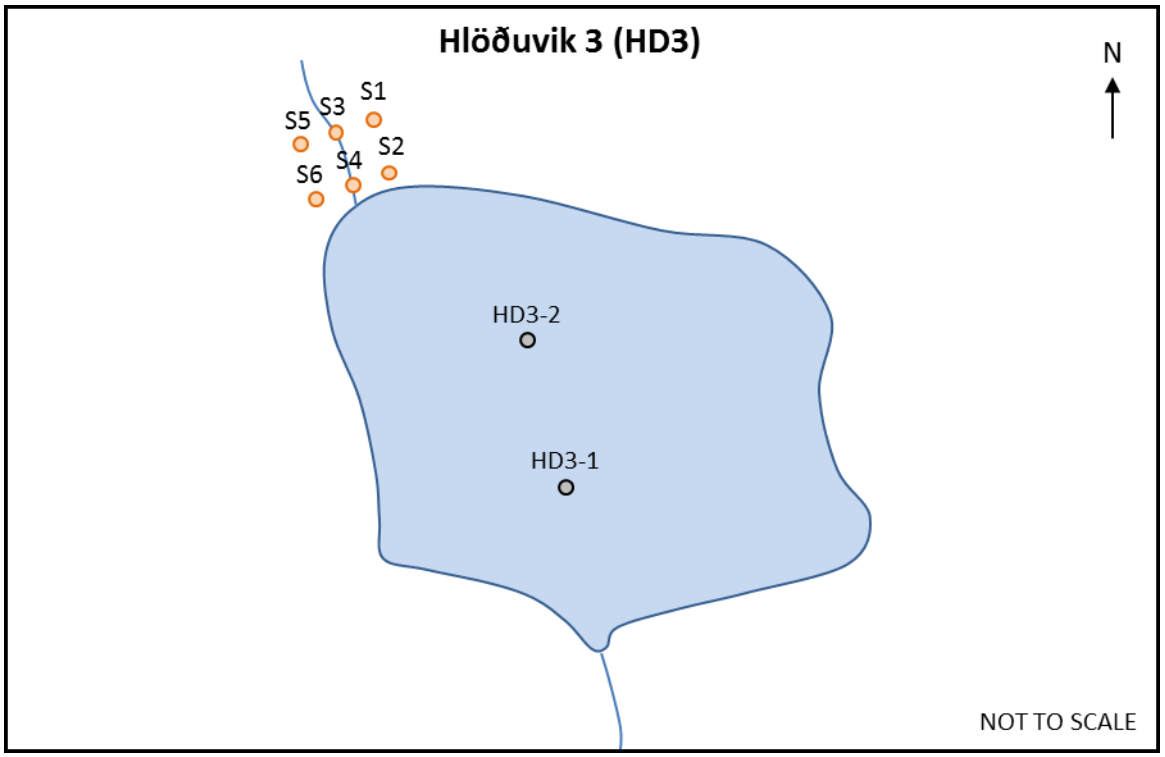

Figure 6.8 – Sill identification at HD3 showing the location of the sill survey points (orange dots), the basin sill (S4) and the sediment core locations (black dots) within the present day lake (blue).

6.5.1.1 Site stratigraphy

A number of sediment cores were extracted from Hlöðuvik 3 (HD3) in order to establish the underlying site stratigraphy. Initially, core samples were not sufficiently deep to allow the establishment of a complete record of environmental change at the site (see Chapter 3 for details). However, samples from the centre of the lake basin produced sufficient material to allow subsequent analysis of the diatom record (HD3-1).

The HD3-1 sediment core is summarised in Fig. 6.9 and Table 6.3. The HD3-1 sediment core comprises 140 cm of sediment, with a distinct tephra layer at its base. Geochemical analysis has identified this as the Saksunarvatn tephra (Fig. 5.3). The sedimentary record from HD3-1 highlights a transition to increasingly organic sediment dominance, with the exception of the upper sand and gravel layer. It is hypothesised that this layer could represent a slope in-wash event, due to the steep-sided nature of the Hlöðuvik area. The sediment record appears to highlight a relatively low energy depositional environment due to the fine grained nature of the sediments present. The mixed organic material noted towards the top of the core section is a mixture of peat, well defined rootlets and unidentifiable organic matter.

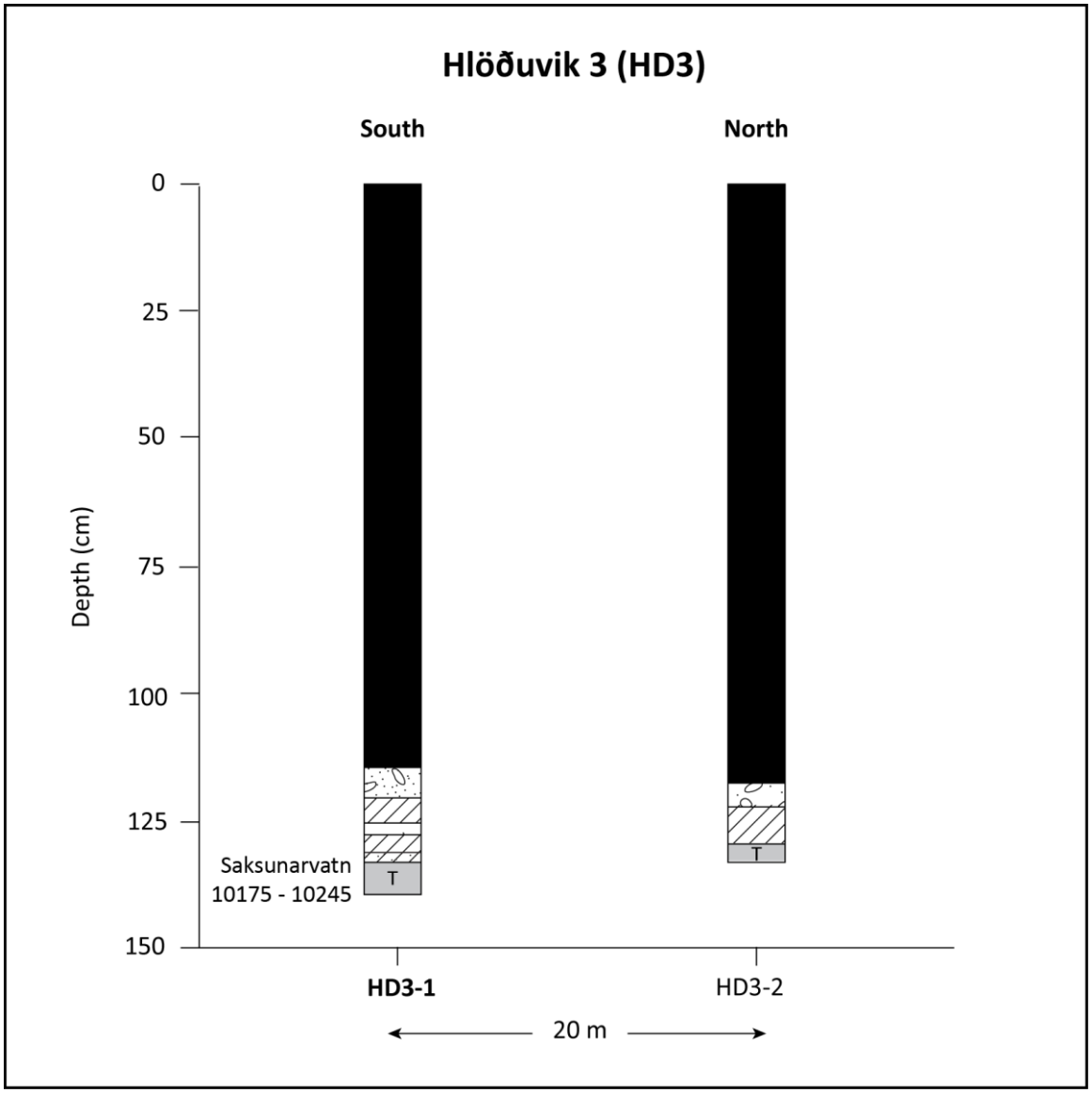

Figure 6.9 – Site stratigraphy at HD3. The key to sediment symbols employed can be found in Section 6.2.

Upper Boundary (cm)	Lower Boundary (cm)	Sediment Description	Tröels-Smith Classification
49	115	Brown mixed organic material with peat	Sh2 Th2
115	120	Grey sand with gravel	Ga2 Gm2
120	125	Olive green/brown limus	Ld4
125	127	Dark brown mixed organic material	Sh4
127	130	Olive green/brown limus	Ld4
130	134	Olive green/brown limus with trace silt	Ld4 Ag+
134	140	Dark grey tephra	Ag4

Table 6.3 – Sediment descriptions and Tröels-Smith (1955) classifications for the Hlöðuvik 3 (HD3-1) sediment core sample.

6.5.1.2 Diatom assemblage

The diatom assemblage at HD3-1 can be divided into two distinct diatom zones (Fig. 6.10). Zone 1 is dominated by freshwater taxa, which make up c. 85% of the total diatom assemblage at the base of the zone. Throughout Zone 1, there is an increase in the percentages of freshwater taxa such as *Fragilaria construens* and *Fragilaria pinnata,* alongside a corresponding decrease in the principal salt intolerant taxa. Zone 2 sees a subsequent increase in the proportion of salt intolerant taxa, principally through greater numbers of *Tabellaria fenestrata.* The total percentages of freshwater and salt intolerant taxa remain approximately constant throughout this zone, representing c. 90% and c. 10% respectively.

6.5.1.3 Environmental summary

It is clear from the diatom assemblage that the site is dominated by freshwater conditions throughout. It is likely that this site was situated above MSL and beyond tidal influence throughout the period represented within the sediment core sample. In order to establish chronological control at the site, one tephra sample was analysed at the base of the sediment core sample, which was identified as the Saksunarvatn tephra (Section 5.2.3). The Saksunarvatn tephra is well constrained throughout Europe and therefore provides a basal age of 10200 cal. a BP (Lohne *et al.*, 2014). It is clear that RSL was lower than the sill elevation at 10200 cal. a BP, which can also be used as a limiting age for marine limit formation in the region.

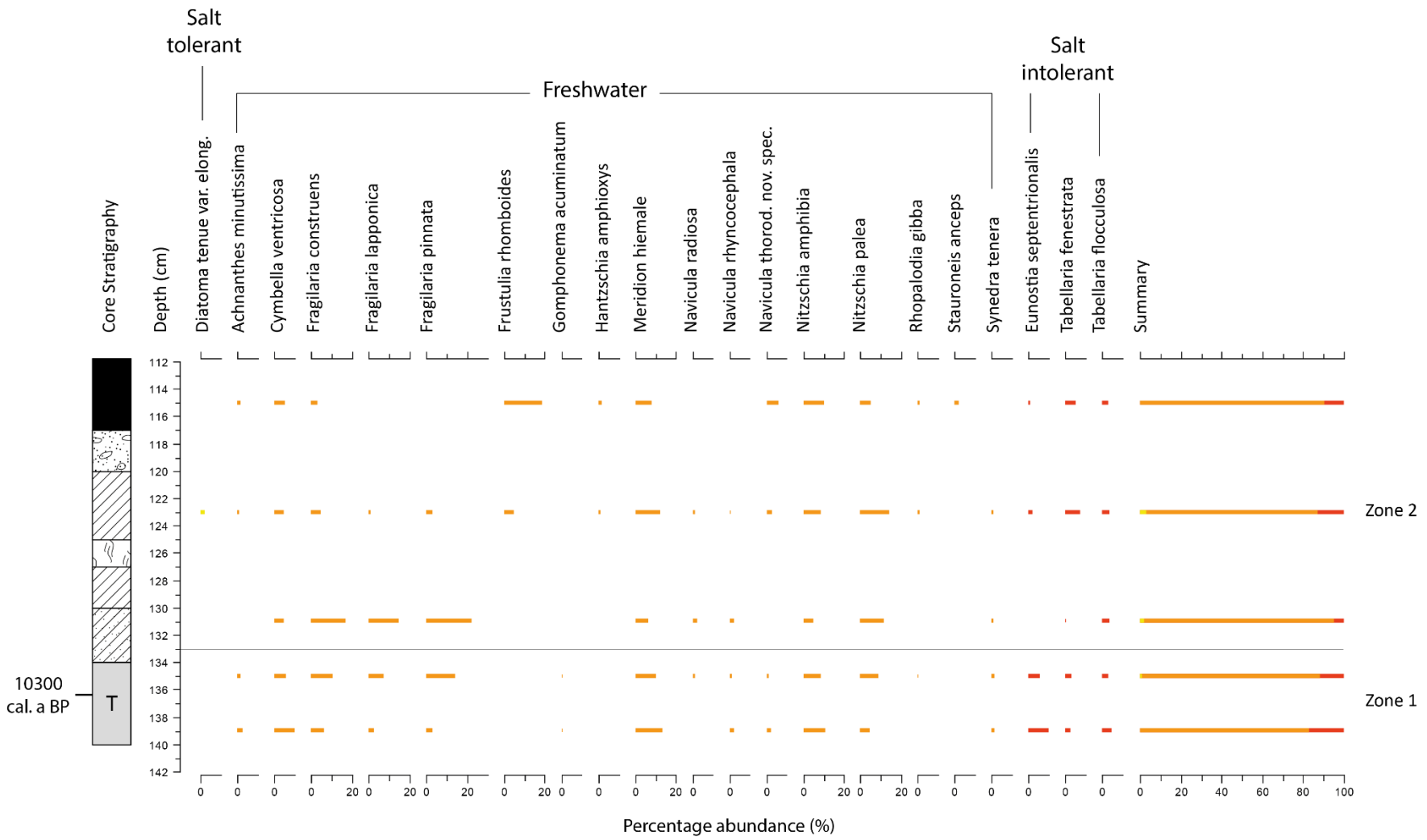

Figure 6.10 – Diatom assemblage from HD3-1 (>3% of the total diatom count) showing the dominance of freshwater conditions at the site. For the key, see Section 6.2.

6.5.2 Hlöðuvik 1 (HD1)

Sill elevation: 18.13 ± 0.30 m asl Site location: 66°25.156'N 22°38.846'W

HD1 is situated close to the marine limit in Hlöðuvik (Section 3.6.1 and Figs. 3.9 and 3.11). The sill was identified through a grid of cores to the southwest of the lake basin (S1, Fig. 6.11).

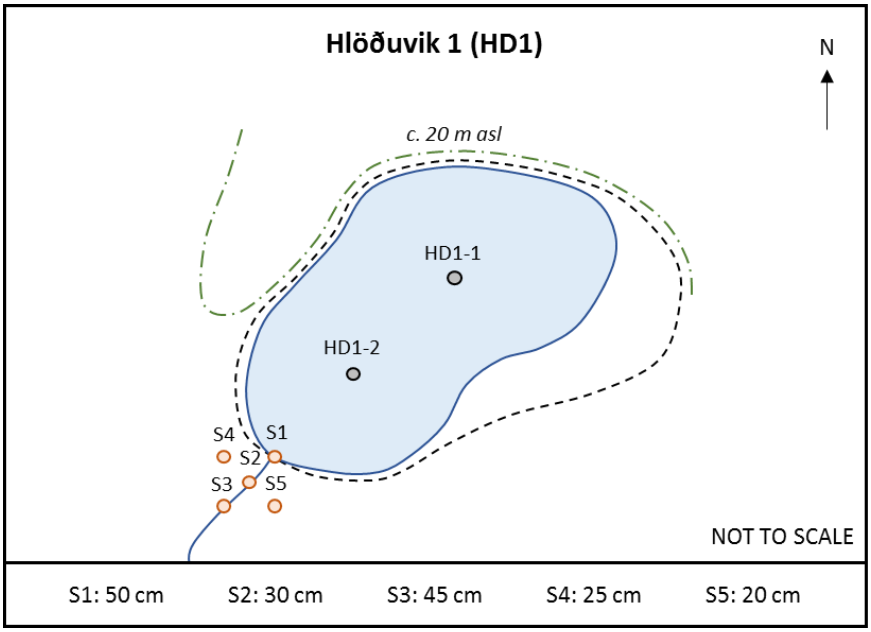

Figure 6.11 – Sill identification at HD1 (S1) alongside sill survey points (orange dots), core locations (black dots), higher topography (green dashed line) and the extent of the basin (black dashed line), alongside the sill core depths to the underlying bedrock.

6.5.2.1 Site stratigraphy

Due to the limited size of the basin, two sediment cores were extracted. The transect demonstrated a uniform site stratigraphy, as demonstrated by Fig. 6.12, characterised by a basal silty clay, overlain by olive green limus. Above this layer, an organic rich layer is evident, overlain by turfa peat. One sediment core sample was extracted at HD1-2 (Table 6.4).

Upper Boundary (cm)	Lower Boundary (cm)	Sediment Description	Tröels-Smith Classification
20	33	Mid brown sphagnum peat	Tb4
33	53	Mixed organic material with peat	Sh2 Th2
53	79	Mid brown mixed organic material	Sh4
79	106	Olive green limus	Ld4
106	120	Blue grey silty clay	As2 Ag2

Table 6.4 – Sediment descriptions and Tröels-Smith (1955) classifications for the Hlöðuvik 1 (HD1-2) sediment core sample.

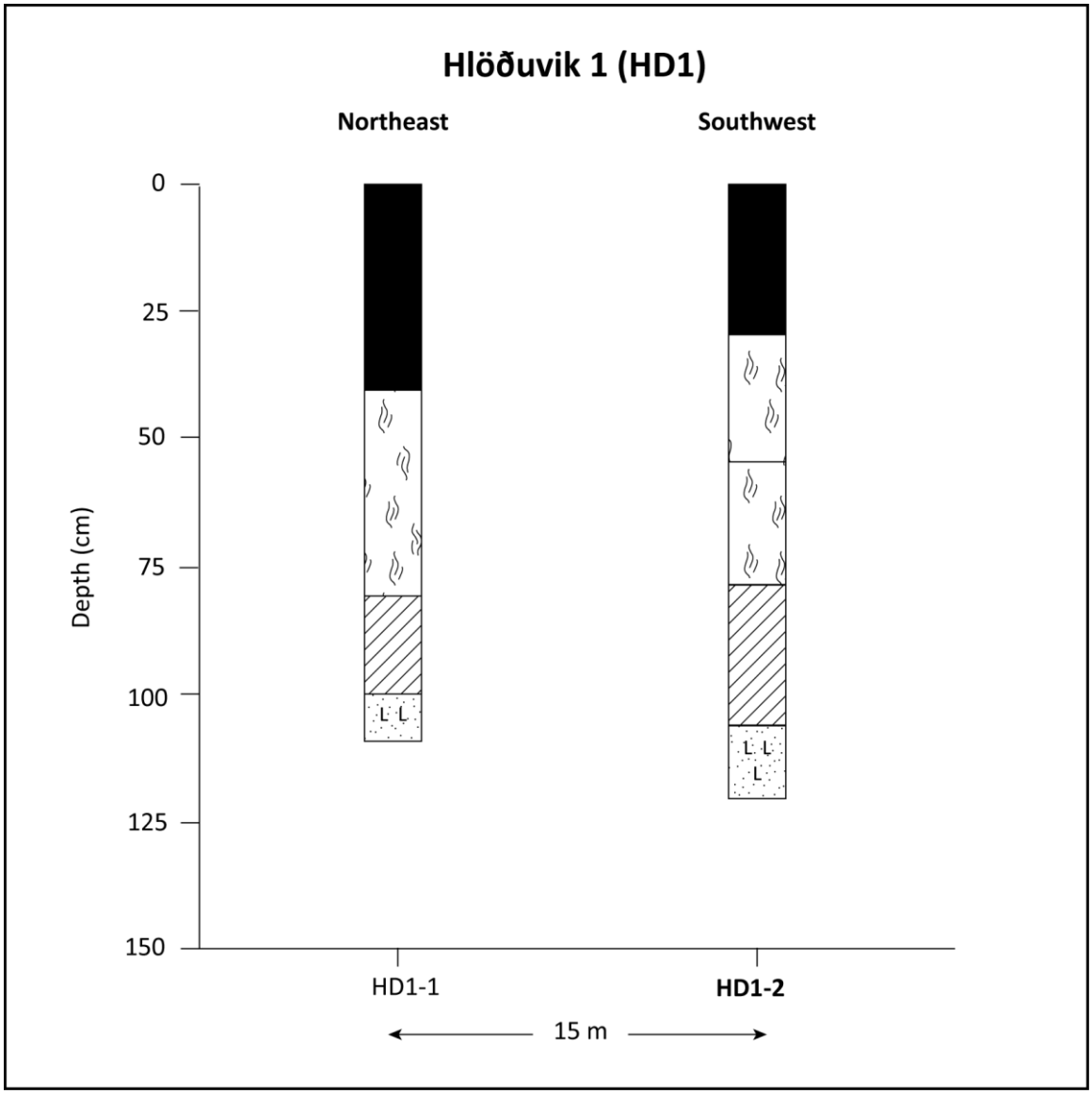

Figure 6.12 – Site stratigraphy at HD1 showing the dominance of organic sedimentation at the site. For the key to sediment symbols used, see Section 6.2.

6.5.2.2 Diatom assemblage

Freshwater taxa dominate the diatom assemblage at HD1-2, which can be divided into two distinct diatom zones (Fig. 6.13). Zone 1 is comprised predominantly of freshwater taxa, such as *Cymbella ventricosa, Meridion circulare* and *Frustulia rhomboides*, making up at least 80% of the total diatom count. There is an increase in the proportion of salt tolerant taxa within the zone, principally through an increase in *Navicula halophila,* alongside limited numbers of salt intolerant taxa. The beginning of Zone 2 is marked by an increase in the percentage of *Fragilaria construens* and *Nitzschia*, alongside the loss of salt tolerant taxa from the diatom record. Over the course of the zone, the levels of *Fragilaria construens* decrease, alongside increases in *Nitzschia sp.* and salt intolerant taxa. There is a corresponding increase in the proportion of salt intolerant taxa within the zone from c. 5% to c. 9% of the total diatom count.

6.5.2.3 Environmental summary

The diatom assemblage at HD1-2 demonstrates a dominance of freshwater conditions at the site (Fig. 6.13). The site is likely situated above the influence of marine conditions at the point of sediment deposition. Due to the lack of a transition within the diatom assemblage and the availability of chronological control at other sites in the area, no radiocarbon samples were taken from the site. The site does however act as a limiting elevation for RSL, alongside that at HD3.

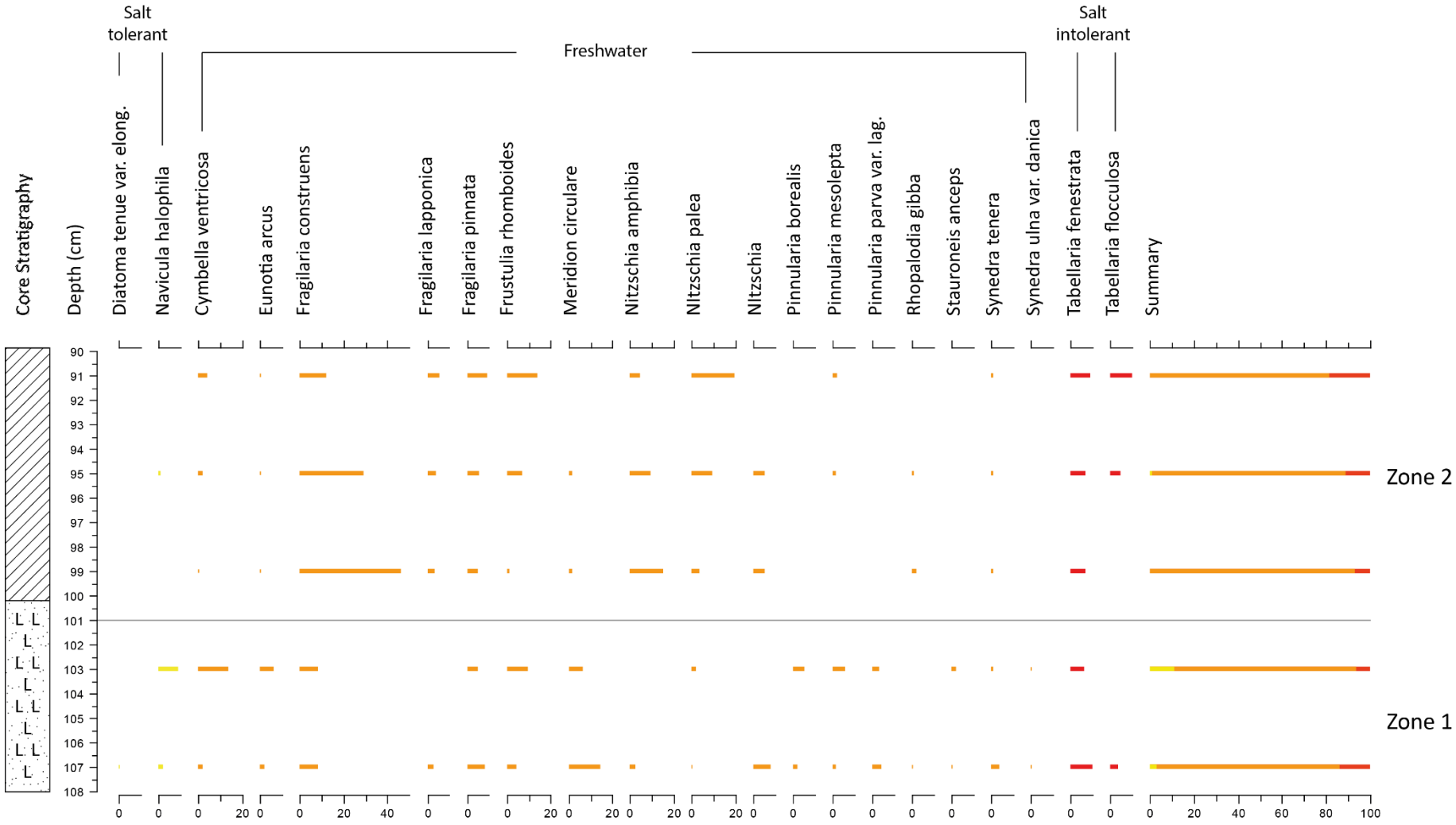

Figure 6.13 – Diatom assemblage at HD1-2 (>3% of the total diatom count) showing the dominance of freshwater conditions at the site. For the key, see Section 6.2.

6.5.3 Hlöðuvik 2 (HD2)

Sill elevation: 18.71 ± 0.30 m asl Site location: 66°25.142'N 22°38.776'W

HD2 is the final isolation basin site studied in Hlöðuvik, situated close to HD1. At HD2, the sill elevation is based on a grid of cores at the lowest topographical point surrounding the present lake (S3, Fig. 6.14).

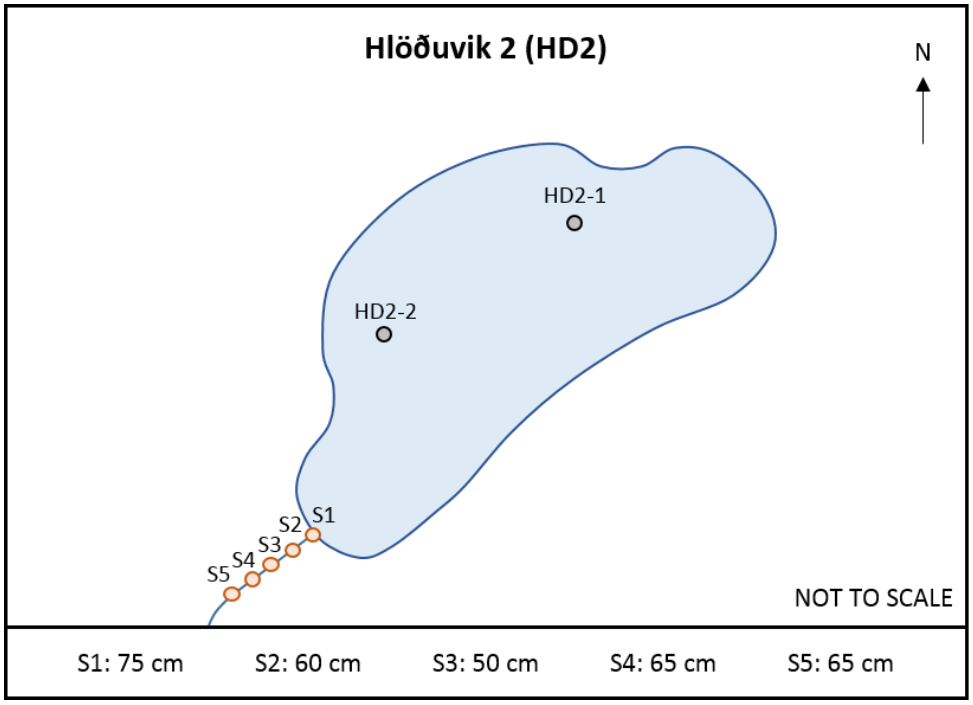

Figure 6.14 – Sill identification at HD2 (S3) including core sample loactions (black) and sill cores (orange).

6.5.3.1 Site stratigraphy

HD2 is a small basin and as a result, two sediment cores were extracted from the site. Both sediment cores demonstrate a similar stratigraphy, with a basal silt being overlain by limus and peat layers (Fig. 6.15). One sediment sample for analysis was extracted from HD2-1. The sample comprises a basal wood layer overlain by a grey silt, olive green limus and mid-brown turfa peat (Table 6.5).

Upper Boundary (cm)	Lower Boundary (cm)	Sediment Description	Tröels-Smith Classification
30	61	Mid brown turfa peat	Th4
61	81	Brown organic material with limus	Sh2 Ld2
81	91	Olive green limus	Ld4
91	93	Grey silt	Ag4
93	95	Wood	Dl4

Table 6.5 – Sediment descriptions and Tröels-Smith (1955) classifications for the Hlöðuvik 2 (HD2-1) sediment core sample.

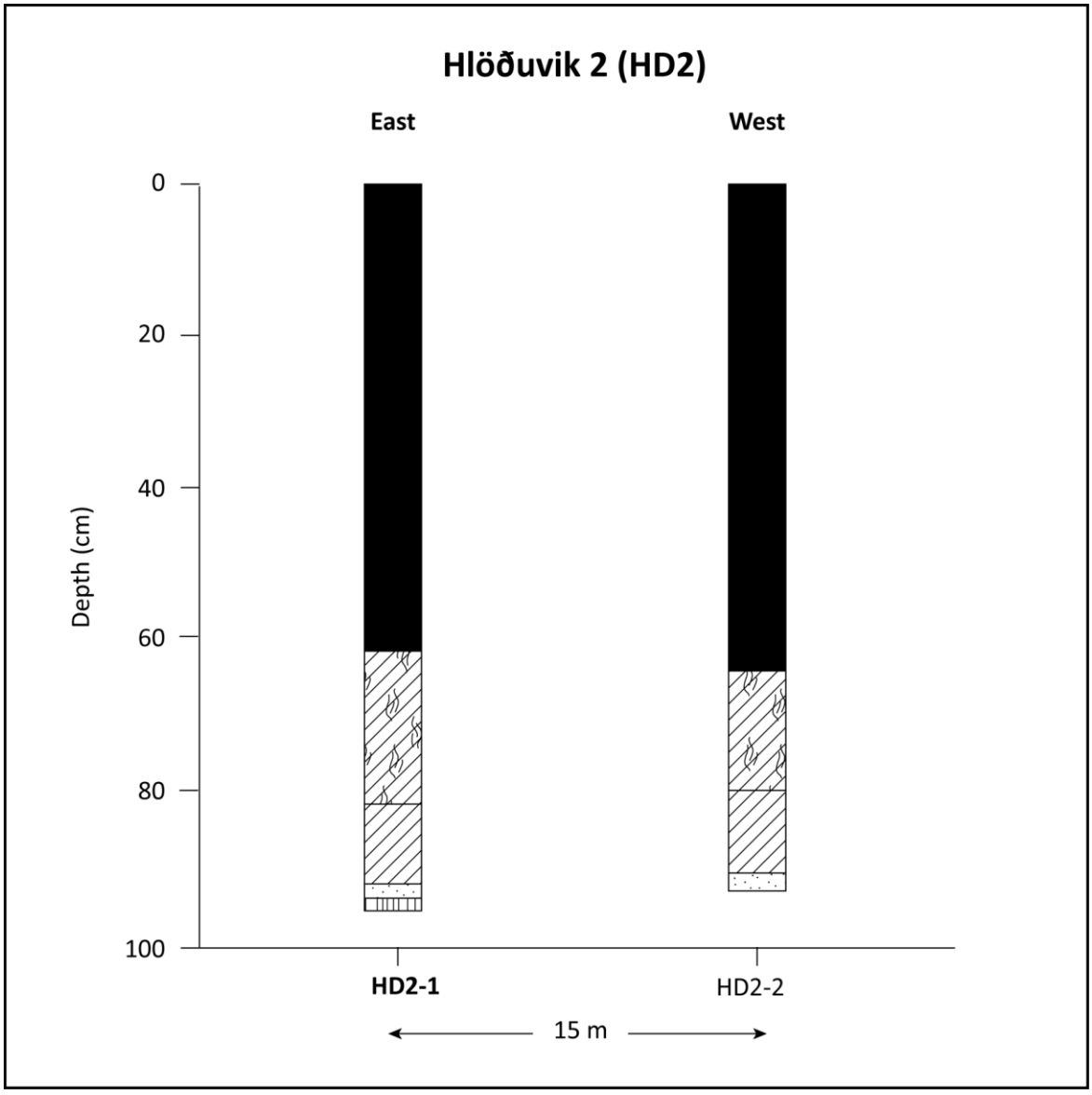

Figure 6.15 – Site stratigraphy at HD2, showing the dominance of organic sediments at the site. For the key to sediment symbols, see Section 6.2.

6.5.3.2 Diatom assemblage

The diatom assemblage at HD2-1 can be divided into two distinct diatom zones (Fig. 6.16). Zone 1 is comprised predominantly of freshwater taxa, which make up c. 95% of the total diatom count. *Nitzschia sp.* are particularly numerous within this zone, which also has a limited number of salt tolerant taxa such as *Navicula halophila*. Zone 2 sees an increase in the proportion of salt intolerant taxa, with greater numbers of *Tabellaria fenestrata* and *Tabellaria flocculosa* present within the zone. Alongside this, salt tolerant taxa are lost from the diatom record at the start of this zone. Freshwater taxa continue to dominate the diatom assemblage, although this is predominantly through greater numbers of *Fragilaria lapponica.*

6.5.3.3 Environmental summary

The diatom assemblage from HD2-1 suggests that the site was situated above the point of marine influence, as freshwater species are dominant throughout the record (Fig. 6.16). There is no record of brackish or marine influence at the site, which corresponds with the results from HD1 and HD3. The site therefore acts as another limiting elevation for postglacial RSL at the location. No tephra layers were evident at this site and no radiocarbon samples were analysed. This is due to the proximity of the site to HD3, which has better chronological control.

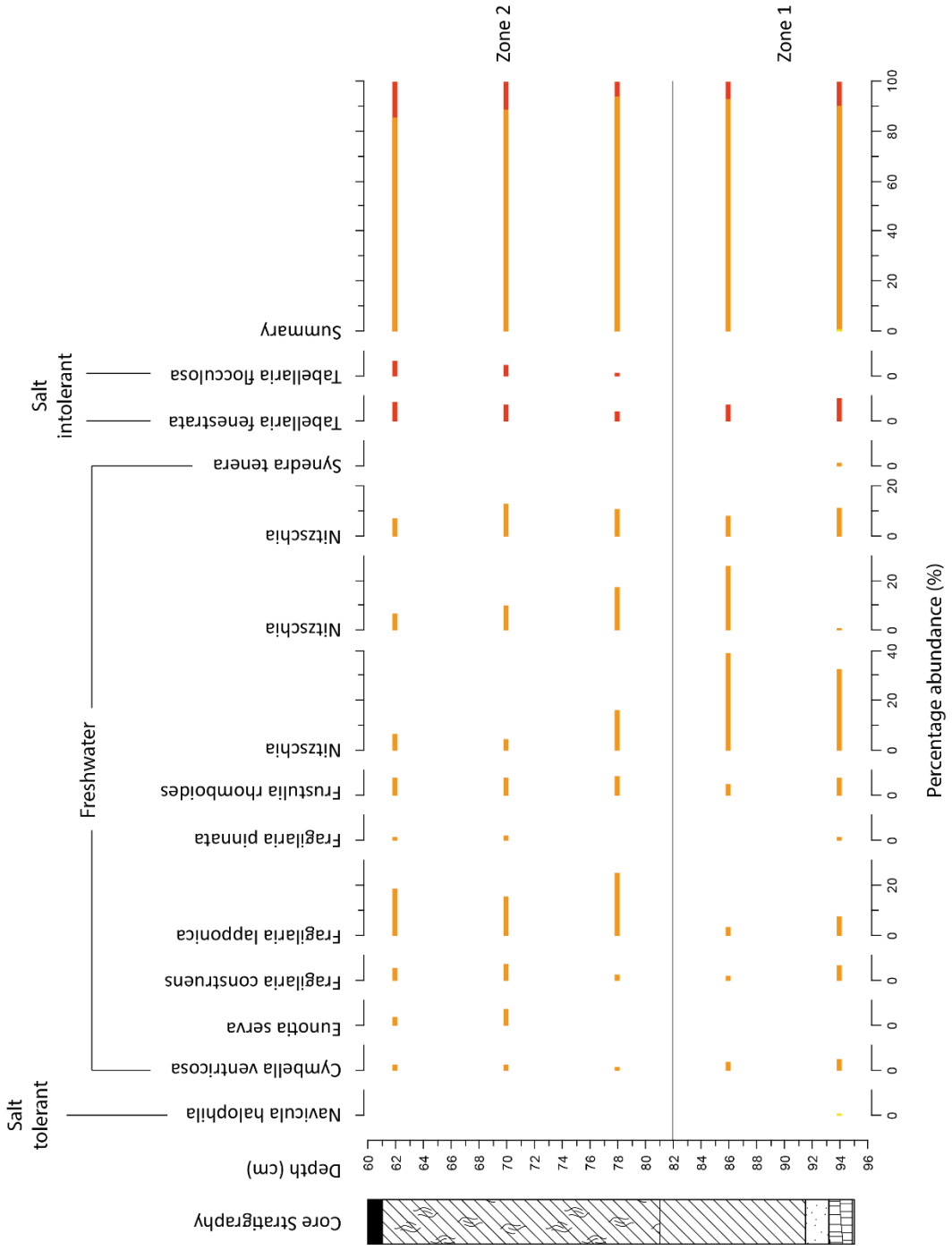

Figure 6.16 – Diatom assemblage at HD2-1 (>3% of the total diatom count) showing the dominance of freshwater conditions at the site. See Section 6.2 for the key to sediment symbols and colour classification.

6.5.4 Rekavik (REK1)

Sill elevation: 18.63 ± 0.50 m asl Site location: 66°24.500'N 23°0.441'W

RK1 is situated in Aðalvik and represents the westernmost point studied in Area D (Fig. 3.3). The sill was identified within the channel draining the present day lake. Survey points were taken within the present drainage channel in order to identify the lowest high point within the sequence (S5, Fig. 6.17). Information about the site can be found in Section 3.6.1 and Figs. 3.12 and 3.13.

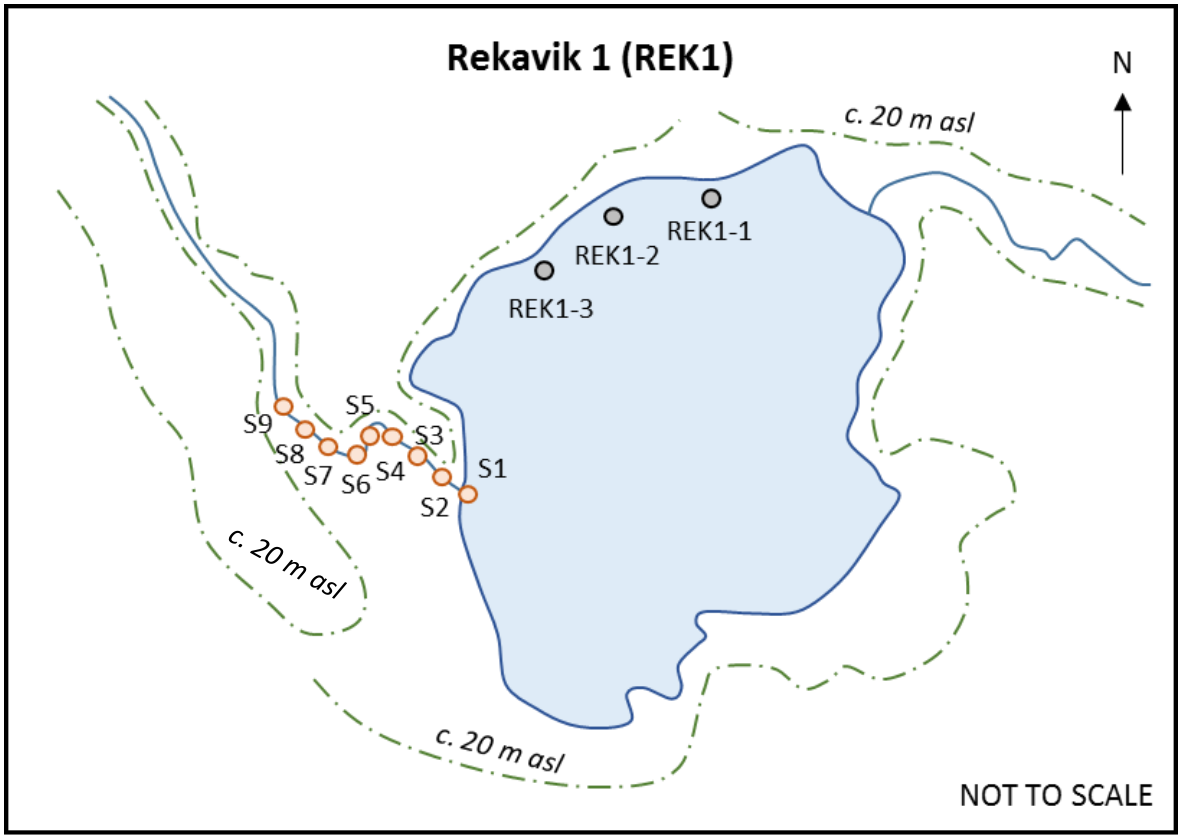

Figure 6.17 – Sill identification at REK1 showing the transect of survey points (orange), core sample locations (black), present lake basin (blue) and surrounding higher topography (green dashed line).

6.5.4.1 Site stratigraphy

Three sediment cores were extracted on the northern side of Rekavik lake in order to establish site stratigraphy (Fig. 6.18). The depth of sediments increased with proximity to the lake centre, with REK 1-3 being the furthest achievable point without use of a boat. A sediment sample was therefore extracted from REK1-3 (Fig. 6.18) for subsequent laboratory analysis. REK1-3 was selected due to the length of the available record and the interest of the core stratigraphy, which is summarised in Table 6.6.

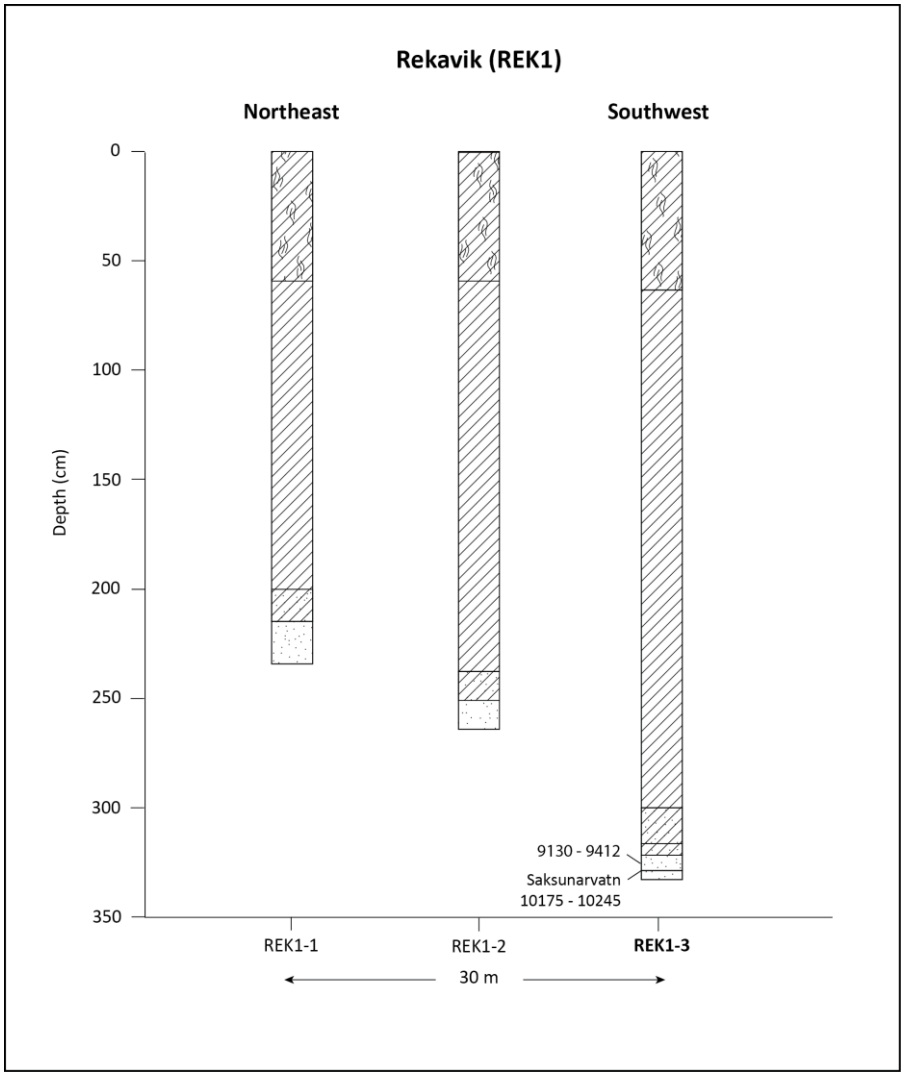

Figure 6.18 – Site stratigraphic profile for REK1. For the key to sediments, see Section 6.2.

Upper Boundary (cm)	Lower Boundary (cm)	Sediment Description	Tröels-Smith Classification
0	68	Mid-brown mixed organic material with limus, rootlets and seeds	Sh3 Ld1 Th+
68	300	Olive green-brown organic rich limus with sphagnum peat	Ld3 Th1
300	319	Olive green limus with grey silt	Ld3 Ag1
319	319.5	Dark grey silt	Ag4
319.5	325.5	Olive green limus with grey silt	Ld3 Ag1
325.5	329.5	Dark grey silt	Ag4
329.5	333	Mid brown silt with clay	Ag2 As2
333		Gravel/tephra	Gmaj4

Table 6.6 – Sediment description and Troels-Smith (1955) classification of the REK1-3 sediment core sample.

6.5.4.2 Diatom assemblage

At REK1-3, seven diatom samples were analysed and the resulting diatom record can be divided into three distinct zones (Fig. 6.19). Zone 1 is dominated by freshwater taxa, such as *Hannea arcus* (c. 40%) and *Meridion hiemale* (c. 18%), with limited numbers of brackish taxa also present. Within Zone 2, the dominant freshwater taxa change to *Fragilaria construens and Fragilaria pinnata*, which both represent c. 30-40% of the total diatom count. Limited numbers of brackish taxa are also present within this zone, but they fail to comprise more than 5% of the total diatom count. Zone 3 is comprised of freshwater and salt intolerant species and sees the loss of brackish taxa from the diatom assemblage. Within this zone, *Fragilaria construens* and *Fragilaria pinnata* continue to dominate the diatom assemblage and levels of *Fragilaria lapponica* increase through the zone.

6.5.4.3 Environmental summary

The diatom assemblage from REK1-3 demonstrates the dominance of freshwater conditions at the site (Fig. 6.19). However the occurrence of limited numbers of brackish taxa towards the base of the core sample suggests that the site may record occasional inundation by highest tide or storm events at the point of deposition. The site was therefore likely situated close to the highest tide level. REK1 is the highest lake basin surveyed in Area D and is situated close to the proposed local marine limit. Hence, the diatom record supports the interpretation of this feature, which likely represents the highest postglacial RSL in the region. One radiocarbon sample was analysed from 330 cm, which produced an age of 8275 ^{14}C a BP (9130-9412 cal. a BP). In addition, the Saksunarvatn tephra was identified at 333 cm (Fig. 5.2.3), which provides a second date for the sediment core sample (10200 cal. a BP; Lohne *et al.*, 2014) and a limiting date for basin isolation and subsequently marine limit formation.

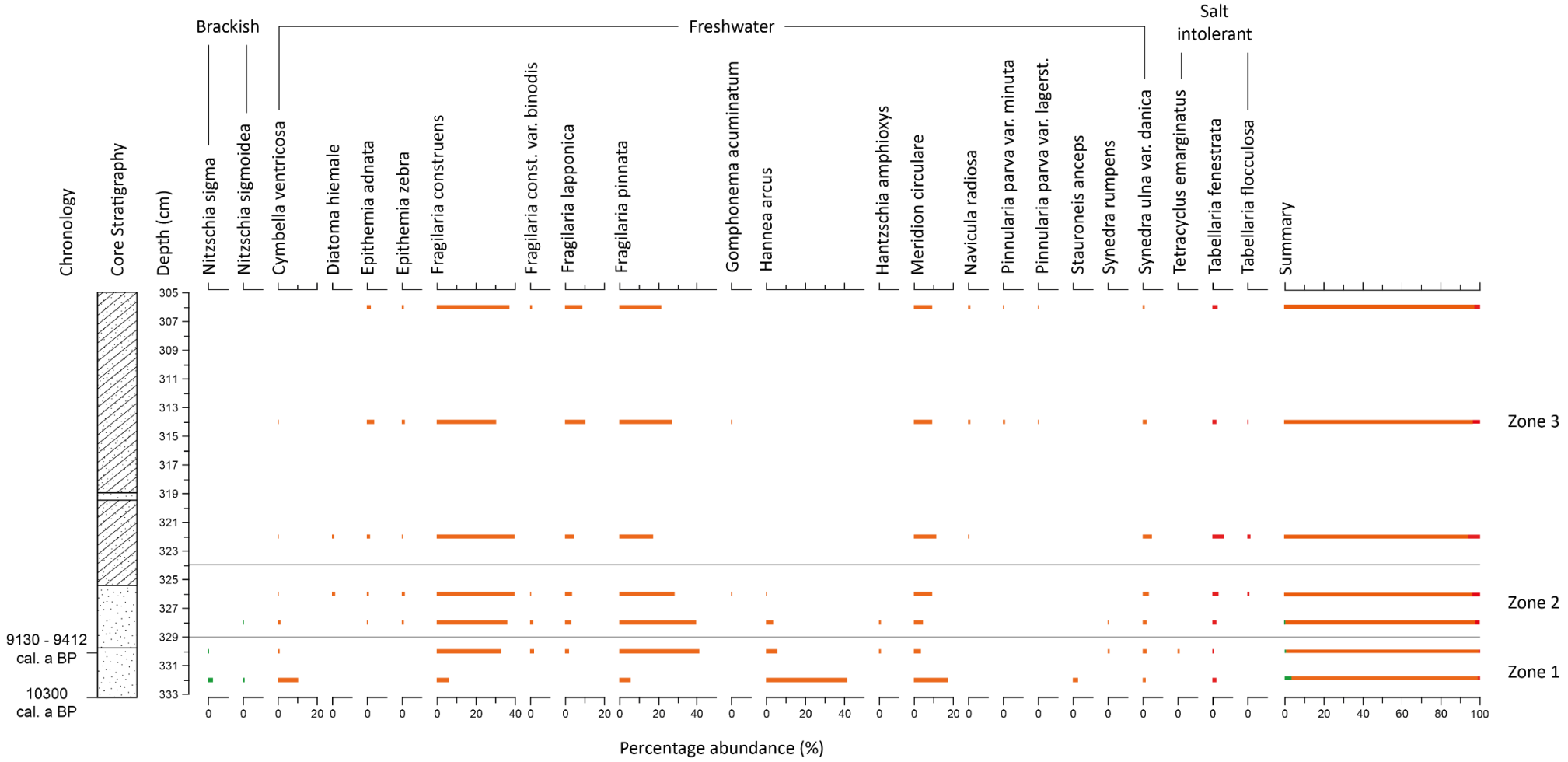

Figure 6.19 – Diatom assemblage at REK1-3 (>3% of the total diatom count), showing the transition from the short-lived brackish phase to freshwater dominance at the site. The key to sediment symbols and colour classification can be found in Section 6.2.

6.6 Area E – Vatnsfjörður, Vestfirðir

Initial investigation in Area E was undertaken by Dr Jeremy Lloyd in 2007 as part of the Vatnsfjörður Project (Milek, 2008), when samples were collected from Sveinhúsvatn (SHV1), Reykjanes 6 (RK6), Vatnsfjörður Home Field (VHF1) and Reykjanes 3 (RK3). Diatom analyses were undertaken on these samples as part of this research, alongside samples retrieved from additional sites. Within this study, samples were collected from Bolsvik Bay (BB1), Reykjanes 10 (RK10), Vatnsfjarðarnes 1 (VAT1), Vatnsfjarðarnes 2 (VAT2) and Grimhólsvatn (GR1). In addition, the marine limit was identified as part of this study at Laugadalur (30 m asl).

6.6.1 Bolsvik Bay (BB1)

Sample elevation: -0.50 ± 0. 25 m asl Site location: 65°56.392'N 22°29.029'W

Bolsvik Bay is an open coast site situated close to Vatnsfjörður farm (Section 3.6.2, Fig. 3.14 and 3.15). The sample elevation represents the top of the sample and was corrected to mean sea level through a timed tide measurement.

6.6.1.1 Site stratigraphy

One sediment sample was extracted using a spade from an archaeological inspection site at Bolsvik Bay (BB1). The sediment section comprised a basal mid-brown gravel-rich silty clay, overlain by a dark gravel-rich turfa peat and an upper gravel-rich silt (Fig. 3.15). The sediment stratigraphy is summarised in Table 6.7.

Upper Boundary (cm)	Lower Boundary (cm)	Sediment Description	Tröels-Smith Classification
0	11	Mid-brown gravel rich silt	Ag2 Gmaj2
11	16	Dark brown gravel rich turfa peat	Th2 Gmaj2
16	28	Mid brown gravel rich silt	Ag2 Gmaj2

Table 6.7 – Sediment stratigraphic profile at BB1.

6.6.1.2 Diatom assemblage

Six diatom samples were analysed for the BB1-1 sediment sample: two samples from the basal silt, two samples from the turfa peat and a final two samples from the upper silt layer (Fig. 6.20). The lowermost diatom samples demonstrate a high proportion of marine taxa such as *Cocconeis scutellum* and *Cocconeis stauroneiformis* within the total percentage composition. Despite this, there is also a clear freshwater influence within these two samples, with *Pinnularia borealis*

making up c. 20% of the total diatom count. Both diatom samples from the turfa peat deposit demonstrate a stronger freshwater influence at the site, with some incidence of salt tolerant and brackish taxa. The uppermost diatom sample, within the upper silt layer, had poor diatom preservation and it was therefore not possible to achieve a statistically reliable count from the sample.

6.6.1.3 Environmental Summary

The diatom assemblage from BB1-1 demonstrates a transition between marine dominance in the lower silt and freshwater dominance in the turfa peat deposit (Fig. 6.20). The diatom assemblage thus suggests a fall in RSL, with the uppermost silt likely representing a subsequent RSL rise to present sea level.. The dark brown gravel-rich turfa peat likely represents a coastal lowland environment. A radiocarbon sample was analysed from the turfa peat deposit; however, the age generated was determined as 'modern'. It was not possible therefore to determine an age for the proposed RSL lowstand recorded at the site.

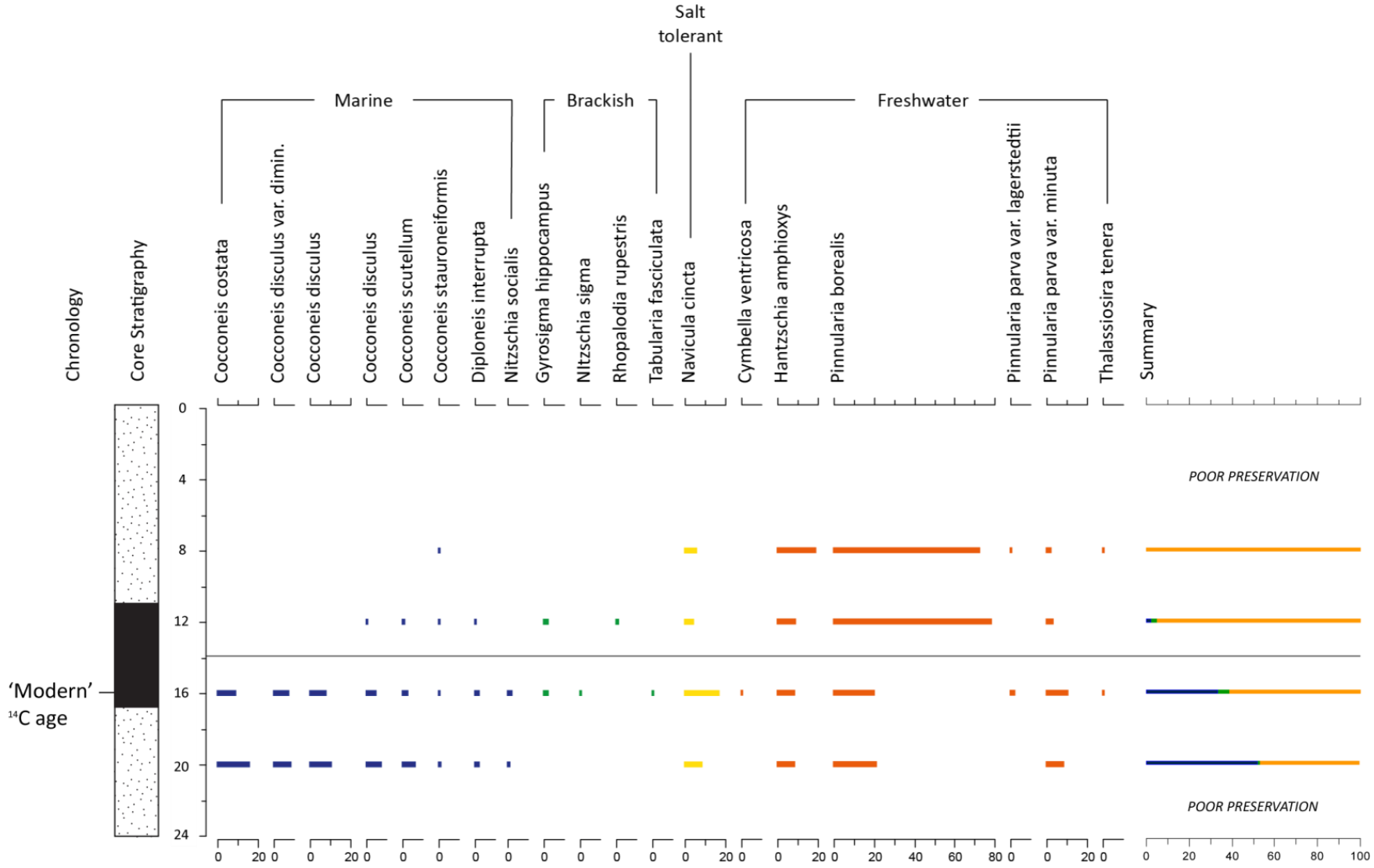

Figure 6.20 – Diatom assemblage from BB1-1 (>3% of the total count), showing the transition from brackish-marine to freshwater dominance. Figure key: Section 6.2.

6.6.2 Sveinhúsvatn (SHV1)

Sill elevation: 1.25 ± 0.30 m asl Site location: 65°56.210'N 22°28.193'W

SHV1 was initially investigated by Dr Jeremy Lloyd in 2007 and 2009 as part of the Vatnsfjörður Project, when two sediment samples were extracted from the site (Milek, 2008; 2011). Tephrochronological analyses were subsequently undertaken by Anderson (unpub.). Diatom analysis and radiocarbon samples from these sediment core samples were then completed as part of this research project. The sill elevation was determined by Dr Jeremy Lloyd (Lloyd, 2011).

6.6.2.1 Site Stratigraphy

Two sediment samples were retrieved from SHV1 in order to determine site stratigraphy. Both sediment cores were from the same location within the lake centre, as it was likely to yield the most complete sedimentary record. The stratigraphic profile of SHV1 can be summarised as grey silty clay with shell fragments, overlain by mid brown-grey silty clays. There are a series of tephra layers present within the stratigraphic sequence. As part of this research, the SVH1-1 sediment core was analysed, which is summarised in Table 6.8.

Upper Boundary (cm)	Lower Boundary (cm)	Sediment Description	Tröels-Smith Classification
135	170	Mid brown silt with clay	As2 Ag2
170	171	Tephra	Ag4
171	220	Mid brown-grey silty clay	As2 Ag2
220	221	Tephra	Ag4
221	245	Mid brown-grey silt with clay	Ag3 As1
245	270	Grey silty clay with shell fragments	Ag2 As1 part test 1
270	271	Tephra	Ag4
271	285	Grey silty clay with shell fragments	Ag2 As1 part test 1
285	295	Sediment lost during core extraction	-----
295	340	Grey silty clay with shell fragments	Ag2 As1 part test 1

Table 6.8 – Sediment composition of the SHV1-1 sediment core extracted in 2009 by Jerry Lloyd. Sediment depths are not corrected for water depth.

6.6.2.2 Diatom assemblage

The diatom assemblage from SHV1-1 can be divided into eight zones, demonstrating the transition from brackish-marine conditions to brackish-freshwater dominance (Fig. 6.21). Zone 1 demonstrates a clear brackish-marine signal, with *Cocconeis scutellum*, *Cocconeis stauroneiformis* and *Tabularia fasciculata* present throughout the zone. In Zone 2, the proportion of brackish species increases, particularly *Tabularia fasciculata* and *Thalassiosira tenera* with corresponding decreases in major marine components. Zones 3-6 demonstrate the transition to brackish water conditions although *Cocconeis scutellum* remains at c. 20% of the total assemblage throughout. In Zone 7, the proportion of freshwater species increases with *Fragilaria construens*, *Fragilaria pinnata* and *Synedra ulna var. danica* increasing to c. 5-10% at the top of the zone. Zone 7 also sees a decrease in the remaining marine species, with *Cocconeis scutellum* decreasing from c. 10% to c. 2% composition. Zone 8 shows the dominance of brackish and freshwater species within the diatom assemblage, with increasing numbers of *Fragilaria construens*, *Fragilaria lapponica* and *Fragilaria pinnata*. A limited number of marine diatoms were also recorded in this zone (c. 2%)

6.6.2.3 Environmental Summary

At SHV1-1, there is a clear transition from brackish-marine to brackish-freshwater dominance in the diatom assemblage from Zone 3 - 6 (Fig. 6.21). As a result, the diatom assemblage demonstrates a decrease in marine influence at the site. The sediment core benefits from good chronological control through both tephra analysis and radiocarbon dating. Three tephra samples were analysed from the SHV1 (Anderson, unpub.), which led to the identification of three distinct layers: Landnam 871AD (1079 cal. a BP), Eldgja 935AD (1015 cal. a BP) and Hekla 1693AD (257 cal. a BP). In addition, two radiocarbon samples were analysed at 218 cm and 228 cm returning dates of 2123 ± 35 ^{14}C a BP (1993-2161 cal. a BP) and 2269 ± 35 ^{14}C a BP (2156-2267 cal. a BP) respectively. It is clear that there is a mismatch between the ages generated by tephra analyses and the radiocarbon analyses, possibly a consequence of the bulk samples analysed at the site.

However, Sveinhúsvatn provides an opportunity to determine environmental and therefore RSL changes over the late Holocene within Area E. It is clear that at the time of settlement (871 ± 2 AD) Sveinhúsvatn was a coastal lagoonal environment, with high percentages of marine and brackish diatom taxa present within the diatom assemblage. Between 1079 cal. a BP and 1015 cal. a BP, the site becomes increasingly dominated by brackish diatom taxa, representing a fall in RSL at the location. This is further demonstrated by the subsequent increases in freshwater taxa within the diatom assemblage. It is clear that the isolation process is not yet complete at Sveinhúsvatn, with the site now representing a brackish-water lake environment close to the limit of regular marine inundation.

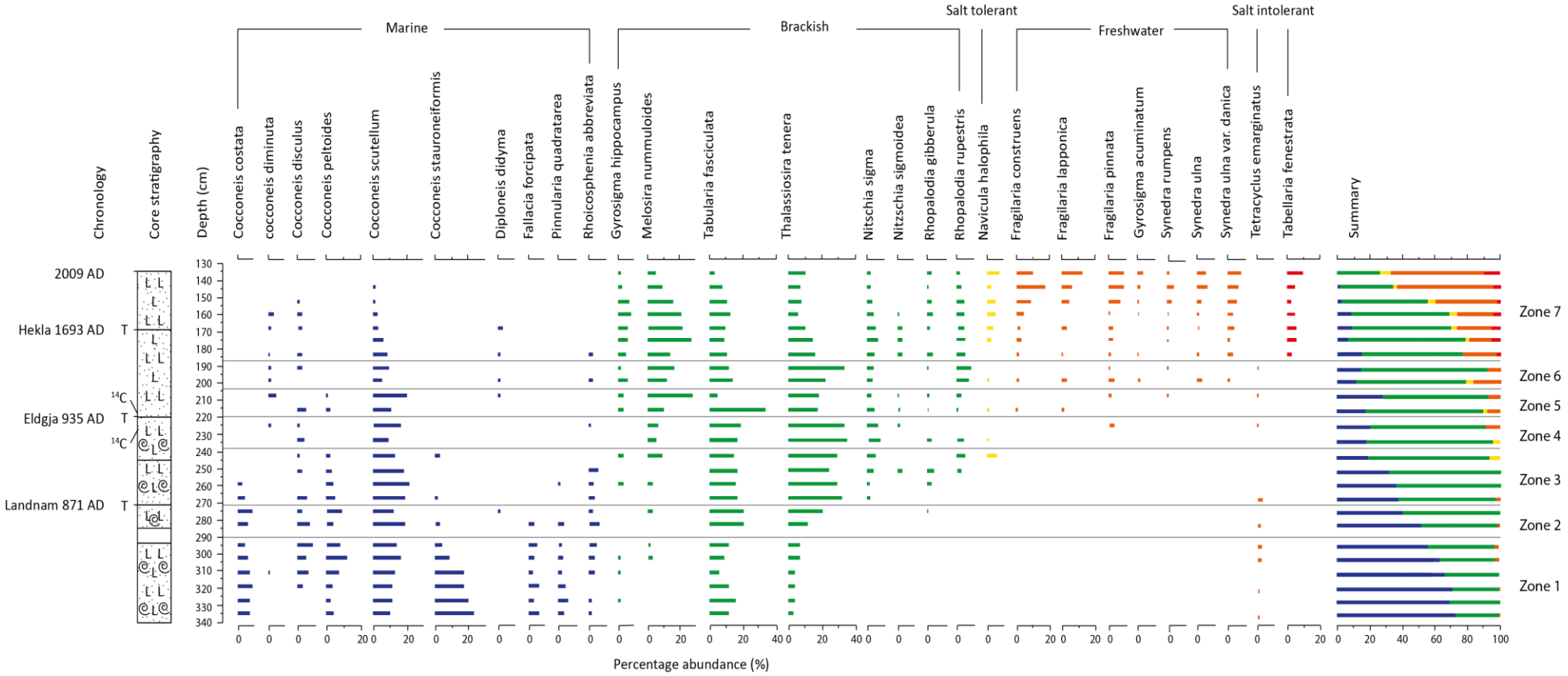

Figure 6.21 – Diatom assemblage from SHV1-1 (>3% of the total count) showing the transition from marine-brackish to brackish-freshwater influence. The site is still connected to the sea at high tide. For the key to sediment symbols and colour classifications, see Section 6.2.

6.6.3 Reykjanes 6 (RK6)

Sill elevation: 2.30 ± 0.30 m asl Site location: 65°55.193'N 22°25.588'W

RK6 was initially investigated by Dr Jeremy Lloyd (Lloyd, unpub.) as part of the Vatnsfjörður Project (Milek, 2011). Sediment samples were extracted from the site and stored at Durham University. Diatom and radiocarbon analyses of these sediment core samples were undertaken as part of the current research. The sill elevation was determined by a grid of cores (Lloyd, unpub.).

6.6.3.1 Site stratigraphy

A total of 16 sediment cores were extracted along two transects in 2009 by Dr Jeremy Lloyd, in order to establish the site stratigraphy. The sediment depth was recorded at each core location to determine the deepest sediment section for subsequent laboratory analysis, with core sample depths ranging from 0.8 m to 1.3 m. Following the determination of site stratigraphy, one sample was extracted from RK6-4 using a Russian Corer. The sediment profile at RK6 comprises a basal olive green organic material, overlain by a lower peat layer, olive green organic material and middle peat layer. Above this, an upper olive green organic layer is recorded, overlain by an upper turfa peat layer. The sediment sample at RK6-4 is summarised in Table 6.9.

Upper Boundary (cm)	Lower Boundary (cm)	Sediment Description	Tröels-Smith Classification
70	75	Dark brown turfa peat	Th4
75	81	Olive green-brown humified organic material	Sh3 Th1
81	107	Brown turfa peat	Th4
107	110	Olive green-brown humified organic material	Sh4
110	113	Brown turfa peat	Th4
113	120	Olive green-grey well humified organic material with silt	Sh3- Ag1+

Table 6.9 – Sediment stratigraphy of the RK6-4 sediment core.

6.6.3.2 Diatom assemblage

Within the RK6-4 diatom assemblage, four diatom zones have been identified (Fig. 6.22). Zone 1 is dominated by brackish and freshwater taxa, each representing c. 40% of the total assemblage. These proportions are made up of a limited number of taxa, such as *Nitzschia ovalis, Fiagilaria pinnata* and *Nitzschia amphibia*. Within the zone, a limited number of marine taxa are also present although no species makes up more than 5% of the total assemblage. Zone 2 sees a

reduction in the percentage of brackish taxa and the loss of all marine taxa from the diatom assemblage. In turn, there is an increase in the percentage and number of freshwater taxa recorded. Zone 3 demonstrates a further reduction in brackish taxa, which now represent c. 10% of the total diatom count. Freshwater taxa now dominate the diatom assemblage and salt intolerant taxa also increase in number. The uppermost zone within the record, Zone 4, comprises freshwater and salt intolerant species, with the remaining brackish species being lost from the assemblage.

6.6.3.3 Environmental summary

The diatom assemblage demonstrates a reduction in the percentages of marine and brackish taxa in the diatom record and subsequent freshwater dominance of the assemblage. The diatomological isolation contact can be identified at 100 cm. The diatom assemblage records a fall in RSL at the site. A bulk organic radiocarbon sample at 100 cm returned an age of 8299 ± 38 ^{14}C a BP (9201 - 9432 cal. a BP), providing an age for this fall in RSL. No tephra deposits were present within the sedimentary record.

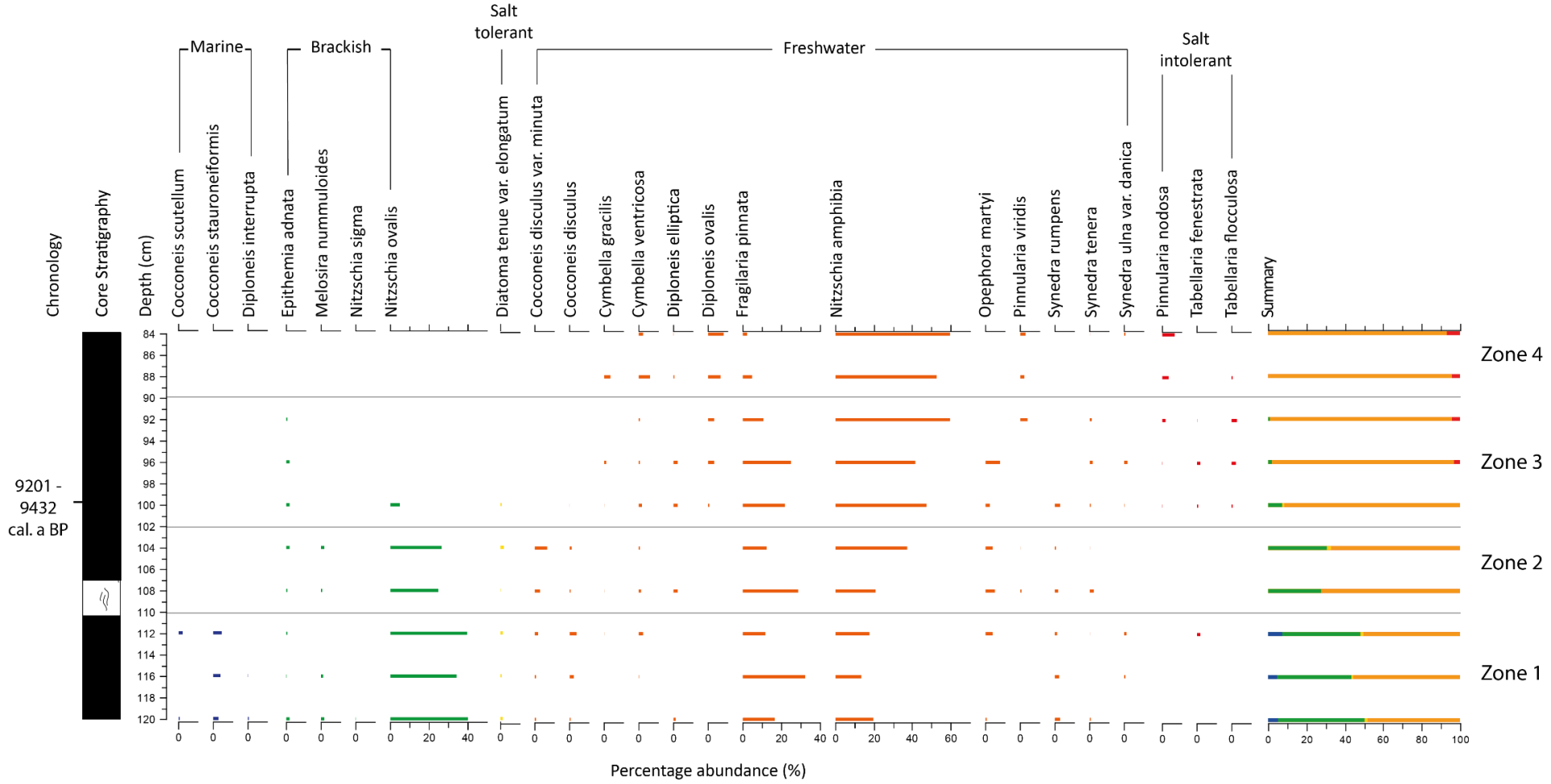

Figure 6.22 – Diatom assemblage from RK6-4 (>3% of the total diatom count) demonstrating the transition from marine-brackish to freshwater dominance at the site. For the key to sediment symbols and colour classification used, see Section 6.2.

6.6.4 Vatnsfjörður Home Field (VHF1)

Sample elevation: 4.50 ± 0.30 m asl Site location: 65°56.324'N 22°30.000'W

VHF1 was initially investigated by Dr Jeremy Lloyd in 2009 (Lloyd, unpub.) as part of the Vatnsfjörður Project (Milek, 2011). Subsequent diatom and chronological analyses were undertaken as part of the current research. The site is a coastal lowland, with the recorded elevation representing the top of the extracted sediment sample. Information about the site location and sample characteristics can be found in Section 3.6.2 and Figs. 3.14 and 3.16.

6.6.4.1 Site stratigraphy

The VHF1 site was surveyed in 2009 by Dr Jeremy Lloyd, with one sediment sample being extracted for subsequent laboratory analysis. The stratigraphy of the site can be summarised as a basal blue-grey sandy gravel (78-90 cm) overlain by extensive turfa peat deposits (0-78 cm). A series of samples were taken from 60-80 cm within the sediment profile (VHF1-1), in order to investigate the diatom assemblage across the sediment transition.

6.6.4.2 Diatom assemblage

Five diatom samples were prepared from the bagged samples retrieved from VHF1-1 (Fig. 6.23). The lowermost diatom sample at 79 cm demonstrated poor preservation and so it was not possible to achieve a statistically reliable sample. The remaining diatom samples can be divided into two zones. Zone 1 demonstrates a higher proportion of brackish taxa than Zone 2, making up c. 10% of the total diatom assemblage. Zone 2 has a lower brackish component at c. 5% of the diatom assemblage. There is a clear dominance of freshwater diatom taxa throughout the site assemblage.

6.6.4.3 Environmental summary

The diatom assemblage from VHF1-1 shows a dominance of freshwater taxa throughout the sediment profile, with the levels of brackish taxa diminishing up-profile, suggesting a decreased marine influence at the site through time (Fig. 6.23). The low proportion of brackish taxa and lack of marine diatoms suggest that the site records conditions at higher elevations within the tidal frame. One radiocarbon sample was taken from the site at 69 cm and returned an age of 4886 ± 36 ^{14}C a BP (5584 - 5664 cal. a BP).

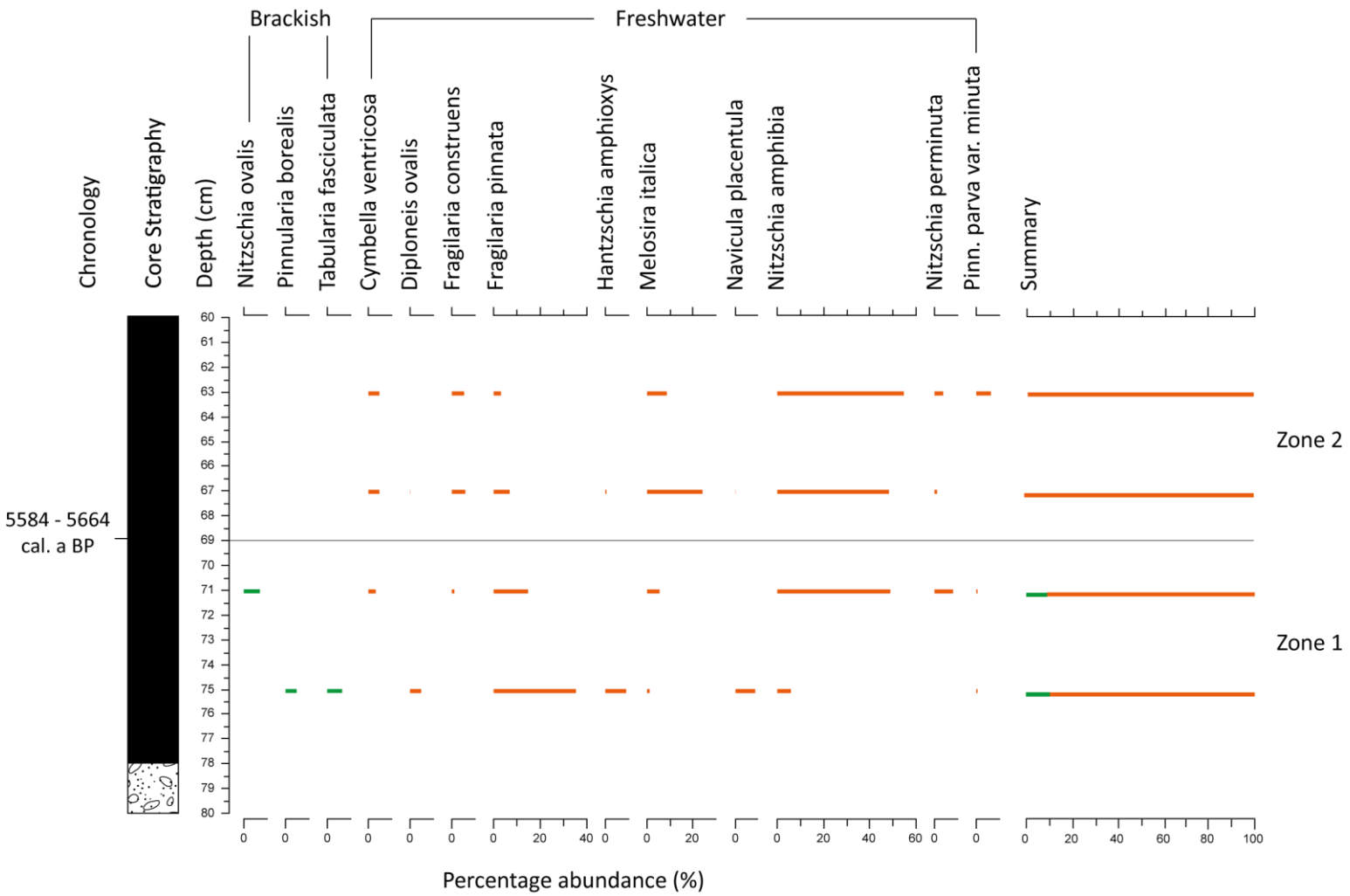

Figure 6.23 – Diatom assemblage from VHF1-1 (>5% of the total diatom count) showing the transition from brackish to freshwater dominance at the site. Figure key: Section 6.2.

6.6.5 Reykjanes 3

Sill elevation: 6.20 ± 0.30 m asl Site location: 65°54.171'N 22°25.069'W

RK3 was initially surveyed by Dr Jeremy Lloyd in 2009 (Lloyd, unpub,) as part of the Vatnsfjörður Project (Milek, 2011). One sediment sample was retrieved from the isolation basin site and stored at Durham University for subsequent laboratory analysis. Diatom and tephrochronological analyses were undertaken on this sediment core sample as part of the current research. Information about the location and morphology of the isolation basin can be found in Section 3.6.2 and Figs. 3.14 and 3.16.

6.6.5.1 Site stratigraphy

Two transects were cored at RK3 to establish site stratigraphy. Sediment depths ranged from 0.8 m to 2.4 m, with a sediment core for subsequent laboratory analysis being extracted from the deepest section sampled (RK3-5). The site stratigraphy comprised a basal brown mixed organic material with silt overlain by a grey silt, brown mixed organic material and upper peats. The sediment composition of the sediment core (RK3-5) is summarised in Table 6.10.

Upper Boundary (cm)	Lower Boundary (cm)	Sediment Description	Tröels-Smith Classification
125	150	Dark brown organic material with some silt and abundant rootlets	Sh3 Th1 Ag+
150	162	Dark grey silt with some organic material and abundant rootlets	Ag3 Sh1 Th+
162	175	Olive green-brown organic material with rootlets and some silt	Sh3 Ag1+ Th+

Table 6.10 – Sediment stratigraphy of the RK3-5 core sample.

6.6.5.2 Diatom assemblage

Five zones can be identified within the diatom assemblage from RK3-5 (Fig. 6.24). Zone 1 is dominated by brackish taxa, which represent c. 85-90% of the total diatom count within the zone. In particular, there are high percentages of *Melosira nummuloides* and *Tabularia fasciculate* within the zone. In addition, there is a small percentage of marine taxa present within the zone, such as *Tryblionella apendiculata.* Within Zone 2, the percentage of freshwater taxa within the record increases, predominantly through the occurrence of *Fragilaria pinnata* that represents c. 20% of the diatom count. There is a reduction in *Tabularia fasciculata* within this zone, although numbers of *Melosira nummuloides* remain constant at c. 60% of the total diatom count. Within Zone 3, the proportion of brackish species reduces greatly, with *Melosira nummuloides* reducing

to c. 10% of the total diatom count at the end of the zone. This reduction in brackish species is linked to an increase in freshwater diatom taxa such as *Fragilaria pinnata.* Zone 3 also has a limited number of salt tolerant species recorded, which represent c. 10% of the total diatom count. Zone 4 is characterised by the loss of the majority of brackish taxa, although limited numbers of individual species are still present. Finally, Zone 5 is characterised by freshwater and salt intolerant taxa.

6.6.5.3 Environmental summary

The diatom assemblage demonstrates a decrease in marine-brackish influence at the site (Fig. 6.24), representing a fall in RSL. The limited numbers of marine taxa in the basal sample suggests that the basal section of the retrieved core sample represents an environment part way through the isolation process. Full marine conditions are thus not represented in the retrieved sample. One radiocarbon sample was sampled from 145 cm, which returned an age of 3602 ± 37 ^{14}C a BP (3862 - 3931 cal. a BP). No tephra deposits were recorded within the sediment core sample.

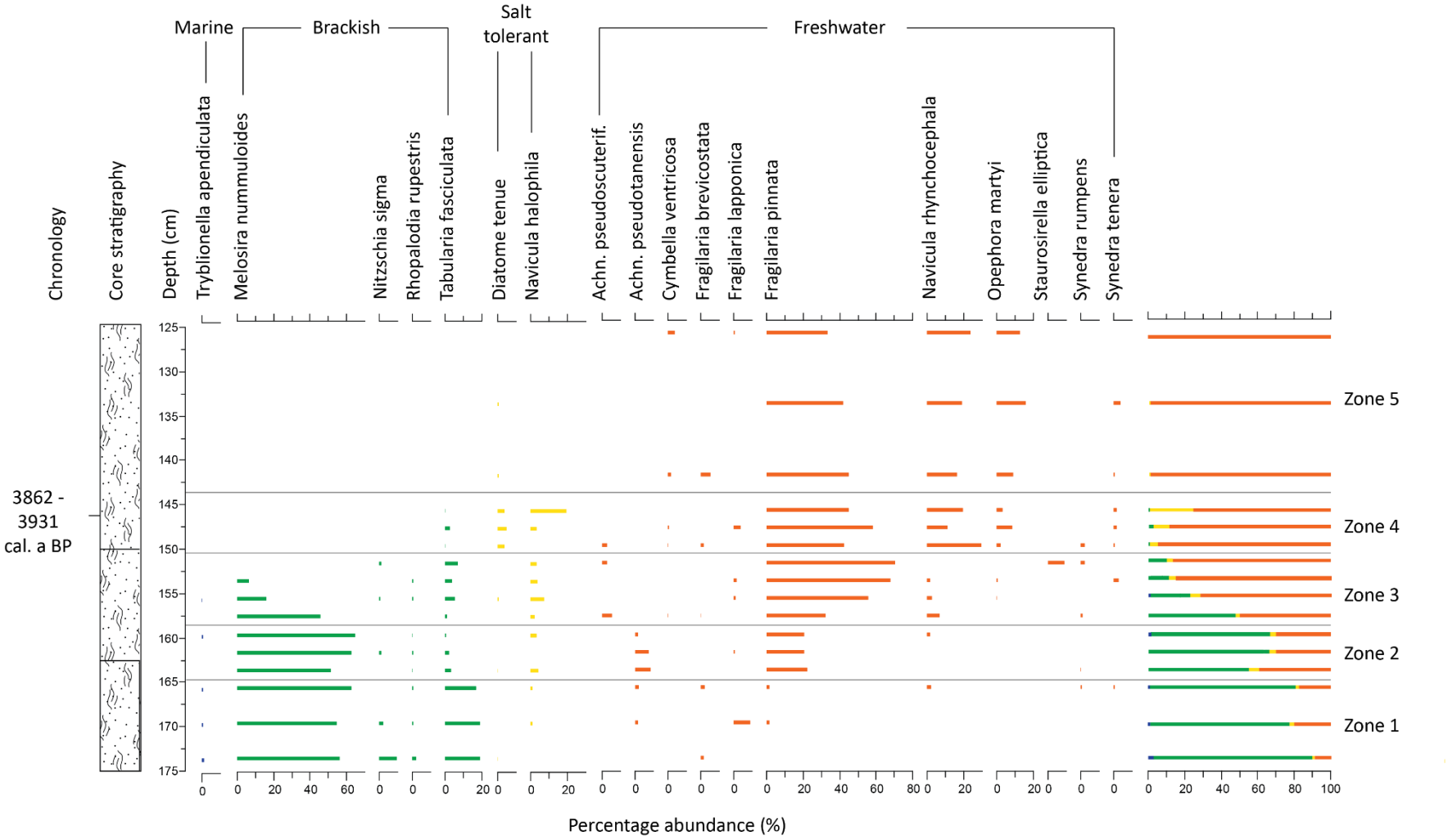

Figure 6.24 – Diatom assemblage from RK3-5 (>3% of the total diatom count) showing the transition from marine-brackish to freshwater dominance at the site. Key: Section 6.2.

6.6.6 Reykjanes 10 (RK10)

Sill elevation: 16.50 ± 0.30 m asl Site location: 65°54.321'N 22°25.184'W

RK10 is an isolation basin site which was sampled as part of this research project. The sill elevation is based on a grid of cores to the east of the isolation basin, at the lowest point in the surrounding topography (S7, Fig. 6.25). Information about the site location can be found in Section 3.6.2 and Figure 3.14.

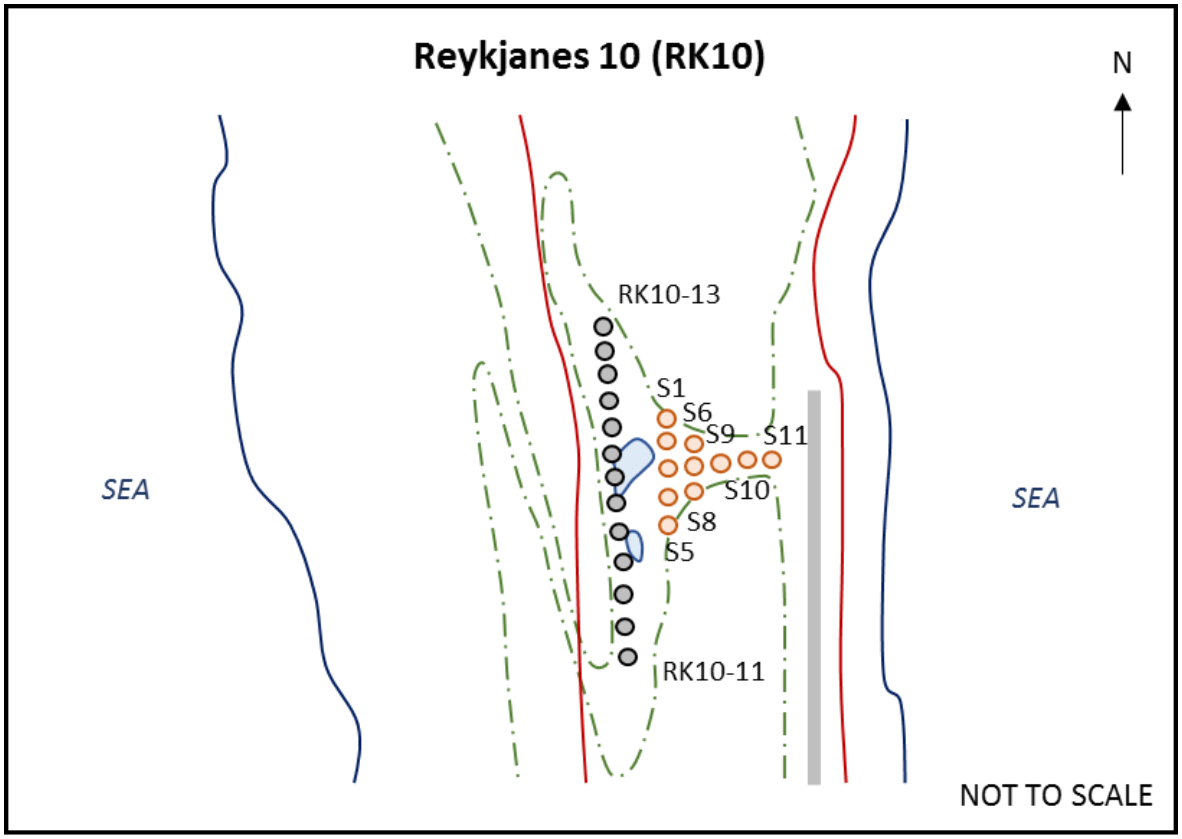

Figure 6.25 – Sill identification at RK10 (S7), including the sill core locations (orange), sediment core locations (black), present lakes (light blue), present coastline (dark blue), road (red solid line), airstrip (grey line) and higher topography (green dashed line). For clarification of core numbers, see Fig. 6.26.

6.6.6.1 Site stratigraphy

Thirteen sediment cores were extracted along one transect across the Reykjanes 10 (RK10) site in order to establish the underlying stratigraphy. RK10 is characterised by extensive limus deposits overlain by turfa peat (Fig. 6.26). All of the sediment cores terminated in gravel and several cores recorded tephra deposits of variable thickness. One sediment sample was retrieved at RK10-5 which is summarised in Table 6.11.

Upper Boundary (cm)	Lower Boundary (cm)	Sediment Description	Tröels-Smith Classification
0	201	Dark brown turfa peat	Th4
201	248	Olive green limus with plant fragments	Ld3 Sh1
248	280	Dark grey tephra	Ag4
280	289	Olive green grey limus	Ld4
289	296	Gravel	Gmaj4

Table 6.11 – Sediment composition of the RK10-5 sediment core sample.

6.6.6.2 Diatom assemblage

The diatom assemblage from RK10-5 can be divided into two distinct diatom zones (Fig. 6.27). At the beginning of Zone 1, marine taxa represent c. 30% of the total diatom count, reducing to c. 5% at the termination. This is predominantly caused by a decrease in the percentage of *Cocconeis stauroneiformis*. There is a concurrent increase in the proportion of salt tolerant and freshwater species through this zone, principally caused by increases in *Fragilaria pinnata* and *Navicula thorodsseni nov. spec.* Within the upper zone, Zone 2, brackish and marine taxa are no longer recorded within the diatom assemblage. The proportions of salt tolerant and freshwater species remain relatively constant throughout this zone, although there if variability in the percentages of individual taxa. Two principal changes in Zone 2 relate to the percentages of *Fragilaria construens* and *Navicula thorodsseni nov. spec* (Fig. 6.27).

6.6.6.3 Environmental Summary

Within the diatom assemblage from RK10-5, there is a clear reduction in the proportion of marine and brackish diatom taxa (Fig. 6.27). The diatomological isolation contact is therefore evident at 237 cm, denoting a fall in RSL at the site. The chronology for the site is based on one radiocarbon sample, which was taken at 238 cm and returned an age of 8894 ± 41 ^{14}C a BP (9887-10190 cal. a BP). As noted in Chapter 5, the Saksunarvatn tephra has also been identified within the core sample at 248 cm (10200 cal ka BP).

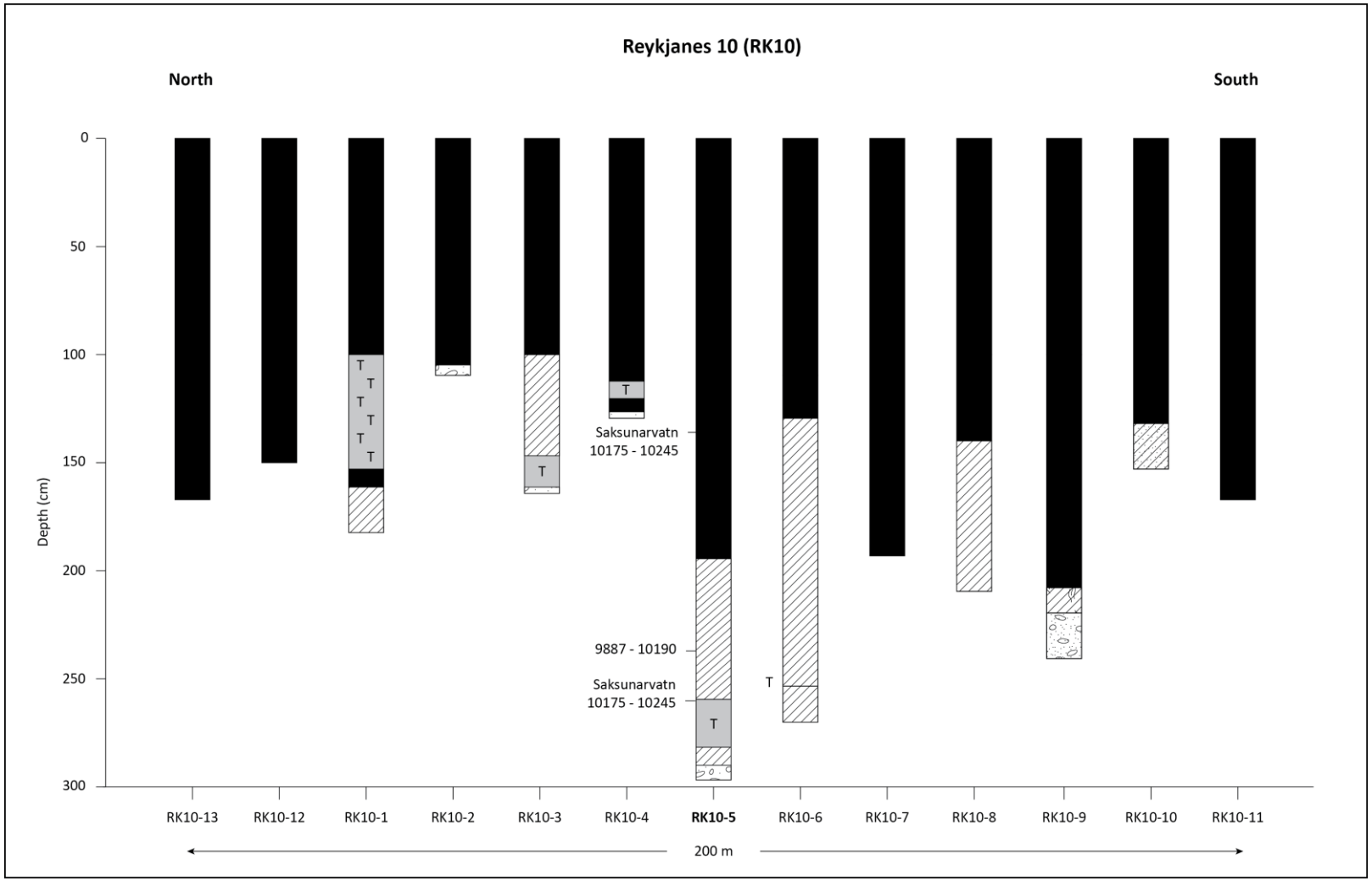

Figure 6.26 – Site stratigraphy at RK10 showing the extensive peat deposits at the site, alongside the variable quantities of tephra. Key to sediment symbols: Section 6.2.

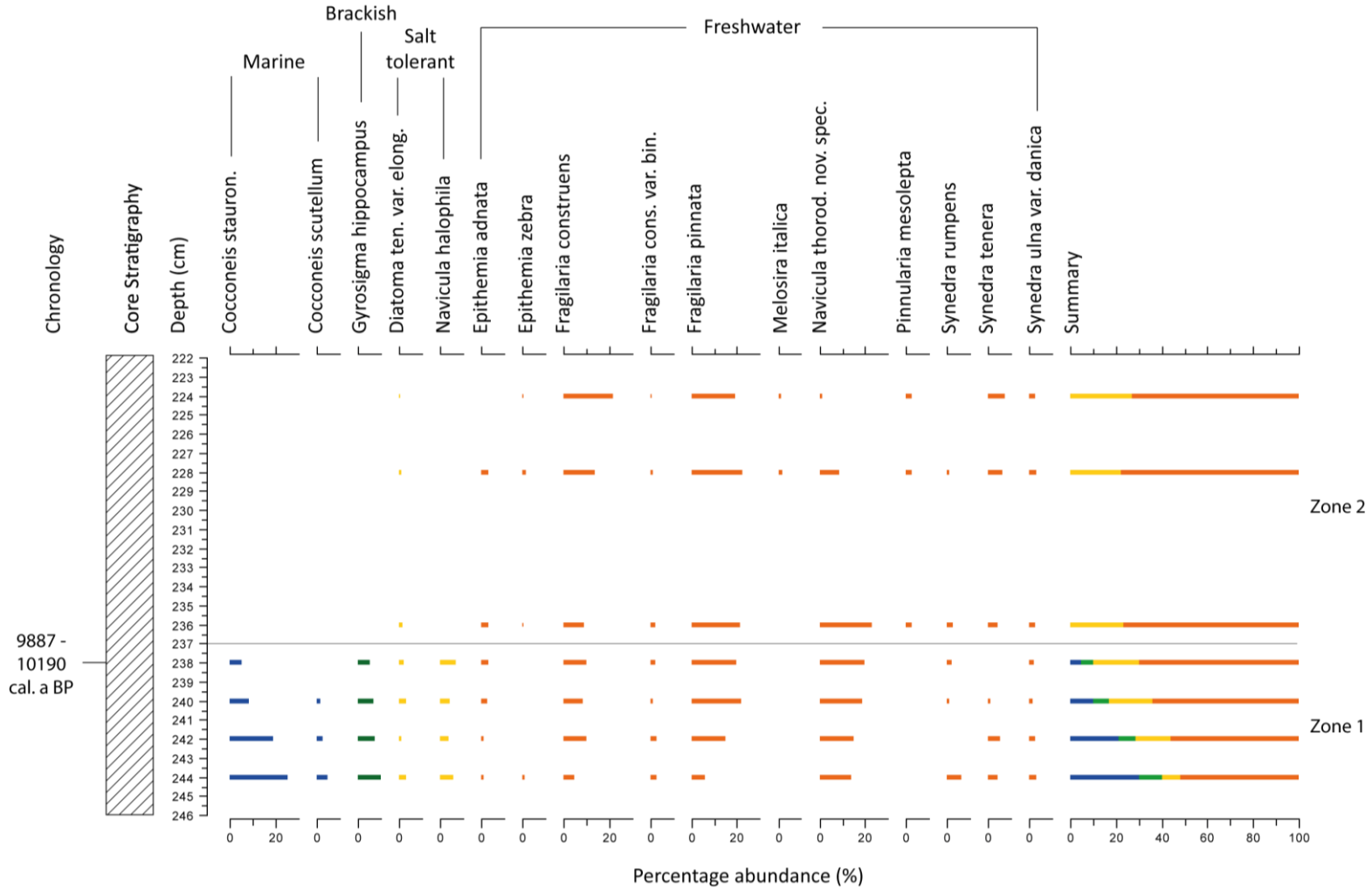

Figure 6.27 – Diatom assemblage at RK10-5 (>5% of the total diatom count) showing the transition from marine-brackish to freshwater dominance at the site. Figure key: Section 6.2.

6.6.7 Vatnsfjarðarnes 1 (VAT1)

Sill elevation: 22.2 ± 0.30 m asl Site location: 66°25.142'N 22°38.776'W

VAT 1 is situated on the Vatnsfjarðarnes peninsula, Vatnsfjörður, Vestfirðir (Section 3.6.2; Fig. 3.14), with sediment samples being retrieved as part of this research. The sill was identified through a grid of cores to the northwest of the basin (S9, Fig. 6.28). Information about the morphology of the site can be found in Fig. 3.16.

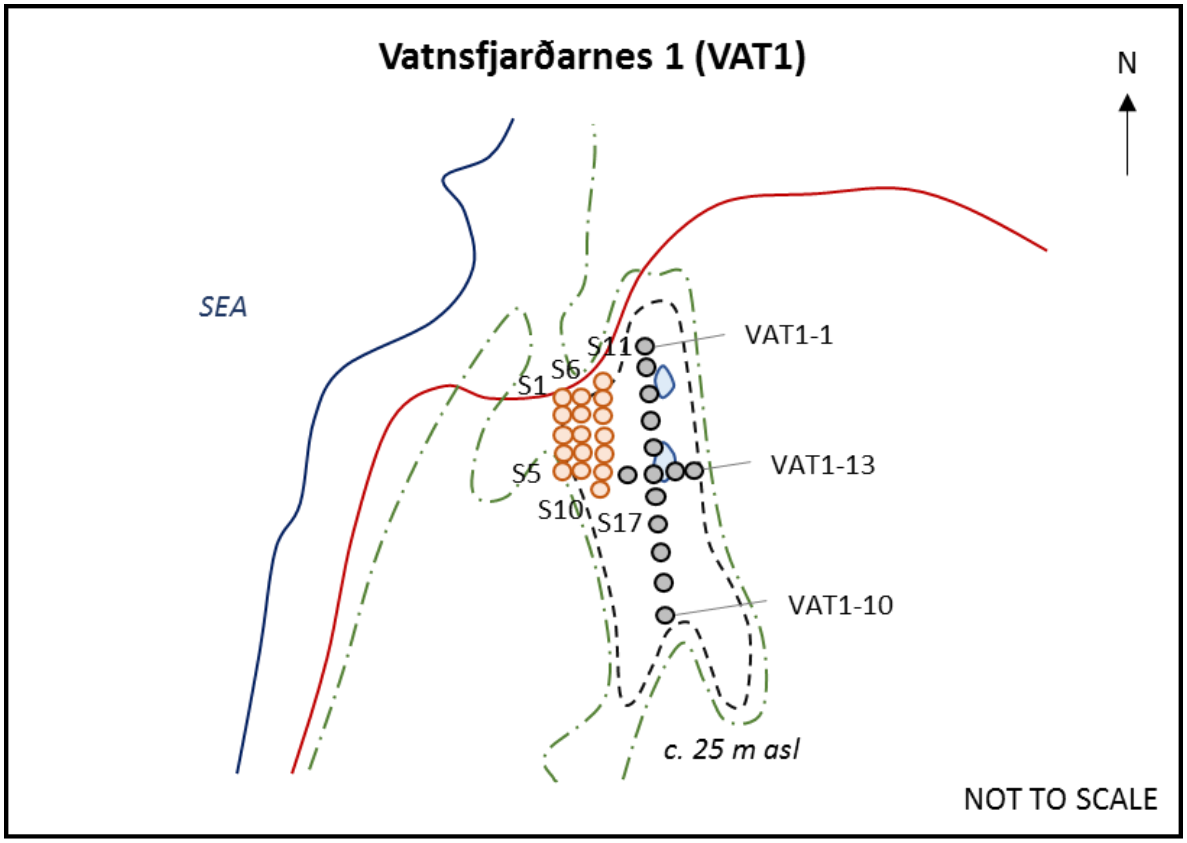

Figure 6.28 – Sill identification at VAT 1, showing the location of the sill survey points (orange dots), sample core locations (black dots), present coastline (dark blue line), infilled basin (black dashed line), road (red solid line) and higher surrounding topography (green dashed line).

6.6.7.1 Site stratigraphy

Thirteen sediment cores were extracted along two perpendicular transects at the VAT 1 site in order to establish the underlying stratigraphy. Transects 1 and 2 record a basal gravel overlain by silty sand, limus and peat deposits (Fig. 6.29 and 6.30). Tephra deposits were present in a number of the extracted sediment cores although the thickness of these layers varied between core samples. One sediment sample was extracted at VAT1-6 (Fig 6.29 and 6.30), which provided the deepest sediments. The composition of the core sample is summarised in Table 6.12.

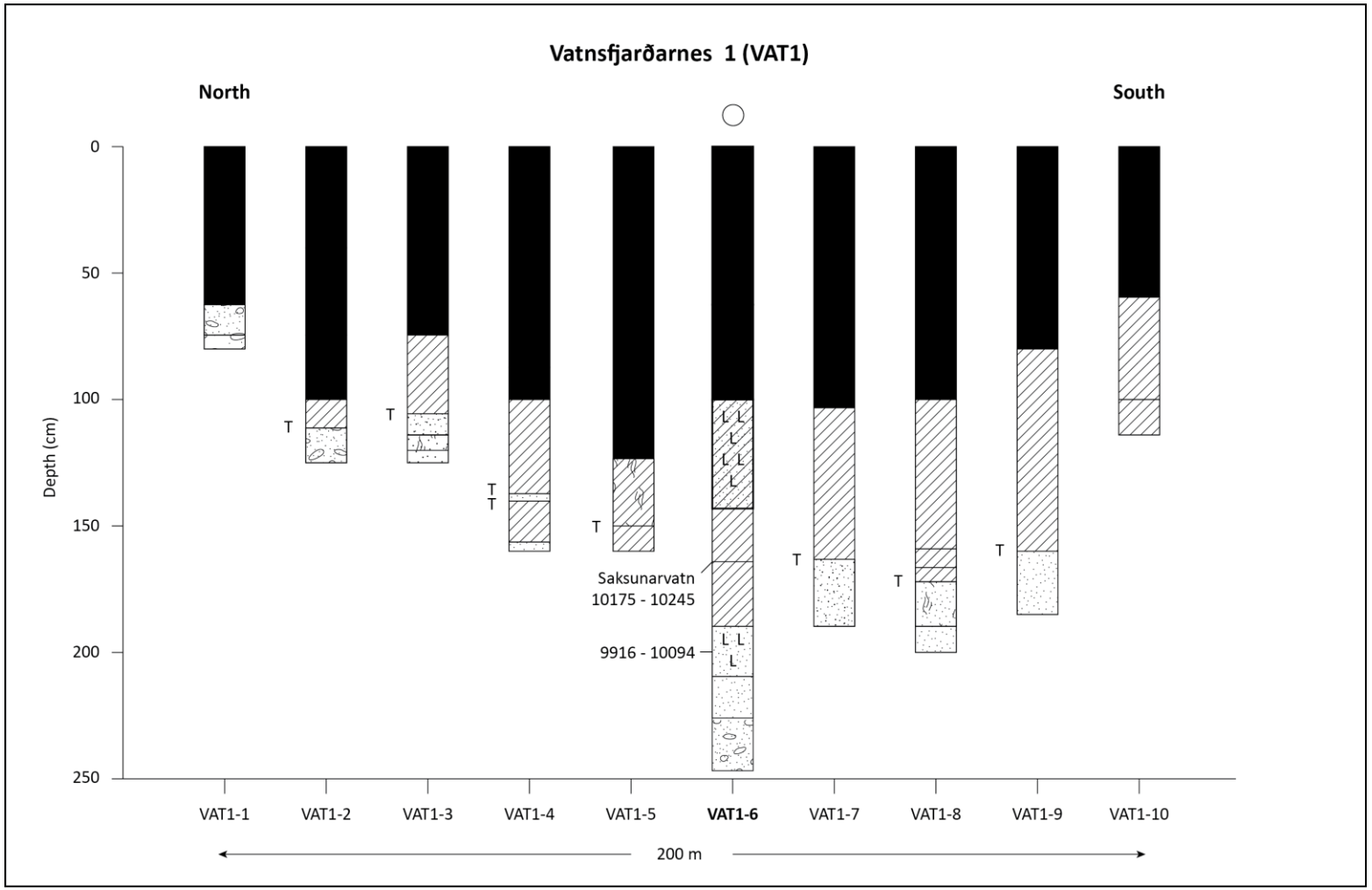

Figure 6.29 – Site stratigraphic long profile at VAT1 demonstrating the underlying sediment composition. VAT1-6 represents the centre point of the two transects. Key: Section 6.2.

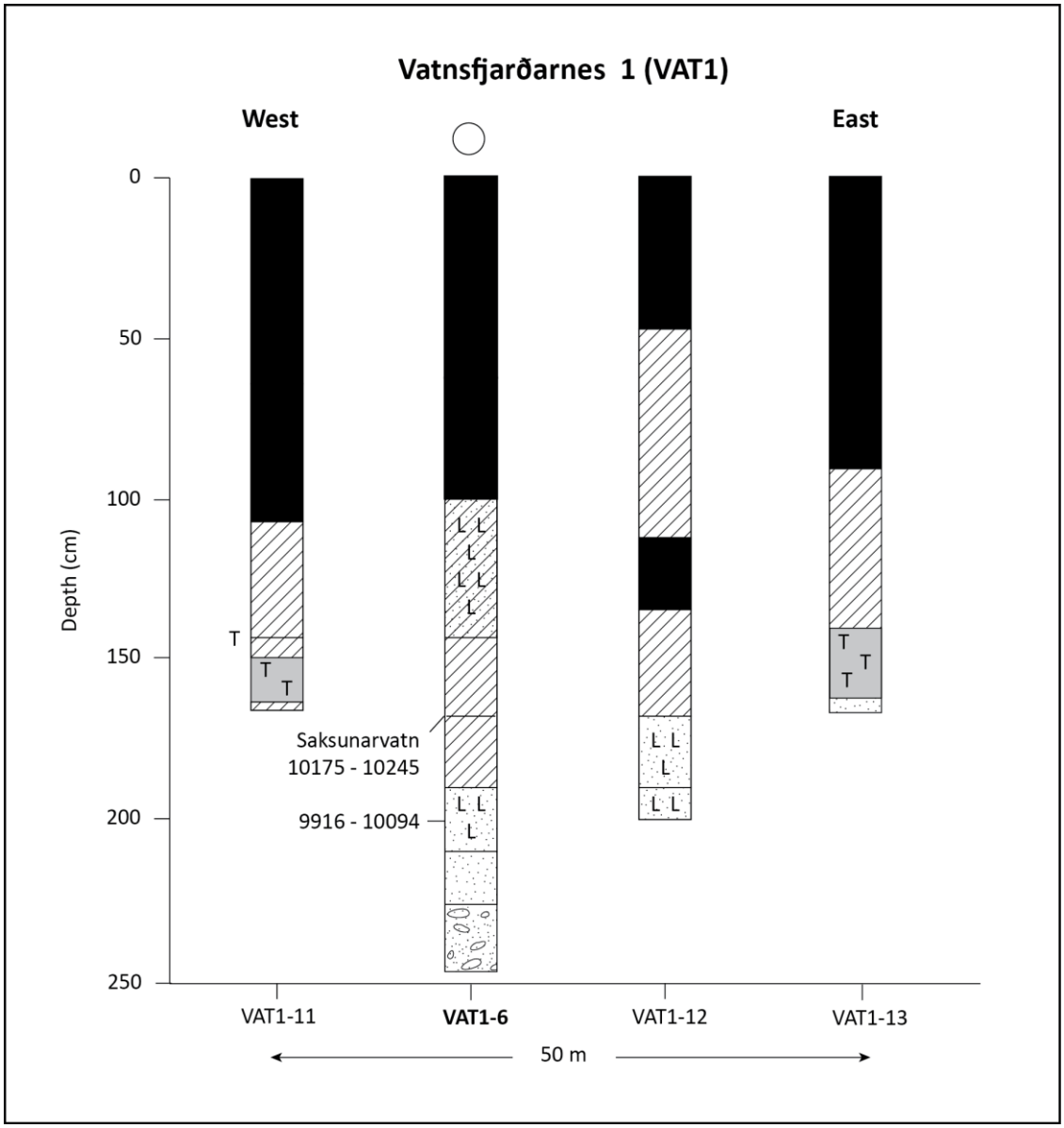

Figure 6.30 – Site cross-profile at VAT1 highlighting the stratigraphic profile of the site. Key: Section 6.2.

Upper Boundary (cm)	Lower Boundary (cm)	Sediment Description	Tröels-Smith Classification
0	100	Dark brown turfa peat	Th4
100	144	Olive green limus with silt and clay	Ld2 As1 Ag1
144	163	Olive green limus	Ld4
163	165	Dark grey tephra	Ag4
165	180	Olive green limus	Ld4
180	210	Grey silt with clay	Ag3 As1
210	225	Grey silt	Ag4
225	247	Gravel	Gmaj4

Table 6.12 – Sediment composition of the VAT1-6 sediment core sample.

6.6.7.2 Diatom assemblage

The diatom assemblage from VAT1-6 demonstrates a clear transitional sequence and can be divided into four distinct diatom zones (Fig. 6.31). Zone 1 is dominated by brackish-marine taxa, with lesser percentages of salt tolerant taxa also present. Within Zone 2, there is a reduction in the numbers of brackish diatom taxa and marine taxa are lost from the diatom record. There is a concurrent increase in freshwater diatom taxa, both in terms of the range and percentages of individual taxa. Zone 3 sees a further reduction in the percentage of brackish diatom taxa and an increase in a number of freshwater taxa, such as *Fragilaria brevicostata, Fragilaria construens* and *Fragilaria pinnata.* The percentage of *Diatoma tenue var. elongatum* also increases through this zone, but the overall proportion of salt tolerant species remains constant. The uppermost zone, Zone 4, is dominated by freshwater conditions, shown by further increases of freshwater taxa and reductions in the salt intolerant taxa such as *Diatoma tenue var. elongatum.* The diatomological isolation contact is identified at 204 cm.

6.6.7.3 Environmental summary

The diatom assemblage from VAT1-6 demonstrates a decrease in marine influence at the site, representing a fall in RSL at the location, as shown by the transition from Zone 1 to Zone 4 (Fig. 6.31). One radiocarbon sample was analysed from VAT1-6 at the isolation contact and returned an age of 8947 ± 39 ^{14}C a BP (9916 - 10094 cal. a BP). The tephra sample at 163 cm returned a geochemical signature similar to the Saksunarvatn tephra. This older age may mean that the isolation at VAT1 is more likely to have occurred at the older point of the calibrated age range from the radiocarbon sample.

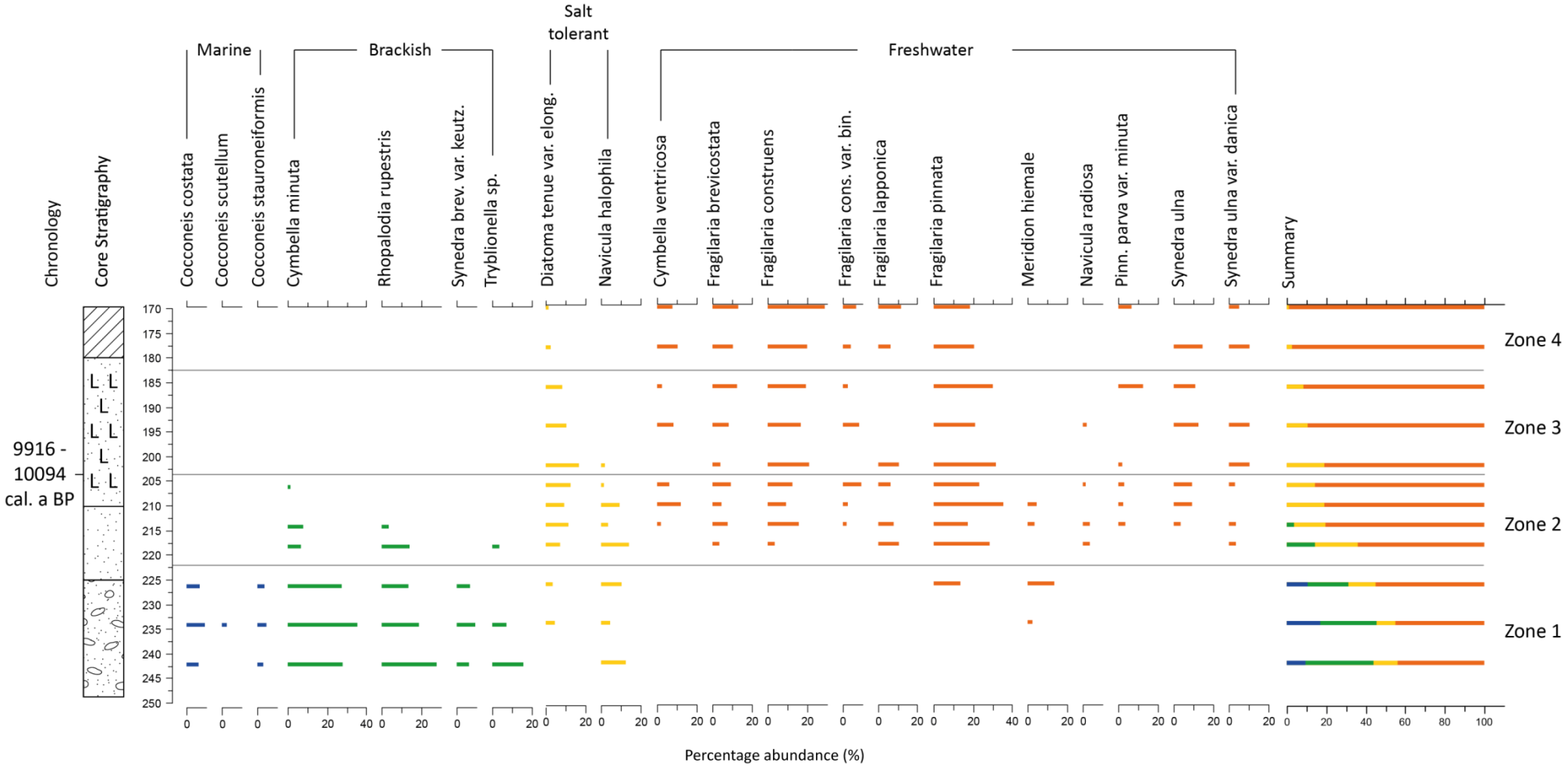

Figure 6.31 – Diatom assemblage from VAT1-6 (>3% of the total diatom count) showing the transition from brackish-marine to freshwater dominance at the site. For the key to sediment symbols and colour classifications, see Section 6.2.

6.6.8 Vatnsfjarðarnes 2 (VAT2)

Sill elevation: 29.50 ± 0.30 m asl Site location: 65°57.553'N 22°30.956'W

VAT 2 was first investigated as part of this PhD research and the sill was identified through a transect of cores within the present drainage channel to the north of the basin. The lowest highpoint within this transect was identified as the sill location (S5, Fig. 6.32). Information about the basin morphology and location can be found in Section 3.6.2 and Figs. 3.14 and 3.17.

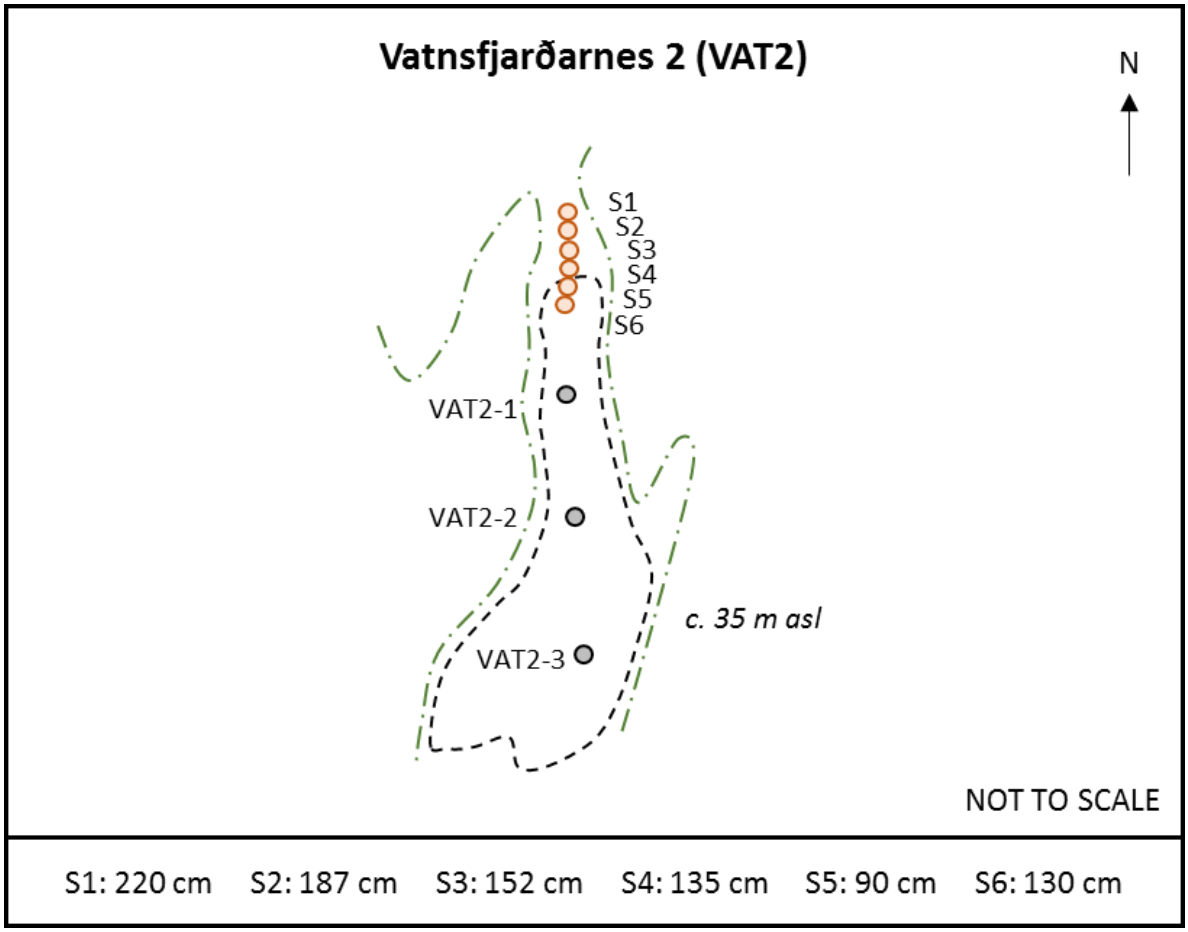

Figure 6.32 – Sill identification at VAT2 (S5), showing the transect of sill cores (orange dots), core sample locations (black dots), basin extent (black dashed line) and higher surrounding topography (green dashed line), alongside the sill core depths to the underlying bedrock.

6.6.8.1 Site stratigraphy

Three sediment cores were retrieved from VAT 2 in order to establish the underlying site stratigraphy (Fig. 6.33). The deepest sediment core comprised a basal silty clay, overlain by limus and peat deposits. VAT2-2 and VAT2-3 both terminated at gravel, whilst VAT2-1 terminated on rock. A sample for laboratory analysis was retrieved from VAT2-1. The sediment composition of this sample is summarised in Table 6.13.

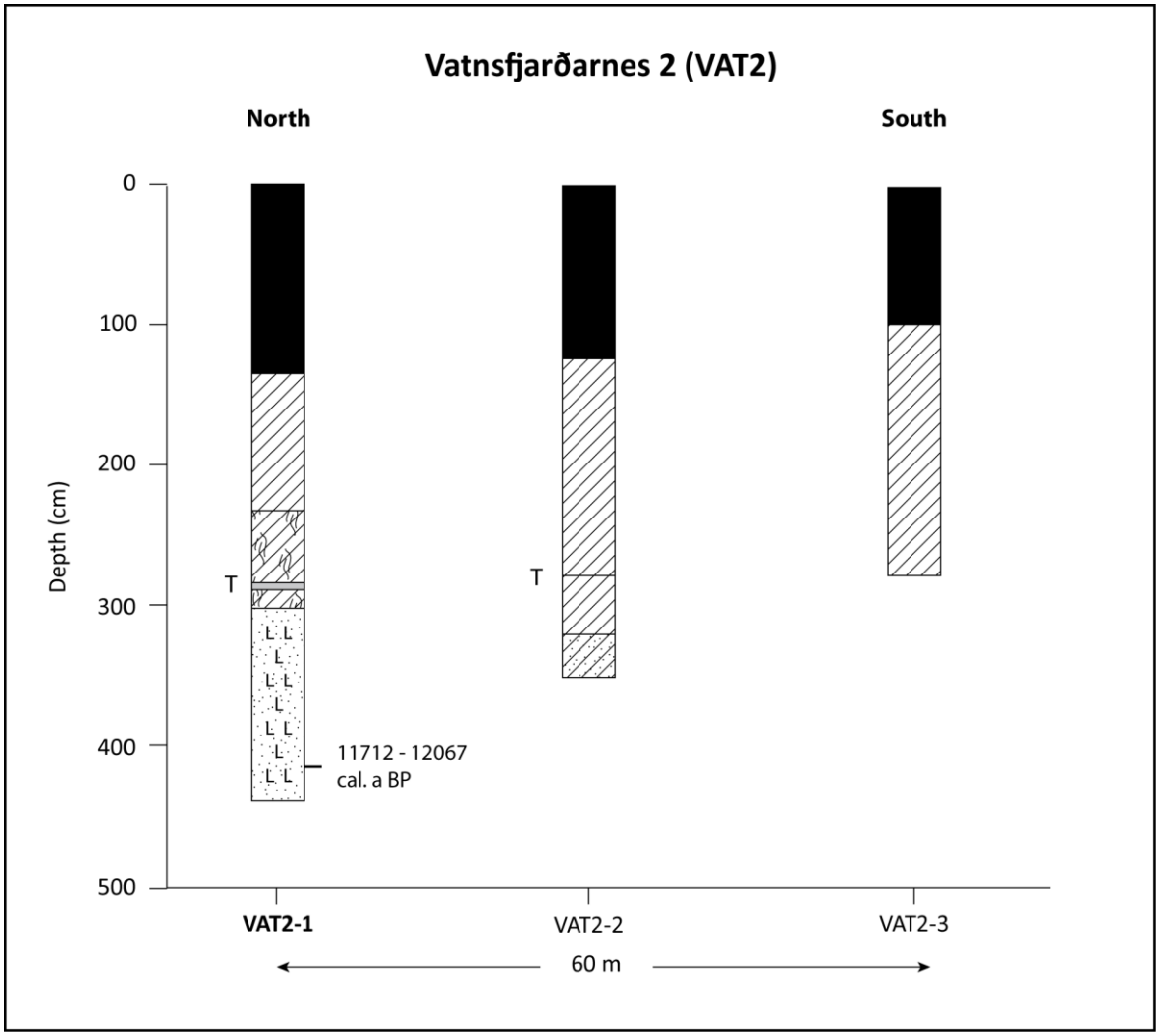

Figure 6.33 – Site stratigraphic profile for VAT2 showing the dominance of organic sediments at the site.

Upper Boundary (cm)	Lower Boundary (cm)	Sediment Description	Tröels-Smith Classification
0	130	Dark brown turfa peat	Th4
130	230	Olive green limus	Ld4
230	278	Olive green limus with abundant organic material	Ld3 Sh1
278	287	Dark grey tephra	Ag4
287	301	Olive green limus with abundant organic material	Ld3 Sh1
301	442	Grey silt with clay	Ag3 As1

Table 6.13 – Sediment composition of the VAT2-1 sediment core sample.

6.6.8.2 Diatom assemblage

The diatom assemblage from VAT2-1 can be divided into two zones, with each zone being dominated by freshwater taxa (Fig. 6.34). The lowermost zone, Zone 1, comprises predominantly freshwater taxa, with a limited percentage of salt tolerant taxa, such as *Diatoma tenue var. elongatum* and *Navicula halophila.* The percentage of *Fragilaria lapponica* increases through this zone, alongside a reduction in *Fragilaria construens var. binodis.* Similar transitions between *Fragilaria* species have been noted in other diatom assemblages from Area E. Within Zone 2, *Firagilaria lapponica* becomes the dominant taxa within the diatom assemblage, representing between 40% and 60% of the total diatom count within the zone. In addition, there is a small number of brackish diatom taxa recorded, although freshwater taxa continue to make up c.95% of the total diatom count.

6.6.8.3 Environmental summary

The diatom assemblage from VAT2-1 suggests that the site was dominated by freshwater conditions and therefore situated above tidal inundation (Fig. 6.34). Thus, the diatom record suggests that the sill was situated above MHWST. The short lived brackish event within the diatom assemblage may therefore represent a storm event rather than a prolonged higher RSL. A clear transitional sequence is not evident within the diatom assemblage. It is possible that the sediment sample is not sufficiently deep to record a previous marine-brackish influence at the site, but the termination of the sediment core on rock would suggest that this is unlikely. One radiocarbon sample was analysed from the site at 428 cm, which returned an age of 10188 ± 42 ^{14}C a BP (11712 - 12067 cal. a BP). Due to the lack of a clear transitional sequence within the VAT2-1 sediment sequence, the tephra deposit at the site did not undergo geochemical analysis.

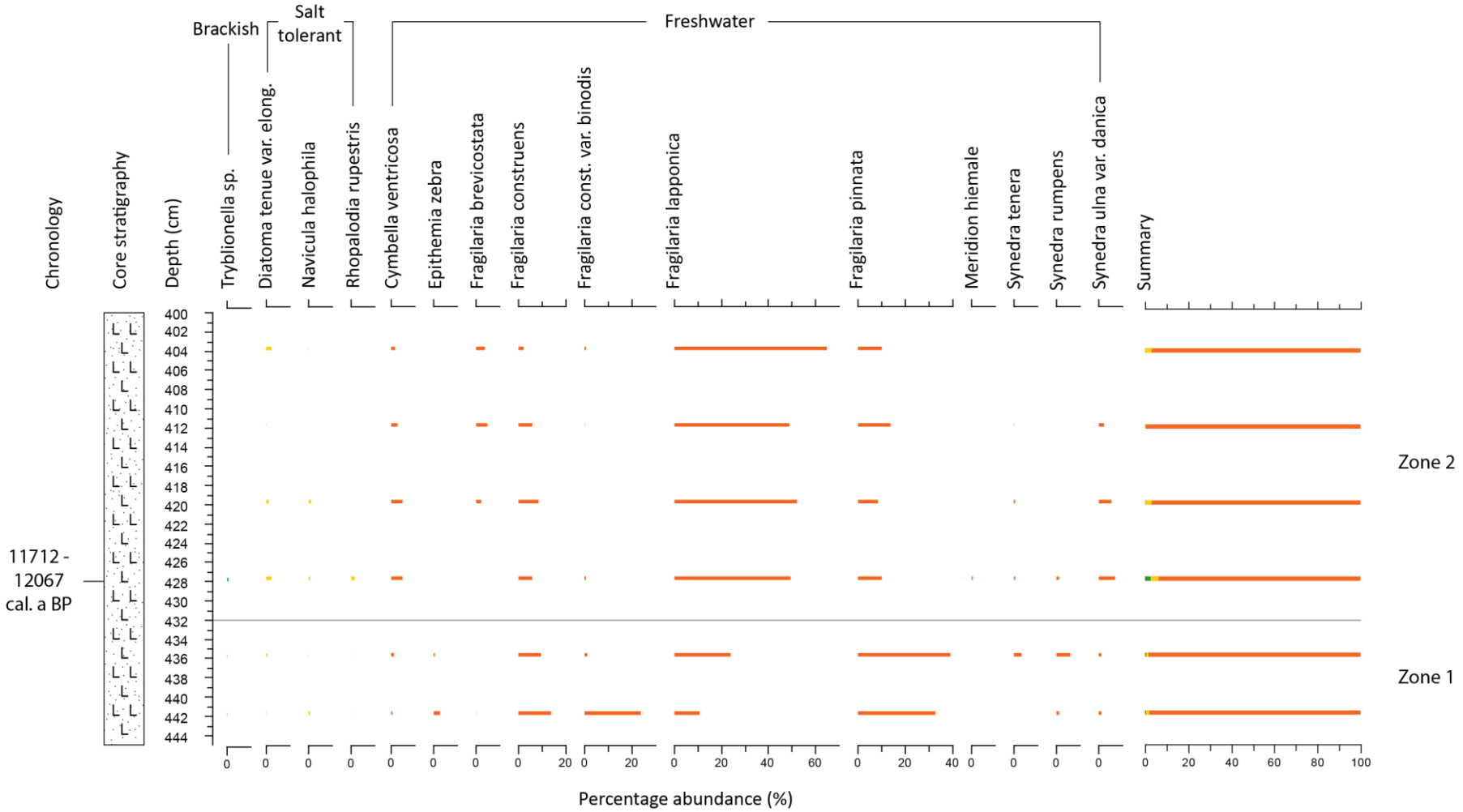

Figure 6.34 – Diatom assemblage from VAT2-1 (>5% of the total diatom count) showing the dominance of freshwater species at the site. For the key to sediment symbols and colour classifications, see Section 6.2.

6.6.9 Grimhólsvatn (GR1)

Sill elevation: 28.60 ± 0.30 m asl Site location: 66°0.053'N 22°39.353'W

GR1 was initially investigated as part of this research and is situated close to the local marine limit (Section 3.6.2 and Fig. 3.14 and 3.17). The sill was identified within the present drainage channel through the coring of a transect of cores (S2, Fig. 6.35). The sill was determined as the lowest high point along this transect.

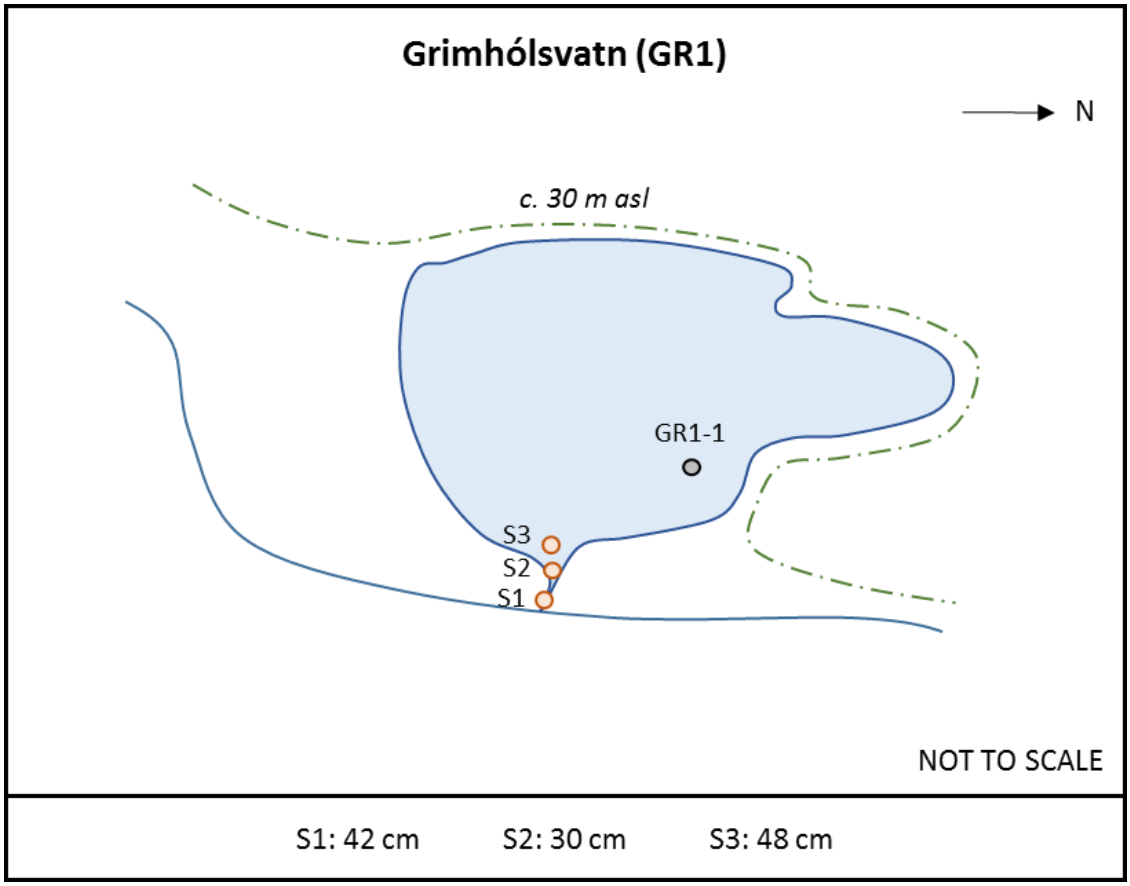

Figure 6.35 – Sill identification at GR1 (S2), showing the sill core locations (orange), lake basin (blue) and sample location (black dot), alongside the higher surrounding topography (green dashed line) alongside the sill core depths to the underlying bedrock.

6.6.9.1 Site stratigraphy

A series of sediment cores were extracted from the present-day lake at GR1 in order to establish the underlying stratigraphy. At the majority of core locations, less than one metre of sediment was retrieved and therefore failed to meet the requirements outlined in Section 3.4. However, one sediment sample from the site provided a longer sediment sequence and was retrieved for subsequent laboratory analysis. GR1 is characterised by limus deposits, with a basal silty brown limus overlain by an olive green limus layer. The sediment composition of the extracted sediment core from GR1-1 is summarised in Table 6.14.

Upper Boundary (cm)	Lower Boundary (cm)	Sediment Description	Tröels-Smith Classification
100	145	Olive green-mid brown limus with trace of silt	Ld4 Ag+
145	224	Mid brown limus with silt and gravel	Ld2 Ag1 Gmaj1

Table 6.14 – Sediment composition of the GR1-1 sediment core sample.

6.6.9.2 Diatom assemblage

The diatom assemblage from GR1-1 can be divided into three distinct diatom zones (Fig. 6.36). Zone 1 is dominated by brackish and freshwater taxa, with brackish species making up 30-45% of the total composition. *Cymbella minuta, Navicula sp. (brackish)* and *Surirella brebissoni var. keutzingi* all present within the diatom record from Zone 1. Towards the top of the zone, the proportion of freshwater taxa increases, mostly through increases in *Fragilaria construens.* Within Zone 2, the percentage of brackish taxa reduces, with freshwater taxa making up c. 90% of the diatom assemblage. There are occasional incidences of brackish and salt tolerant taxa throughout this zone. Zone 3 is comprised of similar total percentages of freshwater taxa, but the abundance of individual species differs to those recorded in Zone 2.

6.6.9.3 Environmental summary

The diatom assemblage from GR1-1 demonstrates a decrease in marine influence at the site and therefore records a fall in RSL. The occasional brackish occurrences higher up within the record are likely caused by individual storm events or brackish incursions into the basin. One radiocarbon sample at 212 cm provides an age for the diatomological isolation contact of 9377 ± 47 ^{14}C a BP (10495-10794 cal. BP).

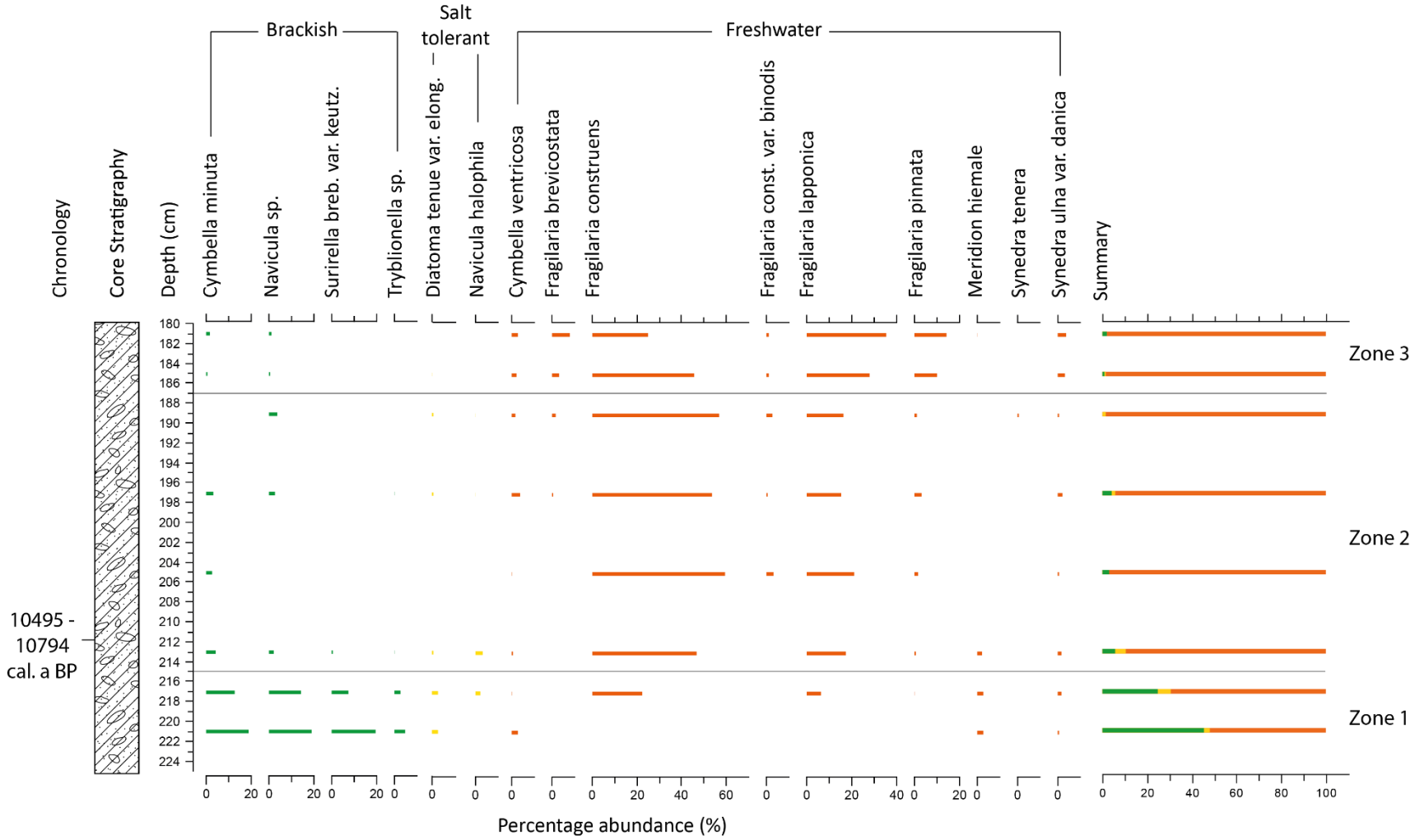

Figure 6.36 – Diatom assemblage from GR1-1 (>3% of the total diatom count) showing the decreased brackish influence at the site through time. Figure key: Section 6.2.

6.7 Area F – Hvammstangi, Vatnsnes

Area F has not previously been the subject of RSL research and so coastal lowland and isolation basin sites were sought from the proposed marine limit to present sea level. In total, one coastal lowland and seven isolation basin sites were investigated in order to establish the pattern of postglacial RSL in the region. There is a lack of suitable mid-elevation sites (c. 15 – 40 m asl) in Area F.

6.7.1 Kolbeinsánes 2 (KB2)

Sample elevation: 1.09 ± 0.30 m asl Site location: 65°25.978'N 21°11.793'W

KB2 is situated to the rear of an isolation basin, which is flooded at high tide. As a result, the sample elevation is employed as the altitude of the sea-level index point in this location, as the sample is situated above the sill elevation. The sill was identified through a survey of the isolation basin sill, which is identified as exposed bedrock (S3, Fig. 6.37). Information about the location and morphology of the isolation basin and KB2 coastal lowland can be found in Section 3.6.3 and Figs. 3.18 and 3.19.

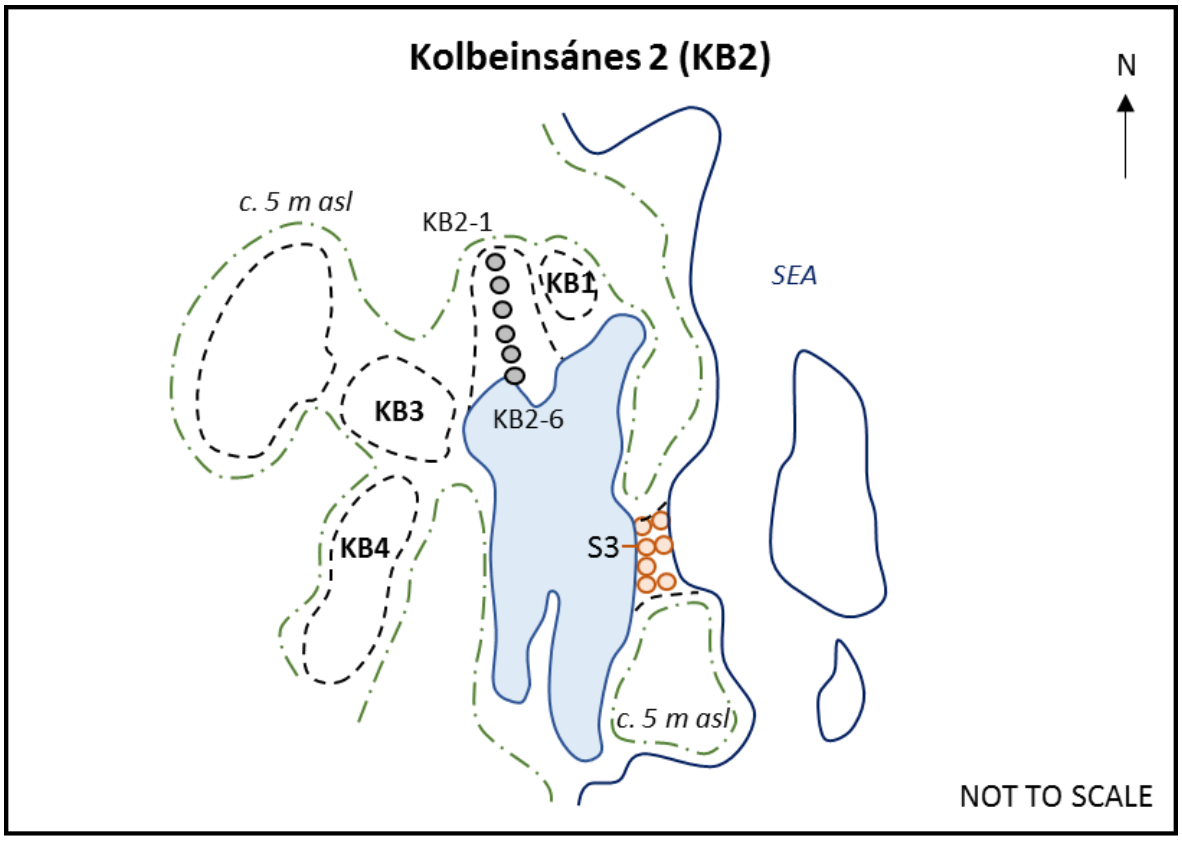

Figure 6.37 – Sill identification at KB2, showing the location of the sill at S3. Schematic provides an overview of the site, including sediment core sample locations (KB2-1 to KB2-6), higher surrounding topography (green dashed lines), present coastlines (dark blue solid line) and proximity to other basins (dashed lines).

6.7.1.1 Site stratigraphy

Kolbeinsánes 2 (KB2) is a small coastal lowland site situated close to present sea level. One transect of cores was surveyed from the back of the coastal lowland to the present lake basin, with four cores being extracted. The transect highlighted various depths of sediment across the coastal lowland, with sediment depths ranging from 47 cm (KB2-5) to 440 cm (KB2-6). In general, the site stratigraphy comprised a basal blue grey silt, subsequent blue grey clay layers and an overlying sphagnum peat layer (Fig. 6.38). Despite the deepest sediments being retrieved from KB2-6, a sample for later analysis was extracted from point KB2-4, due to ease of extraction and the quality of sedimentary record preserved.

The KB2-4 sediment core comprises a basal blue grey clay with silt, overlain by a blue grey silt and overlying sphagnum peat layer. The sediments extracted from the site suggest a low energy environment, which is consistent with the position of the site to the rear of a small tidal inlet. No tephra deposits were identified at the site. The core stratigraphy is summarised in Table 6.15.

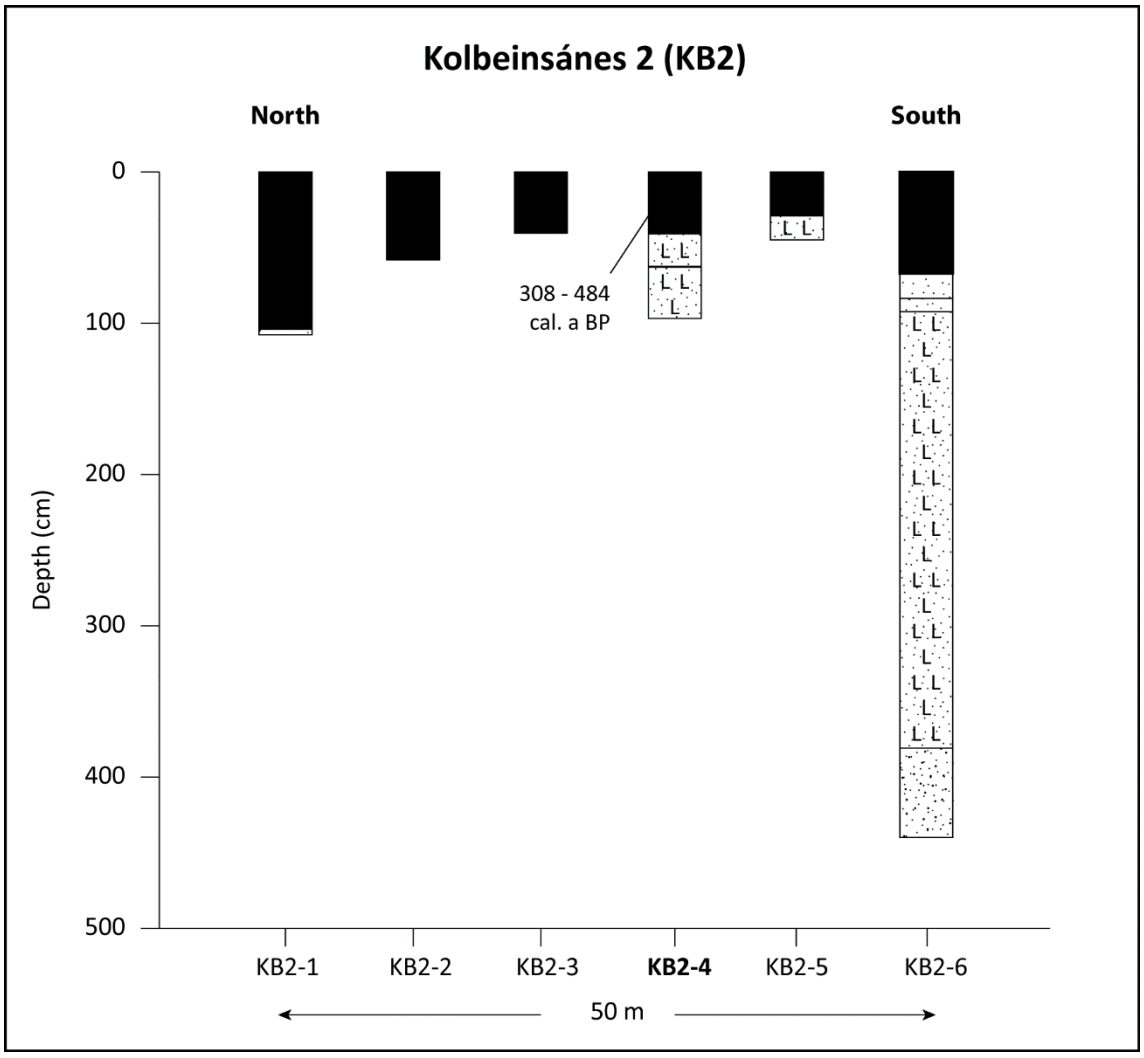

Figure 6.38 – Site stratigraphy at KB2. For the key to sediment symbols, see Section 6.2.

Upper Boundary (cm)	Lower Boundary (cm)	Sediment Description	Tröels-Smith Classification
0	39	Sphagnum peat	Tb4
39	72	Blue-grey silt with clay	Ag3 As1
72	94	Firm blue grey clay with silt	As2 Ag2
94	97	Blue grey clay with silt and gravel	As2 Ag1 Gm1

Table 6.15 – Sediment descriptions and Tröels-Smith (1955) classifications for the Kolbeinsánes 2 (KB2-4) sediment core sample.

6.7.1.2 Diatom assemblage

The diatom assemblage at KB2-4 demonstrates a gradual transition from brackish-marine dominance to an increase in freshwater taxa presence (Fig. 6.39). However, the diatom assemblage can be divided into two distinct zones. Zone 1 is characterised by a number of marine and brackish taxa which are present within the diatom assemblage, including *Navicula forcipata, Navicula peregrina, Nitzschia sigma* and *Rhopalodia rupestris.* At the beginning of Zone 2, there is an increase in the number and percentage of freshwater taxa, demonstrating the gradual isolation of the site.

Unfortunately, it was not possible to process samples to the present ground surface at the location due to the nature of the sediments. Upon attempted extraction, the upper layer of sphagnum peat suffered from intense compaction. It was not therefore possible to assess whether the sediment depths recorded were representative of the true sample elevation.

6.7.1.3 Environmental summary

The sediment sample from KB2-4 is taken from a coastal lowland environment within the infilled section of an isolation basin. The isolation basin (which was not sampled as part of this research) is still connected to the sea at high tide and so the influence of marine and brackish species within the assemblage is to be expected.

The diatom assemblage from KB2 shows the gradual decrease in marine influence at the site, as demonstrated by the increase in the percentage of freshwater species in the record (Fig. 6.39). As the sample is situated above the elevation of the isolation basin sill, the altitude of the sea-level index point is taken as the altitude of the sample rather than the sill elevation. One radiocarbon sample was taken from the site at 30 cm, which returned an age of 338 ± 37 ^{14}C a BP (308 - 484 cal. a BP). These results provide a useful constraint on recent RSL change in Area F, which has a lack of low elevation sites. No visible tephra layers were present within the core sample.

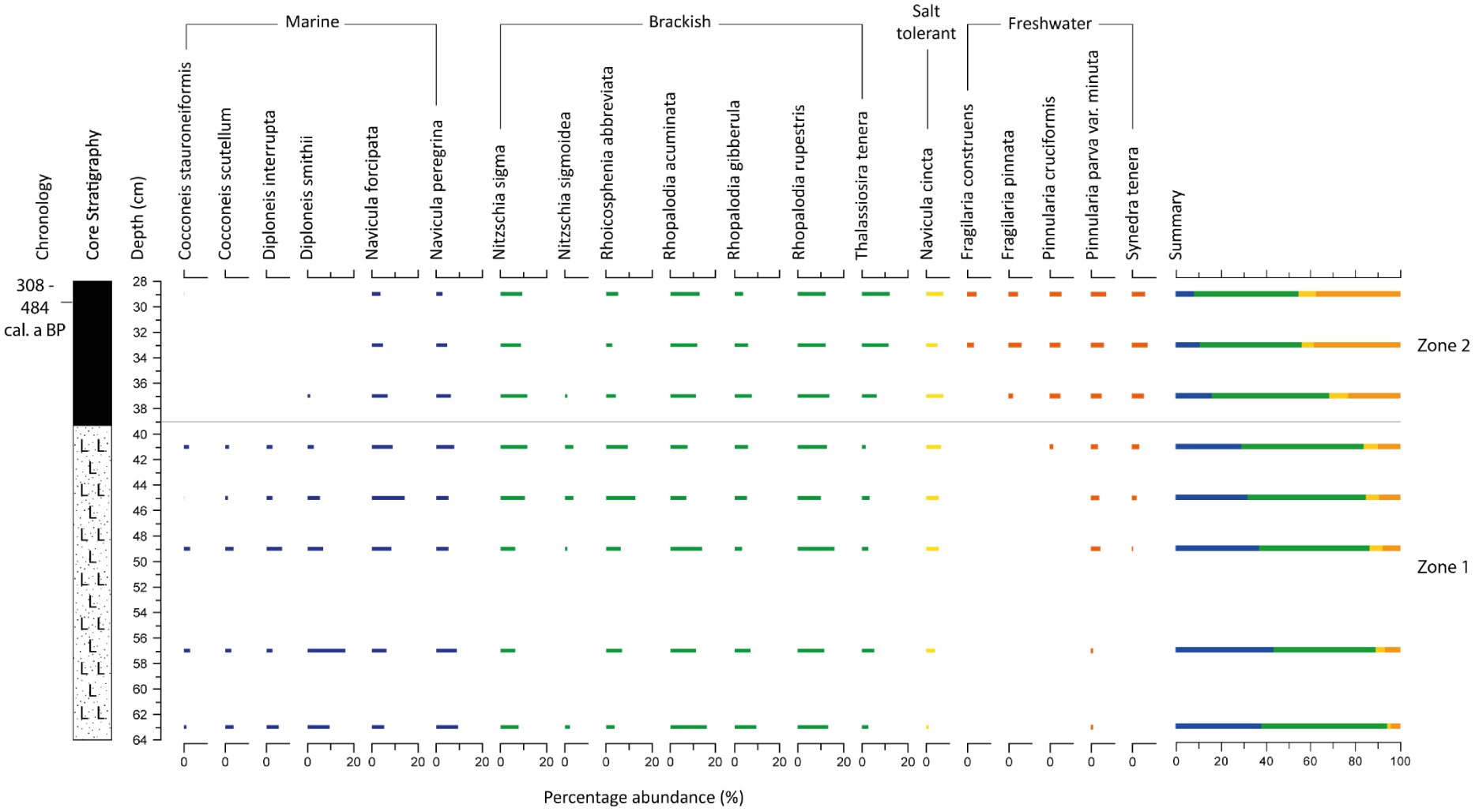

Figure 6.39 – Diatom assemblage from KB2-4 (>3% of the total diatom count), showing the ongoing isolation of the site. For the key to sediments and colour classification, see Section 6.2.

6.7.2 Kolbeinsánes 4 (KB4)

Sill elevation: 2.24 ± 0.30 m asl Site location: 65°25.906'N 21°11.992'W

The sill at KB4 was identified through the coring of a grid of cores across the lowest point in the surrounding topography (S5, Fig. 6.40). The sill was taken as the lowest high point within this grid (see Fig. 4.2). Information about the morphology and location of the basin can be found in Section 3.6.3 and Figs. 3.18 and 3.19.

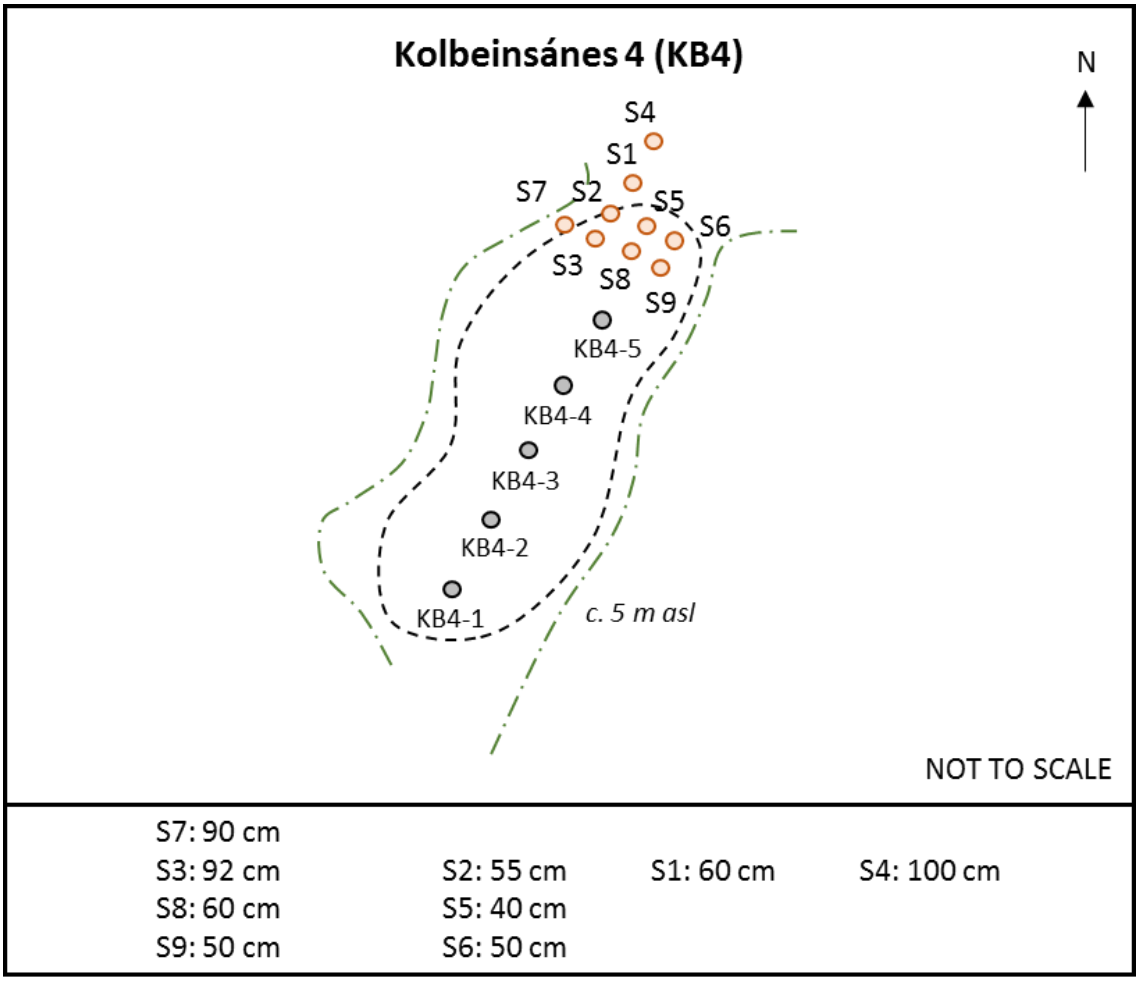

Figure 6.40 – Sill identification at KB4, with sill cores (orange), core sample locations (black) and higher surrounding topography (green dashed line), alongside the sill core depth to the underlying bedrock.

6.7.2.1 Site stratigraphy

A total of six sediment cores were extracted from the Kolbeinsánes 4 site in order to establish the underlying site stratigraphy (Fig. 6.33). The transect highlights the consistent stratigraphic profile, which comprises a lower silty clay, organic rich limus and overlying turfa peats. One sediment sample was retrieved from KB4 for subsequent laboratory analyses. KB4-2 was selected as it provided the most comprehensive record of sedimentary changes at the site (Fig. 6.41). The sediment composition of the sample is summarised in Table 6.16.

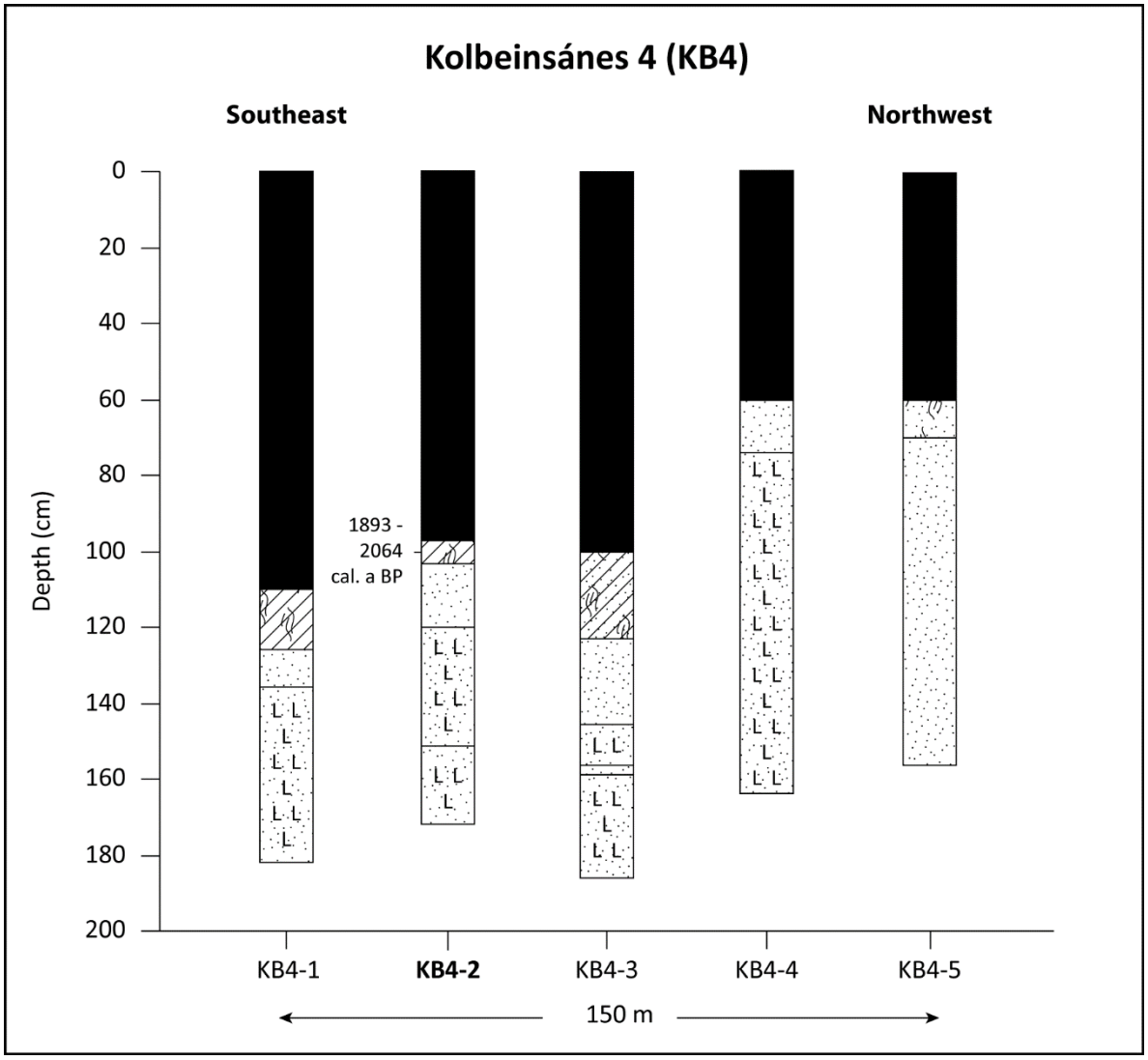

Figure 6.41 – Site stratigraphy at KB4, showing the underlying sediment profile.

Upper Boundary (cm)	Lower Boundary (cm)	Sediment Description	Tröels-Smith Classification
0	97	Sphagnum peat	Tb4
97	103	Olive green limus with mixed organic material	Ld3 Sh1
103	121	Blue grey silt	Ag4
121	154	Blue grey silt with clay	Ag2 As2
154	155	Blue grey silt	Ag4
155	172	Blue grey silt with clay	Ag2 As2

Table 6.16 – Sediment descriptions and Tröels-Smith (1955) classifications for the Kolbeinsánes 4 (KB4-2) sediment core sample.

6.7.2.2 Diatom assemblage

The diatom assemblage from KB4-2 can be divided into two distinct zones (Fig. 6.42). Zone 1 is comprised of brackish, marine and freshwater taxa, with freshwater taxa increasing in percentage through the zone. Individual freshwater taxa only increase marginally but the cumulative increase is notable, leading to an increase from c. 20% to c. 65% of the total diatom count. Salt tolerant taxa also increase in abundance through the zone, despite decreases in brackish and marine taxa. Zone 2 sees the loss of brackish and marine taxa from the diatom record. The upper zone within the assemblage is comprised of c. 10-15% salt tolerant and c. 85-90% freshwater taxa.

6.7.2.3 Environmental summary

The diatom assemblage from KB4-2 shows a decrease in the percentages of marine and brackish species within the diatom assemblage, representing a fall in RSL at the site. One radiocarbon sample was analysed from the site at 100 cm, which returned an age of 2024 ± 37 ^{14}C a BP (1890 - 2064 cal. a BP). This radiocarbon age provides a valuable sea-level index point for the late Holocene, which are currently lacking in northwest Iceland. No tephra layers were present at the location.

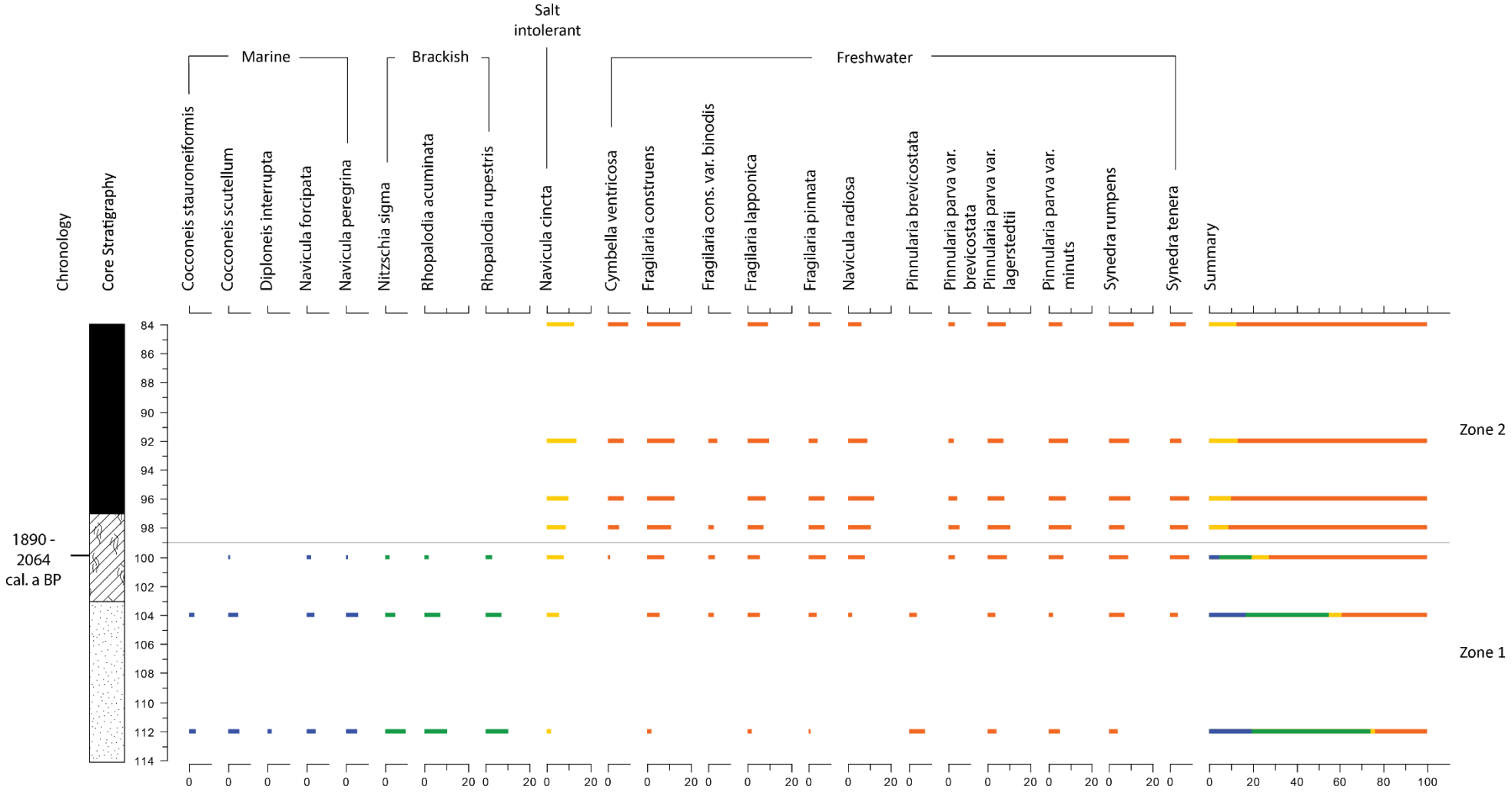

Figure 6.42 – Diatom assemblage from KB4-2 (>3% of the total diatom count) showing the transition from brackish-marine to freshwater conditions at the site. Figure key: Section 6.2.

6.7.3 Kolbeinsánes 1 (KB1)

Sill elevation: 3.45 ± 0.30 m asl Site location: 65°25.984'N 21°11.756'W

The sill at KB1 is based on a transect of cores at the current drainage channel, with the sill being identified as the lowest high point within this transect (S5, Fig. 6.43). Information about the morphology and location of the isolation basin can be found in Section 3.6.3 and Figs. 3.18 and 3.19.

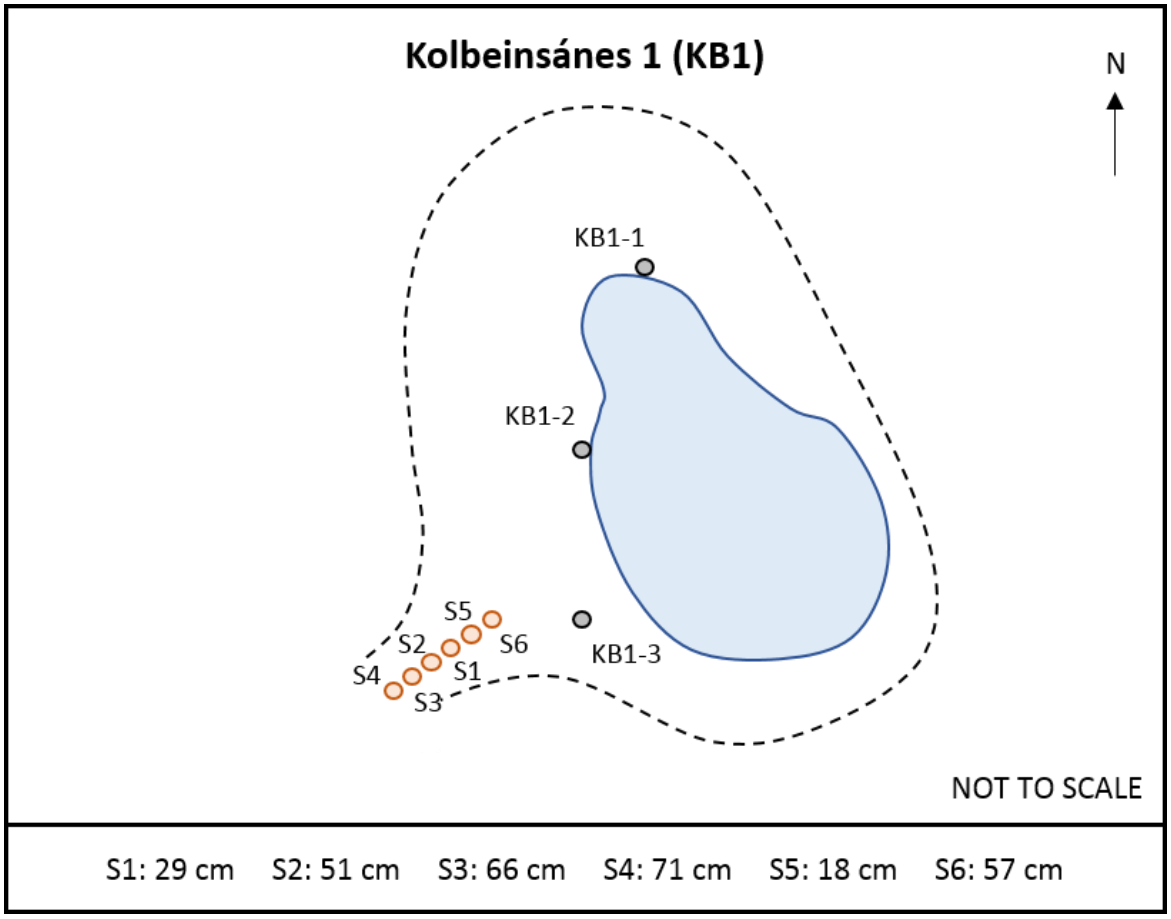

Figure 6.43 – Sill identification at KB1, showing the depths of sill cores (S1-S6). Schematic also shows the sediment core locations at KB1.

6.7.3.1 Site stratigraphy

Three sediment cores were extracted from the site at Kolbeinsánes 1 (KB1) in order to establish the site stratigraphy. Kolbeinsánes 1 (KB1) is a small lake basin and as such, core samples were collected across the width of the site. The site stratigraphy can be summarised as blue grey silty clay, overlain by brown mixed organic material and a subsequent limus layer. The underlying stratigraphy is summarised in Fig. 6.44.

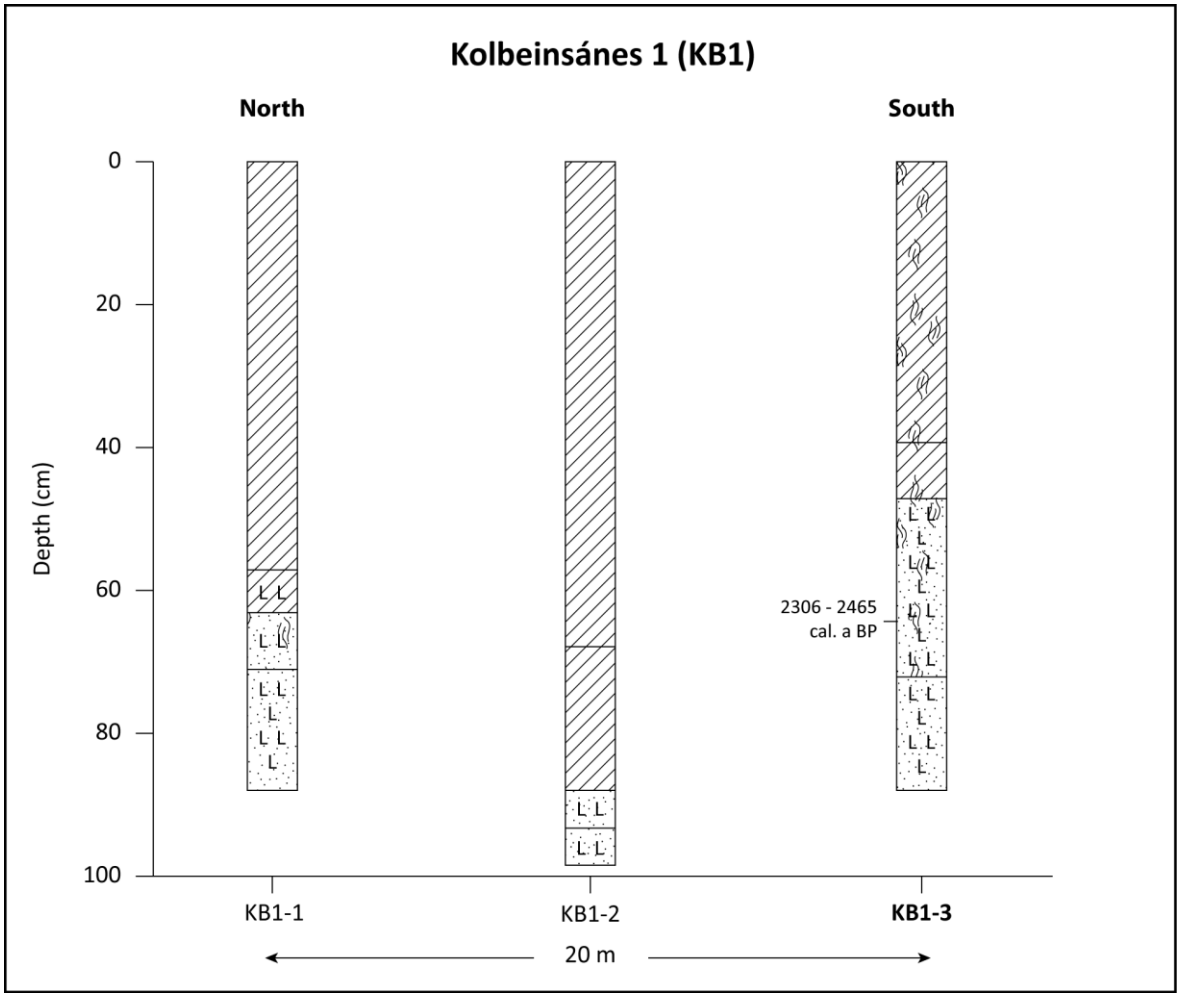

Figure 6.44 – Site stratigraphy at Kolbeinsánes 1, highlighting the underlying sediment profile.

A sediment core for diatom analysis was extracted from KB1-3, which represented the most complete record of changes in the stratigraphic profile at the site (Fig. 6.44). The sediment core comprises a basal blue grey silt, overlain with an organic rich clay and subsequent olive green limus layer. The sediment core is indicative of a low energy environment, being made up of fine grained sediments. The stratigraphy of the core is summarised in Table 6.17 and Fig. 6.44.

Upper Boundary (cm)	Lower Boundary (cm)	Sediment Description	Tröels-Smith Classification
0	39	Olive green limus with mixed organic material	Ld3 Sh1
39	47	Olive green/brown limus with abundant rootlets	Ld2 Sh2
47	72	Mid brown clay with silt and organic material	As2 Ag1 Sh1
72	90	Blue grey silt with clay	Ag3 As1

Table 6.17 – Sediment descriptions and Tröels-Smith (1955) classifications for the Kolbeinsánes 1 (KB1-3) sediment core sample.

6.7.3.2 Diatom assemblage

Nine diatom samples were analysed from KB1-3, which revealed two zones within the diatom record (Fig. 6.45). Zone 1 demonstrates a mixed assemblage, with marine, brackish, salt tolerant and freshwater taxa being recorded. The percentage of freshwater taxa increases through the zone due to increases in the range of freshwater taxa present. *Navicula cincta* is present throughout the record, representing up to c. 10% of the total diatom count. Within Zone 2, the percentage of marine taxa decreases to c. 5% of the total diatom assemblage. This decrease in marine influence is coupled with an increase in the percentage of freshwater taxa, including *Fragilaria construens, Navicula radiosa* and *Synedra rumpens*, Zone 3 is marked by a further increase in the proportion of freshwater taxa within the diatom assemblage, alongside low percentages of brackish and salt tolerant taxa. Marine taxa are not recorded in Zone 3.

6.7.3.3 Environmental summary

The diatom record from KB1-3 demonstrates a gradual decrease in marine influence at the site through decreases in the recorded percentages of marine and brackish diatom taxa (Fig. 6.45). This gradual decrease in marine influence is linked to a fall in RSL at the site. One radiocarbon sample was analysed from the sediment core sample at 65 cm, which produced an age of 2332 ± 37 ^{14}C a BP (2306 - 2465 cal. a BP). No tephra samples were recorded within the sediment sample.

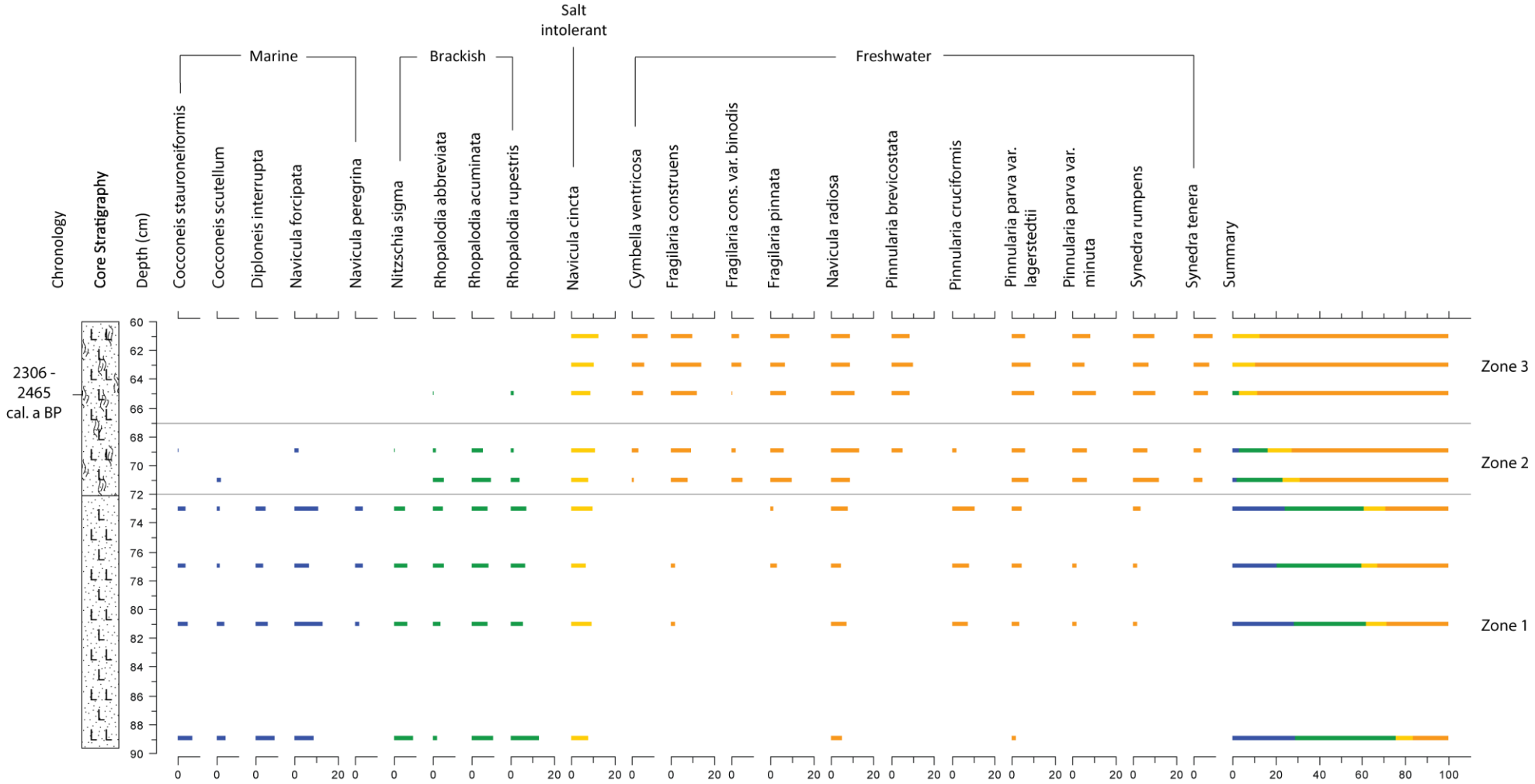

Figure 6.45– Diatom assemblage from KB1-3 (>3% of the total diatom count) showing the transition from marine-brackish to freshwater dominance at the site. Figure key: Section 6.2.

6.7.4 Sandar 2 (SN2)

Sill elevation: 46.51 ± 0.30 m asl Site location: 65°20.026'N 20°59.230'W

The sill at SN2 was identified by a grid of cores at the lowest point within the surrounding topography. The sill is covered by overlying sediments and was taken as the lowest highpoint within the transect of cores (S2-3, Fig. 6.46). Information about the location of the isolation basin can be found in Section 3.6.3 and Fig. 3.18.

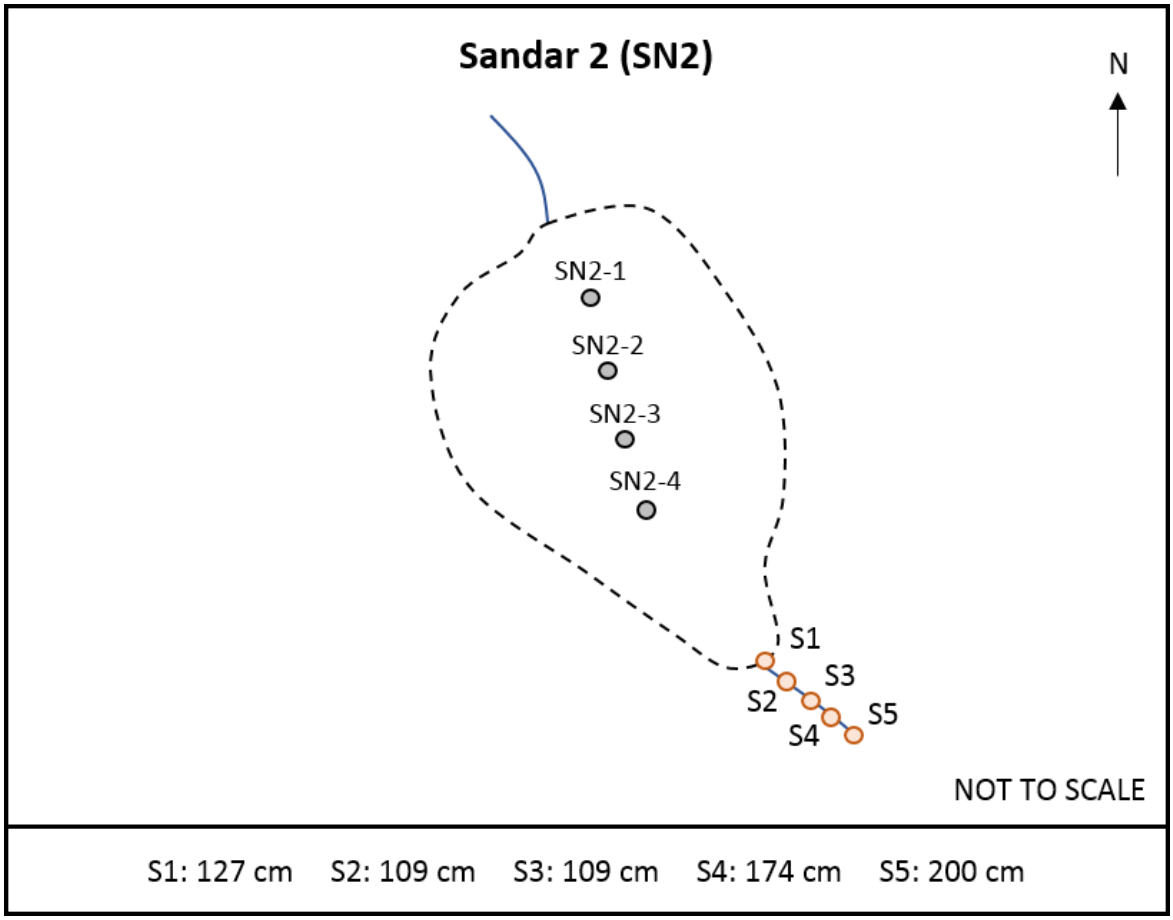

Figure 6.46 – Sill identification at SN2, including sill core locations (orange dots), sediment core samples (black dots) and present infilled basin (black dashed line).

6.7.4.1 Site stratigraphy

Four sediment cores were extracted from SN2 in to establish the underlying stratigraphy of the site. SN2 is an infilled basin and as such the transect was undertaken from the northernmost section to the centre of the basin. The basin stratigraphy can be summarised as a basal silt overlain by organic rich limus with tephra layers and an uppermost turfa peat layer (Fig. 6.47).

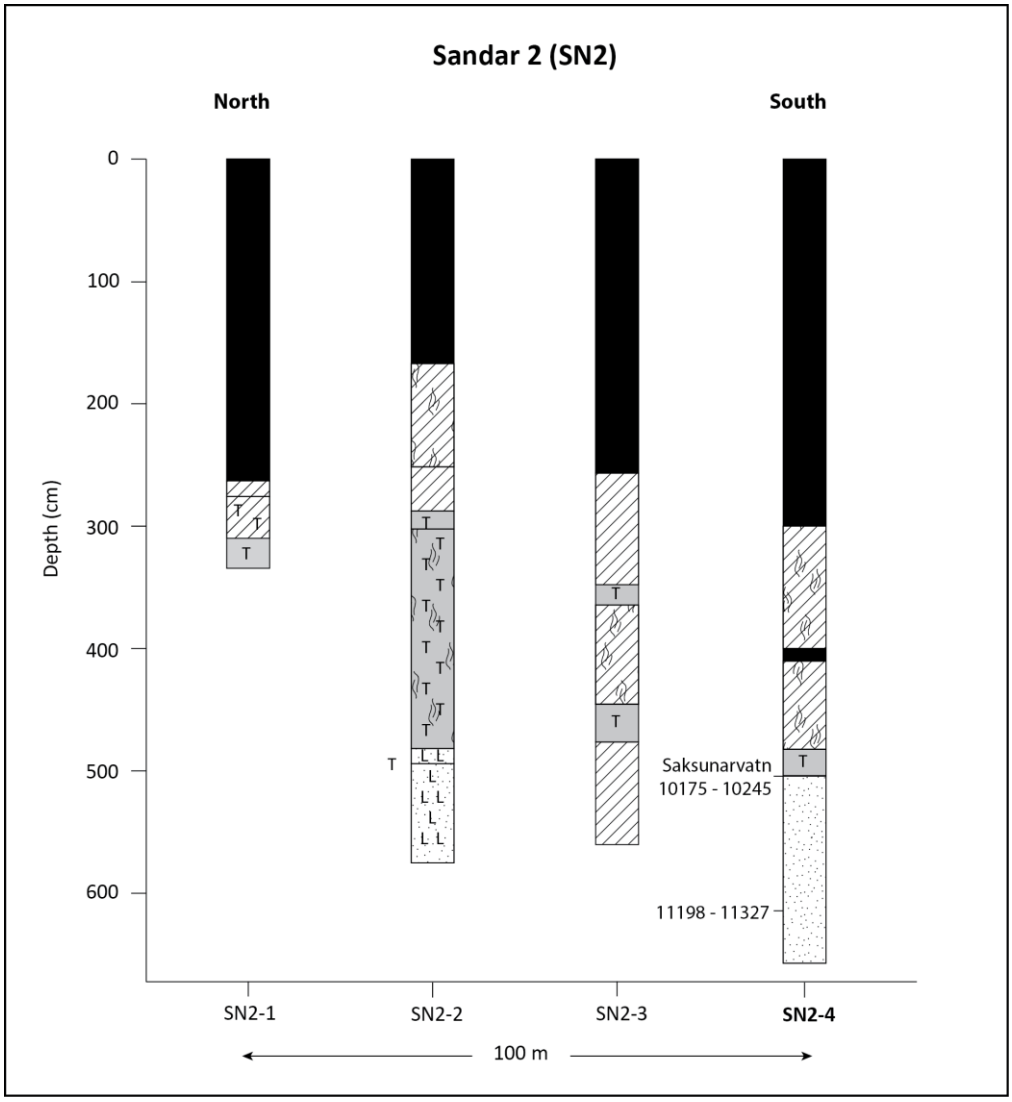

Figure 6.47 – Site stratigraphic profile at Sandar 2. Ages presented are calibrated ages before present.

One sediment core was extracted from SN2 for subsequent diatom analysis. The sediment core, SN2-4, represented the most comprehensive record of sedimentary changes at the site, being extracted from the centre of the basin (Fig. 6.47). The core comprises a basal blue grey silty clay, overlain be an olive green limus layer. Within the limus layer, the Saksunarvatn tephra is present (Fig. 5.6). The core stratigraphy is summarised in Table 6.18 and Fig. 6.47.

Upper Boundary (cm)	Lower Boundary (cm)	Sediment Description	Tröels-Smith Classification
470	499	Olive green limus with mixed organic material	Ld3 Sh1
499	509	Dark grey tephra	Ld2 Sh2
509	550	Olive green/grey limus with some silt	As2 Ag1 Sh1
550	640	Blue grey silty clay	Ag3 As1

Table 6.18 – Sediment descriptions and Tröels-Smith (1955) classifications for the Sandar 2 (SN2-4) sediment core sample.

6.7.4.2 Diatom assemblage

The diatom assemblage from SN2-4 can be divided into three distinct zones (Fig. 6.48). Zone 1 demonstrates a clear brackish-marine influence on the diatom assemblage, with *Cymbella minuta* and *Gyrosigma hippocampus* both making up c. 15 % of the total abundance. Freshwater species are also present throughout this zone, suggesting that basin isolation is taking place. Towards the bottom of this zone, diatom preservation was poor and samples at both 626 cm and 620 cm failed to produce counts of at least 250 taxa. Zone 2 demonstrates the loss of all brackish and marine species from the diatom assemblage,leading to an increased proportion of freshwater species. *Fragilaria construens, Fragilaria lapponica* and *Synedra ulna var. danica* are particularly populous within this zone, which also sees salt intolerant species making up <10% of the total percentage abundance and a reduction in salt tolerant taxa. Zone 3 is marked by the loss of the remaining salt tolerant taxa and freshwater dominance.

6.7.4.3 Environmental summary

The diatom assemblage from SN2-4 demonstrates a reduction in marine-brackish influence at the site and therefore a clear transitional sequence, with final basin isolation occurring at 614 cm as RSL fell below the altitude of the rock sill. One radiocarbon age was generated at the site at 610 cm that produced an age of 9850 ± 41 ^{14}C a BP (11198 - 11327 cal. a BP). In addition, one tephra layer was analysed from the sediment core sample, which was identified as the Saksunarvatn tephra at 509 cm (Fig. 5.3.3; 10200 cal. a BP, Lohne *et al.*, 2014). The isolation of Sandar 2 is well constrained both by the diatom and chronological datasets.

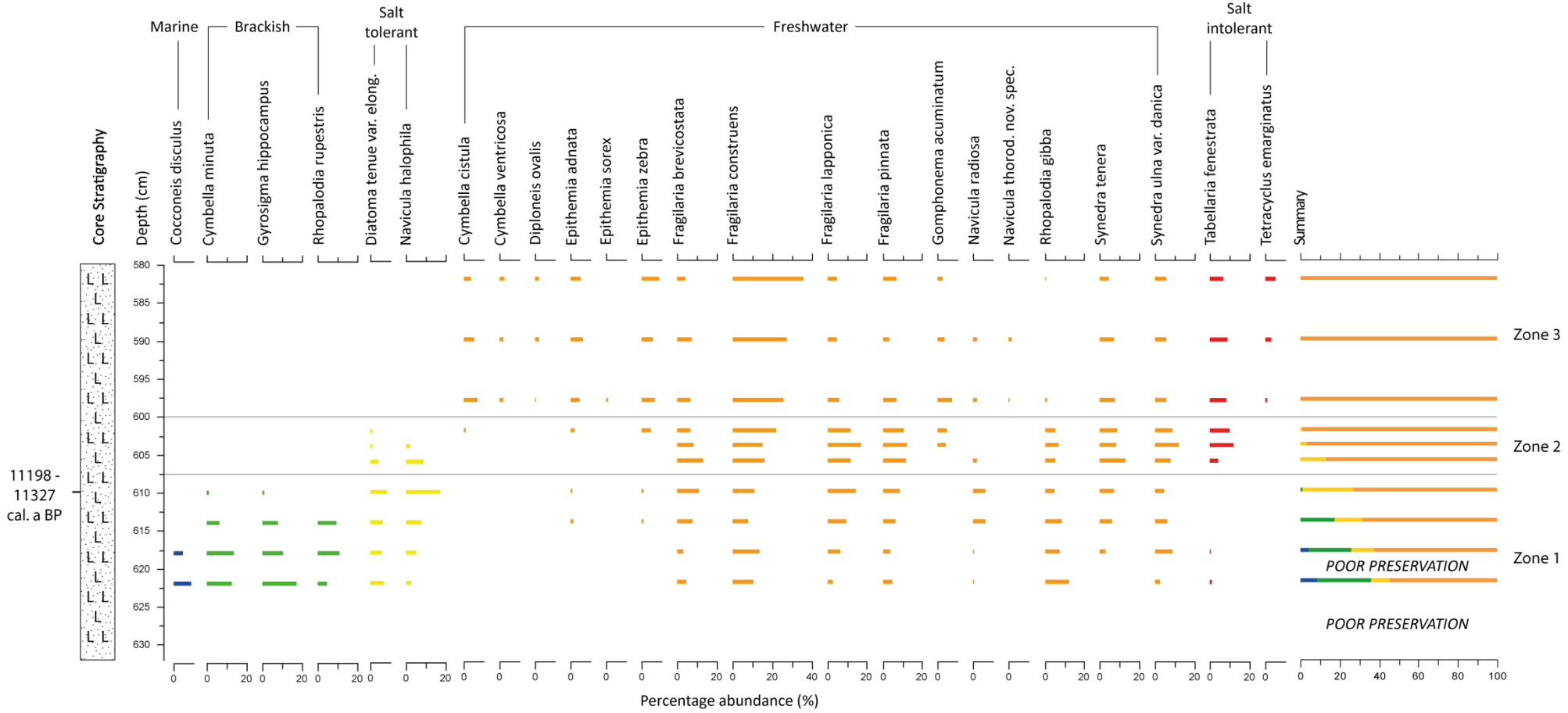

Figure 6.48 – Diatom assemblage from SN2-4 (>3% of the total diatom count) showing the decrease in marine and brackish influence at the site. For the key to sediment symbols and colour classification, see Section 6.2.

6.7.5 Sandar 1 (SN1)

Sill elevation: 51.02 ± 0.30 m asl Site location: 65°20.249'N 20°59.381'W

The sill at SN1 was identified by a survey transect across the lowest point (exposed bedrock) within the surrounding topography using an EDM (S2, Fig. 6.49). The sill represents the lowest high point within this transect. Information about the basin morphology can be found in Section 3.6.3 and Figs. 3.19 and 3.20.

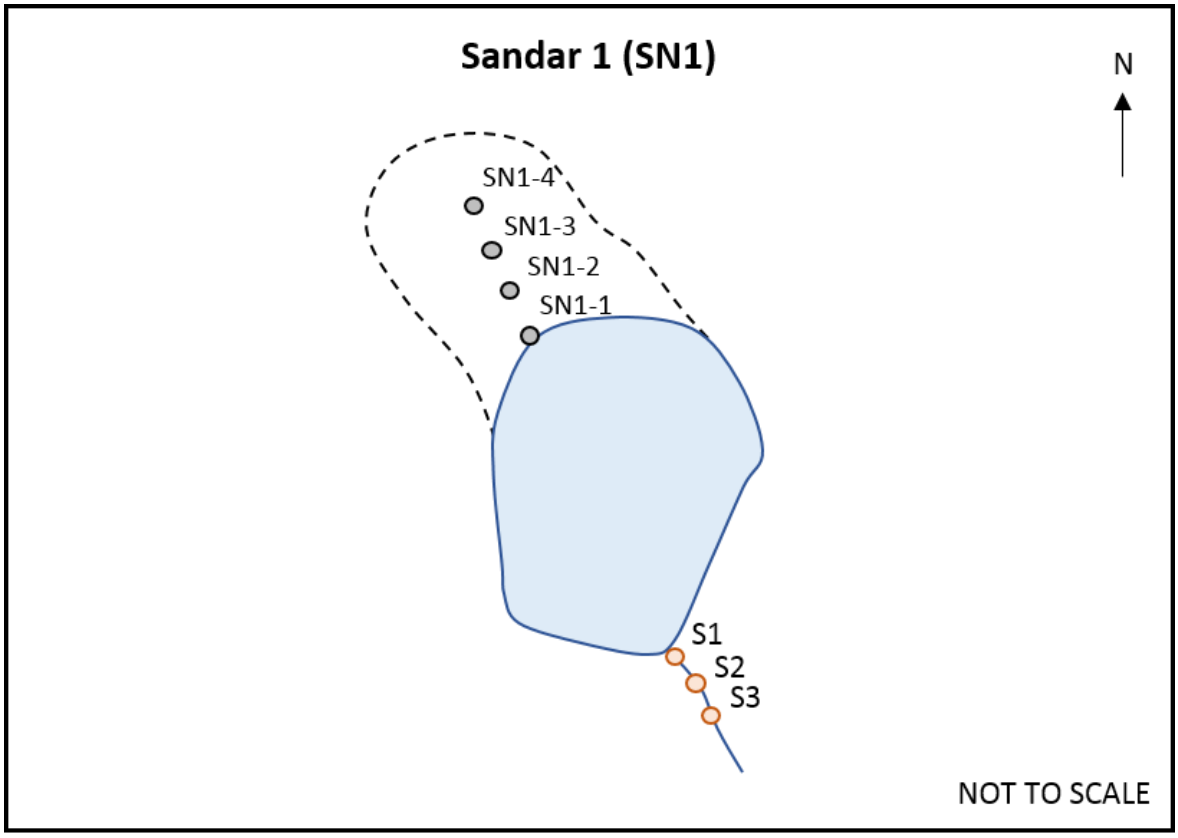

Figure 6.49 – Sill identification at SN1, showing the location of the sill survey points (orange dots), sediment core sample locations (black dots), present lake (blue) and the extensive infilled section (black dashed line).

6.7.5.1 Site stratigraphy

The SN1 basin presently comprises a lake and large infilled section. As a result, a series of cores were extracted from the infilled section of the basin, due to the difficulties associated with site access and operating the boat. Four sediment cores were retrieved in total from the centre of the basin to the basin edge. The sediment profile is comprised of a basal blue grey silt with overlying limus layer and a surface turfa peat layer. Between the silt and limus layers, a dark grey tephra was evident in a number of core samples. The fine grained sediments in SN1 suggest a relatively low energy depositional environment. The site stratigraphy is summarised in Fig. 6.50.

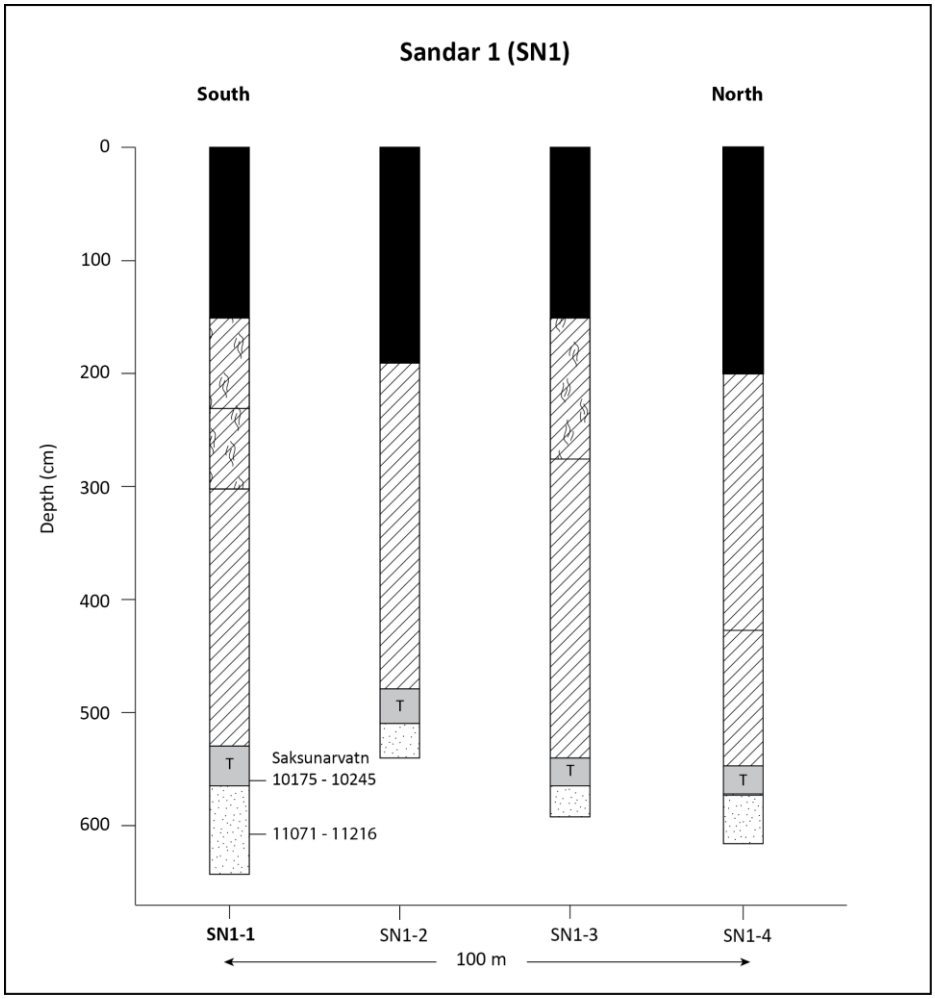

Figure 6.50 – Site stratigraphy at Sandar 1. Sediment key: Fig. 6.1.

The SN1-1 sediment core represents a comprehensive record of environmental change at the site, being extracted from the centre of the lake basin. The sediment core comprises a basal blue-grey silt layer, with overlying dark grey tephra. As outlined in Chapter 5, this tephra has been identified as the widespread Saksunarvatn tephra, following geochemical analyses on the tephra sample. The top of the core sample is an olive green limus, with variable levels of humification. The SN1-1 sediment core is summarised in Table 6.19 and Fig. 6.50.

Upper Boundary (cm)	Lower Boundary (cm)	Sediment Description	Tröels-Smith Classification
450	510	Olive green well humified limus	Ld4
510	560	Olive green/grey limus	Ld4
560	575	Dark grey tephra	Ag4
575	609	Blue grey silt with some clay	Ag3 As1
609	644	Blue grey firm silt	Ag4

Table 6.19 – Sediment descriptions and Tröels-Smith (1955) classifications for the Sandar 1 (SN1-1) sediment core sample.

6.7.5.2 Diatom assemblage

The diatom assemblage from SN1-1 demonstrates a clear transitional sequence from brackish to freshwater dominance (Fig. 6.51). The site assemblage is divided into five distinct zones, which are based on shifts in the principal diatom taxa. Zone 1 demonstrates a decrease in brackish species, such as *Gyrosigma hippocampus* from c. 35% to c. 5% of the total assemblage, alongside an increase in freshwater species such as *Fragilaria construens* from c. 15% to c. 45% of the total percentage composition. Zone 2 is dominated by freshwater species, with *Fragilaria construens* peaking at c. 50% of the total diatom assemblage. Zones 3-5 are all dominated by freshwater diatom taxa, with variability in the percentage composition leading to the designation of individual zones.

6.7.5.3 Environmental summary

The basal section of the diatom assemblage represents a brackish environment, with a change to freshwater conditions recorded in Zone 2. The diatom assemblage therefore demonstrates a fall in RSL at the site. One radiocarbon date was produced from the site at 610 cm, which generated an age of 9689 ± 40 ^{14}C a BP (11071 - 11216 cal. a BP). In addition, tephra analyses determined the presence of Saksunarvatn tephra at 575 cm (Fig. 5.3.3) providing an additional limiting age for basin isolation.

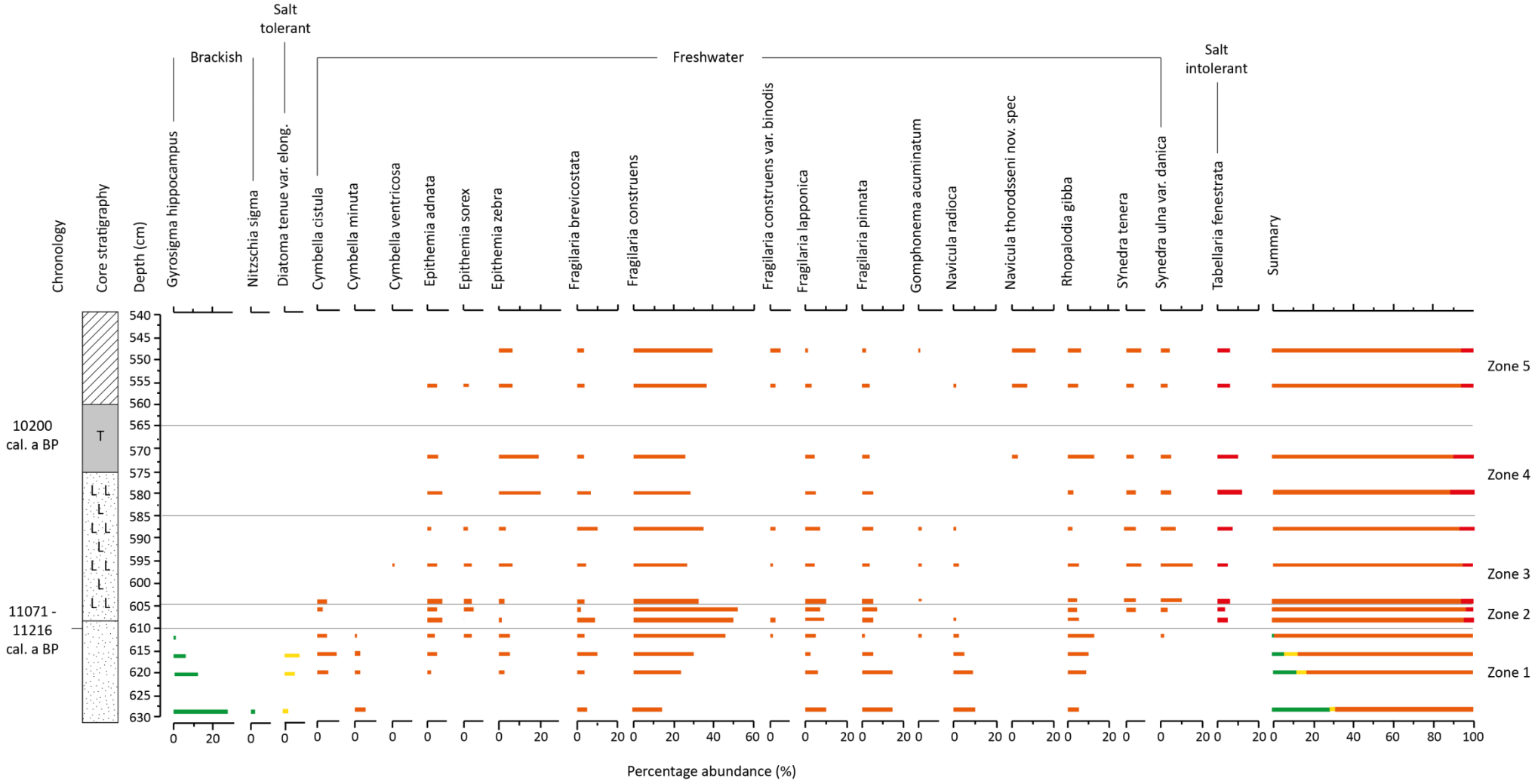

Figure 6.51 – Diatom assemblage from SN1-1 (>3% of the total diatom count), showing the transition from brackish-freshwater to freshwater dominance. Figure key: Section 6.2.

6.7.6 Myrar (MY1)

Sill elevation: 57.90 ± 0.30 m asl Site location: 65°18.253'N 21°02.401'W

The sill at MY1 was identified within the present drainage channel, through a transect of cores (S7, Fig. 6.52). The lowest highpoint recorded along this transect denoted the basin sill. Information about the morphology and location of the isolation basin can be found in Section 3.6.3 and Figs. 3.18 and 3.20.

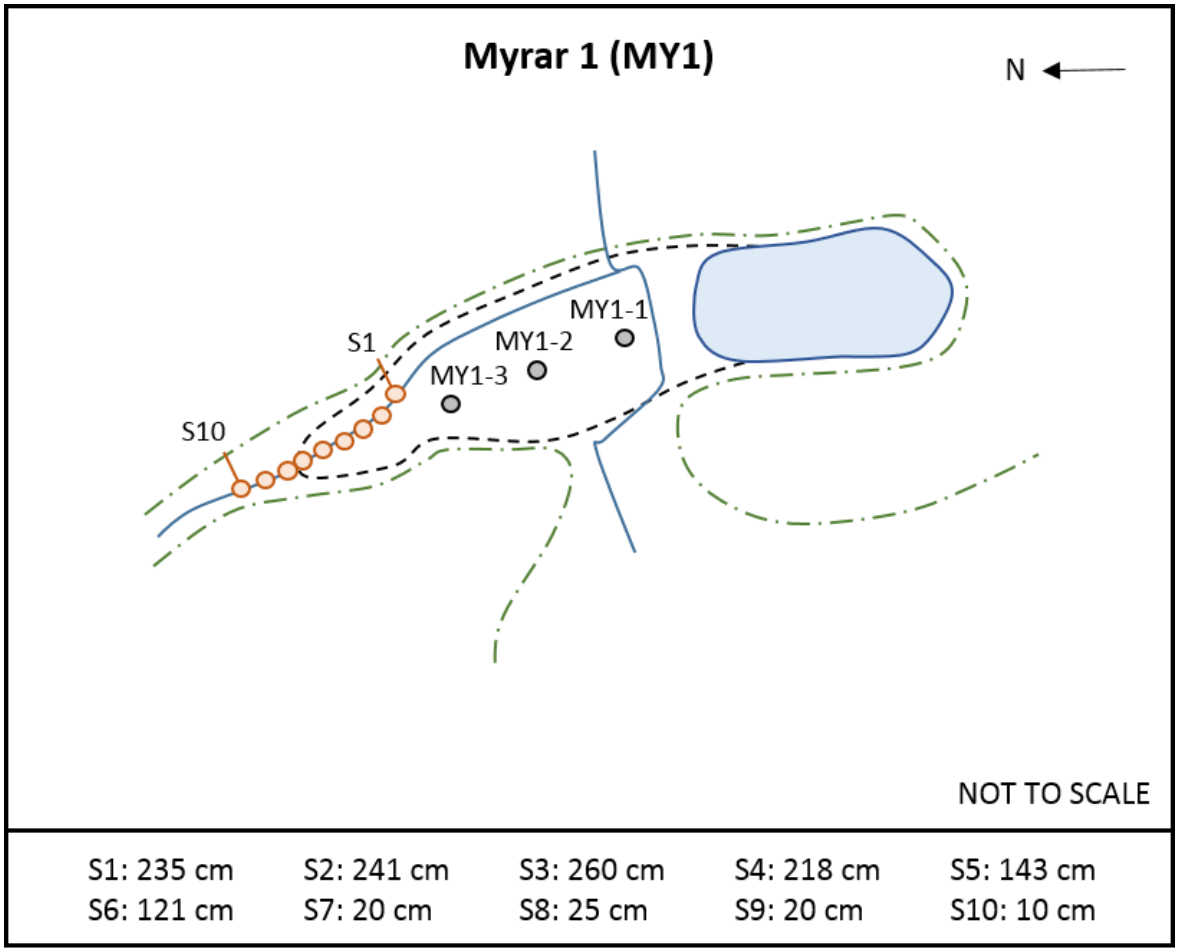

Figure 6.52 – Sill identification at MY1, showing the sill core locations (orange dots), sediment core locations (black dots), infilled section (black dashed line), present lake (blue), and higher surrounding topography (green dashed line). Due to the sloping nature of the sill location, the lowest highpoint within the sequence is found at S7, when corrected for sediment depth.

6.7.6.1 Site stratigraphy

A transect of three sediment cores was completed in order to establish the site stratigraphy at Myrar 1 (MY1). Each sediment core presented a similar stratigraphic profile, comprising a basal gravel with overlying blue grey silts and clays, mixed organic sediments and uppermost peat layer (Fig. 6.53). Within the sedimentary profile, a number of tephra layers were also identified.

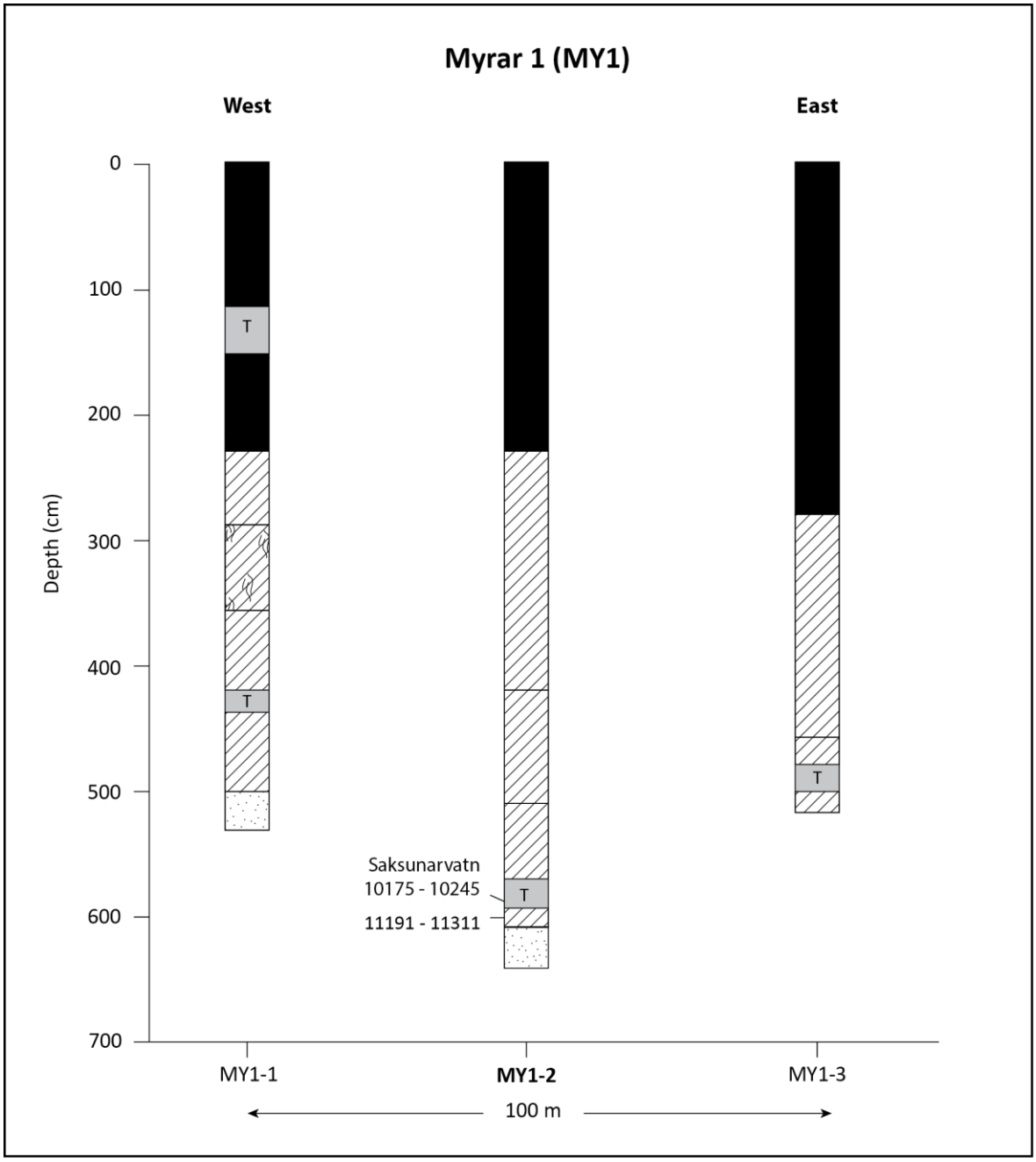

Figure 6.53 – Site stratigraphy at Myrar 1 (MY1). For the key to sediment symbols, see Section 6.2.

The sediment sample at MY1-2 (Fig. 6.53) was chosen as a representative sample for diatom analysis. The sediment core comprises a basal blue grey clay and overlying olive green limus, within which a distinct tephra layer is evident. As outlined in Chapter 5, the tephra layer underwent geochemical analysis and was identified as the Saksunarvatn tephra. The fine grained nature of the sediments preserved at the site suggests a low energy depositional environment. The sediment core stratigraphy is summarised in Table 6.20 and Fig. 6.53.

Upper Boundary (cm)	Lower Boundary (cm)	Sediment Description	Tröels-Smith Classification
550	572	Olive green limus with organic material and plant fragments	Ld3 Th1
572	594	Dark grey tephra	Ag4
594	617	Olive green limus with plant fragments	Ld3 Th1
617	636	Blue grey silty clay	Ag3 As1

Table 6.20 – Sediment descriptions and Tröels-Smith (1955) classifications for the Myrar 1 (MY1-2) sediment core sample.

6.7.6.2 Diatom assemblage

Within the diatom assemblage from MY1-2, three distinct zones can be identified (Fig. 6.54). Zone 1 shows a clear marine-brackish composition, with *Cocconeis scutellum, Cocconeis stauroneiformis* and *Tabularia fasciculata* each representing >15% of the total diatom assemblage. Zone 2 is characterised by a decrease in brackish and marine species, with an increase in freshwater taxa such as *Fragilaria construens, Fragilaria pinnata* and *Synedra ulna var. danica.* The uppermost zone, Zone 3, comprises salt tolerant, freshwater and salt tolerant taxa, with marine and brackish species disappearing from the diatom assemblage. Within Zone 3, the percentages of individual taxa remain approximately constant.

6.7.6.3 Environmental summary

The diatom assemblage from MY1-2 demonstrates a decrease in marine influence at the location and thus a fall in RSL. One radiocarbon sample was analysed from the isolation contact at 612 cm which returned an age of 9831 ± 42 ^{14}C a BP (11191 - 11311 cal. a BP). In addition, the Saksunarvatn tephra was identified at the site at 594 cm (Fig. 5.6) providing additional support for the chronology of this site.

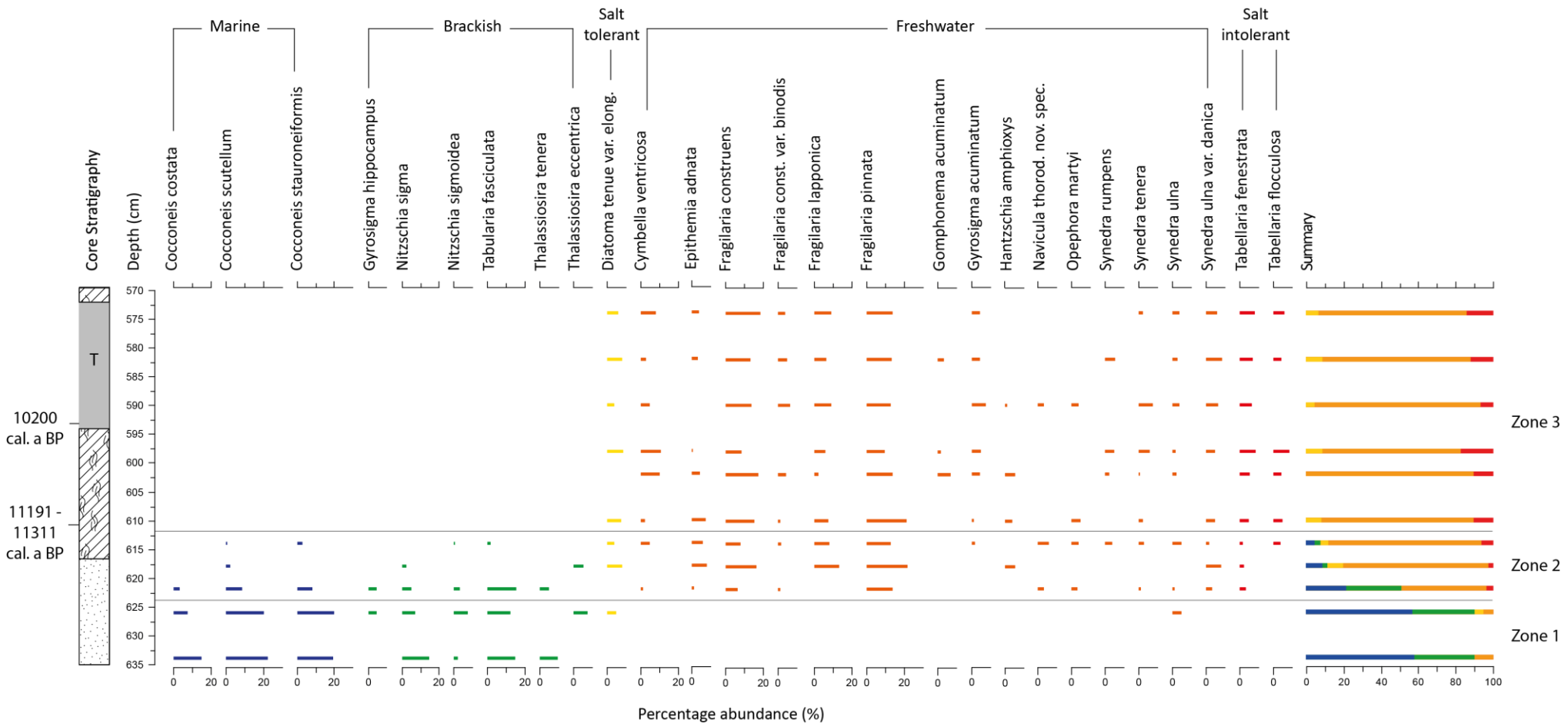

Figure 6.54 – Diatom assemblage and summary plot for MY1-2 (>3% of the total diatom count), showing the transition from brackish-marine to freshwater dominance at the site. For the key to sediment symbols and colour classifications, see Section 6.2.

6.7.7 Arnhóll 2 (AH2)

Sill elevation: 68.22 ± 0.30 m asl Site location: 65°17.601'N 20°55.978'W

The sill at AH2 is based on a transect of cores at the lowest point within the surrounding basin topography (S4, Fig. 6.55). The lowest high point within this grid was taken as the sill elevation. Information about the morphology and location of the site can be found in Section 3.6.3 and Figs. 3.18 and 3.20.

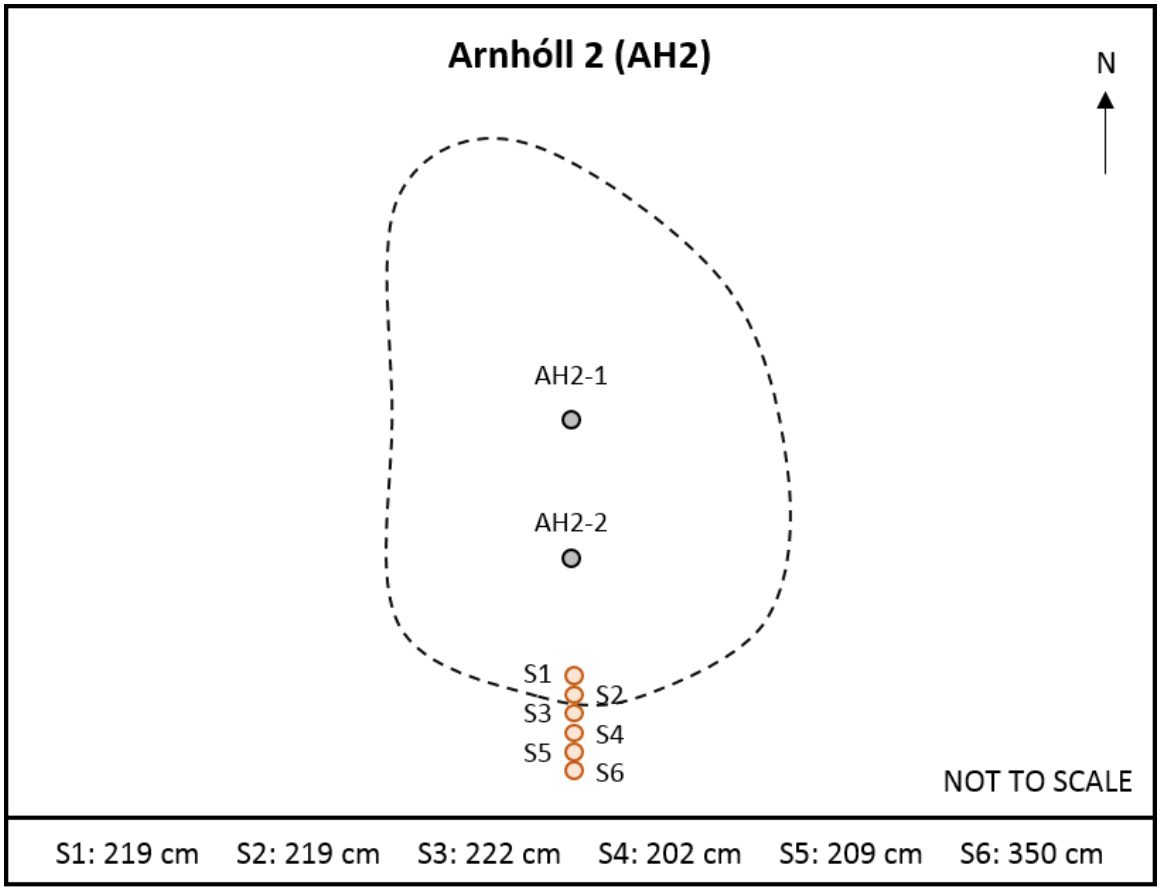

Figure 6.55 – Sill identification at AH2, showing sill (orange dots) and core (black dots) locations, alongside the extent of the basin (black dashed line). In addition, the depth of sill cores to underlying bedrock is outlined for each point.

6.7.7.1 Site stratigraphy

Two core samples were extracted from Arnhóll 2 (AH2) in order to establish the site stratigraphy. Samples were extracted within the infilled section of the basin, due to ease of access and the difficulties associated with operating the boat at the location. The transect was completed from the basin centre towards the eastern edge of the basin. Both sediment cores had a basal blue grey sand layer, overlain by a silty clay and an olive green limus. Tephra was also evident within the limus layer in both locations. The site stratigraphy is summarised in Fig. 6.56.

The AH2-2 sediment core was chosen for subsequent diatom analyses, as it provided a representative sample of basin stratigraphy. The sediment core comprises a basal sand with some gravel, overlain by a blue grey silty clay and olive green limus. Within the upper limus layer, a dark grey tephra was sampled and identified as the Saksunarvatn tephra following geochemical analyses. The decreased grain size of the sediment sample suggests a decrease in the energy of the depositional environment over time. The sediment core stratigraphy is summarised in Table 6.21 and Fig. 6.56.

Upper Boundary (cm)	Lower Boundary (cm)	Sediment Description	Tröels-Smith Classification
580	588	Olive green organic rich limus	Ld3 Th1
588	594	Dark grey tephra	Ag4
594	605	Olive green limus	Ld4
605	620	Dark grey silty clay	Ag3 As1
620	630	Blue grey sand with some gravel	Ga3 Gm1

Table 6.21 – Sediment descriptions and Tröels-Smith (1955) classifications for the Arnhóll 2 (AH2-2) sediment core sample.

6.7.7.2 Diatom assemblage

Eight diatom samples were analysed at AH2-2 to establish the environmental changes recorded at the site; however, the deepest two samples produced insufficient diatoms to produce a reliable count (Fig. 6.57). The resulting diatom record demonstrates a dominance of freshwater diatom taxa, with *Fragilaria construens* being particularly prevalent throughout the assemblage. There is a minor brackish element within the lowest recorded diatom sample. The percentages of individual diatom taxa remains approximately constant throughout the profile, with the exception of *Fragilaria construens.*

6.7.7.3 Environmental summary

The diatom record from AH2-2 suggests a freshwater dominance at the site (Fig. 6.57). The minor brackish element in the sample from 632 cm may suggest that the site was situated just above tidal inundation at the point of deposition. One radiocarbon sample from 632 cm returned an age of 9751 ± 41 ^{14}C a BP (11121 – 11242 cal. a BP). As outlined in Section 5.2.5, the Saksunarvatn tephra was identified at 594 cm, providing a limiting age of 10200 cal. a BP (Lohne *et al.*, 2014).

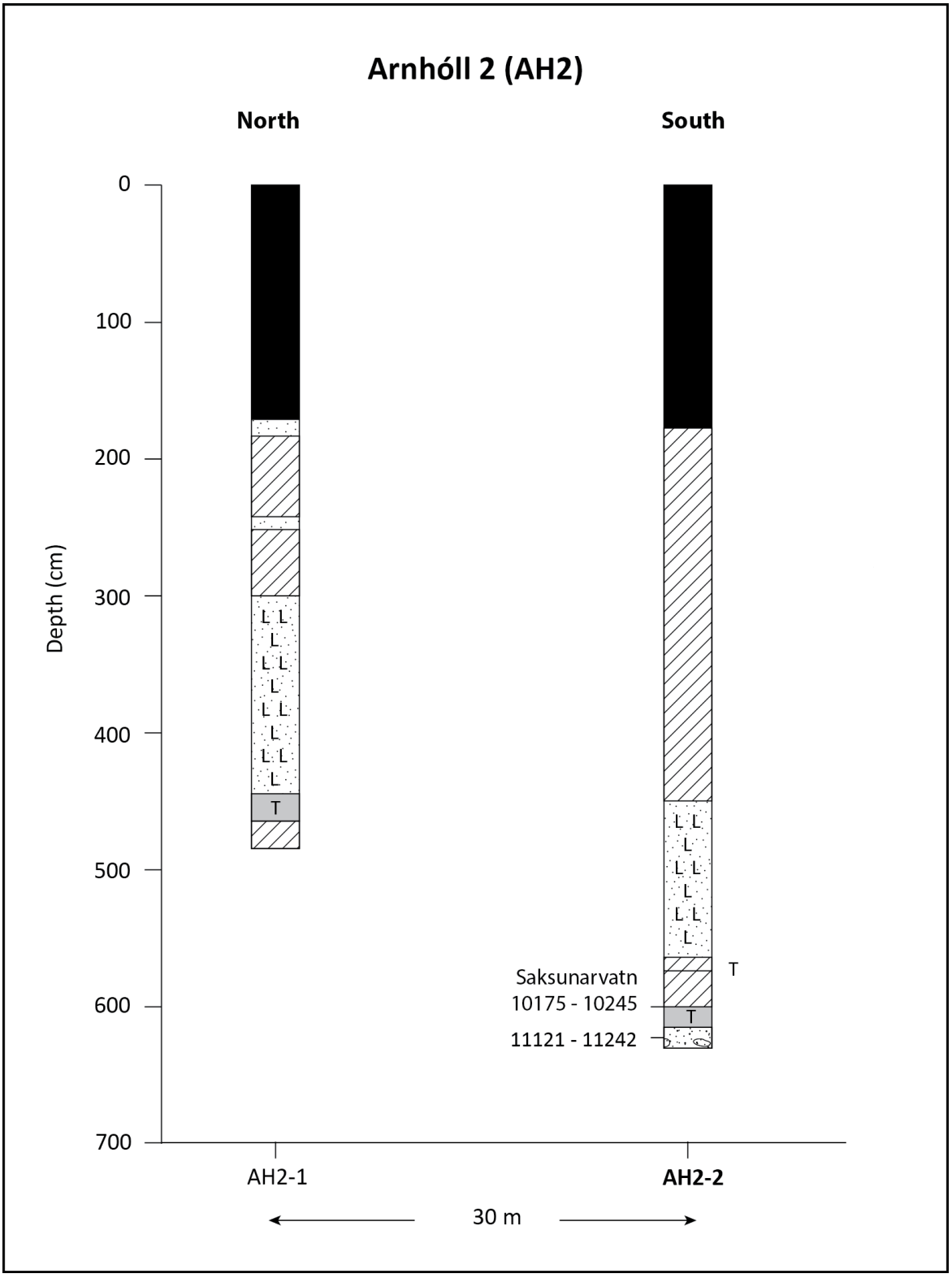

Figure 6.56 – Site stratigraphic profile from Arnhóll 2. For the key to sediment symbols, see Section 6.2. Ages presented are calibrated ages before present (cal. a BP).

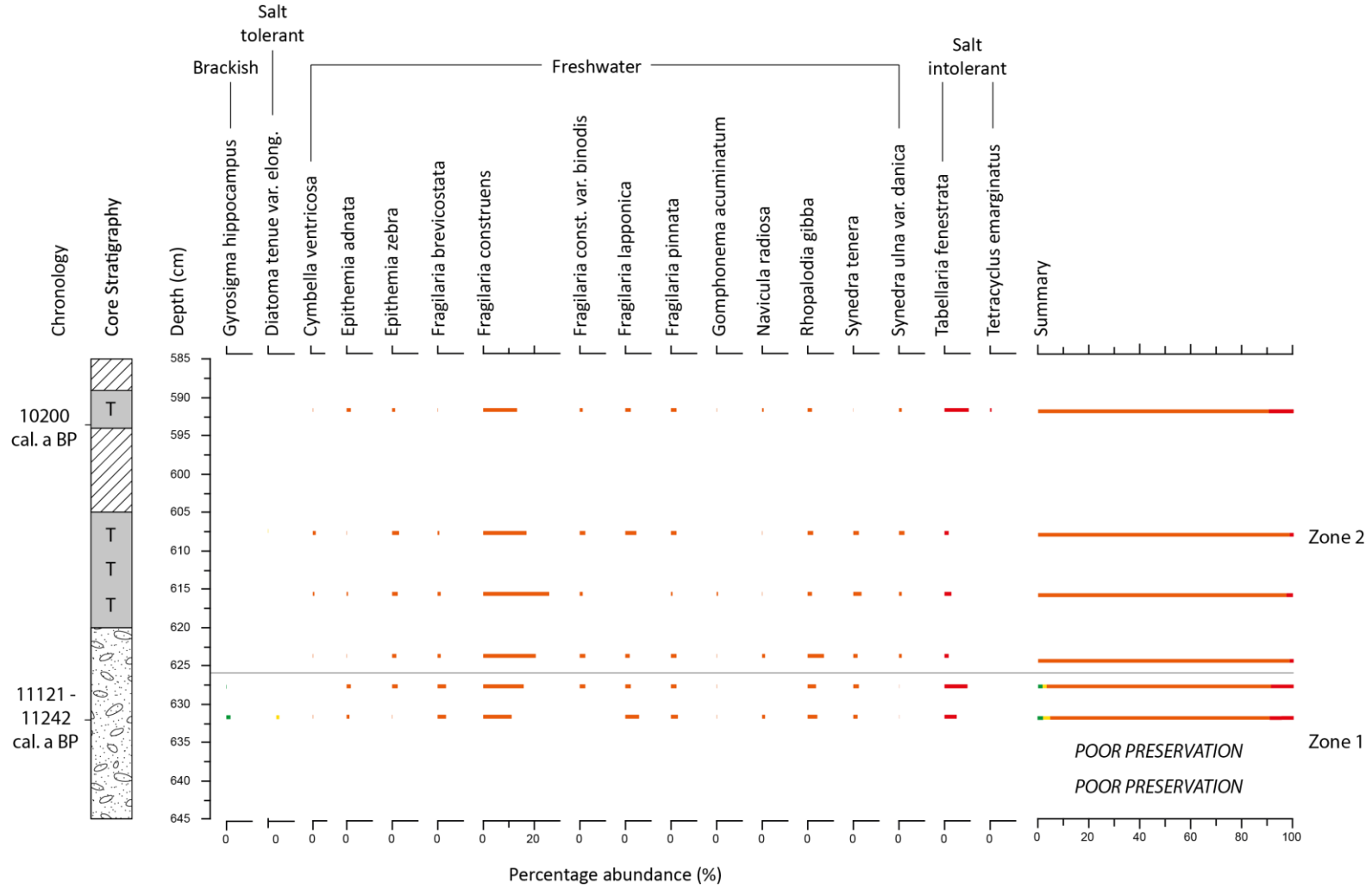

Figure 6.57– Diatom assemblage from AH2-2 (>3% of the total diatom count) showing the weak brackish influence recorded at the base of the sample. Figure key: Section 6.2.

6.7.8 Arnhóll 1 (AH1)

Sill elevation: 70.62 ± 0.30 m asl Site location: 65°17.657'N 20°55.821'W

The sill at AH1 was identified through a grid of cores, with the lowest high point representing the basin sill (S4, Fig. 6.58). Information about basin morphology can be found in Section 3.6.3.

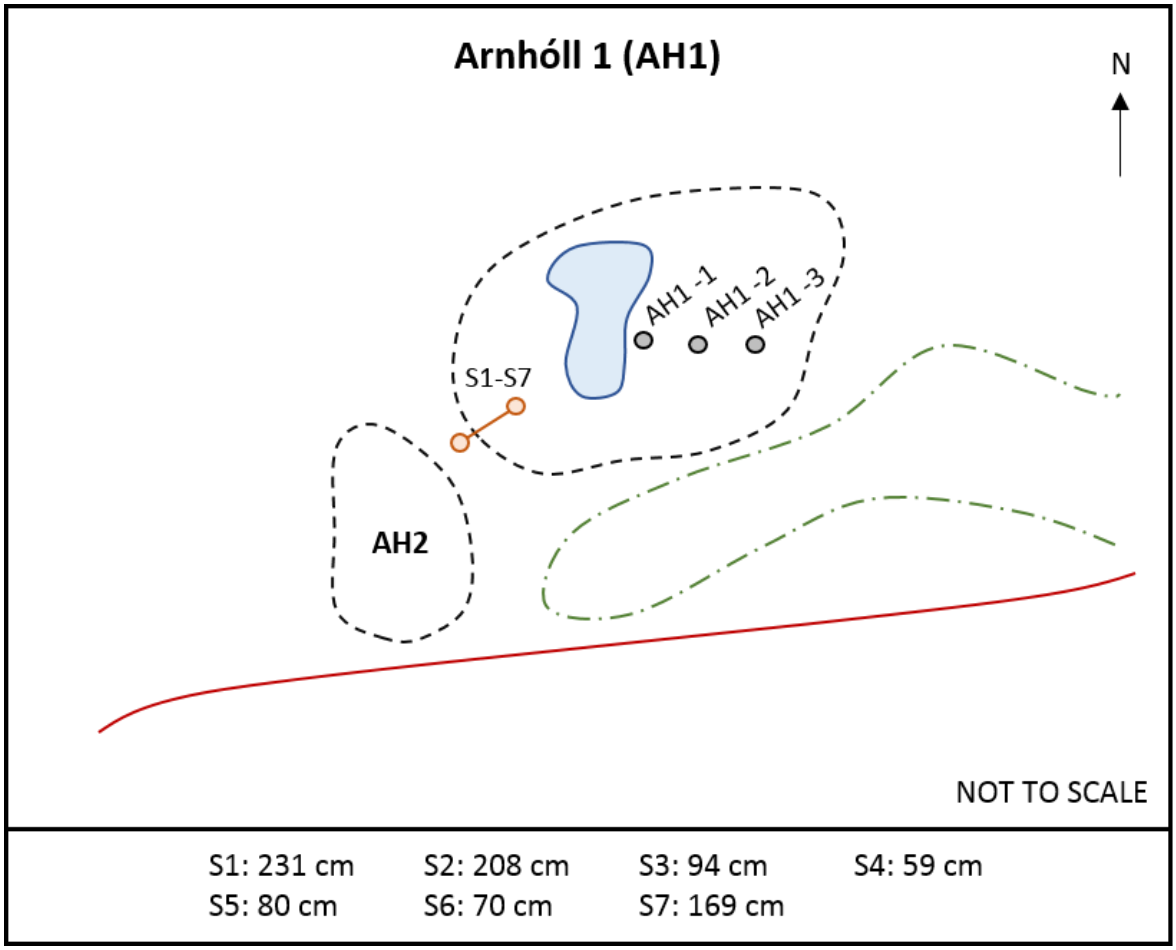

Figure 6.58 – Sill identification at AH1, showing the sill core locations (orange), sediment core locations (black dots), road (red solid line), present lake (blue), infilled section (black dashed line) and higher surrounding topography (green dashed line). The sill was identified at S4.

6.7.8.1 Site stratigraphy

A transect of three cores were extracted at AH1 (Fig. 6.59). Samples were extracted within the infilled section of the basin, due to ease of access and the difficulties associated with operating the boat at the location. The transect was completed from the basin centre towards the eastern edge of the basin. Each of the three sediment cores returned similar compositions, comprising a basal blue grey clay and silty clay overlain by an olive green limus. Within the limus layer, a distinct dark grey tephra layer was evident in each of the cores extracted. The site stratigraphy is summarised in Fig. 6.59.

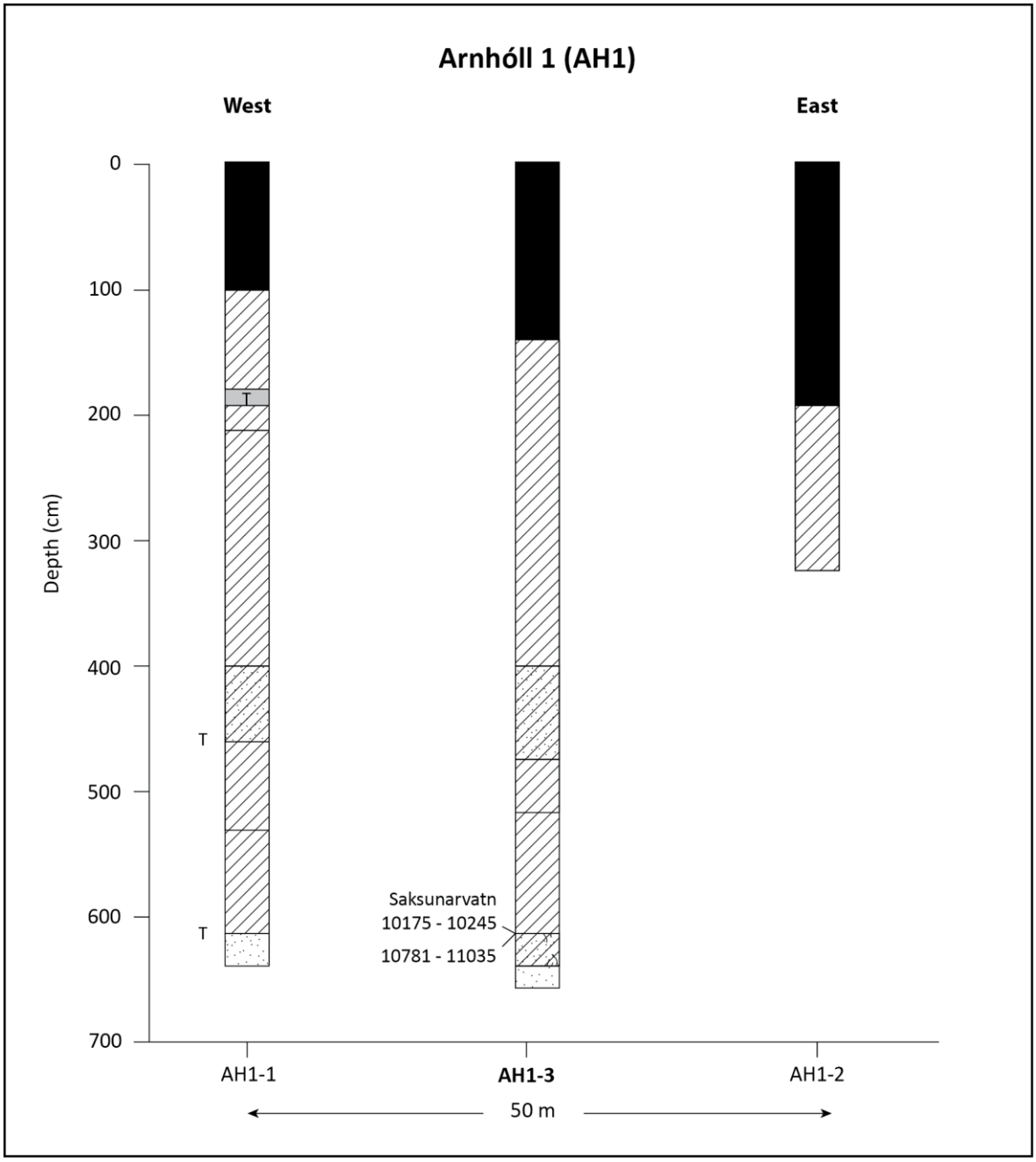

Figure 6.59 – Site stratigraphy at Arnhóll 1 (AH1). For the key to sediment symbols, see Section 6.2.

AH1-3 was selected as a suitable sediment core for diatom analysis, due to the representative nature of the core sample. The AH2-2 sediment core comprises a basal blue grey clay with sand, overlying silty clay and extensive limus layer. Within the limus layer, a 3 cm tephra layer is present. This sample underwent geochemical analysis and was identified as the Saksunarvatn tephra layer, as outlined in Chapter 5 and Fig. 5.6. The sediment core is summarised in Table 6.22 and Fig. 6.59.

Upper Boundary (cm)	Lower Boundary (cm)	Sediment Description	Tröels-Smith Classification
591	609	Olive green organic rich limus	Ld3 Th1
609	612	Dark grey tephra	Ag4
612	630	Olive green limus with some organic material and silt	Ld2 Sh1 Ag1
630	641	Blue grey silt with clay	Ag3 As1

Table 6.22– Sediment descriptions and Tröels-Smith (1955) classifications for the Arnhóll 1 (AH1-3) sediment core sample.

6.7.8.2 Diatom assemblage

In total, nine diatom samples were analysed from the AH1-3 sediment core, but the lowest two samples failed to produce sufficient diatoms to generate a reliable count (Fig. 6.60). The diatom assemblage from AH1-3 therefore comprises seven samples and demonstrates a dominance of freshwater taxa throughout the assemblage. Despite this, the assemblage can be divided into three distinct zones. Zone 1 is characterised by high percentages of *Fragilaria sp.*, particularly *Fragilaria construens, Fragilaria Lapponica* and *Fragilaria pinnata.* Zone 2 sees a reduction in the percentage of *Fragilaria construens,* alongside the first occurrence of *Navicula thorodsseni nov. spec*, which increases to c. 30% of the total diatom count at the end of the zone. Within Zone 3, there is an increase in salt intolerant species, alongside a return to a freshwater assemblage similar to Zone 1.

6.7.8.3 Environmental summary

The diatom assemblage from AH1-3 demonstrates freshwater conditions at the site (Fig. 6.60). The lack of marine or brackish diatom taxa within the assemblage suggests that the site may have been located above highest postglacial RSL (above the marine limit). One radiocarbon sample was produced an age of 9625 ± 40^{14}C a BP (10781 – 11035 cal. a BP) at 613 cm and the Saksunarvatn tephra at 612 cm (Fig. 5.5) provides a limiting date for RSL i.e. RSL must be situated below the altitude of this site at this point in time.

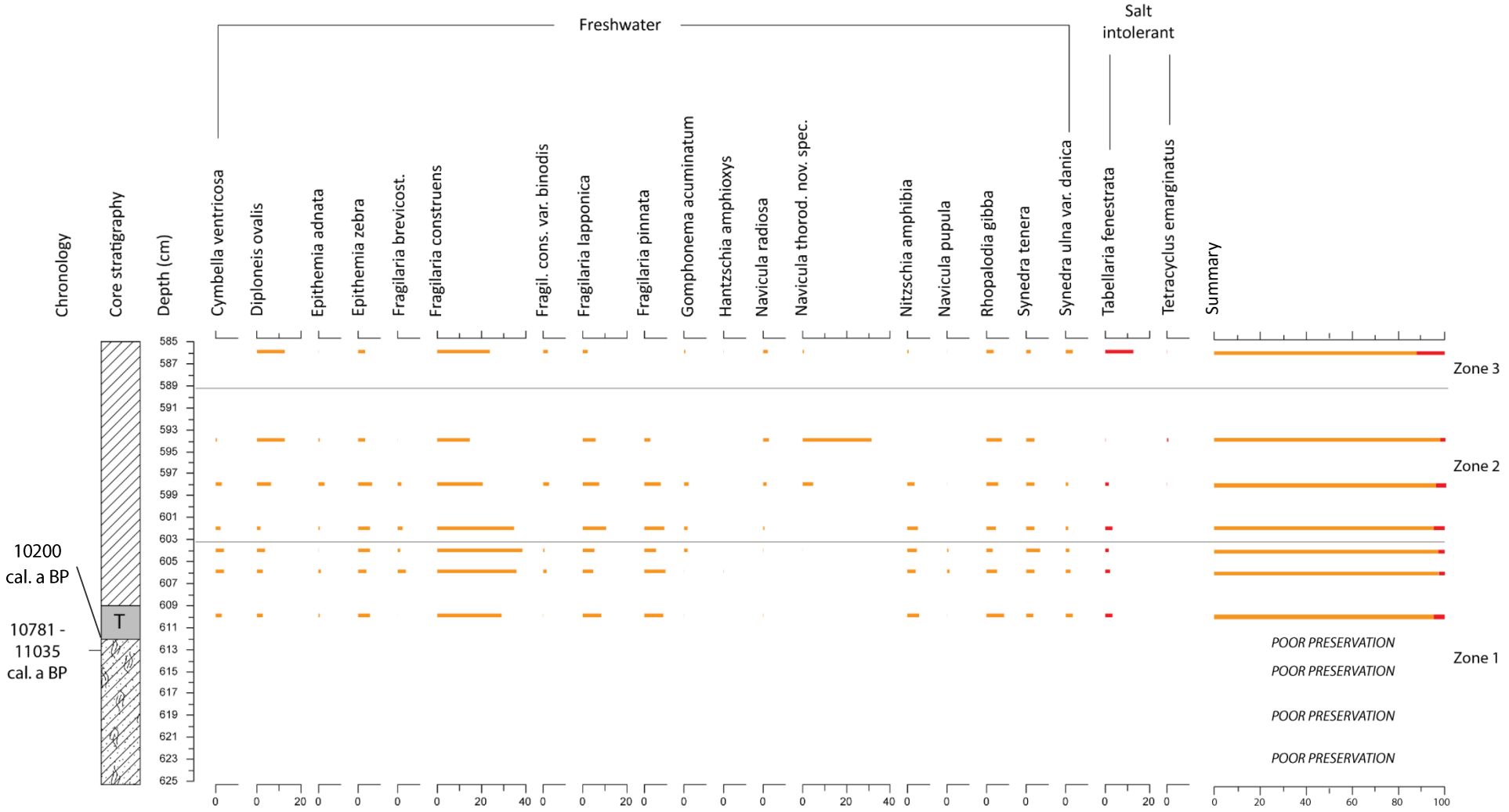

Figure 6.60 – Diatom assemblage from AH1-3 (>3% of the total diatom count) showing the freshwater dominance in the available diatom record. Figure key: Section 6.2.

6.8 Area G – Breiðavik, Vestfirðir

6.8.1 Breiðavik 10 (BR10)

Sill elevation: 4.40 ± 0.30 m asl Site location: 65°32.631'N 24°25.081'W

BR10 is an isolation basin site close to present sea level (Section 3.6.4, Fig. 3.21). The sill was identified within the present drainage channel through the surveying of a series of points along the channel bed using an EDM (S2, Fig. 6.61). The sill was taken as the lowest high point along this transect.

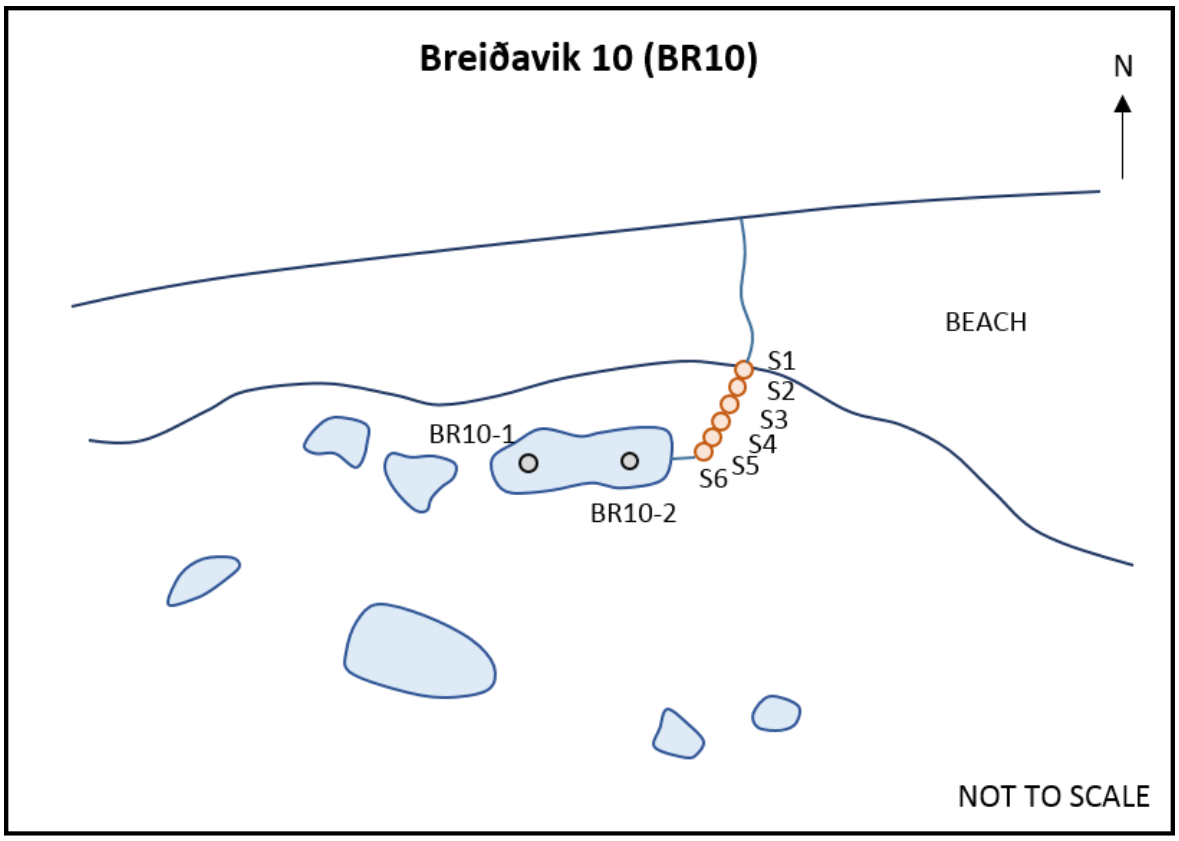

Figure 6.61 – Sill identification at BR10, showing the location of sill survey points (orange dots) and sediment core samples (black dots), with the sill identified at S2. In addition, the present lake (blue infilled shapes) drainage channel (mid-blue solid line) and present coastline (dark blue line) can be seen.

6.8.1.1 Site stratigraphy

In order to establish the underlying stratigraphy at BR10, two sediment cores were extracted. The site stratigraphy can be summarised as a basal sand overlain by a sandy peat and silty clay layer. Above this, an organic rich silt was noted, overlain by limus and organic rich silts. The site stratigraphy can be summarised in Fig. 6.62. One sample was retrieved from BR10-1 to allow subsequent laboratory analyses. The analysed sediment sample is summarised in Table 6.23.

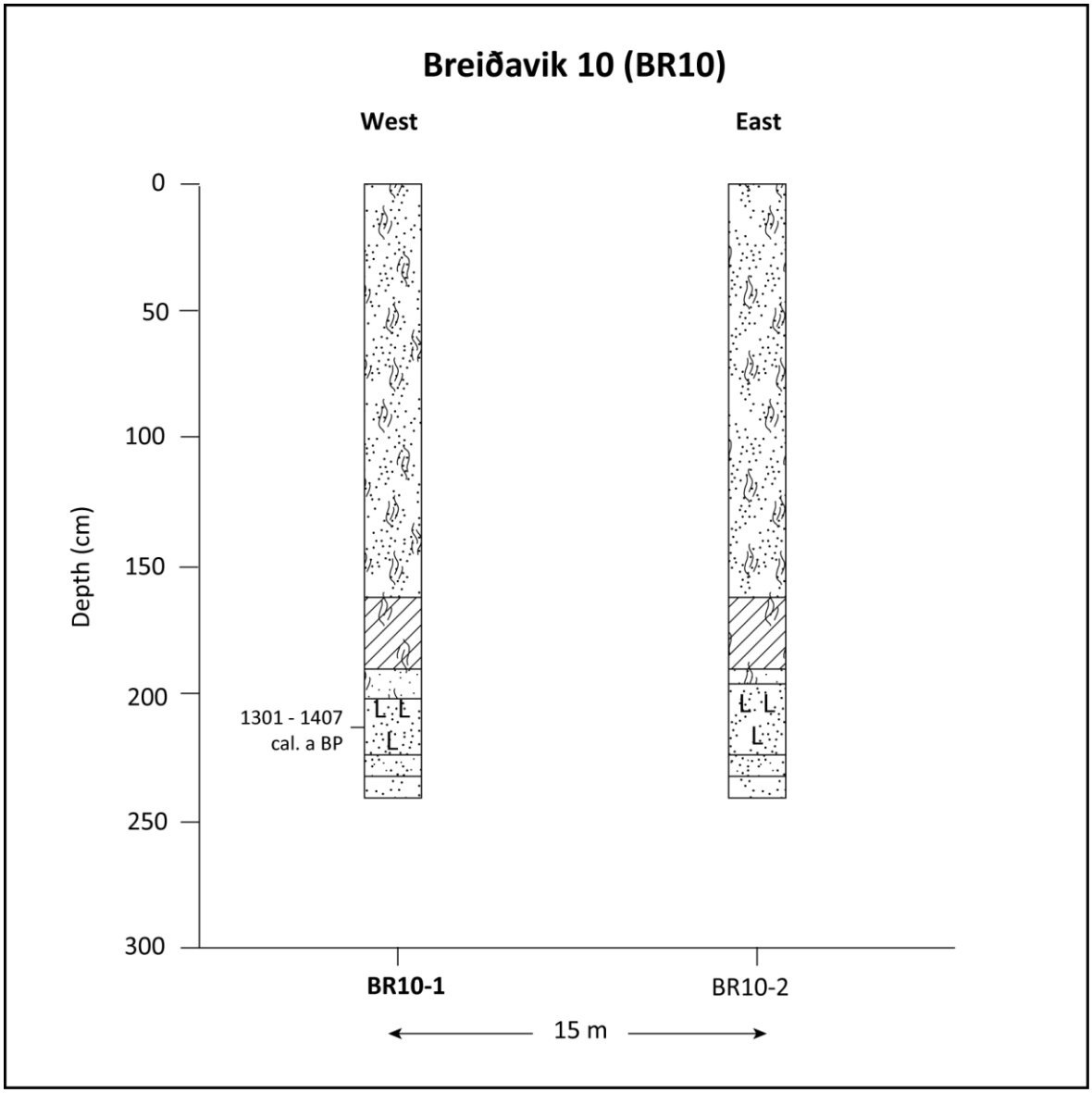

Figure 6.62 – Site stratigraphic profile at BR10. For the key to sediment symbols, see Section 6.2.

Upper Boundary (cm)	Lower Boundary (cm)	Sediment Description	Tröels-Smith Classification
190	202	Dark grey organic rich silt with shell fragments	Ag3 Sh1 part test+
202	228	Dark grey silty clay with organic material, shell fragments and sand	Ag1 As1 Sh1 Gmin1 part test+
228	236	Dark grey sandy silt	Ag3 Gmin1
236	240	Dark grey coarse sand with shell fragments and organic material	Gmin3 Sh1 part test+

Table 6.23 – Sediment composition of the BR10-1 sediment core sample.

6.8.1.2 Diatom assemblage

The diatom assemblage from BR10-1 can be divided into four distinct zones (Fig. 6.63). Zone 1 has a mixed assemblage, with c. 35% marine, c. 15% brackish and c. 45% freshwater taxa at the start of the zone. Through the course of Zone 1, the proportion of marine taxa decreases to c. 25%, with a resulting increase in freshwater taxa. Zone 2 is characterised by a continuation in the increase in freshwater taxa, with further reductions in the percentages of marine and brackish taxa, such as *Tabularia fasciculata* and *Cocconeis scutellum*. At the end of Zone 2, freshwater taxa comprise c. 90% of the diatom assemblage. Within Zone 3, marine taxa are no longer present within the diatom assemblage. There is however an increase in salt intolerant taxa within the record, particularly in the presence of *Tabellaria flocculosa* and *Tabellaria fenestrata.* Zone 4 sees a return of marine taxa within the diatom assemblage, rising to c. 10% of the diatom assemblage at the end of the zone. In addition, there is reoccurrence of brackish taxa within the zone. Levels of freshwater taxa reduce within this zone, falling from c. 85% to c. 70% of the total diatom count.

6.8.1.3 Environmental Summary

The diatomological isolation contact at BR10 is identified at 218 cm. One radiocarbon sample was analysed at the site, which returned an age of 1301-1407 cal a BP. No tephra deposits were recorded within the sediment sample (Fig. 6.62) and so the radiocarbon sample anaysed acts as the chronological control for the location.

There are three potential interpretations of the BR10 diatom record:

a) That the diatom assemblage at BR10-1 represents a reduction and subsequent increase in marine influence at the site. The diatom assemblage would therefore represent a RSL fall then RSL rise over the course of the record. If so, the BR10 sea-level index point would have both a positive and negative tendency due to the pattern recorded in the diatom record;
b) That the diatom record shows evidence for storm activity post-isolation at 218 cm. This interpretation may be supported by the sandy deposits towards the top of the sediment core. Such deposits may represent wind-blown material or storm deposits; or
c) That basin isolation is still in progress at the site, as marine and brackish diatom taxa are still evident towards the top of the analysed section of the core.

The preferred interpretation is for a rise and subsequent fall in RSL at the location, given the dominant trends within the dataset.

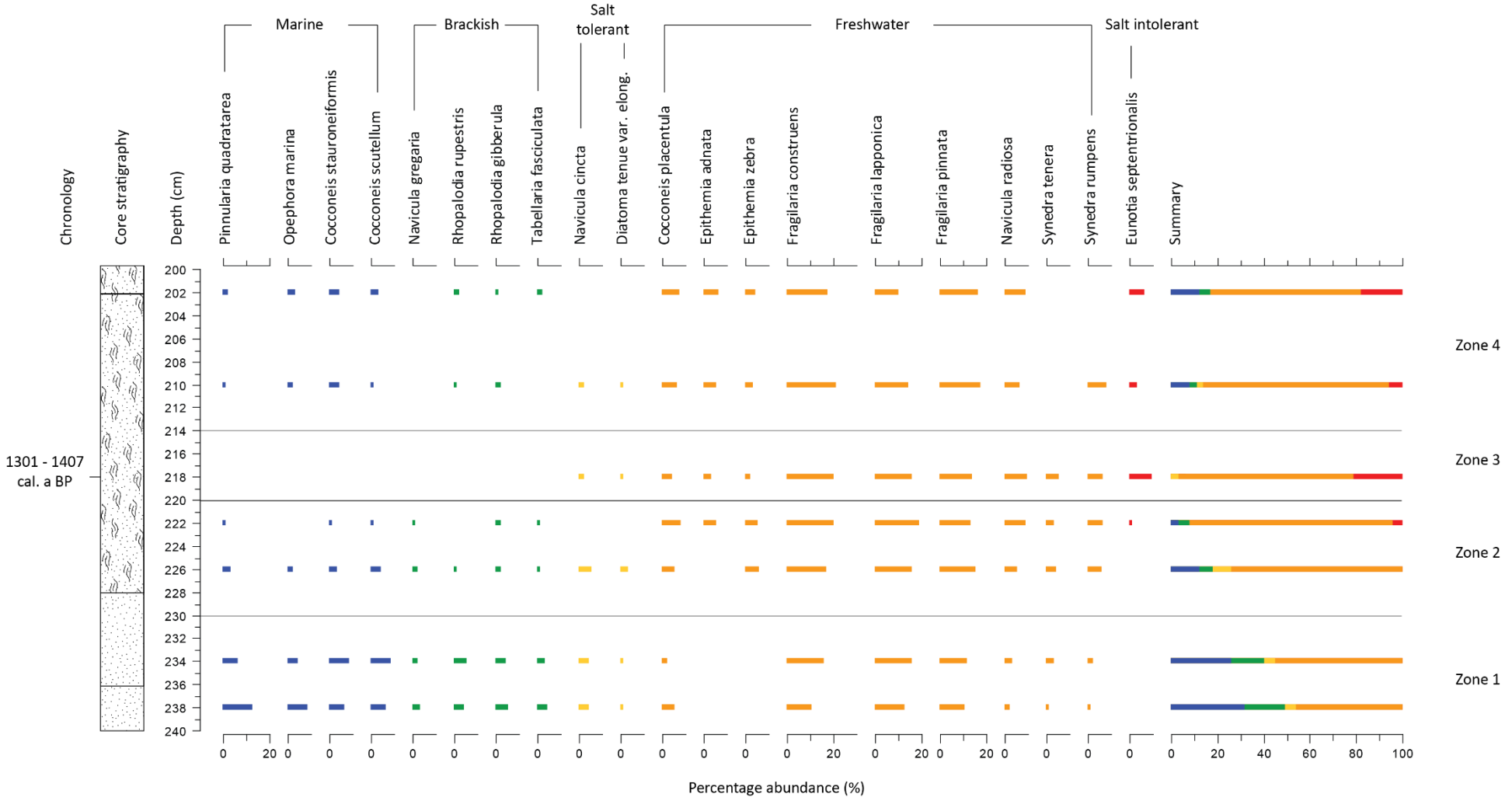

Figure 6.63 – Diatom assemblage from BR10 (>3% of the total count), showing the reduction and reintroduction of marine influence at the site. Key: Section 6.2

6.8.2 Hvallátur 4 (HV4)

Sill elevation: 65.45 ± 0.30 m asl Site location: 65°30.876'N 24°27.746'W

The sill at HV4 was identified within the present drainage channel through the surveying of a series of points within the channel bed on exposed bedrock using an EDM. The sill was identified as the lowest high point along this transect (S3, Fig. 6.64). Information about the site location and morphology can be found in Section 3.6.4 and Fig. 3.23.

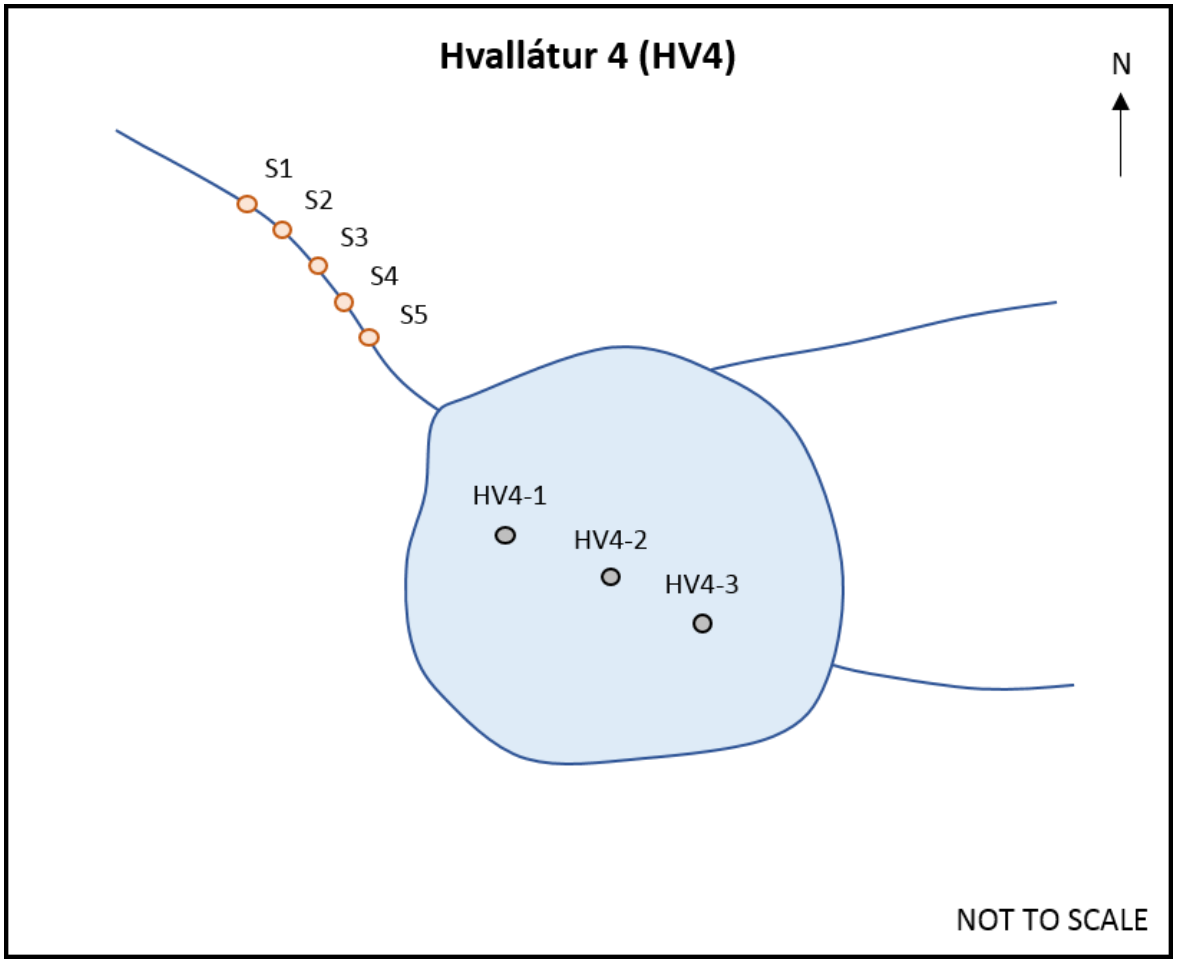

Figure 6.64 – Sill identification at HV4 showing the transect of survey locations (orange dots) within the present drainage channel to the northwest of the lake basin. The location of the sediment samples are also shown (black dots).

6.8.2.1 Site stratigraphy

Three sediment cores were extracted from HV4 in order to establish the site stratigraphy, which is summarised in Fig. 6.65. Due to the length of record available, a sample for laboratory analysis was extracted from HV4-1. The sediment composition of this core sample is summarised in Table 6.24.

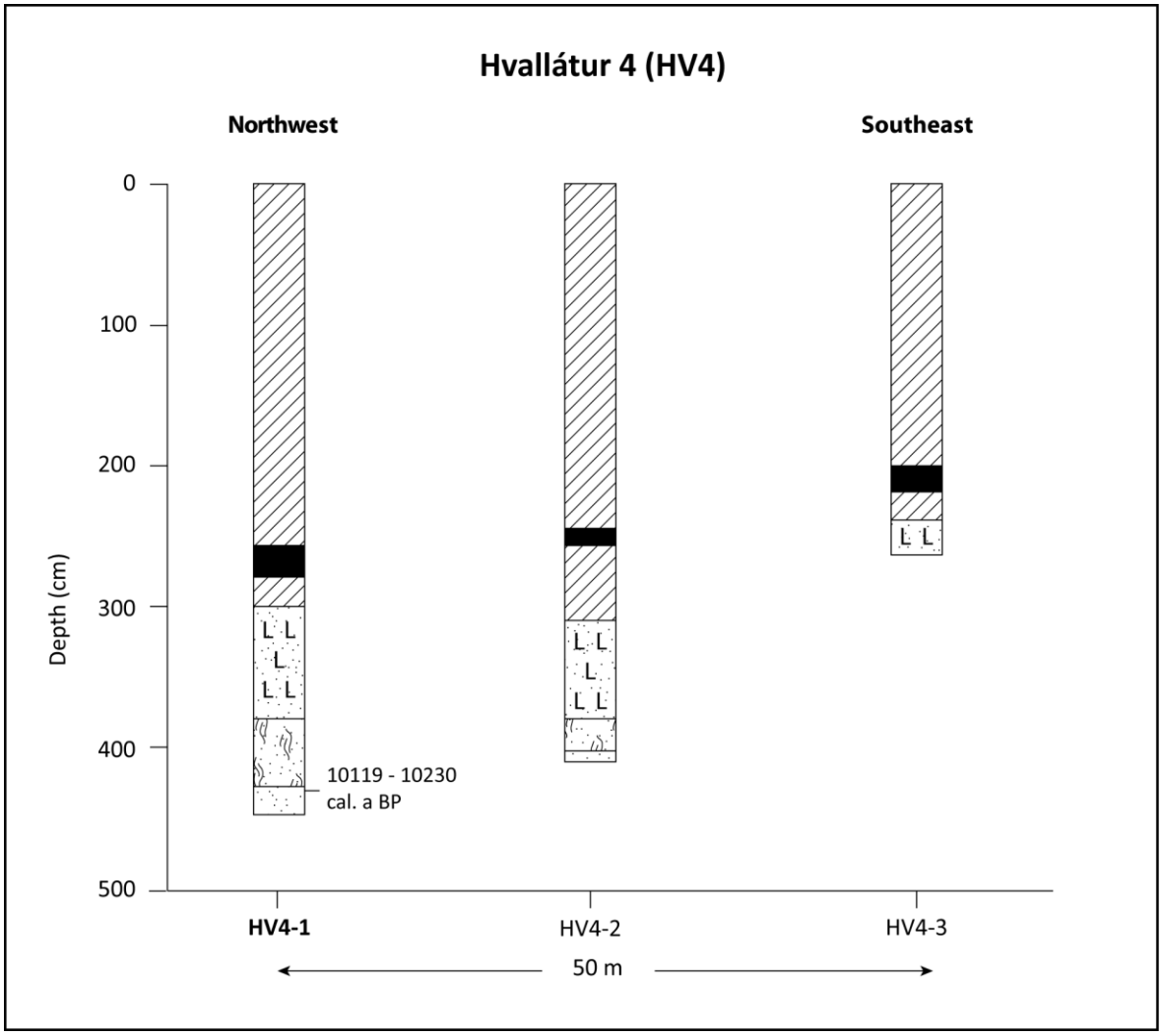

Figure 6.65 – Site stratigraphy at HV4, showing the uniform nature of the sediment composition. For the key to sediment symbols, see Section 6.2.

Upper Boundary (cm)	Lower Boundary (cm)	Sediment Description	Tröels-Smith Classification
405	430	Olive green mixed organic material with silt	Ld3 Ag1
430	455	Grey silt	Ag4

Table 6.24 – Sediment composition of the HV4-1 sediment core sample.

6.8.2.2 Diatom assemblage

The diatom assemblage at HV4-1 can be divided into four distinct zones (Fig. 6.66). Zone 1 is dominated by marine (c. 40%) and brackish (c. 60%) diatom taxa, including *Cocconeis scutellum, Cocconsis stauroneiformis* and *Tabularia fasciculata.* Within Zone 2, the proportion of marine and brackish taxa decreases, with the introduction of freshwater species to the diatom record from the site. The proportion of freshwater taxa increases through the zone from c. 20% to c. 30% through the introduction of *Cymbella ventricosa* and *Fragilaria sp.*

Zone 3 is marked by an increase in the range of freshwater taxa recorded in the diatom assemblage and the introduction of a limited number of salt intolerant taxa, such as *Tabellaria fenestrata.* The levels of marine and brackish taxa reduce through Zone 3, representing c. 5% of the total diatom count respectively at the termination. Levels of freshwater and salt intolerant taxa increase to mark the start of Zone 4. This uppermost zone has a limited percentage of brackish taxa within the first diatom sample, which are subsequently lost from the diatom record. The proportion of individual freshwater and salt intolerant taxa remain approximately constant throughout this zone and represent c. 80% and c. 20% of the total diatom count respectively.

6.8.2.3 Environmental Summary

There is a clear reduction in marine influence within the diatom assemblage from HV4-1, as demonstrated by the reduced percentages of marine and brackish taxa in the upper zones (Fig. 6.66). The diatom record from HV4 therefore suggests a RSL fall at the site. The diatomological isolation contact is identified at 432.5 cm, which is the boundary between Zone 2 and Zone 3. One radiocarbon sample was analysed from the site at 435 cm, which provided an age of 8972 ± 41 ^{14}C a BP (10119 - 10230 cal. a BP). No tephra deposits were found in Area G and there were therefore no samples analysed from HV4.

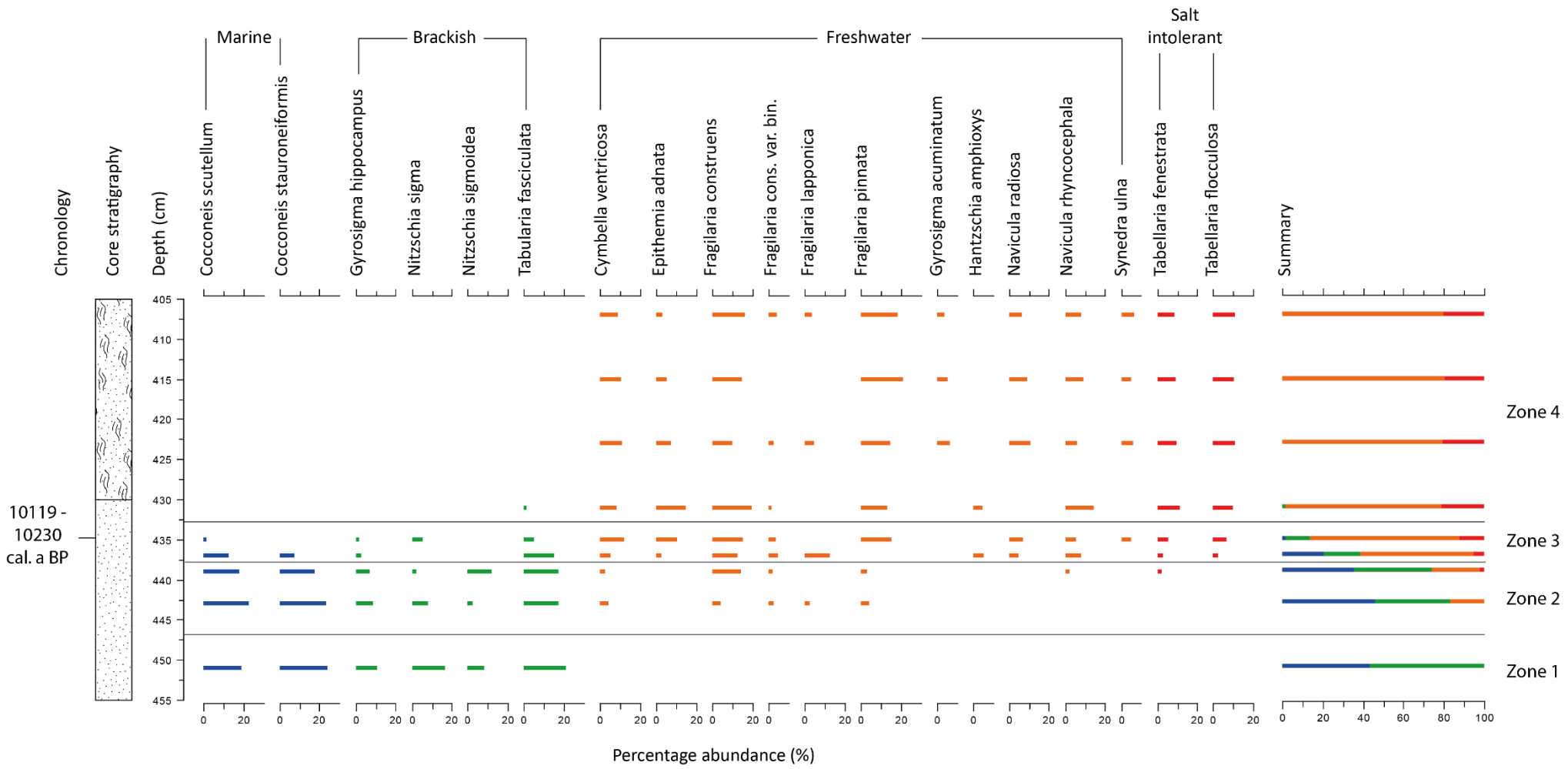

Figure 6.66 – Diatom assemblage from HV4-1 (>3% of the total diatom count), showing the transition from brackish-marine to freshwater dominance at the site. Figure key: Section 6.2.

6.8.3 Hvallatur 3 (HV3)

Sill elevation: 68.70 ± 0.30 m asl Site location: 65°30.889'N 24°27.504'W

The sill at HV3 was identified in the present drainage channel, which exits to the west of the present lake. A series of elevation measurements were taken within the channel using an EDM, with the lowest high point along this transect representing the sill elevation (S2, Fig. 6.67). Information about the morphology can location of the basin can be found in Section 3.6.4 and Fig. 3.23.

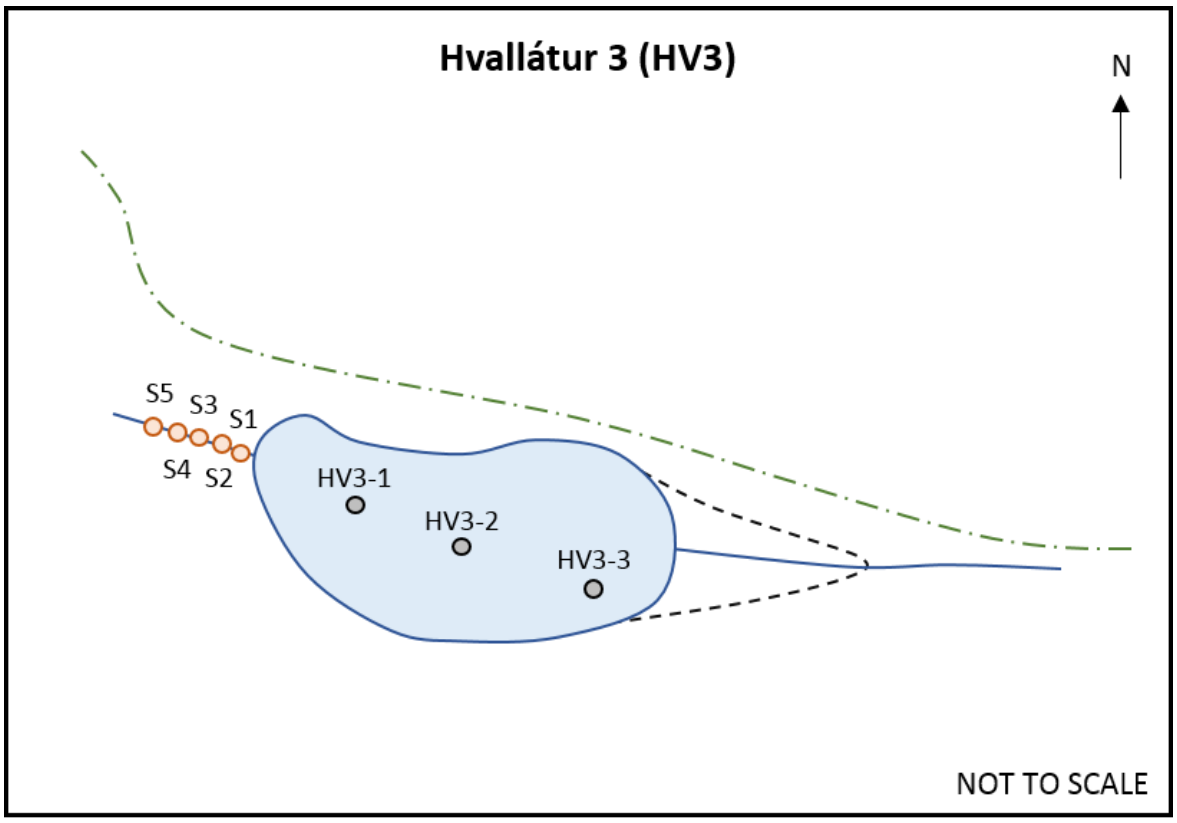

Figure 6.67 – Sill identification at HV3 showing the location of the transect of survey points (S1-S6; orange dots) and the position of sediment core samples (black dots), alongside the present lake (blue), basin (black dashed line) and higher surrounding topography (green dashed line).

6.8.3.1 Site stratigraphy

In order to establish the underlying site stratigraphy, three sediment cores were extracted from HV3. The site stratigraphy can be summarised as a basal grey silt, overlain by olive green silty limus and olive green limus deposits (Fig. 6.68). One sample was retrieved at HV3-1 (Fig. 6.68) for subsequent laboratory analysis due to the completeness of the available record. The sediment composition of this sample is summarised in Table 6.25.

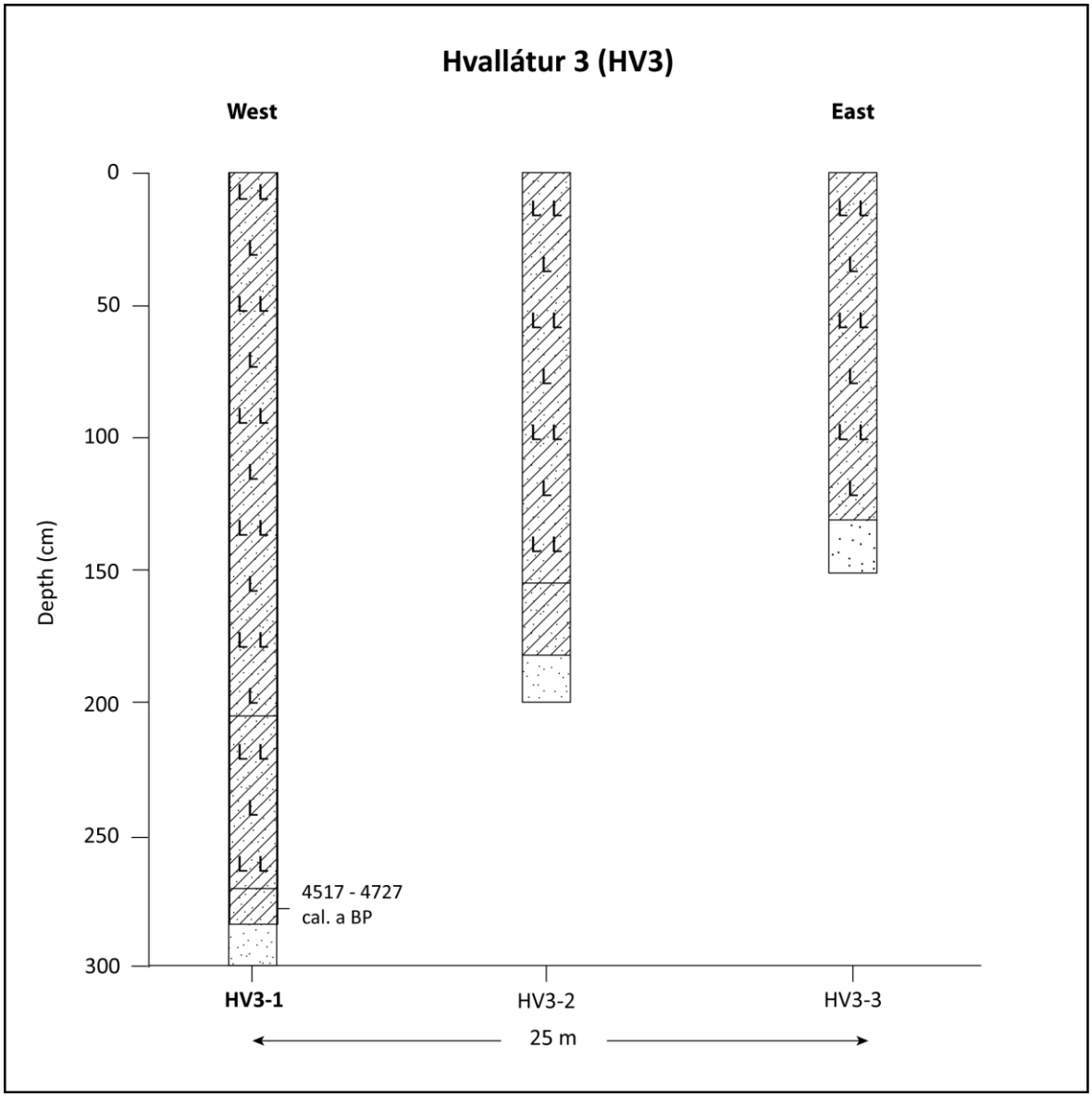

Figure 6.68 – Site stratigraphy at HV3, showing the variability in sediment depth recorded at the site.

Upper Boundary (cm)	Lower Boundary (cm)	Sediment Description	Tröels-Smith Classification
260	271	Olive green limus with silt and clay	Ld2 As1 Ag1
271	281	Olive green limus with silt	Ld3 Ag1
281	300	Blue-grey silt	Ag4

Table 6.25 – Sediment composition of the HV3-1 sediment core sample.

6.8.3.2 Diatom assemblage

At HV3-1, the diatom assemblage can be divided into two zones (Fig. 6.69). Zone 1 is characterised by a mixed composition, with brackish, marine and freshwater taxa present throughout the zone. Unfortunately, several lower samples from HV3 were poorly preserved, so

it was not possible to generate statistically reliable diatom counts. However, there is a clear reduction in the proportion of brackish and marine taxa through the zone. Freshwater taxa represent c. 18% of the total count at 298 cm. Toward the top of Zone 1, there is an increase in the proportion of freshwater taxa, making up c. 85% of the total count for the uppermost sample in the zone at 278 cm. Zone 2 is comprised predominantly of freshwater taxa. A small number of *Gyrosigma hippocampus* is present within the lowermost sample within this zone, but all brackish taxa are lost from the record thereafter. The level of salt tolerant taxa within this zone fluctuates, principally through levels of *Navicula cincta*, whereas the percentage of most freshwater and salt intolerant species remains roughly constant throughout.

6.8.3.3 Environmental Summary

There is a clear transitional sequence present within the diatom data from HV3-1, which represents a decrease in marine influence at the site, denoting a fall in RSL at the location. The diatomological isolation contact is identified at 276 cm, following the loss of the majority of brackish and marine taxa from the site record. No tephra layers were found within the sediment sample, but chronological control was achieved through a radiocarbon sample at 278 cm. The sample returned an age of 4102 ± 38 ^{14}C a BP (4517 - 4727 cal. a BP).

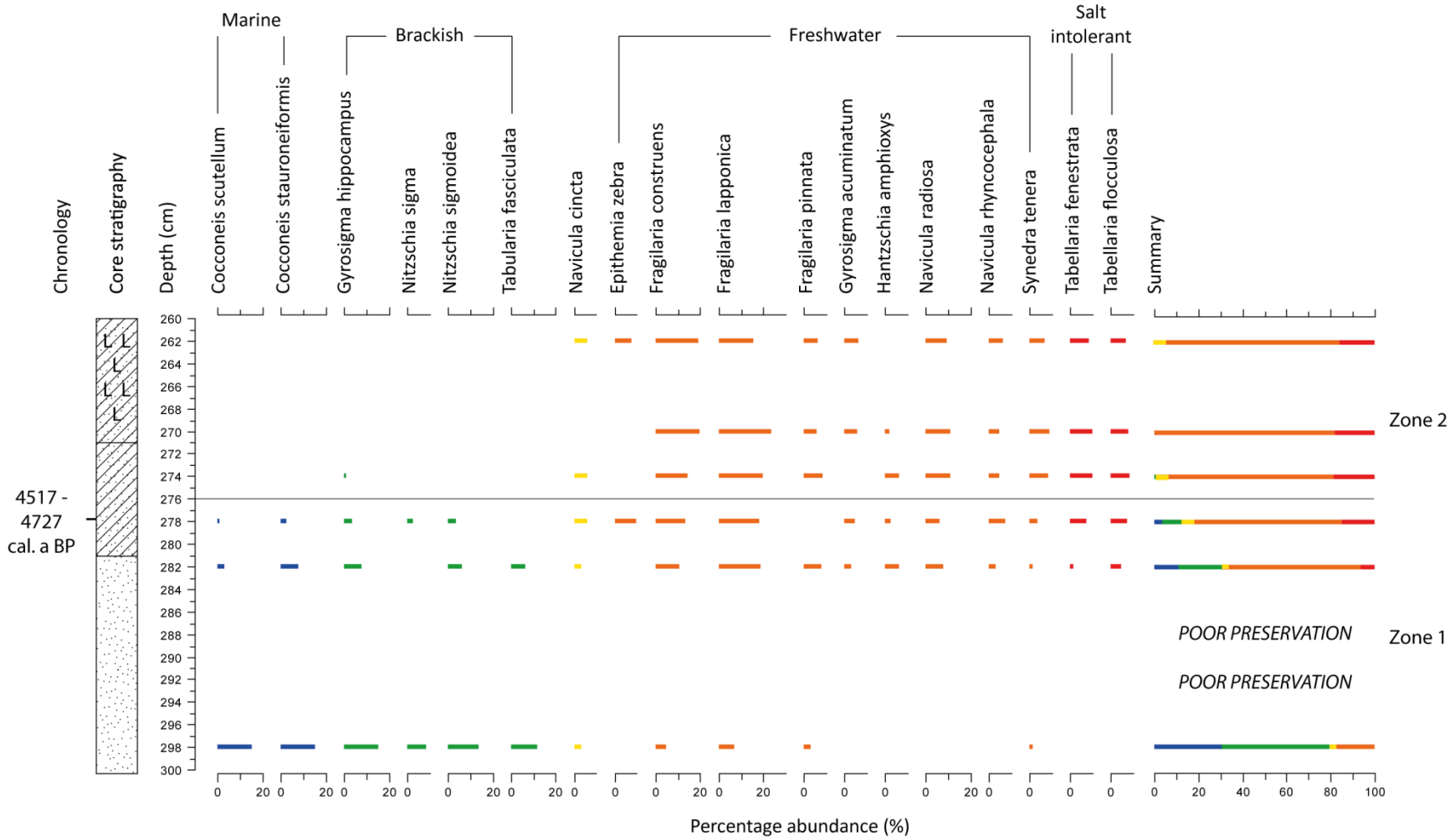

Figure 6.69 – Diatom assemblage from HV3-1 (>3% of the total diatom count) showing the transition from brackish-marine dominance to freshwater dominance. Figure key: Section 6.2.

6.8.4 Breiðavik 1 (BR1)

Sill elevation: 74.70 ± 0.30 m asl Site location: 65°32.322'N 24°21.266'W

The potential sill locations were identified during analysis of the surrounding morphology. The sill at BR1 was therefore identified through a grid of cores in two locations at the basin edge, with the lowest high point identified as the basin sill (Fig. 6.70).

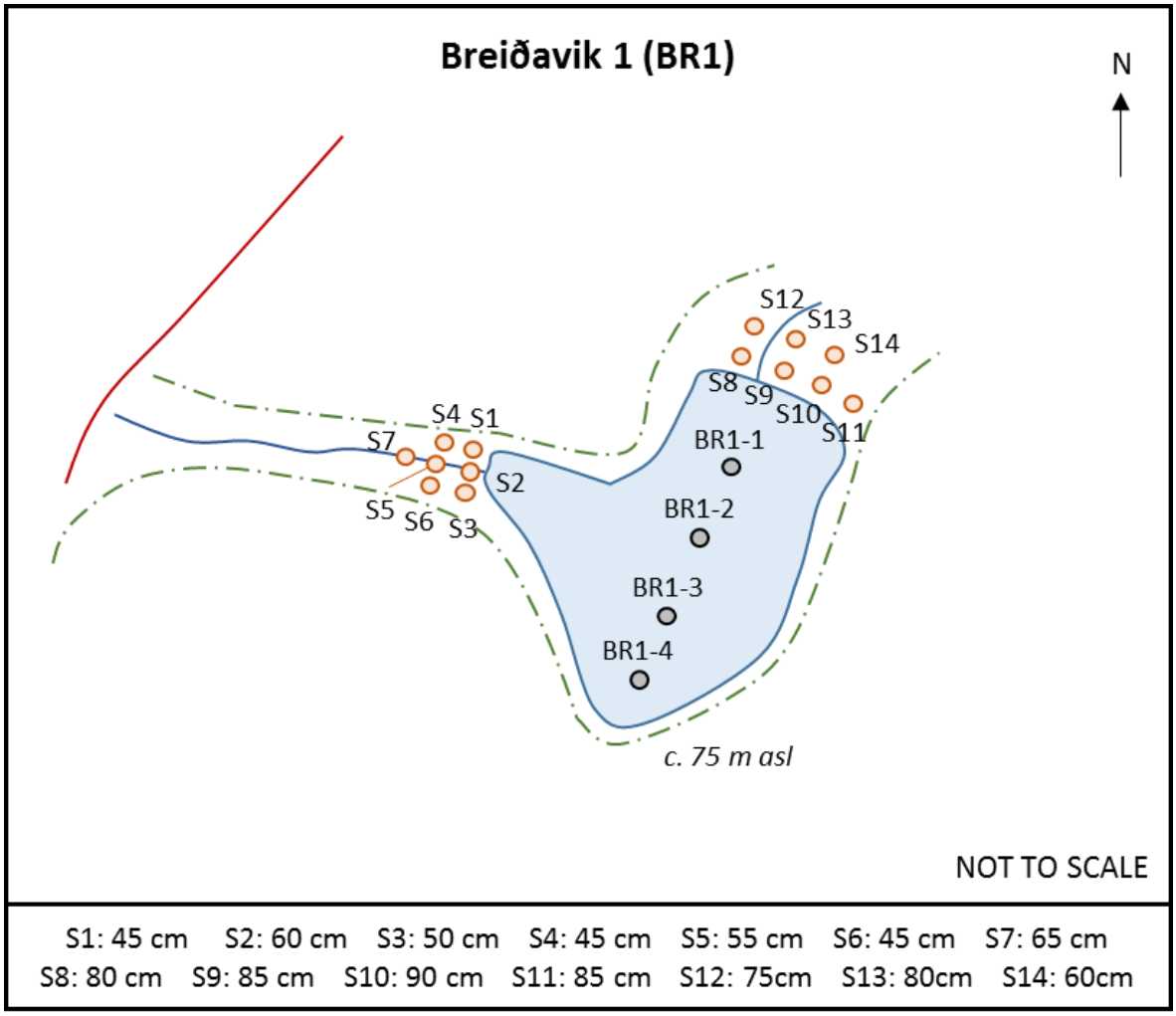

Figure 6.70 – Sill identification at BR1 showing the location of the two grids of survey points on underlying bedrock (orange dots) and sediment core locations (black dots). In addition, the surrounding higher topography (green dashed line), road (red solid line) and sill core depths to underlying bedrock are recorded.

6.8.4.1 Site stratigraphy

BR1 is the highest basin surveyed in Area G, being situated close to the proposed local marine limit at c. 85 m asl (Norðdahl and Pétursson, 2005). Four sediment cores were extracted to establish the underlying site stratigraphy, which is summarised in Figure 6.71. The most complete record was retrieved from BR1-1 and a sample was therefore retrieved for subsequent diatom analysis. The composition of the BR1-1 sediment core is summarised in Table 6.26.

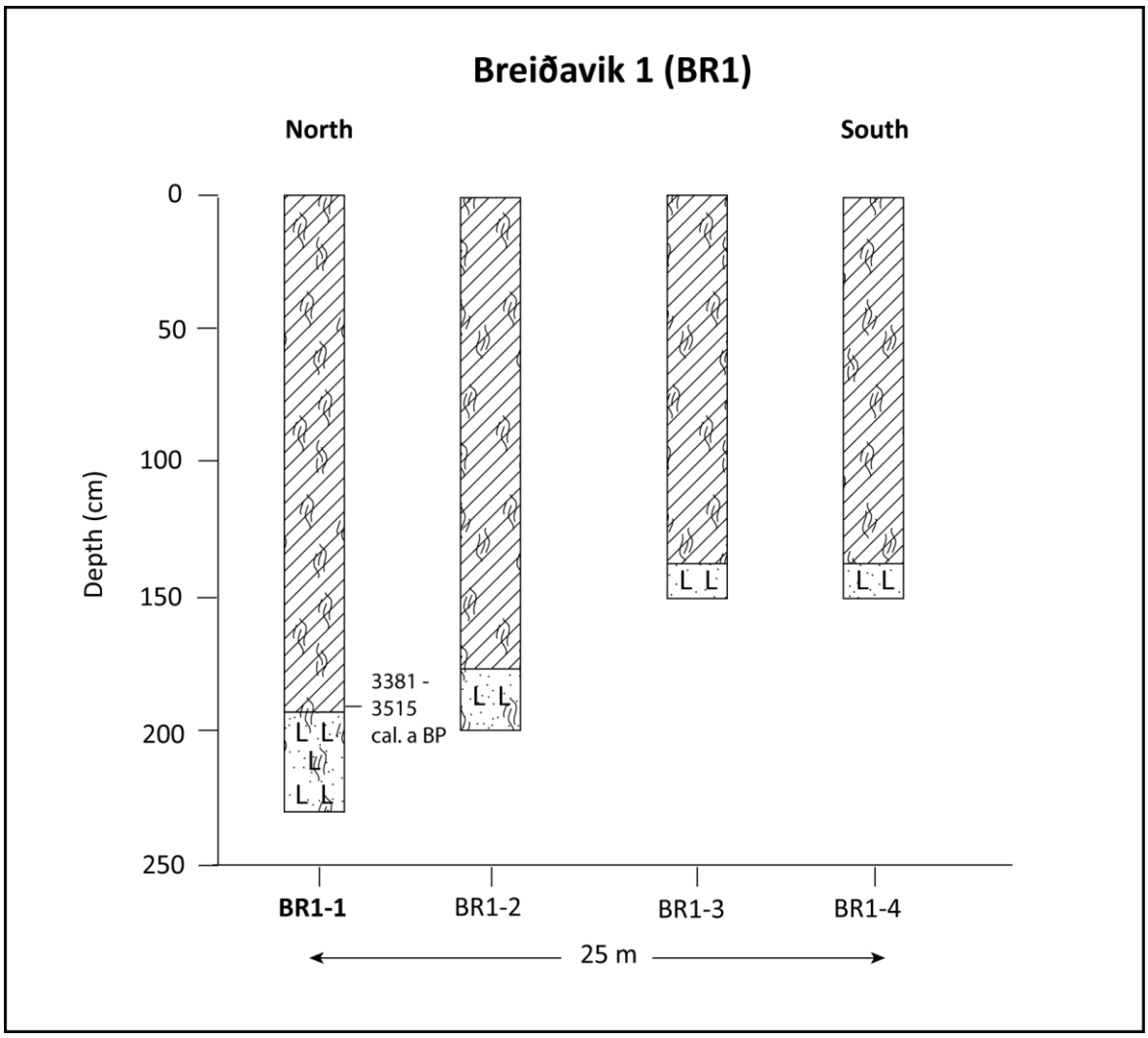

Figure 6.71 – Site sediment stratigraphy at BR1, Area G. For the key to sediment symbols, see Section 6.2.

Upper Boundary (cm)	Lower Boundary (cm)	Sediment Description	Tröels-Smith Classification
0	190	Olive green limus with abundant organic material	Ld3 Sh1
190	235	Mid brown silt with clay and organic material	Ag2 As1 Sh1

Table 6.26 – Sediment composition of the BR1-1 sediment core sample.

6.8.4.2 Diatom assemblage

The diatom assemblage at BR1-1 can be divided into two zones (Fig. 6.72). Zone 1 has a minor marine and brackish influence, principally through the presence of *Gyrosigma hippocampus*, *Tabularia fasciculata* and *Cocconeis scutellum* within the record. The zone is however dominated by freshwater taxa, including *Fragilaria construens, Fragilaria pinnata* and *Fragilaria lapponica.* The zone also contains c. 10% salt intolerant taxa, such as *Tabellaria fenestrata.* Zone 2 is marked by the loss of marine and brackish taxa from the diatom record. The proportion of salt intolerant

taxa increases through the zone, rising to c. 20% of the total diatom count at 66 cm. Diatom samples analysed at lower depths within the sediment core suffered from poor preservation.

6.8.4.3 Environmental Summary

The diatom record at BR1-1 demonstrates very weak marine influence at the base of the sample, suggesting that the sediment core records the final stages of isolation at the site. In particular, Zone 2 records the decreased brackish-marine influence at the site over time. Consequently, the core records a fall in RSL at the site. One radiocarbon sample was retrieved from the site at 90 cm, which returned an age of 3233 ± 37 ^{14}C a BP (3381 - 3515 cal. a BP). No tephra deposits were found at the location.

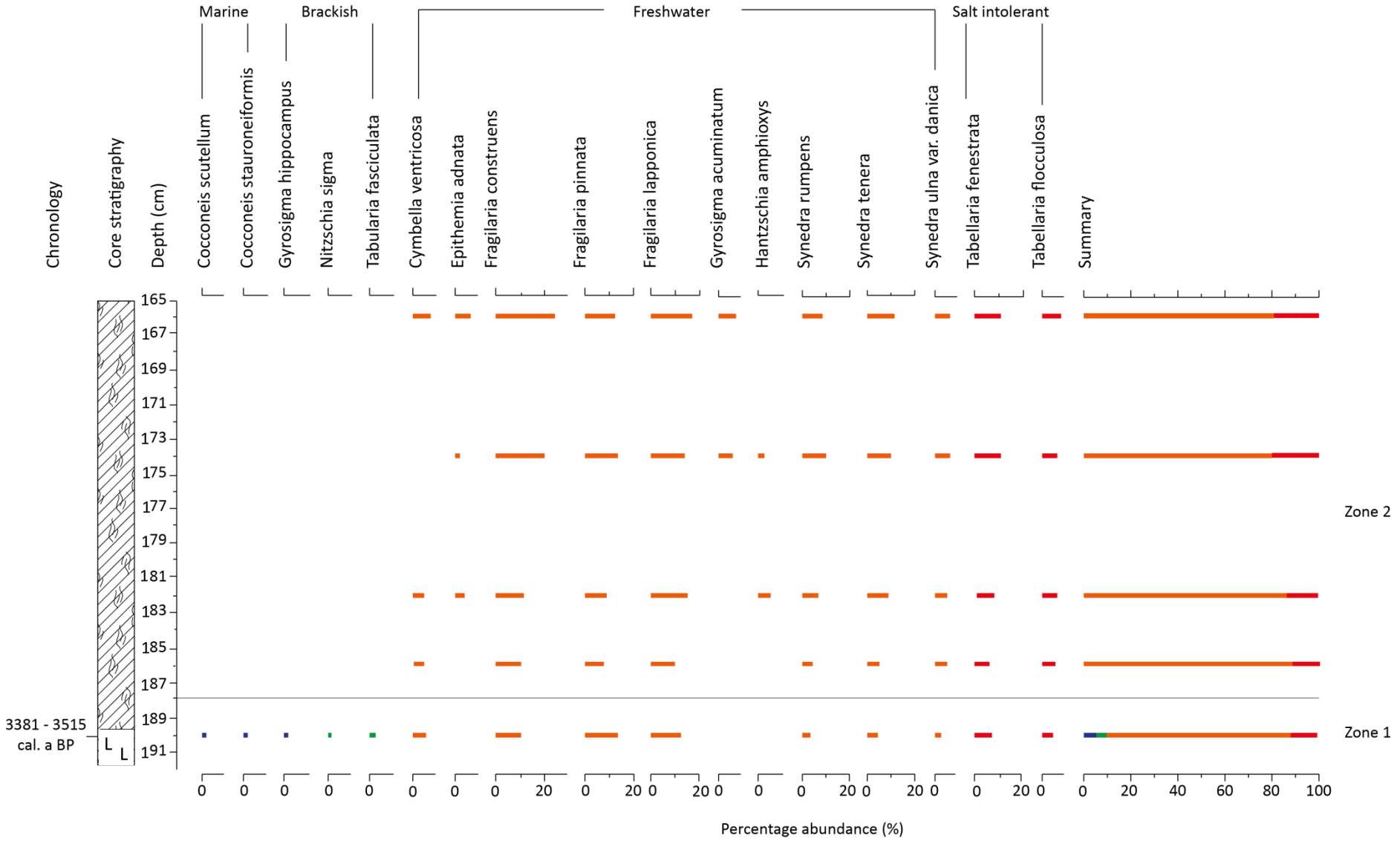

Figure 6.72 – Diatom assemblage for BR1-1 (>3% of the total diatom count) showing the minor brackish influence at the base of the analysed section. Figure key: Section 6.2.

6.9 New RSL index points for northwest Iceland

The diatom analyses at sites in Areas A, C, D, E, F and G (Fig. 3.3) have allowed the investigation of environmental changes at locations throughout northwest Iceland. Where these environmental changes are supported by suitable chronological control, whether radiocarbon analyses or tephrochronology, it has been possible to generate a series of new sea-level index points. As outlined in Chapter 4, sea-level index points were calculated through identification of the indicative meaning from diatom analyses of individual isolation basins. Where appropriate, corrections for marine and freshwater reservoir effects have been undertaken.

The completed analyses have allowed the identification of 22 new sea-level index points for northwest Iceland (Table 6.27). Table 6.27 contains information on sample identification, site name, site elevation (m), radiocarbon age (1 σ), calibrated age (2 σ), indicative meaning and corrected RSL (m). Using these data, it is possible to generate a series of new RSL curves which can be used to test the modelled RSL changes presented in Chapter 7. The new sea-level index points can be summarised by field research area as below:

Area A

One new sea-level index point was generated for Area A, providing an age for deglaciation and marine limit formation in the region (Fig. 6.73). The age constraint for the sea-level index point was calculated by extrapolation of the tephrochronological analyses undertaken at the site, due to the anomalous radiocarbon age produced (Table 6.28). These results are presented alongside the sea-level index points generated in Area A by Rundgren *et al.* (1997; Table 6.27).

Area B

No new sea-level index points were generated in Area B as part of this research project. The results from Lloyd *et al.* (2009) are presented in Table 6.27 and Fig. 6.74 to provide an insight into the sea-level index points generated for the field research area.

Area C

One sea-level index point was generated in Area C as part of this research (Fig. 6.75). The sea-level index point from YBR1 provides a limiting age for marine limit formation in the region, with the age constraint being produced via extrapolation from tephrochronological analyses at the site. Two additional radiocarbon ages are presented for the site, but these are significantly older results than previously found in Iceland (Brader *et al.,* submitted). In addition to this new sea-level index point, the results of previous research are presented to provide an overview of the present RSL record from the region (Brader *et al.*, submitted; Table 6.27)

Area D

One new sea-level index point was generated in Area D, from diatom analyses at REK1 (Fig. 6.76). The sample provides an age for marine limit formation in the region, due to the close proximity of the site to the local marine limit. Due to the limited marine influence recorded at the site, this location will not be employed to test the GIA model outputs.

Area E

Eight new sea-level index points were generated in Area E, ranging from present sea level to the local marine limit (Fig. 6.77). The results from this area are supported by both radiocarbon and tephrochronological analyses. Unfortunately, radiocarbon analyses at BB1, the closest site to present sea level, provided a 'modern' age, which cannot therefore be used as a reliable sea-level index point. If an index point could have been generated at BB1, a timing of RSL below present would have been possible.

Area F

A further eight new sea-level index points were produced in Area F, with the majority of sites either close to present sea level or the marine limit (Fig. 6.78). As previously outlined, there is a lack of suitable locations for isolation basin research at mid-elevations within the postglacial RSL profile. The index point from AH1 acts as a minimum age for RSL, as the diatom assemblage demonstrates that RSL had fallen below the sill elevation at the time recorded.

Area G

Five sea-level index points were generated in Area G (Fig. 6.79). However, there are a number of issues regarding the dates produced. The result from BR10 appears to be reliable, but results from higher elevations appear to be significantly younger than would be anticipated, possibly due to contamination from rootlets and other sources of younger carbon. Observations from core extraction and sediment analysis at HV3 and HV4 record the presence of modern rootlets within the sediment record.

The isolation basin and coastal lowland sea-level index points from northwest Iceland add to the existing RSL dataset for Iceland, which were included within *sealevel.dat* in SELEN. The criteria employed for inclusion within this Iceland-wide dataset are outlined in Chapter 4.

Area	Site Code	Lab Code	^{14}C age (1σ) BP	cal. age (2σ) BP	Uncorr. sill/ core elv. (m MHWST-sill)	Corr. sill/core elv. (m asl)	Core depth (cm)	Reference wtr. level	Indicative Meaning (m)	Relative sea level (m)	
A	OS1	Unreported	9050	10100	-	1.5	-	-	1.2	0.3	Rundgren *et al.* (1997)
	OS1	Unreported	9100-9200	10200	-	1.5	-	-	1.2	0.3	
	NE1	Unreported	9600-9650	10900	-	13	-	-	1.2	11.8	
	KO1	Unreported	9850	11300	-	22	-	-	1.2	20.8	
	GE1	Unreported	9900	11350	-	26	-	-	1.2	24.8	
	HRA	Unreported	10900	12700	-	42	-	-	1.2	40.8	
	TO1	ESTIM.	11300	13000	-	47	-	-	1.2	45.8	
	TJ1	SUERC-54836	6180 ± 37	6955 - 7174	69.75 ± 0.15	71.25 ± 0.3	226	>HAT	N/A	Limiting	This Study
	TJ1	ESTIM.	-	14558	69.75 ± 0.15	71.25 ± 0.3	226	>HAT	N/A	Limiting	
B	HR2	GU-13956	10500 ± 45	12346 - 12700	-	94.1	290	>HAT	2.5	<91.6	Lloyd *et al.* (2009)
	HR1	ESTIM.	12185 ± 100	13785 - 14463	-	79.1	548	MHWST	2.0	77.1	
	BF1	Poz-15684	11400 ± 90	13106 - 13421	-	51.1	401	MHWST	2.0	49.1	
	HSN1	Poz-15682	9670 ± 60	11060 - 11215	-	41.1	431	>HAT	2.5	38.6	
	HSN1	GU-14335	9975 ± 45	11254 - 11620	-	41.1	433	MHWST	2.0	39.1	
	HFN1	GU-14336	11690 ± 40	13416 - 13673	-	24.7	395	MHWST	N/A	N/A	
	HFN1	Poz-15813	11730 ± 70	12414 - 12746	-	24.7	398	HAT	N/A	N/A	
	HFN1	Saksunarvatn	9030 ± 110	9857 - 10439	-	24.7	374	>HAT	2.5	22.2	

	MA1	Poz-15683	3135 ± 35	3319 - 3444	-	3.0	14	MHWST	2.0	1.0	
	SG1	GU-14474	2375 ± 35	2337 - 2490	-	3.0	145	MHWST	2.0	1.0	
C	BO10	Poz-43545	6240 ± 40	7148 - 7259	0.3 ± 0.15	1.8 ± 0.25	50	HAT	2.4 ± 0.45	-0.5 ± 0.7	Brader (2012)
	BO11	SUERC-47976	8931 ± 39	9915 - 10097	1.8 ± 0.15	3.3 ± 0.25	104	HAT	2.4 ± 0.45	0.9 ± 0.7	
	SK1	SUERC-47977	9973 ± 44	11253 - 11619	3.1 ± 0.15	4.6 ± 0.3	548	MHWST-HAT	2.1 ± 0.45	2.44 ± 0.75	
	TH1	Poz-43546	9710 ± 60	11066 - 11241	3.8 ± 0.15	5.3 ± 0.3	505	MHWST-HAT	2.1 ± 0.45	3.21 ± 0.75	
	SA1	SUERC-47983	10455 ± 43	12135 - 12544	7.5 ± 0.15	9.0 ± 0.3	332	MHWST-HAT	2.1 ± 0.45	6.84 ± 0.75	
	HE1	SUERC-47981	9914 ± 42	11224 - 11408	11.3 ± 0.15	12.8 ± 0.3	620	MHWST-HAT	2.1 ± 0.45	10.64 ± 0.75	
	SA3	Poz-43547	10670 ± 60	12544 - 12722	14.7 ± 0.15	16.2 ± 0.3	808	MHWST-HAT	2.1 ± 0.45	14.1 ± 0.75	
	YBR1	SUERC-47984	6972 ± 35	7702 - 7869	56.5 ± 0.15	57.6 ± 0.3	210	N/A	N/A	N/A	This study
	YBR1	SUERC-48878	16841 ± 76	20074 - 20536	56.5 ± 0.15	57.6 ± 0.3	448	MHWST	1.5 ± 0.45	56.1 ± 0.75	
	YBR1	BETA-0314	20140 ± 60	24340 - 24075	56.5 ± 0.15	57.6 ± 0.3	440	HAT	2.4 ± 0.45	55.2 ± 0.75	
	YBR1	ESTIM.	-	13800	56.5 ± 0.15	57.6 ± 0.3	468	MHWST	N/A	Limiting	
D	REK1	SUERC-54842	8275 ± 39	9130 - 9412	17.5 ± 0.15	18.63 ± 0.3	310	MHWST	1.1 ± 0.3	17.7 ± 0.6	
	HD3	Saksunarvatn	-	10175 - 10245	16.91 ± 0.15	18.01 ± 0.3	120	>HAT	N/A	Limiting	
E	BB1	SUERC-47973	MODERN	N/A	-0.5 ± 0.15	-0.5 ± 0.25	15	N/A	N/A	N/A	
	SHV1	SUERC-47963	2123 ± 35	1993 - 2161	0.2 ± 0.15	1.25 ± 0.3	218	MHWST	1.05 ± 0.3	0.2 ± 0.6	
	SHV1	SUERC-47964	2269 ± 35	2156 - 2267	0.2 ± 0.15	1.25 ± 0.3	288	MHWST-MTL	0.65 ± 0.55	0.6 ± 0.85	
	VHF1	SUERC-47967	4886 ± 36	5584 - 5664	3.45 ± 0.15	4.5 ± 0.3	69	MHWST	1.05 ± 0.3	3.45 ± 0.6	

	RK3	SUERC-47965	3602 ± 37	3862 - 3931	5.15 ± 0.15	6.2 ± 0.3	147	MHWST	1.05 ± 0.3	5.15 ± 0.6	This study
	RK6	SUERC-47966	8299 ± 38	9201 - 9432	1.25 ± 0.15	2.3 ± 0.3	100	MHWST	1.05 ± 0.3	1.45 ± 0.6	
	RK10	SUERC-47970	8894 ± 41	9887 - 10190	15.45 ± 0.15	16.5 ± 0.3	238	MHWST	1.05 ± 0.3	15.45 ± 0.6	
	VAT1	SUERC-47971	8947 ± 39	9916 - 10094	21.15 ± 0.15	22.2 ± 0.3	204	MHWST	1.05 ± 0.3	21.15 ± 0.6	
	VAT2	SUERC-47972	10188 ± 42	11712 - 12067	28.45 ± 0.15	29.5 ± 0.3	428	>HAT	N/A	Limiting	
	GR1	SUERC-48877	9377 ± 47	10495 - 10724	27.55 ± 0.15	28.6 ± 0.3	212	MHWST	1.05 ± 0.3	27.55 ± 0.6	
F	KB1	SUERC-54844	2332 ± 37	2306 - 2465	2.75 ± 0.15	3.45 ± 0.3	65	MHWST	0.7 ± 0.25	2.75 ± 0.55	
	KB2	SUERC-54845	338 ± 37	308 - 484	0.4 ± 0.15	1.09 ± 0.3	30	HAT	1.2 ± 0.25	-0.1 ± 0.55	
	KB4	SUERC-54846	2024 ± 37	1890 - 2064	1.55 ± 0.15	2.24 ± 0.3	100	MHWST	0.7 ± 0.25	1.55 ± 0.55	
	MY1	SUERC-54839	9831 ± 42	11191 - 11311	57.2 ± 0.15	57.9 ± 0.3	614	HAT	1.2 ± 0.25	56.7 ± 0.55	
	SN1	SUERC-47986	9689 ± 40	11071 - 11216	50.3 ± 0.15	51.02 ± 0.3	610	MHWST	0.7 ± 0.25	50.3 ± 0.55	
	SN2	SUERC-47987	9850 ± 41	11198 - 11327	45.8 ± 0.15	46.51 ± 0.3	610	MHWST	0.7 ± 0.25	45.8 ± 0.55	
	AH2	SUERC-47974	9751 ± 41	11121 - 11242	67.5 ± 0.15	68.22 ± 0.3	632	HAT	1.2 ± 0.25	67.0 ± 0.55	
	AH1	SUERC-47985	9625 ± 40	10781 - 11035	69.9 ± 0.15	70.62 ± 0.3	612	>HAT	N/A	Limiting	
G	BR10	SUERC-54849	1465 ± 35	1301 - 1407	2.9 ± 0.15	4.4 ± 0.3	218	MHWST	1.5 ± 0.3	2.9 ± 0.6	
	BR1	SUERC-54840	3233 ± 37	3381 - 3515	73.2 ± 0.15	74.7 ± 0.3	90	MHWST	1.5 ± 0.3	73.2 ± 0.6	
	HV4	SUERC-54841	8972 ± 41	10119 - 10230	63.95 ± 0.15	65.45 ± 0.3	435	MHWST	1.5 ± 0.3	63.95 ± 0.6	
	HV3	SUERC-54912	4102 ± 38	4517 - 4727	67.2 ± 0.15	68.7 ± 0.3	278	HAT	2.1 ± 0.3	66.7 ± 0.6	

Table 6.27 – RSL index points for northwest Iceland including sites studied by Rundgren et al. (1997); Lloyd et al. (2009), Brader (2012) and new sea-level index points generated as part of this research. 'Uncorrected' elevation gives the elevation difference between sill and MHWST. Corrected elevation gives the value relative to MSL.

6.10 New RSL curves for NW Iceland

As a result of the current and previous RSL research undertaken in NW Iceland, seven RSL records are available as a test for GIA model outputs (Figs. 6.73 -6.79).

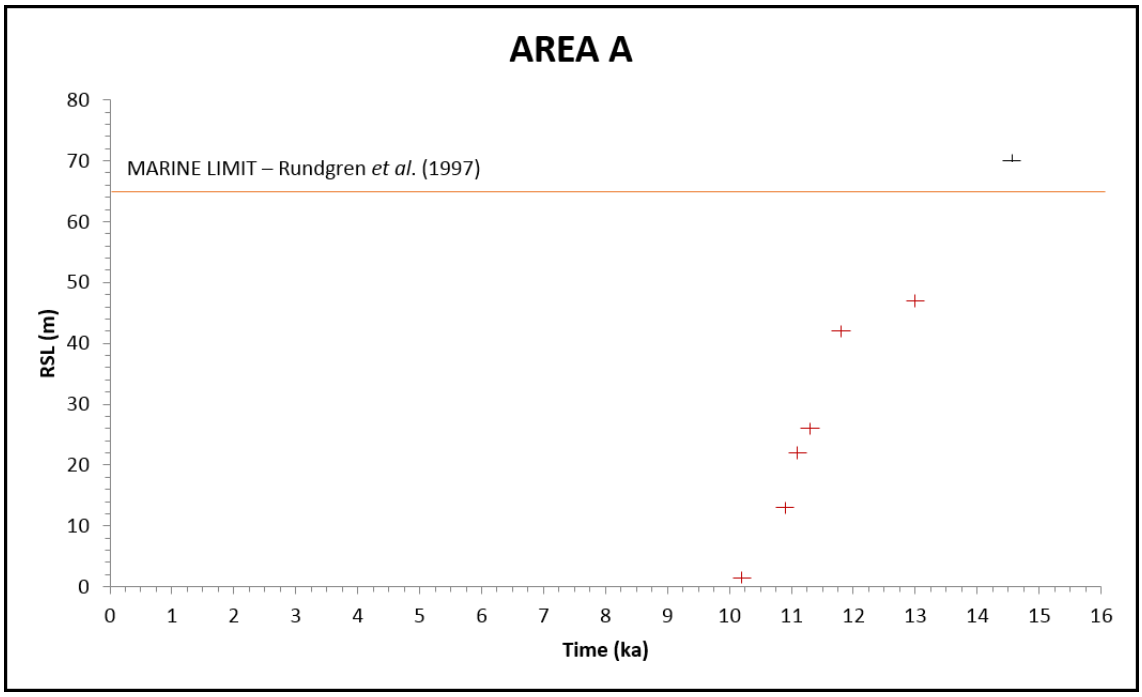

Figure 6.73 – RSL for Area A including data from Rundgren et al. (1997; red) and the this thesis (black)

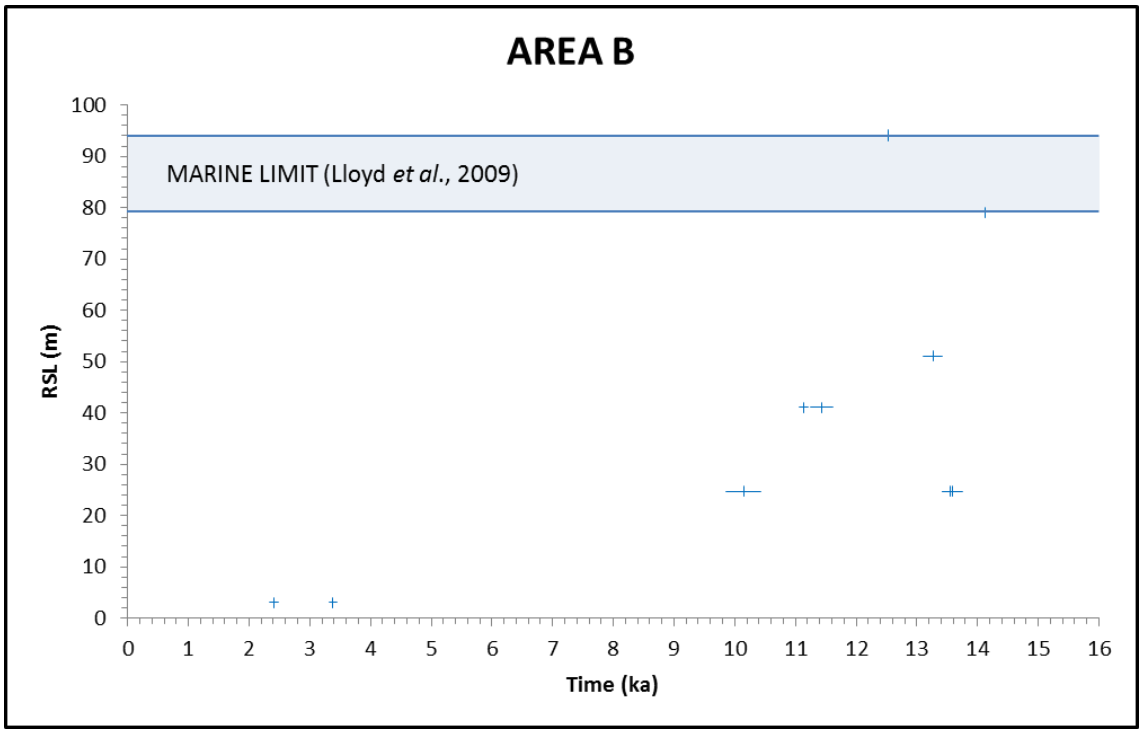

Figure 6.74 – RSL curve for Area B, generated by Lloyd et al. (2009, blue)

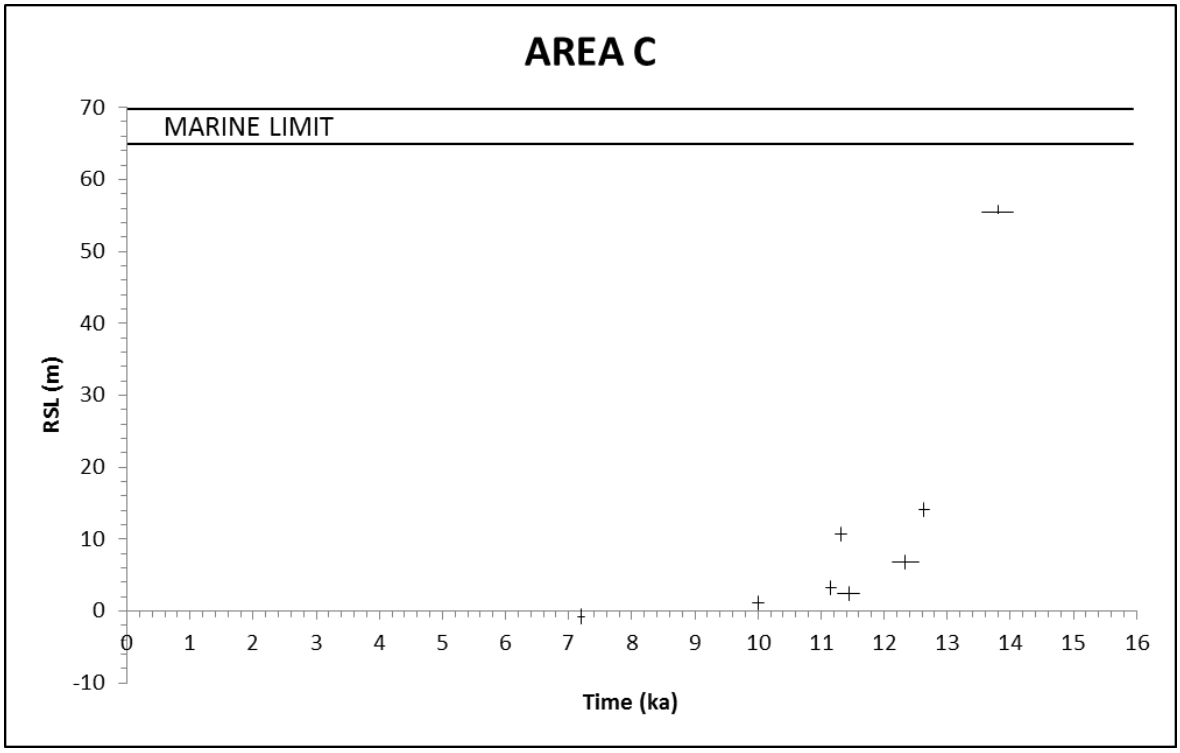

Figure 6.75 – RSL curve for Area C as presented in Brader et al (submitted).

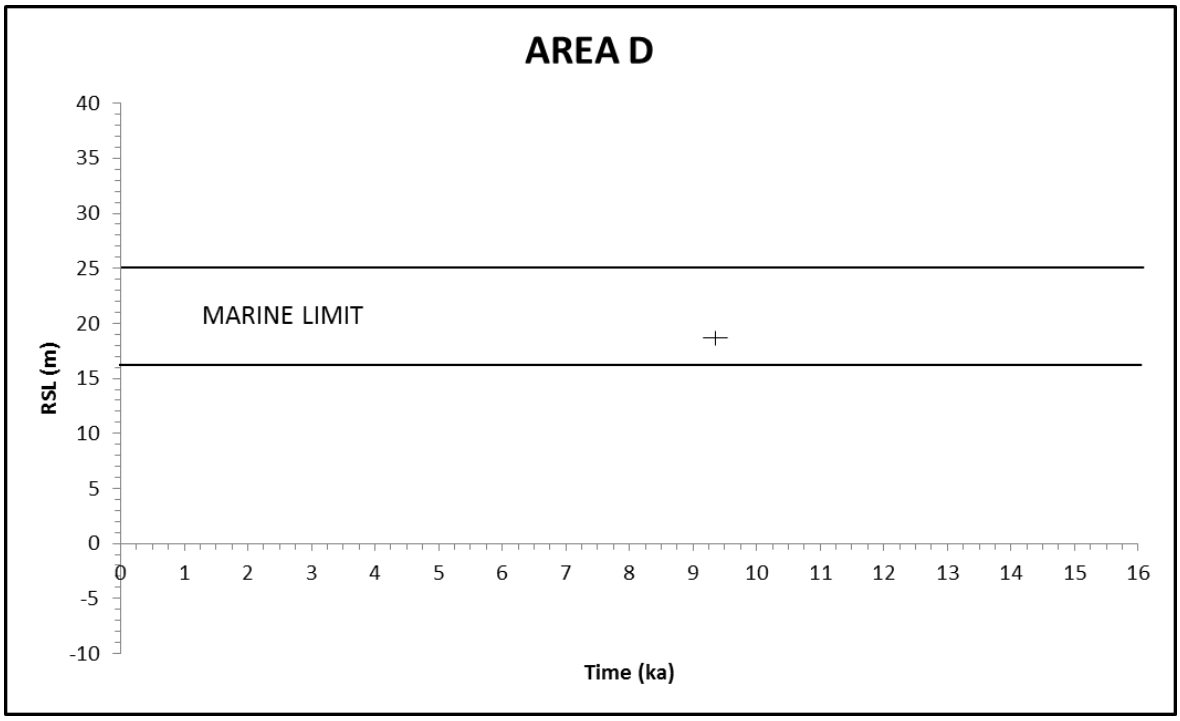

Figure 6.76 – RSL record for Area D showing the elevation of the marine limit recorded and the tentative SLIP from Rekavik 1 (this thesis).

Due to the limited marine influence recorded in the diatom assemblages from Area D, the marine limit elevation is reported in Fig. 6.76. The marine limit was recorded in the present study and correlates with the elevations presented by Hjort *et al.* (1985).

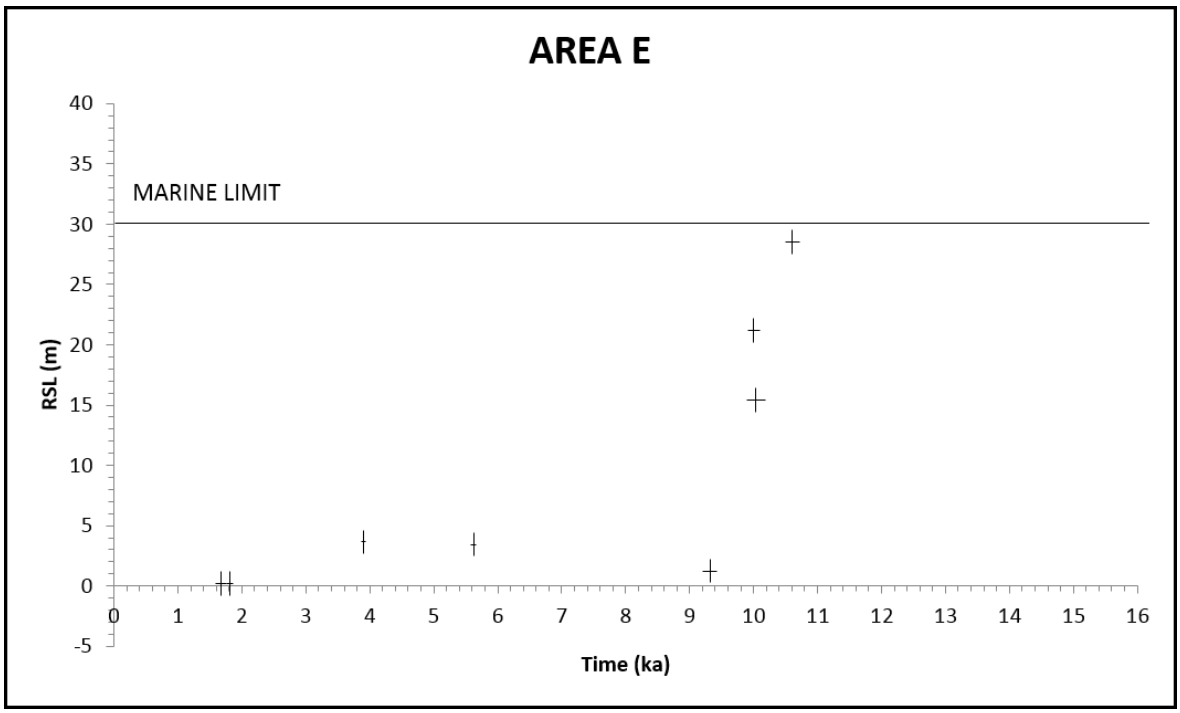

Figure 6.77 – RSL curve for Area E using data generated as part of this research.

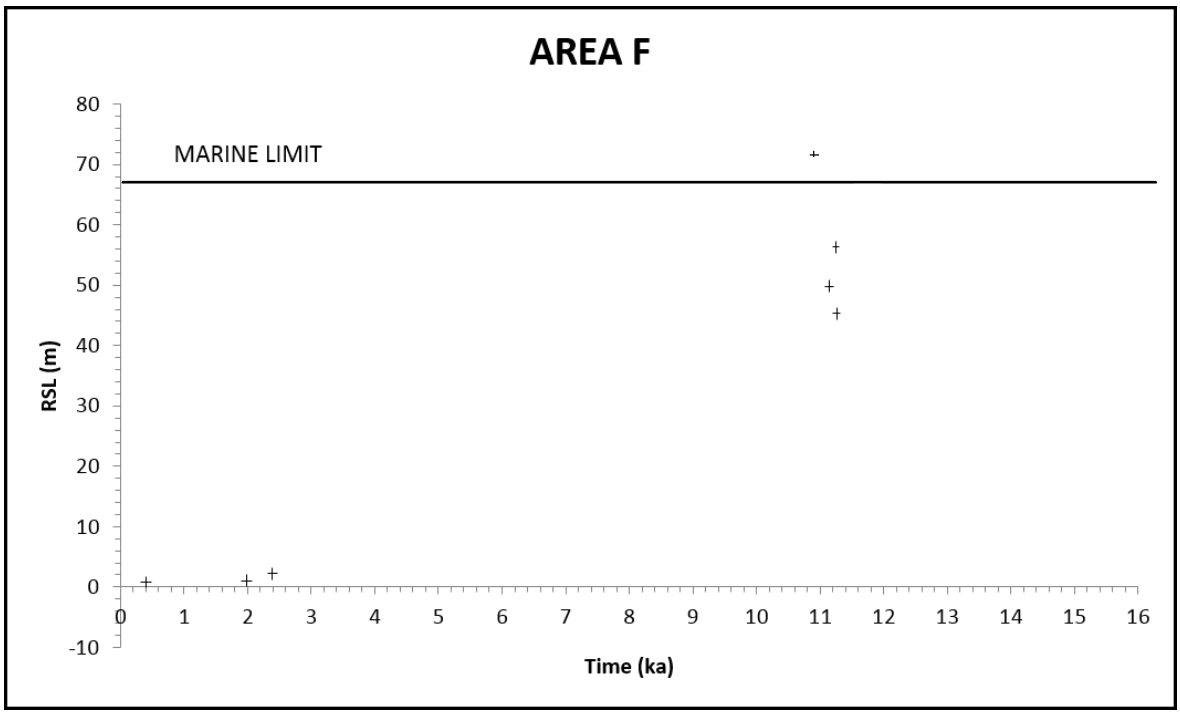

Figure 6.78 – RSL curve for Area F demonstrating the sea-level index points and limiting date generated as part of this research, including the lack of data for mid-elevation sites.

As outlined in Section 6.7, a number of the sites investigated in Area G suffer from poor chronological control, possibly due to contamination by modern carbon from rootlet penetration. Only the marine limit recorded in the region is therefore presented in Fig. 6.79 rather than the full suite of sea-level index points generated.

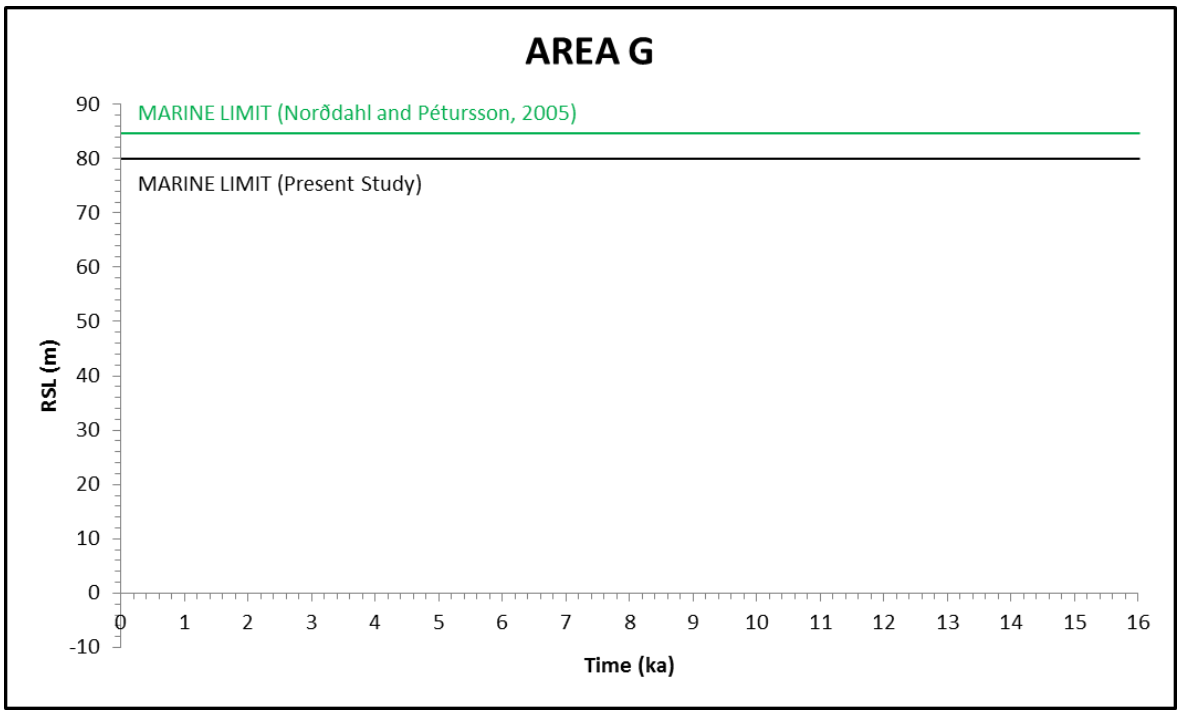

Figure 6.79 – RSL record from Area G showing the elevation of the marine limit recorded by the current and previous study.

6.11 Additional sites

In addition to the sites outlined within Chapter 6, diatom samples were extracted from a series of further sites, which are shown in Chapter 3. These sites were not used in the generation of the RSL curves for particular locations due to poor preservation of diatoms, incomplete records of environmental change or duplication of samples from the same elevation. These sites are therefore not outlined in detail within this thesis.

6.12 Summary

New isolation basin and coastal lowland records have allowed the generation of three new RSL curves for northwest Iceland, as well as providing additional SLIPs and limiting points for three further regions. Litho- and biostratigraphic analysis has allowed the identification of environmental changes at 27 sites, with radiocarbon and tephrochronological analyses providing chronological control. Radiocarbon samples from Area C and Area G suffer from contamination. As a result, Area G suffers from limited SLIPs. In addition, there is a lack of mid-elevation sites in Area F. In total, 20 new SLIPs and 7 limiting points have been generated for northwest Iceland.

The patterns of RSL change in northwest Iceland are spatially variable along the two perpendicular transects across the region (see Fig. 3.4). The new RSL curves will act as a useful test for GIA model outputs for Iceland. Chapter 7 outlines the GIA model outputs generated for Iceland as part of this research, using a suite of ice and Earth characteristics.

CHAPTER 7

Glacio-isostatic adjustment (GIA) Modelling

7.1 Introduction

This chapter outlines the results of a suite of glacio-isostatic adjustment (GIA) model runs for Iceland. Four ice models were employed (Table 4.2), alongside a range of rheological profiles (Table 4.3), in order to determine modelled RSL changes in Iceland for comparison with the new and existing field evidence outlined in Chapter 2 and Chapter 6. The RSL outputs from individual ice models and rheological profiles are presented for four modelling 'control' locations around Iceland and seven field areas in the Northwest (Fig. 4.7). Two suites of model output are presented for each IIS model in this chapter, demonstrating the differences in RSL change produced. The range of locations explored also allows the investigation of areas of better or lesser fit between the GIA model outputs and field datasets through chi^2 testing. Elevations presented are relative to MSL and time is presented as calibrated years before present.

7.2 Notation and Abbreviations

Within this chapter, the following abbreviations have been used:

Abbreviation	Definition
RES	Tegmark resolution (see Section 4.4.1)
NP	Number of pixels
LMAX	Spherical harmonics
LT	Lithospheric thickness (km)
υ_{UM}	Upper mantle viscosity (Pa s)
υ_{LM}	Lower mantle viscosity (Pa s)
HP_MAX	Maximum Glaciation Model (Patton, unpub.)
HP_OPT	Optimum Glaciation Model (Patton, unpub.)
HP_MIN	Minimum Glaciation Model (Patton, unpub.)
ICE5G_ICL	Iceland Component of ICE5G (Peltier, 2004)

7.3 ICE5G in Iceland with VM2 Rheology

Initial GIA modelling was completed using the ICE5G ice loading history (Peltier, 2004; Fig. 7.1) and its associated averaged VM2 rheological profile provided in SELEN (LT 90 km, υ_{UM} 4 x 10^{20} Pa s, υ_{LM} 2.7 x 10^{21} Pa s), hereafter referred to as ICE5G_VM2. ICE5G_VM2 provides an opportunity to determine RSL changes in Iceland using a global ice model, where the equivalent sea level (ESL) within the ice load is 127.6 m since the LGM (Peltier, 2004). The ESL of the ICE5G_ICL component is 0.4 m.

When the ice and Earth characteristics of ICE5G_VM2 are used, the SELEN modelled RSL change generally under-predicts the postglacial RSL changes recorded by the field data (Fig. 7.1). This mismatch between the modelled RSL changes and field evidence is notable in both the modelling 'control' locations (Fig. 7.1) and the NW Iceland field areas (Fig. 7.2). Whilst the ICE5G_VM2 ice and Earth model inputs are able to replicate the west-east contrast in marine limit elevations noted in the geomorphological evidence, the model outputs from SELEN fail to reproduce the marine limit elevations from any of the research locations (Fig. 7.1 and 7.2). This is particularly evident for sites in eastern Iceland, where postglacial RSL is modelled as rising no more than 4.6 m asl in Location 4 (Fig. 7.1). Indeed, in Location 3, the SELEN ICE5G_VM2 model results suggest that postglacial RSL has never been above present sea level (Fig. 7.1). This is in contrast to the extensive raised shoreline evidence noted by Norðdahl and Pétursson (2005) in the region.

A number of model outputs at several locations demonstrate a RSL fall below present in the early Holocene, which has been noted in geomorphological records from northern and western Iceland (e.g. Ingólfsson *et al.*, 1995; Norðdahl and Pétursson, 2005). This is demonstrated by the modelled RSL changes for the field areas in northwest Iceland, such as Areas A, B and C (Fig. 7.2; Rundgren *et al.*, 1997; Lloyd *et al.*, 2009; Brader *et al.*, submitted). However, the magnitude of this lowstand is much greater in the geomorphological record (e.g. Ingólfsson *et al.*, 1995) at -40 m below present sea level than that predicted by the results of the SELEN ICE5G_VM2 GIA model (see Fig. 7.2).

Analysis of the NW Iceland dataset demonstrates the clear mismatch between the modelled RSL outputs and field datasets (Fig. 7.2). The SELEN ICE5G_VM2 model fails to reproduce either the broad regional patterns of RSL change or subtle local differences (Fig. 7.2). This is demonstrated through the residual values for model predictions, which show a consistent under-prediction in the Lateglacial and early-mid Holocene (Fig. 7.3). When employed with the VM2 rheology, there appears to be insufficient ice loading in the ICE5G ice model to replicate the field evidence in Iceland.

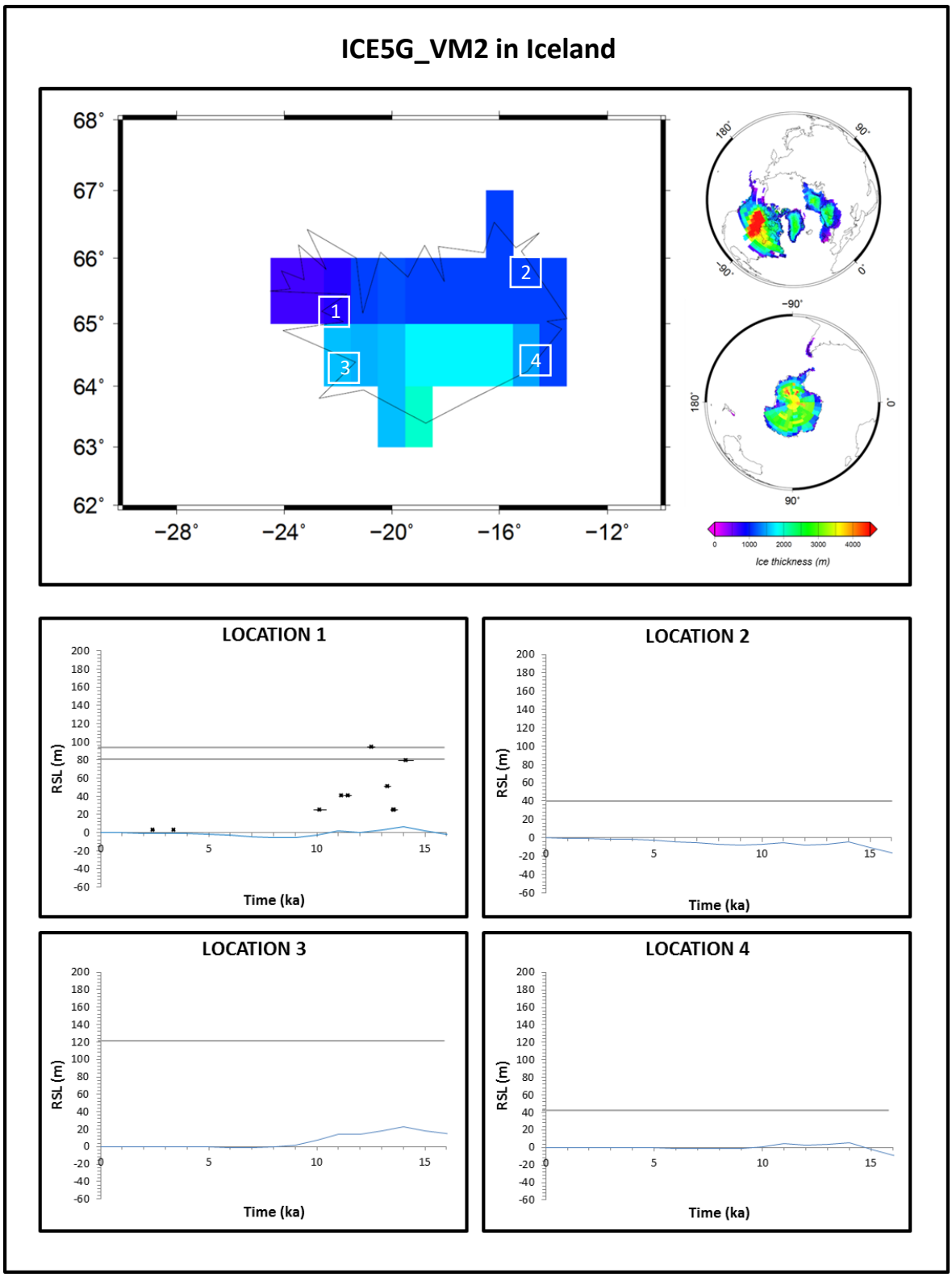

Figure 7.1 – RSL outputs (blue lines) for ICE5G at four modelling locations (see Fig. 4.6) in Iceland (blue lines) alongside published RSL data (Location 1: Lloyd et al (2009); Location 2-4: Norðdahl and Pétursson (2005). The local marine limit for each location is denoted by the solid horizontal grey line.

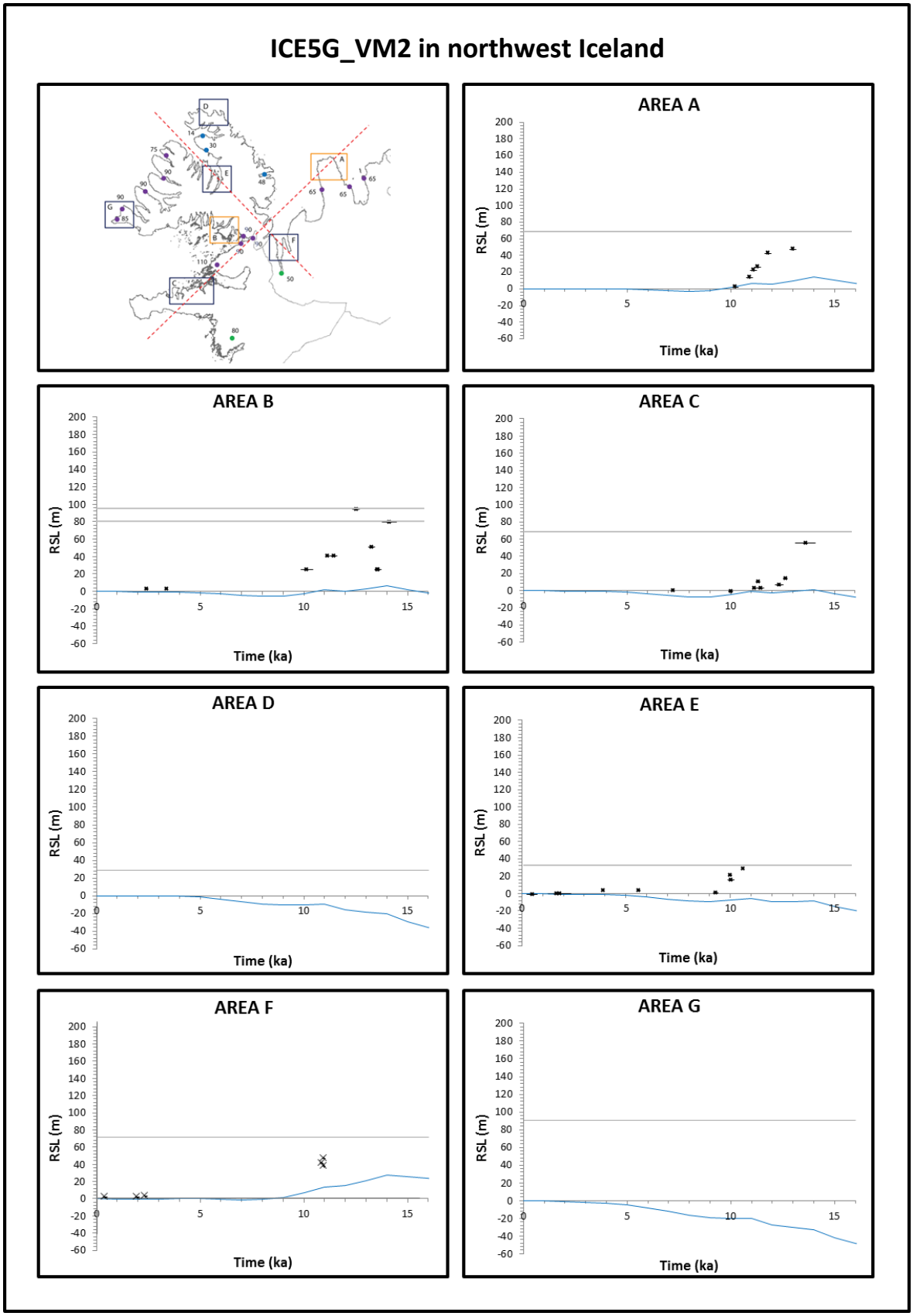

Figure 7.2 – Modelled RSL outputs for locations in NW Iceland from ICE5G (VM2) plotted against the existing field dataset for the region. Sources: ICE5G (VM2) (Peltier, 2004); Area A – Rundgren et al. (1997); Area B – Lloyd et al. (2009), Area C – Brader et al (submitted), Area D – F – current study; Area G – Norðdahl and Pétursson, 2005). The local marine limit for each location is denoted by the solid horizontal grey line.

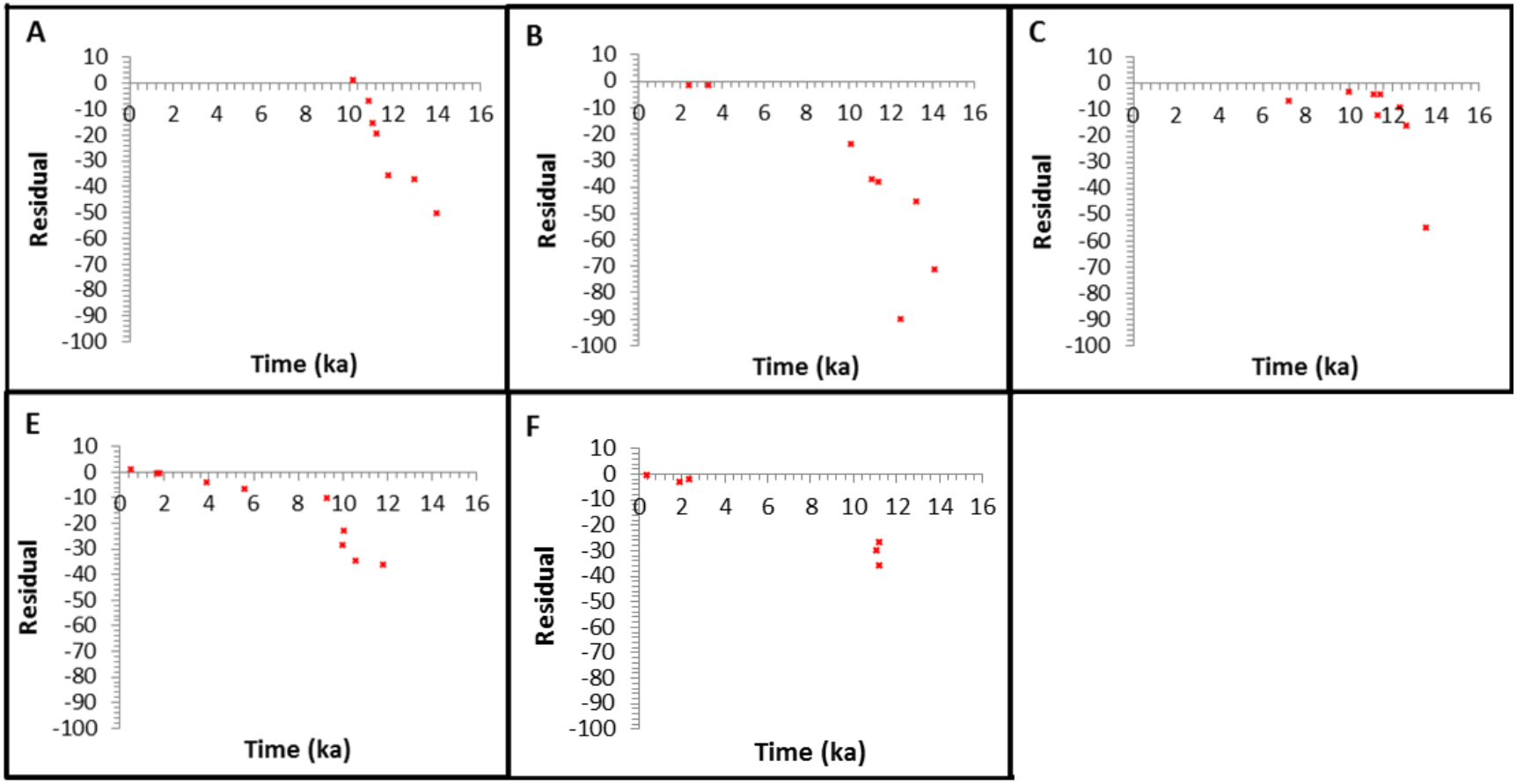

Figure 7.3 – Residuals of RSL prediction from ICE5G (VM2) in NW Iceland (Areas A, B, C, E and F), highlighting the under-prediction of RSL changes at the majority of locations. Areas D and G are not presented due to the limitations of the SLIPs generated in the regions.

The pattern of deglaciation and ice volume within ICE5G, alongside the high viscosity VM2 rheology, leads to an under-prediction of RSL changes in Iceland, when compared to field data. In addition, the exponential decrease in ice thicknesses during deglaciation (Peltier, 2004) omits any ice re-advance during the LGM deglaciation sequence, which is evident within the field evidence (e.g. Norðdahl and Pétursson, 2005) during the Younger Dryas. The GIA model fails to reproduce the decreased rates of RSL fall noted during the Younger Dryas in Area B (Lloyd *et al.*, 2009), for example (Fig. 7.3).

It is therefore evident that there are three issues with the ICE5G_VM2 model:

a) ice thicknesses within ICE5G_ICL;
b) the upper mantle viscosity value of VM2 (x 10^{21} Pa s), which is designed for mid-plate locations and is relatively high compared to published values for Iceland, and;
c) the lack of Younger Dryas ice thickness increases within the ICE5G_ICL ice model.

In order to address the first of these limitations, additional GIA model runs were undertaken with adjustments to the ice loading component. The ICE5G_ICL150% ice loading input was developed by increasing the ice load of the Icelandic component of ICE5G by 50%, whilst keeping the distribution of ice the same as the original ICE5G_ICL ice model. This adjustment produces an overall ESL change within the GIA model of 127.8 m due to the increase in the Icelandic component by 0.2 m ESL.

ICE5G_ICL150% ice and VM2 rheology inputs results in model outputs with higher estimations of marine limit elevations in Iceland (Fig. 7.4). However, this increase in ice thickness also leads to an over-prediction of highest postglacial RSL in eastern Iceland and an under-prediction in western Iceland (Fig. 7.4 and 7.5). In NW Iceland, the ICE5G_ICL150%_VM2 SELEN model does produce RSL predictions which correspond to the marine limit elevations recorded in Area C and E (Fig. 7.5). As noted for ICE5G_VM2, the model is unable to reproduce the subsequent postglacial RSL changes of the field locations in NW Iceland (Fig. 7.5), due to the pattern of deglaciation within the ice model. In addition, the ICE5G_ICL150%_VM2 model is unable to produce the early Holocene fall below present sea level or the subsequent mid-Holocene highstand, which has been noted in a number of locations (e.g. Lloyd *et al.*, 2009; Brader *et al.*, submitted). The limited field evidence available in Locations 2 – 4 mean that the Holocene RSL changes produced by both the ICE5G_VM2 and ICE5G_ICL150%_VM2 SELEN models are more difficult to assess (Fig. 7.1 and 7.4). Residual values (Fig. 7.6) for the ICE5G_ICL150%_VM2 GIA model demonstrate a closer fit to the field evidence than ICE5G_ICL_VM2. However, the poor overall fit means that both the ICE5G_VM2 and ICE5G_ICL150%_VM2 GIA models cannot produce RSL outputs which replicate the geological dataset.

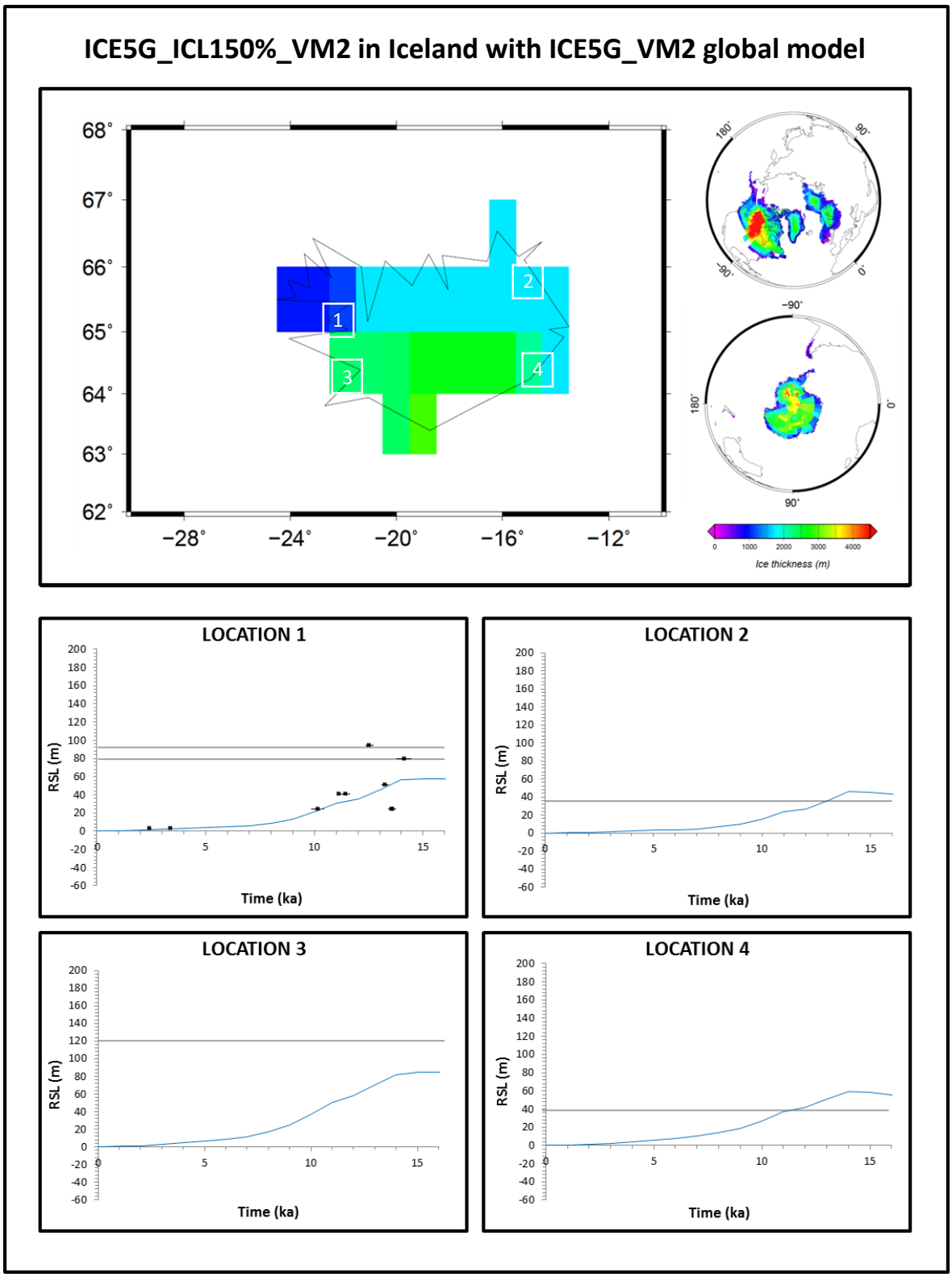

Figure 7.4 – Ice distribution and RSL outputs for Iceland from ICE5G 150% (VM2). Modelled RSL outputs are plotted against the existing field dataset. Sources – Location 1: Lloyd et al. (2009); Location 2 – 4: Norðdahl and Pétursson (2005). The local marine limit is shown by the solid grey horizontal line.

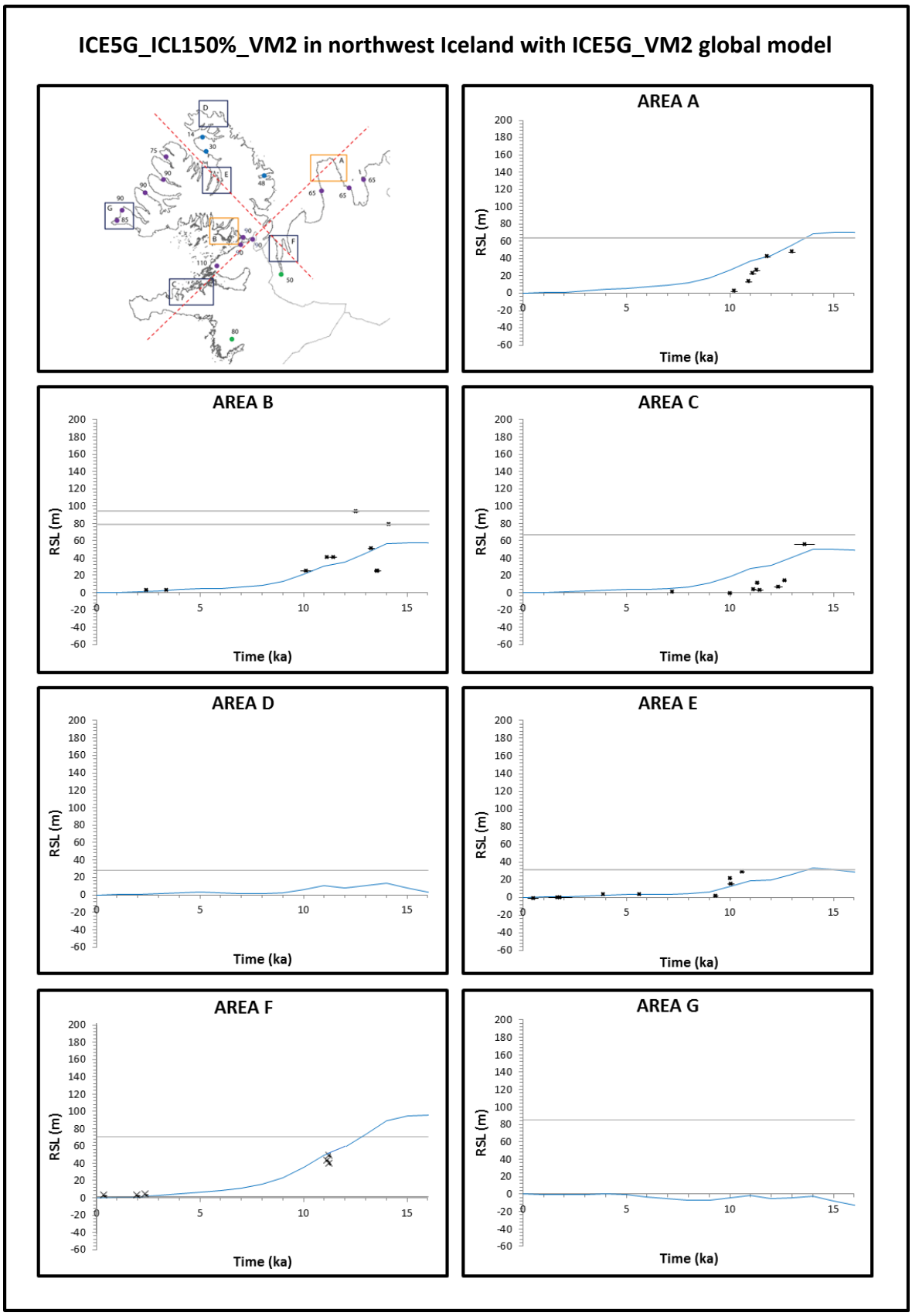

Figure 7.5 – Modelled RSL outputs for locations in NW Iceland from ICE5G 150% (VM2) plotted against the existing field dataset for the region. Sources: ICE5G (VM2) (Peltier, 2004); Area A – Rundgren et al. (1997); Area B – Lloyd et al. (2009), Area C – Brader et al (submitted), Area D – F – current study; Area G – Norðdahl and Pétursson, 2005). The local marine limit is shown by the solid grey horizontal line.

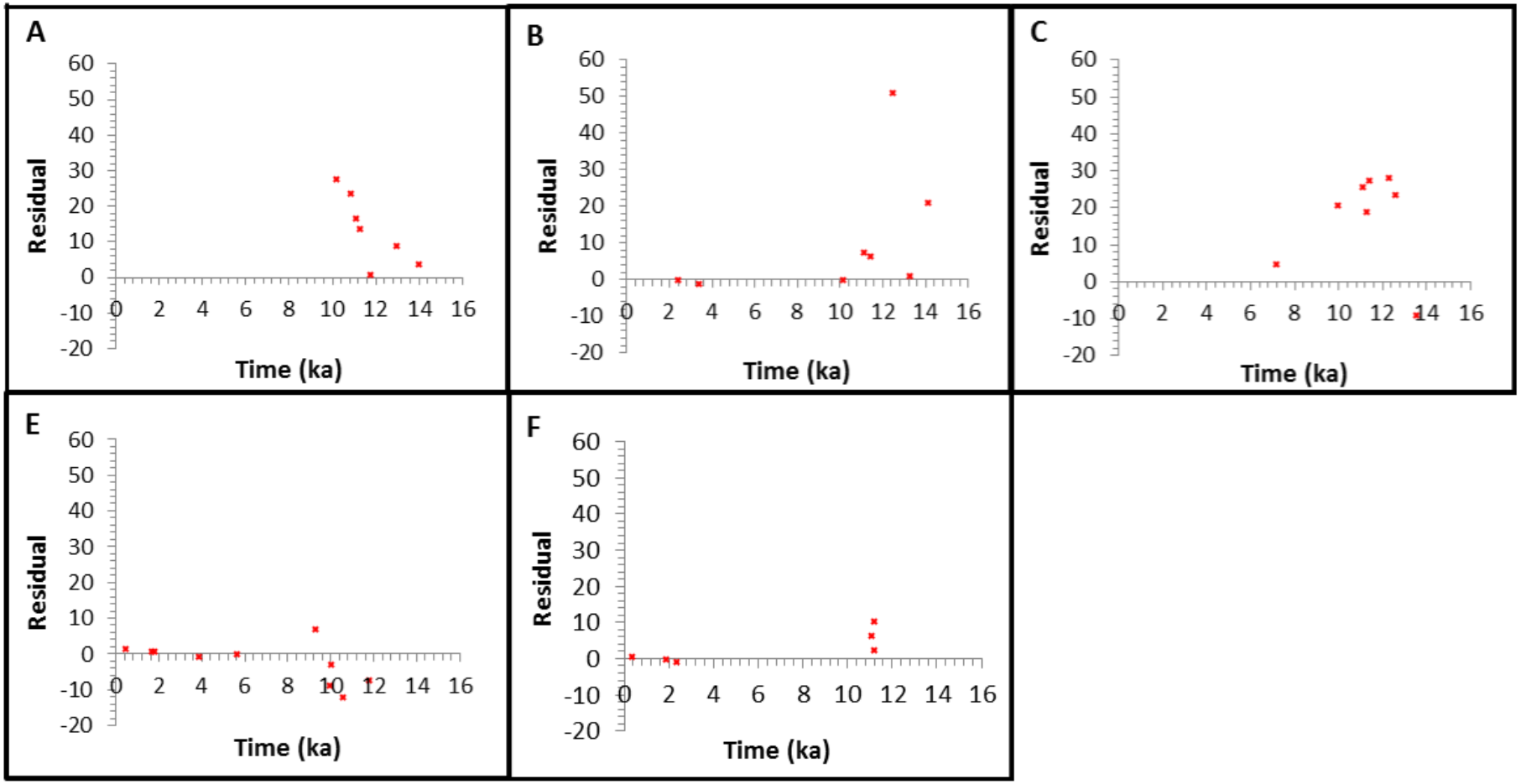

Figure 7.6 – Residuals of RSL prediction from ICE5G 150% (VM2) in NW Iceland (Areas A, B, C, E and F). Areas D and G are not presented due to the limitations of the SLIPs in the regions.

An alternative approach to improve the GIA model fit with the field evidence is through adjustment of the rheological profile. However, in both NW Iceland and the wider modelling 'control' locations, the RSL outputs from the ICE5G_IcelandicRheology (see Table 2.1) SELEN models cannot be reconciled with the field data (Fig. 7.7 and 7.8). Analysis of chi^2 values of these model runs demonstrates that the best fit ICE5G_IcelandicRheology model has a LT of 40 km and υ_{UM} of 5 x 10^{20} Pa s. Chi^2 plots are not presented for the ICE5G ice model due to the limited number of viscosity and lithospheric thickness values tested (LT 30 km, 40 km, 60 km, 100 km and υ_{UM} of 5 x 10^{18} Pa s, 5 x 10^{19} Pa s, 1 x 10^{20} Pa s and 5 x 10^{20} Pa s), which gave a low number of points for surface plots. Adjustment of the υ_{LM} had a negligible effect on the modelled RSL change, being equivalent to the elevational error of individual sea-level index points. However, the modelled RSL changes in particular field areas still differ greatly from the geomorphological and isolation basin based RSL reconstructions (Fig. 7.7 and 7.8). It is not possible to produce the RSL changes recorded by the field evidence, either through adjustment to ICE5G ice thicknesses or the associated viscosity profiles as this ice model has been tuned for mid-plate locations and 'tectonically stable' coastlines such as eastern USA (Peltier, 2004).

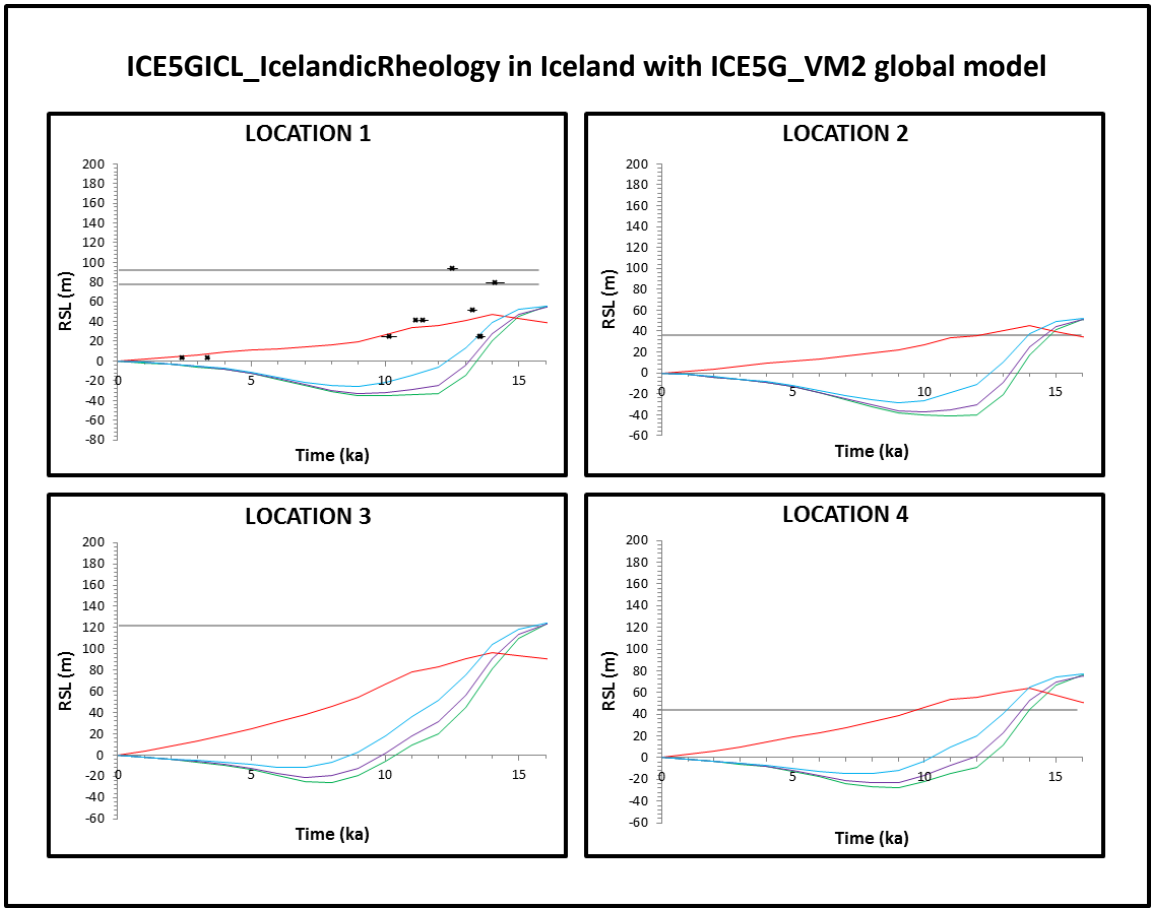

Figure 7.7 – Modelled RSL changes from ICE5GICL (Icelandic Rheology) with ICE5G global ice loading plotted against the existing field database. Sources – ICE5G (VM2); Peltier, (2004); Location 1 – Lloyd et al. (2009); Location 2 – 4: Norðdahl and Pétursson (2005). The local marine limit is shown by the solid grey horizontal line within each location figure.

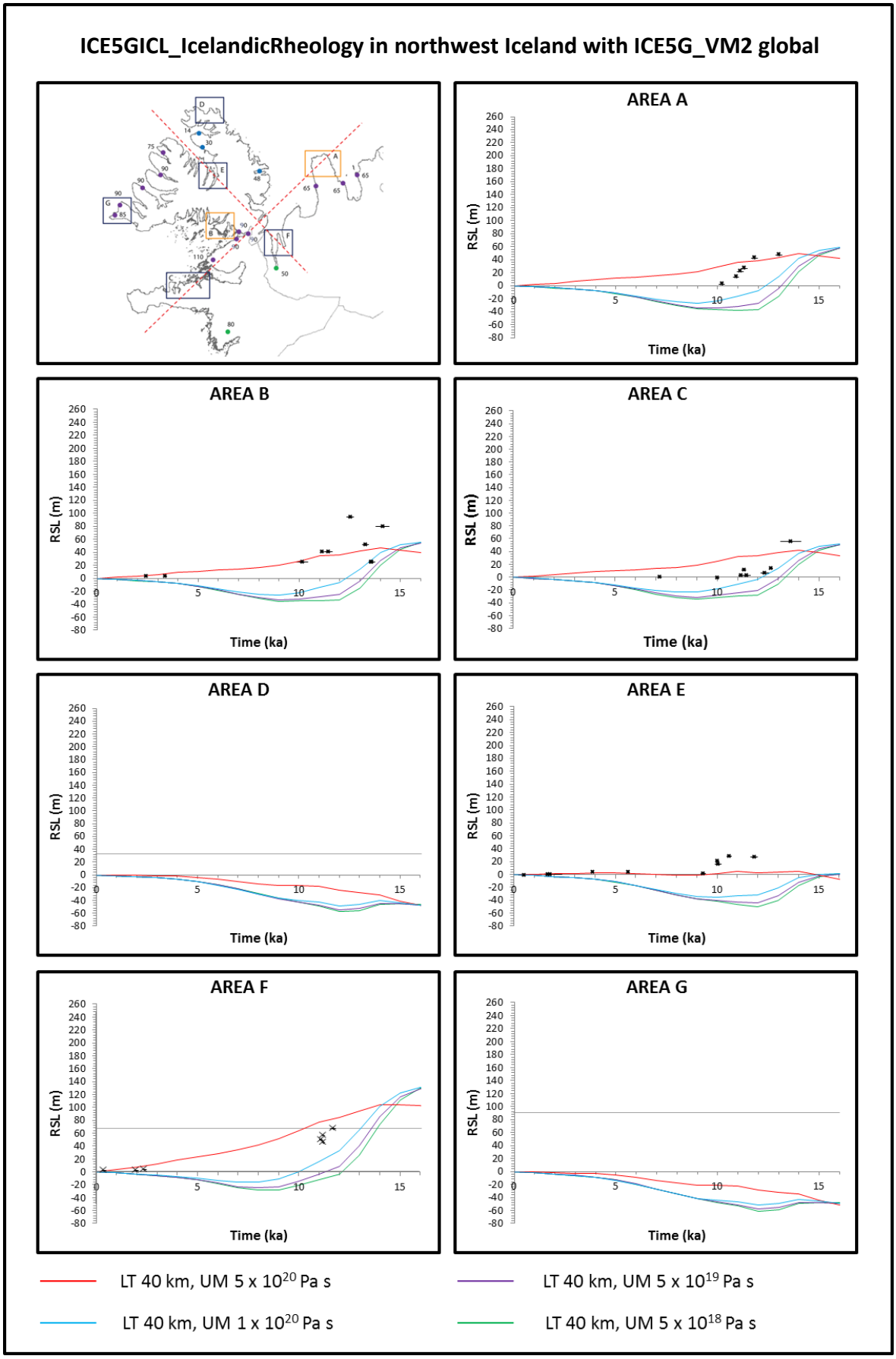

Figure 7.8 – RSL outputs for NW Iceland from ICE5GICL (Icelandic Rheology) in Iceland with ICE5G global ice loading. Sources – ICE5G: Peltier, (2004); Area A – Rundgren et al. (1997); Area B - Lloyd et al. (2009); Area

C – Brader et al. (submitted); Area D – F: Present Study; Area G: Norðdahl and Pétursson (2005). The local marine limit is shown by the solid grey horizontal line within each location figure.

7.4 Icelandic Ice Sheet (IIS) Models with VM2 Rheology

Following the exploration of ICE5G ice loading and the demonstrable lack of fit with the field data, the HP_MAX, HP_MIN and HP_OPT ice models (Patton, unpub.) were adopted in SELEN (see Section 4.4.2 for methodological overview). Initial GIA model runs were completed with a VM2 rheological input (Peltier, 2004). ESLs within the models are 128.2m (HP_MAX and ICE5G), 127.95 m (HP_OPT and ICE5G) and 127.87 m (HP_MIN and ICE5G) respectively. Outputs of the HP_MAX_VM2, HP_MIN_VM2 and HP_OPT_VM2 GIA models in SELEN are able to reproduce the west-east contrast in marine limit elevations and RSL changes shown by field evidence (e.g. Norðdahl and Pétursson, 2005). This is clearly demonstrated by the modelled RSL outputs (see Fig. 7.9), which show higher marine limits in western Iceland and therefore clearly contrasts with the spatial pattern of RSL changes when using ICE5G ice loading (Fig. 7.1). The RSL outputs further highlight the differences in ice loading patterns between the individual GIA models.

HP_MAX_VM2 generally predicts RSL higher than ICE5G_VM2, with HP_MIN_VM2 and HP_OPT_VM2 modelling lower RSLs than ICE5G_VM2 (Fig. 7.9). The HP_MIN_VM2 and HP_OPT_VM2 models generate similar patterns of postglacial RSL change at the four modelling 'control' locations (Fig. 7.9). This is unsurprising, as the ice loading patterns are similar in the two ice models, both in terms of deglacial timing and ice thicknesses (Patton, unpub.). The HP_MAX_VM2 model produces higher RSLs then either HP_MIN_VM2 or HP_OPT_VM2; however, these modelled RSL changes also fall below the marine limit in Locations 2-4 (Fig. 7.9). The HP_MAX_VM2 model also fails to replicate the early-Holocene lowstand noted in a number of field-based RSL reconstructions in western Iceland (e.g. Ingólfsson *et al.*, 1995; Lloyd *et al.*, 2009; Fig. 7.9). However, the HP_MAX_VM2 model does provide a reasonable RSL prediction for Location 1 (Lloyd *et al.,* 2009; Fig. 7.9) during the Lateglacial and early Holocene.

Following the modelling of RSL changes at the four 'control' locations, additional outputs were generated for the field data areas in NW Iceland (Fig. 7.10). These model runs were completed to allow comparison to subsequent regional ice model based RSL reconstructions. HP_MIN_VM2 and HP_OPT_VM2 SELEN models both fail to produce a postglacial RSL above present in Areas C, D, E and G, despite a range of geomorphological evidence in these locations suggesting higher postglacial RSLs (Fig. 7.10). Furthermore, the modelled marine limit is at a lower elevation than those recorded in the remaining field data areas (Fig. 7.10). When coupled with VM2 rheology, it is clear that the HP_MIN and HP_OPT (Patton, unpub.) ice models require further development for use in these locations.

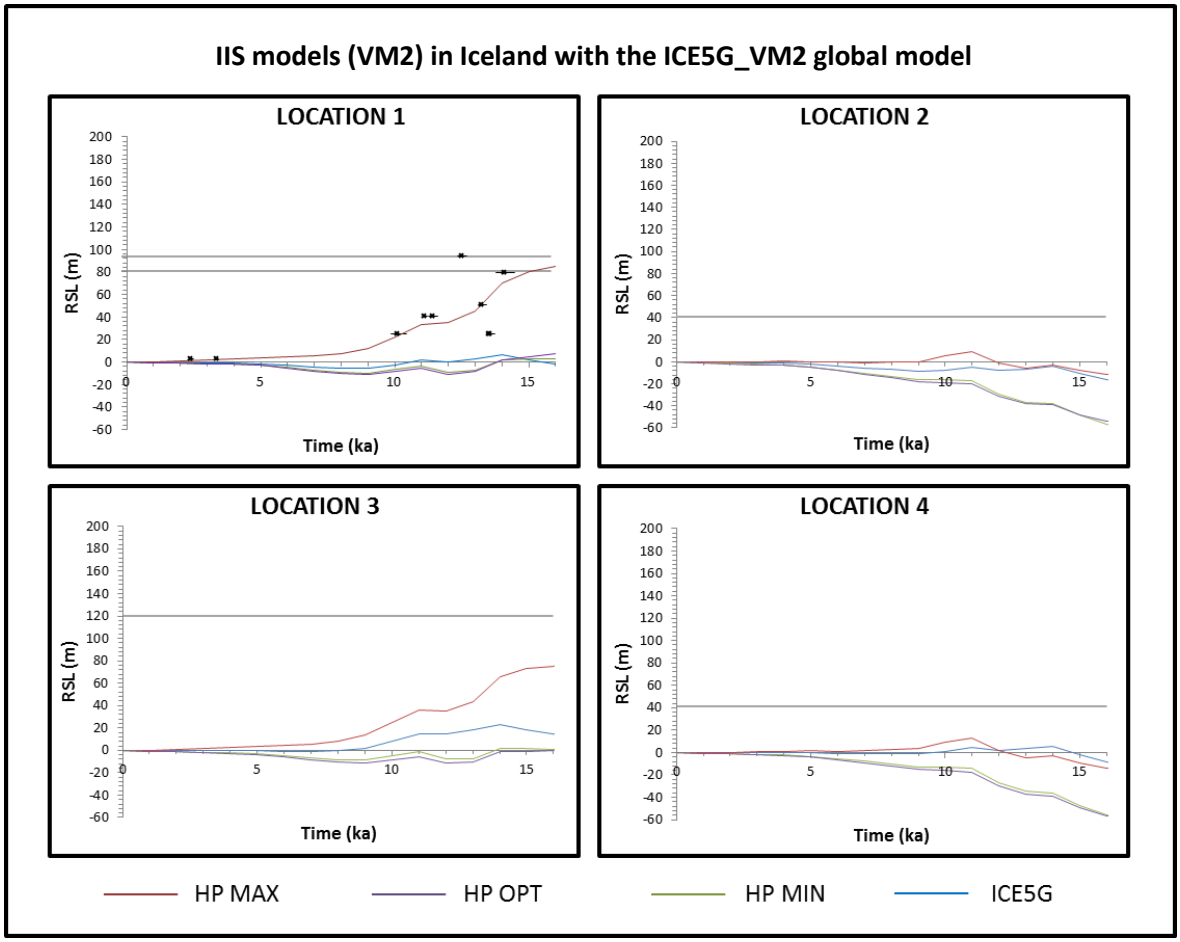

Figure 7.9 – Modelled RSL outputs for Locations 1-4 around Iceland using the ICE5G, HP_MAX, HP_OPT and HP_MIN ice models with the VM2 rheological profile. The curves show modelled RSL changes (solid lines) alongside the existing field data (black crosses; Location 1 – Lloyd et al. (2009); Location 2 and 3 – Norðdahl and Pétursson, 2005; Location 4 – Norðdahl and Einarsson, 2001). Marine Limit: grey line.

In contrast, HP_MAX_VM2 produces higher postglacial RSLs but does not predict the early Holocene lowstand or subsequent mid Holocene highstand noted in the field evidence (e.g. Ingólfsson *et al.*, 1995). The modelled RSL at deglaciation is close to that recorded in the field evidence for a number of the field areas (Fig. 7.10). However, there is a subsequent deviation between modelled RSL output and field based RSL reconstructions at a number of sites, particularly Area C (Brader *et al.*, submitted). Hence, it is necessary to test a range of viscosity profiles to determine whether the two datasets can be better reconciled.

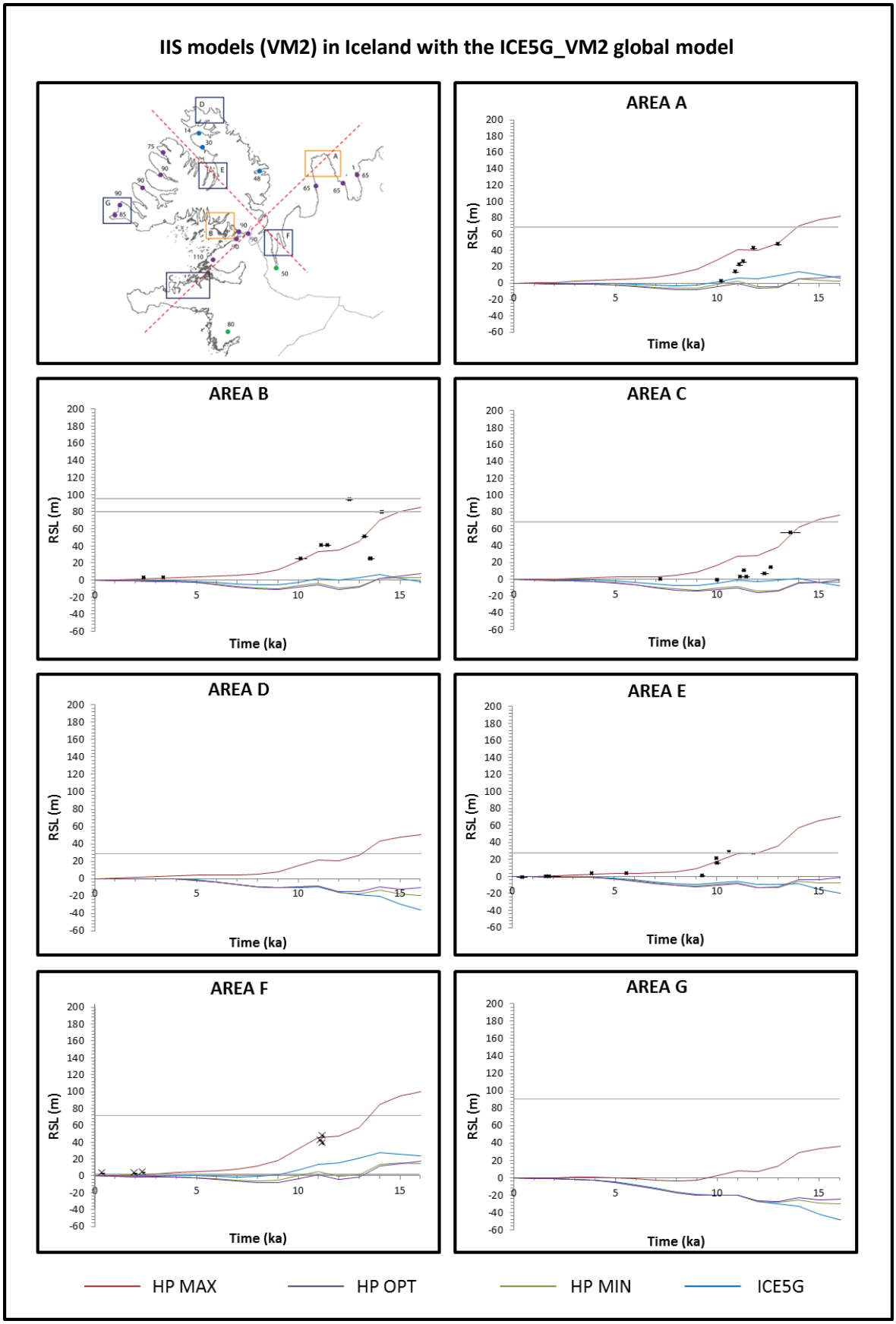

Figure 7.10 – RSL outputs for the ICE5G, HP_MAX, HP_OPT and HP_MIN ice models with VM2 rheology for locations in NW Iceland. Each graph shows the modelled RSL change (solid lines) and the existing field datasets (black crosses) for individual locations. Marine limit elevations are shown by the solid grey horizontal lines in each location figure.

7.5 Icelandic Ice Sheet (IIS) Models with Icelandic Rheology

7.5.1 HP_MAX (Icelandic Rheology)

HP_MAX was run with a suite of rheological profiles, covering a range of lithospheric thicknesses, and upper mantle viscosity values (Table 4.4). Variation of the lower mantle viscosity produced little difference in the resultant RSL record, equivalent to the vertical error of individual sea-level index points. GIA modelling thus concentrated on the effects of lithospheric thickness and upper mantle viscosities. The modelled RSL outputs generated by HP_MAX (Patton, unpub.) are presented in Figure 7.11A, which highlights the consequence of individual upper mantle viscosities whilst the lithospheric thickness remains constant at 40 km, which has been reported as suitable for Iceland (e.g. Árnadóttir *et al.*, 2009; Barnhoorn *et al* ., 2011).

As outlined by Fig. 7.11A, HP_MAX (LT 40 km) is able to reproduce the west-east contrast in marine limit elevations (see Fig. 2.4) regardless of the upper mantle viscosity used. The RSL outputs generated using the HP_MAX (LT 40 km) models reach close to the (hypothesised) marine limit in each of the four modelling 'control' locations when the upper mantle viscosity is less than 5 x 10^{20} Pa s (Fig. 7.11A). There appears to be a notable difference in the RSL output produced by the HP_MAX model once the upper mantle viscosity is increased to 5 x 10^{20} Pa s (Fig. 7.11A). However, the RSL predictions from GIA models employing upper mantle viscosity values of 1 x 10^{20} Pa s, 2 x 10^{20} Pa s, 3 x 10^{20} Pa s and 4 x 10^{20} Pa s in Iceland show that these modelled RSL changes occur in a regular, stepped pattern. Figure 7.11B shows these RSL predictions for Area B using each of these upper mantle viscosity values. This apparently contrasting pattern of RSL change is therefore not unusual but stems from the change in upper mantle viscosity value for Iceland. Although the HP_MAX (LT 40 km) models exceed the marine limit in Locations 1 and 3 when the upper mantle viscosity is less than 5 x 10^{20} Pa s, the model produces estimates of RSL close to the marine limit, when the proposed timing of deglaciation is considered in each location (Fig. 7.11A). However, the modelled timing of marine limit formation appears to occur later than recorded in the field data in Location 1 (Lloyd *et al*, 2009), within the HP_MAX (40 km) model outputs (Fig. 7.11A).

Location 1 and 3 also demonstrate the ability of the HP_MAX ice model (Patton, unpub.) to reproduce the effects of Younger Dryas ice re-advance on the RSL record (Fig. 7.11A). Furthermore, the early Holocene lowstand and subsequent mid-Holocene highstand noted in the two locations are both replicated by the GIA model, when the upper mantle viscosity is lower than 5 x 10^{20} Pa s (Fig. 7.11A). The magnitude of these events corresponds more closely to the field record than when a VM2-type rheology is used; however, the early Holocene lowstand is greater than recorded when the υ_{UM} is less than 5 x 10^{19} Pa s (Fig. 7.11A).

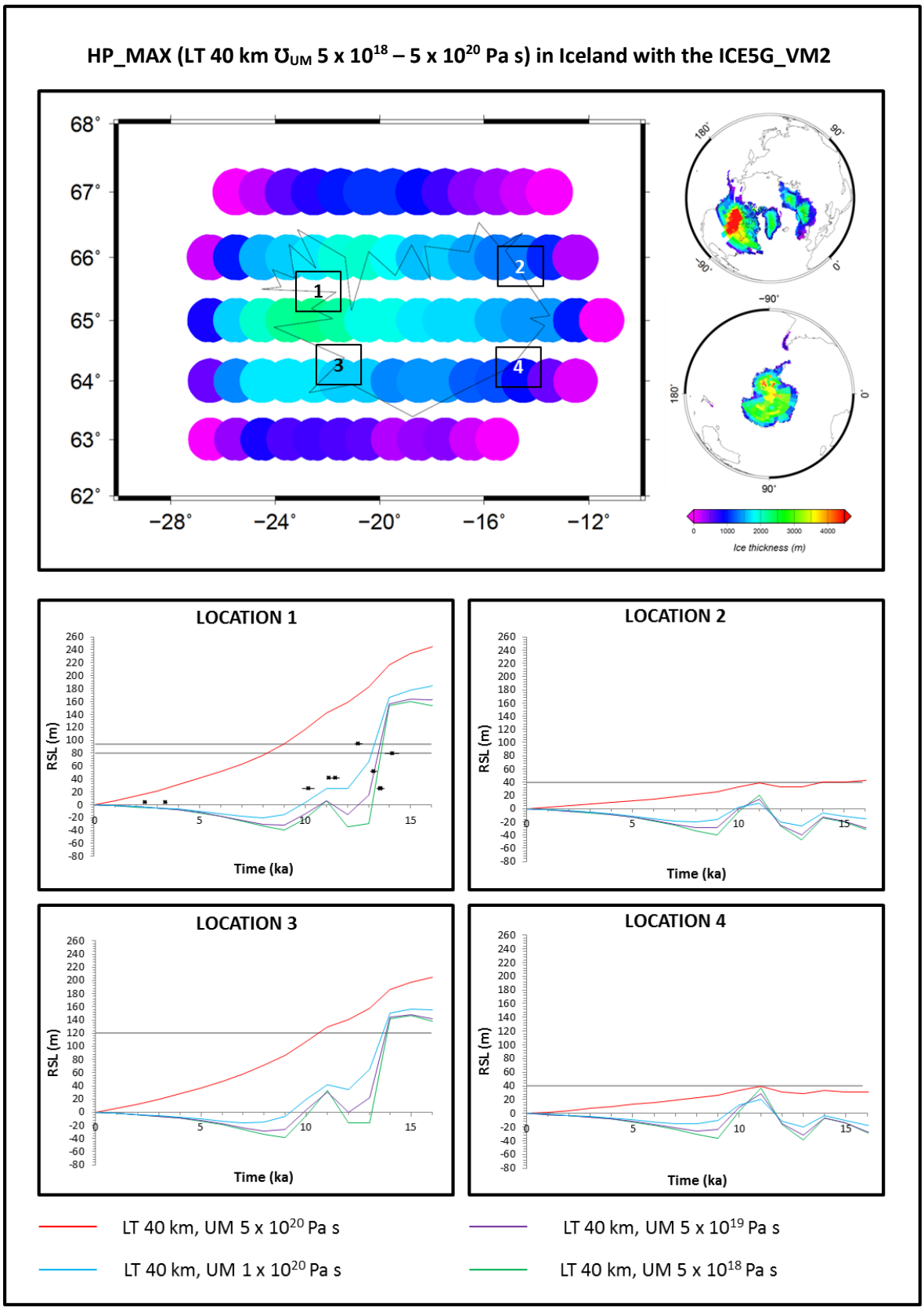

Figure 7.11A – RSL outputs from HP_MAX (40km LT) with ICE5G (VM2) global ice loading in Iceland, alongside ice distribution within the model. The implications of ice loading in Iceland can be seen through the contrasting RSL outputs for western and eastern Iceland. Sources: HP_MAX original file (Patton, unpub), ICE5G original file (Peltier, 2004), Location 1 RSL data (Lloyd et al. 2009), Location 2-4 RSL data (Norðdahl and Pétursson, 2005). The local marine limit is shown by the solid grey horizontal line within each location.

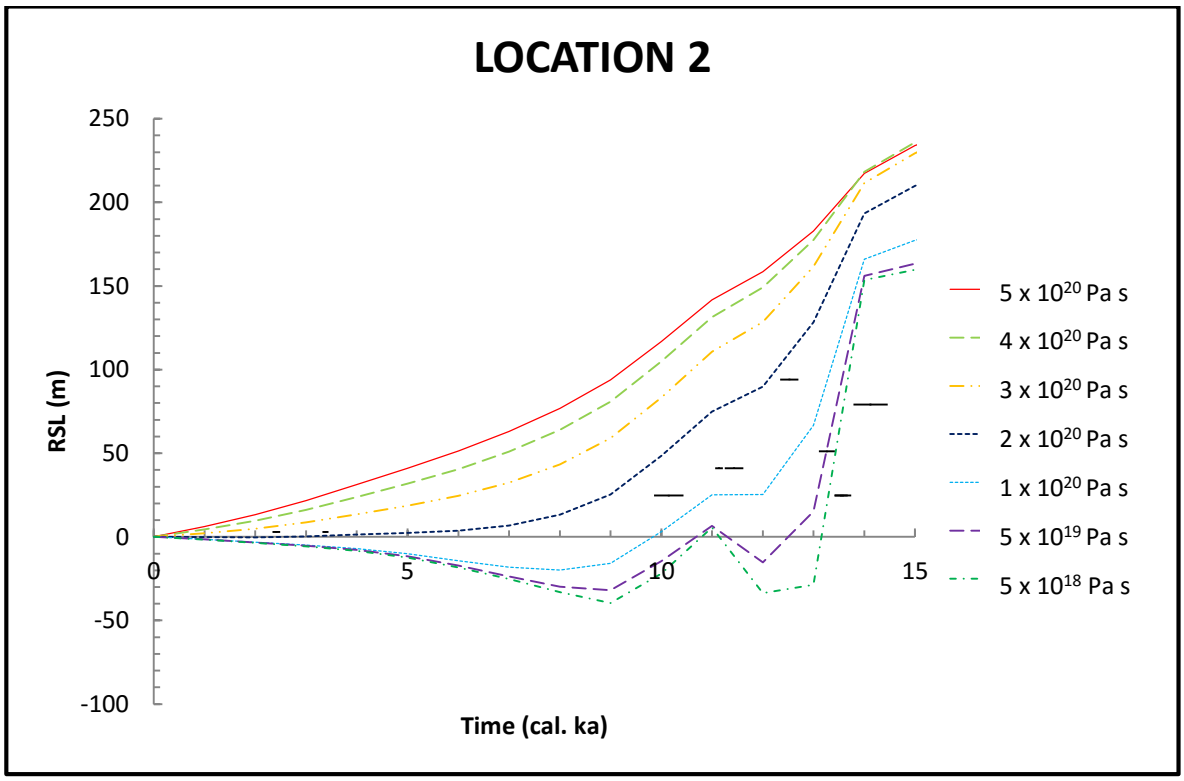

Figure 7.11B – RSL outputs for the HP_MAX (LT 40 km, υ_{UM} 1 x 10^{20} – 5 x 10^{20} Pa s) models for Area B, demonstrating the predicted RSL changes under each scenario. The plots demonstrate that the result from HP_MAX (LT 40 km, υ_{UM} 5 x 10^{20} Pa s) is not unusual when compared to other HP_MAX υ_{UM} 10^{20} Pa s model outputs.

In NW Iceland, the HP_MAX (LT 40 km) models appear to have a good fit with the new field evidence in the majority of locations, with the exception of HP_MAX (LT 40 km, υ_{UM} 5x 10^{20} Pa s; Fig. 7.12). HP_MAX (LT 40 km, υ_{UM} 5 x 10^{20} Pa s) consistently over-predicts postglacial RSL change in NW Iceland and so this ice-Earth model combination can be rejected. None of the HP_MAX (LT 40 km) models are able to produce the mid-Holocene highstand noted in previous records from the region (e.g. Lloyd *et al.*, 2009; Brader *et al.*, submitted).

In Area A (Rundgren *et al.*, 1997), the results of HP_MAX (LT 40 km, υ_{UM} 5x 10^{18} – 1 x 10^{20} Pa s) appear to produce reasonable estimations of postglacial RSL change (Fig. 7.12). Each GIA model is able to provide an approximation of the timing of marine limit formation, as well as the impact of Younger Dryas ice re-advance on the RSL record (Fig. 7.12). In addition, the three GIA models are able to produce the early Holocene lowstand noted in western Iceland (e.g. Norðdahl and Pétursson, 2005). Chi^2 tests of the three outputs suggest that HP_MAX (LT 40 km, υ_{UM} 5 x 10^{19} Pa s) provides the best fit maximum glaciation model for Area A (Fig. 7.13).

The HP_MAX (LT 40 km, υ_{UM} 5 x 10^{18} – 1 x 10^{20} Pa s) model results also provide good approximations of postglacial RSL change in Area B (Lloyd *et al.*, 2009). However, it appears that marine limit formation occurs too late within the HP_MAX ice model (Patton, unpub.), as the highest isolation basin presented by Lloyd *et al.* (2009) provides an age older than the modelled

RSL changes suggest (Area B; Fig. 7.12). The HP_MAX (LT 40 km, υ_{UM} 5 x 10^{18} – 1 x 10^{20} Pa s) GIA models are each able to produce the reduced rate of RSL change at the Younger Dryas, as well as the early Holocene fall of RSL below present, within the model outputs (Fig. 7.12). Both of these GIA model results have been noted within field-based reconstructions for the region (Lloyd *et al.*, 2009). Chi^2 tests of the three outputs suggest that the HP_MAX (LT 40 km, υ_{UM} 5 x 10^{19} Pa s) GIA model results also generate the best fit to the field data from this region (Fig. 7.13).

In Area C, it is clear that the timing of deglaciation for the HP_MAX (LT 40 km, υ_{UM} 5 x 10^{18} and 5 x 10^{19}) GIA models is close to the estimated timing of isolation at Ytra-Baravatn (Brader *et al.*, submitted). There is also generally good agreement with the field evidence and the model outputs using these upper mantle viscosities during the Lateglacial and early Holocene (Fig. 7.12). Brader *et al.* (submitted) note the relatively limited influence of Younger Dryas ice readvance in Snæfellsnes and this is replicated in the model outputs for the region, particularly for HP_MAX (LT 40 km, υ_{UM} 1 x 10^{20} Pa s; Fig. 7.12). It appears that the timing of the early Holocene RSL fall below present is also well represented in the HP_MAX (LT 40 km, υ_{UM} 1 x 10^{20} Pa s) model, although the timing of the subsequent mid Holocene highstand appears to occur too late within in the model output (Fig. 7.12). The HP_MAX (LT 40 km, υ_{UM} 5 x 10^{19} Pa s) model is highlighted as the best fit model by the chi^2 testing in Area C, as noted for Areas A and B (Fig. 7.13). However, this result may be influenced by the direct correlation of the marine limit point with the modelled RSL change, as the chi^2 testing does not take age error into account. It is worth noting here that if the large age uncertainty surrounding the marine limit point were considered, the HP_MAX (LT 40 km, υ_{UM} 1 x 10^{20} Pa s) model may perform almost as well as the preferred model, given the fit with the other geological data presented.

Each of the three HP_MAX (LT 40 km, υ_{UM} 5 x 10^{18} – 1 x 10^{20} Pa s) SELEN models under-predict the RSL changes noted in the field evidence from Area E (Fig. 7.12). This mismatch between the datasets stems from the Younger Dryas ice thicknesses within the HP_MAX ice model. An increase in ice thickness at the Younger Dryas in the region would lead to a better fit with the field evidence, with the modelled RSL curve demonstrating the correct pattern of RSL fall since deglaciation (Fig. 7.12). Chi^2 tests highlight the preferred maximum ice and earth model combination for Area E is HP_MAX (LT 40 km, υ_{UM} 1 x 10^{20} Pa s; Fig. 7.13).

When considering the results of chi^2 tests on the individual model outputs, it is clear that there is some consistency in the preferred HP_MAX models – HP_MAX (LT 40 km, υ_{UM} 5 x 10^{19} Pa s) and HP_MAX (LT 40 km, υ_{UM} 1 x 10^{20} Pa s; Fig. 7.13) – between sites. This is replicated in the chi^2 tests for the entire modelled dataset for HP_MAX_Icelandic Rheology in northwest Iceland (Fig. 7.14).

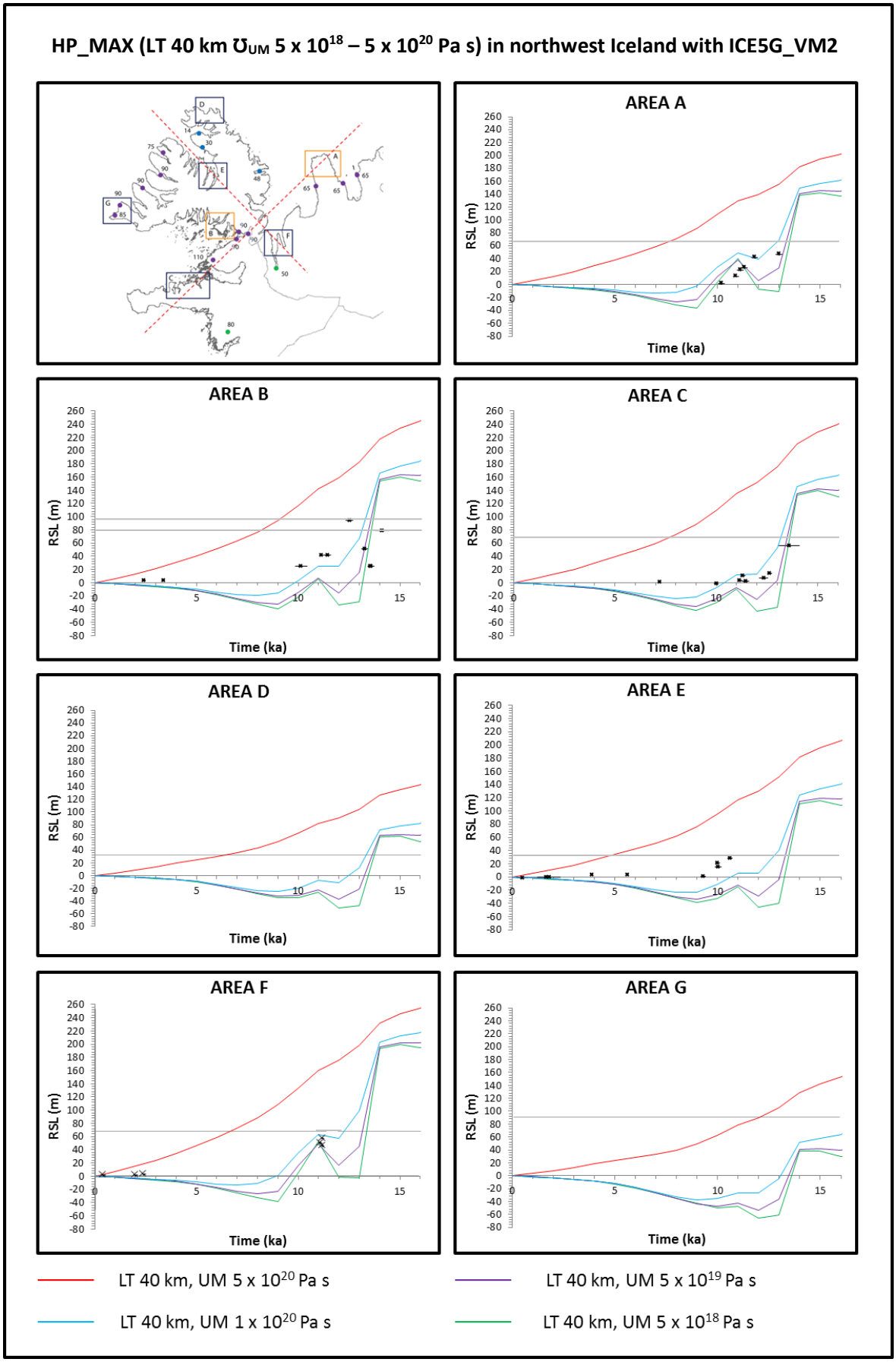

Figure 7.12 – RSL outputs from HP_MAX (40 km LT) with ICE5G (VM2) global ice loading in NW Iceland. Sources: HP_MAX original file (Patton, unpub), ICE5G original file (Peltier, 2004), AREA A RSL data (Rundgren et al 1997), AREA B RSL data (Lloyd et al. 2009), AREA C RSL data (Brader et al., submitted), AREA D-G RSL data (current study). The local marine limit is shown by the solid grey horizontal line.

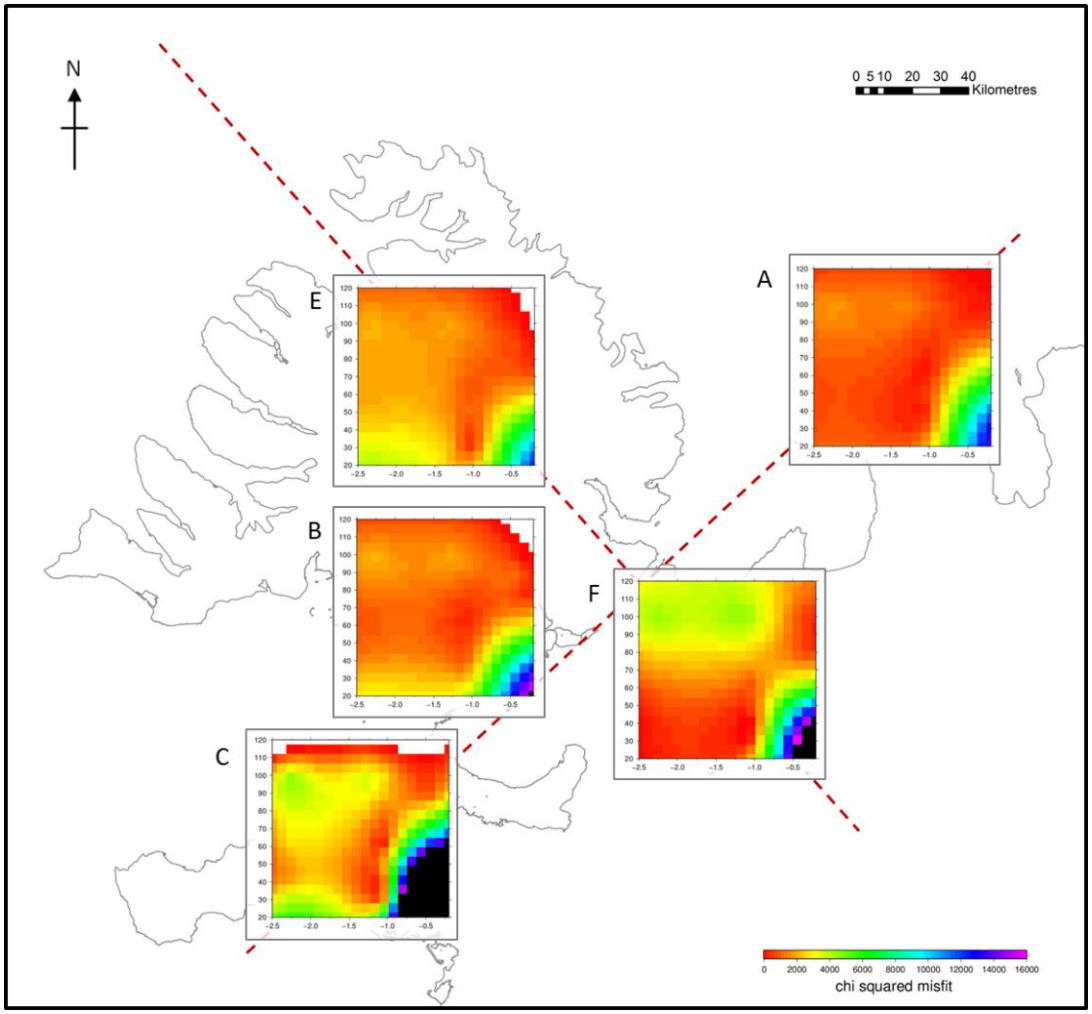

Figure 7.13 – Chi^2 results for the HP_MAX (Patton, unpub) model with Icelandic rheological profiles for the five field locations in northwest Iceland, highlighting the best fit model with the field dataset. For individual plots, the axes are: x - log υ_{UM} and y - LT. Outputs are provided for locations with reliable chronological control only. For reference, log (υ_{UM}) values are as follows: -0.3: 5 x 10^{20} Pa ; -1.3: 5 x 10^{19} Pa s; -2.3: 5 x 10^{18} Pa s. Better fit between the model output and field evidence is demonstrated by red shading. Areas of white or black within the chi^2 plots are points where the interpolation method is unable to provide a suitable value.

Additional testing of the HP_MAX ice model (Patton, unpub.) was undertaken through adjustment of the LT to 100 km (Barnhoorn *et al.*, 2011). HP_MAX (LT 100 km υ_{UM} 5 x 10^{18} – 5 x 10^{20} Pa s) GIA models are still able to replicate the west-east divide in marine limit elevations recorded within the existing geomorphological evidence (Fig. 7.15). However, none of the HP_MAX (LT 100 km υ_{UM} 5 x 10^{18} – 5 x 10^{20} Pa s) GIA models are able to reproduce the marine limit elevations recorded in the field evidence (Fig. 7.15). The results of each HP_MAX (LT 100 km, υ_{UM} 5 x 10^{18} - 5 x 10^{20} Pa s) GIA model do however demonstrate the influences of the Younger Dryas ice readvance, although the HP_MAX (LT 100 km, υ_{UM} 5 x 10^{20} Pa s) GIA model appears to show the best fit to the available field evidence (Fig. 7.15). Whilst the HP_MAX (LT 100km, υ_{UM} 5 x 10^{20} Pa s) GIA model produces a reasonable prediction of postglacial RSL change in Location 1, the marine limit elevation is still poorly constrained by the model (Fig. 7.15). Despite this, the model has a good fit with the geological dataset, with a chi^2 value of 59.2 in Area B (Fig. 7.13).

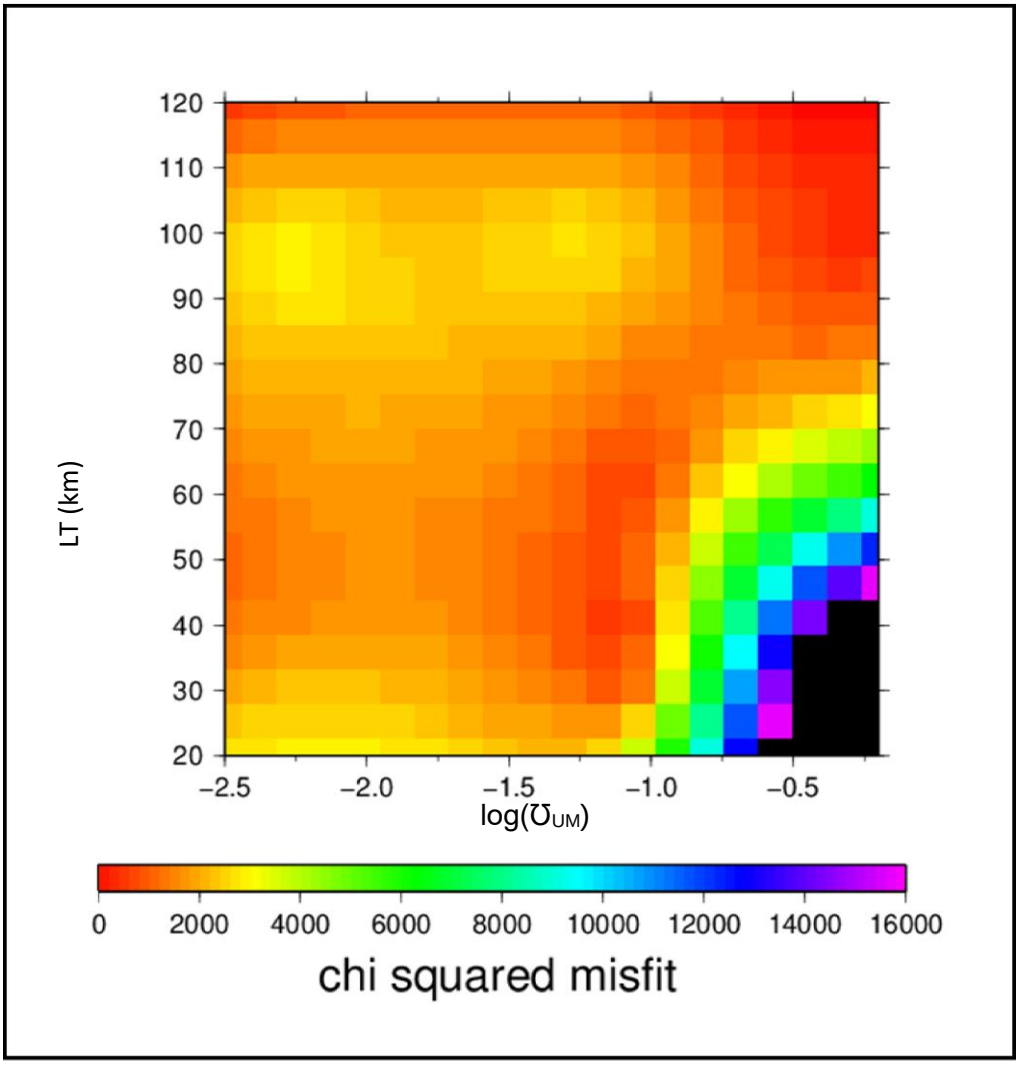

Figure 7.14 – Chi² results for the HP_MAX model in northwest Iceland (regional scale) at a range of rheological profiles, highlighting the preference for a LT 40km and ʊUM between 5 x 10¹⁹ Pa s and 1 x 10²⁰ Pa s. For reference, log (ʊUM) values are as follows: -0.3: 5 x 10²⁰ Pa ; -1.3: 5 x 10¹⁹ Pa s; -2.3: 5 x 10¹⁸ Pa s.

Similar results for the HP_MAX (LT 100 km) models can be seen for the modelled locations in NW Iceland (Fig. 7.16). HP_MAX (LT 100 km, ʊUM 5 x 10^{20} Pa s) GIA models are able to provide reasonable estimations of postglacial RSL change in the majority of field research locations (Fig. 7.16). However, the HP_MAX (LT 100 km, ʊUM 5 x 10^{20} Pa s) GIA model fails to reproduce the early Holocene RSL fall below present or the subsequent mid-Holocene highstand noted in Area B (Lloyd *et al.*, 2009) or Area C (Brader *et al.*, submitted). The HP_MAX (LT 100 km, ʊUM 5 x 10^{18} - 1 x 10^{20} Pa s) GIA models clearly produce RSL changes which are consistently lower than that suggested by the field evidence, such as in Area G (Fig. 7.16). The HP_MAX (LT 100 km ʊUM 5 x 10^{18} – 5 x 10^{20} Pa s) GIA models can therefore be excluded from further testing, with the Barnhoorn *et al.* (2011) estimation of LGM lithospheric thickness appearing too large for use throughout the Holocene.

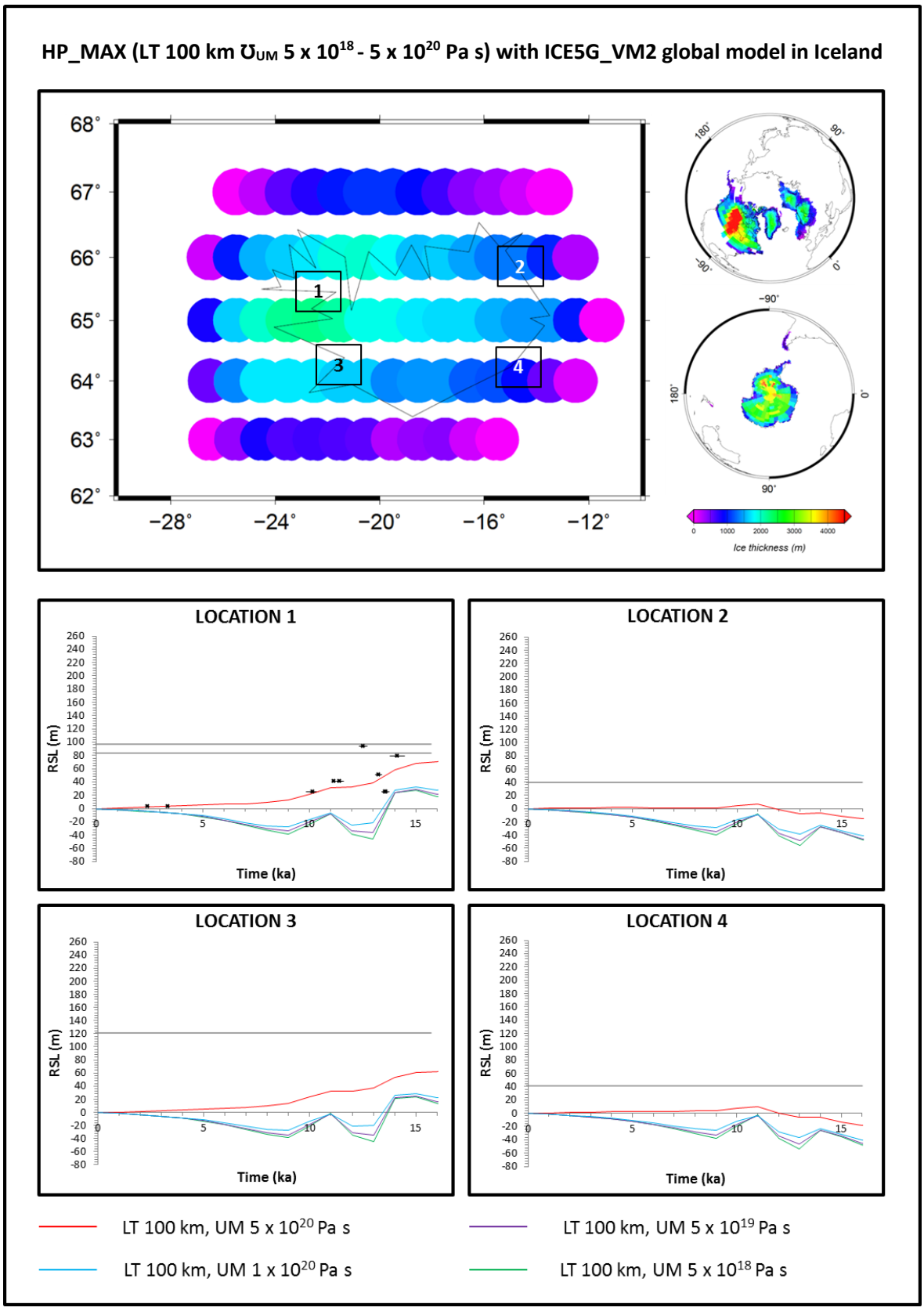

Figure 7.15 – Ice loading distribution and modelled RSL changes in Iceland from HP_MAX (100 km LT) with ICE5G (VM2) global ice loading and rheological profile. Modelled RSL changes are plotted against the existing field dataset. Sources: HP_MAX: Patton (unpub).; ICE5G: Peltier (2004); Location 1 – Lloyd et al. (2009); Location 2 – 4: Norðdahl and Pétursson (2005). The local marine limit is shown by the solid grey horizontal line within each location figure.

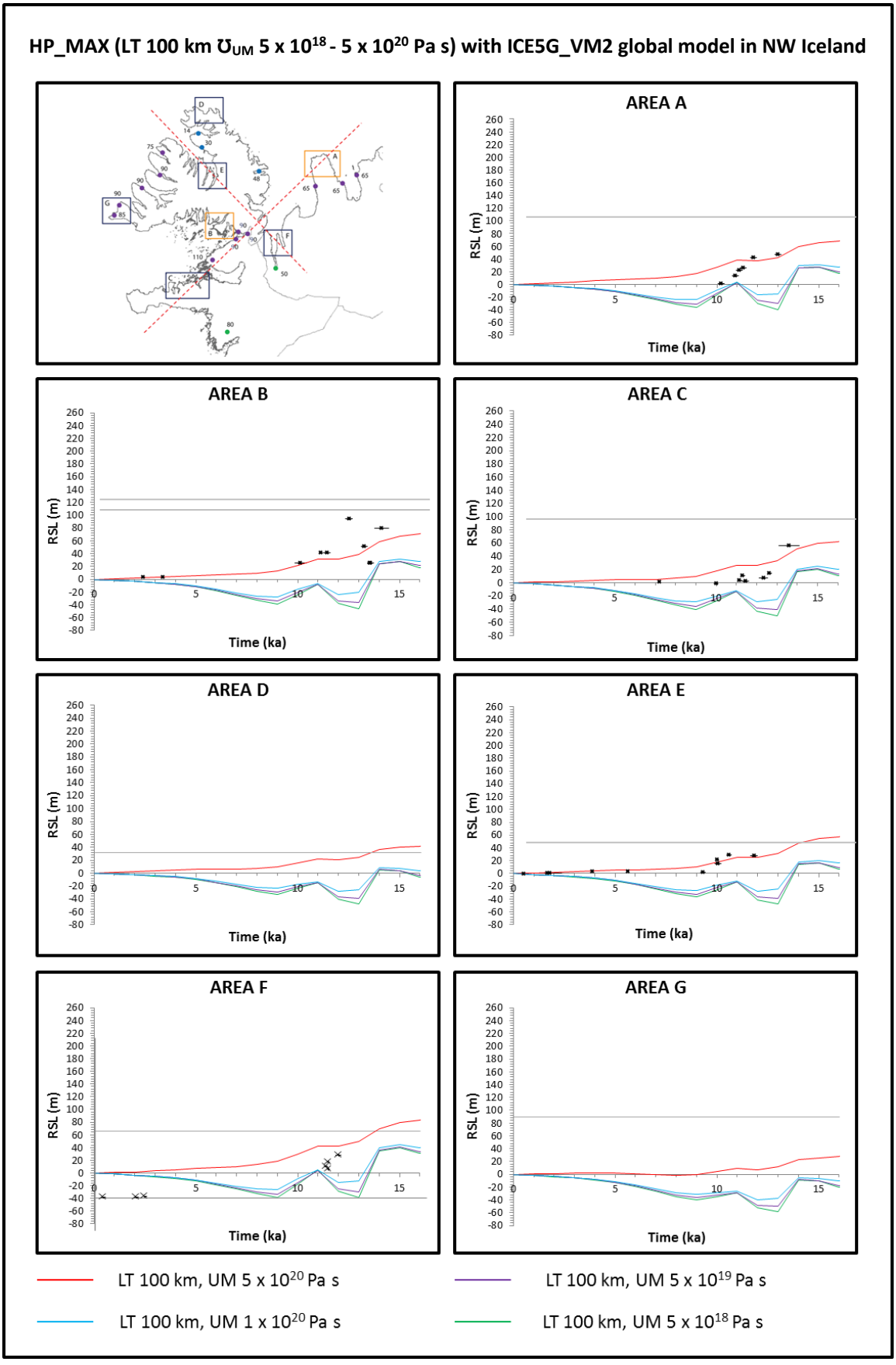

Figure 7.16 –RSL changes in NW Iceland from HP_MAX (100 km LT) with ICE5G (VM2) global ice loading and rheological profile. Modelled RSL changes are plotted against the existing field dataset. Sources: HP_MAX: Patton (unpub).; ICE5G: Peltier (2004); Area A: Rundgren et al. (1997); Area B: Lloyd et al. (2009); Area C: Brader et al. (submitted); Area D – F: Present Study; Area G: Norðdahl and Pétursson (2005). The local marine limit is shown by the solid grey horizontal line within each location figure.

7.5.2 HP_OPT (Icelandic Rheology)

A suite of model runs are presented for the HP_OPT ice model (LT 40 km υ_{UM} 5 x 10^{18} – 5 x 10^{20} Pa s; Fig. 7.17 and 7.18). The HP_OPT ice model has less contrast in ice loading between west and east Iceland, and this is translated to the resultant RSL outputs from the GIA models (Fig. 7.17). There is therefore a lesser contrast between the marine limit elevations of western and eastern Iceland modelled using HP_OPT (Fig. 7.17). In each of the four modelling 'control' locations, the HP_OPT (LT 40 km υ_{UM} 5 x 10^{18} – 5 x 10^{20} Pa s) models fail to reach the marine limit elevations when the upper mantle viscosity is less than 5 x 10^{20} Pa s (Fig. 7.17). However, the HP_OPT (LT 40 km, υ_{UM} 5 x 10^{20} Pa s) model does not produce the patterns and elevation of Lateglacial to Holocene RSL change to match the existing isolation basin field data (see Location 1; Fig. 7.17).

In NW Iceland, the HP_OPT (LT 40 km, υ_{UM} 5 x 10^{18} – 1 x 10^{20} Pa s) GIA models also produce RSL outputs which are lower than recorded by the field evidence (Fig. 7.18). The only HP_OPT GIA model to consistently generate RSL predictions above present sea level is HP_OPT (LT 40 km, υ_{UM} 5 x 10^{20} Pa s; Fig 7.18). There is a particular contrast between the field-based RSL record and modelled RSL changes in Area G (Fig. 7.18). The best fit HP_OPT (LT 40 km) model in NW Iceland varies between field areas (Fig. 7.19). HP_OPT (LT 40 km, υ_{UM} 1 x 10^{20} Pa s) is the preferred ice and Earth model for Areas A and C, with HP_OPT (LT 40 km, υ_{UM} 5 x 10^{20} Pa s) being favourable in Areas B, E and F (Fig. 7.18 and 7.19). Through comparison between the field data and modelled RSL outputs, it is clear that the HP_OPT (LT 40 km, υ_{UM} 5 x 10^{18} Pa s) and HP_OPT (LT 40 km, υ_{UM} 5 x 10^{19} Pa s) models can be excluded for use in NW Iceland (Fig. 7.18 and 7.19). Both models produce RSL outputs which under-estimate the RSL changes at each field research location and have high chi^2 values (Fig. 7.19). The poor fit between the model and field-based RSL reconstructions for northwest Iceland is further demonstrated by the regional chi^2 results (Fig. 7.20).

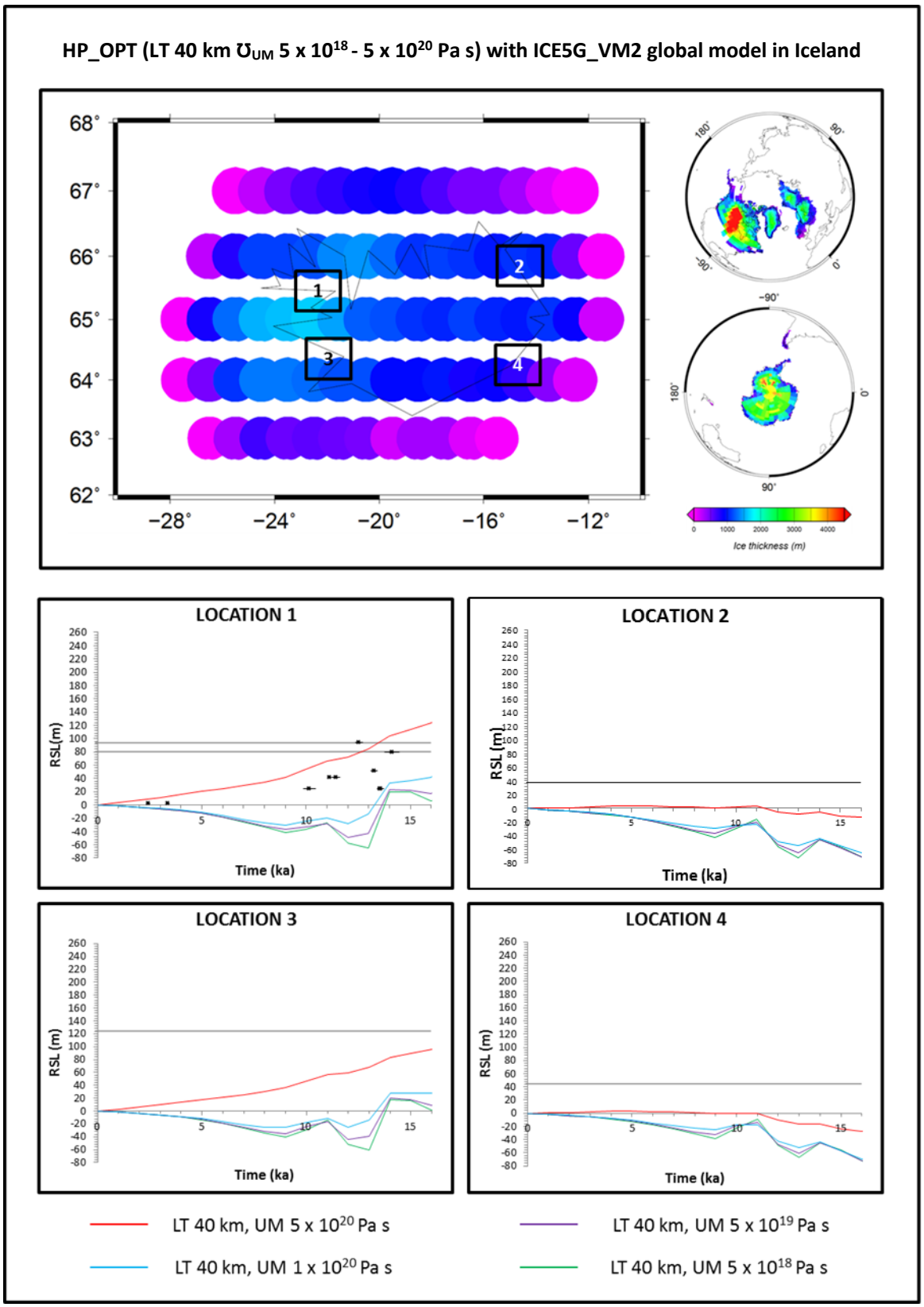

Figure 7.17 – RSL outputs from HP_OPT (Icelandic Rheology) with ICE5G (VM2) global ice loading in Iceland, alongside ice distribution within the model. The implications of ice loading in Iceland can be seen through the contrasting RSL outputs for western and eastern Iceland. Sources: HP_MAX original file (Patton, unpub), ICE5G original file (Peltier, 2004), Location 1 RSL data (Lloyd et al. 2009), Location 2-4 RSL data (Norðdahl and Pétursson, 2005). The local marine limit is shown by the solid grey horizontal line in the location figures.

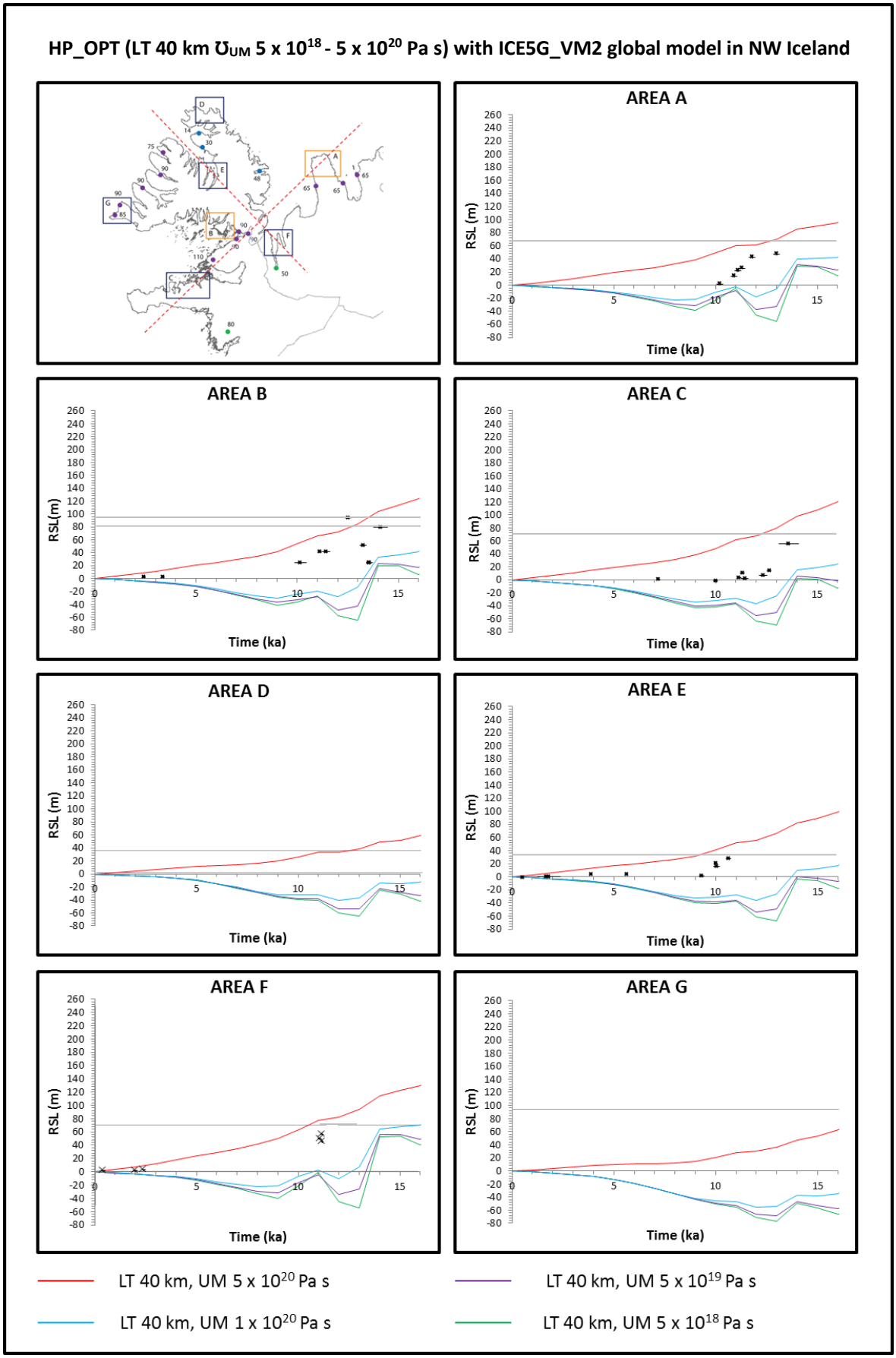

Figure 7.18 – RSL outputs from HP_OPT (Icelandic Rheology) with ICE5G (VM2) global ice loading in NW Iceland. Sources: HP_MAX (Patton, unpub), ICE5G original file (Peltier, 2004), AREA A RSL data (Rundgren et al 1997), AREA B RSL data (Lloyd et al. 2009), AREA C RSL data (Brader et al., submitted), AREA D-G RSL data (current study). The local marine limit is shown by the solid grey horizontal line in the location figures.

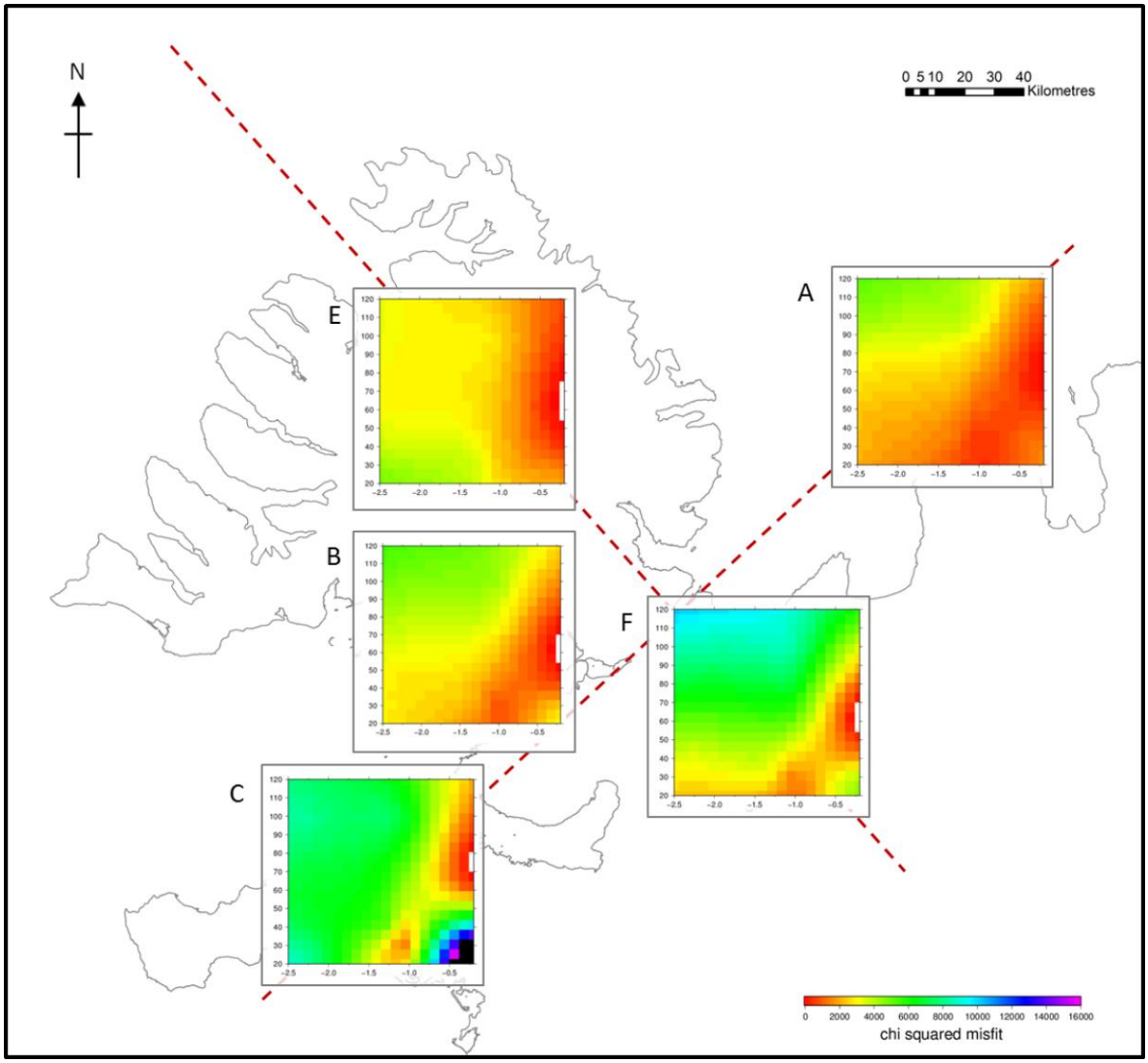

Figure 7.19 – Chi^2 outputs for the HP_OPT (Patton, unpub.) model for five field locations in northwest Iceland, highlighting the best fit model for the optimum glaciation scenario in each area. Outputs are provided for locations with reliable chronological control only. For reference, log (υ_{UM}) values are as follows: -0.3: 5 x 10^{20} Pa ; -1.3: 5 x 10^{19} Pa s; -2.3: 5 x 10^{18} Pa s. Areas of white or black within the chi^2 plots are points where the interpolation method is unable to provide a suitable value.

As for the HP_MAX ice models (Patton, unpub.), additional testing of the ice distribution was undertaken for HP_OPT (Patton, unpub.), with the lithospheric thickness increased to 100 km (Barnhoorn *et al.*, 2011; Fig. 7.21). The HP_OPT (LT 100 km υ_{UM} 5 x 10^{18} – 1 x 10^{20} Pa s) models demonstrate an under-prediction of postglacial RSL changes at all of the modelling 'control' and field research locations (Fig. 7.21 and 7.22). The field area and regional chi^2 results, generated through model runs between LT 30 – 100 km and υ_{UM} 5 x 10^{18} – 5 x 10^{20} Pa s, suggest that the preferred earth model for use with the HP_OPT ice model is likely (Fig. 7.20) *LT 60 km υ_{UM} 5 x 10^{20} Pa s.*

The regional overview also demonstrates the generally poor fit between the GIA model outputs and geological datasets for northwest Iceland for the rheological profiles presented.

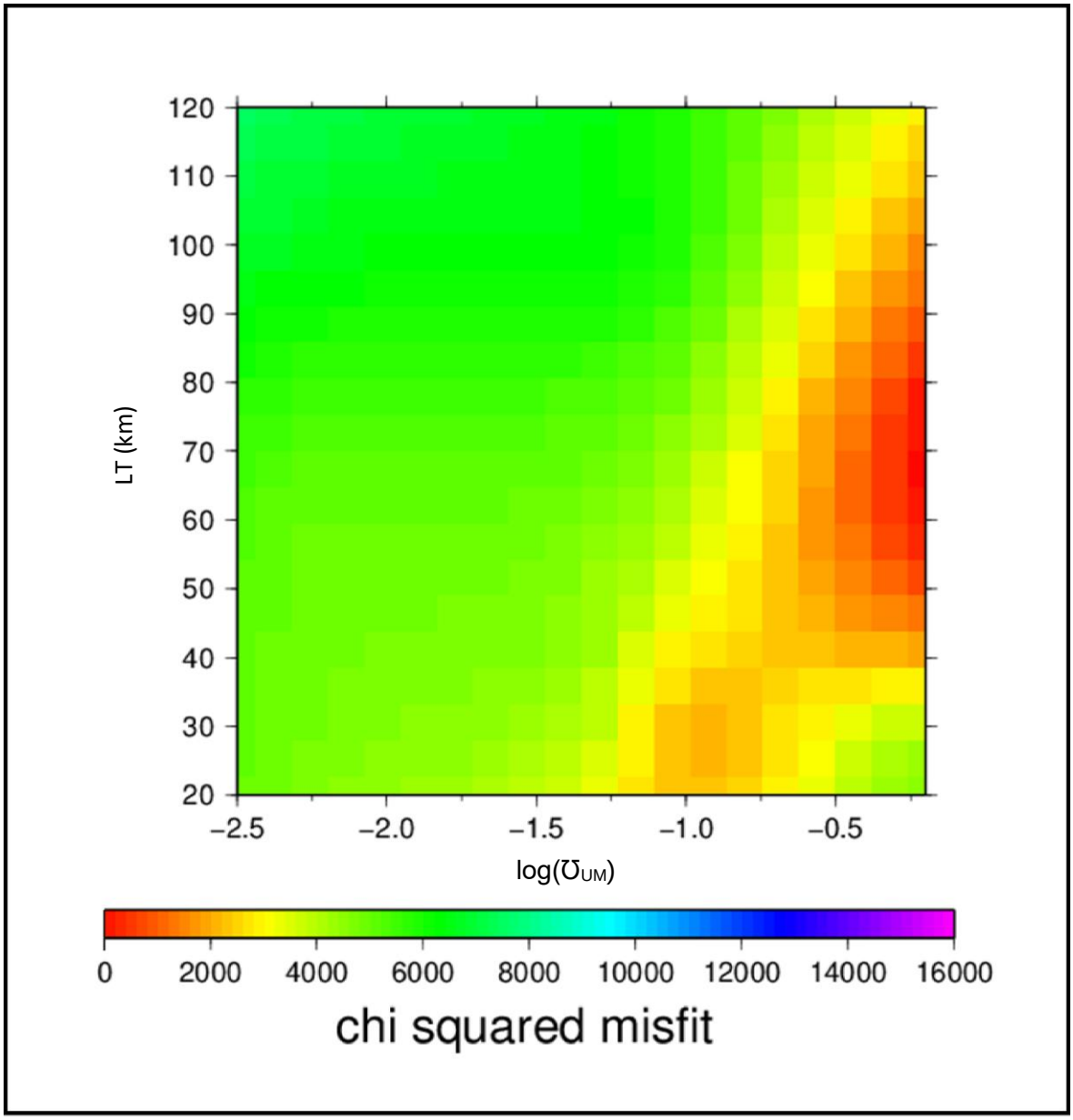

Fig. 7.20 – Chi^2 results of the HP_OPT ice model for sites in northwest Iceland, showing the preference for a LT of 30km and ʊ$_{UM}$ of c. 1 x 10^{20} Pa s. For reference, log (ʊ$_{UM}$) values are as follows: -0.3: 5 x 10^{20} Pa ; -1.3: 5 x 10^{19} Pa s; -2.3: 5 x 10^{18} Pa s.

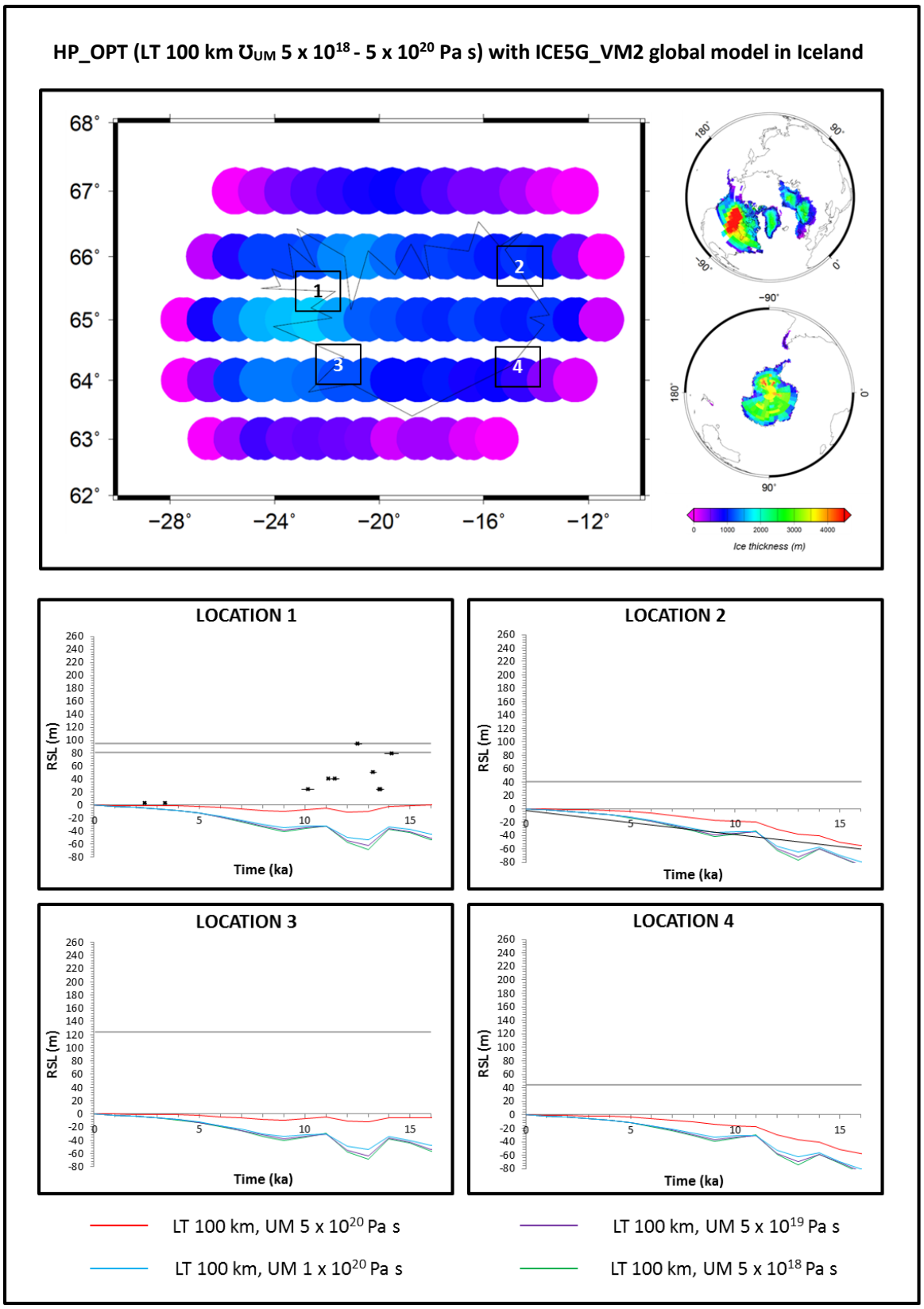

Figure 7.21 – RSL changes in Iceland from HP_OPT (100 km lithosphere) with ICE5G (VM2) global ice loading and rheological profile. Modelled RSL changes are plotted against the existing field dataset. Sources: HP_MAX: Patton (unpub); ICE5G: Peltier (2004); Location 1: Lloyd et al. (2009); Location 2 - 4: Norðdahl and Pétursson (2005). The marine limit is shown by the solid grey horizontal line within each location figure.

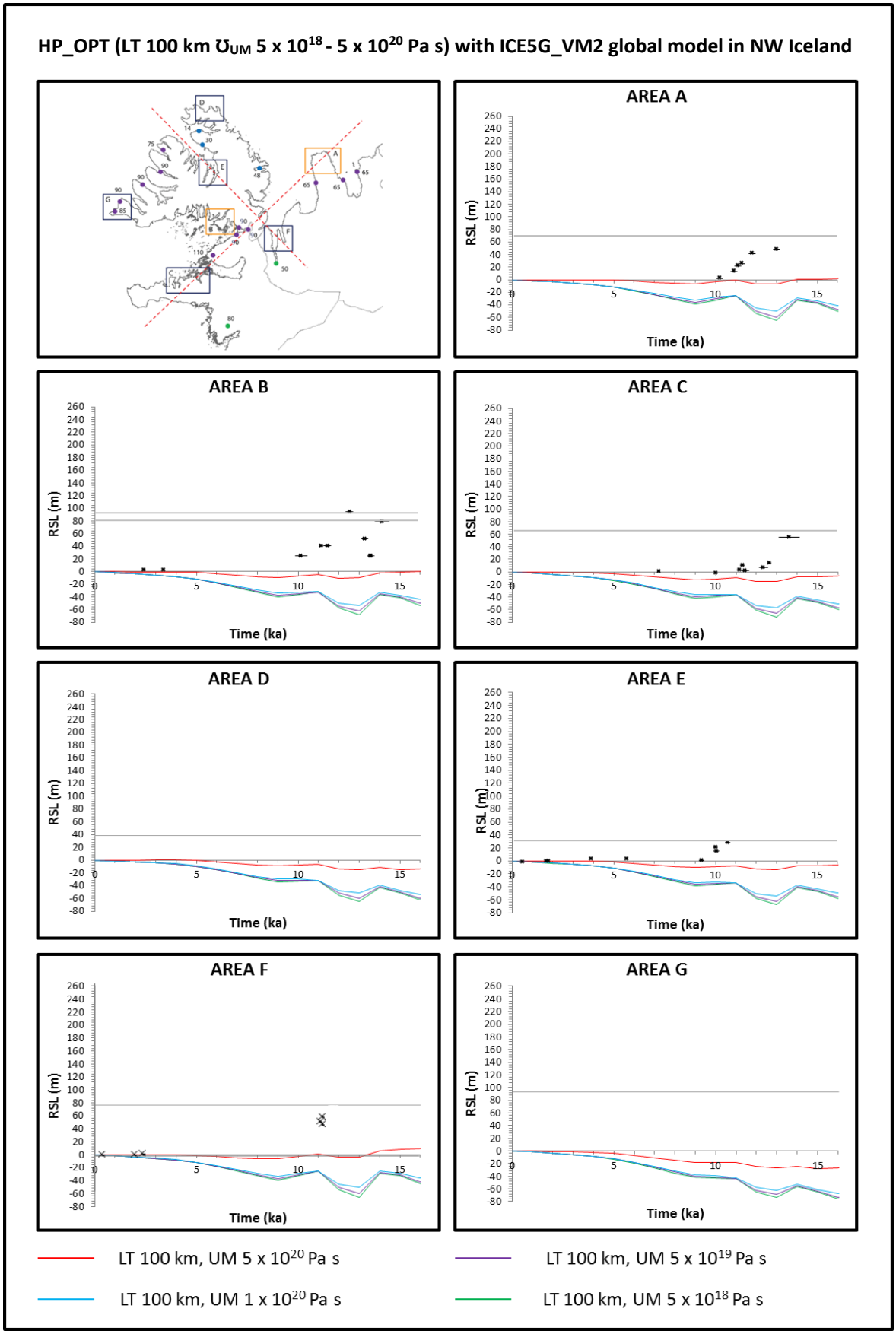

Figure 7.22 – RSL changes in NW Iceland from HP_OPT (100 km lithosphere) with ICE5G (VM2) global ice loading and rheological profile. Modelled RSL changes are plotted against the existing field dataset. Sources: HP_MAX: Patton (unpub).; ICE5G: Peltier (2004); Area A: Rundgren et al. (1997); Area B: Lloyd et al. (2009); Area C: Brader et al. (submitted); Area D – F: Present Study; Area G: Norðdahl and Pétursson (2005). The local marine limit is shown by the solid grey horizontal line within each location figure.

Consequently, the LT 100 km model characteristic is not suitable for use throughout the Holocene when employing the HP_OPT ice model and υ_{UM} 5 x 10^{18} – 5 x 10^{20} Pa s. The chi^2 testing shows an improved fit between field data and model outputs, when GIA models employ lower LT and υ_{UM} values (Fig. 7.20).

7.5.3 HP_MIN (Icelandic Rheology)

The final ice model to be examined was HP_MIN (Patton, unpub.), which represents the minimum glaciation scenario (Section 4.4.2; Fig. 7.23). As noted with the other ice models, variation of the lower mantle viscosity had little effect on the predicted RSL changes - any difference in the results of modelled RSL change between individual GIA model runs was equivalent to the vertical error associated with the generation of individual sea-level index points.

RSL outputs from the HP_MIN (LT 40 km υ_{UM} 5 x 10^{18} - 5 x 10^{20} Pa s) models demonstrate the west-east division of marine limit elevations noted within the field record (Fig. 7.23). This is a consequence of the ice distribution within the HP_MIN ice model, where greater ice thicknesses are found at Breiðafjörður, western Iceland (Fig. 7.23). In western Iceland, the HP_MIN (LT 40 km υ_{UM} 5 x 10^{20} Pa s) model provides the best fit to the empirical dataset (Fig. 7.23). HP_MIN (LT 40 km υ_{UM} 5 x 10^{20} Pa s) is able to produce higher marine limit elevations in Location 1 (Fig. 7.23), although the model is unable to replicate the fall below present during the early Holocene or subsequent mid-Holocene highstand noted by Lloyd *et al.* (2009). Similarly, in Location 3 (Fig. 7.23), the HP_MIN (LT 40 km υ_{UM} 5 x 10^{20} Pa s) model is able to reproduce the marine limit elevation, yet subsequent RSL changes are not correctly predicted. For example, a previous study has demonstrated a lowstand of -17 to -30 m in southwest Iceland, which is not produced by the HP_MIN ice model (Ingólfsson *et al.*, 1995). It is clear that the HP_MIN (LT 40 km υ_{UM} 5 x 10^{18} – 1 x 10^{20} Pa s) lower υ_{UM} models are unable to produce RSL outputs which correspond with the field data. In eastern Iceland, the HP_MIN (LT 40 km) models failed to predict RSL higher than 10 m asl over the course of the Lateglacial and Holocene (Fig. 7.23). As a result, the predictions generated by the GIA model are substantially lower than demonstrated by the geomorphological evidence.

It is also clear that there are differences between the modelled and field based RSL changes (Fig. 7.24). With the chosen rheological profiles, it is not possible to reconcile the field evidence with any of the HP_MIN (LT 40 km) models (Fig. 7.24). The HP_MIN (LT 40 km, υ_{UM} 5 x 10^{20} Pa s) is the preferred model in Areas B, E and F, with HP_MIN (LT 40 km, υ_{UM} 1 x 10^{20} Pa s) having the lowest chi^2 values in Area A and C (Fig. 7.27).

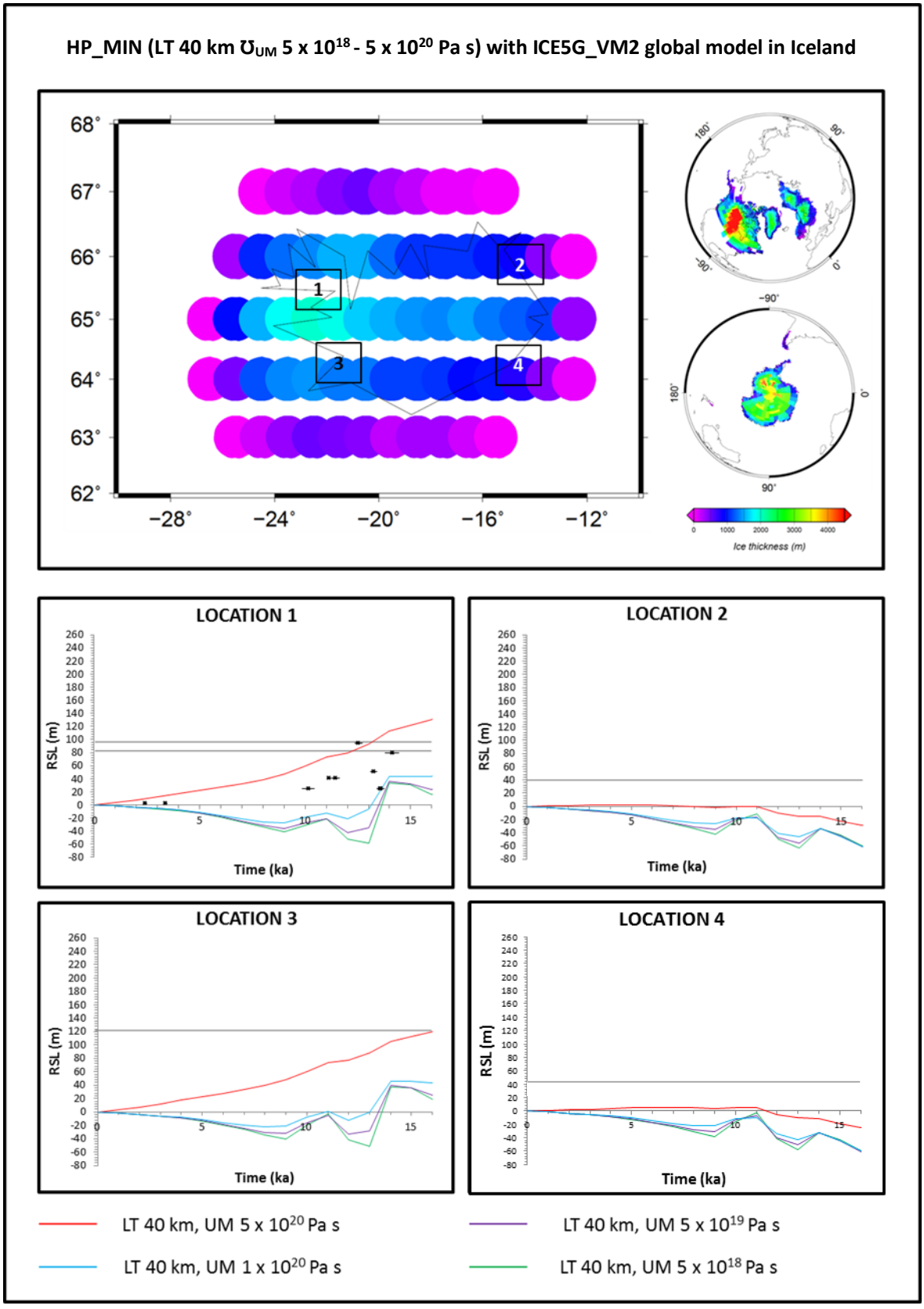

Figure 7.23 – RSL changes in Iceland from HP_MIN (40 km lithosphere) with ICE5G (VM2) global ice loading and rheological profile. Modelled RSL changes are plotted against the existing field dataset. Sources: HP_MIN: Patton (unpub); ICE5G: Peltier (2004); Location 1: Lloyd et al. (2009); Location 2 - 4: Norðdahl and Pétursson (2005). The local marine limit is shown by the solid grey horizontal line within each location figure.

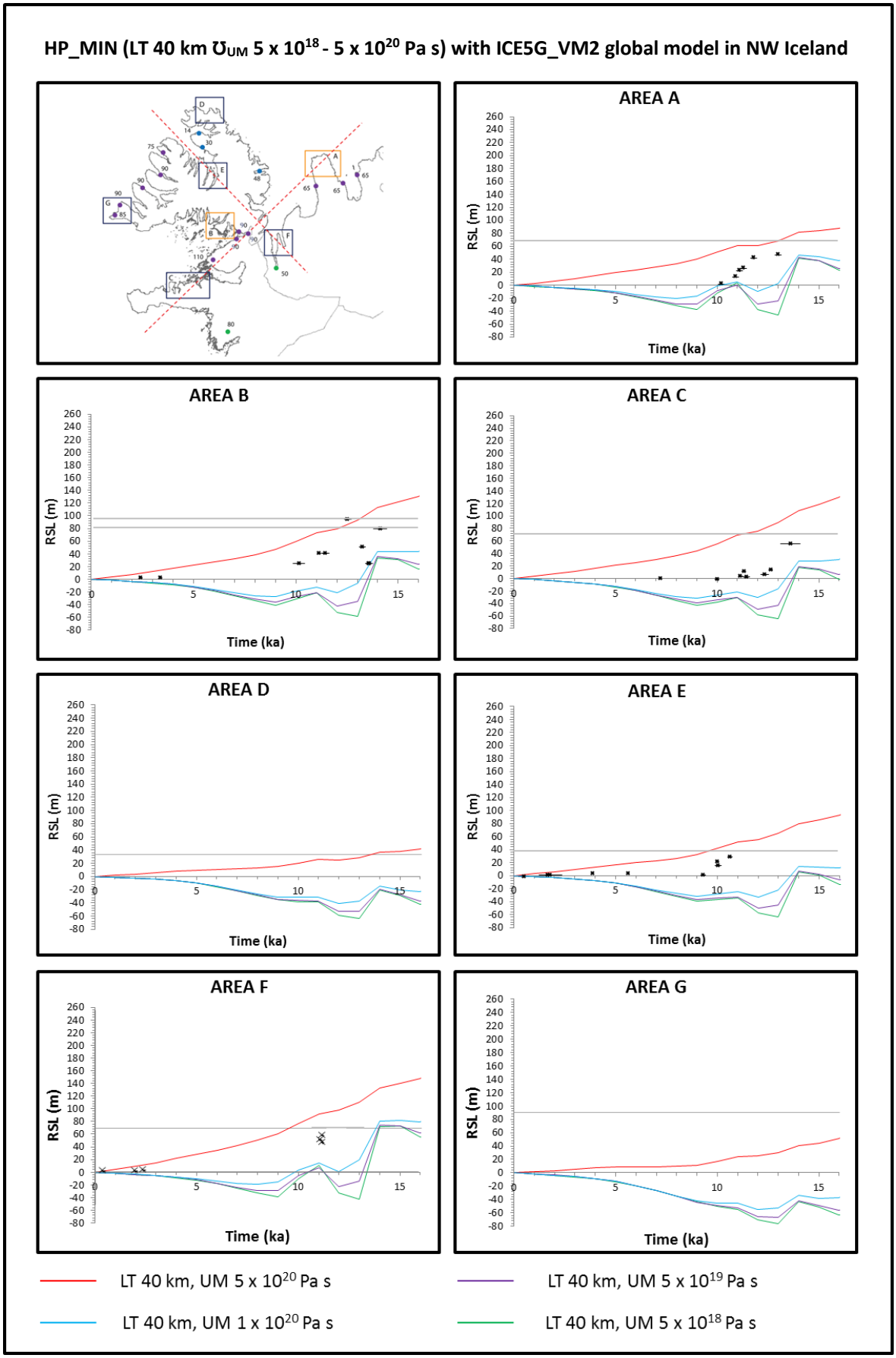

Figure 7.24 – RSL changes in NW Iceland from HP_MIN (40 km lithosphere) with ICE5G (VM2) global ice loading and rheological profile. Modelled RSL changes are plotted against the existing field dataset. Sources: HP_MAX: Patton (unpub.); ICE5G: Peltier (2004); Area A: Rundgren et al. (1997); Area B: Lloyd et al. (2009); Area C: Brader et al. (submitted); Area D – F: Present Study; Area G: Norðdahl and Pétursson (2005). The local marine limit is shown by the solid grey horizontal line within each location figure.

The HP_MIN (LT 40 km, υ_{UM} 5 x 10^{18} – 5 x 10^{19} Pa s) can be excluded for use in NW Iceland. It is evident that with the chosen rheological profiles investigated, there is insufficient ice loading to produce the higher RSLs recorded in the geomorphological and isolation basin evidence from the region.

RSL outputs from the HP_MIN (LT 100 km, υ_{UM} 5 x 10^{18} – 5 x 10^{19} Pa s) models for the four modelling 'control' locations suggest that postglacial RSL has not been above present (Fig. 7.25). This is in clear contrast to the geomorphological and isolation basin records from these locations (Norðdahl and Einarsson, 2001; Norðdahl and Pétursson, 2005; Lloyd *et al.*, 2009). In NW Iceland, similar modelled patterns of RSL change are noted, with RSL being below present throughout the postglacial period in Areas B, C, E and G (Fig. 7.26). When the LT is increased to 100 km, it is clear that the preferred model has the greatest upper mantle viscosity, which leads to less deformation of the UM and therefore produces modelled RSL changes, which better fit the field-based reconstructions (e.g. Rundgren *et al.*, 1997; Lloyd *et al.*, 2009). However, the HP_MIN (υ_{UM} 5 x 10^{20} Pa s) models are unable to replicate the distinct patterns of postglacial RSL change in any of the research areas. It is therefore clear that the ice models of the minimum glaciation scenario require further development. Modification to the rheological profile fails to allow the replication of the field evidence, unless LT and υ_{UM} were to be adjusted to extreme levels.

The completion of GIA model runs for the HP_MIN ice model at LT 30 – 100 km and υ_{UM} 5 x 10^{18} – 5 x 10^{20} Pa s suggest that overall the preferred Earth models for employment with the HP_MIN ice model is LT 60 km υ_{UM} 5 x 10^{20} Pa s (Fig. 7.27 and 7.28). This is clearly demonstrated in the field area and regional chi^2 results and correlates with the preferred Earth models for the HP_OPT ice model. However, the model outputs from both the HP_OPT and HP_MIN models have a poor fit with the geological data in comparison to HP_MAX (Fig. 7.13 and 7.14).

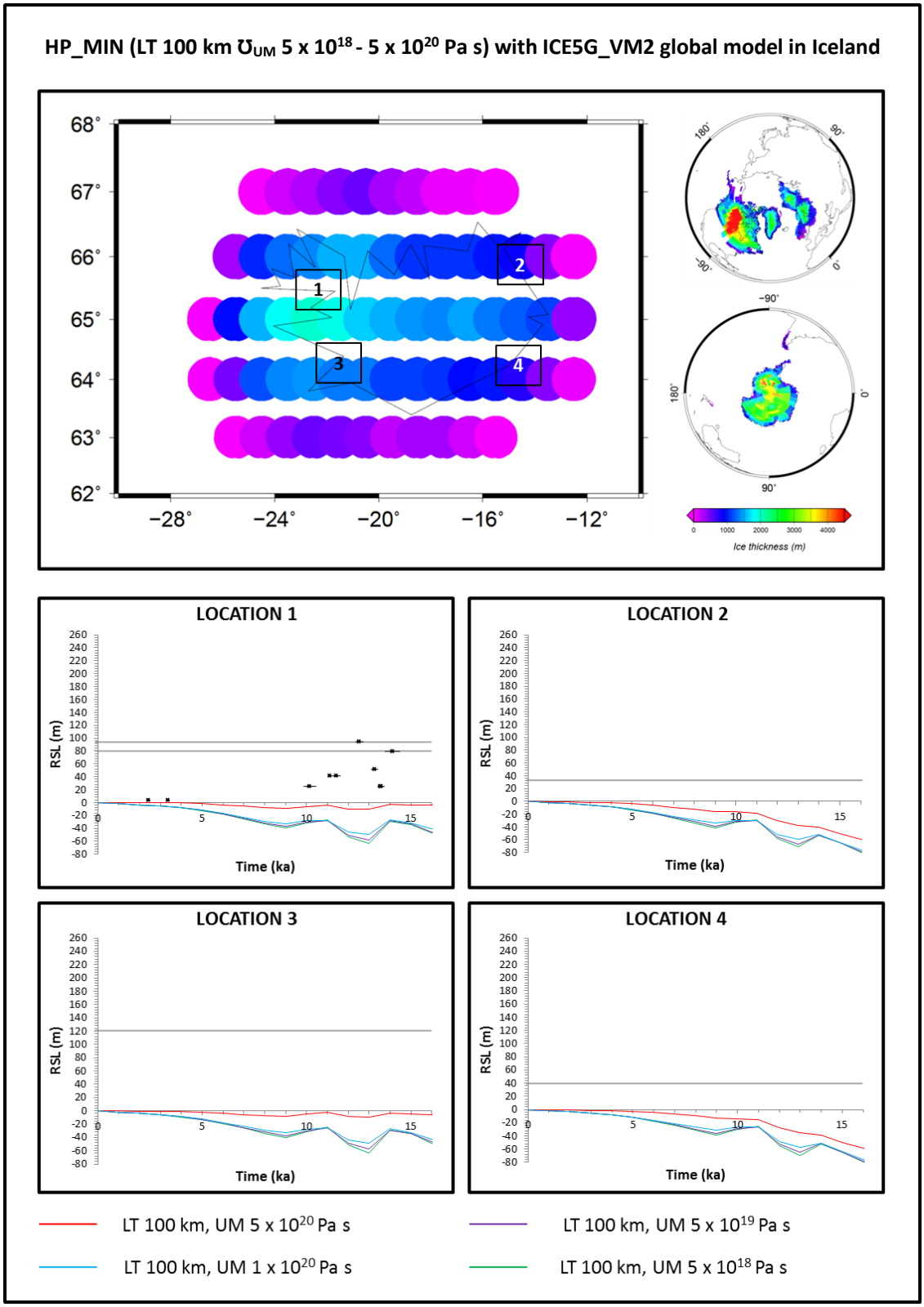

Figure 7.25 – RSL changes in Iceland from HP_MIN (100 km lithosphere) with ICE5G (VM2) global ice loading and rheological profile. Modelled RSL changes are plotted against the existing field dataset. Sources: HP_MIN: Patton (unpub).; ICE5G: Peltier (2004); Location 1: Lloyd et al. (2009); Location 2 - 4: Norðdahl and Pétursson (2005). The local marine limit is shown by the solid grey horizontal line within the location figures.

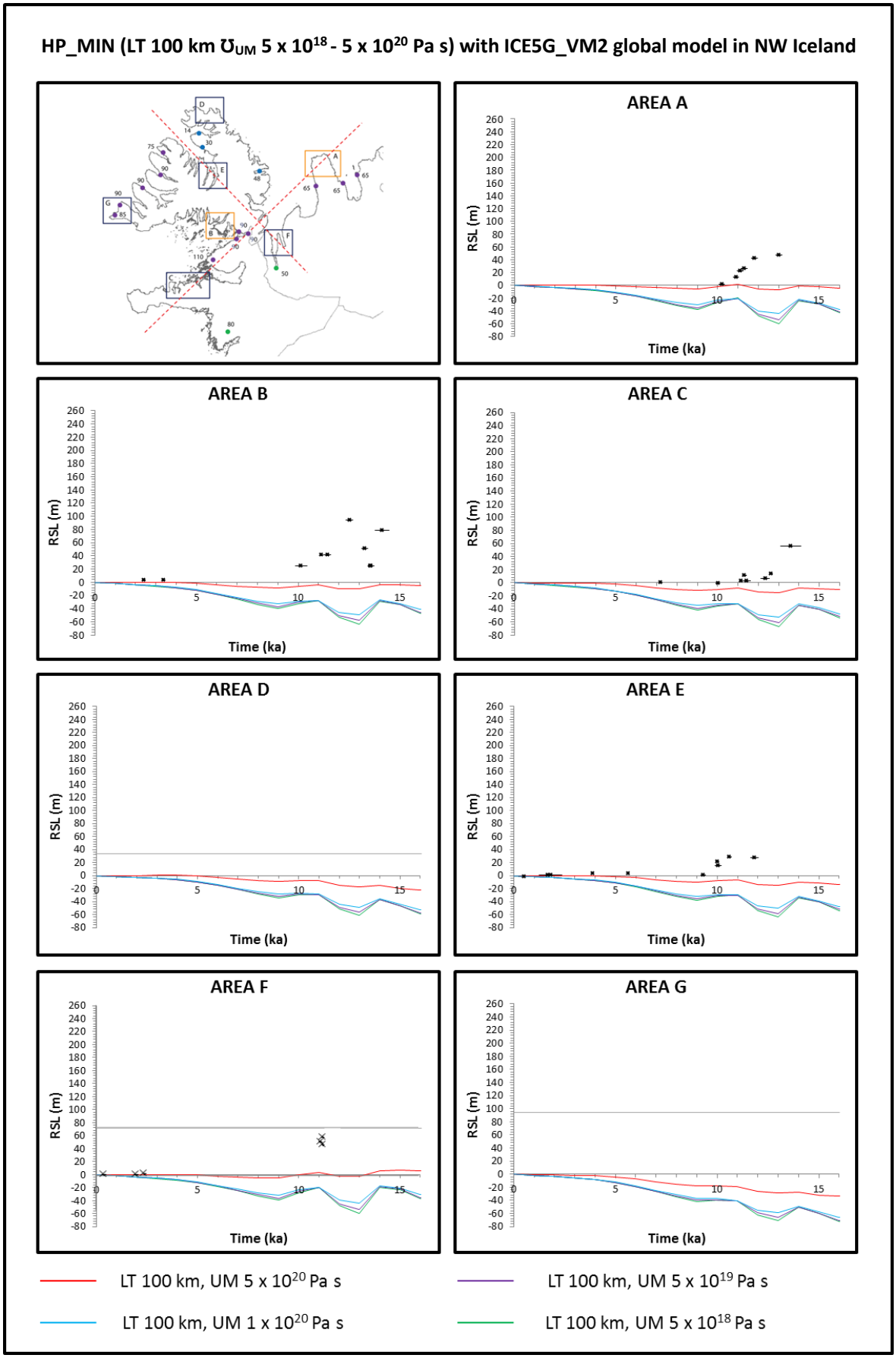

Figure 7.26 – RSL changes in NW Iceland from HP_MIN (40 km lithosphere) with ICE5G (VM2) global ice loading and rheological profile. Modelled RSL changes are plotted against the existing field dataset. Sources: HP_MAX: Patton (unpub).; ICE5G: Peltier (2004); Area A: Rundgren et al. (1997); Area B: Lloyd et al. (2009); Area C: Brader et al. (submitted); Area D – F: Present Study; Area G: Norðdahl and Pétursson (2005). The local marine limit is shown by the solid grey horizontal line in the location figures.

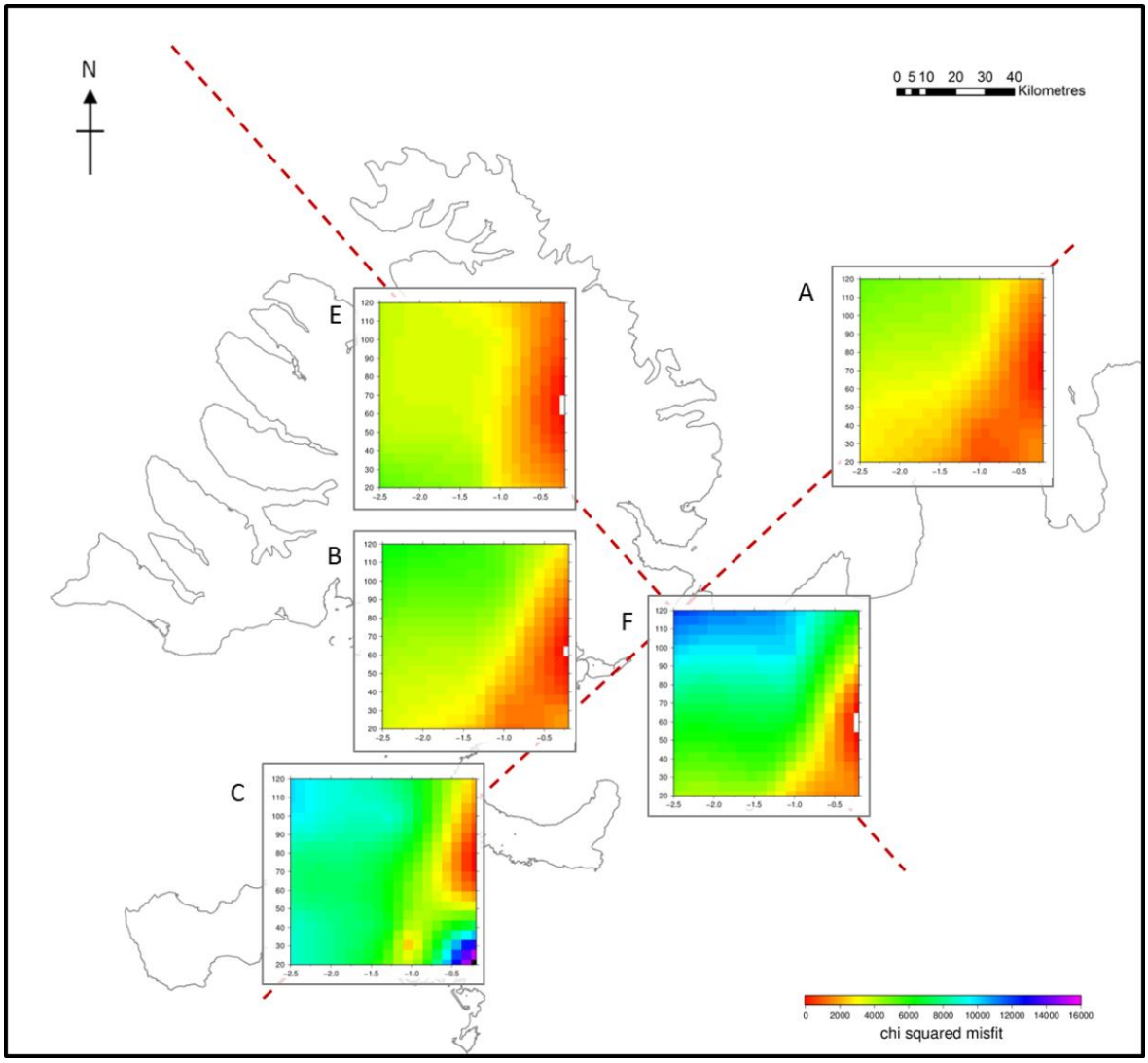

Figure 7.27 – Chi² results for the HP_MIN ice model for individual field areas in northwest Iceland, demonstrating the preferred rheological profile in each area. Outputs are provided for locations with reliable chronological control only. For reference, log (υ_{UM}) values are as follows: -0.3: 5 x 10^{20} Pa ; -1.3: 5 x 10^{19} Pa s; -2.3: 5 x 10^{18} Pa s. Areas of white within the chi² plots are points where the interpolation method is unable to provide a suitable value.

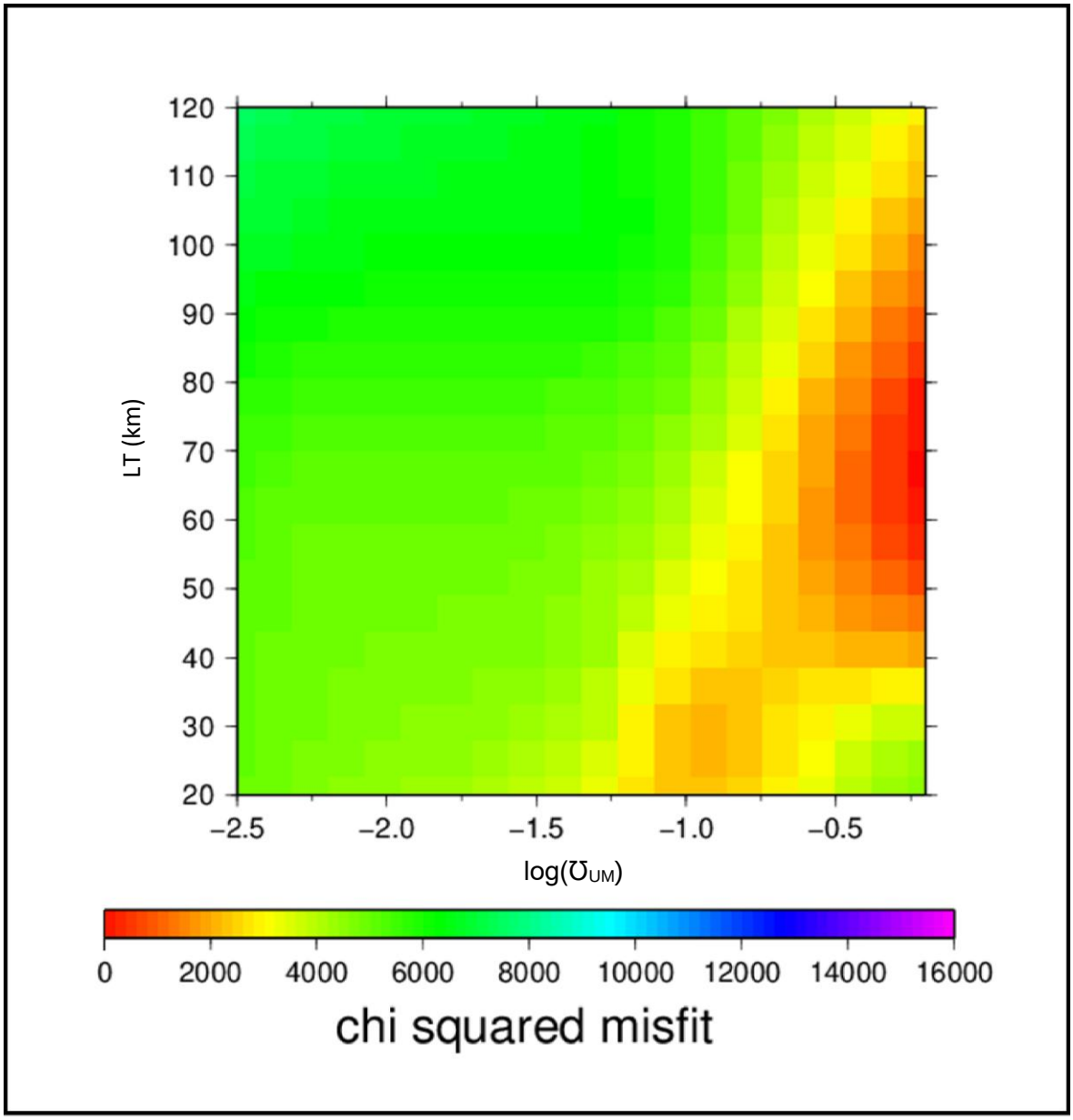

Figure 7.28 – Chi² results for northwest Iceland, showing the preferred rheological characteristics at the regional scale. For reference, log (ʊUM) values are as follows: -0.3: 5 x 10²⁰ Pa ; -1.3: 5 x 10¹⁹ Pa s; -2.3: 5 x 10¹⁸ Pa s.

7.6 Summary

GIA model runs have demonstrated that the preferred ice model is HP_MAX, which is particularly effective when coupled with the LT 40km, ʊUM 5 x 10¹⁹ - 1 x 10²⁰ Pa s Earth models, demonstrating good fit with the majority of field sites. However, differences between the GIA model output and field based RSL reconstructions are evident, suggesting that further development of the ice and Earth models are required. In particular, it is evident that additional ice loading is required at the LGM in Area Gin order to reproduce the elevation of the proposed marine limit. Additional ice loading during the Younger Dryas is also required in Areas B, D and E, if the HP_MAX (LT 40km, ʊUM 5 x 10¹⁹ - 1 x 10²⁰ Pa s) model is accepted. Furthermore, the HP_MAX (LT 40km, ʊUM 5 x 10¹⁹ - 1 x 10²⁰ Pa s) model fails to re-produce the RSL highstand recorded in the field evidence for

northwest Iceland. Adjustment to the Earth characteristics may be able to mitigate some of these differences between the model and geological datasets, although the proposed viscosity characteristics fit well with previously published estimates.

The GIA modelling completed has also highlighted the differing potential impact of Younger Dryas ice re-advance on the RSL records from NW Iceland, which has important implications for the configuration of the LGM IIS. There is clear evidence for a lesser influence of this ice re-advance in Area C, when compared to Areas A and B. Chapter 8 will discuss these results alongside the new RSL data presented in Chapter 6 in the context of existing records of the LGM IIS and postglacial RSL changes.

CHAPTER 8

Discussion

8.1 Introduction

This chapter provides an overview of the principal outputs of this research in the context of previous geomorphological, relative sea level (RSL) and glacio-isostatic adjustment (GIA) modelling studies undertaken in Iceland. In particular, the chapter highlights the potential implications for the proposed scale, extent and volume of the Last Glacial Maximum (LGM) Icelandic Ice Sheet (IIS). Initially, the results of marine limit and isolation basin studies will be reviewed, followed by a discussion of the patterns and style of deglaciation outlined by these results. Subsequently, the GIA modelling results will be discussed, in particular the preferred ice and Earth models will be examined, alongside a review of the fit between model predictions and the new geological datasets.

8.2 Marine limit in northwest Iceland

The elevation of the marine limit is a product of ice thickness, the timing of deglaciation and, to a more limited extent, variation in lithospheric thickness and Earth viscosity characteristics. Within this study, variations in the viscosity profile are assumed to be limited in NW Iceland, meaning that the principal controls on marine limit elevation are ice loading patterns and the timing of deglaciation. Exploring variations in the viscosity profile requires three dimensional modelling of the Earth structure, which is beyond the scope of this thesis. However, mapping and dating of the marine limit provides a valuable insight into glacial loading and unloading, as well as rates of postglacial rebound (e.g. Andrews, 1970; Ingólfsson, 1991). Where ice re-advance has occurred, such as during the Younger Dryas, evidence for the postglacial marine limit can be limited. Thus, the marine limit is likely to be associated with either the LGM deglaciation (e.g. Lloyd *et al.*, 2009) or the Younger Dryas re-advance (e.g. Norðdahl and Ásbjörnsdóttir, 1995).

In Iceland, previous research has highlighted the rapid nature of isostatic rebound, due to the low viscosity of the upper mantle (Norðdahl, 1991; Sigmundsson, 1991; Ingólfsson *et al.*, 1995; Rundgren *et al.*, 1997; Ingólfsson and Norðdahl, 2001; Le Breton *et al.*, 2010). It has been suggested that postglacial rebound in Iceland is largely complete within 1000 years of deglaciation (Sigmundsson, 1991). Marine limits recorded with similar ages can thus be taken as proxies of ice thickness, as rebound rates would be dependent on glacial loading. The pattern of marine limit elevation along Transect 2 therefore suggests greater ice thicknesses with proximity to the proposed principal ice loading centre at Vatnajökull, as suggested under the maximum glaciation

hypothesis (Fig. 2.3). If there had been an independent secondary ice loading centre in Vestfirðir, the marine limit in Area E would likely be found at a higher elevation in comparison to Areas B and F (see Fig. 3.4; 8.1), due to the greater ice thickness over central Vestfirðir in this secnario.

Geomorphological studies have highlighted the differences in recorded elevation and timing of formation of the marine limit in Iceland (e.g. Hjort *et al.*, 1985; Ingólfsson, 1991; Rundgren *et al.*, 1997; Norðdahl and Einarsson; 2001; Principato, 2008). Within this existing dataset, distinct differences in the elevation of the marine limit have been noted between sites in western and eastern Iceland (Fig. 2.5). There are, however, also notable differences in the recorded marine limit elevation at a regional scale, particularly in the northwest (e.g. Principato and Geirsdóttir, 2002; Norðdahl and Pétursson, 2005; Principato, 2008; Fig. 8.1). The additional data points generated as part of this study add to this regional complexity but also allow local differences in marine limit elevation to be explored.

It is clear from the marine limit dataset that ice thickness values and timing of deglaciation were likely different throughout northwest Iceland (Fig. 8.1).

With the exception of sites in innermost Breiðafjörður, the marine limit elevations along Transect 1 (Areas A, B and C) are approximately uniform, ranging from 65 – 80 m asl (Fig. 8.1; Hansom and Briggs, 1991; Rundgren *et al.*, 1997; Brader *et al.*, submitted). The uniform nature of these marine limit elevations suggests similar ice thicknesses at the LGM, particularly considering the agreement between deglacial ages along the ABC transect. Higher marine limit elevations in innermost Breiðafjörður (90-110 m asl; Norðdahl and Pétursson, 2005; Fig. 8.1) may suggest greater ice thicknesses in these inner fjord locations or earlier deglaciation, although the latter would seem unlikely given the location of the sites. In Area A, Rundgren *et al.* (1997) produced a deglacial age of 14 cal. ka BP, following the investigation of isolation and raised shoreline evidence, which has been supported by this research from the basin at TJ1 (Section 6.3.1). Lloyd *et al.* (2009) report that deglaciation occurred at 14 cal. ka in Area B and the present research has determined that deglaciation occurred in Area C at c. 13.8 cal. ka BP. Similar ice thickness values would support the maximum glaciation hypothesis, which would suggest approximately similar ice loading patterns at locations equidistant to the principal ice loading centre at Vatnajökull (Fig. 2.3). This exploration of ice loading patterns is possible due to the two key characteristics of the new marine limit data for northwest Iceland – age and elevation - which have been determined for each of the field areas along Transect 1.

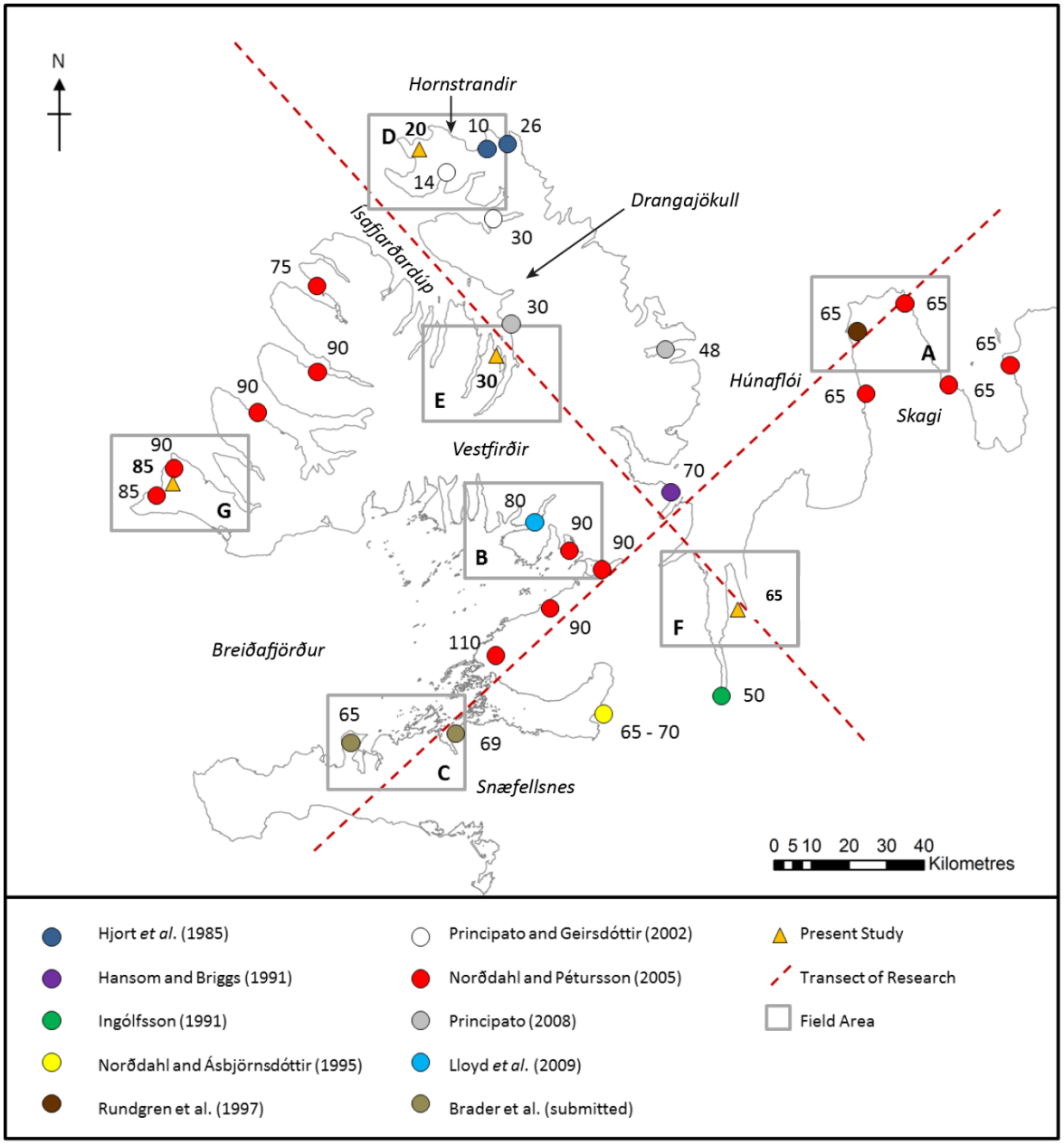

Figure 8.1 – Marine limit in NW Iceland, demonstrating the differences in recorded marine limit elevation (metres asl) in previous research and the present study.

Along Transect 2 (Areas D, E, and F), the marine limit elevation increases towards the SE. However the recorded elevations are more variable than Transect 1, likely as a consequence of the proximity of Areas D and E to post-LGM ice loading from small ice caps, such as that found at Drangajökull (Fig. 2.1, 8.1). This is demonstrated by the lower marine limit values recorded in Hornstrandir (Hjort *et al.*, 1985, Principato and Geirsdóttir, 2002) and innermost Ísafjarðardúp, as well as the low marine limit elevation surveyed in eastern Vestfirðir (48 m, Principato, 2008; Fig. 8.1). The marine limits in Hornstrandir (Hlöðuvik and Aðalvik) and innermost Ísafjarðardjúp are both dated to c. 10200 – 11500 cal. a BP by this research, which suggests formation following the Younger Dryas ice re-advance. In addition, the marine limit in Area F is also dated to the Younger Dryas and is situated at c. 75-80 m asl (Fig. 8.1). Consequently, the relatively low elevation of the

marine limit is likely a consequence of later deglaciation or Younger Dryas readvance, rather than simply lower ice thicknesses at the LGM.

In addition to the broad patterns highlighted by Transects 1 and 2, the marine limit elevation records from northwest Iceland provide an insight into local and regional patterns of ice loading in NW Iceland. In Hornstrandir (Area D), the recorded marine limit elevation is variable, suggesting that some valleys, such as Hlöðuvik, may have remained glaciated for longer periods and therefore deglaciated later (Hjort *et al.*, 1985; Fig. 8.2). The propensity for later deglaciation within individual valleys has been linked to valley morphology, with Hlöðuvik containing a greater number of cirque glaciers than neighbouring locations, such as Hælavik, which has a higher local marine limit (Hjort *et al.*, 1985; Fig. 8.2). Such complexity highlights the importance of detailed mapping and dating of the marine limit (and thus the determination of timing of deglaciation) in northwest Iceland, in order to avoid misinterpretation of local signals within broader regional trends. In addition, several of the marine limits recorded in this region have poor chronological control, due to limited dateable material or suitable lake basins, which adds to the difficulties of interpretation of these data.

The recorded marine limit elevation in eastern Vestfirðir (42 - 48 m asl; Principato, 2008, Fig. 8.1) is also of interest for exploration of ice loading patterns within Húnaflói (Fig. 2.1). Previous research has highlighted that Húnaflói may have acted as an important ice stream at the LGM (Bourgeois *et al.*, 2000) and therefore mapping of the marine limit around the fjord may provide a valuable insight into ice thicknesses and patterns of deglaciation. Unfortunately, Principato (2008) notes a lack of dateable material at the location and so direct dating of the marine limit is not possible. However, if ice loading and deglaciation had been uniform across Húnaflói, higher marine limit elevations would be expected in eastern Vestfirðir than presently recorded, correlating to marine limit elevations presented in Skagi and innermost Húnaflói (Fig. 8.1), assuming it formed following the LGM deglaciation. It is however evident that the elevation of the marine limit in eastern Vestfirðir is approximately equivalent to that of the isolation basin at Torfadalsvatn, northernmost Skagi (Area A, Rundgren *et al.*, 1997; Fig. 3.5 and Table 3.1). The isolation of Torfadalsvatn has been dated to 11500-11600 cal. a BP (Rundgren *et al.*, 1997) and therefore if similar ice loading conditions were present across Húnaflói, the eastern Vestfirðir marine limit may represent a Younger Dryas shoreline. Under either scenario, the marine limit elevations surrounding Húnaflói provide an insight into potential patterns of ice loading and deglaciation.

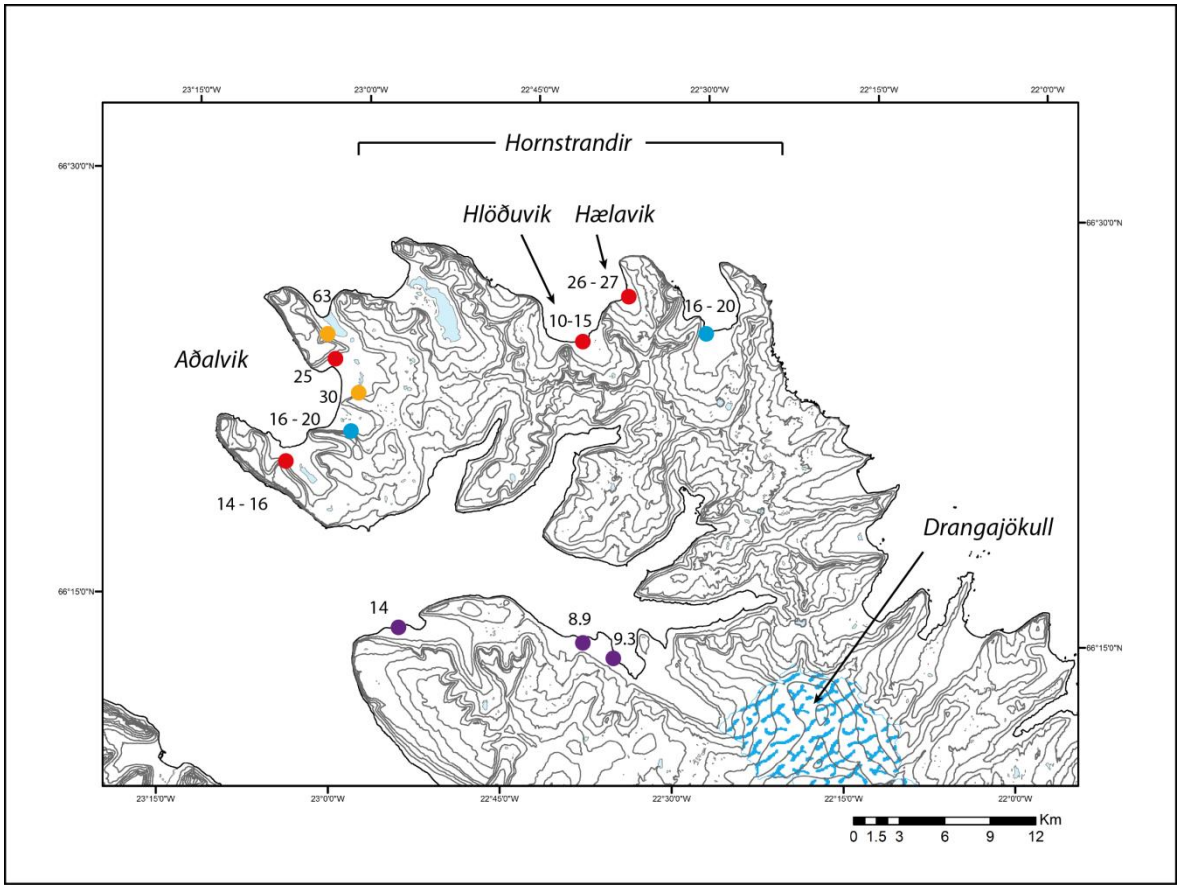

Figure 8.2 – Marine limit elevations in Hornstrandir (Area D) and northernmost Vestfirðir based on raised terraces (adapted from Hjort et al., 1985), showing the variability in recorded elevations (metres asl) from Thoroddsen (1892; orange), Simonarson (1979; blue), Hjort et al. (1985; red) and Principato (2008; purple).

Furthermore, the marine limit elevations surrounding Breiðafjörður provide a useful insight into the patterns of ice loading at the LGM. Marine limit investigation in Area B (southern Vestfirðir; Lloyd *et al.*, 2009) and Area C (northern Snæfellsnes; Brader *et al.*, submitted) based on lake basin evidence has shown that these features formed c. 13800 – 14000 cal. a BP (see Fig. 8.1). This is in contrast to the results of Norðdahl and Ásbjörnsdóttir (1995) who suggest Younger Dryas ages for the marine limit recorded at sites in innermost Breiðafjörður (Fig. 8.1). However, the marine limit elevations in Breiðafjörður are amongst the highest recorded in the region, suggesting that the thickest ice at the LGM may have been found within the fjord. Furthermore, there are clear differences in proposed ice thicknesses on the northern and southern coastlines due to the distinct patterns of marine limit elevations with similar ages of formation (Fig. 8.1). It is proposed here that ice thicknesses were greater on the northern coastline of the fjord based on the higher recorded marine limit elevations. Bourgeois *et al.* (2000) has suggested that Breiðafjörður represented a major ice stream at the LGM. The development of RSL histories from this region are particularly important and are further developed in Section 8.3.3.

It is clear therefore that marine limit records have the potential to provide valuable insights into the patterns of ice loading and deglaciation in northwest Iceland, if suitable chronological control

can be established. There are distinct patterns of marine limit elevation along the two principal transects of research (Fig. 8.1), as well as important sequences surrounding the regions two proposed major ice streams in Húnaflói and Breiðafjörður. Additional chronological constraint is required in some areas to further develop this geomorphological record. However, when coupled with isolation basin data, these marine limit results have the potential to act as useful tests for ice models and therefore ice loading scenarios for the region (e.g. Hubbard *et al.,* 2006).

8.3 Relative sea-level change in northwest Iceland

It is clear that the patterns of postglacial relative sea-level change in northwest Iceland are spatially variable, as demonstrated by the investigations taken along the two transects of research (Fig. 3.3). As a result, the two transects are discussed separately here (Section 8.3.1 and 8.3.2), with subsequent discussion of the implications for Breiðafjörður (Section 8.3.3). As outlined in Section 3.3, the two transects were designed to highlight the potential differences in RSL change produced under the contrasting LGM glaciation scenarios for Iceland (Fig. 8.3). Therefore, these discussions should be considered alongside Figure 8.3, which highlights the potential RSL scenarios resulting from the two glaciation scenarios.

8.3.1 Transect 1 (A, B, C)

8.3.1.1 Area A – Skagi (Rundgren et al., 1997 and this thesis)

Rundgren *et al.* (1997) provide a useful overview of the postglacial RSL changes of northernmost Skagi, having sampled sites from 47 m asl to present sea level. In doing so, the RSL record from Skagi demonstrates a relatively rapid fall in RSL following deglaciation, with a reduction in this rate of RSL fall during the Younger Dryas (Rundgren *et al.*, 1997). Following the Younger Dryas, the rate of RSL fall increases, dropping below present at c. 10000 cal. a BP (Rundgren *et al.*, 1997). There is little evidence for recent RSL changes in the Rundgren *et al.* (1997) record, due to a lack of low elevation isolation basins in the location.

Whilst the record generated by Rundgren *et al.* (1997) provides a useful overview of the postglacial RSL changes of Skagi, there are some limitations which require consideration when analysing the outputs presented in Chapter 7. Two of the sites presented - Hraunsvatn (42 m asl and Kallusákurvatn (22 m asl) – have gaps in the diatom assemblage (Rundgren *et al.*, 1997). Consequently, the likely patterns of RSL change are inferred rather than direct attributions from the diatom assemblage. In addition, the low numbers of brackish taxa within the Torfadalsvatn (42 m asl) and Geitakarlsvötn (26 m asl) sequences are proposed as being indicative of proximity to sea level (Rundgren *et al.*, 1997). However, there is no evidence of marine incursion at either location, despite a sea-level index points being generated. It should also be noted that the age of deglaciation in the area is calculated through extrapolation rather than a direct or limiting date

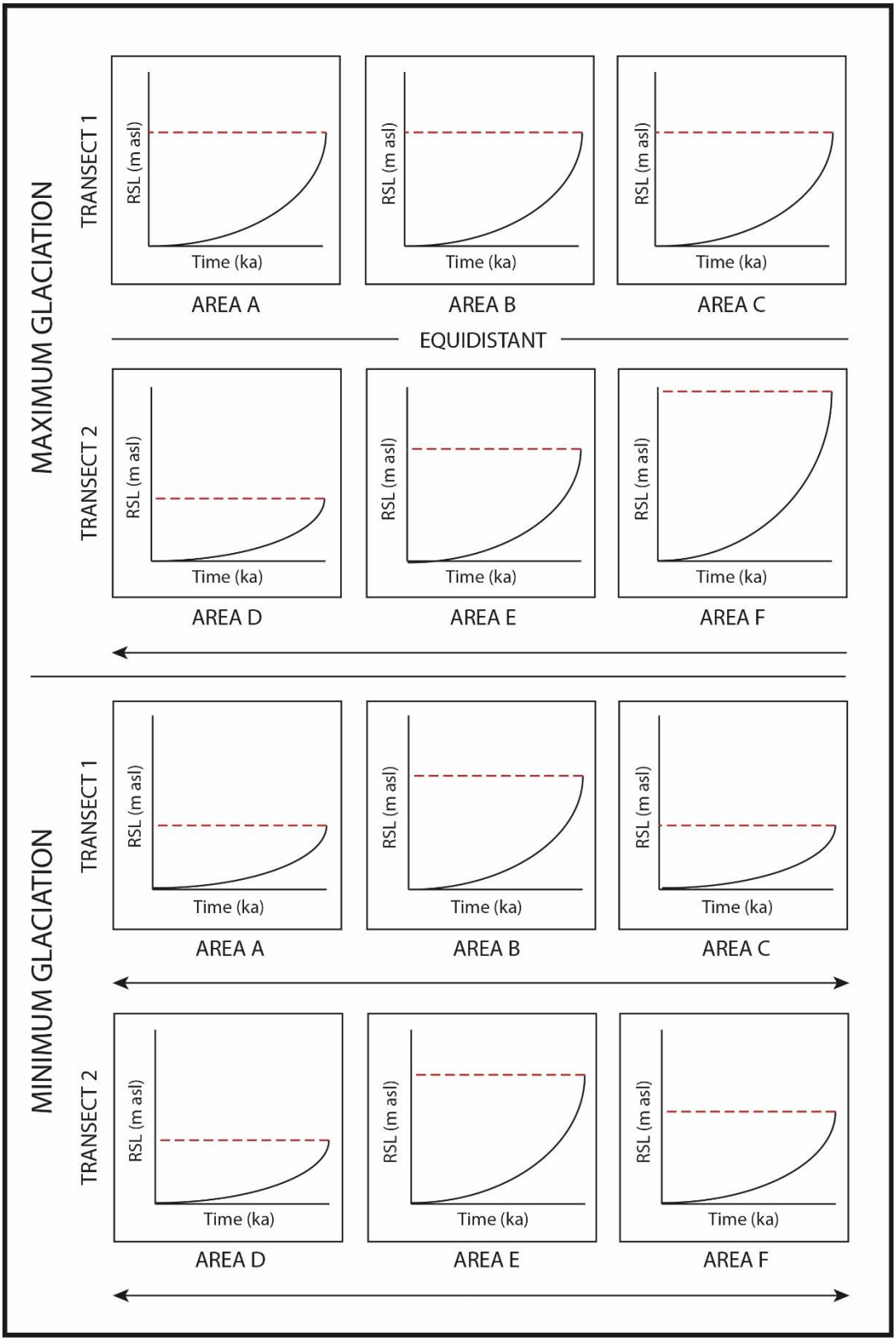

Figure 8.3 - Proposed patterns of RSL change for the two LGM glaciation scenarios in NW Iceland. Arrows denote distance from the loading centre and red dashed lines show the marine limit (relative elevations). Under the maximum scenario, Transect 1 experiences similar patterns of RSL change due to equidistance from the proposed loading centre. Transect 2 sees a decrease in the marine limit elevation with distance away from the loading centre. Under the minimum scenario, highest marine limit elevations will be recorded at the centre points of both research transects due to the secondary loading centre in Vestfirðir. See Fig. 3.4A for contextual information regarding the transect locations and glaciation scenarios.

from the hypothesised marine limit. Despite these limitations, the RSL curve from Rundgren *et al.* (1997) remains the most comprehensive published record of postglacial RSL for Area A.

The results of diatom analysis at Tjörn in this thesis have provided a limiting age for the formation of the marine limit in Skagi (Fig. 6.4). Tjörn (TJ1; Section 6.3.1), situated above the proposed marine limit, demonstrates an entirely freshwater assemblage and the presence of the Vedde Ash allows the extrapolation of a basal age of c. 14500 cal. a BP. Unfortunately, the basal radiocarbon sample produced an age younger than the Vedde Ash layer at 6180 ± 37 ^{14}C a BP, despite being situated lower within the stratigraphic sequence. It is likely that this sample has suffered from contamination by modern carbon and is therefore rejected. Accordingly, the proposed deglacial age of 14000 cal. a BP (Rundgren *et al.*, 1997) is supported by this research if the extrapolated basal age is accepted (Fig. 8.4). Whilst it is unlikely that sedimentation rates have remained constant throughout the sediment profile, the sediment composition and therefore likely depositional environment remains constant within the section through which extrapolation takes place. It is therefore likely that deglaciation occurred between c. 14000 and 14500 cal. a BP (Rundgren *et al.*, 1997) in Area A (Skagi).

8.3.1.2 Area B – Bjarkarlundur, Vestfirðir (Lloyd et al., 2009)

Lloyd *et al.* (2009) provides a comprehensive record of RSL change for southern Vestfirðir (Area B), with sites from the marine limit to present. No additional RSL study was undertaken in this region, but the RSL record is discussed here to highlight the principal limitations of and patterns present within the reconstruction. Within the RSL record from Area B, the radiocarbon sample from Hafrafellsvatn is anomalous and therefore is not used to constrain the RSL curve from the region (Lloyd *et al.*, 2009). Instead, tephrochronology was used as the chronological control for this site through identification of the Saksunarvatn tephra following geochemical analysis. Following deglaciation at c. 14000 cal. a BP, RSL fall was rapid at a rate of 38 mm cal. a^{-1} from c. 80 m asl to c. 50 m asl at c. 13200 cal. a BP (Lloyd *et al.*, 2009; Fig. 8.4). These initial rates of RSL fall fit well with the regional trends in RSL change noted along Transect 1. In addition to these rapid initial rates of RSL change, Lloyd *et al.* (2009) report a notable decrease in the rate of RSL fall during the Younger Dryas (Lloyd *et al.*, 2009).

The influence of the Younger Dryas ice readvance on the RSL record from Bjarkarlundur is relatively well constrained due to the analysis of isolation basins at Berufjarðarvatn (51.1 m asl) and Hrishólsvatn (41.1 m asl; Lloyd *et al.*, 2009). As a result, Lloyd *et al.* (2009) suggest that any RSL fluctuation was less than 10 m in amplitude. However, there is potential for a rise in RSL during the period, which cannot be constrained by the dataset (Lloyd *et al.*, 2009). In the regional context, there is some variability of the proposed effects of the Younger Dryas glaciation on RSL change (e.g. Norðdahl and Ásbjörnsdóttir, 1995; Rundgren *et al.*, 1997). In innermost

Breiðafjörður, Norðdahl and Ásbjörnsdóttir (1995) note a rise in RSL, whereas Rundgren *et al.* (1997) note a reduction in the rate of RSL fall in northernmost Skagi. Despite this, the RSL record produced at Bjarkarlundur (Area B) demonstrates a rapid initial rate of RSL fall, alongside a clear influence of Younger Dryas ice re-advance at the location. These characteristics will be important when exploring the regional patterns and drivers for RSL changes in NW Iceland (Section 8.3.1.4, 8.3.3.2 and 8.4).

8.3.1.3 Area C – Snæfellsnes (Brader, 2012; Brader et al., submitted; this thesis)

Initial research by Brader (2012) highlighted marine-freshwater transitions within a number of isolation basin sequences from Snæfellsnes. In total, five isolation basin and two coastal lowland sites were investigated in the region (Brader, 2012). The research presented here has extended the Brader (2012) study by sampling a site close to the marine limit (Ytra-Baravatn, YBR1) and thus has allowed the completion of the RSL curve for the region (Brader *et al.*, submitted; Fig. 6.75). As outlined in Section 8.2, the marine limit was identified at 65-69 m asl (Brader, 2012) and likely formed c. 13800 – 14000 cal a BP (Brader *et al.*, submitted). The RSL record from Snæfellsnes demonstrates a rapid RSL fall in the Lateglacial at a rate of 35.5 mm cal a^{-1} until 12600 cal a BP (Brader *et al.*, submitted; Fig. 8.4). It is notable that these rates of RSL change and timings of marine limit formation are similar to those found in Bjarkarlundur (Lloyd *et al.*, 2009), which is situated on the opposite coastline of Breiðafjörður. After *c.* 12600 cal a BP, the rate of RSL fall decreased in Snæfellsnes, falling below present during the early Holocene (by *c.* 10 cal ka BP; Brader *et al.*, submitted). The RSL record from Snæfellsnes demonstrates an exponential decrease in the rate of RSL change within the region (Fig. 8.4).

There are however limitations to the RSL reconstruction generated for northern Snæfellsnes, principally associated with the chronology produced for Ytra-Baravatn, which is employed as a limiting age for marine limit formation and therefore deglaciation (Brader *et al.*, submitted). Radiocarbon samples from the site returned ages which are considerably older than previous samples from the region or elsewhere in Iceland (e.g. Rundgren *et al.*, 1997; Lloyd *et al.*, 2009). It is likely that the samples are affected by the inwashing of old carbon from the landscape (Björck and Wohlfarth, 2001), reservoir effects (e.g. Ascough *et al.*, 2011) or local lignite deposits (e.g. Lloyd *et al.*, 2009).

A chronology for this site, however, can be developed based on the presence of the Saksunarvatn tephra identified higher within the sediment core sample (Section 5.2.2), which can be used as a limiting age for the site. Using this chronological marker, it is possible to extrapolate an age for basin isolation, as undertaken in Tjörn, Skagi (Area A). However, two assumptions must be accepted: a) the radiocarbon samples extracted from the sediment sample are affected by contamination and b) sedimentation has remained constant throughout the stratigraphic profile

(Section 6.3.1). If accepted, the timing of basin isolation and therefore marine limit formation in the region can be inferred as c. 13600 cal. a BP. It is likely that this represents a minimum age for marine limit formation, as the sedimentation rate was likely to be lower immediately after basin isolation due to the limited organic productivity during that period (Brader *et al.,* submitted).

8.3.1.4 Transect 1 – Summary

The RSL reconstructions from Areas A (this thesis; Rundgren *et al.*, 1997), B (Lloyd *et al.*, 2009) and C (Brader, 2012; Brader *et al.*, submitted) provide valuable information for sites which are approximately equidistant from the proposed principal ice loading centre at Vatnajökull (Fig. 2.1; Fig. 8.1). In turn, the locations provide a valuable opportunity to assess whether a mono-domed Vatnajökull-centric ice loading pattern consistent with maximum glaciation model is preferred. If this hypothesised ice loading were dominant at the LGM, it is anticipated that the timing of deglaciation and subsequent patterns of RSL change would be approximately similar between the three locations (Areas A, B and C) depending on the proximity to subsequent ice re-advances, such as the Younger Dryas (Fig. 2.4). The RSL records along Transect 1 demonstrate broad similarities between locations (Figs. 6.73, 6.74, 6.75, 8.4).

Areas A and C demonstrate similar marine limit elevations, ranging from 65 – 69 m asl (this thesis; Rundgren *et al.*, 1997; Brader, 2012; Brader *et al.*, submitted; Fig. 8.1), suggesting similar ice thickness values at the LGM, if the rheological profile is assumed uniform throughout the region (see Chapter 6). In contrast, higher marine limit elevations are found in Area B at 85-90 m asl (Lloyd *et al.*, 2009), suggesting greater ice thicknesses in this location at the LGM, as noted in Section 8.2. This greater ice thickness may be associated with the preferable environment for ice accumulation on the northern coastline of Breiðafjörður at the LGM (Brader *et al.,* submitted), which is also supported by the higher marine limit elevations recorded in innermost Breiðafjörður (Norðdahl and Pétursson, 2005).

Following the formation of the marine limit, the pattern of RSL change is similar in Areas A and B, with a notable reduction in the rate of RSL fall during the Younger Dryas (Rundgren *et al.*, 1997; Lloyd *et al.*, 2009). As outlined in Section 8.3.1.2, Lloyd *et al.* (2009) also note the possibility of a reversal of RSL fall during the period, although this is not well constrained by the current dataset. However, the exponential decrease in the rate of RSL fall in Area C differs from this regional pattern, suggesting a limited influence of Younger Dryas ice re-advance at this location (Brader *et al.*, submitted). This is perhaps unsurprising, due to the limited land surface available on the peninsula for ice accumulation in comparison to Areas A and B (Fig. 2.1; Fig. 8.1).

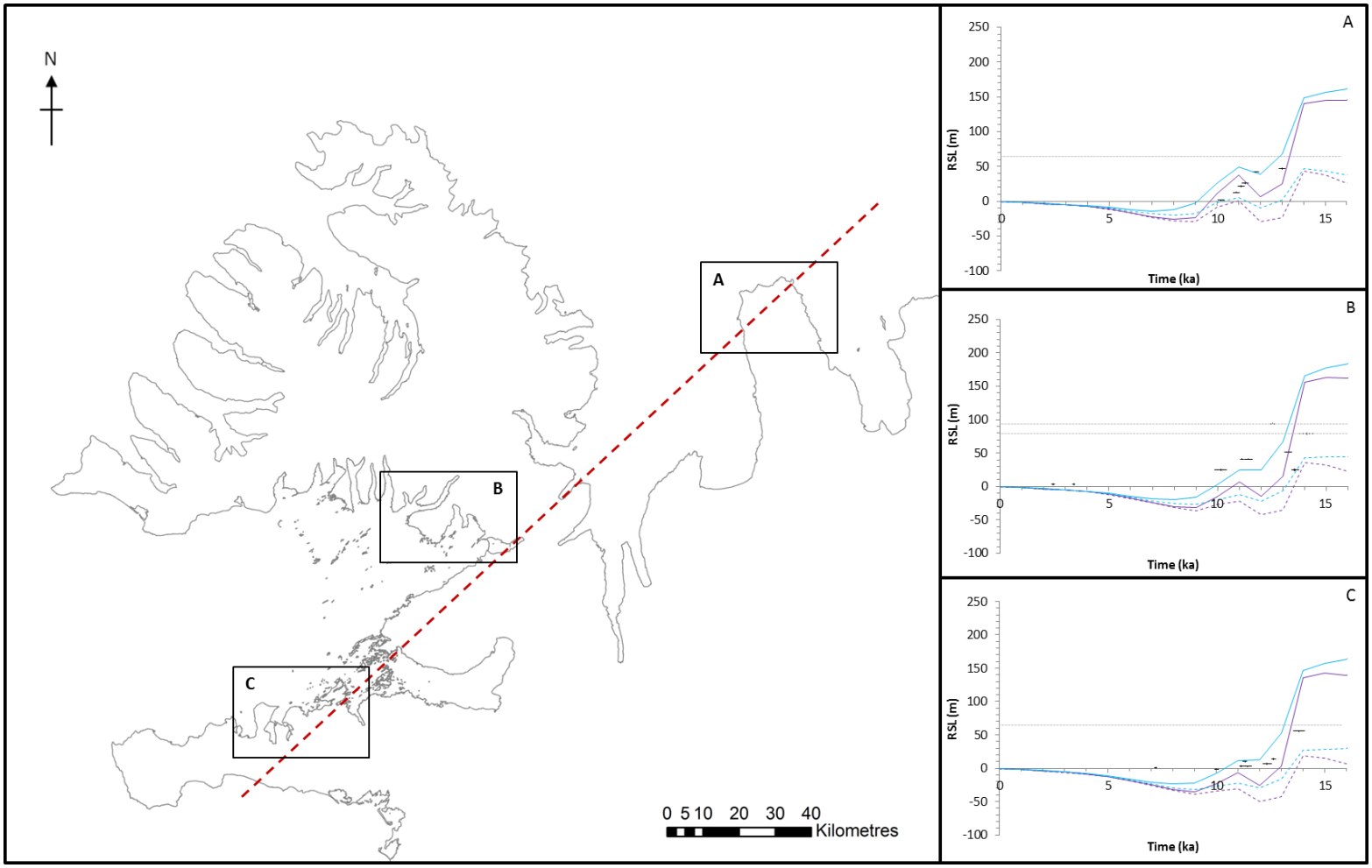

Figure 8.4 – RSL changes along Transect 1 plotted alongside HP_MAX (solid lines) and HP_MIN (dashed lines) ice model outputs when employed alongside the LT 40 km $\mho_{UM}$ 1 x 10^{20} Pa s (blue) and LT 40 km $\mho_{UM}$ 5 x 10^{20} Pa s (purple) Earth models. The grey horizontal dashed lines represent the highest raised terrace recorded in each location.

There are however similarities between RSL records during the early Holocene, which demonstrate a fall below present sea level between 8000 and 10000 cal. a BP (Rundgren *et al.*, 1997; Lloyd *et al.*, 2009; Brader *et al.*, submitted; Fig. 8.4). This correlates well with locations elsewhere in Iceland, such as the southwest, where RSL fell below present at 9400 cal. a BP (Ingólfsson *et al.*, 1995). This fall below present during the early Holocene is not currently well constrained by field evidence in northwest Iceland, but previous research has suggested that RSL may have fallen as low as 40 m below present sea level in the north (e.g. Meyer and Venzke, 1987; Moriwaki, 1990) and southwest (e.g. Norðdahl and Pétursson, 2005). Despite this, the agreement between sites relating to a RSL fall below present in the early Holocene is important in terms of the implications for the position of ice margins during this time period.

It is also clear that RSL was above present sea level during the mid-late Holocene in Areas B and C (Fig, 6.74, 6.75, 8.4; Lloyd *et al.*, 2009; Brader *et al.*, submitted). It is anticipated that the patterns of relative sea-level change around Breiðafjörður over the mid-late Holocene would likely be similar, due to the proximity of the two locations. A mid-late Holocene marine transgression is not recorded within the samples analysed by Rundgren *et al.* (1997) for Area A, with an assumed rise to present levels over the late Holocene. Within the study, low elevation sites are surveyed (Rundgren *et al.*, 1997), suggesting a lack of evidence for a mid-Holocene highstand in the area. This may result from differences in the patterns of postglacial uplift, with the influence of eustatic sea-level rise outpacing isostatic rebound in the area over the mid-late Holocene. It is however interesting to note that the GIA model outputs fail to reproduce a mid-Holocene highstand in any of these locations (Chapter 6) whether under the maximum or minimum glaciation scenario.

Despite this, there is evidence for broadly similar patterns of RSL change between the three research areas along Transect 1 during the Lateglacial, particularly in terms of the marine limit elevation (Fig. 8.1) and the rapid rates of RSL change following deglaciation. However, the influence of Younger Dryas ice re-advance in the three locations is varied, suggesting a limited Younger Dryas ice cap in Snæfellsnes when compared to Vestfirðir (Brader *et al.*, submitted). There are also differences in the timing of the early Holocene fall below present, although there is broad agreement with locations elsewhere in Iceland. Finally, the mid-late Holocene RSL records produced in the three field areas shows regional variability in the patterns of recent RSL changes, possibly resulting from differential uplift rates in northwest Iceland (Fig. 8.4).

8.3.2 Transect 2 (D, E, F)

8.3.2.1 Area D – Hornstrandir and Aðalvik

The marine limit in Hornstrandir is situated at c. 18 - 26 m asl and is characterised by a basal till overlain by beach deposits at Hlöðuvik and Hælavik (Hjort *et al.*, 1985; Fig. 8.1). Lake basin

samples from close to or above the altitude of the raised terraces in the region demonstrated entirely freshwater assemblages and therefore support the interpretation of the raised terrace deposits at the mouth of the valley as the local marine limit (Hjort *et al.*, 1985; Section 6.5). The presence of the Saksunarvatn tephra within the lake sediments implies that the location was ice-free by 10210 ± 35 cal. a BP (Lohne *et al.*, 2014) and provides a limiting age for marine limit formation. The marine limit in this location is therefore assigned this minimum age, as the marine sediments are deposited above the glacial till (Hjort *et al.,* 1985).

In contrast, the isolation basin study in Rekavik (Aðalvik) has identified a brackish influence at 18.6 m asl and thus provides a constraint on postglacial RSL in the location (Fig. 6.19). The elevation of the site, close to the proposed local marine limit (Area D; Fig. 8.2), also allows the radiocarbon age for isolation (9130 – 9412 cal. a BP) and the Saksunarvatn tephra (10210 ± 35 cal. a BP; Lohne *et al.*, 2014) to be adopted as the minimum age for marine limit formation and therefore deglaciation in the area. The marine limit in this area is located at c. 20 m asl and is assigned the same minimum age as Hlöðuvik (10210 ± 35 cal. a BP).

Due to the nature of the local deglaciation and location of the study area, there are limited opportunities to determine the subsequent patterns of postglacial RSL change. Hjort *et al.* (1985) highlight that ice remained in Hlöðuvik longer than other valleys in northwest Iceland and so the opportunity for isolation basins to record RSL changes in these locations is limited. In addition, many sites in Aðalvik are dominated by gravel and sand deposits, meaning that an accurate record of environmental changes at these sites in the westernmost section of Area D cannot be guaranteed. Hence, the testing of GIA model outputs for this location is reliant upon only two limiting points.

The low elevation of the marine limit in this location is expected under both the maximum (e.g. Hubbard *et al.*, 2006) and minimum (e.g. Hansom and Briggs, 1991) LGM glaciation scenarios. Area D is located at the furthest terrestrial location from the proposed ice loading centre under the maximum glaciation hypothesis and from the secondary ice-loading centre in northwest Iceland proposed under the minimum glaciation scenario. However, the limiting ages for marine limit formation are beneficial for the testing of IIS ice models, which still have significantly different ice thicknesses in this region (Patton, unpub.).

8.3.2.2 Area E – Vatnsfjörður, Vestfirðir

The rate of RSL change was relatively low at Vatnsfjörður following initial deglaciation at c. 12000 cal. a BP. From the marine limit at ca. 30 m asl, RSL fell at a rate of 21.5 mm cal. a^{-1} until the isolation of Reykjanes 6 at 9201 - 9432 cal. a BP, after which RSL fell below present sea level (Fig. 6.77, 8.5). The initial lower rate of RSL fall may be a consequence of the proximity of the field

sites to the ice margin in the Lateglacial and early Holocene, which would have reduced the rates of isostatic rebound in comparison to other field areas. The subsequent RSL fall below present is well constrained by the isolation of Reykjanes 6 (RK6) at 2.3 m asl and corresponds well with the records produced along Transect 1 (this thesis; Rundgren *et al.*, 1997; Brader *et al.*, submitted) and elsewhere in Iceland (e.g. Moriwaki, 1990; Ingólfsson *et al.*, 1995; Norðdahl *et al.*, 2008).

The RSL record from Vatnsfjörður also fits well with reconstructions of RSL change produced by a recent palaeoceanography study in Ísafjarðardjúp (Quillman *et al.*, 2010). Quillman *et al.* (2010) present palaeoclimatic, paleoceanographic and palaeo-sea-level reconstructions for the fjord system based on two sediment cores located in inner and outer Ísafjarðardjúp (Fig. 2.1, 8.5). Quillman *et al.* (2010) note a termination of glacio-marine conditions within Ísafjarðardjúp at c. 10200 cal. a BP, with a lowering of RSL between c. 10600 and c. 8900 cal. a BP and subsequent rise to present between c. 8900 and c. 5500 cal. a BP in the inner fjord. The Vatnsfjörður RSL record correlates well with these data, particularly when the potential timing of deglaciation along the fjord is taken into consideration (Fig. 8.5). At Vatnsfjörður, deglaciation and the subsequent RSL fall below present appears to occur later than in the RSL record proposed by Quillman *et al.* (2010). This pattern of RSL change is likely as a consequence of Vatnsfjörður being located closer to the centre of ice loading in Vestfirðir and the retreat of ice along Ísafjarðardjúp.

The RSL reconstruction presented by Quillman *et al.* (2010) notes a rise in RSL above present at c. 5500 – 6000 cal. a BP, which also fits well with the RSL curve produced in Vatnsfjörður (Area E; Fig. 8.5). The site therefore appears to follow the previously suggested fjord-scale patterns of RSL change (Quillman *et al.*, 2010). This is further demonstrated by the agreement of the Vatnsfjörður RSL curve with the proposed Little Ice Age and late-Holocene raised beaches surveyed by Principato (2008) in Ísafjarðardjúp. The Little Ice Age raised beach is recorded at 0.3 - 0.5 m asl and dated to 85 – 177 cal. a BP, with the 3000 cal. a BP raised beach surveyed at 5 m asl (Principato, 2003; Fig. 8.4). The agreement between these independent records of RSL changes support the reconstruction produced in Area E (Fig. 8.4 and 8.5).

Late Holocene RSL changes in Area E appear to demonstrate fluctuation, as shown by the radiocarbon ages from Sveinhúsvatn (1993 - 2161 cal. a BP and 2156 – 2267 cal. a BP; 1.25 m asl), the age of the LIA raised beach in Ísafjarðardjúp (85 – 177 cal. a BP; 0.4 m asl; Principato, 2008) and Bolsvik Bay ('modern'; - 0.5 m asl). Previous research has demonstrated RSL rise over the past 500 years in western Iceland (e.g. Gehrels *et al.*, 2006; Saher *et al.*, 2015) but the record from Area E might suggest a more complex pattern in Ísafjarðardjúp.

It is clear that the magnitude of RSL changes recorded in Area E differ from those generated along Transect 1 (Fig. 8.4; Rundgren *et al.*, 1997; Lloyd *et al.*, 2009; Brader *et al.*, submitted). However,

there are similarities between the patterns of RSL change noted in these locations, including a relatively rapid fall below present sea level in the early Holocene (e.g. Lloyd *et al.*, 2009), a subsequent RSL lowstand (e.g. Norðdahl and Pétursson, 2005) and then RSL rise above present in the mid Holocene (Fig. 8.5; e.g. Brader *et al.*, submitted). It is also evident from the RSL record produced in Area E that there has likely been a fluctuation in RSL over the late Holocene, adding to the complexity of recent RSL changes in northwest Iceland identified from Transect 1.

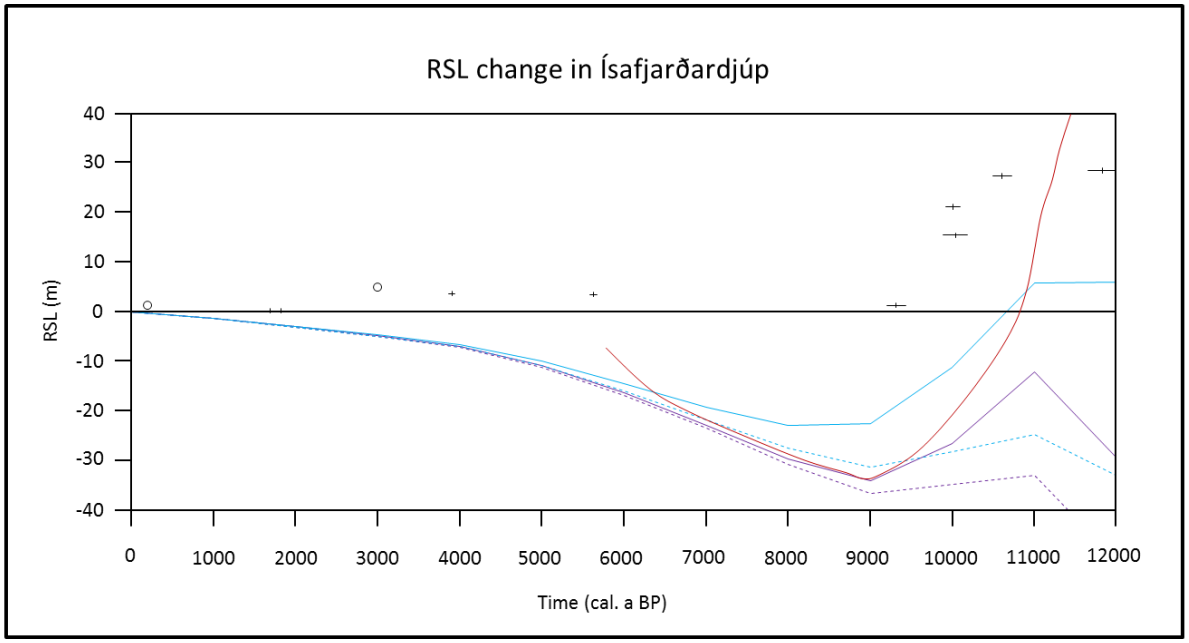

Figure 8.5 – RSL curves for Ísafjarðardjúp including data from Quillman et al. (2010; red solid line), Principato (2008; open black circle) and the present study (black crosses). In addition, modelled RSL change under the maximum (solid light blue and purple lines) and minimum (dashed light blue and purple lines) glaciation scenarios are presented with the LT 40 km υ_{UM} 1 x 10^{20} Pa s (light blue) and LT 40 km υ_{UM} 5 x 10^{20} Pa s (purple) earth models.

8.3.2.3 Area F – Hvammstangi, Vatnsnes

The RSL reconstruction from Area F suffers from a lack of mid-elevation study sites and so the rate of RSL change during the early Holocene cannot be accurately constrained (Fig. 6.78). However, the diatom analyses of high elevation sites have provided a good constraint on the age of the proposed marine limit. As shown in Fig. 8.1, the marine limit in Area F has been proposed at c. 65 m asl, which is the elevation of the highest recorded marine influence in the field area. There is little direct evidence of a raised shoreline in the region and the age of isolation at AH1 is taken to represent the marine limit age (10781 – 11035 cal. a BP; Table 6.22; Fig. 6.78).

The highest recorded marine influence is however significantly higher than those measured in Area D or Area E. In addition, the new marine limit elevation presented here for Area F is also notably higher than that proposed for inner Hrútafjörður at 50 m asl (Ingólfsson, 1991). However,

it should also be noted that this innermost marine limit elevation is undated (Ingólfsson, 1991). In addition, previous research has noted a southward decrease in marine limit elevations within fjords in northern Iceland (Cossart *et al.*, 2014), due to differences in deglacial timing. In neighbouring Skagafjörður, for example, Cossart *et al.* (2014) reported a southward decrease in marine limit elevation of 1m km^{-1}. Within Hrútafjörður, the same rate of change is evident for the reported marine limit elevations.

The marine limit in Area F likely formed at the Younger Dryas, which correlates well with the other RSL records from Transect 2. The elevation of the marine limit along Transect 2 appears to show support for the maximum glaciation hypothesis, which proposes an increase in marine limit elevation with proximity to the ice loading centre (Fig. 2.2). As a result of similar formation ages, it is likely that there was significantly thicker ice in Area F than Areas D and E. This greater ice thickness may be a result of proximity to the principal ice loading centre in central Iceland or proximity to major former ice streams at the LGM in Breiðafjörður or Húnaflói (Bourgeois *et al.*, 2000; Spagnolo and Clark, 2009) fed from this loading centre.

The RSL curve from Area F provides some useful information for the testing of GIA models and comparison to other RSL records from northwest Iceland (e.g. Lloyd *et al.*, 2009). In particular, diatom analyses at Kolbeinsánes 1 - 4 (1.1 – 3.45 m asl; Area F) provide a useful overview of late Holocene RSL changes for comparison to other field areas and published records of recent RSL change in Iceland (e.g. Gehrels *et al.,* 2006; Saher *et al.*, 2015). It is clear from the RSL reconstruction that Area F has been experiencing recent RSL fall, likely from a mid-Holocene highstand, as noted elsewhere in northwest Iceland (e.g. Lloyd *et al.*, 2009).

8.3.2.4 Transect 2 – Summary

The records from Transect 2 offer valuable datasets for the further testing of the hypothesised RSL changes associated with the maximum (e.g. Hubbard *et al.*, 2006) and minimum (e.g. Hansom and Briggs, 1991) glaciation hypotheses. There is clear evidence for an increase in marine limit elevation with proximity to the proposed LGM ice loading centre, as outlined by the maximum glaciation scenario, in central Iceland (Fig. 8.6). Within the records from Areas E and F, there is evidence for an influence of Younger Dryas ice re-advance, with both areas likely ice covered or close to the ice margin (Fig. 8.6). In addition to the marine limit, the elevations of sea-level index points are generally higher in Area F than Area E and D at equivalent time periods (Fig. 8.6). This pattern of RSL change may therefore be indicative of greater ice thicknesses in Area F that in Areas D and E, supporting the maximum glaciation hypothesis (Hubbard *et al.*, 2006). It is also notable that there is evidence for a mid-Holocene highstand within the RSL data from Areas E and F, demonstrating a recent fall in RSL to present (Fig. 6.77, 6.78 and 8.6).

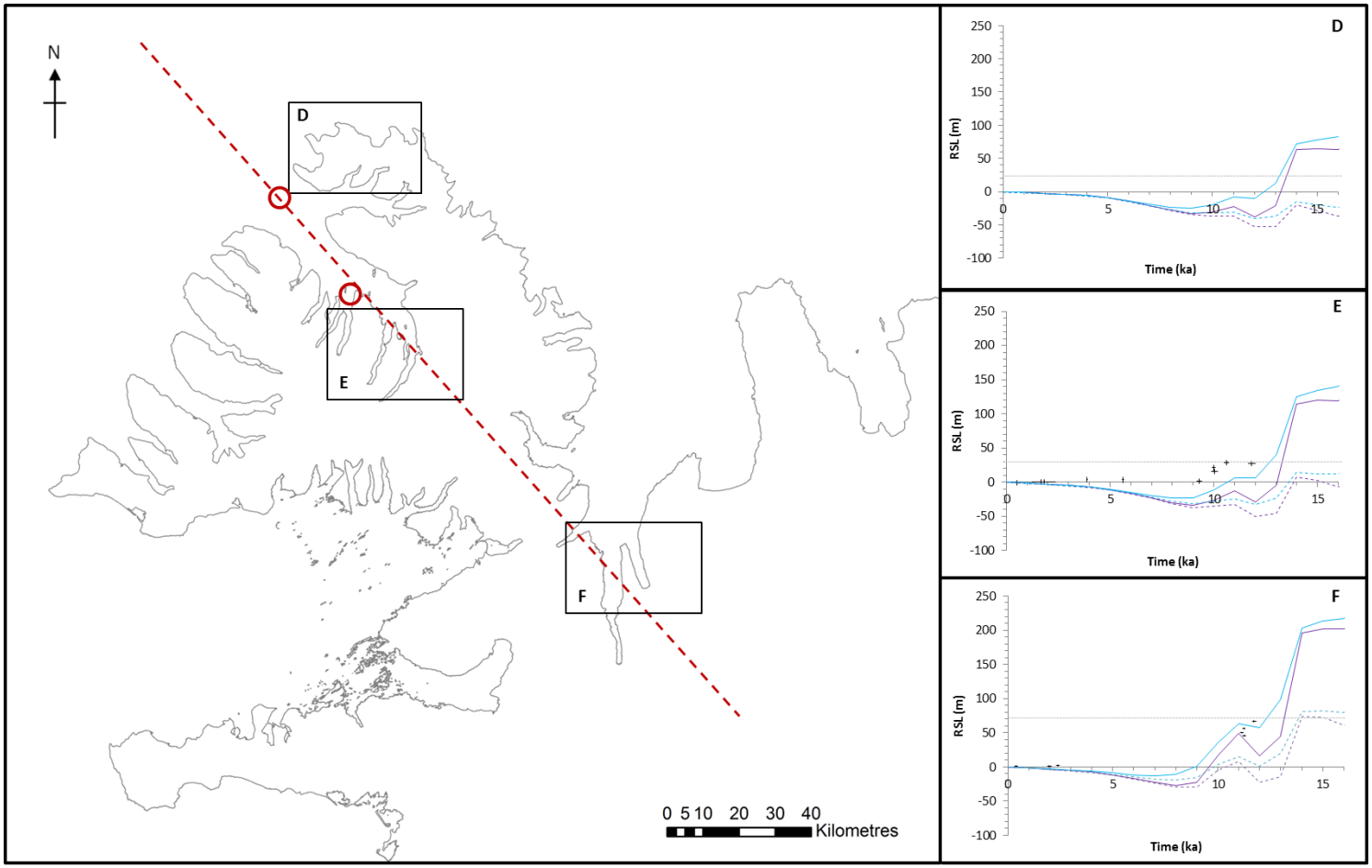

Figure 8.6 - RSL changes along Transect 2 plotted alongside HP_MAX (solid lines) and HP_MIN (dashed lines) ice model outputs when employed alongside the LT 40 km υ_{UM} 1 x 10^{20} Pa s (blue) and LT 40 km υ_{UM} 5 x 10^{20} Pa s (purple) Earth models. The grey horizontal dashed lines represent the highest raised terrace recorded in each location. Quillman et al. (2010) core locations are also shown (red circles).

8.3.3 Breiðafjörður, western Iceland

8.3.3.1 Area G – Breiðavik, Vestfirðir

Area G offers the opportunity to further explore the RSL changes of northwest Iceland, specifically in relation to the elevation of the proposed marine limit and therefore the proposed ice loading of outer Breiðafjörður at the LGM. Previous research has identified the marine limit at 85 – 90 m asl (Norðdahl and Pétursson, 2005; Fig. 8.1) which is the highest marine limit recorded on the Vestfirðir peninsula. These high marine limit values in Area G suggest either early deglaciation or greater ice thicknesses at the LGM. Mapping of the marine limit in Area G supports this previous research (Fig. 8.1) and diatom analyses have identified a marine-brackish influence in isolation basins at c. 65 – 70 m asl (see Section 6.8). Unfortunately, the large size of higher lake basins in the area meant that they were unable to be cored with the equipment available.

Despite the records of marine influence generated from individual site analyses, the chronological control on the RSL record produced in Area G is relatively poor. As outlined in Section 6.8, radiocarbon analyses from Area G returned ages considerably younger than expected for the elevation of individual sites. This is likely a consequence of contamination by younger carbon, possibly through rootlet penetration. Consequently, no sea-level index points are presented for Area G, due to the uncertainty in the reliability of the chronological control (Fig. 6.79). Unfortunately, the position of Area G, at the westernmost point of the Vestfirðir peninsula, away from the tephra distribution centres of most Icelandic volcanic centres, means that relatively few tephra deposits are present and thus a secondary chronological framework is not available. As a result, the RSL record from Area G is reliant upon the assignment of proposed ages for marine limit formation, taken from other studies in the fjord (e.g Lloyd *et al.*, 2009; Brader *et al.*, submitted), which is a major limitation for the RSL reconstruction for the region.

The higher marine limit values are likely a consequence of earlier deglaciation based on Area G´s location at the westernmost point of the northern coast of Breiðafjörður. The high marine limit elevation may also be a consequence of greater ice thickness values, with similar marine limit elevations being found in Area B (Fig. 8.4). Unfortunately, the driver for high marine limit elevation – early deglaciation or greater ice thicknesses - is unclear in Area G, due to the poor chronological control on isolation basin sediments close to the marine limit (see Section 6.8). However, thicker ice would appear less likely in this location, on the outer edge of Breiðafjörður.

There is however good chronological control on lower elevation sites, with the record from Breiðavik 10 suggesting a RSL fall and subsequent rise over the late Holocene. Recent RSL rise has been noted in saltmarsh studies in western Iceland (e.g. Gehrels *et al.*, 2006; Saher *et al.*, 2015) and the results from Area G contrast with late Holocene RSL changes derived from isolation basins

in other field locations (e.g. Lloyd *et al*., 2009). This may suggest that Area G is experiencing low rates of rebound at present, due to the distance from the principal proposed ice loading centre and proposed early deglaciation in the area.

8.3.3.2 – Breiðafjörður – Summary

The RSL records generated for northwest Iceland provide a valuable opportunity to explore the ice loading history of Breiðafjörður, especially when examined alongside previous research (e.g. Norðdahl and Ásbjörnsdóttir, 1995; Lloyd *et al.*, 2009; Spagnolo and Clark, 2009; Brader *et al.*, submitted). In particular, the RSL records produced highlight differences in ice loading conditions in and around Breiðafjörður prior to deglaciation. In southern Breiðafjörður (Area C), the marine limit is recorded at 65 – 69 m asl (Brader *et al.*, submitted), which is considerably lower than the marine limits presented on the northern coastline (e.g. Lloyd *et al.*, 2009; Area B and G; Fig. 8.7). There is therefore evidence to indicate greater ice thicknesses in southern Vestfirðir than northern Snæfellsnes prior to deglaciation (Fig. 8.7; Brader *et al.*, submitted). Alternatively, this may relate to greater ice thicknesses in northern Breiðafjörður, possibly linked to the proposed ice stream in the region (Bourgeois *et al*., 2000).

Following deglaciation, RSL fell rapidly around Breiðafjörður on both the northern and southern coastlines (Area B and C; Lloyd *et al.*, 2009; Brader *et al.*, submitted; Fig. 8.6). The rates of RSL fall recorded in Area B (Lloyd *et al.*, 2009) and C (Brader, 2012; Brader *et al.*, submitted) correlate well and are greater than those recorded elsewhere in northwest Iceland, such as in Area E. This rapid postglacial RSL fall indicates that the ice was thicker and retreated more rapidly in Breiðafjörður than other fjord systems studied as part of this research (see Section 8.3.2.2; Fig. 8.7).

This rapid ice retreat may be a consequence of the rapid disintegration of the proposed major ice stream present within Breiðafjörður at the LGM (e.g. Bourgeois *et al.*, 2000; Hubbard *et al.*, 2006; Spagnolo and Clark, 2009). The rapid disintegration of this section of the LGM IIS could also have had important consequences for IIS stability and in turn the overall pattern of deglaciation. Breiðafjörður would have represented a major marine-based component of the LGM IIS (Hubbard, 2006). This sector of the LGM IIS would have been particularly sensitive to rising eustatic sea level, penetration of warmer water masses onto the inner shelf, and calving during deglaciation (Hubbard, 2006), which would have led to the rapid disintegration (Ingólfsson and Norðdahl, 2001) and fall in RSL noted in the records from the region (e.g. Lloyd *et al.,* 2009; Brader *et al.*, submitted).

In addition, the RSL records generated around Breiðafjörður provide valuable information about the influence of Younger Dryas ice re-advance in the region. Records from Area B (Lloyd *et al.*, 2009), Area F and innermost Breiðafjörður (Norðdahl and Ásbjörnsdóttir, 1995) suggest a strong

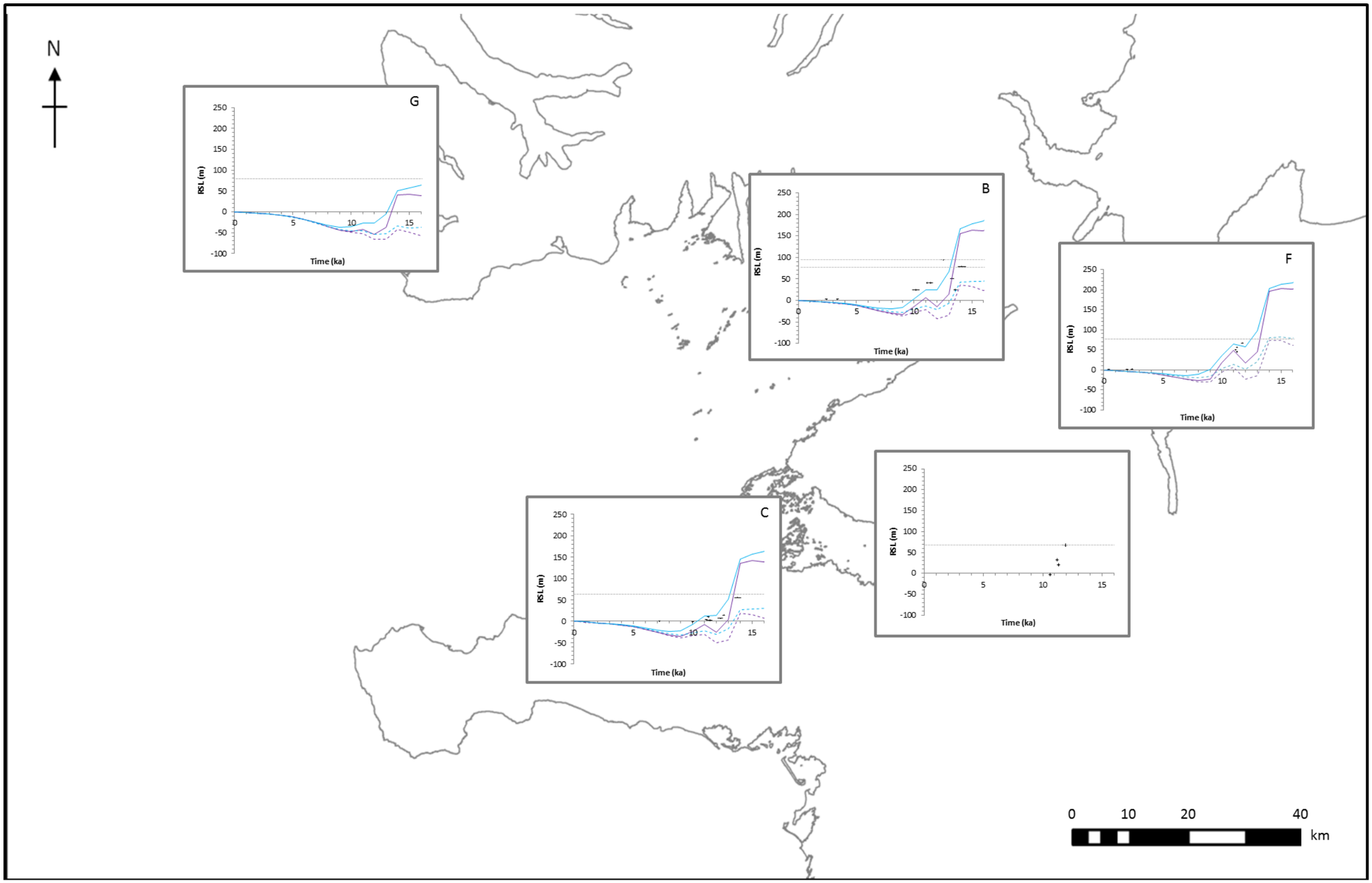

Figure 8.7 – RSL changes around Breiðafjörður plotted alongside HP_MAX (solid lines) and HP_MIN (dashed lines) ice model outputs when used alongside the LT 40 km υ_{UM} 1 x 10^{20} Pa s (blue) and LT 40 km υ_{UM} 5 x 10^{20} Pa s (purple) Earth models. The grey horizontal dashed lines represent the highest raised terrace recorded in each location.

influence of Younger Dryas ice re-advance on the rates of RSL change. Lloyd *et al.* (2009) note a reduction in the rate of RSL fall, with Norðdahl and Ásbjörnsdóttir (1995) recording a RSL rise over the period. There is however no evidence of a transgression within the record from Area C (Brader *et al.*, submitted) which supports the proposed differences in ice loading patterns during the Younger Dryas in northwest Iceland. In addition, it is likely that the influence of Younger Dryas ice regrowth was relatively localised around Breiðafjörður, due to the limited impact recorded in Area C (Brader *et al.,* submitted).

There is evidence from sites in northern and southern Breiðafjörður that RSL fell below present in the early Holocene (Fig. 8.7; Norðdahl and Ásbjörnsdóttir, 1995; Lloyd *et al.*, 2009; Brader *et al.*, submitted), which corresponds with records elsewhere in southwest, western and northern Iceland (e.g. Meyer and Venzke, 1987; Moriwaki, 1990; Thors and Helgadóttir, 1991; Ingólfsson *et al.*, 1995; Norðdahl and Pétursson, 2005; Norðdahl *et al.*, 2008). The extent of this RSL fall below present is currently poorly constrained in Breiðafjörður, although it is likely that RSL fell no lower than c. 40 m below present sea level in western Iceland (Ingólfsson *et al.*, 1995; Norðdahl and Pétursson, 2005; Norðdahl *et al.*, 2008; Quillman *et al.*, 2010).

On the northern and southern coastlines of Breiðafjörður, there is evidence for a transgression during the mid-Holocene (see Area B and C in Fig. 8.7; Lloyd *et al.*, 2009; Brader *et al.*, submitted). The timing of this transgression differs between these new field-based RSL records, yet the limited availability of data from lower elevations in the study areas can account for some of these differences. In Areas B and C, there is an assumed RSL fall to present, following a mid-late Holocene highstand (Fig. 8.4). This is however in contrast to the results from Area G, which suggest that RSL has fallen below and subsequently risen to present over the late Holocene. Saltmarsh studies in southern Snæfellsnes have identified RSL rise over the last 2000 years using foraminiferal and diatom assemblages (e.g. Gehrels *et al.*, 2006; Saher *et al.*, 2015). It is therefore unclear whether RSL is rising on a regional scale, due to the lack of data for recent RSL change in Areas B and C (Fig. 8.4), although it is clear that the pattern of recent RSL changes in northwest Iceland is complex.

The RSL records from Breiðafjörður provide a valuable insight into the potential patterns of ice loading at the LGM. There is evidence for thicker ice along the northern coastline, with deglaciation and ice retreat within Breiðafjörður being both rapid and potentially catastrophic for ice sheet stability. The influence of Younger Dryas ice re-advance on the RSL record appears to be different on the northern and southern coastlines of Breiðafjörður, having consequences for the patterns of RSL change throughout the Holocene. Variability in the proposed recent RSL changes suggests a complex pattern across western Iceland. However,

the addition of further low elevation sites would allow for these trends to be better constrained.

8.4 Implications for models of the LGM Icelandic Ice Sheet

Support for the maximum glaciation scenario is further demonstrated by the fit between the geological dataset and GIA model outputs for northwest Iceland (Figs 8.4 - 8.7). The GIA model including the HP_MAX ice model (Patton, unpub.) and Earth model of LT 40 km, υ_{UM} 5 x 10^{19} Pa s is able to replicate the high marine limit values in northwest Iceland, as well as reproduce the intricacies of RSL changes during the Holocene, with the exception of the mid-Holocene highstand noted in several field locations (Fig. 8.4 - 8.6). In addition, GIA models employing the HP_MAX ice loading are able to generate the differences in RSL changes produced by the field evidence around Breiðafjörður at the LGM and Younger Dryas (Fig. 8.7) when employed alongside Icelandic rheological characteristics.

From the GIA model outputs, it is clear that the HP_OPT and HP_MIN ice models can be excluded from use in northwest Iceland, when the preferred Icelandic rheological characteristics are adopted (Fig. 7.19, 7.20, 7.27, 7.28). RSL outputs from GIA models employing HP_MIN (Patton, unpub.) ice loading demonstrate that insufficient ice is present within the model, which is unable to replicate the elevation of marine limit limiting points and isolation basin derived SLIPs in northwest Iceland (Fig. 8.4, 8.6, 8.7).

There are a clear suite of implications of the RSL records produced from northwest Iceland for models of the LGM IIS. The new marine limit and isolation basin data suggest an extensive, relatively thick mono-domed ice sheet at the LGM (e.g. Hubbard *et al.*, 2006), with little support for an independent ice loading centre in Vestfirðir based on the marine limit and isolation basin evidence from Transect 2 (e.g. Hansom and Briggs, 1991). If the minimum glaciation scenario were favoured, a higher marine limit elevation would be expected in Area E in comparison to Areas D and F along Transect 2 (see Fig. 8.3).

The newly-established pattern of deglaciation for northwest Iceland could have important consequences for patterns of sea-level change within global models, beyond the proposed additional Equivalent Sea Level (ESL) outlined in Chapter 7. It is clear from GIA model outputs that the ESL of the LGM IIS is under-represented within global ice models (e.g. Peltier, 2004). SELEN models of the HP_MAX ice model suggest that the ESL for the LGM IIS is equivalent to 1.0 m ESL (Patton, unpub.) (cf. 0.4 m for ICE-5G). This could have important implications for the role of IIS meltwater on oceanic circulation, given the proximity of Iceland to sensitive areas of deepwater formation in the North Atlantic.

Geological evidence from northwest Iceland also suggests the need for a significant ice re-advance during the Younger Dryas within ice models of the IIS (Fig. 8.4, 8.6 and 8.7). At present, such an ice re-advance is not evident within the global ice model employed (ICE5G), which assumes an exponential decrease in ice thickness following deglaciation (Peltier, 2004). Within the HP_MAX ice model (Patton, unpub.), there is a clear Younger Dryas re-advance, which is able to replicate the patterns of RSL change noted in Transects 1 and 2 (Fig. 8.4 and 8.6). The regional ice model (HP_MAX; Patton, unpub.) produces a superior representation of ice loading in Iceland, when used alongside the preferred rheological characteristics.

Despite the preferable ice loading scenario in HP_MAX, there are demonstrable improvements which could be made to the ice model, as outlined by the RSL outputs and chi^2 results for the region (Fig. 7.12 and 7.13). The GIA models employing the HP_MAX ice loading provide RSL predictions which are slightly lower than suggested by the geological dataset, likely as a consequence of insufficient ice loading (Patton, unpub.). Furthermore, the HP_MAX based GIA models are unable to replicate the mid-Holocene highstand recorded in northwest Iceland RSL datasets, when employed alongside the preferred rheological characteristics for Iceland (Fig. 7.12).

In order to provide an improved fit to the geological dataset, the ice model requires either:

a) later ice loading in Iceland than present within the HP ice models, where ice loading is assumed as constant after 10 cal. ka BP (Patton, unpub.), or;
b) increased influence of Antarctic ice sheet meltwater during the mid-Holocene (e.g. Ingólfsson and Hjort, 1999).

Previous research has highlighted the influence of meltwater from the Antarctic Ice Sheets (AIS) on RSL change in the North Atlantic (Mitrovica *et al*., 2009). Ingólfsson and Hjort (1999) suggest that the mid-Holocene highstand found in locations in the North Atlantic may be a consequence of the later deglaciation of the AISs, which led to a major meltwater input to the oceans between 7 and 5 cal. ka BP. Northern Hemisphere ice sheets are unlikely candidates for the source of this meltwater, as they had mostly disappeared by 8-7 cal ka BP (Ingólfsson and Hjort, 1999).

Although there are evidently areas for further improvement on individual model outputs, the GIA modelling undertaken has been able to differentiate between the two proposed LGM glaciation scenarios for Iceland. The maximum glaciation scenario is the preferred ice loading history for the region.

8.5 Preferred rheological characteristics in northwest Iceland

An additional output of the modelling work has been to provide a preferred rheological model for NW Iceland. Based on the completed GIA model runs, the preferred Earth characteristics for northwest Iceland are LT 30 - 40 km and υ_{UM} 5 x 10^{19} – 1 x 10^{20} Pa s (see Section 7.5), which are particularly effective at fitting the data when used alongside the HP_MAX ice model for Iceland (Patton, unpub.). This rheological profile appears to provide the best fit with the geological dataset (see Fig. 7.13 and 7.14). The preferred Earth characteristics correspond with the higher end of proposed values from previously published models, mostly derived from other approaches to determining Earth structure (see Table 2.1). The testing of thinner lithospheric values has demonstrated poor fit with the field evidence from a number of the sites in northwest Iceland (Fig. 7.13), which is also highlighted in the regional GIA model overview (7.14). The GIA modelling undertaken thus supports the proposal for a relatively thicker lithosphere (e.g. Bjarnason *et al.*, 1993) for northwest Iceland in comparison to central regions. However, this thicker Icelandic scenario would be thin in comparison to mid-plate locations, such as those used in ICE5G (Peltier, 2004). Du and Foulger (1999) noted that the crustal thickness in northwest Iceland was likely c. 30 km based on the modelling of receiver functions and the velocities of regional surface phase waves, whilst similar values have also been calculated for the northeast (White *et al.*, 1996).

Furthermore, the preferred Earth characteristics agree with the results of Biessy *et al.* (2008) and are similar to those presented by Árnadóttir *et al.* (2009), Le Breton *et al.* (2010) and Barnhoorn *et al.* (2011). Adjustments to the ice loading within the HP_MAX ice model (Patton, unpub.) may lead to differences in the preferred rheological characteristics, with some field areas suggesting a mismatch between the geological evidence and GIA model outputs (Fig. 7.14).

GIA modelling involving the HP_OPT and HP_MIN ice models suggest a second preferred rheological profile based on chi^2 outputs, which comprises a LT of 60 km and υ_{UM} of 5 x 10^{20} Pa s (Fig. 7.19, 7.20, 7.27, 7.28). The pattern of RSL change produced by these GIA models does not fit that recorded within the field dataset, failing to produce the intricacies of Holocene RSL changes at individual sites, despite the proposed fit. Consequently, the LT 30 – 40 km, υ_{UM} 5 x 10^{19} – 1 x 10^{20} Pa s Earth model is taken as the preferred rheological profile for employment with the HP_MAX ice model (Patton, unpub.) investigated as part of this study.

Although the modelling has demonstrated a clear preference of Earth model, there are a number of limitations to the preferred characteristics presented herein. In particular, the potential for lateral variations of the Icelandic lithosphere and upper mantle viscosity has been

demonstrated by a number of previous studies (e.g. Bijwaard and Spakman, 1999; Du and Foulger, 1999; Kumar *et al.*, 2007; Barnhoorn *et al.*, 2011; Schmidt *et al.*, 2012). In turn, the selection of a single rheological model may not reflect real-world complexity, as has been noted for many other GIA studies (e.g. Whitehouse *et al.*, 2012; Argus *et al.*, 2014). Such lateral variability in Iceland is probable because of its location on a ridge axis (Barnhoorn *et al.* 2011). Furthermore, the two dimensional rheological profile employed fails to account for a hotspot or mantle plume, which has been proposed beneath Iceland (e.g. Wolfe *et al.*, 1997; Shen *et al.,* 2002). The influence of rheological characteristics on postglacial RSL changes in Iceland is likely different throughout the country and the uplift rates modelled may under- or over-estimate the rates in particular locations. However, this approach of two dimensional rheological modelling has been adopted in a range of previous studies in similar locations (e.g. Le Breton *et al.*, 2010; Whitehouse *et al.*, 2012). A limited number of three-dimensional Earth models have been developed for Iceland (Schmidt *et al.*, 2012), but this study has adopted the approach outlined by Le Breton *et al.* (2010) due to the comparatively uniform geology of the Vestfirðir peninsula, situated away from the mantle plume.

Previous work has highlighted variability in Earth relaxation time in Iceland, which has been assigned to differences in lithospheric thickness rather than mantle viscosity values (Le Breton *et al.*, 2010). This characteristic has been used as justification for use of a uniform upper mantle viscosity in Iceland within previous GIA modelling studies (Le Breton *et al.*, 2010). Following GIA modelling within this research, the RSL outputs generated have demonstrated the influence of adjustment to the lithospheric thickness employed within the Earth model (Fig. 7.14, 7.20 and 7.28), although the magnitude of this influence is highly dependent on the ice model used.

8.6 The pattern and style of deglaciation of northwest Iceland

The new RSL records and GIS model outputs from northwest Iceland suggest that following the LGM, deglaciation in Iceland was rapid, particularly in Breiðafjörður (Fig. 8.7). Within the RSL record, rapid deglaciation is demonstrated by the high rates of RSL fall and isostatic rebound reported from the field areas during the Lateglacial (Fig. 8.4, 8.6 and 8.7). The rapid deglaciation of northwest Iceland was likely a consequence of a series of factors, including ice sheet configuration (e.g. Hubbard *et al.*, 2006), oceanic circulation (e.g. Ingólfsson and Norðdahl, 2001), eustatic sea-level rise (e.g. Deschamps *et al*, 2012) and warming of the climate during the Bølling period (e.g. Norðdahl and Pétursson, 2005).

Previous research has highlighted that a considerable ice mass covered Iceland at the LGM (Ingólfsson *et al.*, 2010), which is supported by the patterns of RSL change noted in northwest

Iceland (e.g. this thesis, Rundgren *et al*, 1997; Lloyd *et al.*, 2009; Brader *et al.*, submitted) and the GIA modelling undertaken in this thesis, which supports the maximum glaciation scenario. In turn, substantial sectors of the LGM IIS were largely marine-based, extending to the shelf edge in a number of locations (Ólafsdóttir, 1975; Ingólfsson and Norðdahl, 2001; Norðdahl and Pétursson, 2005; Hubbard *et al.*, 2006). Marine based sectors of ice sheets are particularly sensitive to changes in eustatic sea level (Hughes, 1973; Bentley, 1984; Hubbard, 2006) and changes in the temperature of the oceans (Schmidtko *et al.*, 2014).

Oceanographic research in Antarctica has highlighted the potential influences of basal melt on ice sheet stability, due to ocean-ice interactions (Schmidtko *et al.,* 2014). Schmidtko *et al*. (2014) highlight increased access of warmer waters to the ice shelf linked to increased heat content on the continental slope. The process drives enhanced basal melt of the ice shelf and resultant freshwater discharge and sea-ice formation (Schmidtko *et al.,* 2014). Basal melt from ocean circulation-derived heat influx has been proposed as a driver for ice shelf loss by several studies in Antarctica (e.g. Pritchard *et al*., 2012; Depoorter *et al*., 2013; Joughlin *et al,* 2014; Schmidtko *et al*., 2014).Increases in total ocean volume associated with Meltwater Pulse 1A (14600 – 14300 cal. a BP; Deschamps *et al.*, 2012) and correspondingly warmer southerly surface waters from the North Atlantic will have had significant impacts on the position of the grounding line, causing thinning of the ice stream and an increase in the rate of calving within Breiðafjörður and other similar fjord systems (Fig. 8.8). Evidence for an increase in iceberg production has been demonstrated during this period, through increases in the rates of Icelandic ice-rafted debris (IRD) deposition within sediment core samples from the Irminger Basin (Elliot *et al.*, 1998). The IRD layers demonstrated an average age of 15000 ± 700 cal. a BP, with an average duration of 1700 ± 700 cal. a (Elliot *et al.*, 1998), suggesting an early deglaciation phase around 1000 years earlier than the proposed marine limit formation ages. Increases in sea-surface temperature (SST) are noted following deposition of these layers, suggesting that the main meltwater source area was located north of the core site in western Iceland (Elliot *et al.*, 1998).The rapid rates of RSL fall recorded within Transect 1 and around Breiðafjörður therefore signal patterns of catastrophic ice stream collapse within Breiðafjörður and possibly Húnaflói, likely as the result of an unsustainable retreat of the grounding line (Fig. 8.8). Similar patterns have been posited for Faxaflói in southwest Iceland following the investigation of high marine limit elevations (Ingólfsson and Norðdahl, 2001), with the RSL records corresponding well with oceanographic studies on the Icelandic shelf (e.g. Andrews *et al.*, 2000; Elliot *et al.*, 2008).

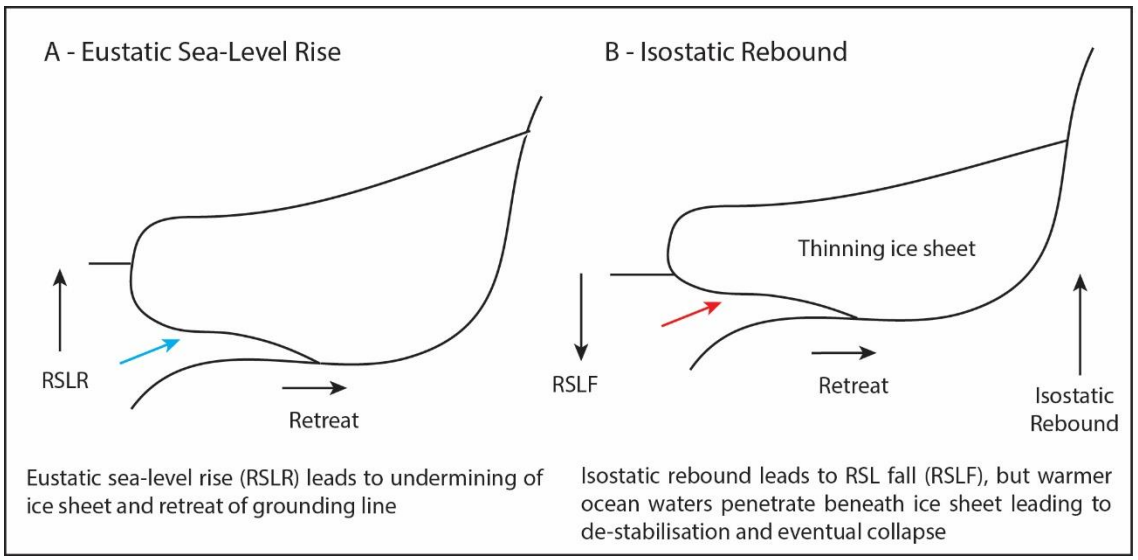

Figure 8.8 – Ice sheet dynamics during deglaciation, highlighting the importance of grounding line position, adapted from Schmidtko et al. (2014). Initial retreat occurs as a result of eustatic sea-level rise (A), which is compounded by subsequent isostatic rebound (B) following the thinning of the overlying ice sheet.

An amelioration of environmental conditions based on proxy evidence from ocean cores off northern Iceland between 16000 and 15500 cal a BP has been used as evidence for the arrival of warmer surface waters (Eiriksson *et al.*, 2000), with the impacts likely to have been felt earlier in southwest and western Iceland due to the prevailing oceanic circulation patterns (Fig. 3.2; Ingólfsson and Norðdahl, 2001). If, as suggested, deglaciation occurred rapidly in northwest Iceland, the ages presented by Eiriksson *et al.* (2000) appear to be relatively early. The results of the current study suggest that deglaciation occurred c. 1500 a after this proposed date for warmer conditions (Eiriksson *et al.*, 2000), which correlates well with studies in the southwest (Ingólfsson and Norðdahl, 2001). Alternatively, this difference could be explained through retreat rates during deglaciation, demonstrating the period of time taken for retreat from the shelf edge to the present coastline.

It is however clear that the North Atlantic and Irminger Currents would have transported the warm southern waters around the western coastline of Iceland prior to deglaciation, leading to the flotation and eventual collapse of the western ice shelves (Ingólfsson and Norðdahl, 2001). In addition to these characteristics, increased volcanism during deglaciation likely reinforced the rapid rates of ice retreat, although the order of these processes is still under debate (MacLennan *et al.*, 2002).

In contrast, the RSL records generated for Area E suggest that deglaciation occurred at a slower rate in Ísafjarðardjúp than Breiðafjörður (Areas B, C and G) and Húnaflói (Area A and F). Quillman *et al.* (2010) suggest that glacio-marine conditions were dominant in inner

Ísafjarðardjúp until c. 10200 cal. a BP, with deglaciation occurring at c. 11500 cal. a BP, which correlates well with the results generated in Area E (innermost Ísafjarðardjúp) that show deglaciation occurring at c. 11900 cal. a BP (see Section 6.10). This is in contrast to the rapid rates of glacial retreat noted in southwest Iceland, where the ice sheet retreated from its maximum position to the present coastline within 200 years (Ingólfsson and Norðdahl, 2001). Differences in the rate of deglaciation within these fjord systems may relate to one of three factors: a) the influence of warmer surface waters due to prevailing oceanic currents (e.g. Quillman *et al.*, 2010), b) the morphology of the fjord, leading to prolonged glacio-marine conditions in particular sections (e.g. Carr *et al.*, 2013) or c) increased resistance of the fjord glacier due to the narrower basin width (Raymond, 1996).

Quillman *et al.* (2010) note a progressive increase in fjord water temperatures in inner Ísafjarðardjúp, whilst outer fjord conditions appear to be relatively warm throughout, suggesting a gradual increase in the influence of warmer waters within the fjord over time. The landward migration of warmer water temperatures within the fjord may explain the pattern of deglaciation noted in the region (Fig. 8.5 and 8.7). Alternatively, a decreasing influence of glacial meltwater may also account for this slow increase in water temperature over time. The sedimentological and palaeoceanographic records from the fjord suggest that this water temperature increase occurred over a prolonged period (Quillman *et al.*, 2010) in comparison to wider fjord systems, such as Breiðafjörður (Fig. 8.7).

In addition to this prolonged introduction of warm water into Ísafjarðardjúp, the morphology of the fjord basin may also have added to the longer period of deglaciation. Uniform fjord systems tend to have slower retreat rates particularly when the termini of glaciers are located in the narrowest sections ('pinning points') of the fjord (Carr *et al.*, 2014). Furthermore, the narrow width of Ísafjarðardjúp may have led to increased opportunity for pinning points, reducing the rate of ice retreat, as demonstrated in systems within Novaya Zemlya, Russian Arctic (Carr *et al.*, 2014). Raymond (1996) has also demonstrated a reduction in ice retreat in narrow fjord systems, as a result of the increased influence of side drag on the central sectors of the ice stream or glacier.

It is clear that there are distinct patterns of postglacial RSL fall, which correspond to differences in the rates of ice retreat in northwest Iceland. Wider fjord systems appear to have deglaciated earlier and experienced more rapid ice retreat rates and therefore greater rates of isostatic rebound and RSL fall (Breiðafjörður and Húnaflói). Where fjord sites are more restricted in width, deglaciation appears to occur at a slower rate, influencing resultant RSL

records. This interpretation of the deglacial pattern is supported by a range of evidence, including palaeoceanography, sedimentology and glaciology.

Establishment of the style and pattern of deglaciation of Iceland is important, as freshwater input into the North Atlantic may have had significant implications for oceanic circulation, particularly the Atlantic Meridional Overturning Circulation (AMOC; Fig. 3.2; e.g. Alley and Águstsdóttir, 2005; Thornalley *et al.*, 2010; Lewis *et al,* 2012). The AMOC represents a key component of the climate system and therefore any reduction or strengthening of this current could have implications for global climate (Hubbard *et al.*, 2006; Thornalley *et al.*, 2009). Modelling studies have demonstrated the weakening of the AMOC and subsequent cooling of the North Atlantic following freshwater input (Le Grande *et al.*, 2006; Clarke *et al.*, 2009), which has also been supported by proxy data (McManus *et al.*, 2004; Thornalley *et al.*, 2010), including at sites in Iceland (e.g. Geirsdóttir *et al*., 2009; Larsen *et al*., 2012).

Thornalley *et al.* (2010) note the importance of determining accurate deglacial histories for the North Atlantic in particular, due to the presence of a sensitive area of deepwater production in the Nordic Seas and northern North Atlantic. Determination of the volume of ice present in Iceland at the LGM is important, due to the potential impact on the AMOC and deepwater formation (Hubbard *et al.*, 2006). In addition, meltwater events in the North Atlantic have frequently taken place prior to cold events, such as the Younger Dryas, suggesting an important link between these two phenomena (Thornalley *et al.*, 2010).

South of Iceland, Thornalley *et al*. (2010, 2011) produced a reconstruction of meltwater input and hydrography of the North Atlantic using Mg/Ca-$\delta^{18}O$ from planktonic foraminifera. Six freshwater events were identified from the record between 15.8 and 12.6 cal. ka BP, with the likely source being meltwater release from the Saint Lawrence river (Thornalley *et al*., 2010). Peaks in freshwater correlate with cooling in the North Atlantic (Thornalley *et al*., 2010), which Thornalley *et al*. (2011) attribute to reduced AMOC as a result of extensive sea-ice in the North Atlantic. Investigation into the influences of Icelandic freshwater input is limited, although iceberg discharge from circum Nordic Sea ice sheets may have had an impact on ocean colling (Thornalley *et al*., 2011). Ocean core studies suggest that the Younger Dryas re-advance was not coupled with a strong freshwater signal within the record (Thornalley *et al*., 2011).

Following initial deglaciation during the Bølling Period (14700 – 12700 cal. a BP), it is clear that there was a considerable ice re-advance during the Younger Dryas based on the RSL data presented. Previous research has noted that the Younger Dryas ice margin terminated onshore in western Iceland (Vikingsson, 1978; Eíriksson *et al.*, 1997; Geirsdóttir *et al.*, 1997; Norðdahl and Pétursson, 2005) and this is supported by the RSL records from Breiðafjörður

(Fig. 8.5). There is a notable difference along Transect 2 (Fig. 8.6), which suggests that coastal locations may have been ice-covered at the Younger Dryas. However, the extent of the Younger Dryas ice limit proposed in previous reconstructions appears to be in broad agreement with these new RSL datasets along Transect 2 (e.g. Ingólfsson *et al.*, 2010; Fig. 2.3). It should however be noted that the influence of Younger Dryas re-advance is variable between records and may have been spatially limited, as demonstrated by the RSL reconstructions from Areas B and C (Fig. 8.3 and 8.4).

8.7 Summary

This chapter has discussed the results of RSL study and GIA modelling in northwest Iceland in the context of previous research. It is clear that the field-based RSL records from northwest Iceland support the maximum glaciation hypothesis, as demonstrated by the marine limit and isolation basin datasets. In addition, there is evidence for variations in ice thickness across Breiðafjörður at the LGM. Reconstruction of RSL change in northwest Iceland suggests that deglaciation was relatively rapid, particularly in Breiðafjörður, leading to rapid rates of RSL fall following deglaciation. The influence of Younger Dryas ice readvance has been shown to differ between locations, highlighting differences in ice loading conditions during the period.

There is also evidence for an early Holocene RSL fall below present in a number of locations, although the magnitude of such a lowstand is not currently well constrained. RSL records have highlighted a mid-Holocene highstand in a number of locations, with new results supporting existing geological and palaeoceanographic records from northwest Iceland. It is evident that patterns of late Holocene RSL change are complex in northwest Iceland, with proposed RSL rise (Area A), RSL fall (Area B, C, F) and fluctuating sea level (Area E) being suggested by the new and existing RSL records.

The marine limits, RSL records and modelling have clear consequences for models of the LGM IIS. It is evident from the model outputs presented that there is good agreement between the HP_MAX ice model and the geological dataset, particularly when coupled with the LT 30 – 40 km, υ_{UM} 5 x 10^{19} – 1 x 10^{20} Pa s Earth Model. This Earth model, preferred by the maximum glaciation scenario, is a new estimation for the rheological characteristics in northwest Iceland. The preferred ice and Earth model suggests that the ESL of the LGM IIS may have been as high as 1.0 m, which is significantly larger than estimations within current global ice models (ICE-5G). The minimum glaciation scenario can be rejected based on the field evidence and GIA modelling undertaken in this thesis. The conclusions of this research are presented in Chapter 9, alongside a discussion of limitations of the current research and areas for future study.

Chapter 9

Conclusions

9.1 Introduction

This chapter provides an overview of the main conclusions of this research project, alongside a discussion of the principal limitations and areas for future study.

9.2 Principal Conclusions

This research has investigated the Last Glacial Maximum (LGM) ice loading histories and crustal characteristics of northwest Iceland, using a suite of new and existing relative sea-level (RSL) data through the achievement of a series of key objectives. These objectives are outlined below, alongside the subsequent outcomes:

1. *Collection of field data (isolation basin sediments and marine limit elevations)*

In most field research locations, it has been possible to reconstruct postglacial RSL changes through a combination of isolation basin and marine limit evidence. However, there are some evident issues regarding chronological control in Area G, which limits the employability of the RSL record produces. In addition, the low elevation of the marine limit in Area D meant that suitable isolation basin sites were uncommon.

2. *Palaeoenvironmental reconstruction (sediment and microfossil analyses, radiocarbon dating and tephrochronology) to provide RSL records*

The majority of isolation basin sediments have yielded complete environmental records through diatom analysis (Chapter 6), which when coupled with tephrochronology (Chapter 5) and radiocarbon analysis (Section 6.9), has allowed the generation of a series of new RSL curves for NW Iceland (Section 6.10). A limited number of sites suffered from poor preservation of the diatom record and were therefore not used in the generation of the RSL curves.

3. *Assessment of the spatial patterns of relative sea-level (RSL) changes in northwest Iceland*

Isolation basin records from northwest Iceland allow the determination of spatial variability within the RSL record. These differences in RSL are demonstrated by the elevation of the marine limit and rates of subsequent RSL changes (Rundgren *et al*., 1997; Lloyd *et al*., 2009;

Brader *et al*., submitted; this thesis). RSL reconstructions from several field areas demonstrate rapid rates of RSL fall following marine limit formation (Area A, B, C, F). These high rates of RSL fall are associated with the rapid response of the Icelandic lithosphere to the removal of glacial loading (Sigmundsson, 1991; Hubbard, 2006). Around Breiðafjörður, these rates of RSL change are relatively high at -35 to -38 mm cal. a^{-1} (Lloyd *et al.*, 2009; Brader *et al.*, submitted), suggesting catastrophic collapse of the ice present within the fjord.

There is also evidence from the majority of field research areas that RSL fell below present in the early Holocene. The magnitude of this lowstand is currently poorly constrained in northwest Iceland, but RSL was likely no lower than 40 m below present sea level, as shown by estimations from northern and southwest Iceland (Moriwaki, 1990; Ingólfsson *et al.*, 1995). In addition, there is evidence for a mid-Holocene highstand in a number of the field areas, including Areas B, C, E and F.

4. *Modelling of glacio-isostatic adjustment (GIA) to test regional ice models and rheological characteristics*

GIA modelling has allowed the determination of the preferred ice model. HP_MAX (Patton, unpub.) has been shown to provide the best fit with the field datasets (Chapter 7). The HP_MAX ice model which has a significantly larger equivalent sea-level value that frequently used in global ice models (Patton, unpub.). The ESL of the LGM IIS may be as high as 1.0 m and therefore under-represented in global ice models at 0.4 m (e.g. Peltier, 2004).

GIA modelling in Iceland has also highlighted a preferred Earth model, which produces the lowest chi^2 values when used alongside the regional ice models (Patton, unpub.). The rheological characteristics presented correspond with the higher end of the range of published values (e.g. Biessy *et al.*, 2008) determined independently from other geophysical techniques. Variations in the viscosity of the lower mantle had a limited effect on modelled RSL changes and so this work does not provide firm constraints on lower mantle viscosity.

Consequently, the achievement of these research objectives allows the principal research question to be addressed:

5. *Did Iceland experience a maximum or minimum glaciation at the Last Glacial Maximum?*

Evidence from marine limit and isolation basin data along two perpendicular transects in northwest Iceland has demonstrated support for the maximum glaciation hypothesis for LGM IIS extent. Marine limit elevations increase with proximity to the proposed principal ice loading centre at Vatnajökull, with limited evidence to support a secondary ice loading centre

in Vestfirðir (e.g. Hansom and Briggs, 1991). Sites along Transect 1 demonstrate responses to similar ice loading conditions at the LGM, with sites on Transect 2 showing ice coverage until the termination of the Younger Dryas.

Marine limit data show that the greatest ice thicknesses in northwest Iceland were found along the northern coastline of Breiðafjörður, likely due to favourable conditions for ice accumulation. The greater ice thicknesses in Breiðafjörður may relate to the presence of an ice stream proposed to have existed within the fjord at the LGM (Bourgeois *et al.*, 2000; Hubbard *et al.*, 2006).

RSL reconstructions from isolation basin records in northwest Iceland have demonstrated the differing influence of Younger Dryas ice readvance on the rates of RSL change recorded (Norðdahl and Ásbjörnsdóttir, 1995; Rundgren *et al.*, 1997; Lloyd *et al.*, 2009; Brader *et al.*, submitted). Evidence from geological data and GIA modelling suggests differences in ice loading between Snæfellsnes and Vestfirðir (Brader *et al.*, submitted), likely as a consequence of the available land area for ice accumulation.

The employment of a suite of new and existing RSL datasets has allowed the testing of the contrasting glaciation scenarios for Iceland. In turn, GIA modelling has allowed the preferred ice loading and rheological characteristics to be identified. There is clear evidence to support the maximum glaciation scenario for Iceland.

9.3 Limitations to the research

9.3.1 Data availability

It has not been possible to assess isolation basin samples from the marine limit to present in all field research areas, particularly in Area F and G. The ability to test modelled RSL changes in these areas is therefore limited. The availability of isolation basin and coastal lowland sites in each field location is therefore a key limitation in the exploration of GIA model outputs.

9.3.2 Chronological control for isolation basin SLIPs

Several sites have demonstrated issues surrounding the production of a suitable chronological framework to accurately assess environmental and therefore RSL changes. Isolation basin sediment samples from Area A and G have generated radiocarbon ages which are substantially younger than anticipated and are contradictory to tephrochronological analysis. In addition, analysis at Ytra-Baravatn (Area C) has suffered from contamination by older carbon within the landscape. There is uncertainty over the validity of individual SLIPs employed to test GIA model outputs. Adjustment to the material dated may alleviate some of these issues.

9.3.3 Marine limit chronologies

Previous research has posited that the marine limit in Iceland formed synchronously. However, there is generally poor chronological control on the formation of these features, which represent the elevation of highest postglacial RSL. Hence, the marine limit in Iceland may be diachronous, with the age of formation of similar stratigraphic units occurring over different time periods. Increased chronological control of marine limit formation would therefore confirm the interpretation of these features which are used for the testing of GIA model outputs.

9.3.5 2-dimensional, incompressible Earth model

As outlined in Chapter 2, the crustal structure of Iceland has high lateral variability due to its location on a ridge axis (Barnhoorn *et al.*, 2011). The uniform two dimensional rheological profile adopted in this study may therefore over- or under-represent the postglacial rebound experienced in particular locations. Furthermore, the two-dimensional Earth model fails to account for the proposed mantle plume below Iceland, which has particularly low viscosity values.

Within SELEN, the software program, TABOO, employs an incompressible Earth structure, meaning that the volume of the Earth does not vary due to external pressures, in this case ice loading. The introduction of a compressible Earth structure may lead to very different RSL predictions for Iceland, as compressibility would allow changes to the volume of the Earth with the addition of loading. Further exploration of RSL changes in Iceland using compressible Earth models will be important in further assessing the pattern of ice loading at the LGM.

9.4 Recommendations for future research

9.4.1 GIA Modelling in Vestfirðir

The new HP ice models for Iceland provide an opportunity to explore the LGM ice loading in NW Iceland at a higher resolution than undertaken within this study. Modelling at a higher resolution may allow the exploration of ice loading within particular valley systems and thus provide predictions for specific localities. In order to facilitate this, greater computing power is required than available in the present study. At present, the RSL predictions generated are produced from a comparatively low (one degree) resolution.

In addition, the influence of other proximal ice sheets could be further explored, particularly the Greenland Ice Sheet, using higher resolution ice loading scenarios than available within ICE5G. This may allow the deconstruction of influences on the Icelandic RSL records and

therefore provide an insight into possible locations for additional work to identify the meltwater fingerprints of individual ice sheets (e.g. Antarctica/Greenland).

9.4.2 Mid-Holocene highstand in northwest Iceland

There is a range of evidence to suggest that northwest Iceland experienced a RSL highstand during the mid-Holocene, such as the *Nucella* beach (Hansom and Briggs, 1991). However, evidence for the mid-Holocene highstand in isolation basin sediments is limited, as a regression-transgression-regression sequence is not evident within the samples collected as part of this study. As a result, it is important to sample additional isolation basin samples between 4 and 8 m asl in order to further explore this possible highstand and the possible effects of the Storegga tsunami in northwest Iceland. Determination of the highstand elevation is also important in providing an insight into the possible mechanisms for this pattern of RSL change, such as meltwater from Antarctic or the influence of hydro-eustacy (Ingólfsson and Hjort, 1999).

9.4.3 Early Holocene Lowstand

It is clear from the isolation basin data and modelling outputs that RSL fell below present in northwest Iceland during the early Holocene. However, the depth to which RSL fell below present is currently poorly constrained. Where research has been undertaken, sea-level index points often have large vertical errors and poor chronological control due to methodological limitations. It is therefore important to undertake additional research in northwest Iceland to determine the elevation of RSL fall below present. Establishment of this early Holocene RSL lowstand could provide key information on the drivers of mid-late Holocene RSL changes in the region, particularly in relation to the timing of eustatic sea-level rise.

9.4.4 Modern diatom training set

It would be greatly beneficial to gain further understanding of the modern diatom distribution in northwest Iceland. The establishment of a modern diatom training set would allow position of individual taxa within the tidal frame in Iceland to be identified and clarified. The position of individual species could have important consequences for interpretation of Icelandic diatom assemblages and may allow the development of suitable transfer functions to further investigate RSL changes.

9.4.5 SLIPs in Eastern Vestfirðir

In order to further test the ice loading scenarios for NW Iceland, additional SLIPs from eastern Vestfirðir would be beneficial. The investigation of isolation basins in eastern Vestfirðir would

allow the exploration of sea-level changes in outer Húnaflói, acting as a useful comparison to analyses conducted in Area F and the results of ocean drilling by Andrews *et al.* (2000). The generation of a series of SLIPs for eastern Vestfirðir would therefore allow the further exploration of environmental conditions in this important fjord system.

9.4.6 SLIPs for Northeast and East Iceland

Testing of ice loading scenarios on an Iceland-wide scale is restricted due to the limited availability of comprehensive records of postglacial RSL change for northeast and eastern Iceland. Previous study has highlighted the *potential* for ice-free areas in northeast Iceland at the LGM and this region might provide important new data for the assessment of deglacial patterns. Furthermore, an increase in field based RSL data from eastern Iceland would allow a better assessment of fit between field evidence and modelled RSL changes.

Appendix

Full diatom counts and tephra geochemical data are available from the author upon request.

A1 – SELEN Model task_1.dat input file – example

For a full explanation of the code employed, please see Spada and Melini (2013) SELEN User Guide.

```
Active

Harmonic_Degrees
1 128
0
1

Make_Model
3
0                    User defined model
40.0                 Lithospheric thickness (km)
2.7                  Mantle viscosity (lower)
0.005
0.005                Mantle viscosity (upper)

Normalized_Residues
1 1 1

El_Fluid_Viscel
1 1 1
```

References

A, G.; Wahr, J. and Zhong, S. (2013) Computations of the viscoelastic response of a 3-D compressible Earth to surface loading: an application to Glacial Isostatic Adjustment in Antarctica and Canada *Geophysical Journal International Vol. 192 No. 2 Pg. 557-572.*

Ægisdóttir, H. H. and Þórhallsdóttir, Þ. E. (2005) Theories on migration and history of the North Atlantic flora: a review *Jökull Vol. 54 Pg. 1-16.*

Admiralty Tide Tables (2006) Admiralty Tide Tables – Europe (excluding United Kingdon and Ireland, Mediterranean Sea and Atlantic Ocean Volume 2 *Taunton, UK: United Kingdon Hydrographic Office*

Alley, R. B. and Águstsdóttir, A. M. (2005) The 8k event: cause and consequences of a major Holocene abrupt climate change *Quaternary Science Reviews Vol. 24 Pg. 1123-1149*

Anderson, J. (unpub.) Sveinhúsvatn Interim Report *Source: Dr Jerry Lloyd*

Andrews, J. T (1970) A geomorphological study of postglacial uplift: with particular reference to Arctic Canada *London: Institute of British Geographers 156pp.*

Andrews, J. T.; Hardardóttir, J.; Helgadóttir, G.; Jennings, A. E.; Geirsdóttir, Á.; Sveinbjörnsdóttir, Á. E.; Schoolfield, S.; Kristjánsdóttir, G. B.; Smith, L. M., Thors, K. and Syvitski, J. P. M. (2000) The N and W Iceland Shelf: insights into Last Glacial Maximum ice extent and deglaciation based on acoustic stratigraphy and basal radiocarbon AMS dates *Quaternary Science Reviews Vol. 19 Pg. 619-631*

Antonioli, F.; Ferranti, L.; Fontana, A.; Amorosi, A.; Bondesan, A.; Braitenberg, C.; Dutton, A.; Fontolan, G.; Furlani, S.; Lambeck, K.; Mastronuzzi, G.; Monaco, C.; Spada, G. and Stocchi, P. (2009) Holocene relative sea-level changes and vertical movements along the Italian and Istrian coastlines *Quaternary International Vol. 206 No. 1-2 Pg. 102-133*

Argus, D. F.; Peltier, W. R.; Drummond, R. and Moore, A. W. (2014) The Antarctica component of postglacial rebound model ICE-6G_C (VM5a) based on GPS positioning, exposure age dating

of ice thicknesses and relative sea-level histories *Geophysical Journal International Vol. 198 No. 1 Pg. 537-563*

Árnadóttir, T.; Lund, B.; Jiang, W.; Geirsson, H.; Björnsson, H.; Einarsson, P. and Sigurdsson, T. (2009) Glacial rebound and plate spreading: results from the first countryside GPS observations in Iceland *Geophysical Journal International Vol. 177 No. 2 Pg. 691-716*

Ásbjörnsdóttir, L. and Norðdahl, H. (1995) Götungar í sjávarsetlögum við Mela á Skarðsströnd. In, Hróarsson, B.; Jónsson, D.; Jónsson, S. S. (eds.) Eyjar í Eldhafi *Reykjavik: Gott mál Pg. 179-188*

Ascough, P. L.; Cook, G. T.; Hastie, H.; Dunbar, E.; Church, M. J.; Einarsson, Á.; McGovern, T. H. and Dugmore, A. J. (2011) An Icelandic freshwater radiocarbon reservoir effect: implications for lacustrine 14C chronologies *The Holocene Vol. 21 No. 7 pg. 1073-1080*

Auriac, A.; Spaans, K. H.; Sigmundsson, F.; Hooper, A.; Schmidt, P. and Lund, B. (2013) Iceland rising: solid Earth response to ice retreat inferred from satellite radar interferometry and viscoelastic modelling *Journal of Geophysical Research: Solid Earth Vol. 118 No. 4 Pg. 1331-1344*

Balascio, N. L.; Zhang, Z.; Bradley, R. S.; Perren, B. Dahl, S. O. and Bakke, J. (2011) A multi-proxy approach to assessing isolation bains stratigraphy from the Lofoten Islands, Norway *Quaternary Research Vol. 75 No. 1 Pg. 288-300*

Ballantyne, C. K.; McCarroll, D. and Stone, J. O. (2006) Vertical dimensions and age of the Wicklow Mountains ice dome, eastern Ireland, and implications for the extent of the last Irish ice sheet *Quaternary Science Reviews Vol. 25 Pg. 2048-2058*

Ballantyne, C. K.; McCarroll, D. and Stone, J. O. (2007) The Donegal ice dome, NW Ireland: dimensions and chronology *Journal of Quaternary Science Vol. 22 Pg. 773-783*

Ballantyne, C. K.; Stone, J. O. and McCarroll, D. (2008) Dimensions and chronology of the last ice sheet in western Ireland *Quaternary Science Reviews Vol. 27 Pg. 185-200*

Bárðarson, G. G. (1910) Traces of changes of climate and level at Húnaflói, northern Iceland *Postglaziale Klimaveränderungen Pg. 347-352*

Bárðarson, G. G. (1923) Fornar Sjávarminjar vid Borgarfjörd og Hvalfjörd. *Rit Visinda-felags Islendinga Vol. 1 Akureyri, Iceland*

Barker, D. S. (1983) Igneous Rocks *Prentice-Hall: Englewood Cliffs, New Jersey, USA.*

Barnhoorn, A.; van der Wal, W. And Drury, M. R. (2011) Upper mantle viscosity and lithospheric thickness under Iceland *Journal of Geodynamics Vol. 52 No. 3-4 Pg. 260-270*

Battarbee, R.W. (1986) Diatom Analysis In, Berglund, B.E. (ed.) Handbook of Holocene palaeoecology and palaeohydrology *Chichester: Wiley* p. 527-570

Bell, T. (1996) the last glaciation and sea-level history of Fosheim Peninsula, Ellesmere Island, Canadian High Arctic *Canadian Journal of Earth Sciences Vol. 33 No. 7 Pg. 1075-1086*

Bentley, C. J. (1984) Some aspects of the Cryosphere and its Role in Climatic Change, in Hansen, J. E. and Takahashi, T. (eds.) Climate Processes and Climate Sensitivity Washington DC: *American Geophysical Union doi: 10.1029/GM029p0207*

Bentley, M. J.; Hodgson, D. A.; Smith, J. A. and Cox, N. J. (2005) Relative sea-level curves for South Shetland Islands and Marquerite Bay, Antarctic Peninsula *Quaternary Science Reviews Vol. 24 No. 10-11 Pg. 1203-1216*

Biessy, G.; Dauteuil, O.; Van Vliet-Lanoë, B. and Wayolle, A. (2008) Fast and partitioned postglacial rebound of southwestern Iceland *Tectonics Vol. 27 No. 3 DOI: 10.1029/2007TC002177*

Bijwaard, H. and Spakman, W. (1999) Tomographic evidence for a narrow whole mantle plume below Iceland *Earth and Planetary Science Letters Vol. 166 No. 3-4 Pg. 121-126*

Bingham, R.; Hulton, N. and Dugmore, A. J. (2003) Modelling the southern extent of the last Icelandic Ice Sheet *Journal of Quaternary Science Vol. 18 No. 2 Pg. 169-181*

Bjarnason, I. T.; Manke, W.; Flovenz, O. G. and Caress, D. (1993) Tomographic image of the mid-Atlantic plate boundary in south-western Iceland *Journal of Geophysical Research Vol. 98 Pg. 6607-6622*

Björck, S. and Wohlfarth, B. (2001) 14C chronostratigraphic techniques in paleolimnology In, Last, W. M. and Smol, J. P. (eds.) Tracking Environmental change using lake sediments Volume 1: basin analysis, coring and chronological techniques *Dordrecht, The Netherlands: Kluwer Academic Publishers Pg. 205-245*

Björck, S.; Ingólfsson, Ó.; Hafliðason, H.; Hallsdóttir, M. and Anderson, N. J. (1992) Lake Torfadalsvatn: a high resolution record of the North Atlantic Ash Zone 1 and the last glacial-interglacial environmental changes in Iceland *Boreas Vol. 21 Pg. 15-22*

Boulton, G. S.; Jarvis, J. and Thors, K. (1988) Dispersal of glacially derived sediment over part of the continental shelf of south Iceland and the geometry of the resultant sediment bodies *Marin Geology Vol. 83 Pg. 193-223*

Bourgeois, O.; Dauteuil, O. and Van Vliet-Lanoe, B. (1998) Pleistocene subglacial volcanism in Iceland: tectonic implications *Earth and Planetary Science Letters Vol. 164 Pg. 165-178*

Bourgeois, O.; Dauteuil, O. and Van Vliet-Lanoe, B. (2000) Geothermal control on flow patterns in the Last Glacial Maximum Ice Sheet of Iceland *Earth Surface Processes and Landforms Vol. 25 Pg. 59-76*

Bjarnason, I. Th.; Menke, W.; FLovenz, O. G. and Caress, D. (1993) Tomographic image of the Mid-Atlantic plate boundary in southwestern Iceland *Journal of Geophysical Research Vol. 98 Pg. 6607-6622*

Brader, M. D. (2012) Lateglacial to Holocene relative sea-level changes at Stykkishólmur, northern Snæfellsnes, Iceland *Durham University: Unpublished Masters Thesis*

Brader, M. D.; Lloyd, J. M.; Bentley, M. J. and Newton, A. J. (submitted) Lateglacial to Holocene relative sea-level changes at Stykkishólmur, northern Snæfellsnes, Iceland *Journal of Quaternary Science*

Bradley, S. L. ; Milne, G. A. ; Shennan, I. and Edwards, R. (2011) An improved glacial isostatic adjustment model for the British Isles *Journal of Quaternary Science Vol. 26 No. 5 Pg. 541-552*

Brun, J. (1965) Diatomées des Alpes et du Jura *Amsterdam: Asher and Co.*

Buckland, P. and Dugmore, A. (1991) 'If this is a Refugium, why are my feet so bloody cold?' The origins of the Icelandic biota in the light of recent research In, Caseldine, C. and Maizels, J. K. (eds) *Environmental Change in Iceland: Past and Present Dordrecht: Kluwer Pg. 107-125*

Carr, J. R.; Vieli, A. and Stokes, C. (2013) Influence of sea ice decline, atmospheric warming and glacier width on marine-terminating outlet glacier behaviour in northwest Greenland at seasonal to interannual timescales *Journal of Geophysical Research: Earth Surface Vol. 118 No. 3 Pg. 1210-1226*

Clague, J. J. and James, T. S. (2002) History and isostatic effects of the last ice sheet in southern British Colombia *Quaternary Science Reviews Vol. 21 No. 1-3 Pg. 71-87*

Clarke, G. K. C.; Bush, A. B. G.; and Bush, J. W. M. (2009) Freshwater discharge, sediment transport and modelled climate impacts of the final drainage of Glacial Lake Agassiz *Journal of Climate Vol. 22 Pg. 2161-2180*

Compton, K.; Bennett, R. A. and Hreinsdóttir, S. (2015) Climate-driven vertical acceleration of Icelandic crust measured by continuous GPS geodesy *Geophysical Research Letters Early View DOI: 10.1002/2014GL062446*

Corner, G. D.; Kolka, V. V.; Yevzerov, V. Y. and Møller, J. J. (2001) Postglacial relative sea-level change and stratigraphy of raised coastal basins on Kola Peninsula, northwest Russia *Global and Planetary Change Vol. 31 No 1-4 Pg. 155-177*

Cossart, E.; Mercier, D.; Decaulne, A.; Feuillet, T.; Jónsson, H. P. and Sæmundsson, Þ. (2014) Impacts of post-glacial rebound on landslide spatial distribution at a regional scale in northern Iceland (Skagafjörður) *Earth Surface Processes and Landforms Vol. 39 No. 3 Pg. 336-350*

Darbyshire, F. A.; Bjarnason, I. Th.; White, R. S. and Flovenz, O. G. (1998) Crustal structure above the Iceland mantle plume imaged by the ICEMELT refraction profile *Geophysical Journal International Vol. 135 Pg. 1131-1149.*

Darbyshire, F. A.; White, R. S. and Priestley, K. F. (2000) Structure of the crust and uppermost mantle of Iceland from a combined seismic and gravity study *Earth and Planetary Science Letters Vol. 181 No. 3 Pg. 409-428*

Davies, S. M.; Turney, C. S. M. and Jowe, J. J. (2001) Identification and significance of a visible, basalt-rich Vedde Ash layer in a Late-glacial sequence on the Isle of Skye, Inner Hebrides, Scotland *Journal of Quaternary Science Vol. 16 No. 2 Pg. 99-104*

Depoorter, M. A.; Bamber, J. A.; Griggs, J. A.; Lenaerts, J. T. M.; Ligtenberg, S. R. M.; van den Broeke, M. R. and Moholdt, G. (2013) Calving fluxes and basal melt rates of Antarctic ice shelves *Nature Vol. 502 Pg. 89-92*

Deschamps, P.; Durand, N.; Bard, E.; Hamelin, B.; Camoin, G.; Thomas, A. L.; Handerson, G. M.; Okuno, J. and Yokoyama, Y. (2012) Ice-sheet collapse and sea-level rise at the Bølliing warming 14,600 years ago *Nature Vol. 483 Pg. 559-564*

Dickson, B.; Yashayaev, I.; Meincke, J.; Turrell, B.; Dye, S. and Holfort, J. (2002) Rapid freshening of the deep North Atlantic Ocean over the past four decades *Nature Vol. 416 Pg. 832-837*

Du, Z. J. and Foulger, G. R. (1999) The crustal structure beneath the northwest fjords, Iceland, from receiver functions and surface waves *Geophysical Journal International Vol. 139 No. 2 Pg. 419-432*

Du, Z. J. and Foulger, G. R. (2001) Variation in the crustal structure across central Iceland *Geophysical Journal International Vol. 145 No. 1 Pg. 246-264*

Du, Z. J. and Foulger, G. R. (2002)

Du, Z. J.; Foulger, G. R.; Julian, B. R.; Allen, R. M.; Nolet, G.; Morgan, W. J.; Bergsson, B. H.; Erlendsson, P.; Jakobsdóttir, S.; Ragnarsson, S.; Stefansson, R. and Vogfjord, K. (2002) Crustal structure beneath western and eastern Iceland from surface waves and receiver functions *Geophysical Journal International Vol. 149 No. 2 Pg. 349-363*

Dugmore, A. J. and Newton, A. J. (2012) Isochrons and beyond: maximising the use of tephrochronology in geomorphology *Jökull Vol. 62 Pg. 39-52*

Dugmore, A. J.; Newton, A. J.; Sugden, D. E. and Larsen, G. (1992) Geochemical stability of fine grained silicic Holocene tephra in Iceland and Scotland *Journal of Quaternary Science Vol. 7 Pg. 173-183*

Dugmore, A. J.; Larsen, G. And Newton, A. J. (1995a) Seven tephra isochrones in Scotland *The Holocene Vol. 5 Pg. 257-266*

Dugmore, A. J.; Shore, J. S.; Cook, G. T.; Newton, A. J.; Edwards, K. J. and Larsen, G. (1995b) The radiocarbon dating of Icelandic tephra layers in Britain and Ireland *Radiocarbon Vol. 37 No. 2 Pg. 286-295*

Dugmore, A. J.; Newton, A. J.; Edwards, K. J.; Larsen, G. Blackford, J. J. and Cook, G. T. (1996) Long-distance marker horizons from small-scale eruptions: british tephra deposits from the AD 1510 eruption of Hekla, Iceland *Journal of Quaternary Science Vol. 11 Pg. 511-516*

Dugmore, A. J.; Gisladóttir, G.; Simpson, I. A. and Newton, A. J. (2009) Conceptual models of 1200 years of Icelandic soil erosion reconstructed using tephrochronology *Journal of the North Atlantic Vol. 2 Pg. 1-18*

Dyke, A. S.; McNeely, R. N. and Hooper, J. (1996) Marine reservoir corrections for bowhead whale radiocarbon age determinations *Canadian Journal of Eath Sciences Vol. 33 No. 12 Pg. 1628-1637*

Egloff, J. and Johnson, G. L. (1979) Erosional and depositional structures of the Southwest Iceland insular margin: thirteen geophysical profiles In, Watkins, J. S.; Montadert, L. and Dickerson, P. W. (edits.) Geological and geophysical investigations of continental margins *Tulsa, OK: AAPG Pg. 43-63*

Einarsson, Th. (1967) Zu der Ausdehnung der weichselzeitlichen Verseiung Nordislands Sonderoffentlichungen des Geologischen Institutes der Universitat Koln 13 Pg. 167-173

Einarsson, Th. (1968) Jarðfræði. Saga bergs og lands *Reykjavik: Mál og Menning*

Einarsson, Th. (1973) Geology of Iceland In, Pitcher, M. G. (edit.) *Arctic Geology: Memoirs of the American Association of Petroleum Geologists Vol. 19 Pg. 171-175*

Einarsson, Th. (1979) The deglaciation of Iceland *Norsk Geologisk Förening Medlemsblad 13 Pg. 18*

Einarsson, M. A. (1984) Climate of Iceland In, van Loon, H. (ed.) *World Survey of climatology No. 15 Climates of the Oceans Amsterdam: Elsevier Pg. 673-697*

Einarsson, T. and Albertsson, K. J. (1988) The glacial history of Iceland during the past three million years *Philosophical Transactions of the Royal Society of London Series B Vol. 318 Pg. 637-644*

Eiríksson, J.; Simonarson, L. A.; Knudsen, K. L. and Kristensen, P. (1997) Fluctuations of the Weichselian ice sheet in SW Iceland: a glaciomarine sequence in Sudurnes, Seltjarnes *Quaternary Science Reviews Vol. 16 Pg. 221-240*

Eiríksson, J., Simonarson, L. A. and Sveinbjörndóttir, A. (1998) Heimsókn ad Bae í Hrutafirdi: Aflaedi og loftslagsbreytingar a nutima og ny timasetning med kolefnisgreiningum og gjoskulagatimatali Jardfrædafelag Islands *Vorradstefna 1998 Agrip erinda og veggspjalda Pg. 20-22*

Eiríksson, J.; Knudsen, K. L.; Hafliðason, H. and Henriksen, P. (2000) Late-glacial and Holocene palaeoceanography of the North Icelandic Shelf *Journal of Quaternary Science Vol. 15 No. 1 Pg. 23-42*

Elliot, M.; Labeyrie, L.; Bond, G.; Cortijo, E.; Turon, J.-L.; Tisnerat, N. and Duplessy, J.-C. (1998) Millennial-scale iceberg discharges in the Irminger Basin during the Last Glacial Period: Relationship with the Heinrich events and environmental settings *Paleoceanography Vol. 13 No. 5 Pg. 433-446*

Evans, D. J. A. (1990) The last glaciation and relative sea-level history of northwest Ellesmere Island, Canadian High Arctic *Journal of Quaternary Science Vol. 5 Pg. 67-82*

Fabel, D.; Ballantyne, C. K. and Xu, S. (2012) Trimlines, blockfields, mountain-top erratics and the vertical dimensions of the last British-Irish Ice sheet in NW Scotland *Quaternary Science Reviews Vol. 55 Pg. 91-102*

Fairbanks, R. G. (1989) A 17000 year glacio-sea-level record: influence of glacial melting rates on the Younger Dryas event and deep-ocean circulation *Nature Vol. 342 Pg. 637-642*

Farrell, W. E. and Clark, J. A. (1976) On postglacial sea-level *Geophysical Journal International Vol. 46 No. 3 Pg. 647-667*

Farrington, A. (1947) Unglaciated areas in southern Ireland *Irish Geography Vol. 1 Pg. 89-97*

Fjeldskaar, W. (1994) Viscosity and thickness of the asthenosphere detected from the Fennoscandian uplift *Earth and Planetary Science Letters Vol. 126 No. 4 Pg. 399-410*

Fleming, K. and Lambeck, K. (2004) Constraints on the Greenland Ice Sheet since the Last Glacial Maximum from sea-level observations and glacial-rebound models *Quaternary Science Reviews Vol. 23 Pg. 1053-1077*

Fleming, K.; Johnston, P.; Zwartz, D.; Yokoyama, Y.; Lambeck, K. and Chappell, J. (1998) Refining the eustatic sea-level curve since the Last Glacial Maximum using far- and intermediate-field sites *Earth and Planetary Science Letters Vol. 163 No. 1-4 Pg. 327-342*

Fleming, K. Martinec, Z. and Wolf, D. (2007) Glacial-isostatic adjustment and the viscosity structure underlying the Vatnajökull Ice Cap, Iceland *Pure and Applied Geophysics Vol. 164 No. 4 Pg. 751-768*

Flovenz, O. G. (1992) Properties of the crust and upper mantle below Iceland from geophysical measurements *Edlisfraedi Islandi VI Pg. 89– 104*

Foged, N. (1974) Freshwater diatoms in Iceland *Bibliotheca Phycologica No. 15 118pp.*

Foulger, G. R. (2006) Older crust underlies Iceland *Geophysical Journal International Vol. 165 No. 7 Pg. 672-676*

Foulger, G. R. and Anderson, D. L. (2005) A cool model for the Iceland hotspot *Journal of Volcanology and Geothermal Research Vol. 141 No. 1-2 Pg. 1-22*

Foulger, G. R.; Du, Z. and Julian, B. R. (2003) Icelandic type crust *Geophysical Journal International Vol. 155 No. 2 Pg. 567-590*

Freund, H.; Gerdes, G.; Streif, H.; Dellwig, O. and Watermann, F. (2004) The indicative meaning of diatoms, pollen and botanical macro fossils for the reconstruction of palaeoenvironments and sea-level fluctuations along the coast of Lower Saxony; Germany *Quaternary International Vol. 112 No. 1 Pg. 71-87*

Gehrels, W. R.; Marshall, W. A.; Gehrels, M. J.; Larsen, G.; Kriby, J. R.; Eiriksson, J.; Heinemeier, J. and Shimmield, T. (2006) Rapid sea-level rise in the North Atlantic Ocean since the first half of the nineteenth century *The Holocene Vol. 16 No. 7 Pg. 949-965*

Geirsdóttir, Á.; Hardardóttir, J. and Eiriksson, J. (1997) The depositional history of the Younger Dryas-Preboreal Búði moraines in south-sentral Iceland *Arctic and Alpine Research Vol. 29 Pg. 13-23*

Geirsdóttir, Á.; Miller, G. H.; Axford. Y. and Ólafsdóttir, S. (2009) Holocene and latest Pleistocene climate and glacier fluctuations in Iceland *Quaternary Science Reviews Vol. 28 Pg 2017-2118*

Grönvold, K.; Óskarsson, N.; Johnsen, S. J.; Clausen, H. B.; Hammer, C. U.; Bond, G. And Bard, E. (1995) Ash layers from Iceland in the Greenland GRIP ice core correlated with oceanic and land sediments *Earth and Planetary Science Letters Vol. 135 Pg. 149-155*

Gudmundsson, A. (1986) Mechanical aspects of postglacial volcanism and tectonics of the Reykjanes peninsula, southwest Iceland *Journal of Geophysical Research Vol. 91 No. 12 Pg. 711-721*

Gudmundsson, A. (2000) Dynamics of volcanic systems in Iceland: example of tectonism and volcanism at juxtaposed hot spot and mid-ocean ridge systems *Annual review of Earth and Planetary Sciences Vol. 28 Pg. 107-140*

Guillard, R. R. L. and Kilham, P. (1977) Chapter 12: The ecology of marine planktonic diatoms In, Werner, D. with Burnett, J. H.; Baker, H. G.; Beevers, H. and Whatley, F. R. The Biology of Diatoms *Berkeley and Los Angeles: University of California Press*

Guiry, M. D. and Guiry, G. M. (2013) Algaebase: worldwide electronic publication *Galway: National University of Ireland*

Hafliðason, H.; Eiriksson, J. and van Kreveld, S. (2000) The tephrochronology of Iceland and the North Atlantic region during the Middle and Late Quaternary: a review *Journal of Quaternary Science Vol. 15 No. 1 Pg. 3-22*

Hansom, J. D. and Briggs, D. J. (1991) Sea-level change in Vestfirðir, North West Iceland In, Maizels, J. L. and Caseldine, C. J. (edits.) *Environmental Change in Iceland: Past and Present Dordrecht: Kluwer Pg. 79-91*

Hardardóttir, J.; Geirsdóttir, Á. And Sveinbjörnsdóttir, Á. E. (2001) Seismostratigraphy and sediment studies of Lake Hestvatn, southern Iceland: implications for deglacial history of the region *Journal Of Quaternary Science Vol. 16 Pg. 167-179*

Hartley, B.; Barber, H. G.; Carter, J. R. and Sims, P. A. (1996) An Atlas of British Diatoms *Bristol: Biopress*

Hayward, C. (2012) High spatial resolution electron probe microanalysis of tephras and melt inclusions without beam-induced chemical modification *The Holocene Vol. 22 No. 1 Pg. 119-125*

Hedenström, A. and Risberg, J. (1999) Early Holocene shore-displacement in southern central Sweden as recorded in elevated isolation basins *Boreas Vol. 28 No. 4 Pg. 490-504*

Helgadóttir, G. and Thors, K. (1998) Setlög í Ísafjarðardjúpi, Jökulfjörðum og Djúpál (In Icelandic). Geoscience Society of Iceland, Spring Meeting 1998, p. 12

Hjartarson, A. (1991) A revised model of Weichselian deglaciation in south and southwest Iceland, In, Maizels, J.K. and Caseldine, C. (eds.) Environmental Change in Iceland, Past and Present *Dordrecht: Kluwer Academic Pg. 67-77*

Hjartarson, A. and Ingólfsson, Ó. (1988) Preboreal glaciation of Southern Iceland *Jökull Vol. 38 Pg. 1-16*

Hjort, C.; Ingólfsson, Ó. and Norðdahl, H. (1985) Late Quaternary geology and glacial history of Hornstrandir, Northwest Iceland: a reconnaissance study *Jökull Vol. 35 Pg. 9-29*

Hodder, A. P. W.; de Lange, P. J. and Lowe, D. J. (1991) Dissolution and depletion of ferromagnesian minerals from Holocene tephra layers in an acid bog, New Zealand, and implications for tephra correlation *Journal of Quaternary Science Vol. 6 No. 3 Pg. 195-208*

Hoppe, G. (1968) Grimsey and the maximum extent of the last glaciation of Iceland *Geografiska Annaler Vol 50 Pg. 16-24*

Hoppe, G. (1982) The extent of the last inland ice sheet of Iceland *Jokull Vol. 35 Pg. 3-11*

Hubbard, A. (2006) The validation and sensitivity of a model of the Icelandic Ice Sheet *Quaternary Science Reviews Vol. 25 Pg. 2297-2313*

Hubbard, A.; Sugden, S.; Dugmore, A.; Norðdahl, H. and Pétursson, H. G. (2006) A modelling insight into the Icelandic Last Glacial Maximum ice sheet *Quaternary Science Reviews Vol. 25 Pg. 2283-2296*

Hughes, T. (1973) Is the west Antarctic Ice Sheet disintegrating? *Journal of Geophysical Research Vol. 78 No. 33 Pg. 7884-7910*

Hunt, J. B. and Hill, P. G. (1993) Tephra geochemistry: a discussion of some persistent analytical problems *The Holocene Vol. 3 No. 3 Pg. 271-278*

Ingólfsson, Ó. (1984) A review of late Weichselian studies in the lower part of the Borgarfjörður region, western Iceland *Jökull Vol. 34 pg. 117-130*

Ingólfsson, Ó. (1985) Weichselian Glacial Geology of the Lower Borgarfjörður, Western Iceland: a preliminary report *Arctic Vol. 38 No. 3 Pg. 210-213*

Ingólfsson, Ó. (1987) The late Weichselian glacial geology of the Melabakkar-Asbakkar coastal cliffs, Borgarfjörður, W-Iceland *Jökull Vol. 37 Pg. 57-80*

Ingólfsson, Ó. (1988) Glacial history of the lower Borgarfjörður area, western Iceland G*eologiska Föreningens i Stockholm Förhandlingar Vol. 110 Pg. 293-309.*

Ingólfsson, Ó. (1991) A review of the Late Weichselian and early Holocene glacial and environmental history of Iceland In, Caseldine, C. and Maizels, J. K. (edits.) *Environmental Change in Iceland: Past and Present Dordrecht: Kluwer Pg. 13-29*

Ingólfsson, A. (2009) A marine refugium in Iceland during the last glacial maximum: fact or fiction? *Zoologica Scripta Vol. 38 Pg. 663-665.*

Ingólfsson, Ó. and Hjort, C. (1999) The Antarctic contribution to Holocene global sea level rise *Polar Research Vol. 18 No. 2 Pg. 323-330*

Ingólfsson, Ó. and Norðdahl, H. (1994) A review of the environmental history of Iceland, 13000-9000 yr BP *Journal of Quaternary Science Vol. 9 No. 2 Pg. 147-150*

Ingólfsson, Ó. and Norðdahl, H. (2001) High relative sea level during the Bølling Interstadial in Western Iceland: a reflection of ice-sheet and extremely rapid glacial unloading *Arctic, Antarctic and Alpine Research Vol. 33 No. 2 Pg. 231-243*

Ingólfsson, Ó.; Norðdahl, H. and Hafliðason, H. (1995) Rapid isostatic rebound in southwestern Iceland at the end of the last deglaciation *Boreas Vol. 24 Pg. 245-259*

Ingólfsson, Ó.; Björck, S.; Hafliðason, H. and Rundgren, M. (1997) *Glacial and climatic events in Iceland reflecting regional North Atlantic climatic shifts during the Pleistocene-Holocene transition* Quaternary Science Reviews Vol. 16 Pg. 1135-1144

Ingólfsson, Ó.; Norðdahl, H. and Schomacker, A. (2010) Deglaciaiton and Holocene Glacial History of Iceland In, Schomacker, A.; Krüger, J. and Kjær, K. H. (edits.) The Mýrdalsjökull Ice Cap, Iceland: Glacial Processes, Sediments and Landforms on an active volcano *Developments in Quaternary Science 13 Pg. 51-68*

Ivins, E. R. and James, T. S. (2004) Bedrock response to Llanquihue Holocene and present-day glaciation in southernmost South America *Geophysical Research Letters Vol. 31 No. 24 DOI:* 10.1029/2004GL021500

Jakobsson, S.P.; Honsson, J. and Shido, F. (1978) Petrology of the western Reykjanes Peninsula, Iceland. *Journal of Petrology Vol. 19 Pg. 669-705.*

Jennings, A.; Syvitski, J.; Gerson, L.; Grönvold, K.; Geirsdóttir, Á.; Hardardóttir, J.; Andrews, J. and Hagen, S. (2000) Chronology and palaeoenvironments during the late Weichselian deglaciation of the south west Iceland shelf *Boreas Vol. 29 Pg. 167-183*

Jóhannesson, H. (1985) Um endaslepptu hraunin undir Eyjafjöllum og jökla síðasta jökulskeiðs *Jökull Vol. 35 Pg. 83-95*

John, B. (1975) Marine mollusca from Vestfirðir strandlines. *Durham University Vestfirðir Project 1975 Fieldwork Report and Research Notes Pg. 41-45.*

Joughin, I.; Smith, B. E. and Medley, B. (2014) Marine Ice Sheet Collapse Potentially Under Way for the Thwaites Glacier Basin, West Antarctica *Science Vol. 344 Pg. 735-738*

Jowsey, P. C. (1966) An Improved Peat Sampler *New Phytologist Vol. 65 No. 2 Pg. 245-248.*

Juggins, S. (2005) C2 Release 1.4 *University of Newcastle, United Kingdom*

Jull, M. and McKenzie, D. (1996) The effect of deglaciation on mantle melting beneath Iceland *Journal of Geophysical Research Vol. 101 No. 21 Pg. 815-828*

Keith, D. B. and Jones , E. W. (1935) Grimsey, North Iceland *Geographical Journal Vol. 86 Pg. 143-152*

Kjemperud, A. (1986) Late Weichselian and Holocene shoreline displacement in the Trondheimsfjord area, central Norway *Boreas Vol. 15 no. 1 Pg. 61-82.*

Kumar, P.; Kind, R.; Priestley, K. and Dahl-Jensen, T. (2007) Crustal structure of Iceland and Greenland from receiver function studies *Journal of Geophysical Research: Solid Earth Vol. 112 No. B3* DOI: 10.1029/2005JB003991

Lambeck, K. and Purcell, A. P. (2001) Sea-level change in the Irish Sea since the Last Glacial Maximum: constraints from isostatic modelling *Journal of Quaternary Science Vol. 16 No. 5 Pg. 497-506*

Lane, C. S.; Blockley, S. P. E.; Mangerud, J.; Smith, V. C.; Lohne, Ø. S.; Tomlinson, E. L., Matthews, I. P. and Lotter, A. F. (2012) Was the 12.1 ka Icelandic Vedde Ash one of a kind? *Quaternary Science Reviews Vol. 33 Pg. 87-99*

Larsen, G. and Eiriksson, J. (2008) Late Quaternary terrestrial tephrochronology of Iceland – frequency of expolsive eruptions, type and volume of tephra deposits *Journal of Quaternary Science Vol. 23 No. 109-120*

Larsen, C. F.; Motyka. R. J.; Freymueller, J. T.; Echelmeyer, K. A. and Ivins, E. R. (2005) Rapid viscoelastic uplift in southeast Alaska caused by post-Little Ice Age glacial retreat *Earth and Planetary Science Letters Vol. 237 Pg. 548-560*

Larsen, D.; Miller, G. H.; Geirsdóttir, Á. and Ólafsdóttir, S. (2012) Non-linear Holocene climate evolution in the North Atlantic: a high resolution, multi-proxy record of glacier activity and environmental change in Hvítárvatn, central Iceland *Quaternary Science Reviews Vol. 39 Pg 14-25*

Larsen, G.; Dugmore, A. J. and Newton, A. J. (1999) Geochemistry of historical-age silicic tephras in Iceland *The Holocene Vol. 9 Pg. 463-471*

Le Breton, E.; Dauteuil, O. and Biessy, G. (2010) Post-glacial rebound of Iceland during the Holocene *Journal of the Geological Society of London Vol. 167 Pg. 417-432*

Le Grande, A. N.; Schmidt, G. A.; Shindell, D. T.; Field, C. V.; Miller, R. L.; Koch, D. M.; Faluvegi, G. and Hoffmann, G. (2006) Consistent simulations of multiple proxy responses to an abrupt climate change event *Proceedings of the National Academy of Science Vol. 103 No. 4 Pg. 837-842*

Lefébure, P. (1947) Atlas pour la détermination des Diatomées *Paris: Laboratoire de Micrographie*

Lewis, C. F. M.; Miller, A. A. L.; Levac, E.; Pipera, D. J. W. and Sonnichsen, G. V. (2012) Lake Agassiz outburst age and route in Labrador Current and the 8.2 cal ka cold event *Quaternary International Vol. 260 Pg 83-97.*

Lloyd, J. M. and Evans, J. R. (2002) Contemporary and fossil foraminifera from isolation basins in northwest Scotland *Journal of Quaternary Science Vol. 17 No. 5-6 Pg. 431-443*

Lloyd, J. M.; Norðdahl, H.; Bentley, M. J.; Newton, A. J.; Tucker, O. and Zong, Y. (2009) Lateglacial to Holocene relative sea-level changes in the Bjarkarlundur area near Reykhólar, North West Iceland *Journal of Quaternary Science Vol. 24 No. 7 Pg. 816-831*

Lohne, Ø. S.; Mangerud, J. and Birks, H. H. (2014) IntCal13 calibrated ages of the Vedde and Saksunarvatn ashes and the Younger Dryas boundaries from Kråkanes, western Norway *Journal of Quaternary Science Vol. 29 No. 5 Pg. 506-507*

Long, A. J.; Woodroffe, S. A.; Dawson, S.; Roberts, D. H.; Bryant, C. (2009) Late Holocene relative sea-level rise and the Neoglacial history of the Greenland Ice Sheet *Journal of Quaternary Science Vol. 24 Pg. 345-359*

Long, A. J.; Woodroffe, S. A.; Roberts, D. H. and Dawson, S. (2011) Isolation basins, sea-level changes and the Holocene history of the Greenland Ice Sheet *Quaternary Science Reviews Vol. 30 Pg. 3748-3768*

Long, A. J.; Woodroffe, S. A.; Milne, G. A.; Bryant, C. L.; Simpson, M. J. R. and Wake, L. M. (2012) Relative sea-level change in Greenland during the last 700 years and ice sheet response to the Little Ice Age *Earth and Planetary Science Letters Vol. 315-316 Pg. 76-85*

Lowe, D. J. (2011) Tephrchronology and its application: a review *Quaternary Geochronology Vol. 6 Pg. 107-153*

Lowe, J. J. and Walker, M. J. C. (1997) Reconstructing Quaternary Environments *Pearson Prentice Hall: Harlow, UK*

MacLennan, J.; Jull, M.; McKenzie, D.; Slater, L. and Grönvold, K. (2002) The link between volcanism and deglaciation in Iceland G*eochemistry, Geophysics, Geosystems Vol. 3 No. 11 1062 doi: 10.1029/2001GC000282*

Mangerud, J.; Lie, S. E.; Furnes, H.; Kristianssen, I. L. and Lomo, L. (1984) A Younger Dryas ash bed in western Norway and its possible correlation with tephra in cores from the Norwegian Sea and the North Atlantic. *Quaternary Research Vol. 21 Pg. 85–104.*

Mangerud, J.; Furnes, H. J. and Johannessen, J. (1986) A 9000 year old ash bed on the Faroe Islands *Quaternary Research Vol. 26 Pg. 262-265*

McManus, J. F.; Francois, R.; Gherardi, J.-M.; Keigwin, L. D. and Brown-Leger, S. (20040 Collapse and rapid resumption of Atlantic meridional circulation linked to deglacial climate changes *Nature Vol. 428 Pg. 834-837*

Meyer, H. H. and Venzke, J.-F. (1987) Deglaciation and sea-level changes in the vicinity of Blönduós, northern Iceland, in late glacial and early Holocene times: a preliminary report *Norden Vol. 4 pg. 47-64.*

Mineter, M. J. and Hulton, N. R. J. (2001) Parallel processing for finite difference modelling of ice sheets *Computers and Geosciences Vol. 27 Pg. 829-838*

Mitrovica, J. X.; Tamisiea, M. E.; Davis, J. L. and Milne, G. A. (2001) Recent mass balance of polar ice sheets inferred from patterns of global sea-level change *Nature Vol. 409 Pg. 1026-1029*

Mitrovica, J. X.; Gomez, N. and Clark, P. U. (2009) The sea-level fingerprint of West Antarctic Collapse *Science Vol. 323 No. 5915 Pg. 753*

Moriwaki, H. (1990) Late and postglacial shoreline displacement and glaciation in and around the Skagi peninsula, northern Iceland *Geographical Reports of Tokyo Metropolitan University Vol. 25 Pg. 81-97*

Motyka, R. J. (2003) Little Ice Age Subsidence and Post Little Ice Age Uplift at Juneau, Alaska inferred from Dendrochronology and Geomorphology *Quaternary Research Vol. 59 Pg. 300-309*

Newton, A.J. (1996) Tephrabase: A Tephrochronological Database. *Quaternary Newsletter Vol. 78 Pg. 8-13*.

Newton, A.J., Dugmore, A.J. and Gittings, B.M. (2007) Tephrabase: tephrochronology and the development of a centralised European database. *Journal of Quaternary Science Vol. 22 Pg. 737-743*

Norðdahl, H. (1991) A review of the glaciation maximum concept and the deglaciation of Eyjafjörður, North Iceland In, Maizels, J. K. and Caseldine, C. (eds.) Environmental changes in Iceland: past and Present *Dordrecht: Kluwer Academic Publishers Pg. 31-47.*

Norðdahl, H. and Ásbjörnsdóttir, L. (1995) Ísaldarlok í Hvammsfirði In, Hróarsson, B.; Jónsson, D.; Jónsson, S. S. (edits.) *Eyjar í Eldhafi Reykjavik: Gott mál Pg. 117-131*

Norðdahl, H. and Einarsson, T. (2001) Concurrent changes of relative sea-level and glacier extent at the Weichselian-Holocene boundary in Berufjörður, eastern Iceland *Quaternary Science Reviews Vol. 20 Pg. 1607-1622*

Norðdahl, H. and Hjort, C. (1987) Aldur jökulhörfunar í Vopnafirði, Abstract Volume, *Reykjavik: Jarðfræðafélag Íslands Pg. 18-19*

Norðdahl, H. and Pétursson, H. G. (2005) Relative sea-level changes in Iceland: new aspects of the Weichselian deglaciation of Iceland In, Caseldine, C.; Russell, A.; Harðardóttir, J. and

Knudsen, O. (eds.) Iceland: Modern Processes and Past Environments *Amsterdam: Elsevier Pg. 25-78*

Norðdahl, H. and Ásbjörnsdóttir, L. (1994) Ísaldarlok í Hvammsfirði In, Hróarsson, B.; Jónsson, D.; Jónsson, S. S. (edits.) *Eyjar í Eldhafi Reykjavik: Gott mál Pg. 117-131*

Norðdahl, H. and Hjort, C. (1987) Aldur jökulhörfunar í Vopnafirði, Abstract Volume, *Reykjavik: Jarðfræðafélag Íslands Pg. 18-19*

Norðdahl, H.; Ingólfsson, Ó.; Pétursson, H. G. and Hallsdóttir, M. (2008) Late Weichselian and Holocene environmental history of Iceland *Jökull Vol.58 Pg 343-364.*

Ólafsdóttir, T. (1975) A moraine ridge on the Iceland shelf, west of Breiðafjörður *Natturufredinggurin Vol. 45 Pg. 31-37*

Pagli, C.; Sigmundsson, F.; Lund, B.; Sturkell, E.; Geirsson, H.; Einarsson, P.; Árnadóttir, T. and Hreinsdóttir, S. (2007) Glaio-isostatic deformation around the Vatnajökull ice cap, Iceland, induced by recent climate warming: GPS observations and finite element modelling *Journal of Geophysical research: Solid Earth Vol. 112 No. B8 DOI: 10.1029/2006JB004421*

Pálmason, G. (1971) Crustal structure of Iceland from explosion seismology *Soc. Sci. Icl. Vol. 40 187pp*

Palmer, A. J. M. and Abbott, W. H. (1986) Diatoms as indicators of sea-level change In, van der Plassche, O. (edit.) Sea-Level Research: a Manual for the Collection and Evaluation of Data *Norwich: Geo Books Pg. 457-488*

Patton, H. (unpub.) Modelling the dynamic evolution and sensitivities of two palaeo-ice masses: the Welsh Ice Cap and the Icelandic Ice Sheet *University of Aberystwyth: Unpublished PhD Thesis*

Payne, R. and Gehrels, M. J. (2010) The formation of tephra layers in peatlands: an experimental approach *Catena Vol. 81 Pg. 12-23*

Peltier, W. R. (1998) Postglacial variations in the level of the sea: implications for climate dynamics and solid-Earth geophysics *Reviews of Geophysics Vol. 36 No. 4 Pg. 603-689*

Peltier, W. R. (2004) Global glacial isostacy and the surface of the ice-age Earth: the ICE-5G (VM2) Model and GRACE *Annual Reviews of Earth and Planetary Sciences Vol. 32 Pg. 111-149*

Peltier, W. R.; Argus, D. F. and Drummond, R. (2015) Space geodesy constrains ice age terminal deglaciation: the global ICE-6G_C (VM5a) model *Journal of Geophysical Research: Solid Earth Vol. 120 No. 1 Pg. 450-487*

Persson, C. (1971) Tephrochronological investigations of peat deposits in Scandinavia and on the Faroe Islands. *Sveriges Geologiska Undersokning Arbok Vol. 65 No. 2 Pg. 1-34*

Pollard, A. M.; Blackley, S. P. E. and Ward, K. R. (2003) Chemical alteration of tephra in the depositional environment: theoretical stability modelling *Journal of Quaternary Science Vol. 18 No. 5 Pg. 385-394*

Pollitz, F. F. and Sachs, I. S. (1996) Viscosity structure beneath northeast Iceland *Journal of Geophysical Research: Solid Earth Vol. 101 No. B8 DOI: 10.1029/96JB01074*

Principato, S. M. (2003) The late quaternary history of Eastern Vestfirðir, NW Iceland. *University of Wisconsin-Madison*

Principato, S. M. (2008) Geomorphic evidence for Holocene glacial advances and sea level fluctuations on eastern Vestfirðir, northwest Iceland *Boreas Vol. 37 Pg. 132-145*

Principato, S. and Geirsdóttir, A. (2002) Glacial erosion patterns and moraine sequences on the Northwest Peninsula of Iceland *Programs with Abstracts Vol. 34 Geological Society of America 34 Denver*

Pritchard, H. D.; Ligtenberg, S. R. M.; Fricker, H. A.; Vaughan, D. A.; van den Broeke, M. R. and Padman, L. (2012) Antarctic ice-sheet loss driven by basal melting of ice shelves *Nature Vol. 484 Pg. 502-505*

Quillman, U.; Jennings, A. and Andrews J. (2010) Reconstructing Holocene palaeoclimate and palaeoceanography in Ísafjarðardjúp, northwest Iceland, from two fjord records overprinted by relative sea-level and local hydrographic changes *Journal of Quaternary Science Vol. 25 No. 7 Pg. 1144-1159*

Rae, A. C.; Harrison, S.; Mighall, T. and Dawson, A.G. (2004) Periglacial trimlines and nunataks of the Last Glacial Maximum: the gap of Dunloe, southwest Ireland *Journal of Quaternary Science Vol. 19 Pg. 87-97*

Raymond, C. (1996) Shear margins in glaciers and ice sheets *Journal of Glaciology Vol. 42 No. 140 Pg. 90-102.*

Reimer, P. J.; Bard, E.; Bayliss, A.; Beck, J. W.; Blackwell, P. G.; Bronk Ramsey, C.; Buck, C. E.; Cheng, H.; Edwards, R. L.; Friedrich, M.; Grootes, P. M.; Guilderson, T. P.; Haflidason, H.; Hajdas, I.; Hatté, C.; Heaton, T. J.; Hoffmann, D. L.; Hogg, A. G.; Hughen, K. A.; Kaiser, K. F.; Kromer, B.; Manning, S. W.; Niu, M.; Reimer, R. W.; Richards, D. A.; Scott, E. M.; Southon, J. R.; Staff, R. A.; Turney, C. S. M. and van der Plicht, J. (2013) IntCal13 and Marine13 radiocarbon age calibration curves 0-50,000 years cal BP *Radiocarbon Vol. 55 No. 4 Pg. 1869-1887*

Romundset, A.; Fredin, O. and Høgaas, F. (2014) A Holocene sea-level curve and revised isobase map based on isolation basins from near the southern tip of Norway *Boreas Early View* DOI: 10.1111/bor.12105

Rundgren, M. (1995) Biostratigraphic evidence of the Allerød-Younger Dryas-Preboreal Oscillation in Northern Iceland *Quaternary Research Vol. 44 Pg. 405-416*

Rundgren, M. (1999) A summary of the environmental history of the Skagiu peninsula, northern Iceland, 11300 – 7800 BP *Jökull Vol. 47 Pg. 1-19*

Rundgren, M. and Ingólfsson, Ó. (1999) Plant survival in Iceland during periods of glaciation? *Journal of Biogeography Vol. 26 Pg. 387-396*

Rundgren, M.; Ingólfsson, Ó.; Björck, S.; Jiang, H. and Hafliðason, H. (1997) Dynamic sea-level change during the last deglaciation of northern Iceland *Boreas Vol. 26 Pg. 201-215*

Saher, M. H.; Gehrels, W. R.; Barlow, N. L. M.; Long, A. J.; Haigh, I. D. and Blaauw, M. (2015) Sea-level changes in Iceland and the influence of the North Atlantic Oscillation during the last half millennium *Quaternary Science Reviews Vol. 108 Pg. 23-36*

Sandgren, P.; Snowball, I. F.; Hammarlund, D. and Risberg, J. (1999) Stratigraphic evidence for a high marine shoreline during the Late Weichselian deglaciation on the Kullen peninsula, southern Sweden *Journal of Quaternary Science Vol. 14 No. 3 Pg. 223-237*

Schilling, J.-G. (1973) Iceland Mantle Plume: Geochemical Study of Reykjanes Ridge *Nature Vol. 242 No. 5400 Pg. 565-571*

Schmidt, P.; Lund, B.; Árnadóttir, T. and Schmeling, H. (2011) Accessing the 3D viscosity structure beneath Iceland using glacial isostatic adjustment (GIA): insights into dehydration stiffening and the rheology of the upper mantle *Americal Geophysical Union Fall Meeting 2011 Abstracts*

Schmidt, P.; Lund B.; Árnadóttir, T. and Schmeling, H. (2012) Glacial isostatic adjustment constrains dehydration stiffening beneath Iceland *Earth and Planetary Science Letters Vol. 359-360 Pg. 152-161*

Schmidtko, S.; Heywood, K. J.; Thompson, A. F. and Aoki, S. (2014) Multidecadal warming of Antarctic waters *Science Vol. 346 No. 6214 Pg. 1227-1231*

Shen, Y.; Solomon, S. C.; Bjarnason, I. Th.; Nolet, G.; Morgan, W. J.; Allen, R. M.; Vogfjörd, K.; Jakobsdóttir, S.; Stefánsson, R.; Julian, B. R. and Foulger, G. R. (2002) Seismic evidence for a tilted mantle plume and north-south mantle flow beneath Iceland *Earth and Planetary Science Letters Vol. 197 No. 3-4 Pg. 261-272*

Shennan, I. (2015) Chapter 2: Handbook of sea-level research: framing research questions In, Shennan, I.; Long, A. J. and Horton, B. Handbook of Sea-Level Research *Wiley: Chichester Pg. 3-24*

Shennan, I.; Innes, J.B.; Long, A.J. and Zong, Y. (1994) Late Devensian and Holocene relative sea-level changes at Loch nan Eala, near Arisaig, Northwest Scotland. *Journal of Quaternary Science Vol. 9 Pg. 261-283*

Shennan, I.; Innes, J. B.; Long, A. J. and Zong, Y. (1995) Late Devensian and Holocene relative sea-level changes in northwest Scotland: new data to test existing models *Quaternary International Vol. 26 Pg. 97-123*

Shennan, I.; Milne, G. and Bradley, S. (2012) Late Holocene vertical land motion and relative sea-level changes: lessons from the British Isles *Journal of Quaternary Science Vol. 27 Pg. 64-70*

Sigbjarnarson, G. (1983) The Quaternary Alpine Glaciation and Marine Erosion in Iceland *Jökull Vol. 33 Pg. 87-98*

Sigmundsson, F. (1991) Post-glacial rebound and asthenospheric viscosity in Iceland *Geophysical Research Letters Vol. 18 No. 6 Pg. 1131-1134*

Sigmundsson, F. (2006) Iceland Geodynamics – Crustal Deformation and Divergent Plate Tectonics *Chichester, UK: Praxis Publishing 233pp.*

Sigmundsson, F. and Einarsson, P. (1992) Glacio-isostatic crustal movements caused by historical volume change of the Vatnajökull Ice Cap, Iceland *Geophysical Research Letters Vol. 19 No. 21 Pg. 2123-2126*

Sigurgeirsson, M. Á.; Hauptfleisch, U.; Newton, A. J. and Einarsson, Á. (2013) Dating of the Viking Age Landnám Tephra Sequence in Lake Mývatn Sediment, North Iceland *Journal of the North Atlantic Vol. 21 Pg 1-11*

Sigurvinsson, J. R. (1983) Weichselian glacial lake deposits in the highlands of Northwestern Iceland *Jokull Vol. 33 Pg. 99-109.*

Simonarson, L. A. (1979) Jardfraedi Hornstranda og Jokulfjarda *Kaldbakur 6-7 Pg. 24-33*

Simonarson, L. A. and Leifsdóttir, Ó. E. (2002) Late-Holocene sea-level changes in south and southwest Iceland reconstructed from littoral molluscan stratigraphy *The Holocene Vol. 12 No. 2 Pg. 149-158*

Sjöberg, L. E.; Pan, M.; Erlingsson, S.; Asenjo, E. and Arnason, K. (2004) Land uplift near Vatnajökull, Iceland, as observed by GPS in 1992, 1996 and 1999 *Geophysical Journal International Vol. 159 No. 3 Pg. 943-948*

Smith, G. M. (1950) Freshwater algae of the United States *McGraw-Hill*

Smith, I. R.; Bell, T. and Renouf, M. A. P. (2005) Testing a proposed Late Holocene Sea-Level Oscillation using the isolation basin approach, Great Northern Peninsula, Newfoundland *Newfoundland and Labrador Studies Vol. 20 No. 1 Pg. 33-55.*

Spada, G. (pers. comm. a) Email correspondence regarding build.f90 script

Spada, G. (pers. comm. b) Email correspondence regarding conversion from grid to discs

Spada, G. (2003) The theory behind TABOO *Colorado and Vermont: Samizdat Press*

Spada, G. and Stocchi, P. (2007) SELEN: a Fortran 90 program for solving the "sea-level equation" *Computers and Geosciences Vol. 33 No. 4 Pg. 538-562*

Spada, G.; Antonioil, A.; Boschi, L.; Galvani, G.; Giunchi, C.; Perniola, B.; Agostinetti, N. P.; Piersanti, A. and Stocchi, P. (2004) Modelling Earth's post-glacial rebound *EOS Transactions American Geophysical Union Vol. 85 No. 6 Pg. 62-64*

Spada, G.; Ruggieri, G.; Sørensen, L. S.; Nielsen, K.; Melini, D. and Colleoni, F. (2012) Greenland uplift and regional sea-level changes from ICESat observations and GIA modelling *Geophysical Journal International Vol. 189 No. 3 Pg. 1457-1474*

Spagnolo, M. and Clark, C. D. (2009) A geomorphological overview of glacial landforms on the Icelandic continental shelf *Journal of Maps Vol. 5 No. 1 Pg. 37-52*

Steinþórsson, H. (1967) Tvær nyjar C14-aldursákvardanir á öskulögum úr Snæfellsjökli. *Náttúrufroedingurinn Vol. 37 Pg. 236–238.*

Steindórsson, S. (1962) On the age and immigration of the Icelandic flora *Rit Visindafélags Islendinga Vol. 35 Pg. 1-157*

Steindórsson, S. (1963) Ice age refugia in Iceland as indicated by the present distribution of plant species In, Löve A. and Löve, D. (eds.) North Atlantic biota and their history *Oxford: Pergamon Press Pg. 303-320.*

Streeter, R.; Dugmore, A. J. and Vésteinsson, O. (2012) Plague and landscape resilience in premodern Iceland *Proceedings of the National Academy of Sciences Vol. 109 No. 10 Pg. 3664-3669*

Stocchi, P. and Spada, G. (2009) Influence of glacial isostatic adjustment upon current sea level variations in the Mediterranean *Tectonophysics Vol. 474 No. 1-2 Pg. 56-68*

Stuiver, M. and Braziunas, T. F. (1993) Modelling atmospheric ^{14}C influences and ^{14}C ages of marine samples to 10000 BC *Radiocarbon Vol. 35 Pg. 137-189*

Stuiver, M. and Polach, H. A. (1977) Discussion: Reporting of 14C data *Radiocarbon Vol. 19 No. 3 Pg. 355-363*

Stuiver, M.; Reimer, P. J. and Reimer, R. (2014) CALIB7.1 [online] available from: http://calib.qub.ac.uk/calib/

Svendsen, J. J. and Mangerud, J. (1987) Late Weichselian and Holocene sea-level history for a cross-section of western Norway *Journal of Quaternary Science Vol. 2 pg. 113-132*

Swindles, G. T.; De Vleeschouwer, F. and Plunkett, G. (2010) Dating peat profiles using tephra: stratigraphy, geochemistry and chronology *Mires and Peat Vol. 7 Article 5 Pg. 1-9*

Syvitski, J. P.; Jennings, A. E. and Andrews, J. T. (1999) High resolution seismic evidence for multiple glaciation across the southwest Iceland shelf *Arctic and Alpine Research Vol. 31 Pg. 50-57*

Tamisiea, M. E. and Mitrovica, J. X. (2011) The moving boundaries of sea-level change: understanding the origins of geographical variability *Ocenography Vol. 24 No. 2 Pg. 24-39*

Tegmark, M. (1996) An isohedron-based method for pixelizing the celestial sphere *ApJ Letters Vol. 470 L81-L84*

Thoma, M.; Wolf, D. and Neumeyer, J. (2002) Inverting land uplift near Vatnajökull, Iceland, in terms of lithospheric thickness and viscosity stratification In, Sideris, M. G. Gravity, Geoid and Geodynamics 2000 GGG2000 IAG International Symposium, Alberta, Canada *Berlin/Heidelberg: Springer Pg. 97-102*

Thorodssen, Th. (1892) Islands Jøkler i Fortid og Nutid *Geofrafisk Tidskrift11 (5-6) 1891-1892 Pg. 111-146*

Thorodssen, Th. (1905-1906) Island: Grundiss der geographie und geologie *Justus Perthes: Gotha Pg.358*

Thórarinsson, S. (1944) Tefrokronologiska studier på Island G*eografiska Annaler Vol. 26 Pg. 1-217*

Thórarinsson, S. (1956) Mórinn i Seltjörn [English summary: The submerged peat in Seltjörn] *Nátúrufrædingurinn Vol. 26 Pg. 179-193*

Thórarinsson, S. (1958) The Öræfajökull eruption of 1362 AD *Acta Naturalia Islandica Vol. 2 No. 2 Pg. 1-99*

Thórarinsson, S. (1967) The eruptions of Hekla in historical times *The Eruption of Hekla 1947-1948 Vol. 1 Pg. 1-170*

Thórarinsson, S. (1975) Katla and the annals of Katla tephras (in Icelandic) *Árbók Ferðafélags Islands 1975 Pg. 125-149*

Thordarson, T. And Larsen, G. (2007) Volcanism in Iceland in historical time: volcano types, eruption styles and eruptive history *Journal of Geodynamics Vol. 43 No. 1 Pg. 118-152*

Thornalley, D. J. R.; Elderfield, H. and McGave, I. N. (2009) Holocene oscillations in temperature and salinity of the surface subpolar North Atlantic *Nature Vol. 457 Pg. 711-714*

Thornalley, D. J. R.; McGave, I. N. and Elderfield, H. (2010) Freshwater input and abrupt deglacial climate change in the North Atlantic *Paleoceanography Vol. 25 No. 1 DOI: 10.1029/2009PA001772*

Thors, K. and Boulton, G. S. (1990) Deltas, spits and littoral terraces associated with rising sea level: Late Quaternary examples from northern Iceland *Marine Geology Vol. 98 Pg. 99-112*

Thors, K. and Helgadóttir, G. (1991) Evidence from south west Iceland of low sea-level in Flandrian times In, Maizels, J. K. and Caseldine, C (edits.) Environmental Change in Iceland: Past and Present Pg. 93-104 *Kluwer Academic: Dordrecht*

Thorseth, I. H.; Furnes, H. and Tumyr, O. (1995) Textural and chemimcal effects of bacterial activity on basaltic glass: an experimental approach *Chemical Geology Vol. 119 No. 1-4 Pg. 139-160*

Tröels-Smith, K. (1955) Characterisation of unconsolidated sediments *Danm. Geol. Unders. Ser. IV No. 3 (10).*

Tryggvason, K.; Husebye, E. S. and Stefánsson, R. (1983) Seismic image of the hypothesized Icelandic hot spot *Tectonophysics Vol. 100 No. 1-3 Pg. 97-118*

Tushingham, A. M. and Peltier, W. R. (1991) ICE-3G: A new global model of Late Pleistocene deglaciation based on geophysical predictions of post-glacial relative sea level change *Journal of Geophysical Research: Solid Earth Vol. 96 No. B3 Pg. 4497-4523*

Tushingham, A. M. and Peltier, W. R. (1993) Relative Sea Level Database *IGPB PAGES/World Data Center-A for Paleoclimatology Data Contribution Series 93-106 NOAA/NGDC Paleoclimatology Program, Boulder, USA.*

Verleyen, E.; Hodgson, D. A.; Sabbe, K.; Vanhoutte, K. and Vyverman, W. (2004) Coastal oceanographic conditions in the Prydz Bay region (East Antarctica) during the Holocene recorded in an isolation basin *The Holocene Vol. 14 No. 2 Pg. 246-257*

Vikingsson, S. (1978) The deglaciation of the southern part of the Skagafjördur district, Northern Iceland. *Jökull Vol. 28 Pg. 1–17*

Vogt, P. R. (1983) The Iceland Mantle Plume: Status of the hypothesis after a decade of new work In, Bott, M. H. P.; Saxov, S.; Talwani, M. and Thiede, J. (eds.) Structure and Development

of the Greenland-Scotland Ridge New Methods and Concepts *Nato Conference Series Volume 8 New York: Springer Science and Business Media*

van der Wal, W.; Whitehouse, P. and Schrama, E. J. O. (2015) Effect of GIA models with 3D composite mantle viscosity on GRACE mass balance estimates for Antarctica *Earth and Planetary Science Letters Vol. 414 Pg. 134-143.*

Warren, W. P. (1979) Moraines on the northern slopes and foothills of the Macgillycuddy's Reeks, south-west Ireland In, Schlüchter, C. (ed.) *Moraines and Varves* Pg. 223-236 Balkema: Rotterdam

Weir, N. R. W.; White, R. S.; Brandsdóttir, B.; Einarsson, P.; Shimamura, H. and Shiobara, H. (2001) Crustal structure of the northern Reykjanes Ridge and Reykjanes Peninsula, southwest Iceland *Journal of Geophysical Research: Solid Earth Vol. 106 No. B4 DOI: 10.1029/2000JB900358*

Wessell, P. and Smith, W. H. F. (1991) Free software helps map and display data *EOS Transactions American Geophysical Union Vol. 72 No. 41 Pg. 441-446*

Westgate, J. A. and Gorton, M. P. (1981) Correlation techniques in tephra studies In, Self, S. and Sparks, S. R. J. (edits.) Tephra Studies *Pg. 73-94 Dordrecht: Reidel*

White, R. S.; Minshull, T. A.; Richardson, K. R.; Smallwood, J. R.; Staples, R. K.; McBride, J. H.; Maguire, P. K. H.; Brandsdóttir, B.; Menke, W. and The FIRE Working Group (1996) Seismic images of crust beneath Iceland contribute to long-standing debate *EOS Transactions American Geophysical Union Vol. 77 No. 21 Pg. 197-201*

Whitehouse, P. L.; Bentley, M. J.; Milne, G. A.; King, M. A. and Thomas, I. D. (2012) A new glacio-isostatic adjustment model for Antarctica: calibrated and tested using observations of relative sea-level change and present-day uplift rates *Geophysical Journal International Vol. 190 No. 3 Pg. 1464-1482*

Wolfe, C. J.; Bjarnason, I. T.; Van Decar, J. C.; Solomon, S. C. (1997) Seismic structure of the Iceland mantle plume *Nature Vol. 385 Pg. 245-247*

Wright, W. B. (1927) The Geology of Killarney and Kenmare *Memoirs of the Geological Survey of Ireland: Dublin*

Zeeberg, J.; Lubinski, D. J. and Forman, S. L. (2001) Holocene relative sea-level history of Novaya Zemlya, Russia, and implications for Late Weichselian Ice Sheet Loading *Quaternary Research Vol. 56 Pg. 218-230*

Zillén, L. M.; Wastegård, S. and Snowball, I. F. (2002) Calendar year ages of three min-Holocene tephra layers identified in varved lake sediments in west central Sweden *Quaternary Science Reviews Vol 21 No. 14-15 Pg. 1583-1591*